THE ANATOKI FAULT AND STRUCTURE OF THE ADJACENT BULLER AND TAKAKA TERRANE ROCKS, NORTHWEST NELSON, NEW ZEALAND.

A thesis

submitted in fulfilment

of the requirements for the Degree

of

Doctor of Philosophy in Geology

at the

University of Canterbury

by

RICHARD JONGENS

University of Canterbury

July 1997

Frontispiece: Adelaide Tarn and Mt Douglas (right of photograph) in the heart of Kahurangi National Park. In the background are the Dragons Teeth (centre) and Anatoki Peak (left).

Abstract

The Early Paleozoic rocks exposed in the northwest of the South Island, New Zealand, can be grouped into two terranes. An Ordovician deep water passive margin assemblage makes up the Buller terrane. A Cambrian arc assemblage and an Ordovician to Silurian mainly shallow water passive margin assemblage make up the Takaka terrane. The two terranes are cut by Late Paleozoic and Early Cretaceous plutonic rocks. The terrane boundary is the Anatoki Fault, which is a north-south striking, east dipping structure that steepens southwards. This thesis is a study of the movement history of the Anatoki Fault and a study of structures and microstructures in the flanking lithologies of the Buller and Takaka terranes. The study area is divided into seven areal domains, each containing structural evidence that can be related on an inter-domainal scale.

In the study area, three major deformation events can be recognised in both the Buller and Takaka terrane rocks. Each consecutive deformation event recognised in one of the terranes has structures that can be matched in style, orientation, and timing of development with that in the adjacent terrane. D_1 is represented by upright to overturned towards the west, N-S trending, large scale folds with an axial planar slaty cleavage. D_1 structures are observed in all domains and relate to other N-S trending structures seen in both terranes. Based principally on constraints outside the study area, D_1 is thought to be Early-Middle Devonian in age. A well-developed foliation, which obliterates D_1 structures in close to the Anatoki Fault, represents D_2. The foliation expresses a zone of non-coaxial ductile deformation observed in the north of the study area. Rb-Sr geochronology, and the relationship between the foliation and the adjacent ~111Ma Mt Olympus Pluton, suggest D_2 formed in the Early Cretaceous (soon after ~111Ma). D_3 is represented mainly by mesoscale folds with an axial planar crenulation cleavage. D_3 structures crenulate and refold both D_1 and D_2 structures and are mid-Cretaceous in age.

Two deformations are recognised in the Balloon Mélange of the Takaka terrane. The first deformation is responsible for the mélanging when the protolith was in an unlithified state. This deformation occurred in the Late Cambrian. The second deformation is expressed by a slaty fabric when the mélange was lithified and is thought to be related to D_1. The contact between the Balloon Mélange and other units in the Takaka terrane is thought to be tectonic but locally intrusive.

Most structures in Northwest Nelson can be correlated with D_1, D_2, and D_3 of the study area. However, some N-S trending folds in the Cambrian arc assemblage are thought to be older than D_1 and are here thought to relate to pre-D_1 Late Cambrian deformation recognised in the Balloon Mélange.

The Anatoki Fault records a complex history of both ductile and brittle movement, a history which differs in various segments of the fault. Thus, tectonites from central segments of the study area record ductile east over west reverse-slip associated with D_1, and represent an early stage in its movement history; D_2 tectonites from the northernmost studied segment record Early Cretaceous ductile dextral-slip reactivation; tectonites from the southernmost segment records ductile/brittle dextral normal-slip reactivation that postdates the intrusion of the ~137Ma Crow Granite. The post-137Ma movement, and brittle/ductile movement of unknown age recorded in the remaining segments, may be related to D_2. The Anatoki Fault has also undergone Late Cenozoic brittle reactivation.

A plate tectonic model is developed to explain the earlier structures of the study area and the general structure of Northwest Nelson. It is proposed that an accretionary wedge/fore-arc setting related to a Cambrian island arc subduction zone provides the environment in which pre-D_1 structures formed, and that in the Early-Middle Devonian, the two terranes amalgamated as a result of a convergent strike-slip plate boundary. Much of the Takaka terrane was truncated by the strike-slip movement which dominated the early stages of Devonian deformation whereas convergence related thin-skinned tectonics dominated the latter stages of deformation, and resulted in formation of the D_1 structures. In this model, the Central Belt of the Takaka terrane, which consists primarily of the Cambrian arc assemblage, is interpreted as an uplifted tectonic wedge in which the Anatoki Fault is a back-thrust. D_2 and D_3 relate to an extremely active and changing tectonic period of New Zealand in the Early to mid-Cretaceous.

Twinning in ankerite porphyroblasts in D_2 tectonites was examined to investigate the twin laws and their usefulness as a paleostress indicator. Results show that the twin laws are the same as those in dolomite and that twinning occurs at temperatures above ~250°C. Paleostress axes derived from the analysis provide evidence of microscale strain partitioning in which the porphyroblasts have accommodated a pure shear component. The *c*-axes preferred orientations in dynamically recrystallised calcite tectonites, from the Anatoki Fault zone, most closely resemble those produced in the grain-boundary migration regime of experimental studies. As such, the preferred orientations cannot be used to indicate shear-sense.

TABLE OF CONTENTS

CHAPTER 1

INTRODUCTION

1.1 Northwest Nelson basement geology

The basement geology of Northwest Nelson is made up of Early Paleozoic sedimentary rocks and Late Paleozoic/Early Cretaceous intrusives (mainly granitoids). The sediments are divided into two tectonostratigraphic suspect terranes, Buller terrane in the west and Takaka terrane in the east (Fig. 1.1) (Cooper 1989). The Buller terrane[1] consists of Ordovician quartz-rich sandstone, siltstone, and black shale. The Takaka terrane contains a varied assemblage of Middle to Late Cambrian volcanics, volcaniclastics, limestone, turbidites, and conglomerates; Ordovician limestone, shale, and sandstone; and Silurian quartzite.

Of the two suspect terranes, the Takaka terrane is the most structurally and stratigraphically complex. The terrane comprises of at least 13 north-south trending fault-bounded slices, each with an internally consistent stratigraphy that differs somewhat to that of its neighbours (Cooper and Tulloch 1992; Cooper 1993). The Devil River Fault and its associated zone of ductile deformation (Waingaro Schist; Powell 1985), separates the western Cambrian dominated half of the terrane, referred to here as the Central Belt, from the eastern Ordovician/Silurian dominated half of the terrane, referred to here as the Eastern Belt[2] (Fig. 1.1, 1.2).

Both the Buller and Takaka terranes are cut by Late Paleozoic and Early Cretaceous plutonic rocks, and together make up the Western Province of New Zealand (Landis and

[1] The Buller terrane is historically known as the Western Sedimentary Belt (Cooper 1979a).
[2] Historically the Central and Eastern Belts are known as the Central and Eastern Sedimentary Belts (Cooper 1979a). The word "sedimentary" has been abandoned here because it suggests the two belts are stratigraphically separate.

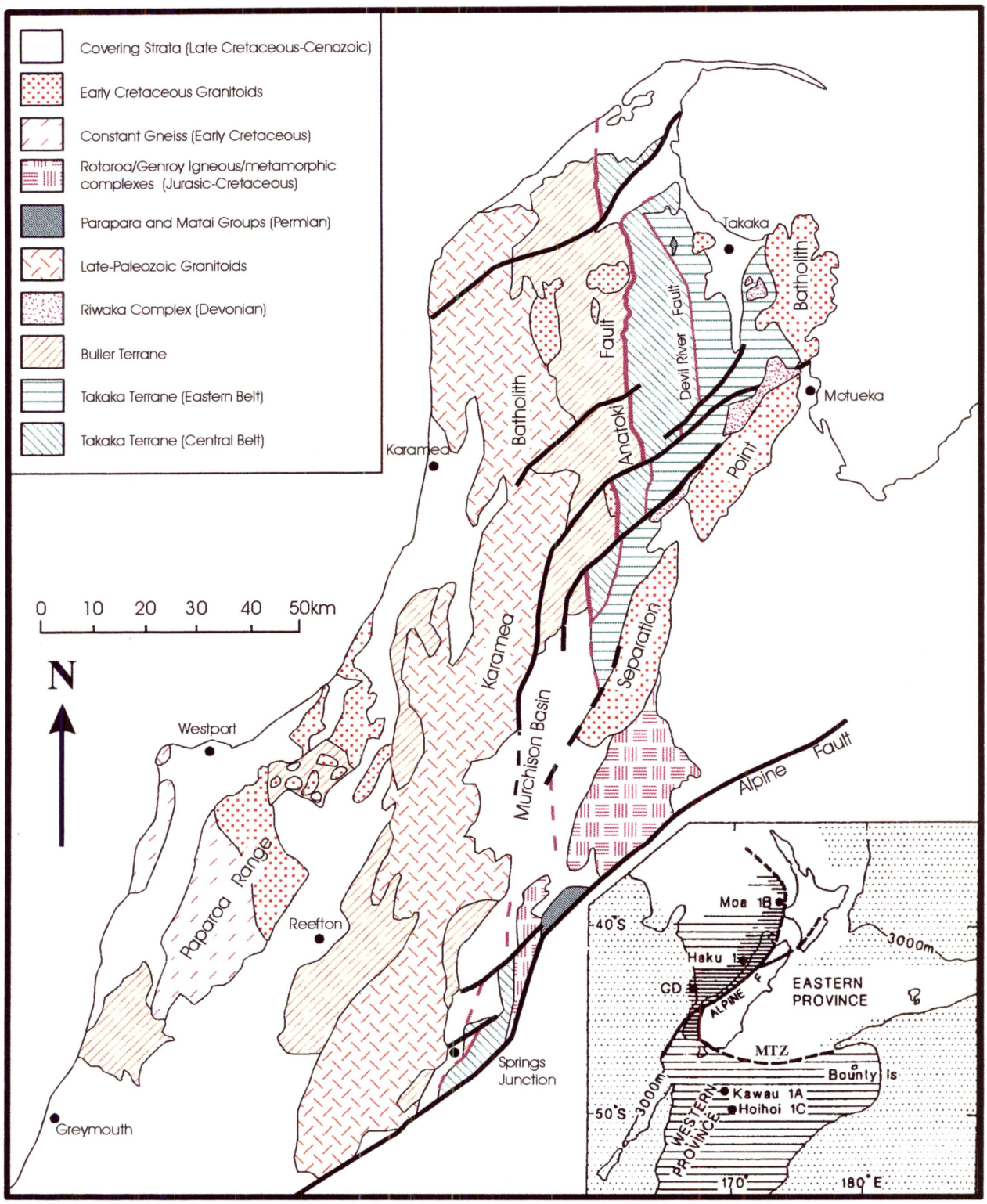

Figure 1.1: Generalised geology of Northwest Nelson - North Westland, South Island, showing distribution of main rock belts and the position of the Anatoki Fault that separates the two Paleozoic terranes. The Insert shows the offshore extent of known and inferred Western Province rocks, and the location of offshore wells that intersect basement rocks. Separating the Western Province from the Eastern Province is the Median Tectonic Zone (MTZ). (Adapted from Cooper and Tulloch 1992 and Muir *et al.* 1996b)

Coombs 1967; Bradshaw 1989). The two terranes have been displaced in a dextral sense by the Late Cenozoic plate boundary (Alpine Fault) and are recognised in southwest Fiordland (Ward 1984, 1986). The Buller terrane is also known to extend offshore and underlies the southern Lord Howe Rise and the Campbell Plateau (Cooper 1979a; Cooper and Tulloch 1992).

1.2 The Anatoki Fault

Separating the two terranes is a fault that is known as the "Anatoki Thrust". The term "Anatoki Thrust" was originally introduced by Grindley (1961). Grindley described the fault as a thrust in the context of his allochthonous Central Belt structural model (see Section 2.4). I propose the "Anatoki Thrust" be renamed the Anatoki Fault for the following reasons. Firstly, Grindley's model is now not thought to be credible (Section 2.4); secondly, little is known about the fault's movement history; thirdly, along at least half of the fault's length, the present day attitude is near vertical and therefore does not have thrust geometry.

As a terrane boundary, the north-south striking Anatoki Fault is the most significant fault in Northwest Nelson. It can be traced for approximately 85 kilometres between the Wakamarama Range in the north to the Wangapeka River in the south. The fault has also been identified further south near Springs Junction (Cooper, unpubl.) and in Fiordland (Ward 1984). The attitude of the fault differs markedly along its length from being at a relatively low angle and dipping east in the north to near vertical further south. The fault is often marked by the presence of prominent limestone bodies. Deformation style in the fault zone varies from brittle to ductile.

1.3 Objective and scope of project

As highlighted by Cooper (1989), very little is known about the Anatoki Fault and structure in the immediately adjacent Buller and Takaka terrane lithologies. Given the terrane boundary status of the Anatoki Fault, a study of the fault and structure in the flanking lithologies is warranted. Therefore, the first objective of the project is to make a thorough determination of the movement history and movement directions of the Anatoki

Fault. To achieve this objective it is necessary to collect and integrate micro-, meso-, and macro-structural evidence from the fault zone, and also from the flanking lithologies of the Buller and Takaka terranes. Thus the second objective, to compare and relate the structural histories of the Buller and Takaka terrane rocks close to the Anatoki Fault, is essentially a by-product of the first.

The project is essentially field based, and microstructural work was undertaken to support the field data. During the course of the study many intriguing geological structures (particularly microstructures) were encountered that could have been potentially relevant to the objectives of this study. However, given the extent and complexity of the study area, only those structures immediately relevant were studied in detail. Some of the microstructures pursued in detail, in the hope that they may be of use to the objectives (e.g. ankerite twinning), proved not to be; nonetheless, these studies have been incorporated into the thesis because they provide valuable information regarding microstructural deformation processes.

1.4 Study area and mapping methods

The study area involves three parts wholly within the newly established Kahurangi National Park, Northwest Nelson (Fig. 1.2)

1. A 24km long, up to 7km wide, corridor following the length of the Anatoki Fault from Boulder Lake in the north to Mt Benson (Cobb Valley) in the south.
2. A 24km^2 area in the middle reaches of the Crow River where a displaced segment of the Anatoki Fault is located.
3. Reconnaissance fieldwork in the Wakamarama Range, Aorere River, Rocky River, Parapara Peak, and Wangapeka River to help elucidate deformational history of Northwest Nelson and constrain the position of the Anatoki Fault trace.

In the study area, the Anatoki Fault and flanking lithologies have been subdivided into seven areal domains (Fig. 1.2). The areal domains are, from north to south, Boulder Lake, Adelaide Tarn, Lonely Lake, Peak 1610, Kakapo Peak, Mt Benson, and Crow River. Each areal domain was carefully mapped, and detailed mesostructural information was recorded. Oriented samples were collected for later microstructural analysis. Some

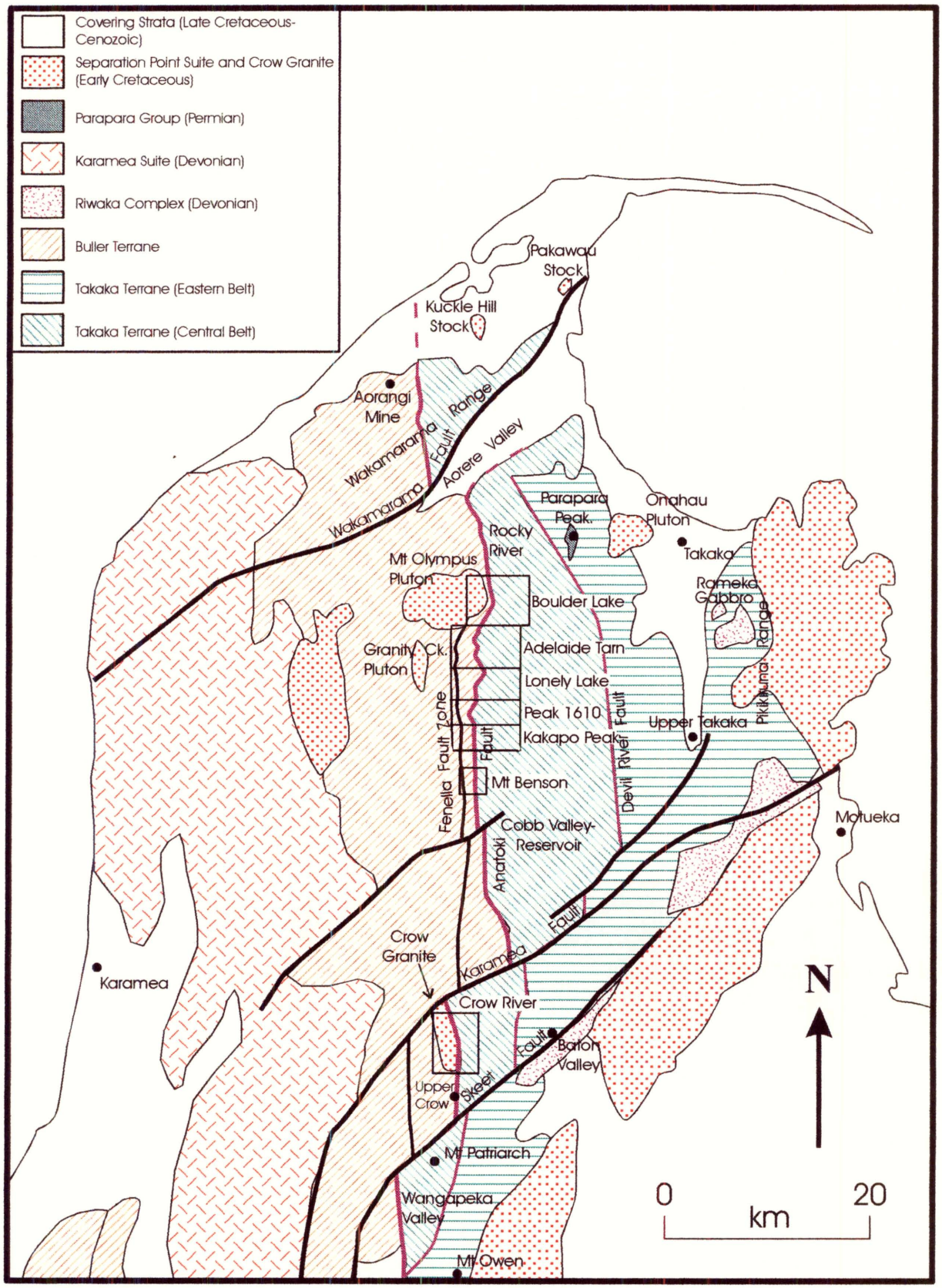

Figure 1.2: Generalised geology of Northwest Nelson. Rectangles outline the seven areal domains which define the study area. Place names referred to in the text are shown on this map. (Adapted from Cooper and Tulloch 1992, and Muir *et al.* 1996b)

of these samples were later selected for dating of foliation surfaces and, in one case, to date a critical intrusion (the Crow Granite).

Airphoto enlargements ranging from 1:5 000 to 1:15 000 were used as base maps in the field. The enlargements originated from Airphoto runs SN 8409 north of the Cobb River, and SNC 5676 south of the Cobb River. The spatial data was transferred to 1:5000 data maps enlarged from NZMS 270 M26 B and D sheets and NZMS 260 M27 sheet. Final interpretive 1:10 000 geology maps were produced to accompany this thesis.

1.5 Physiography

The study area includes some of the more remote areas of Northwest Nelson. The ranges which make up the area are a direct result of transpression since inception of the new plate boundary. Although relatively accessible compared to ranges further south, the terrain is rugged, having mainly been formed by glaciation in the Pleistocene. Modified U-shaped valleys and cirque basins are common. Relief from valley floor to ridge tops is often in excess of 1000m. Vegetation comprises mixed *Nothofagus-Podocarpus* forest and extends from the valley floor to a bushline at about 1300-1400m. Above this elevation, sub-alpine tussock and spaniard predominate.

Access to much of the study area is provided by established walking tracks and routes leading to basic huts or tent sites. Within the study area, access to outcrops was provided by untracked ridge tops, streams, and forest. Some parts of the area (e.g. Dragons Teeth) were not investigated due to a danger factor involved in negotiating high bluffs and waterfalls. The most structurally enlightening outcrop is weathered rock surfaces above the bushline supplemented by outcrop in streams. Outcrops in the bush, where pursued, were consistently poor.

A total of 228 days were spent in the field during the summer seasons of 1993/94, 1994/95 and 1995/96. About one quarter of this time was spent walking to the study area, or spending time in a hut/tent waiting for the rain to stop. Boulder Lake, Adelaide Tarn, Anatoki Forks, Lonely Lake huts, plus tent sites at Upper Snow River, Peaks 1512-1610, Kakapo Peak, Mount Benson and Crow/Little Crow River confluence were used as

base camps. Helicopter support in the first two seasons provided food dumps and facilitated the collection of rock samples.

1.6 Methodology

For most samples selected for detailed microstructural analysis, two thin-sections were made perpendicular to the foliation, one parallel, the other perpendicular to a stretching or intersect lineation. Thin-sections were made using Logitech equipment or in the case of ultrathin-sections, by hand.

Where samples were selected for fabric analysis (e.g. measurement of calcite *c*-axes), an equal number of measurements were made on each of the two perpendicular sections. U-stage measurements were entered on a computer and converted into a format suitable for the stereographic computer software program STEREO (by ROCKWARE). In all cases, measurements made on sections perpendicular to the lineation were rotated 90° and combined with measurements made on sections parallel to the lineation. Fabric stereoplots were then generated for presentation. Where several fabric stereoplots are presented together, they are all presented with a common orientation. The stereoplots are lower hemisphere equal area projections and they have been contoured using the spherical gaussian function.

Stereoplots of field structural data were also generated by STEREO and are lower hemisphere equal area projections. CorelDRAW was used for the presentation of figures. AutoCAD was used to generate base maps from the NZMS 270 topographic map series. Grid references are based on the NZMS 260 topographic map series.

1.7 Classification schemes and terminology

Fold orientation classification is after Fleuty (1964) and fold shape classification is after Hudleston (1973). Fault rock classification is after McClay (1987) which is a modified version of Sibson (1977). Cleavage terminology is a modified version after Powell (1979) and Borradaile *et al.* (1982). The above classifications schemes and terminology are presented in Appendix 3 and should be used as a reference for this thesis.

Strain fringes are here defined as elongate volumes of oriented mineral fibres (usually quartz or carbonate) precipitated adjacent to a rigid crystal or aggregate. Strain shadows are similar but occur as polycrystalline aggregates lacking any fibrous texture. Strain shadows may originate by metamorphic differentiation of matrix material adjacent to a rigid crystal or aggregate, precipitation of a non-fibrous fill adjacent to a rigid crystal or aggregate, or recrystallisation of a strain fringe (terminology adapted from Hanmer and Passchier 1991).

Plunges and dips for lineations and planes respectively are usually referred to as either subhorizontal (0-10°), gentle (10-30°), moderate (30-60°), steep (60-80°), and subvertical (80-90°).

"SPO" and "LPO" are acronyms for "shape preferred orientation" and "lattice preferred orientation" respectively. "PPL" and "CPL" are acronyms of "plane polarised light" and "crossed polarised light" respectively.

The term "microscale" refers to structures observed under the microscope. The term "mesoscale" refers to structures observed on outcrop scale. The term "macroscale" refers to structures inferred from two or more mesoscale observations.

Structural terminology is introduced in Section 2.1.

1.8 Specimens

Thin-sections and rock samples are stored in the University of Canterbury Collection, catalogued with University of Canterbury numbers. Cross references to the field numbers used on the maps and in the text are given in Appendix 4. A brief description of samples is also given in Appendix 4.

1.9 Outline of thesis

As mentioned in Section 1.4, the study area was subdivided into seven areal domains. Chapters 3 to 7 give a complete description and interpretation of the domains in geographical order from north (Boulder Lake) to south (Crow River). An extensive mélange unit in the Takaka terrane (Balloon Mélange) outcrops in several of the areal domains, and is therefore described and interpreted separately in Chapter 8. Chapter 9 integrates all of the results from chapters 3 to 8 and presents a structural synthesis of the Anatoki Fault and adjacent rocks of the Buller and Takaka terranes. Chapter 10 attempts to fuse the conclusions of Chapter 9 into the broader picture of the Western Province and Gondwanaland.

Chapter 2 gives an overview of the deformation events recognised in Chapters 3 to 8, as well as a brief description of stratigraphy relevant to this thesis. This chapter is necessary in order to give the succeeding chapters an appropriate context. The final section in Chapter 2 presents a historical review of models of Northwest Nelson regional structure and stratigraphy.

CHAPTER 2

OVERVIEW

2.1 Structural terminology

I have adopted a chronological notation of structural elements. The chronological notation is inter-domainally consistent in order to make this thesis as readable as possible. This means that, for example, S_3 in the Boulder Lake areal domain is thought to be the same contemporaneous structure as S_3 in the Lonely Lake areal domain. As a result of the inter-domainal consistency, some domains may have, for example, S_1 and S_3 but no S_2. The basis for the inter-domainal chronological designations used is given in Chapter 9, whereas the justification for intra-domainal chronological designations is given in the various areal domain chapters.

In order to keep the chronological notation as simple as possible, all structural elements related to a single deformation event are given the same numerical designation (e.g. S_1 and F_1 relate to D_1; S_2 and F_2 relate to D_2). Where several generations of a structure are thought to relate to one deformation event, due either to progressive deformation and/or deformation partitioning (Tobisch and Paterson 1988), a letter designation alongside the numerical designation is given (e.g. S_{1a} and S_{1b} relate to D_1). Where structural elements cannot be correlated with the inter-domainal chronology, they are given a intra-domainal notation instead using small Roman numerals or abbreviations (e.g. S_{ii}, F_{ii}, or S_{cren}). S_0 is the symbol used for bedding. Intersection lineations symbols (e.g. L_0^2) have a superscript and subscript which refer to the two S surfaces that intersect. The superscript refers to the youngest S surface.

2.2 Overview of deformation events

This section gives an outline of the main deformation events recognised in the Buller and Takaka terrane rocks of the seven areal domains. The purpose is to introduce the inter-domainal structural chronology so that there is no confusion for the reader when

following the chronological designation of structures within individual areal domain chapters. All conclusions presented here are justified in the following chapters.

Three deformation events are recognised in the Buller terrane rocks west of the Anatoki Fault:

- D_1 is a Paleozoic event represented by folding (F_1) and an associated axial planar slaty cleavage (S_1). D_1 structures are observed in the Adelaide Tarn, Lonely Lake, Peak 1610, Kakapo Peak, and Mt Benson domains but have been obliterated by D_2 structures in the Boulder Lake domain. Limited structural data suggests the existence of D_1 structures in the Crow River domain.
- D_2 is an Early Cretaceous event intimately related to movement on the Anatoki Fault. D_2 is observed only in the Boulder Lake domain and is represented by a foliation surface (S_2) and locally developed folds (F_2).
- D_3 is a mid-Cretaceous event represented by prominent mesoscale folds (F_3) and an associated axial planar crenulation cleavage (S_3). D_3 structures are observed in the northern domains (particularly Adelaide Tarn and Lonely Lake domains). F_{ii} and S_{ii} structures, observed in Kakapo Peak and Mt Benson domains, may be related to D_3.

Three deformation events are recognised in the Takaka terrane rocks east of the Anatoki Fault (note that Takaka terrane structure was not studied in the Mt Benson domain):

- D_1 is a Paleozoic event represented by folding (F_1) and an axial planar slaty cleavage (S_1). D_1 structures are observed in the Boulder Lake, Adelaide Tarn, Lonely Lake, Peak 1610, and Kakapo Peak domains. F_i in the Crow River domain is possibly related to D_1.
- D_2 is a Early Cretaceous event represented by a foliation (S_2) that is observed only within close proximity of the Anatoki Fault of the Boulder Lake domain.
- D_3 is a mid-Cretaceous event represented by prominent mesoscale folds (F_3) and an axial planar crenulation cleavage (S_3). D_3 structures are observed in the Boulder Lake, Adelaide Tarn, and Lonely Lake domains only.

All three deformation events recognised in the Buller terrane show similar structural orientations to those in the Takaka terrane. It is shown in the thesis that D_2 and D_3 in the Buller terrane are synchronous with D_2 and D_3 in the Takaka terrane; D_1 in the Buller

terrane is probably related to D_1 in the Takaka terrane, but absolute synchronicity cannot be proven.

Much of the movement recorded on the Anatoki Fault is thought to be related to these deformation events and will be described and discussed in the relevant areal domain chapters and Chapter 9.

2.3 Overview of stratigraphy

Because the subject matter of this thesis concerns two tectonostratigraphic terranes, a large number of named rock units are encountered. The following is an overview of the stratigraphy in the two terranes and should be read in conjunction with Figure 2.1. Group and Formation names used are from Cooper (in prep.) for the 1:250 000 Nelson Q Map. Some of these names may differ from those found in the references given below.

2.3.1 Buller terrane stratigraphy

A sedimentary sequence derived from a passive continental margin (Roser *et al.* 1996) represents the oldest rocks in the Buller terrane (Cooper 1989). At the base of this sequence are latest Cambrian-Early Ordovician quartz-rich sandstones and shales (turbidites) of the Greenland Group (Cooper 1989). In Northwest Nelson, the Greenland Group is represented by the stratigraphically equivalent Roaring Lion and Webb Formations (Cooper 1989). Overlying the Greenland Group is the Golden Bay Group which is subdivided into, from old to young, Aorangi Mine Formation, Leslie and Slaty Creek Formations, and Douglas Formation. The Early Ordovician Aorangi Mine Formation is best exposed in the northern part of Northwest Nelson and consists of thick quartz sandstones, black shales, and blue-grey siltstone (Cooper 1979b). South of the Aorere River, the formation is tectonically thinned and represented within the Fenella Fault Zone, a fault zone that encloses at least two mappable bands of quartz sandstone (Cooper 1989). The Middle Ordovician Leslie and Slaty Creek Formations consist mainly of black shale and quartz sandstone beds (Cooper 1989). The Late Ordovician Douglas Formation is typically a well-laminated siltstone (Cooper 1989). Also in the Golden Bay Group is a dark-grey to black shale/slate unit which has previously been called Peel Formation (Grindley 1980). In the study area, the dark-grey to black

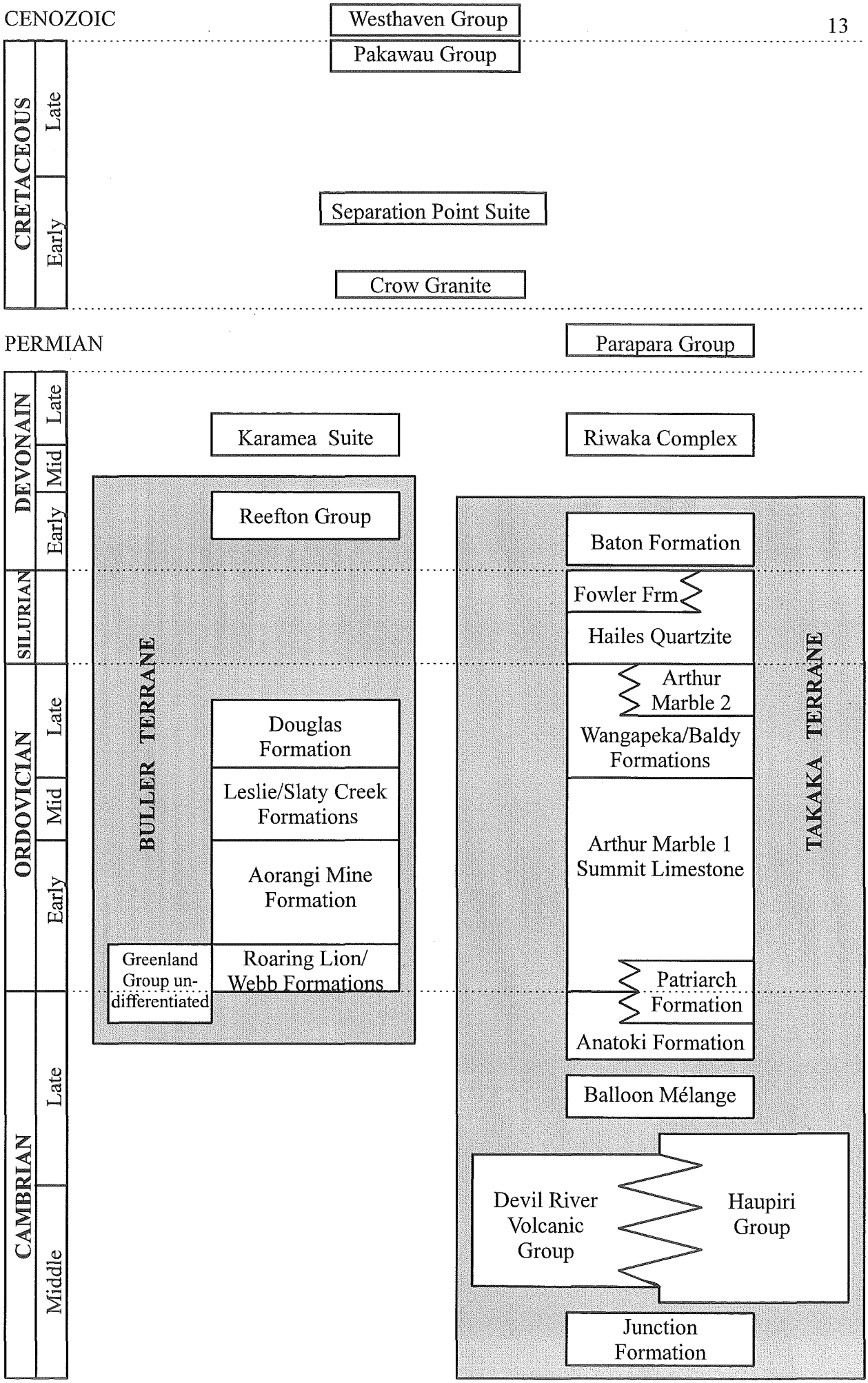

Figure 2.1: A simplified time-lithology diagram representing the current understanding of rock unit relationships in the Buller and Takaka terranes (adapted from Roser *et al.* 1996; Cooper in prep). Note that the Balloon Mélange may have begun forming as early as Mid Cambrian.

shale/slate unit is suspected to be Leslie Formation, and the existence of Peel Formation is questioned (see Section 6.3.4 and 9.3.1). Very low grade schists, slate and phyllite equivalents of the Golden Bay Group rocks are mapped as Bay Schist by Grindley (1971) and Stallard (1994).

The Early Devonian Reefton Group, a carbonate-shale-sandstone shallow marine sequence, is completely fault bounded within the Buller terrane (Bradshaw 1995).

The Buller terrane is cut by volumetrically significant granitoids and subordinate diorites of the Late Devonian Karamea Suite (Muir *et al.* 1996a; 1996b), and also by minor Carboniferous granitoids (Muir *et al.* 1996a).

2.3.2 Takaka terrane stratigraphy

The oldest rocks in the Takaka terrane are the turbiditic sandstones and shales of the Junction Formation (early Middle Cambrian) derived from a passive continental margin (Pound 1993; Cooper 1993). Above the Junction Formation is the Middle to early Late Cambrian island-arc related Devil River Volcanics Group and the contemporaneous and interfingering Haupiri Group sedimentary succession (Roser *et al.* 1996; Münker and Cooper 1997). The Devil River Volcanics Group consists of two volcanic/volcaniclastic units (Benson Volcanics, Mataki Volcanics) and the gabbro/ultramafic Cobb Igneous Complex (Münker and Cooper 1997). The Haupiri Group consists of polymict conglomerates (Christmas, Lockett, and Salisbury Conglomerates: see Pound 1993 and Maclean 1994), and a mixture of turbidite sandstone, shale, limestone, and debris flow conglomerate (Lake Peel, Mount Benson, and Tasman Formations: see Pound 1993 and Münker 1993).

Inclusions of Junction Formation, Devil River Volcanics Group, and Haupiri Group rocks are incorporated into a mélange, termed the Balloon Mélange, thought to have developed in the mid Late Cambrian (Cooper 1997) but possibly as early as Middle Cambrian (Pound 1993).

Following Balloon Mélange development, is a Late Cambrian to Silurian passive margin sequence (Roser *et al.* 1996) consisting of, from old to young, Patriarch Group, Mt

Arthur Group, and Ellis Group. The Patriarch Group is subdivided into the Late Cambrian Anatoki Formation (lithic sandstone, siltstone, granule conglomerate) and latest Cambrian-earliest Ordovician Patriarch Formation (siltstone, sandstone, and silty limestone) (Wright *et al.* 1994). The Mt Arthur Group is subdivided into the Early to Middle Ordovician Arthur Marble 1 and Summit Limestone, Late Ordovician Wangapeka and Baldy Formations (quartz sandstone and shale), and latest Ordovician Arthur Marble 2 (Cooper 1989). The Ellis Group consists of the Silurian Hailes Quartzite and Fowler Formation (sandstone and shale) (Coleman 1981; Cooper 1989).

Above the Ellis Group is the Early Devonian Baton Formation. The formation consists of mudstone, with minor sandstone, limestone, and conglomerate (Willis 1965). Its stratigraphic relationship with Ellis Group is uncertain. In the past, the Devonian has been claimed to be unconformable on older rocks as a result of the pre-Baton tectonic event (Cooper 1989). Current research suggests this interpretation is by no means certain (M. A. Bradshaw pers. comm. 1996).

There are several metamorphic equivalents of the above groups and formations. These include the Wakamarama Schist derived from Haupiri and Devil River Volcanics Group (Cooper in prep.); the Waingaro Schist derived from Haupiri and Devil River Volcanics Group, Balloon Mélange, and Wangapeka Formation (Powell 1984); Onekaka Schist derived from Wangapeka Formation and Hailes Quartzite (Grindley 1971, 1980); and Pikikiruna Schist derived from either Wangapeka Formation (Fig. 11 of Cooper 1979a), or Owen Formation (Grindley 1980) or Hailes Quartzite (Shelley 1981).

In the Eastern Belt, the Ordovician sequence is intruded by the Middle to Late Devonian Riwaka Complex (Rameka Gabbro, Brooklyn Diorite, Campbell Gabbro, Pokororo Pyroxenite) (Grindley 1980; Harrison and McDougall 1980; Muir *et al.* 1996a, 1996b).

A small outlier of Middle Permian metasediments, known as the Parapara Group (quartzite, black slate, siltstone, sandstone and conglomerate), outcrops on Parapara Peak (Clark *et al.* 1965). Its stratigraphic relationship with older Paleozoic rocks is uncertain (Campbell 1996).

2.3.3 Rock units common to both terranes

The earliest Cretaceous Crow Granite intrudes along the Anatoki Fault (see Chapter 7). The Early Cretaceous Separation Point Suite of granitoids intrudes rocks of both the Buller terrane (e.g. Mt Olympus Pluton) and Takaka terrane (e.g. Separation Point Batholith) (Muir *et al.* 1994). Separation Point Suite granitoid plutons are particularly prominent in the north of the two terranes.

Both terranes are unconformably overlain by an extensive latest Cretaceous-Tertiary sedimentary sequence (Pakawau and Westhaven Groups) (Bishop 1971; Grindley 1971; Bal and Lewis 1994).

2.4 A historical review of models of Northwest Nelson regional structure and stratigraphy

This section reviews the history of geological research in Northwest Nelson over the last 118 years in order to explain how we have come to our present understanding of the regional structure and stratigraphy.

Early surveys (1879-1926)

Early reconnaissance by Park (1890), incorporating the work of McKay (1879), established a general north-south structural trend to Northwest Nelson Paleozoic rocks. Park (1890: p.201) observed "a great thickness of green and red slates, greywackes, and slaty breccias of Devonian age" (Central Belt) located within the core of a huge synclinal fold of Silurian slates, schist, and marble (Western and Eastern Sedimentary Belts). The rock ages were determined principally by correlation with other units within New Zealand, and by the overlying fossiliferous Baton River Series.

The first detailed geological exploration of Northwest Nelson was undertaken by Bell *et al.* (1907). They redefined earlier established stratigraphic units into:

- Aorere Series (Western and Eastern Sedimentary Belts)
- Haupiri Series (Central Sedimentary Belt)

The Aorere Series was defined as Ordovician, based on graptolites found in the Western part of Northwest Nelson. Aorere Series rocks found in the eastern part of Northwest Nelson were thought to be the metamorphic equivalents to those of the west. Notably, however, the great massifs of marble found in the east did not have an unmetamorphosed equivalent in the west. Haupiri Series rocks, lacking paleontological data, were thought by Bell *et al.* to unconformably overlie the Aorere Series, the unconformity being marked by conglomerate beds containing supposedly Aorere Series clasts. Structurally, Bell *et al.* confirmed Park's (1890) structural trend and model with Aorere and Haupiri Series rocks being folded into "a great synclinorium" (p.34) of approximately north-south trend.

The Aorere Series of Bell *et al.* was divided into the Mount Arthur Series (marbles and slates) and Aorere Series (argillite and greywacke) by Ongley and Macpherson (1923), and this division was adopted by Henderson *et al.* (1959). Both Ongley and Macpherson (1923) and Henderson *et al.* (1959)* published maps which show Aorere Series rocks to lie exclusively west of the Haupiri Series but the Mount Arthur Series occurring both west and east of the Haupiri Series.

In the 1920's there seemed to be confusion regarding the stratigraphic age relationships of the three "Series". Mount Arthur Series was regarded as the oldest by Ongley and Macpherson (1923) and Henderson *et al.* (1924) but youngest by Henderson *et al.* (1925) and Henderson and Grange (1926). The Haupiri Series was considered by the latter authors to be of an intervening period between Mount Arthur and Aorere Series. No further structural models were advanced during this time.

Paleontological gains (1929-1956)

Confusion over stratigraphic relationships of the three Series spurred Keble and Benson (1929) to undertake detailed investigations of graptolites in samples collected by previous surveys of the region. They found that the graptolite bearing Aorere Series, occurring exclusively in the western parts of Northwest Nelson, was Early Ordovician. The Mount Arthur Series graptolite bearing rocks, outcropping on both the western and eastern flanks of the north trending belt of Haupiri Series rocks, were of Upper

* The fieldwork relating to the published maps of Henderson *et al.* (1959) was carried out between 1923 and 1926.

Ordovician age and apparently conformable with the underlying Aorere Series. Importantly Keble and Benson (1929, p.849) reinforced previous interpretations by stating that "the rocks occurring east and west of the broad belt of Haupiri Series belong to the same group of strata". Keble and Benson went on to say the Haupiri Series "cannot be included as part of the sequence.....probably they owe to folding or faulting their position between belts of Ordovician strata differing little in age".

In 1948, Benson (1956) discovered the first Cambrian trilobites in a lens of limestone within the Haupiri Series. The discovery meant the Ordovician Aorere and Mt Arthur Series were younger than the structurally higher Haupiri Series and a new model for Northwest Nelson Paleozoic rocks was sought.

Allochthonous Central Belt model of Grindley (1961, 1971, 1978, 1980)

The fact that Cambrian rocks were flanked by Ordovician rocks in the shape of a synform prompted Grindley (1961) to propose a radically new structural model for Northwest Nelson. Based on extensive fieldwork for the 1:250 000 and later 1:63 360 New Zealand Geological Survey mapping programmes (Grindley 1971, 1980, Bishop 1971, Coleman 1981), Grindley proposed that the Haupiri Group* (Central Belt) was emplaced as a stack of allochthonous recumbent folds and nappes over autochthonous Aorere/Golden Bay and Mount Arthur Groups (Western and Eastern Belts respectively) (Fig. 2.2a). These first phase folds were said to have east-west axes and to have been thrust from the south, the root zone lying enigmatically somewhere to the south or southeast of the present Central Belt position. Subsequent refolding (second phase) along north-south axes was invoked as the explanation of the present synformal outcrop pattern with recumbent folds now reclined, and the originally flat lying thrust surfaces now steeply dipping (Fig. 2.2b). In Grindley's hypothesis, the elongate but relatively narrow Central Belt must conceal a

* The three "Series" were changed to "Group" status by Grindley (1961). The Mount Arthur Group occurring on the western flank of the Haupiri Group became known as the Golden Bay Group (Grindley 1971).

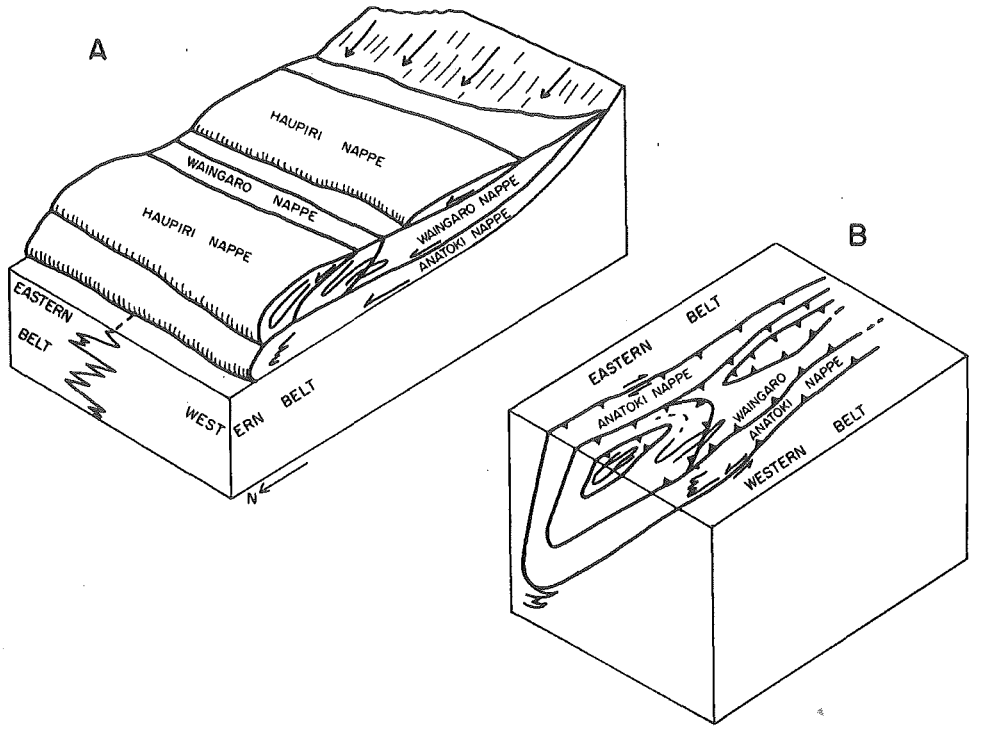

Figure 2.2: Grindley's allochthonous Central Belt model as drawn by Bradshaw (1982). No diagram was ever presented by Grindley to illustrate his model. See text for description of (A) and (B).

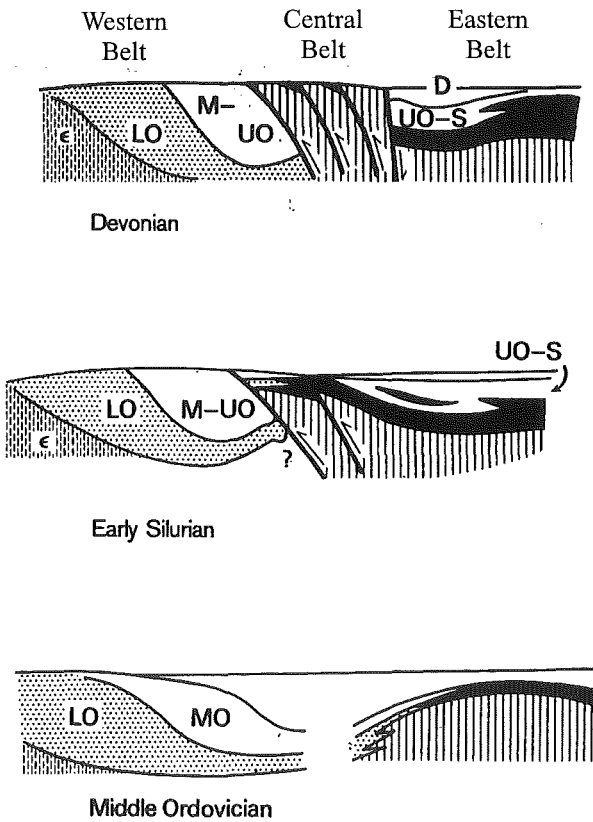

Figure 2.3: The uplifted Cental Belt model of Cooper (1979a). ε = Cambrian, LO = Lower Ordovician, MO = Middle Ordovician, UO = Upper Ordovician, S = Silurian, D = Devonian. Rocks of volcanic arc assemblage are vertical lines; Ordovician carbonates are black. (From Cooper 1979a)

major facies junction between the contrasting stratigraphy of the Eastern and Western Belts.

Grindley named the basal thrust of his allochthonous Central Belt as the "Anatoki Thrust" on the western margin, and its counterpart, the "Devil River Fault (Thrust)" on the eastern margin. The allochthonous Central Belt emplacement and subsequent refolding was termed the "Tuhua Orogeny" by Grindley (1978). This Orogeny was thought to have occurred between the Late Silurian and Devonian based on his interpretation of constraints in the Devonian Baton Formation (Grindley 1978, 1986).

Critical reviews of the allochthonous Central Belt model are given in Bradshaw (1982) and Cooper (1989). The major problems of the model are:

1. The Eastern Belt has a much closer affinity to the Central Belt than to the Western Belt (Cooper 1989). Although no Cambrian rocks are observed in the Eastern Belt, Ordovician Arthur Marble 1 and Wangapeka Formation can be confidently linked with the Summit Limestone and Baldy Formation of the Central Belt respectively, based on litho- and biostratigraphy (Cooper 1989). Bay Schist, once thought to be a lithostratigraphic unit common to the Western and Eastern Belts (Grindley 1971), is now recognised as residing exclusively within the Western Belt (Stallard 1994).

2. The Central Belt and Anatoki Fault have been recognised south of the Alpine Fault in the Dusky Sound area, Fiordland (Ward 1984). The discovery implies the root zone of the allochthonous Central Belt lies south of Dusky Sound and the distance of south to north transport is of the order of 300km (Ward 1986). However, the hypothesised nappes rapidly thin perpendicular, not parallel, to the tectonic transport direction. Thus massive tectonic transport from the south is not demonstrated (Bradshaw 1982). In addition, much of the structural evidence quoted by Grindley (1980) to support his model has been reinterpreted by recent research (Powell 1985; Maclean 1994; Stallard 1994; this thesis).

3. Northwest Nelson Paleozoic rocks involve a large area in which litho- and biostratigraphic control is poor. Recent work by Cooper (1986), Stewart (1988), Cooper and Tulloch (1992), Pound (1993), Maclean (1994), Cooper (1997), and Münker and Cooper (1997), show the stratigraphy of the Central Belt to be far more complicated than

Grindley ever envisaged. Many of the structures shown by Grindley were necessary because he adhered to a simple invariant stratigraphic succession. Thus the recognition of an inverted sequence of discrete nappes, which was considered by Grindley (1980, p.27) as "prima facie evidence" for his model, is based on stratigraphic and structural criteria no longer considered tenable.

The above mentioned major problems, borne out of evidence that has subsequently surfaced since the initial Grindley hypothesis was proposed, have given the allochthonous Central Belt model a somewhat tenuous position.

Migrating arc model of Shelley (1975a)

Shelley (1975a) proposed that Northwest Nelson Paleozoic development could be viewed in terms of subduction zones dipping westward under the New Zealand continent. With time, each successive subduction zone migrated eastwards. Two eastward migrating cycles in the Paleozoic are recognised by Shelley. Each cycle involves three stages of development:

1. Deposition of a "sedimentary belt" east of the continental landmass.
2. A pre-orogenic eastward facing volcanic arc associated with the "sedimentary belt".
3. An orogeny producing a paired metamorphic belt, the median boundary lying between the continental landmass and the "sedimentary belt".

The first cycle in Northwest Nelson began in the Cambrian, and involved the Cambrian part of the Central Belt (pre-orogenic volcanic arc) bordering the east side of a "sedimentary belt" (eastern part of Western Belt). The cycle culminated in a "Pre-Tuhuan" Orogeny in the Late Ordovician, producing a paired metamorphic belt with the median boundary lying along the line of the Karamea Batholith. The second cycle culminated in the "Tuhuan" Orogeny of Late Devonian-Carboniferous age with the median boundary lying along the Devil River Fault. The Eastern Belt represented the "sedimentary belt" and volcanic arc (Riwaka Complex?), and the Central and Western Belts represented newly formed continental landmass. Thus the paired metamorphic belts had migrated eastwards with time.

Shelley's model for two cycles in the Paleozoic was based, in part, on preliminary reports of Ordovician ages for granitoids in the Paparoa Range. Since publication of the model, the Ordovician ages were later invalidated (D. Shelley pers. comm.), in turn invalidating Shelley's first two cycles. Further objections raised by Cooper (1989) are that the model implies the grouping of the Central and Western Belts in Cambrian time, and the separation of Central and Eastern Belts in terms of their Cambrian-Ordovician successions. The model does not deal with specific structural elements recognised in Northwest Nelson Paleozoic rocks.

Crustal evolution model of Crook and Feary (1982)

Crook and Feary (1982) interpret Northwest Nelson Paleozoic rocks in terms of a fore-arc model of crustal evolution. In this model, crustal evolution commences with fore-arc growth during subduction. When subduction ceases, accumulation of post-arc sediments are deposited on top of the fore-arc accretionary prism, the sedimentary character or facies depending on the vertical thickness of the prism. The crustal evolution process culminates in the thermal equilibration of the assembled materials with concomitant deformation, metamorphism and granitoid plutonism that induces continental stability.

The Cambrian part of the Central Belt is thought to represent the fore-arc accretionary prism. Western, Central, and Eastern Belt sediments of Ordovician age or younger, represent the "post-arc sedimentary sequence". In the east, this sedimentary sequence was described as "neritic" whereas in the west the sediments were described as "flysch". This change in facies was interpreted as a result of rapid thinning of the accretionary prism towards the west thus inferring a west facing arc occurring somewhere to the east of the Central Belt (cf. Shelley 1975a). Finally, the "Tuhuan" Orogeny and intrusion of the Karamea Batholith was a response to forces associated with thermal adjustments of the newly formed continental crust.

Like Shelley's model, this model does not deal with major structural elements recognised within Northwest Nelson Paleozoic rocks. The Western, Central and Eastern Belt post-Cambrian sedimentary sequence have been grouped together, an interpretation Cooper (1989) rejects. This grouping assumes abrupt facies changes yet no explanation, which would presumably need to be structurally based, is given. In addition, Crook and Feary

(1982, p.75) admit being unable to explain much of the observed internal structure within sedimentary belts.

Uplifted Central Belt model of Cooper (1979)

Having extensively reviewed the litho- and biostratigraphy, Cooper (1979a) suggested that the Eastern and Central Belts represented a single depositional succession that formed in a region which was not closely related to that of the Western Belt. This led Cooper (1979a) to offer a structural model in which the Central Belt was emplaced against Western Belt by upward and westward directed reverse faulting (Fig. 2.3). The Anatoki Fault was interpreted as an originally east dipping fault (cf. Grindley 1961). Other east dipping faults and overturned isoclinal folds in the Central Belt were also interpreted to have formed during juxtaposition. Reverse faulting was thought to have commenced in the Late Ordovician and continued in the Early Devonian. General uplift of the Western and Central Belt occurred during this time whereas the Eastern Belt subsided and received sediments shed from uplifted western rocks. The uplifted Central Belt model was suggested as an alternative working model to that of Grindley's allochthonous Central Belt model, but at the time there was very little evidence to support or oppose it.

Two suspect terranes

The advent of terrane analysis in the early 1980's, provided the stimulus for Cooper (1984) and Bishop *et al.* (1985) to lump the Eastern and Central Belts together in what is now termed the Takaka terrane*. The Western Belt had been lumped with the Greenland Group sediments of Westland in what is now known as the Buller terrane*. The Anatoki Fault became a terrane boundary. The basis for two separate suspect terranes came about by the genetic grouping of the Eastern and Central Belts (Cooper 1979a), and the contrast in geological history between these two belts with that of the Western Belt (Cooper 1989). The Takaka terrane is interpreted as an island arc assemblage (restricted to the Central Belt), and a latest Cambrian to Silurian passive margin assemblage (common to both the Central and Eastern Belts) that developed on the flanks of the extinct Cambrian

* The Takaka and Buller terranes were originally termed Golden Bay and Karamea terranes respectively by Bishop *et al.* (1985).

arc (Cooper 1989; Cooper and Tulloch 1992). The Buller terrane is interpreted to consist of a passive continental margin assemblage (Cooper 1989; Cooper and Tulloch 1992).

Following on from the uplifted Central Belt model, Cooper (1989) suggested that the final tectonic direction of the Takaka terrane was westward thrusting on to the Buller terrane, and was consistent with structural data obtained from Powell (1985) and Shelley (1981, 1984). The Anatoki Fault was thought to be the basal thrust in a listric system of faults which have tectonically dismembered the Takaka terrane into discrete fault-bounded slices (Fig. 2.4); the Central Belt is the most strongly dismembered. Cooper (1989) suggests, nonetheless, that thrusting may have been preceded by large scale transcurrent movement. In Figure 2.4, the Devil River Fault is interpreted as a back thrust.

Stallard (1994) somewhat refined Cooper's uplifted Central Belt model and suggested that the two terranes amalgamated along a convergent strike-slip margin. The Central Belt was viewed essentially as a "palm tree" structure (Fig. 2.5) which is a typical structure observed in transpression tectonic environments.

An allochthonous passive margin assemblage in the Takaka terrane?

Having investigated recumbent folding in the Eastern Belt which indicate tectonic movement towards the ENE, Shelley (1991) speculated that rocks of the Eastern Belt slid in their entirety over or off the Central Belt; a possible root zone may have existed at the boundary between the Buller and Takaka terranes. It has recently been pointed out by Cooper (1997) that a sedimentary contact between the Cambrian Island Arc assemblage and the latest Cambrian-Silurian passive margin assemblage cannot be demonstrated. In addition, a low angle detachment fault is recorded between the two assemblages in the Springs Junction area (Cooper unpublished). Cooper (1997) has thus suggested the passive margin assemblage of the Takaka terrane may possibly be allochthonous with respect to the island arc assemblage. Given the contrast in lithology between the two assemblages and the lack of a sedimentary contact, the possibility that the Takaka terrane should be subdivided into two suspect terranes should be considered.

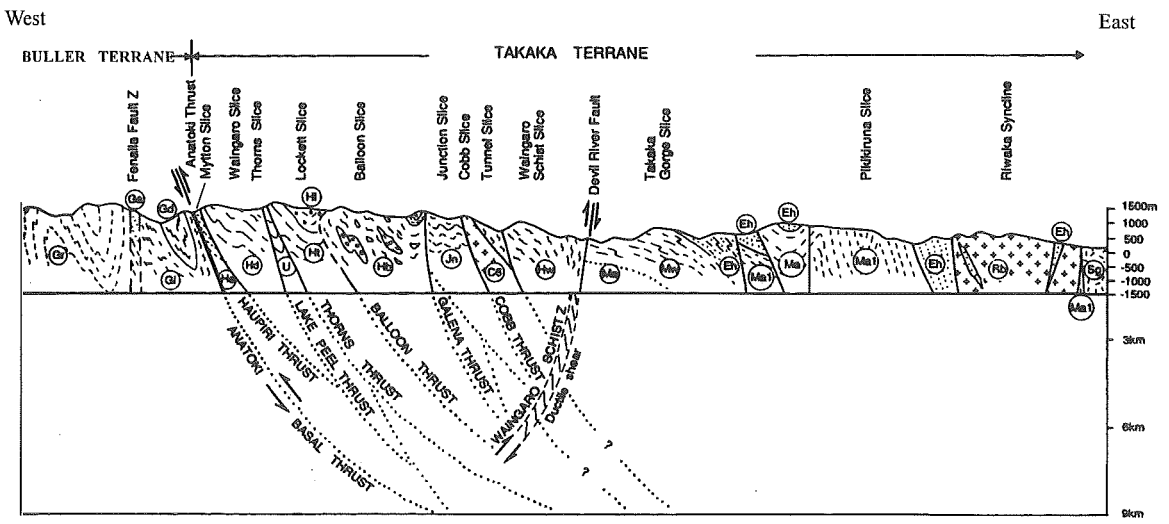

Figure 2.4: Cooper and Tulloch (1992) envisage the Anatoki Fault as a basal thrust in a listric system of faults which have tectonically dismembered the Takaka terrane into discrete fault-bounded slices. Note the overturned syncline immediately west of the Anatoki Fault. Gd = Douglas Formation, Gl = Leslie Formation. (From Cooper and Tulloch 1992)

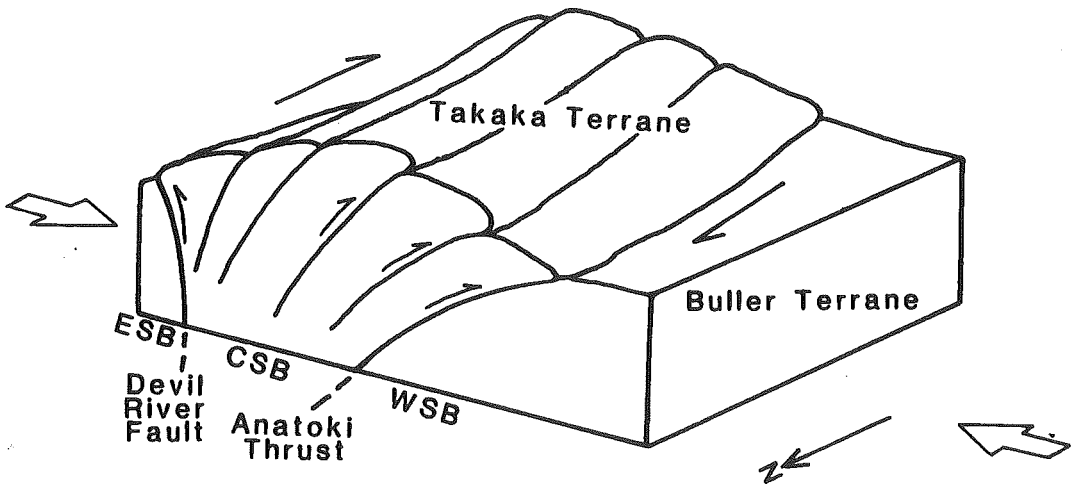

Figure 2.5: The Cental Belt "palm tree" structure of Stallard (1994) which formed along a convergent strike-slip margin. ESB = Eastern Belt, CSB = Central Belt, WSB = Western Belt. (From Stallard 1994)

CHAPTER 3

BOULDER LAKE DOMAIN

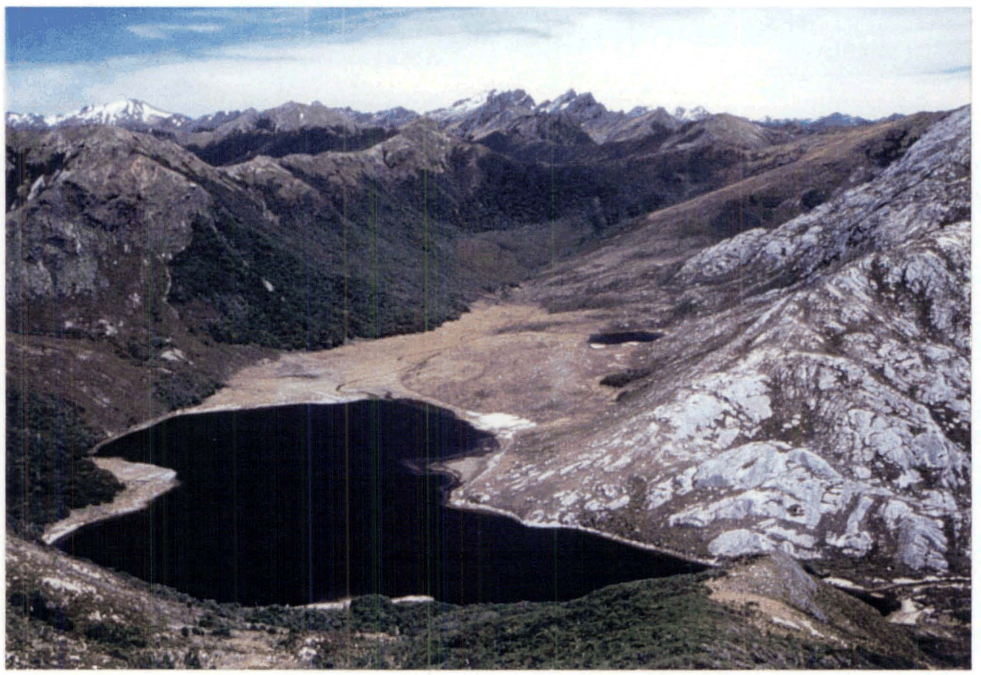

Chapter frontispiece: Boulder Lake from near Cow Saddle. View is towards the south. The light grey rock to the right of the lake is Olympus granite. The Anatoki Fault trace occurs along the left side of the lake and then continues along the bush covered slopes directly behind the lake. Darby Pond is in the centre right. The lake outlet is at the extreme bottom right. Dragons Teeth and Anatoki Peak are in the middle background. Kakapo Peak is the snow covered peak in the extreme left background.

3.1 Introduction

The Boulder Lake domain (Map 1) represents the northernmost segment of the Anatoki Fault studied in detail (Fig. 1.2). The domain differs conspicuously from those further south because the Anatoki Fault trace is deflected from its usual north-south strike to curve around the eastern margin of the Mt Olympus Pluton (Grindley 1961) (Map. 1). A sliver of Buller terrane lithologies occurs between the granite and Anatoki Fault. The curved fault trace is approximately parallel to foliations in the eastern margin of the granite and in metasediments immediately east and west of the Anatoki Fault. A major aspect of studying the Boulder Lake domain is to understand the relationship between the fault trace deflection and foliation development in adjacent rocks.

The area around Boulder Lake is very well-exposed, primarily because Boulder Lake itself now occupies the lower portion of a valley formed by the South Island's northernmost Pleistocene glacier. The glaciation has left the hills and valleys in the Boulder Lake domain poorly vegetated, providing excellent exposures in which to investigate mesoscale and macroscale structures in detail. As a result, I have taken the opportunity to extensively investigate Takaka terrane structure east of the Anatoki Fault. Thus another major aspect of studying the Boulder Lake domain is to understand Takaka terrane structure and to compare and relate it to the foliation observed in the immediate vicinity of the Anatoki Fault.

In the Boulder Lake domain, the lithologies west of the Anatoki Fault encompass the Ordovician Golden Bay Group of the Buller terrane and the eastern margin of the Mt Olympus Pluton; the Takaka terrane lithologies east of the Anatoki Fault include undifferentiated Haupiri Group, Devil River Volcanics Group, and Balloon Mélange. In this chapter, structures in lithologies west of the Anatoki Fault are reported first followed by those east of the Anatoki Fault. Structures on either side of the Anatoki Fault are then compared and a relative timing of deformation established. Previous work by Brathwaite (1968a, 1968b) and Rennison (1992) in the Boulder Lake area will be referred to and discussed in the relevant sections below. A special section on ankerite twinning in the Boulder Lake domain is presented at the end of this chapter (Section 3.10).

3.2 Mt Olympus Pluton: Description

A thorough description of the Mt Olympus Pluton is given in both Brathwaite (1968b) and Rennison (1992), and only a brief description is given here. The Mt Olympus Pluton is roughly elliptical in shape and measures 9 x 6 km. The pluton intrudes Buller terrane metasediments, namely Roaring Lion Formation on its western side, and Leslie and Douglas Formation on its eastern side.

The pluton is a fine to medium grained leucocratic biotite monzogranite (Olympus Granite) and is geochemically related to the Separation Point Suite (Rennison 1992). An emplacement age of 111.4±2.1 Ma has been determined by U-Pb SHRIMP dating of zircons from a sample collected from the eastern margin of the pluton (Muir *et al.* 1992, 1994). This age is slightly younger than the main Separation Point Batholith, dated at 118 Ma, and found 30km to the east (Muir *et al.* 1994).

The eastern margin contact of the pluton is generally sharp and dips outward between 30° and 55° (Rennison 1992). Aplite dikes, interpreted as late stage magmatic differentiates, are common within the granite and some extend into the adjacent country rocks. Thin apophyses of granite also extend into the neighbouring country rock. The two types of intrusions are usually no greater than 1m in thickness and extend no further than 50 metres horizontally from the pluton margin.

3.3 Mt Olympus Pluton: Structure

The most striking structure in the Mt Olympus Pluton is a foliation, primarily defined by aligned biotite, and developed along the eastern margin of the pluton (Brathwaite 1968b; Rennison 1992). This foliation gradually disappears westwards so that the western margin of the granite is structureless (Brathwaite 1968b; Rennison 1992). Measurements by Rennison (1992) show that the foliation is approximately concordant with the eastern margin contact (Map 1 and Fig. 3.1). However, Rennison notes that the foliation varies appreciably over short distances in orientation and intensity, and attributes this to an anastomosing network of high strain zones. The foliation is not necessarily most intense at the contact with country rock.

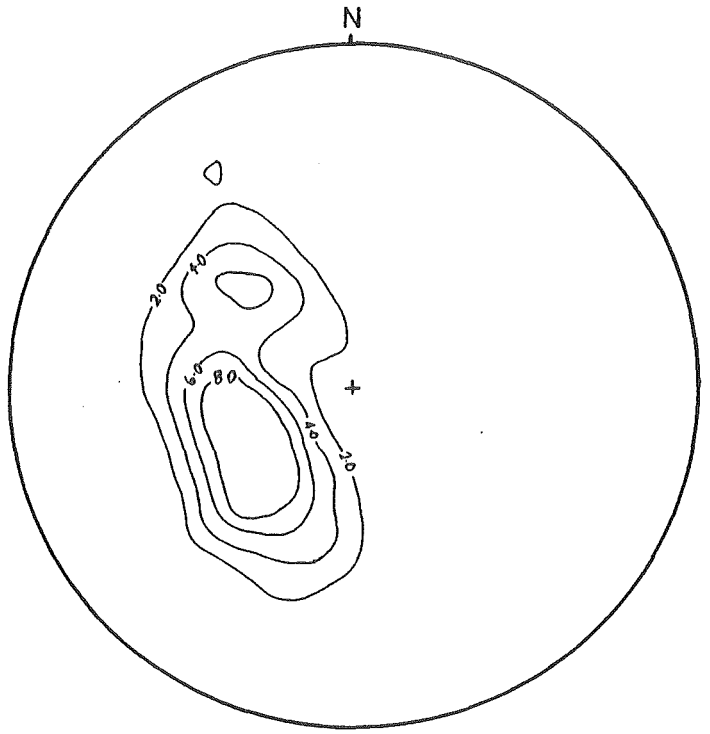

Figure 3.1: Contoured distribution of poles to biotite foliation in granite along the eastern margin of the Mt Olympus Pluton. n=145. Contour interval 2%. (From Rennison 1992)

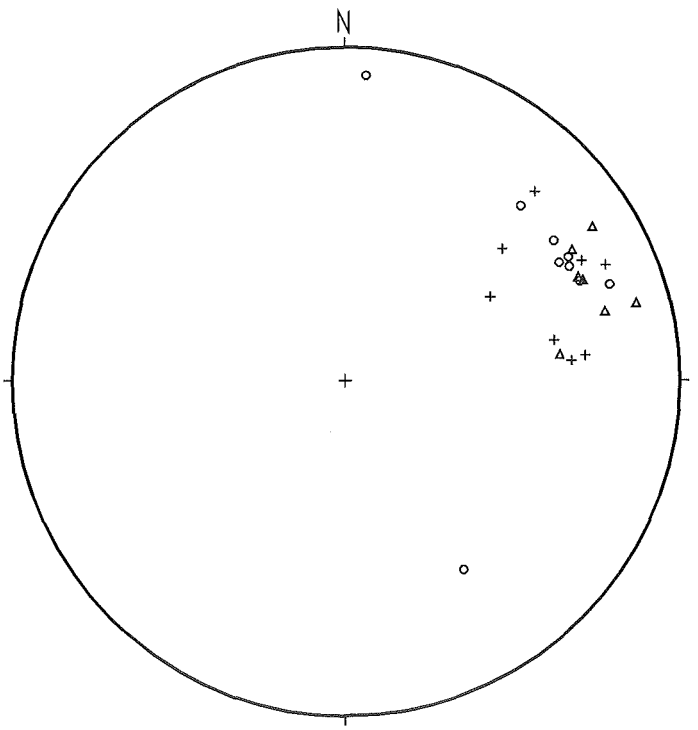

Δ Orator Creek area (my data), n=7
\+ Western side of Boulder Lake (Rennison 1992 data), n=8
O Lake Clara and surrounds (Rennison 1992 data), n=9

Figure 3.2: Stretching lineations from the eastern margin of the Mt Olympus Pluton.

Rennison (1992) showed that the biotite which defines the foliation is metamorphic in origin, and that where the foliation is most intense, appreciable grain size reduction in the granite has taken place, giving an almost mylonitic appearance. Features such as quartz ribbon development, recrystallisation of feldspar to a fine grained matrix, remnant feldspar porphyroclasts with recrystallised tails, together with complete recrystallisation of biotite led Rennison to conclude that the foliation is a result of a solid state, high temperature deformation. Aplite dikes cutting both the granite and country rock possess a biotite/muscovite foliation concordant with the general foliation of the pluton (Rennison 1992). This concordance implies that the formation of the general foliation, at least in part, postdates the late stage magmatic differentiates.

Aside from possessing a foliation, aplite dikes and apophyses which intrude the country rock along the eastern margin of the pluton show other features of deformation. The deformation is intimately related to foliation development in the country rock and will therefore be described in Section 3.5.

Prominent lineations observed within the more intensely foliated granite have been measured close to the eastern margin contact by Rennison (1992) and myself. The lineations plunge consistently towards the NE-E (Fig. 3.2) despite the variation in foliation orientation along the eastern margin. They essentially equate to dip-slip around the western side of Boulder Lake and oblique-slip in the area around Orator Creek. These lineations are interpreted here as stretching lineations for the following reasons:

- Recrystallised quartz ribbons are elongate parallel to the lineation.
- Biotites are elongate parallel to the lineation.
- Porphyroclast tails are elongate parallel to the lineation.
- The lineations are approximately parallel to stretching lineations in the adjacent country rock (Section 3.5).

Of the few samples I collected, only one revealed shear-sense indicators parallel to the lineation. The sample comes from the Orator Creek margin of the pluton and displays asymmetric appendages around feldspar porphyroclasts (Fig. 3.3). The asymmetry indicates reverse dextral shear with top to the SW-WSW.

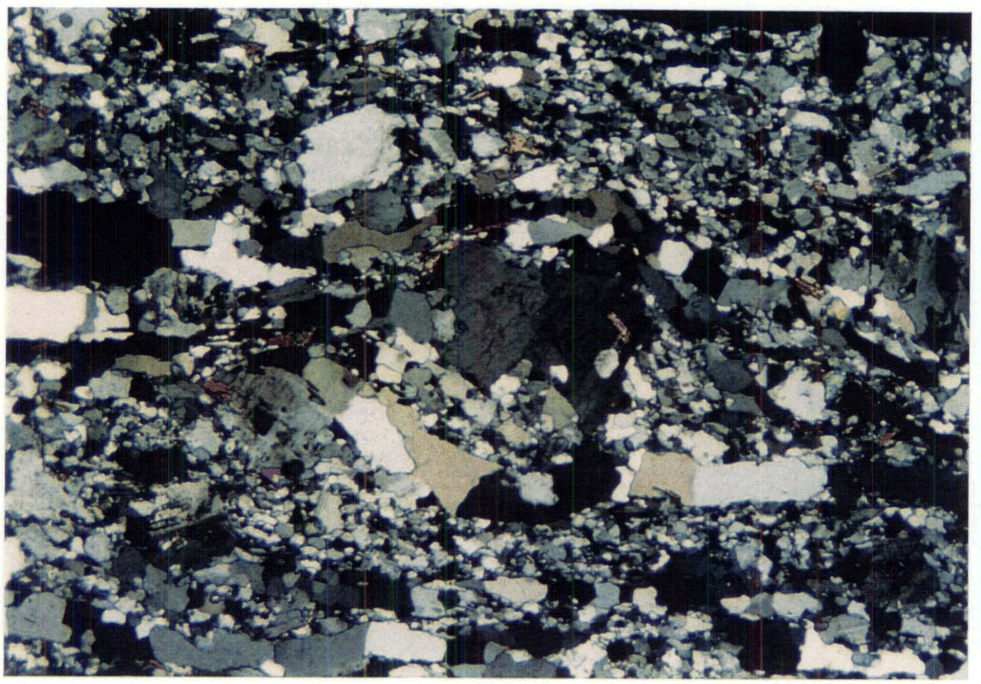

Figure 3.3: Feldspar porphyroclast (centre dark grey grain) with asymmetric appendages consisting of finer grained recrystallised feldspar and quartz. Quartz ribbons asymmetrically anastomose around the porphyroclast. Shear-sense is top to the left. XZ section of RJ299, Olympus granite. CPL.

3.4 Golden Bay Group: Lithology

The bulk of the Golden Bay Group between the Mt Olympus Pluton and the Anatoki Fault consists mainly of light to medium grey semi-pelitic or sandy phyllites. The phyllites possess a typical metamorphic mineral assemblage of quartz + biotite + muscovite + chlorite. Compositionally and texturally, the phyllites are low grade metamorphic equivalents of Douglas Formation seen further south at Adelaide Tarn. The effects of metamorphism increase towards the Mt Olympus Pluton so that minor pelitic horizons become fine grained schists with quartz + biotite + muscovite ± andalusite ± cordierite ± staurolite ± sillimanite assemblages. Randomly oriented retrogressive chlorite plates overprint the phyllites.

Immediately adjacent to the Mt Olympus Pluton eastern margin at the lake outlet, Darby Pond, and in Orator Creek (see Map 1 for location of place names) is a band of predominantly pelitic or semi-pelitic medium to dark grey fine grained schist. Light grey to white quartzite and quartz-rich sandstone beds are interbedded with the pelitic material. Brathwaite (1968b) maps two thick quartzite beds (20m+) around the lake outlet but most quartzite beds are no greater than 80cm in thickness. Thick quartzite beds were not observed south of the lake outlet. The schist commonly has a quartz + muscovite + biotite + opaque assemblage but the more pelitic schist also contains andalusite, cordierite, staurolite and sillimanite. As in the phyllites, randomly oriented retrogressive chlorite plates overprint the fine grained schists. Just downstream from the lake outlet (M26/ 736354), graphitic, quartzose, dark grey to black silty slate occurs between the schist and granite but wedges out towards the SE. This slate also contains quartzite beds. Similar rocks outcrop at M26/ 737336. The graphitic slate, pelitic to semi-pelitic schist, and quartzites have been grouped together by Brathwaite (1968b) as Leslie Formation. I support this grouping in that the parents of these metamorphic rocks were shales and quartz sandstones characteristic of Leslie Formation south of the Boulder Lake domain. Given the position of the Fenella Fault Zone south of Boulder Lake, Aorangi Mine Formation may also be represented here.

Immediately west and parallel to the Anatoki Fault, up to 40m thick, is a semi-continuous horizon of dark grey to black graphitic slate with lesser laminae or beds (up to 20cm) of

quartz siltstone or sandstone. The typical metamorphic mineral assemblage in these rocks is quartz + muscovite/sericite + graphite + chlorite.

Douglas Formation-like lithologies continue south of Green Saddle, within the vicinity of Pt. 1450 (northernmost part of the Adelaide Tarn domain). Here the metamorphic texture and grade drops off rapidly so that the cleavage is slaty rather than phyllitic, and biotite is absent.

A small amphibolitic body occurs in the vicinity of the lake outlet (shown in light green on Map 1). It was not investigated in this study but is described in detail by Brathwaite (1968b).

3.5 Golden Bay Group: Structure

3.5.1 Introduction

In all Golden Bay Group lithologies, the dominant structural feature is a foliation which is subparallel to the eastern margin of the pluton and the Anatoki Fault trace. This contrasts with the lack of foliation in the hornfelsed country rock west of the Mt Olympus Pluton. The foliation is the first deformation feature expressed in the Buller terrane of the Boulder Lake domain. However, as will be seen in later chapters, the foliation is interpreted to postdate an earlier foliation and is therefore referred to as S_2 for regional clarity.

S_2 is noticeably deflected around the pluton, changing from a N-NW strike north of Boulder Lake, to a NE strike south of Boulder Lake. S_2 becomes higher grade and more schistose towards the pluton coinciding spatially with a prominent crenulation (S_{cren}) of S_2 close to the pluton margin. Because of the differences in strike of the foliation and the increase of metamorphism towards the pluton, the Golden Bay Group has been divided into four small structural domains (Fig. 3.4). Two domains occur north of Boulder Lake and two domains occur south of the lake. The Lake Outlet and Orator Creek domains represent the higher grade rocks, and the Beak Creek and Arena Creek domains represent the lower grade rocks. The structural style changes south of Green saddle and therefore

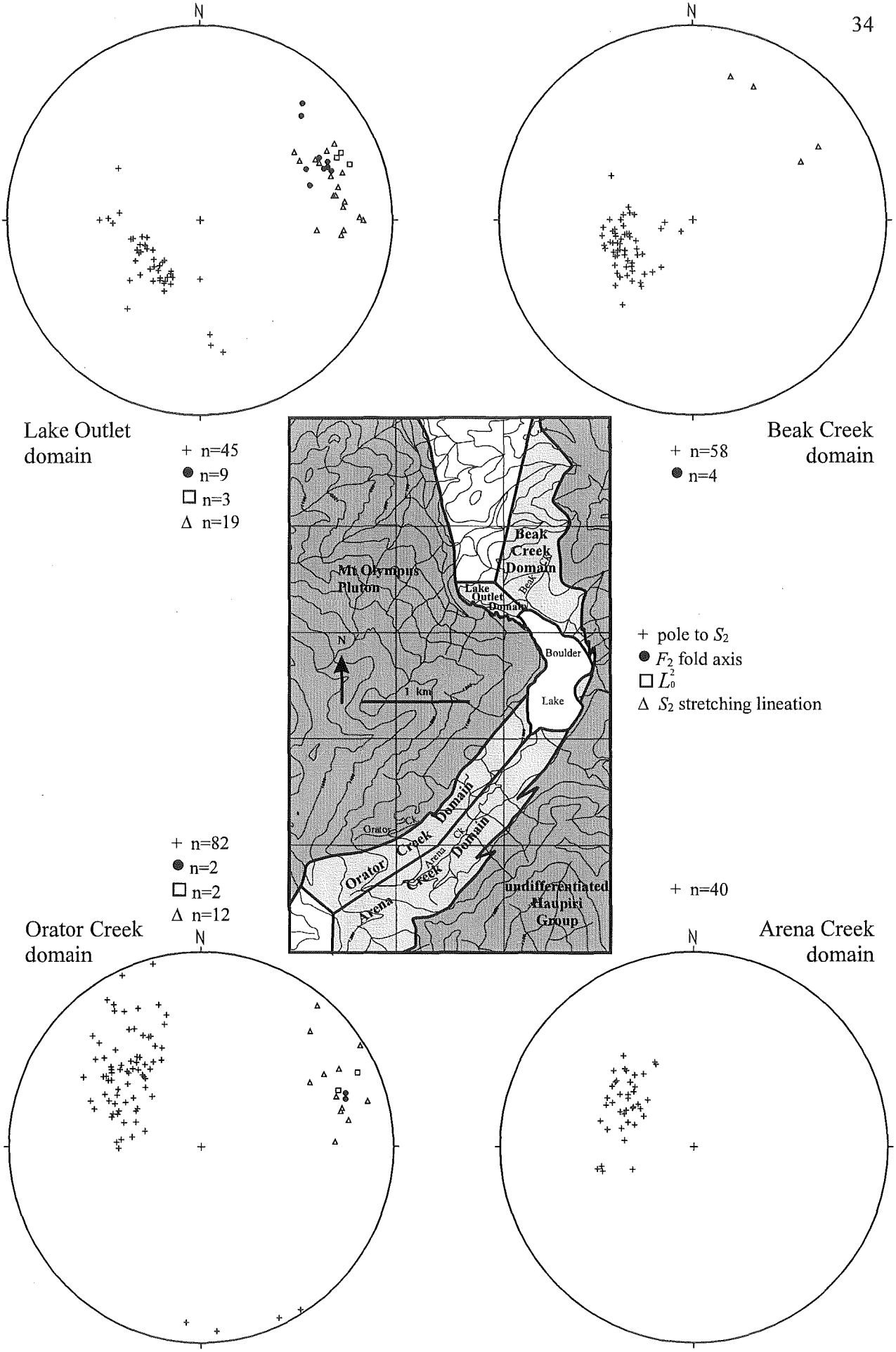

Figure 3.4: The four structural domains of the Golden Bay Group in the Boulder Lake domain. The orientations of F_2, L_0^2, S_2, and S_2 stretching lineations for each structural domain are displayed on stereoplots. Note that for the Lake Outlet domain, the orientations refer to S_{2a}, F_{2a} and L_0^{2a}.

marks the southernmost limit of the Arena Creek domain. Each structural domain is now described in turn.

3.5.2 Orator Creek domain

Orator Creek domain mesoscale structures

In the Orator Creek domain, the majority of schistose S_2 strikes NE, dipping moderately SE (Fig. 3.4). Bedding (S_0) is invariably subparallel to the foliation. However, at M26/ 737336, the bedding in a texturally lower grade graphitic, quartzose, silty slate is folded. S_2 is axial planar to those folds; fold axes and L_0^2 plunge gently towards the ENE (Fig. 3.4).

Quartzose sandstones and quartz veins, subparallel to S_2, often display boudinage. Boudin axes were difficult to measure accurately but generally plunged between ENE and SSE. One quartz vein shows boudinage in two orthogonal directions suggestive of chocolate tablet type boudinage. Obliquely cutting quartz veins commonly display tight to isoclinal folding with S_2 axial planar to the folds.

Aplite dikes and granite apophyses display good evidence of post-intrusion deformation. Evidence includes boudinaging in aplite dikes that parallel S_2 (Fig. 3.5), and pinch and swell structure in granite apophyses (Fig. 3.7). Boudinaged aplites dikes and quartz veins commonly show an asymmetry (Fig. 3.6). This asymmetry is brought about by an overprinting crenulation (see below) and should not be mistaken as a shear-sense indicator.

Overprinting the development of S_2 and associated deformation structures is a crenulation (S_{cren}) of the schistosity. The majority of S_{cren} measurements have a NW-SE strike, dipping moderately NE (Fig. 3.8A). The crenulation is observed throughout the Orator Creek domain but is most intense within pelitic-rich rocks and near the Mt Olympus Pluton contact. The kink-like crenulations typically have wavelengths less than 0.5cm but some are up 4cm. Associated with S_{cren} is a gentle folding most noticeable in sandy layers that are less affected by S_{cren}. Crenulation lineations (L_2^{cren}) and fold axes of larger

Figure 3.5: Boudinaged aplite dike in pelitic schist parallel to S_2 (centre of photograph). A sandstone bed, seen at the bottom of the photograph, is also boudinaged. Orator Creek domain. M26/ 737338. Lens cap for scale.

Figure 3.6: Boudinaged quartz vein showing an asymmetry. The asymmetry is a result of an overprinting crenulation (S_{cren}) as shown in the sketch below. Orator Creek domain. M26/ 727328. Lens cap for scale.

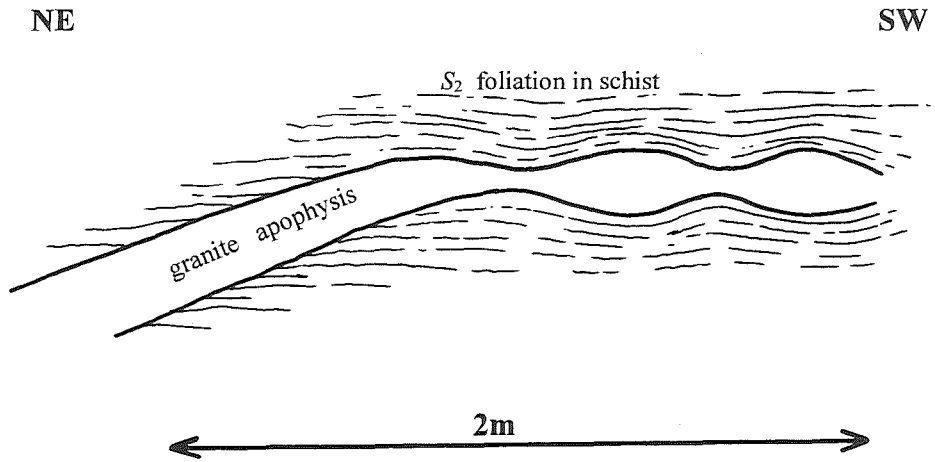

Figure 3.7: Field sketch of granite apophysis, in Orator Creek domain, with pinch and swell structure where the apophysis is parallel to S_2. The reason why the left margin of the apophysis is bent can be explained by either it being bent prior to S_2 deformation, or alternatively, the top half of the outcrop experienced higher strain. In the latter case, the strain may have been either coaxial or non-coaxial with top to the SW shear-sense. M26/ 732332.

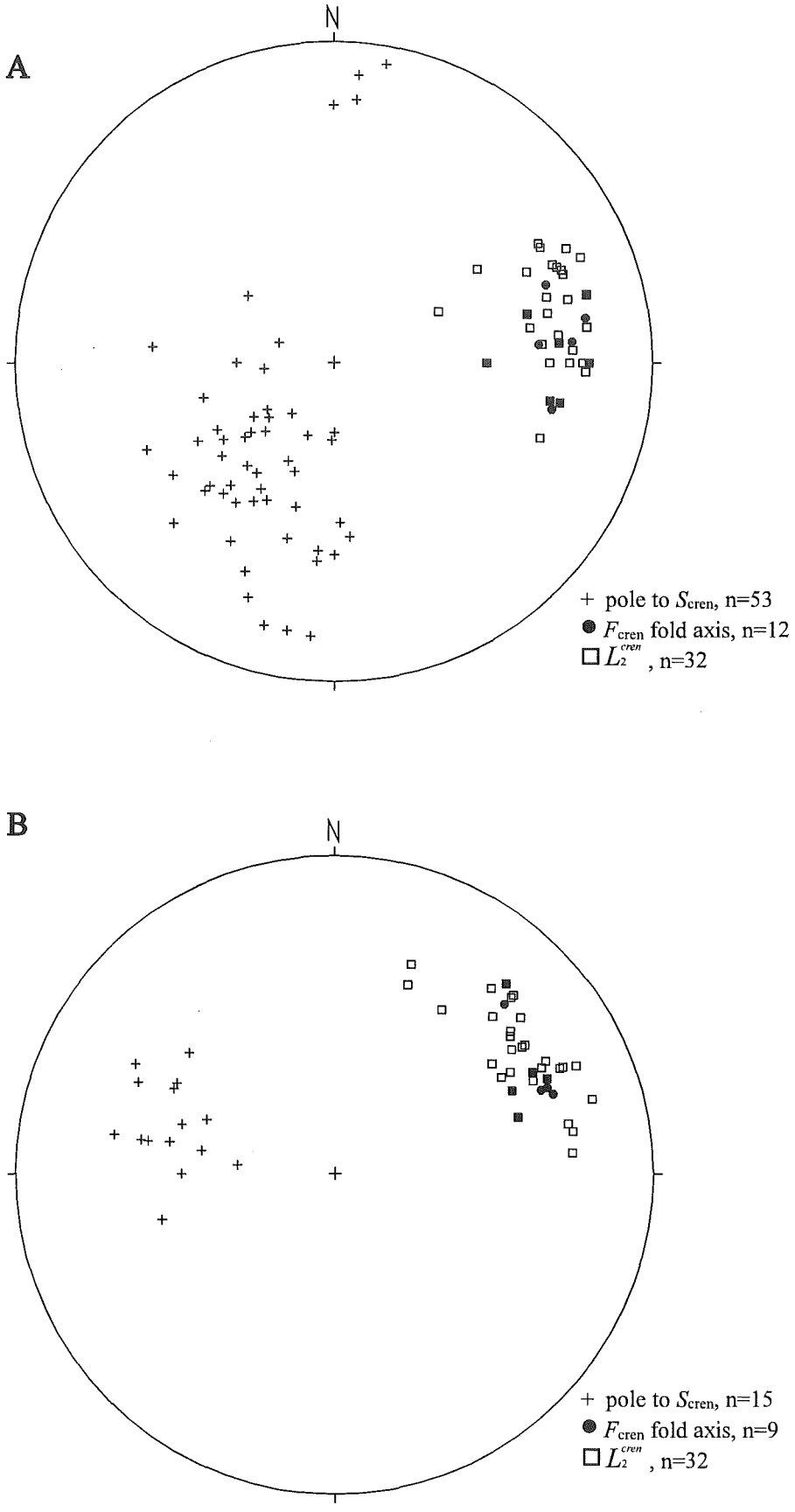

Figure 3.8: S_{cren}, F_{cren}, and L_2^{cren} orientations of the Orator Creek (A) and Lake Outlet (B) domains. Note that filled squares are where filled circle symbols overlap with open square symbols.

crenulations (F_{cren}) plunge fairly consistently towards the ENE-E at a moderate to gentle angle (Fig. 3.8A).

Orator Creek domain microscale structures

S_2 is principally defined by biotite and muscovite. Importantly, the micas wrap around andalusite and cordierite porphyroblasts that are directly related to the Mt Olympus intrusion (Fig. 3.9). The stretching lineation associated with S_2 is defined by the maximum elongation of micas, the maximum elongation of strain shadows adjacent to andalusite, cordierite, and large detrital quartz/feldspar grains, the alignment of andalusite prisms (Fig. 3.10), and the maximum elongation of deformed altered cordierite spots. The latter elongation feature indicates that cordierite had altered pre- or syn-S_2. Stretching lineations plunge gently between NE and E and are essentially parallel to F_2 fold axes and L_0^2 (Fig. 3.4). Curious elongate lenses of chlorite and quartz set in a biotite-muscovite-quartz matrix are parallel to the stretching lineation. The lenses are of uncertain origin but clearly represent compositional differences and may represent highly transposed remnants of bedding.

Strain shadows around andalusite, cordierite, and detrital quartz/feldspar grains usually consist of quartz and lesser biotite and muscovite. The quartz in the strain shadows often exhibits undulatory extinction and deformation bands. Immediately adjacent to the granite, sillimanite occurs amongst quartz in strain shadows around andalusite.

In sections perpendicular to the stretching lineation (i.e. YZ section), strain shadows and elongate micas are less well-developed and the anastomosing schistosity has shorter wavelength. These features indicate that rocks deformed by D_2 are essentially LS-tectonites.

Not all samples collected display a stretching lineation. In these samples, andalusite and/or cordierite are randomly oriented and strain shadows are equally developed in thin-sections perpendicular to each other. Thus it appears that some of the rock in the Orator Creek domain are locally S-tectonites.

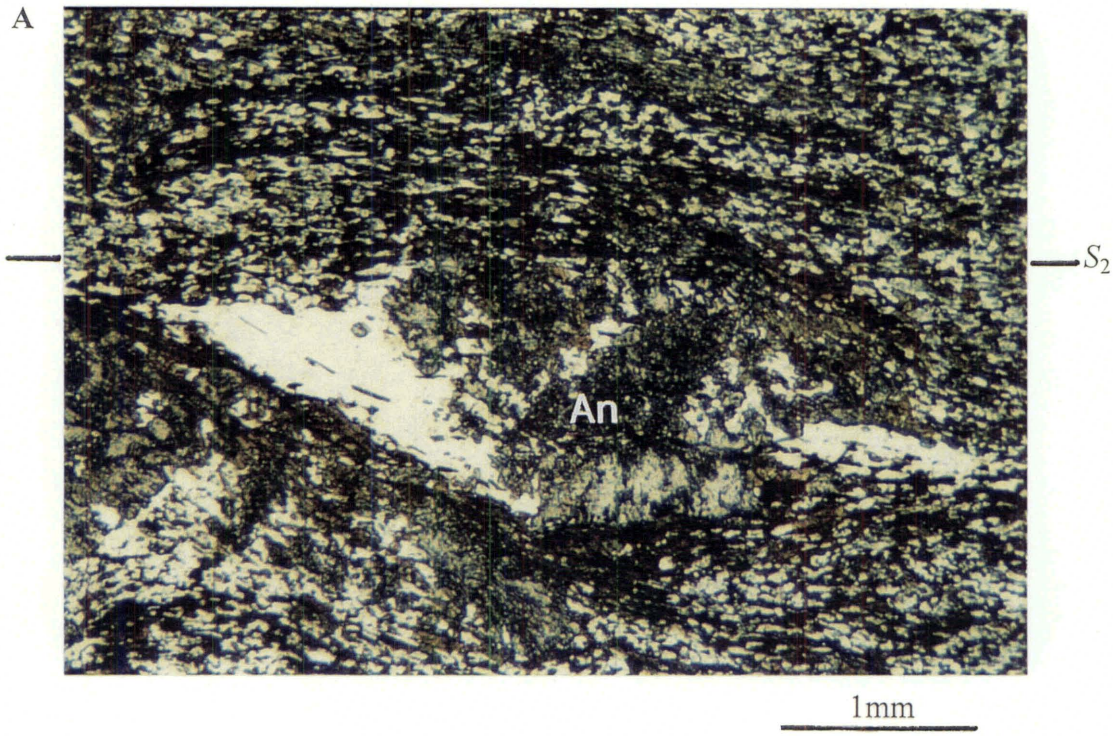

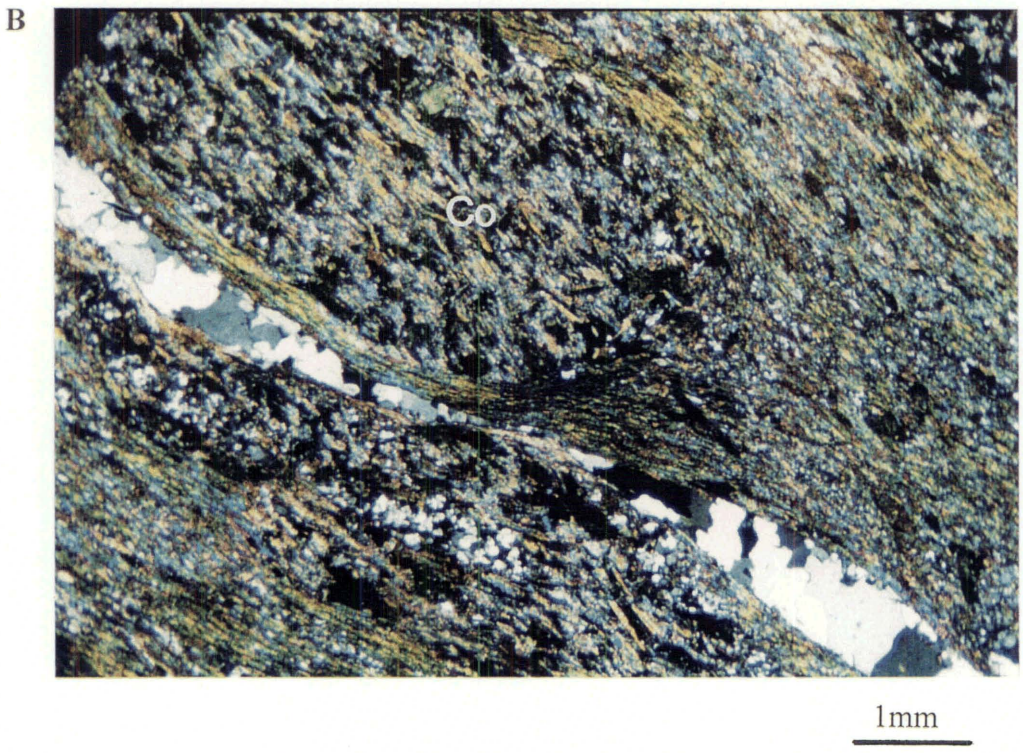

Figure 3.9 (A): S_2 micas wrap around an andalusite porphyroblast (An). The porphyroblast has asymmetric quartz strain shadows which indicate top to the left shear-sense. S_2 XZ section of RJ294. PPL (B): S_2 micas wrap around an elongate altered cordierite porphyroblast (Co). The lack of strain shadow development suggests the cordierite was altered either pre- or syn-S_2, and deformed plastically during D_2. An adjacent quartz vein is boudinaged. S_2 XZ section of RJ364. CPL. Both RJ294 and RJ364 are fine grained schists from the Orator Creek domain.

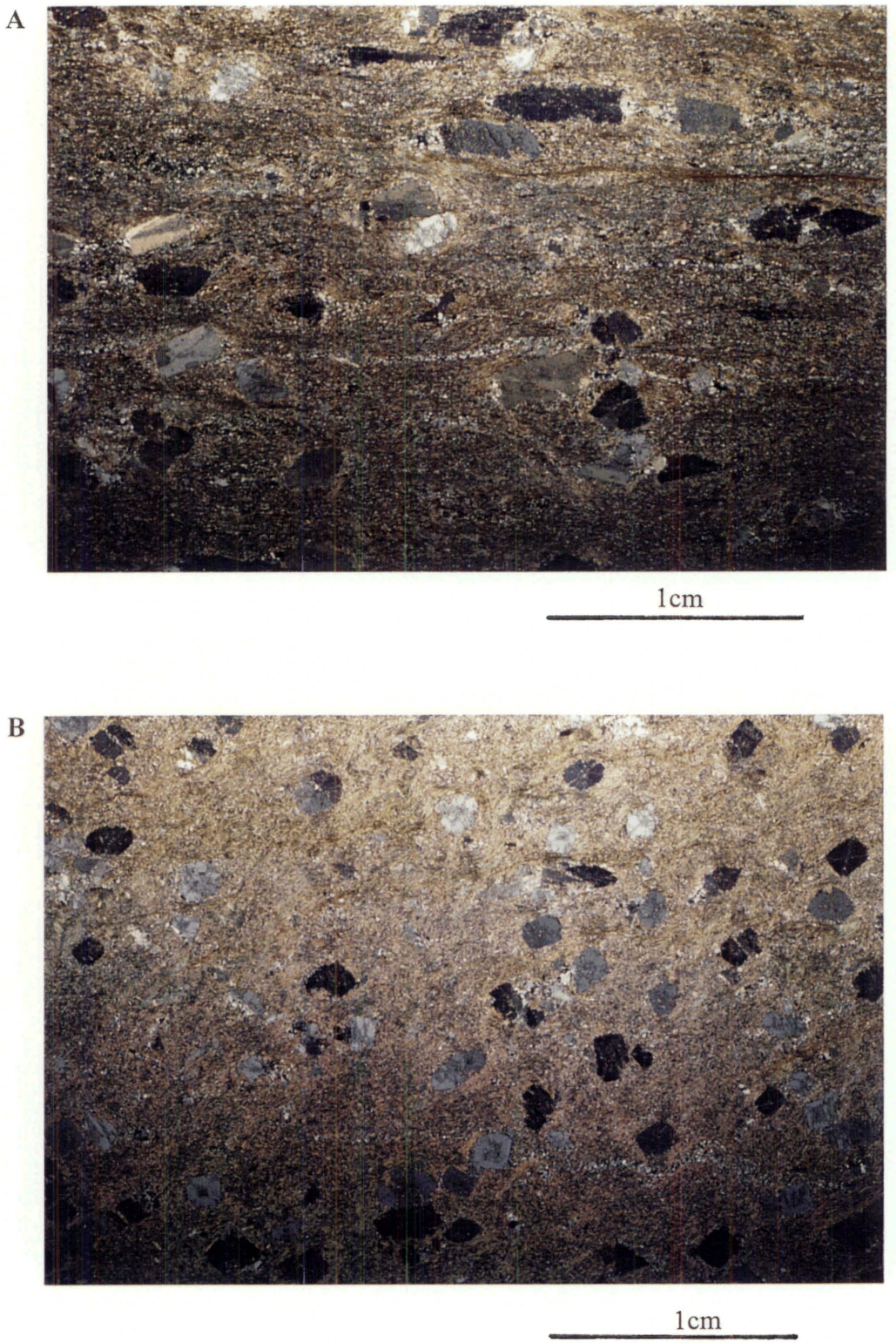

Figure 3.10 (A): Aligned andalusite prisms with maximum strain shadow development define sections parallel to the S_2 stretching lineation. (B): Cross-sections of andalusite prisms and a lack of strain shadow development define sections perpendicular to the S_2 stretching lineation. RJ294, Orator Creek domain. CPL.

Microscopic quartz veins reflect the same features as seen in mesoscale quartz veins in that those oblique to S_2 are isoclinally folded, and those parallel to S_2 are boudinaged (Fig. 3.9B). Boudinaging and folding of quartz veins are observed in both the YZ and XZ sections, but the relative degree of boudinaging in the two sections is difficult to determine. The *c*-axes in the quartz veins, observed with a sensitive tint plate, frequently have a preferred orientation perpendicular to S_2, indicative of basal slip.

In psammitic lithologies, quartz and minor feldspar essentially retain their detrital shape but have been modified to varying degrees by pressure solution with development of overgrowths, strain shadows and minor recrystallisation. Some quartz grains are quite elongate parallel to S_2, and display deformation bands perpendicular to the grain elongation. It is thought that plastic deformation played a role in the elongation as well as solution transfer. In pelitic lithologies, the quartz and feldspar components are recrystallised and no original detrital shapes are preserved.

In the graphitic, quartzose, silty slate, where S_0 is folded by F_2 on the mesoscale (M26/ 737336), S_2 is a crenulation cleavage in contrast to its usual schistose character. S_2 has crenulated a weakly developed slaty cleavage subparallel to S_0. The slaty cleavage could be either S_1 or an earlier S_2 development.

As mentioned in the mesoscale section, S_2 is crenulated by S_{cren}. On the microscale, S_{cren} is defined by bent but also recrystallised and reoriented muscovite and biotite. As a result, the micas display a tiled effect (Fig. 3.11). The more graphitic specimens show pressure solution seam development parallel to crenulation axial planes. In some specimens, quartz grains have been preferentially dissolved along the steeper limbs of the crenulations (Fig. 3.11B). Large chlorite porphyroblasts of more or less random orientation generally overgrow S_{cren} (Fig. 3.12A). However, a few specimens show chlorite porphyroblasts kink banded by S_{cren} (Fig. 3.12B).

Orator Creek domain D_2 shear-sense indicators

Some specimens that were thin-sectioned parallel to the XZ direction of S_2 revealed asymmetric strain shadows implying non-coaxial strain (Fig. 3.9A). Others showed no asymmetry at all in the XZ section indicative of coaxial strain. The asymmetric strain

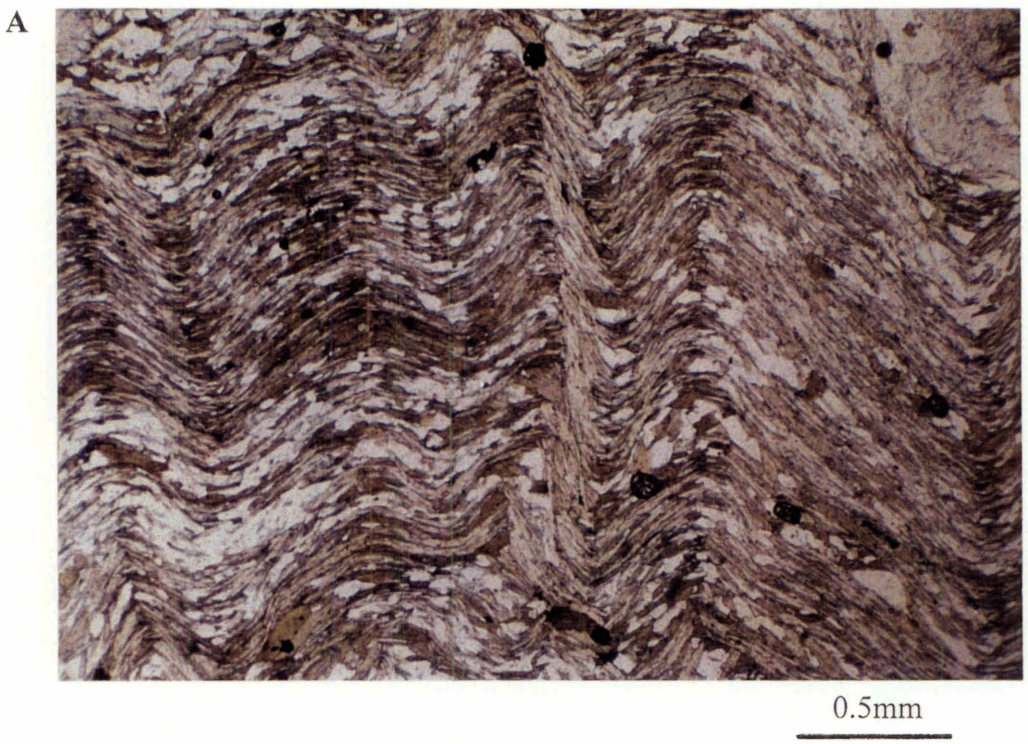

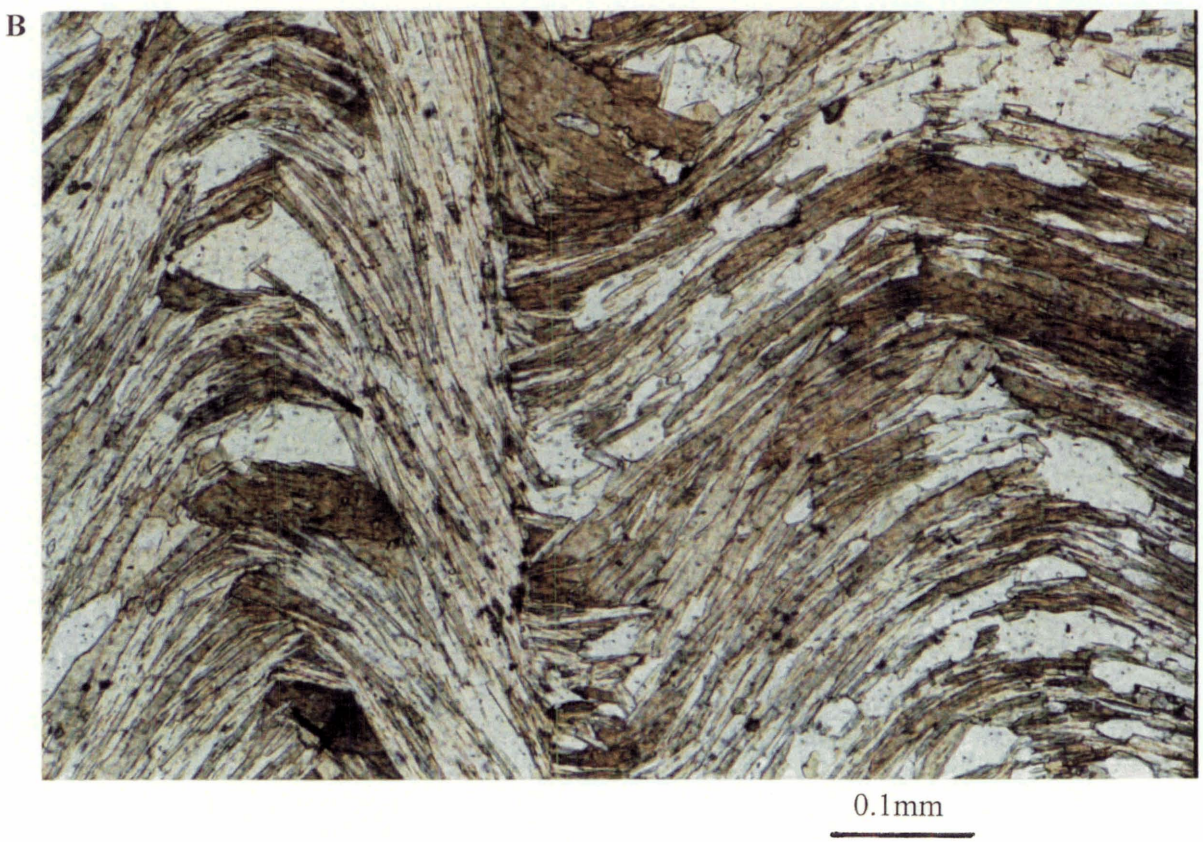

Figure 3.11: (A): S_2 crenulated by S_{cren}. (B): Close-up view of (A) showing a "tiled effect" of biotite and muscovite deformed by S_{cren}. Note how quartz grains have been preferentially dissolved along the steeper limb of a crenulation. RJ370, Orator Creek domain. PPL.

A

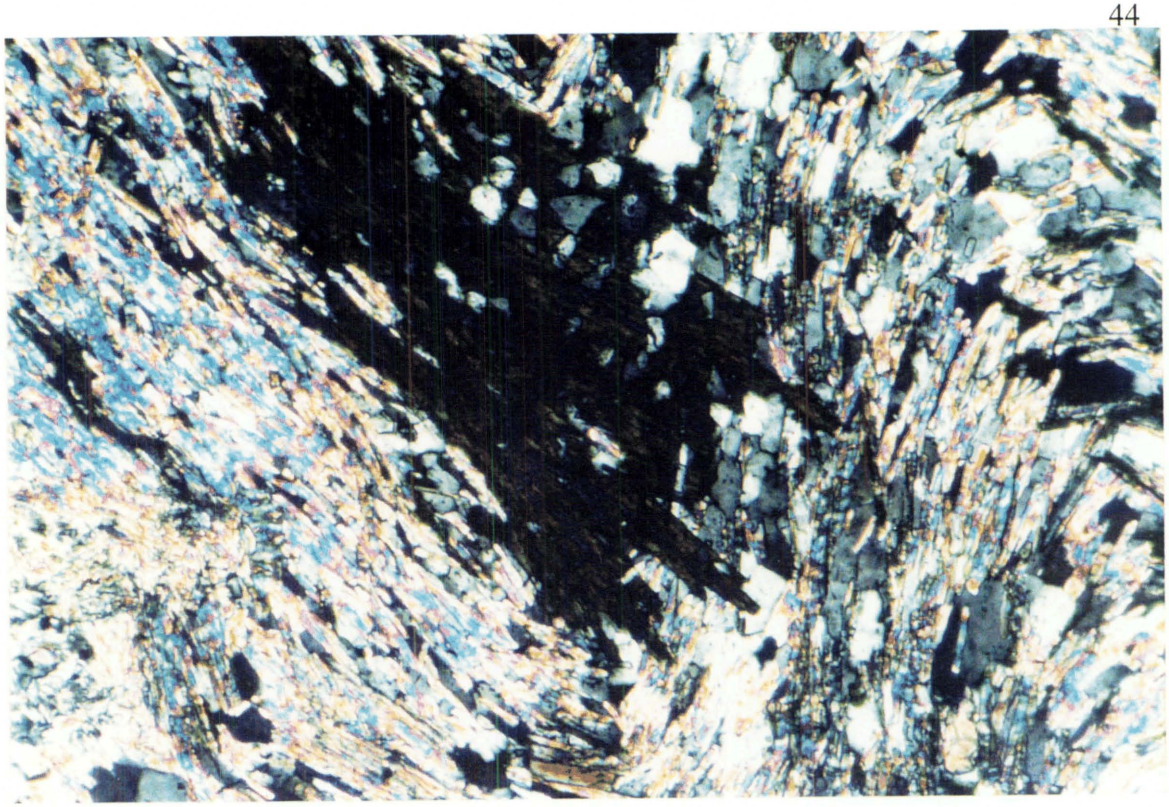

B

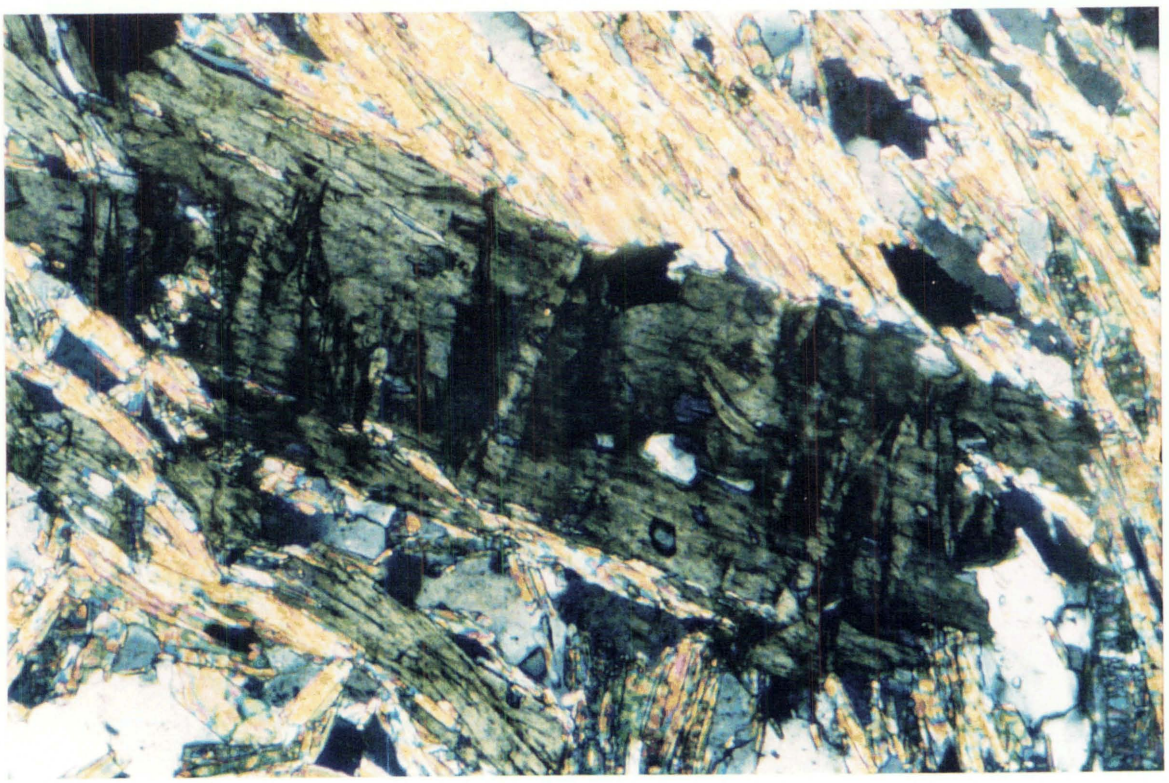

Figure 3.12: (A): Randomly oriented chlorite porphyroblast growing across S_{cren}. Sample M26 (courtesy of Rennison, 1992). CPL. (B): Chlorite porphyroblast kink banded by S_{cren}. RJ291. CPL. Both M26 and RJ291 are from the Orator Creek domain.

shadows provide a dextral reverse sense of shear with top to the SW. If the origin to the bent granite apophysis in Figure 3.7 is a consequence of non-coaxial strain, than the bending is consistent with the microstructural shear-sense indicators.

3.5.3 Lake Outlet domain

Lake Outlet domain mesoscale structures

In contrast to the Orator Creek domain, schistose S_{2a} strikes generally NW and dips gently to moderately NE, directly reflecting the local strike of the Mt Olympus Pluton contact in the Lake Outlet domain (Fig. 3.4). Bedding is commonly subparallel to S_{2a}. Quartzose sandy beds display boudinage or pinch and swell structure. Boudin axes trend between NE and SE, and boudins are often separated from each other by vein quartz necks.

Also in contrast to the Orator Creek domain, bedding is frequently folded close to the pluton contact with S_{2a} axial planar to these folds (Fig. 3.13, 3.14). F_{2a} is close to isoclinal; fold axes and L_o^{2a} plunge gently between NE and ENE (Fig. 3.4). Poles to S_0 fall on a π-girdle in which its axis coincides with measured F_{2a} (Fig. 3.15). Ptygmatic-like F_{2a} fold structures are particularly common at M26/ 736354 where the competence contrast between isolated quartzite beds and graphitic quartzose slate is high (Fig. 3.13B). In some cases F_{2a} folds are truncated by D_2 shear planes (Fig. 3.14).

In addition to the primary folding (F_{2a}), there is a secondary set of folds (F_{2b}) with similar trend (Fig. 3.16) and style to the primary folds. These secondary folds are evidenced particularly well by the refolding of boudinaged sandy beds. Where boudins are separated by vein quartz necks, the necks govern the secondary fold hinge position (Fig. 3.17.; see also Fig. 5 in Brathwaite 1968b). F_{2b} folds have an associated axial planar foliation (S_{2b}) that in some cases is almost as pervasive as the primary schistosity (S_{2a}) it is refolding. Although the secondary foliation is oblique to the primary foliation at any particular outcrop, the attitude of the secondary foliation coincides with primary foliation attitudes elsewhere in the Lake Outlet domain (compare Fig. 3.16 with Fig. 3.4). The refolding of S_{2a}, observed solely in the Lake Outlet structural domain (refolding of F_{2a} is not observed), is a good example of late stage deformation of a single progressive

A

B

Figure 3.13: (A): S_0 is isoclinally folded by F_{2a} in the Lake Outlet domain. M26/ 737353. Lens cap for scale. (B): An isolated quartzite bed with graphitic slaty siltstone is folded by F_{2a}. Fold shape is almost ptygmatic. Lake Outlet domain. M26/ 737353. Lens cap for scale.

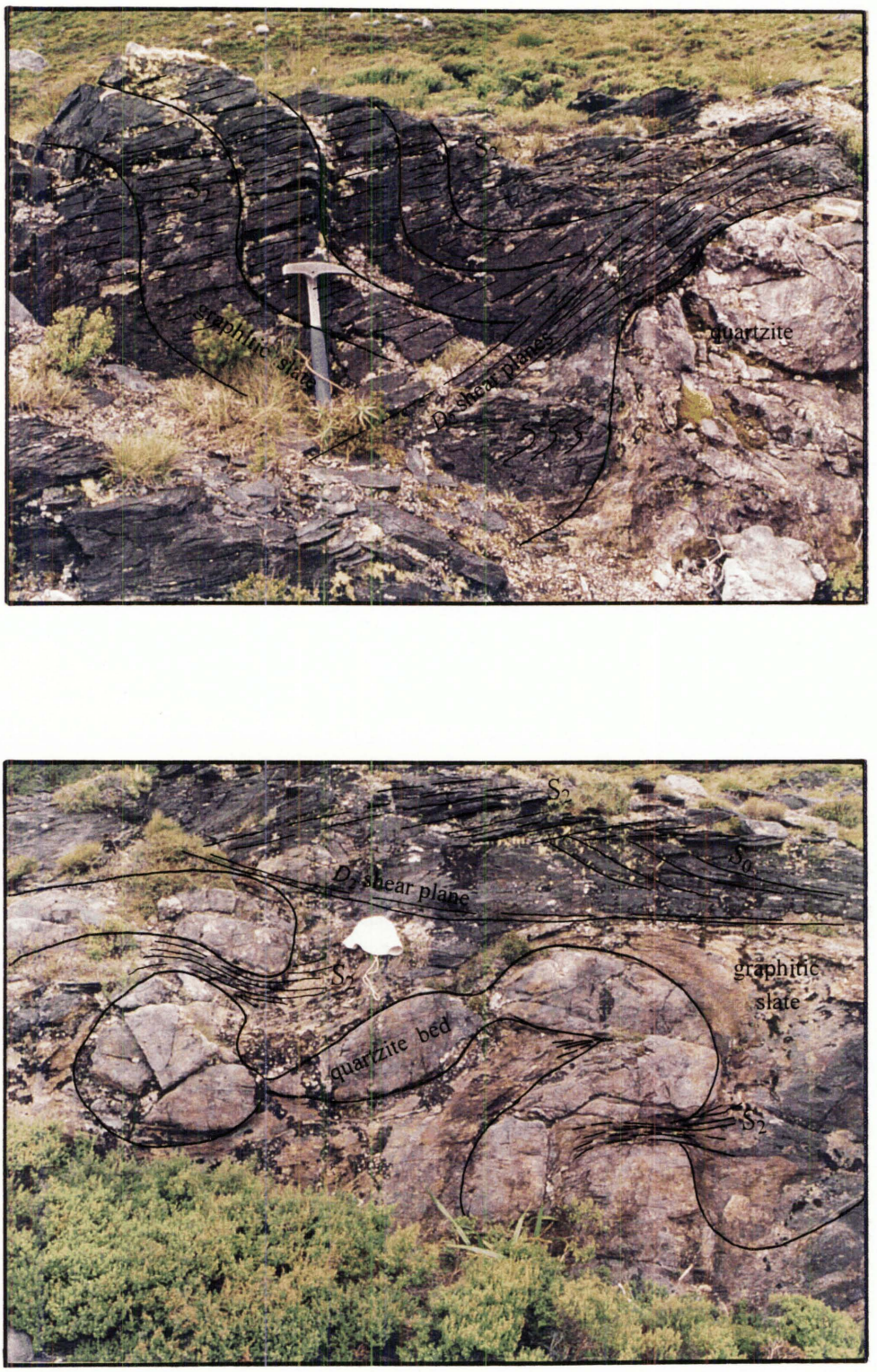

Figure 3.14: F_{2a} folds truncated by D_2 shear planes, Lake Outlet domain. (A) M26/ 737353, (B) M26/ 736354. Hammer and hat for scale.

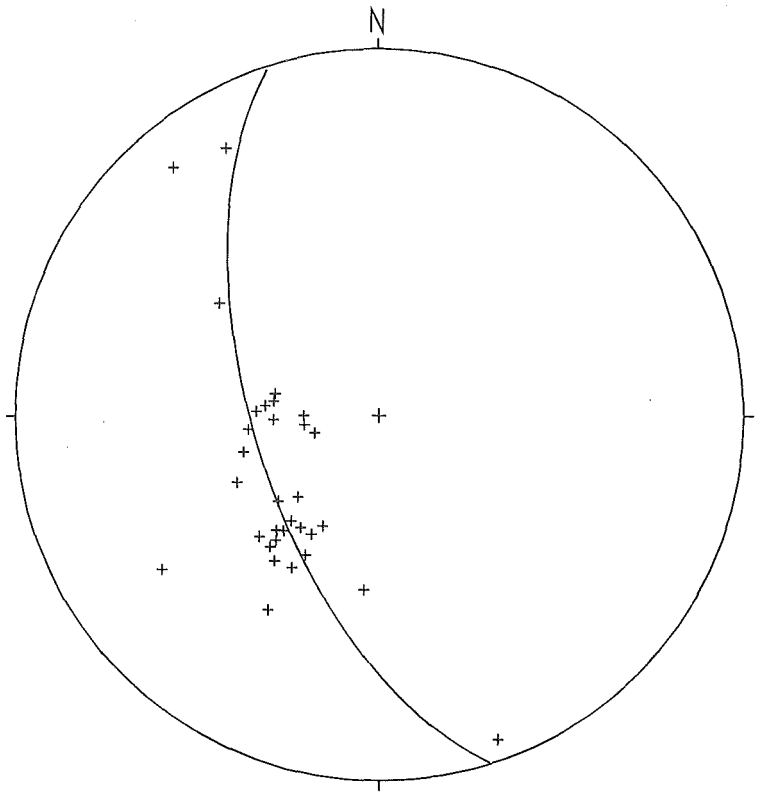

Figure 3.15: Poles to bedding (+) in the Lake Outlet domain. The poles lie on a best fit π -girdle in which the axis (072/28°) is subparallel to measured F_{2a} fold axes. n=32.

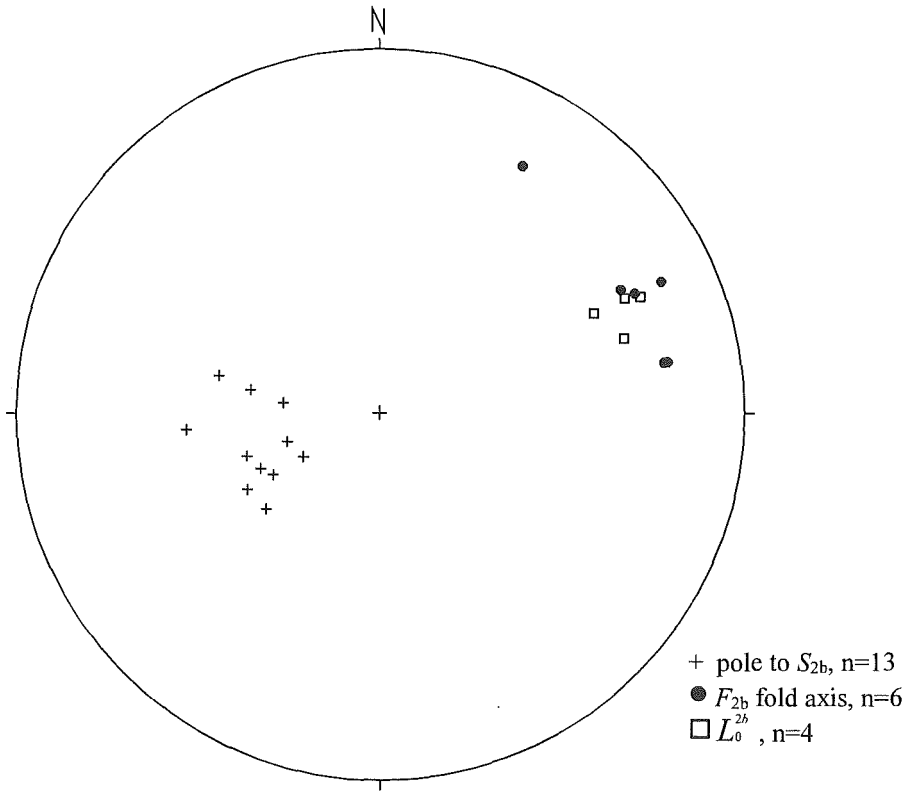

Figure 3.16: S_{2b}, F_{2b}, and L_0^{2b} orientations in the Lake Outlet domain.

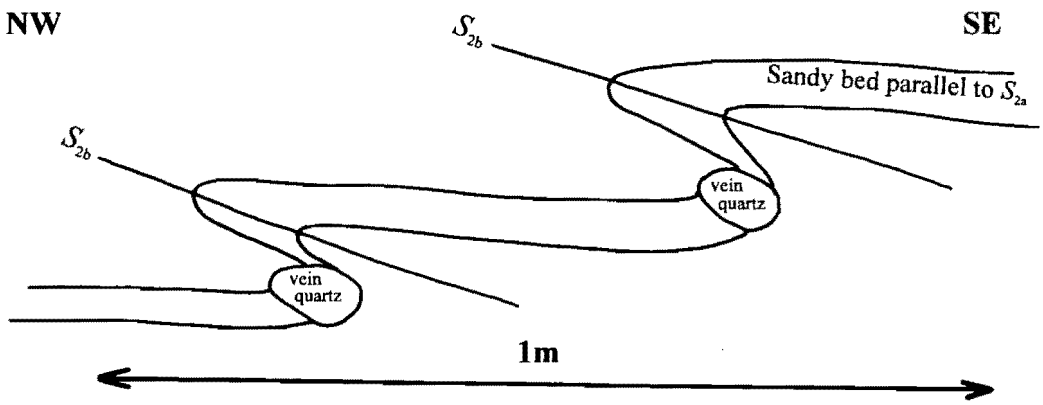

Figure 3.17: Field sketch of a boudinaged sandy bed with vein quartz necks parallel to S_{2a}. The sandy bed outlines F_{2b} fold structures with development of axial planar S_{2b} that is oblique to S_{2a}. The quartz necks govern the secondary fold hinge position. Lake Outlet domain. M26/ 739352.

deformation event. The folding of boudinaged beds is a response to either a change in the principal stress axes or a bulk rotation of the rock.

F_2 folds are both symmetrical and asymmetrical on the outcrop scale with wavelength varying chiefly between 10cm and 2m. Vergence of asymmetrical folds is towards the NW and SE directions with neither of these two directions locally dominant.

Aplite dikes and granite apophyses are invariably deformed by D_2. Both types of intrusions clearly display boudinaging (Fig. 3.18) and folding in exactly the same fashion as adjacent quartzite beds within the same outcrop (see Fig. 7 in Brathwaite 1968b). Occasionally, folds are almost ptygmatic in shape (Fig. 3.19). Figure 3.20 summarises the deformation structure exemplified by the igneous intrusions.

As in the Orator Creek domain, a crenulation (S_{cren}) overprints the development of S_2 (Fig. 3.20). However the orientation is somewhat different in that S_{cren} strikes NNE, dipping moderately to the ESE (Fig. 3.8B). Characteristics of S_{cren} are similar to S_{cren} in the Orator Creek domain and are most likely to be of the same generation. Crenulation lineations (L_2^{cren}) and fold axes of large crenulations (F_{cren}) plunge generally NE to ENE at a gentle to moderate angle (Fig. 3.8B). On some surfaces two sets of crenulation lineations can be identified. The second crenulation lineation plunges between E and SE but its associated crenulation plane was not observed.

Lake Outlet domain microscale structures

Similar microstructures to those seen in the Orator Creek domain are observed in the Lake Outlet domain including stretching lineations, the general appearance of YZ and XZ sections, modification of quartz and minor feldspar grains, random growth of chlorite, and the nature of S_{cren}. Stretching lineations plunge gently to moderately ENE or E, and are essentially parallel to F_2 fold axes and L_0^{2a} (Fig. 3.4). Other important microstructural observations from the Lake Outlet domain are described below.

RJ482 is an excellent example of deformation partitioning and secondary layering associated with S_{2a} in the Lake Outlet domain. In RJ482, flattened cordierite porphyroblasts contain inclusion trails of finer grained minerals than the surrounding

Figure 3.18: Boudinaged aplite dike in pelitic schist parallel to S_{2a}, Lake Outlet domain. M26/ 739352. Compass for scale.

Figure 3.19: F_{2a} folding of an aplite dike in pelitic schist, Lake Outlet domain. Fold shape is almost ptygmatic. M26/ 739352. Lens cap for scale.

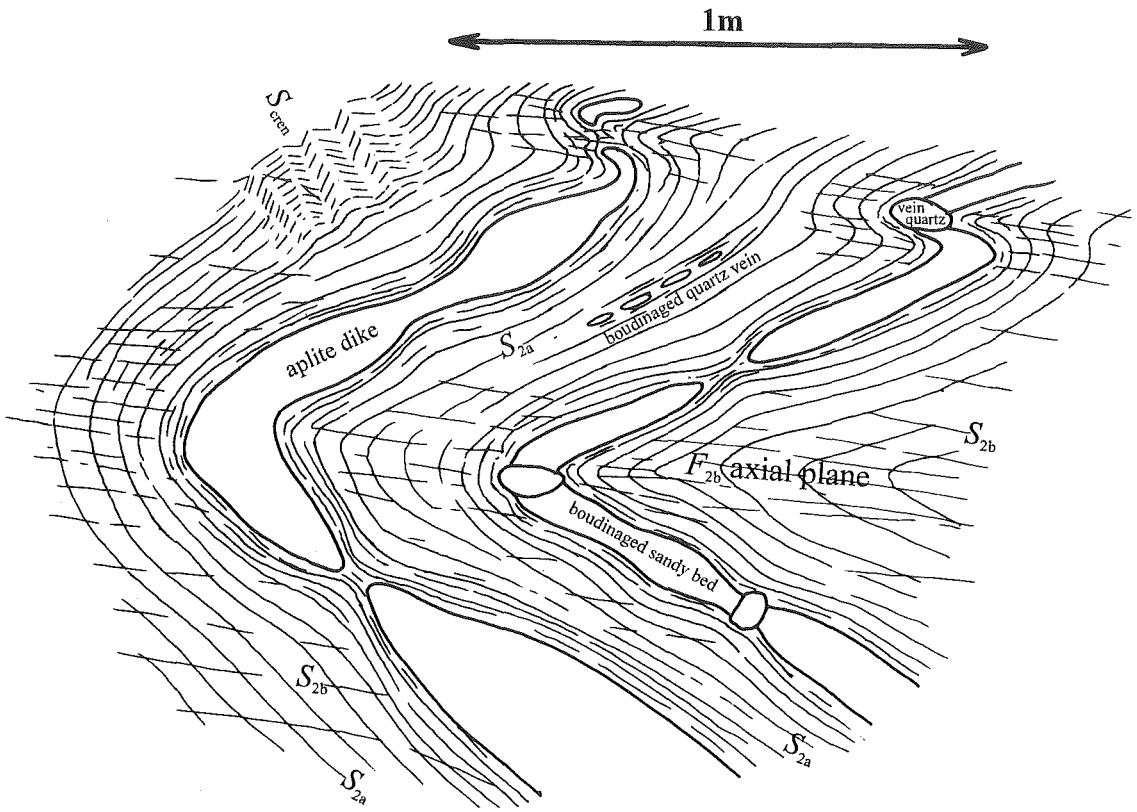

Figure 3.20: Schematic field sketch of D_2 related structures in the Lake Outlet domain. Aplite dikes, quartz veins, and sandy beds have been boudinaged parallel to S_{2a}. S_{2a} has subsequently been folded by F_{2b} with the development of an axial planar foliation (S_{2b}). In places S_{cren} can be observed crenulating both S_{2a} and S_{2b}.

Figure 3.21: Cordierite porphyroblast with inclusion trails oblique to the external S_{2a} foliation. Strain shadows adjacent to the cordierite, and the anastomosing M domain pattern, show an asymmetry that indicates top to the left shear-sense. S_2 XZ section of RJ482, Lake Outlet domain. CPL.

Figure 3.22: Cordierite porphyroblasts with strain shadows parallel to S_{2a} and consisting of quartz, biotite, muscovite, and sillimanite (variety fibrolite). Sillimanite is observed in the middle of the photomicrograph. S_2 XZ section of RJ482, Lake Outlet domain. PPL.

Figure 3.23: Q and M domains in fine grained schist, Lake Outlet domain. The domains are due to strain partitioning around cordierite porphyroblasts. The asymmetry of strain shadows around the porphyroblasts, and the asymmetric M domain anastomosing pattern, indicates top to the left shear-sense. S_2 XZ section of RJ482. PPL.

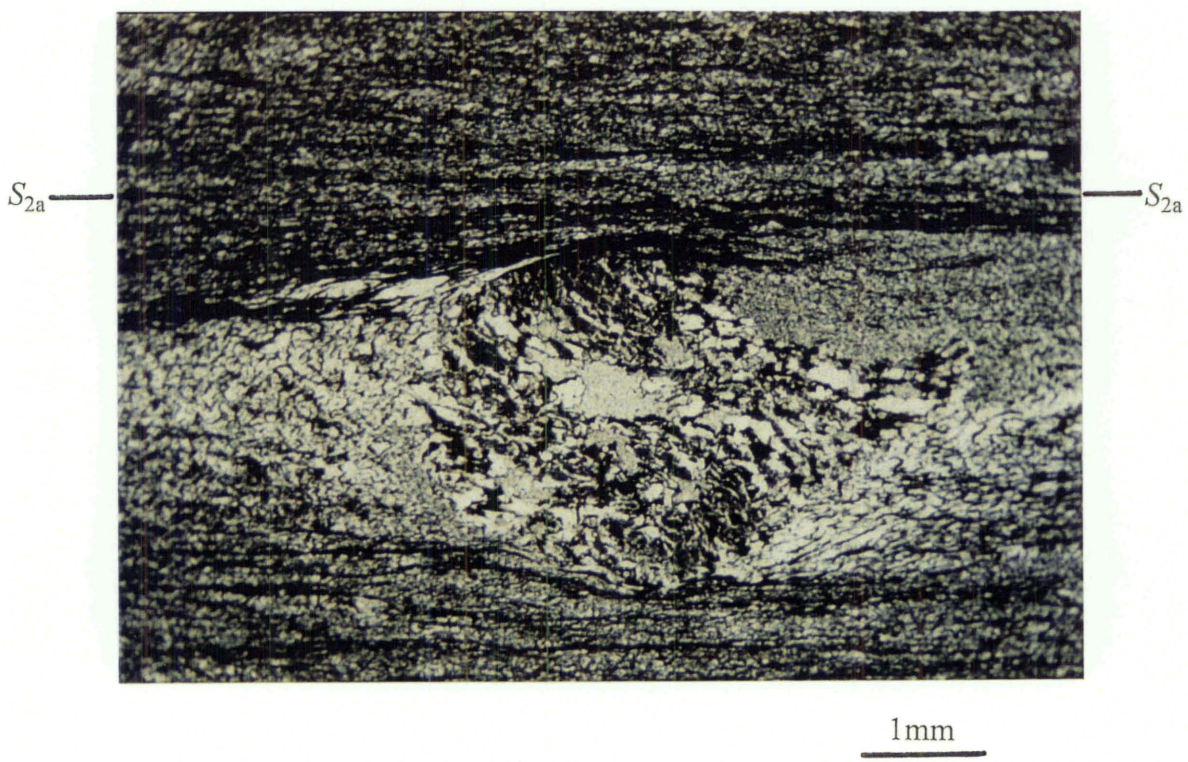

Figure 3.24: S_{2a} wrapping around spots of quartz and graphite. An earlier slaty cleavage is preserved amongst the S_{2a} strain shadows adjacent to the spots. S_{2a} XZ section of RJ335, graphitic slate, Lake Outlet domain. PPL.

matrix (Fig. 3.21). The inclusion trails are straight and tend to be at a high angle to the external foliation (Fig. 3.21). The trails represent either an earlier S_2 development or possibly S_1. If it is assumed the porphyroblasts have not rotated (Bell 1985), the inclusion trails represent the remains of a foliation that has been crenulated and subsequently obliterated by the external schistosity. The external foliation wraps around the cordierite porphyroblasts with maximum strain shadow development in the cordierite elongation direction. Strain shadows consist of quartz + biotite + muscovite ± sillimanite ± opaques (Fig. 3.22). Secondary layering is represented by Q and M domains* parallel to S_{2a}, and is partially a result of strain partitioning around cordierite porphyroblasts (Fig. 3.23).

In the graphitic quartzose black silty slate at M26/ 736354, there are spots with elongate strain shadows parallel to the stretching lineation observed elsewhere (Fig. 3.24). These spots consist of coarser grained quartz and graphite but are of unknown origin. S_{2a} wraps around the spots. An earlier slaty cleavage is preserved within the S_{2a} strain shadows (Fig. 3.24) that may represent either an earlier S_2 development or S_1.

At M26/ 739352, a 5cm aplite dike intrudes and is parallel to a ~4m thick quartzite bed located within 30 metres horizontally of the pluton margin. The dike exhibits a stretching lineation produced by elongate recrystallised quartz ribbons, elongate porphyroclast tails, and aligned muscovite. Also present are mica-fish (Fig. 3.25) and S-C structure. Porphyroclastic feldspars (1-2mm) are themselves elongate parallel to the lineation, and are mantled by finer recrystallised feldspar grains. The matrix is very fine grained (<0.3mm). These features indicate that the aplite has undergone a grain-size reduction as a result of strain. The quartzite immediately adjacent to the aplite dike has a stretching lineation parallel to that of the dike, and is defined by aligned biotites. The quartz is thoroughly recrystallised and exhibits a very strong *c*-axis preferred orientation parallel to the Y strain axis (Fig. 3.26). Such a fabric is compatible with high grade metamorphism (Schmid and Casey 1986) and is indicative of prism <a> slip (Lister and Dornsiepen 1982).

* Q stands for quartz-rich and M stands for mica-rich (Shelley 1993).

Figure 3.25: Mica-fish in a deformed aplite dike. Shear-sense is top to the right. XZ section of RJ479, Lake Outlet domain. CPL.

Figure 3.26: (A): *c*-axis measurements for a quartzite bed (RJ479) adjacent to a deformed aplite dike, Lake Outlet domain. Horizontal line represents S_2 foliation. L= S_2 stretching lineation. (B): Photo-micrograph of RJ479 perpendicular to the S_2 stretching lineation and foliation. The foliation runs diagonally across from bottom left to top right. The sensitive tint plate is inserted showing a strong *c*-axis preferred orientation.

Figure 3.25

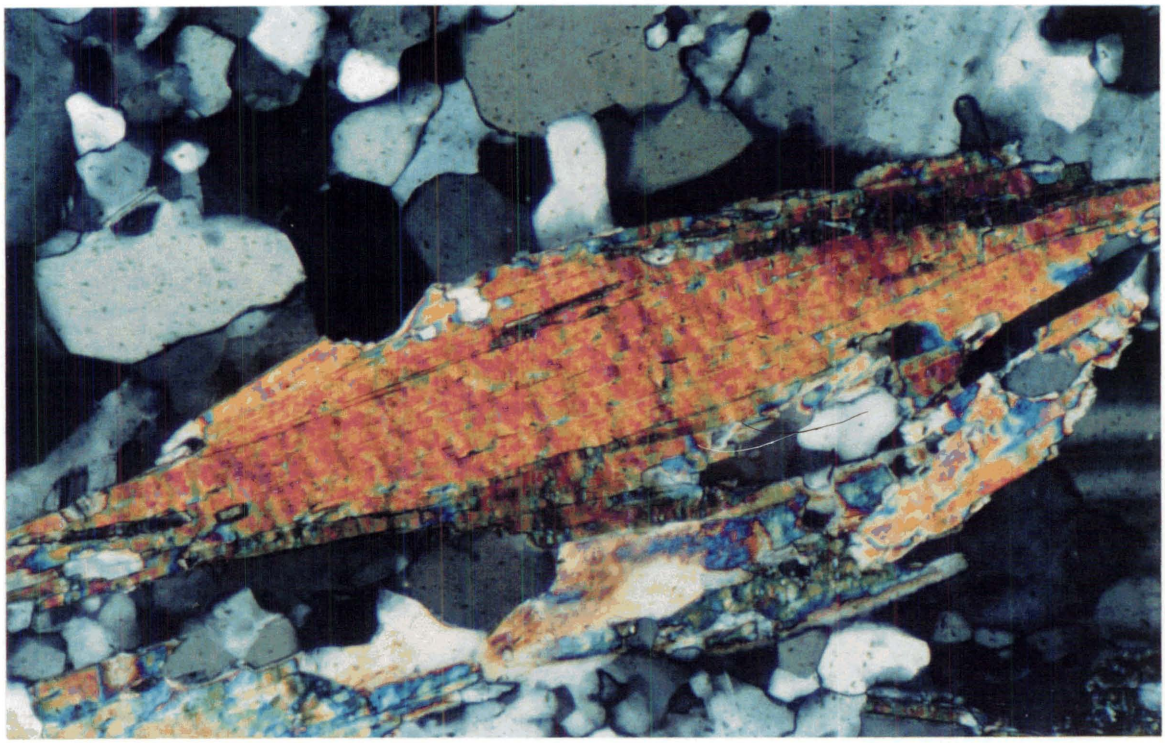

Figure 3.26A

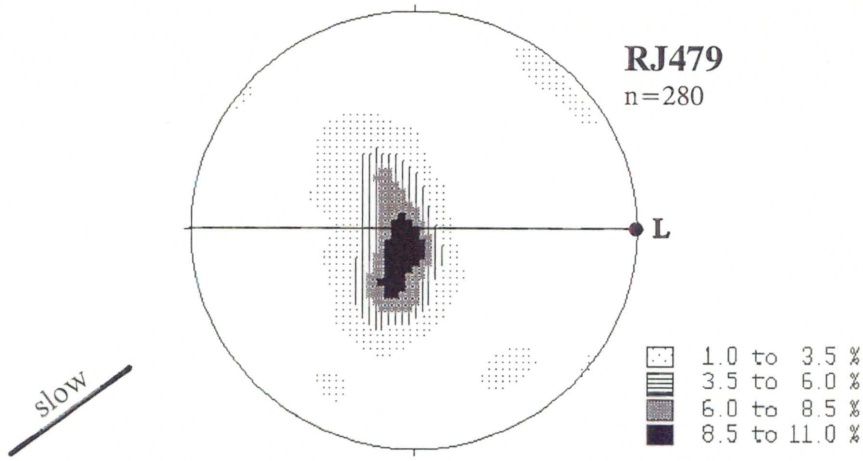

Figure 3.26B

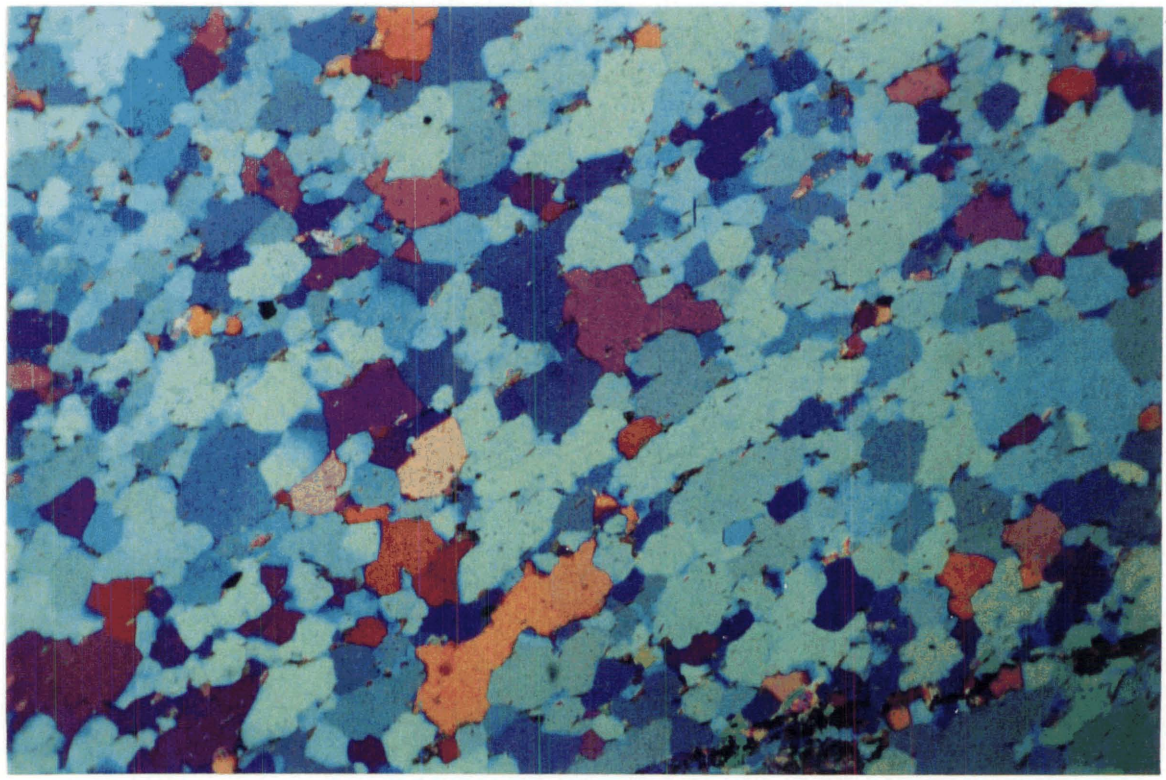

Lake Outlet domain D_2 shear-sense indicators

D_2 shear-senses from only two schistose samples can be determined with confidence, based on the asymmetry of the M domain anastomosing pattern (Bell and Johnson 1992) and asymmetric strain shadows (Fig. 3.21, 3.23). In these samples, a sinistral reverse shear-sense with top to the SW-W is indicated in XZ sections of S_{2a}. Sense of shear determined in the mylonitised aplite is the opposite of that determined in the schistose lithologies, being normal dip-slip shear with top to the ENE.

3.5.4 Beak Creek and Arena Creek domains

The Beak Creek and Arena Creek domains are described together because they display very similar features and differ only in orientation.

Beak Creek and Arena Creek domains: mesoscale structures

In the Beak Creek domain, S_2 strikes between NW and N, dipping gently to moderately NE or E, whereas in the Arena Creek domain, S_2 strikes between N and NE, dipping moderately to the E or SE (Fig. 3.4). Boudinaged quartz veins and bedding are subparallel to S_2 (Fig. 3.27). Folding associated with S_2 is very rare but when observed, bedding is isoclinally folded (Fig. 3.28).

A crenulation cleavage (S_3) is strongly developed in the dark-grey/black graphitic slates adjacent to the Anatoki Fault (Fig. 3.29) but less well-developed, or absent, in the phyllites that make up the majority of the Beak Creek and Arena Creek domains. S_3 strikes generally between NNE and ENE, dipping moderately to steeply SE, in the Beak Creek domain (Fig. 3.30A), whereas in the Arena Creek domain, S_3 strikes between ENE and E, dipping moderately S (Fig. 3.30B). Associated with S_3 are rare open folds (F_3) with wavelengths less than 50cm. F_3 and L_2^3 trend between NE and SE at a gentle to moderate plunge in the Beak Creek domain (Fig. 3.30A), whereas in the Arena Creek domain, they plunge gently to moderately towards the ESE (Fig. 3.30B).

Within the graphitic slates adjacent to the Anatoki Fault, and at the transition between the slates and Douglas Formation phyllites, are brittle shear zones up to 20m thick. These

Figure 3.27: Boudinaged quartz vein and bedding are subparallel to S_2 in graphitic slate/ quartz sandstone, Beak Creek domain. M26/ 745355. Lens cap for scale.

Figure 3.28: Bedding is isoclinally folded by a rare F_2 fold. S_2 is axial planar to the fold. Beak Creek domain. M26/ 740355. Lens cap for scale.

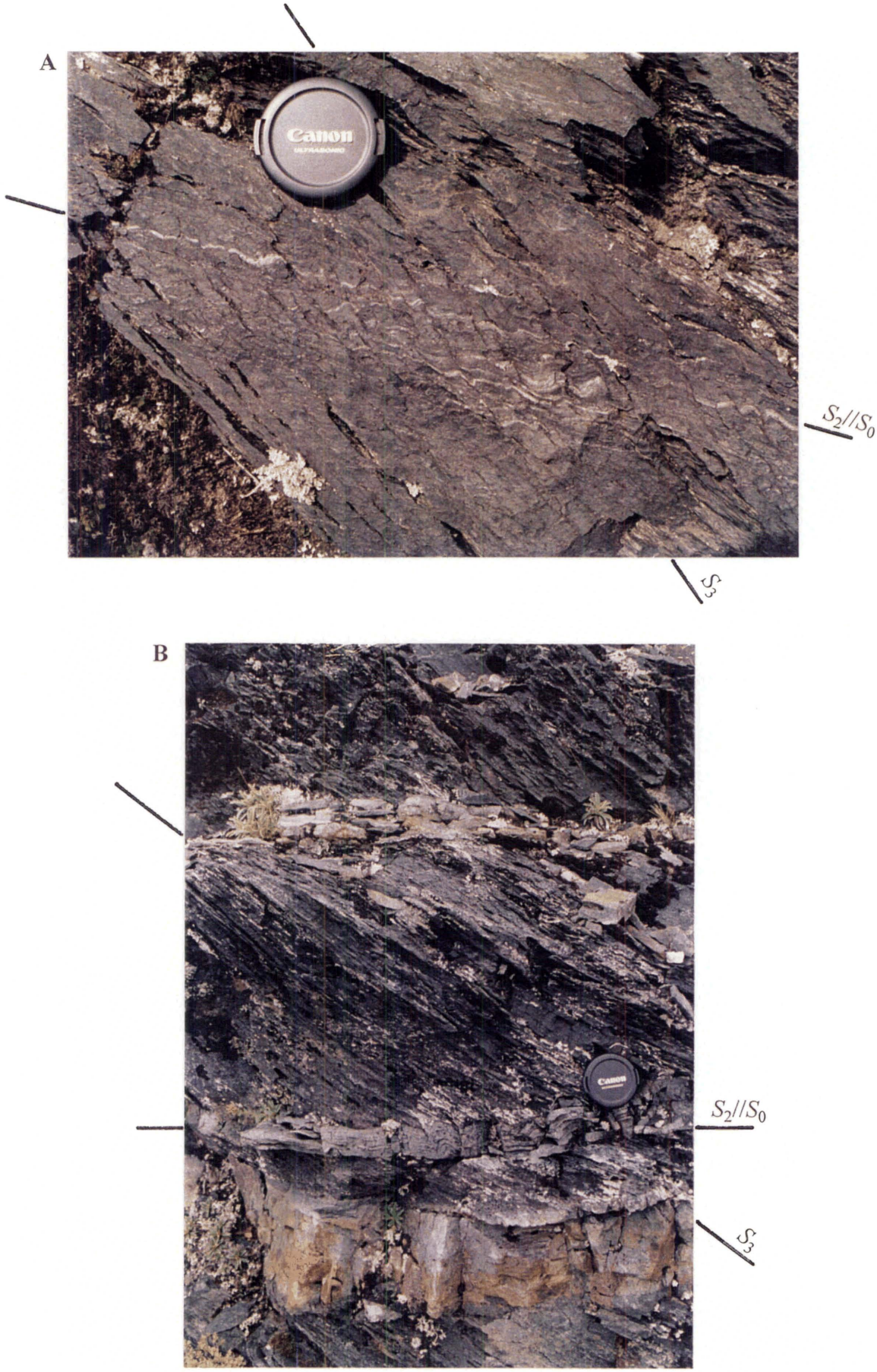

Figure 3.29: S_3 crenulation cleavage in graphitic slate adjacent to the Anatoki Fault (A and B). S_3 crenulates S_2 which is subparallel to S_0. Beak Creek domain. M26/ 745356. Lens cap for scale.

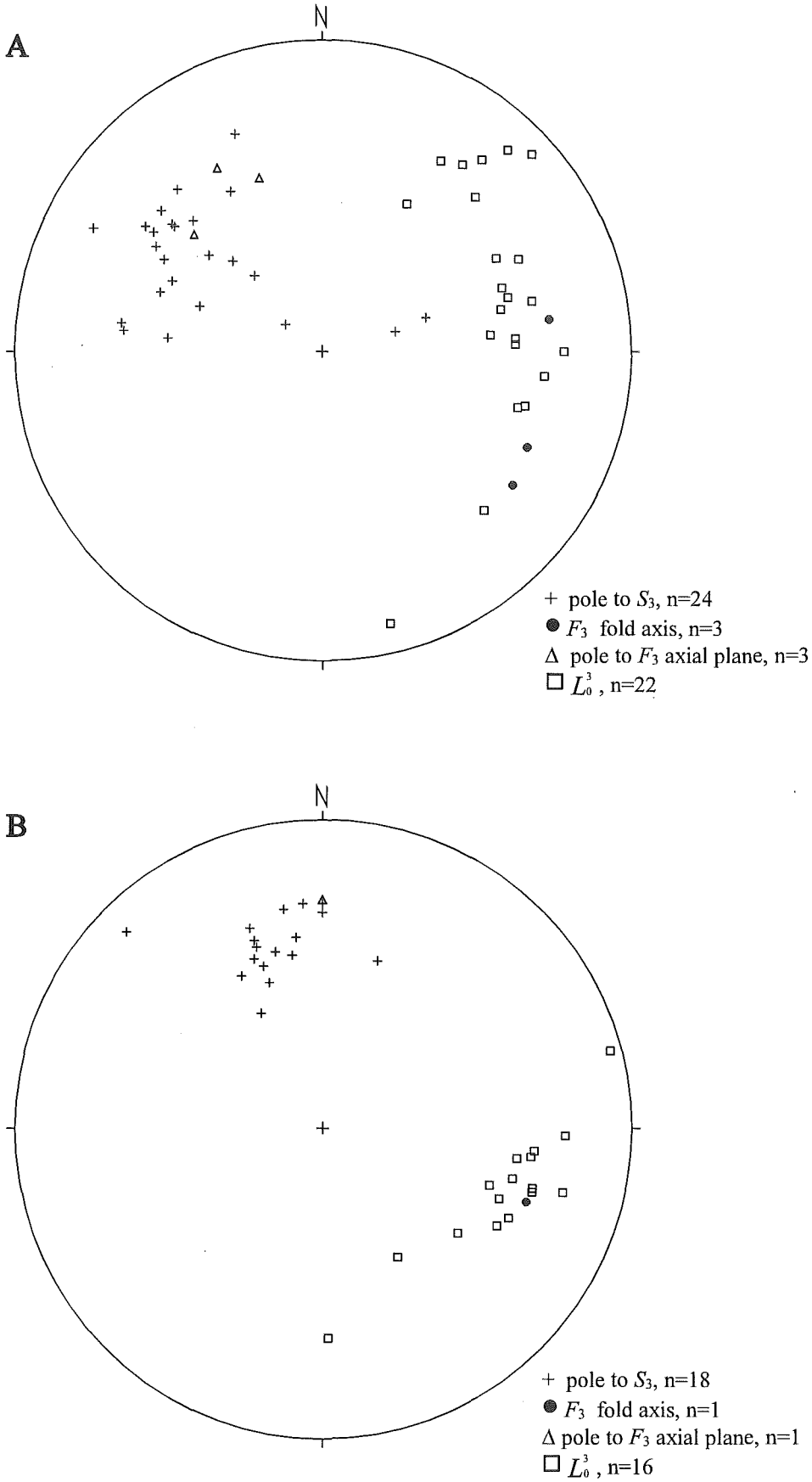

Figure 3.30: F_3, L_0^3, and S_3 orientations in the Beak Creek (A) and Arena Creek (B) domains.

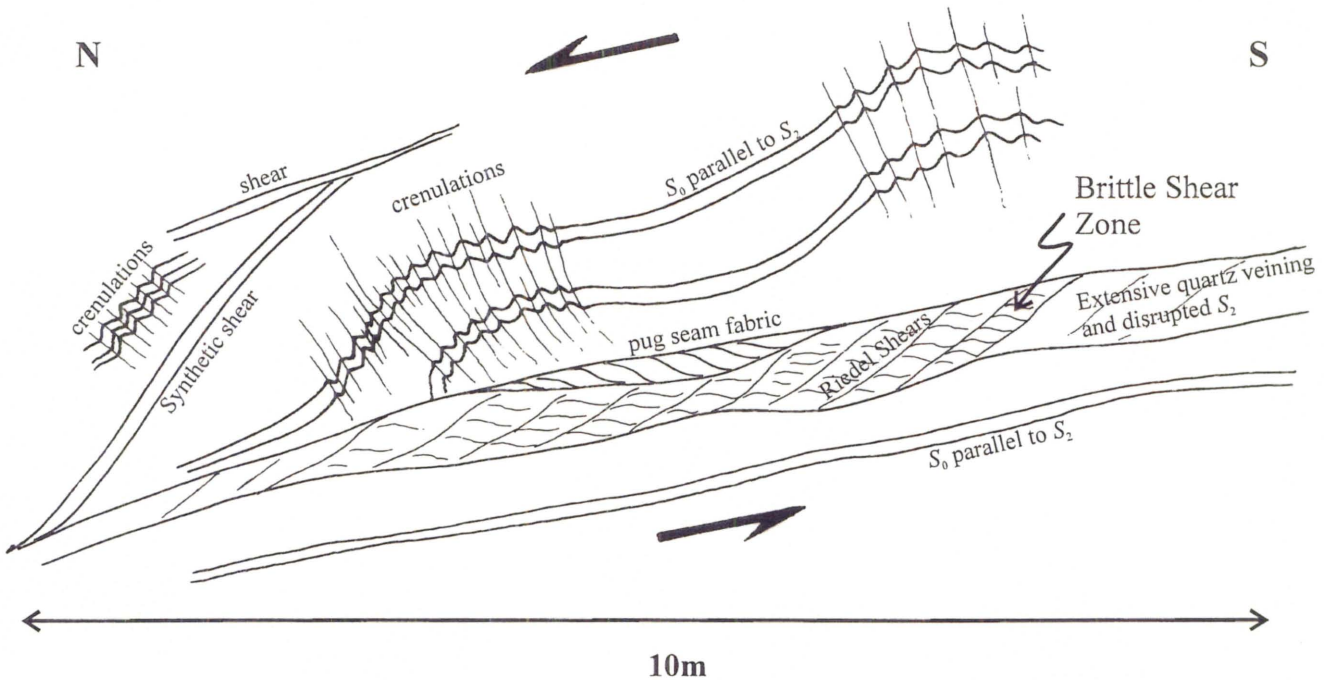

Figure 3.31: A photograph and field sketch of a brittle fault and folded hanging wall located at M26/ 745355, Beak Creek domain. Hammer for scale in photograph.

zones are subparallel to bedding, S_2, and the Anatoki Fault. Expressions of brittle faulting within the zones include an anastomosing network of thin pug seams, sigmoidally shaped pug seams related to small scale duplex structures, Riedel shears, quartz veining, and highly disrupted and irregularly folded bedding. At M26/ 745355 is an excellent exposure of a brittle fault where the hanging wall has been folded during tectonic transport (Fig. 3.31). Associated with the fault related fold are kink-like crenulations of S_2 planes.

Beak Creek and Arena Creek domains: microscale structures

S_2 is defined by the shape preferred orientation of biotite, muscovite, and chlorite in phyllites, and by muscovite and graphite in slate. Ankerite occasionally occurs in rocks immediately adjacent to the Anatoki Fault. Biotite porphyroblasts, reported in Beak Creek domain by Rennison (1992), are overprinted by S_2. Silt-size quartz grains show evidence of solution transfer and grain boundary migration so that original grain shapes are rarely preserved. Occasional sand-size grains tend to retain their detrital shape.

Compositional layering is parallel to S_2. One isoclinal fold of compositional layering has been observed in thin-section. Quartz veins are both isoclinally folded, with S_2 axial planar, and boudinaged along S_2. Quartz vein *c*-axis preferred orientations are typically at a high angle to S_2. RJ317 contains a boudinaged quartz vein that wraps around a large feldspar porphyroclast (Fig. 3.32). Together with *c*-axes at a high angle to S_2, the wrapping suggests this quartz vein has deformed plastically by basal slip.

On S_2 planes in the field, dark micaeous spots, up to 5mm in size, are frequently encountered in phyllites. In general, the spots are round on S_2 planes but occasionally may be elongate. In thin-sections perpendicular to S_2, the spots are lensoidal and elongate parallel to S_2 (Fig. 3.33). The spots consist of quartz and biotite that are coarser than matrix grains. Concentrations of micas and opaques occur on the stressed margins of the spots, perpendicular to S_2, whereas strain shadows are developed parallel to S_2 (Fig. 3.33). It is the mica and opaque concentrations, which wrap around the spots, that give the spots their dark appearance. The spots are of the same dimensions in sections perpendicular to each other and to S_2, indicating the phyllites are S-tectonites. However, occasional differential strain shadow development, corresponding to spot elongation

Figure 3.32: A feldspar porphyroblast with strain shadows parallel to S_2. A boudinaged quartz vein wraps around the porphyroblast. The quartz in the vein has *c*-axes at a high angle to S_2 suggesting the vein deformed by basal slip. RJ317, phyllite, Arena Creek domain. CPL.

Figure 3.33: Spots of quartz and biotite are elongate parallel to S_2. Strain shadows adjacent to the spots also consist of quartz and biotite. Concentrations of mica and opaques occur on the stressed margins of the spots, perpendicular to S_2. RJ331, phyllite, Beak Creek domain. PPL.

Figure 3.34: S_3 discrete crenulation cleavage, outlined by opaque solution seams, crenulates S_2. RJ367, graphitic slate, Arena Creek domain. PPL.

0.5mm

Figure 3.34

S_3

0.5mm

Figure 3.33

0.5mm

Figure 3.32

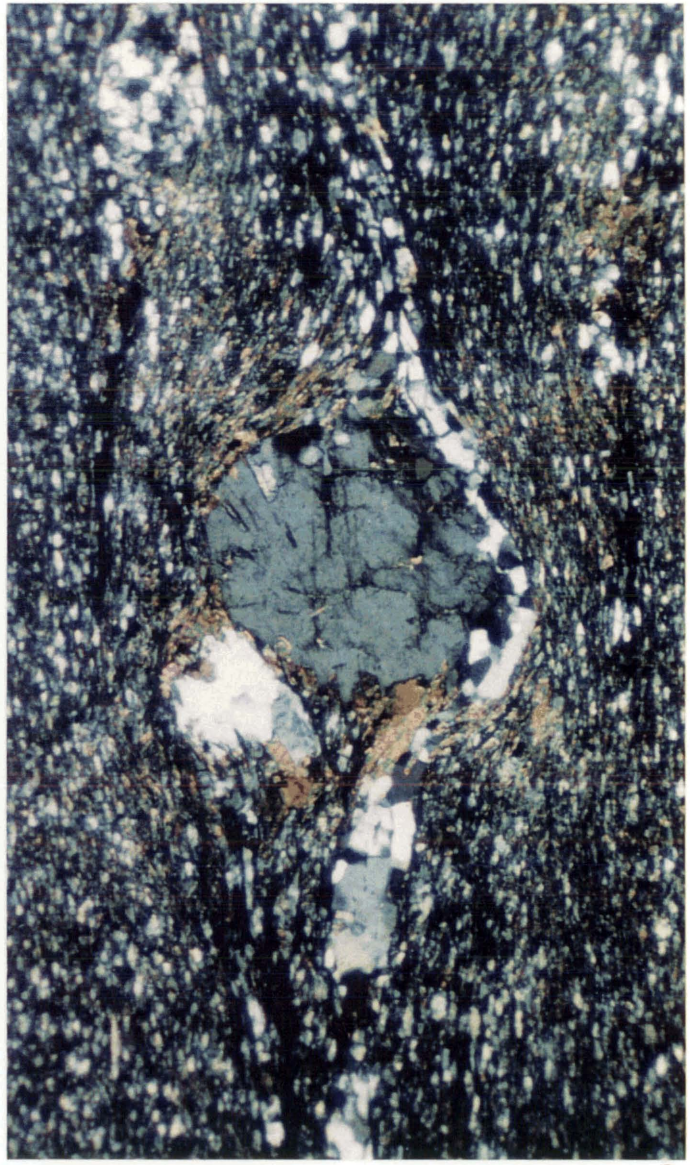

observed in the field, leads to identification of YZ and XZ sections. The few stretching lineations measured plunge gently towards the NNE-NE (Fig. 3.4). The spots are of uncertain origin but may be related to original sedimentary/biogenic structures.

S_3 tends to be a discrete crenulation cleavage outlined by opaque solution seams and some muscovite crystallisation in both phyllite and graphitic slate (Fig. 3.34). Occasionally a zonal crenulation cleavage with sharp boundaries is developed in phyllites, and where this occurs, biotite is conspicuously absent in the cleavage domain.

Beak Creek and Arena Creek domains: D_2 shear-sense indicators

No reliable shear-sense indicators are observed. Most specimens are S-tectonites and where asymmetry of strain shadows is occasionally observed it is difficult to establish the stretching direction.

3.5.5 Discussion of quartz c-axes preferred orientation parallel to S_2

Quartz grains in most pelitic or semi-pelitic Golden Bay Group metasediments of the four structural domains, display a preferential orientation of *c*-axes parallel to S_2 foliation. In Section 4.3.2, a similar observation is found in lower grade Golden Bay Group metasediments of the Adelaide Tarn and Lonely Lake domains. In these more southern domains, the Golden Bay Group has not experienced D_2 deformation, and the orienting process is attributed to mechanical rotation of clastic quartz grains, naturally elongate parallel to *c*, so that their long axes become parallel to S_1 during D_1 deformation (refer to Section 4.3.2 for reasoning). Thus it follows that although the Golden Bay Group quartz grains of the Boulder Lake domain have experienced recrystallisation, the most obvious cause for the observed quartz LPO is an inheritance of the D_1 mechanical rotation fabric. There are, however, several lines of evidence that point against an D_1 mechanical rotation inheritance of fabric:

1. In graphitic quartzose silty slate thin-sections, where an earlier slaty cleavage is preserved in microlithons between S_2 cleavage domains (Orator Creek domain) or in strain shadows around quartz/graphite spots (RJ335, Lake Outlet domain, Fig. 3.24), the quartz *c*-axes preferred orientation in the microlithons and strain shadows are

parallel to S_2 and not to the earlier slaty cleavage. Regardless of whether the slaty cleavage represents S_1 or an earlier S_2 development, the quartz LPO in the microlithons and strain shadows cannot be an inherited D_1 mechanical rotation fabric, given that the earlier slaty cleavage intersects at a high angle to S_2.

2. In the pelitic schist of RJ482, where an earlier cleavage at a high angle to S_2 is preserved in cordierite porphyroblast inclusion trails but not in the strain shadows, *c*-axes preferred orientation within the strain shadows are parallel to S_2. If it is accepted that the porphyroblasts have not rotated, then again, regardless of whether the inclusion trails represents S_1 or an earlier S_2 development, the quartz LPO in the strain shadows cannot be an inherited D_1 mechanical rotation fabric for the same reasons as mentioned above.

3. In the graphitic quartzose silty slate of RJ335, where an earlier slaty cleavage is preserved in strain shadows (Fig. 3.24), two thin-sections were made; one perpendicular to S_2 and parallel to the associated stretching lineation; the other perpendicular to both S_2 and the associated stretching lineation. Insertion of the sensitive tint plate clearly demonstrates a very strong preferred orientation of all quartz grain *c*-axes in the sample to be parallel to the S_2 stretching lineation, thus suggesting the LPO is a result of D_2 deformation.

In the examples described above, other causes for a quartz *c*-axes preferred orientation parallel to S_2 need to be explored. Possible orienting mechanisms include prism <c> slip (Mainprice *et al.* 1986), prism <a> slip, competitive anisotropic growth (Cox and Etheridge 1983), selective dissolution (Hippertt 1994), or in the case of an earlier slaty cleavage preserved at a high angle to S_2, an inherited basal slip fabric. Mechanical rotation of grains, naturally elongate parallel to *c* (Stallard and Shelley 1995), in which their long axes become parallel to S_2, and facilitated by extensive grain boundary sliding, could also be a feasible orienting mechanism. Some of these orienting mechanisms are dependent on temperature and others are dependent on the mica/quartz ratio of the rocks. The orienting mechanisms were not explored in this study but it would not be surprising to expect several of the mechanisms to have been operating at the same time given the range of metamorphic grade and the variable mica/quartz ratios in the Golden Bay Group rocks of the Boulder Lake domain.

3.6 Takaka terrane: Lithology

In the Boulder Lake, Adelaide Tarn, Lonely Lake, Peak 1610, and Kakapo Peak domains, the major rock unit immediately east of the Anatoki Fault is referred to as the Anatoki Formation by Grindley (1961, 1971). At Boulder Lake, the Anatoki Formation is described and discussed in detail by Brathwaite (1968a). Unfortunately the age and designation of this rock unit, east of the Anatoki Fault and between the Boulder Lake and Kakapo Peak domains, is uncertain and in this thesis will be referred to as undifferentiated Haupiri Group (see Appendix 1 for reasoning). All mappable intrusives in the Boulder Lake domain are designated as part of the Devil River Volcanics Group. In addition to the undifferentiated Haupiri Group and Devil River Volcanics Group, there is also an area of Balloon Mélange located in the southeast extremity of the domain. The Balloon Mélange is described and discussed in Chapter 8.

The undifferentiated Haupiri Group rocks east of the Anatoki Fault consist of a varied assemblage of low grade metamorphosed conglomerates, grits, sandstones, shales, and minor tuffs/reworked tuffs.

Bedding ranges from laminations of alternating sandstone and shale to metre scale coarse sandstone, grit, and conglomerate beds. Graded beds, load casts, flame structures, and scour structures are encountered frequently and provide excellent way-up indicators. Conglomerate horizons, up to 30m thick, are typically lensoidal in shape, matrix supported, massive, and commonly contain packets of synsedimentary-deformed sandstone and mudstone, all indicative of deposition by mass flow.

Compositionally, most sedimentary rocks contain varying amounts of basic and/or intermediate volcanic metadetritus, and sandstones are typically metagreywackes. Some sediments, however, are exclusively quartzofeldspathic and micaeous, and appear not to be volcanically derived. Apart from ankerite metasomatised rocks (see later), which are orange on weathered surfaces, the metasedimentary rocks are typically green to grey depending on the relative abundance of metamorphic minerals such as chlorite, epidote or actinolite. Detrital saussuritised calcic plagioclase tends to be ubiquitous. Detrital quartz grains and chert rock fragments are very common but sometimes noticeably absent. Minor bands of recrystallised crystal bearing tuffs and tuffaceous sandstones and

siltstones of basic/intermediate composition are interbedded with other sediments. More than 50% of clasts in conglomerates are lithics, the remainder being vein quartz or chert. Lithic clast types include basic/intermediate volcanics and green, grey or black sandstones and siltstones. In Bray Stream (M26/ 763343), limestone clasts form a significant component of a conglomerate lens.

Immediately east of the Anatoki Fault is a horizon up to 14m thick, but generally about 6m thick, consisting of interbedded black marble, black graphitic slate, and sometimes grey sandstone. This horizon appears to be conformable with undifferentiated Haupiri Group rocks to the east.

Throughout the undifferentiated Haupiri Group rocks are large metamorphosed bodies of basic intrusives (Devil River Volcanics Group) approximately parallel to bedding. Brathwaite (1968a) has described the intrusives in detail and has shown them to be sills that are thought to have intruded shortly after deposition of the sediments. The metamorphic mineralogy of the largest sill (Sill D of Brathwaite, 1968a) includes saussuritised plagioclase, actinolitic and tremolitic hornblende, epidote, chlorite, and altered opaques. Quartz is present (~15%), and its habit suggests it infilled drusy cavities. Relict textures such as feldspar laths and euhedral pyroxene or hornblende shapes of medium grain size indicate this sill was originally a dolerite. Preliminary XRF results of Sill D suggests it is geochemically similar to the Cobb Igneous Complex (C. Münker pers. comm. 1997). A complete description of each sill in the Boulder Lake domain is given in Brathwaite (1968a). However, Sill F of Brathwaite (1968a), located in the headwaters of the Snow River, is interpreted differently here. This body of rock consists predominantly of green volcanic clasts which contain phenocrysts of altered pyroxene. The body of rock is either an agglomerate or a volcanic conglomerate and its western contact is marked by a fault.

3.7 Takaka terrane: Structure

3.7.1 Introduction

The structure within the Takaka terrane rocks is complex. This complexity is not helped by the fact that in some areas, the rocks have experienced soft sediment deformation. Nevertheless, three major deformation events, other than Cenozoic uplift, are recognised: D_1, D_2, and D_3. The deformation associated with D_1 and D_3 affects all Takaka terrane rocks of the Boulder Lake domain whereas D_2 affects rocks only within close proximity of the Anatoki Fault. In sympathy with the deflection of the Anatoki Fault around the Mt Olympus Pluton, bedding and foliations in the Haupiri rocks also are deflected but the amount of deflection is less noticeable than in rocks west of the Anatoki Fault. Because of the lesser deflection, the Haupiri rocks have been subdivided into only two structural domains, one domain north of Grid Northing 34.5 (approximately the position of Portia Creek) and the other south of it (Map. 1). Excluding orientation, the structure and metamorphism are essentially the same in both domains, so rather than describing each domain in turn, the three deformations will be described in turn. Firstly, however, the synsedimentary deformational structures will be described.

3.7.2 Synsedimentary deformation

The most conspicuous expressions of synsedimentary deformation are isoclinal slump folds. Slump folds are generally observed within the vicinity of conglomerate lenses throughout the Boulder Lake domain. They also occur prominently in the lower Snow River and in the vicinity of Brown Cow. At Brown Cow, two thick light grey shale beds outline macroscale slump folds (Fig. 3.35; see also Fig. 4 in Brathwaite 1968a). There is no associated axial planar cleavage. Any cleavage observed always cuts obliquely across the axial plane and is unrelated. Occasionally, thrusts occur in the lower limb of the slump folds (Fig. 3.36). The general rule in the field is that when bedding changes unexpectedly in attitude, slump fold structures will be observed nearby. Features such as synsedimentary faults and disrupted bedding occur in close association with slump folds.

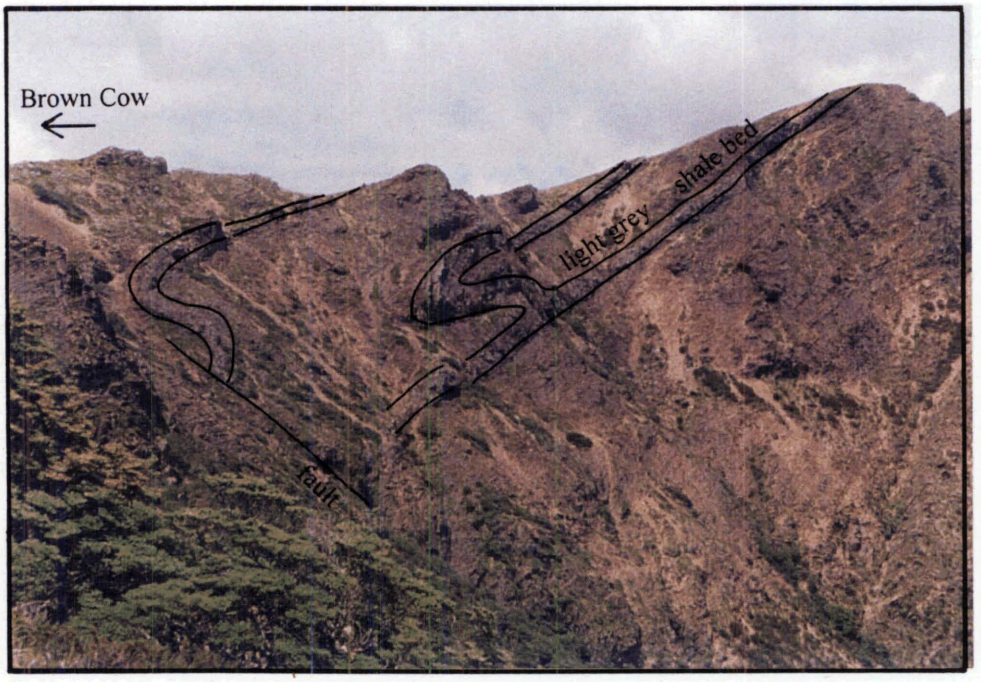

Figure 3.35: Macroscopic slump folds, outlined by light-grey shale beds in undifferentiated Haupiri Group, occur on southwest facing slopes just south of Brown Cow.

Figure 3.36: Slump fold in undifferentiated Haupiri Group sandstone and shale with the lower limb truncated by a thrust. Lower Snow River. M26/ 768363. Lens cap for scale.

3.7.3 D_1 macroscale and mesoscale structures

The first major deformation event to affect the Haupiri rocks is represented by a macroscale folding of bedding (F_1) with an associated axial planar cleavage (S_1). Two major fold structures trending approximately N-S are observed (see Map 1). Brown Cow syncline (Grindley 1971) is the westernmost structure and is best outlined by a large sill that is approximately concordant with bedding in the Haupiri rocks. The corresponding No Man anticline (informal name) lies to the east of Brown Cow syncline. If poles to all bedding measurements are plotted, a diffuse π-girdle is observed in both the North and South domains (Fig. 3.37). The pole to this girdle corresponds to a N to NNE gently plunging fold axis in the North domain and a NE gently to moderately plunging fold axis in the South domain. The diffuse nature of the girdle is primarily a result of later deformation (D_3). Measurements that stray markedly from the girdle are bedding measurements made on F_3 fold structures (see later) or slump folds.

Based on axial plane traces of the Brown Cow and No Man folds (Map 1), F_1 axial planes strike N in the North domain and NNE-NE in the South domain. Brown Cow syncline is moderately inclined and has a steep but upright eastern limb in the North domain which becomes overturned in the South domain (cross-sections A-A' and B-B'). In contrast, No Man anticline is essentially upright (cross-section A-A'and B-B'). In conjunction with the macroscale folds are rare parasitic mesoscale folds observed usually near the major fold hinges. The associated axial planar slaty cleavage (S_1) strikes between NNW and NNE in the North domain, and generally NNE in the South domain (Fig. 3.38). Subvertical cleavage occurs in the No Man anticline whereas moderately E dipping cleavage occurs within the Brown Cow syncline.

Although widespread, S_1 is difficult to measure for three main reasons. Firstly, S_1 is often only weakly developed, secondly a widespread crenulation cleavage (S_3) can obscure S_1, and thirdly S_1 overlaps with S_3 in orientation particularly in the South domain. Many S_1 measurements made in the field proved in thin-section to be a finely spaced S_3 crenulation of the S_1 slaty cleavage. On the mesoscale, S_1 is noticeably refracted from coarse to fine grained layers. In No Man Creek, the S_1 relationship with F_1 is beautifully illustrated: S_1 in fine layers converges towards the No Man anticline whereas S_1 in coarse layers diverges. Refraction is well-displayed in graded beds (Fig. 3.39). Occasionally, small faults of less than 5cm displacement occur parallel to S_1.

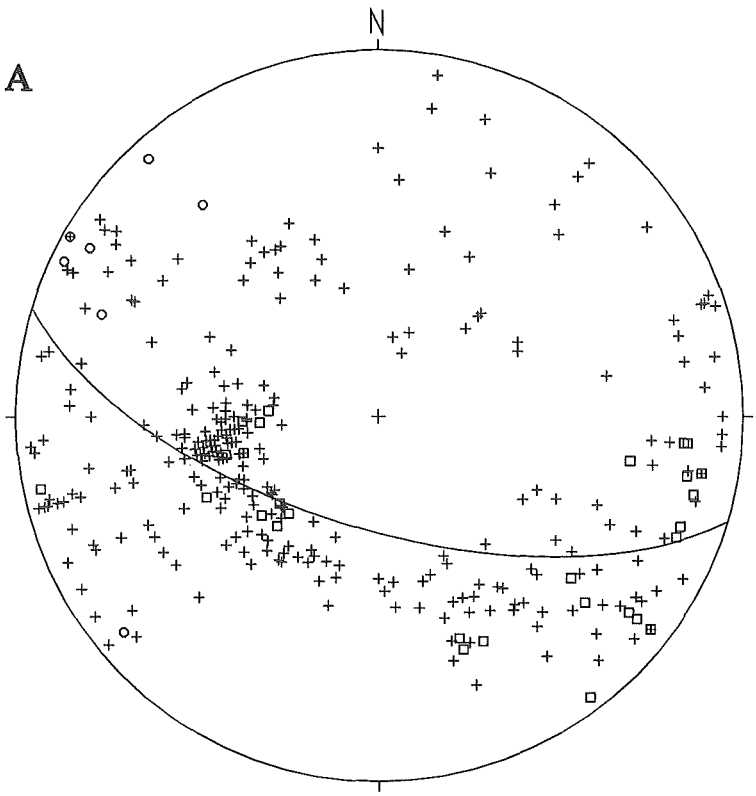

+ pole to bedding with no younging direction, n=284
□ pole to upright bedding, n=28
O pole to overturned bedding, n=7

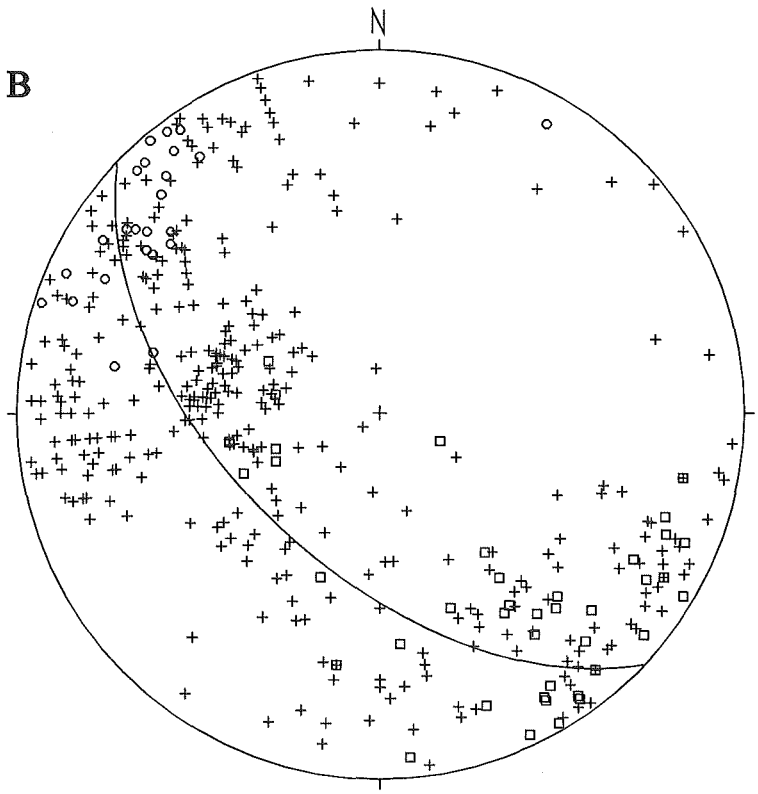

+ pole to bedding with no younging direction, n=358
□ pole to upright bedding, n=41
O pole to overturned bedding, n=24

Figure 3.37: Poles to bedding in the North (A) and South (B) domains, undifferentiated Haupiri Group.

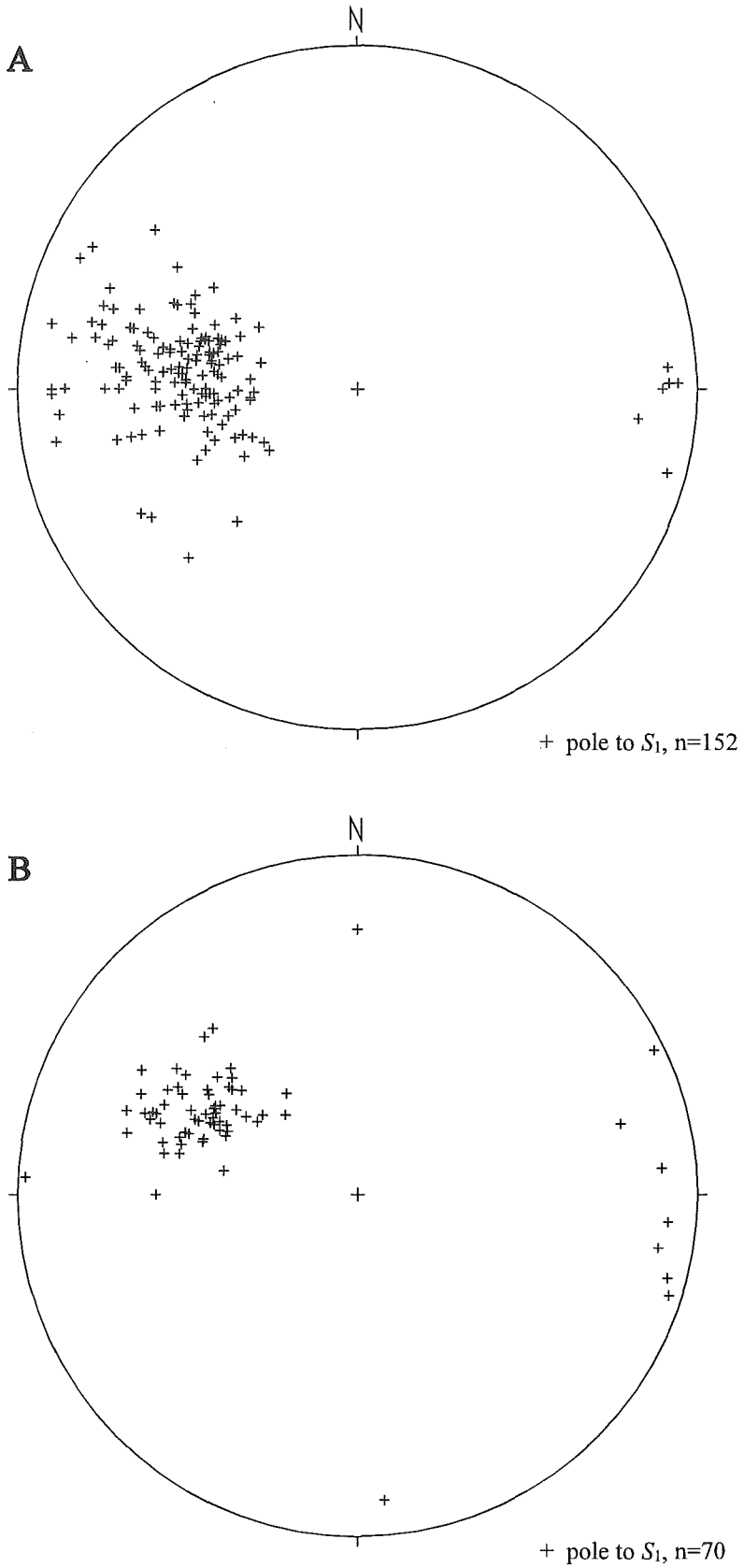

Figure 3.38: Poles to S_1 in the North (A) and South (B) domains, undifferentiated Haupiri Group.

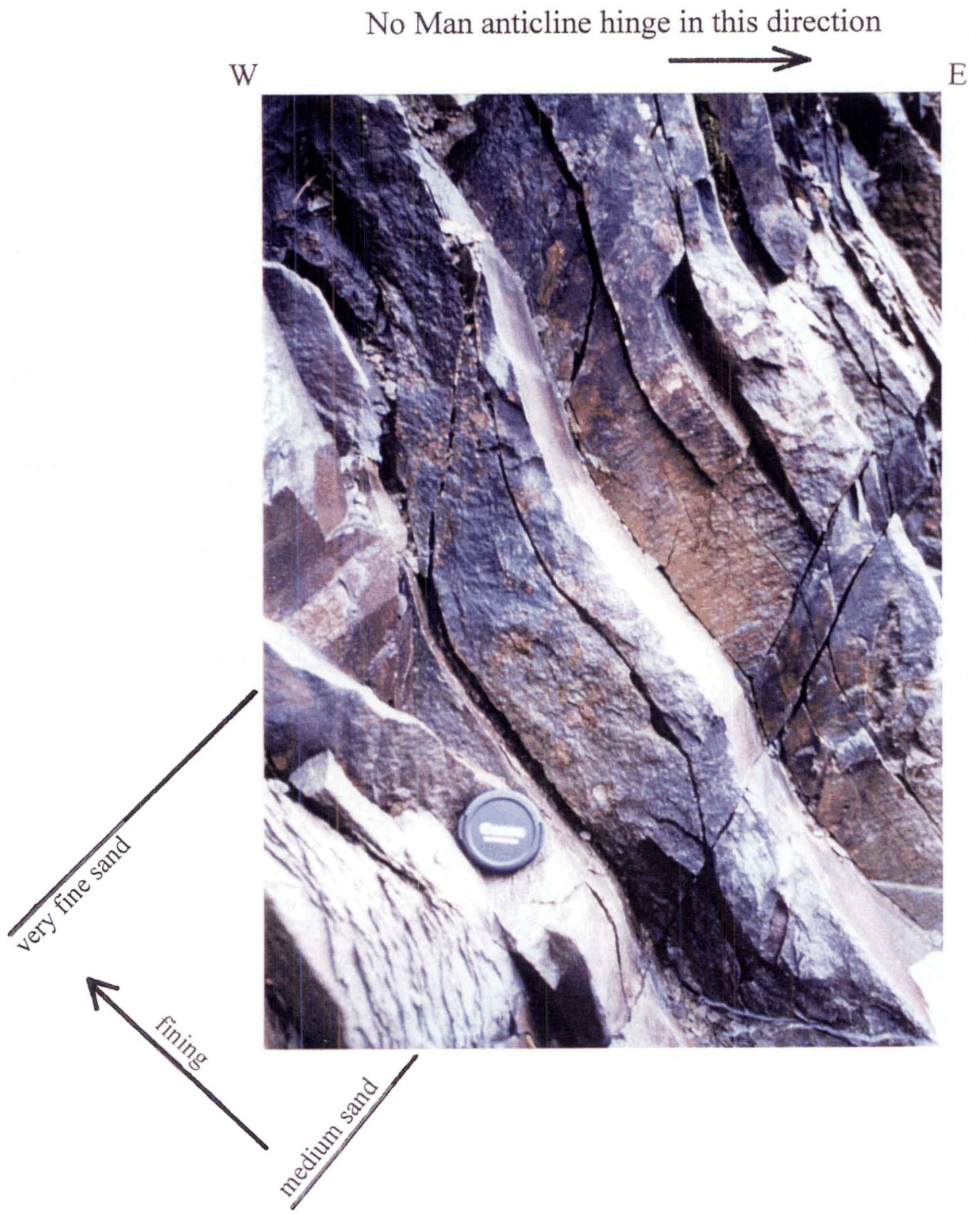

Figure 3.39: Refraction of S_1 cleavage in graded beds on the western limb of the No Man anticline, undifferentiated Haupiri Group. M26/ 761351. Lens cap for scale.

3.7.4 D_1 microscale structures

In silty lithologies, S_1 slaty cleavage is a continuous cleavage on the microscale (Fig. 3.62A) as well as in handspecimen albeit sometimes only poorly developed. Cleavage is defined by aligned sericite, actinolitic hornblende, and chlorite. Other associated metamorphic minerals in D_1 deformed rock include quartz, albitised feldspar, ankerite, calcite, epidote, clinozoisite, and rare biotite. These minerals indicate that D_1 was associated with a low grade metamorphism. In one specimen (RJ483), biotite and quartz occur as strain fringes around pyrite, parallel to S_1. In sandy lithologies, S_1 is represented by rough solution seams.

3.7.5 D_2 mesoscale structures

Within 200m of the Anatoki Fault is a zone of deformation in which the Haupiri rocks are highly strained and possess a well-developed foliation (S_2). The general attitude of the foliation is subparallel to the trace of the Anatoki Fault. In the North domain the foliation strikes N, dipping moderately E, whereas in the South domain the strike is NNE, dipping moderately ESE (Fig. 3.40).

In the field, S_2 is defined by the foliation in phyllites, phyllitic siltstones, slaty sandstone, and highly stretched conglomerates. Bedding is subparallel to S_2. Occasionally, where competency contrasts are large, sandy beds are boudinaged within finer grained beds. However, what is more commonly observed is the boudinaging of quartz veins parallel to S_2 (Fig. 3.41). The long axes of boudins trend mainly between E and SE. Quartz veins are of varying thicknesses, up to 20cm, and often accompanied by pyrite mineralisation. Most veins observed are subparallel to S_2 and boudinaged, but some are oblique to S_2 and tightly folded. Around the margin of quartz vein boudins are concentrations of mica, testimony to significant strain partitioning and solution transfer.

Occasionally, in zones of less than 2m, rock colour significantly darkens from its usual tones of grey and green. This darkened rock is very platy and associated with extensive quartz veining. From thin-section work, the darkening is a result of extreme pressure solutioning that causes strong buildups of opaque material.

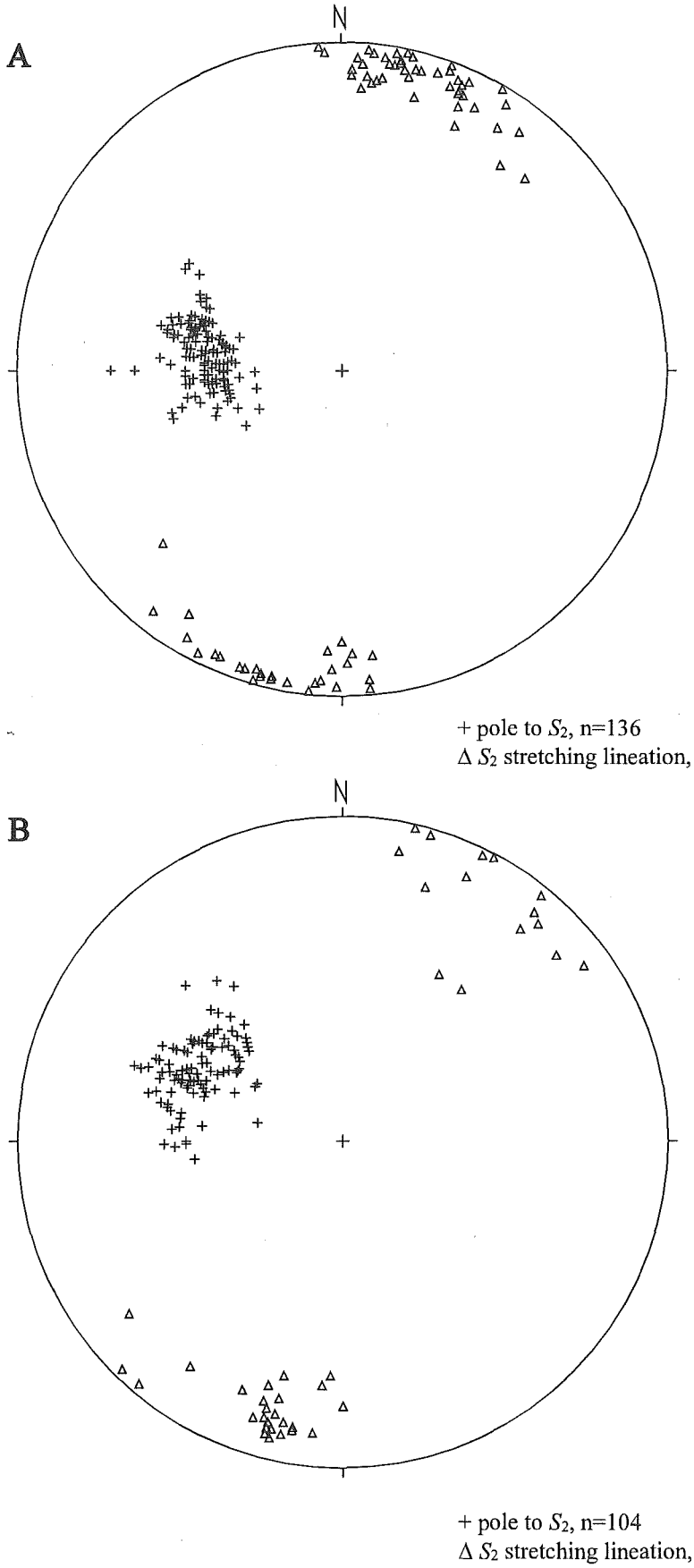

Figure 3.40: S_2 and S_2 stretching lineations in the North (A) and South (B) domains, undifferentiated Haupiri Group .

Figure 3.41: Boudinaged quartz veins parallel to S_2, undifferentiated Haupiri Group. (A) M26/ 749347, sledgehammer for scale. (B) M26/ 745339, lens cap for scale.

Figure 3.42: Elongate ankerites (orange brown spots) on S_2 foliation surface. The ankerites are elongate parallel to the pencil. Undifferentiated Haupiri Group. M26/ 748351, pencil for scale.

Figure 3.42

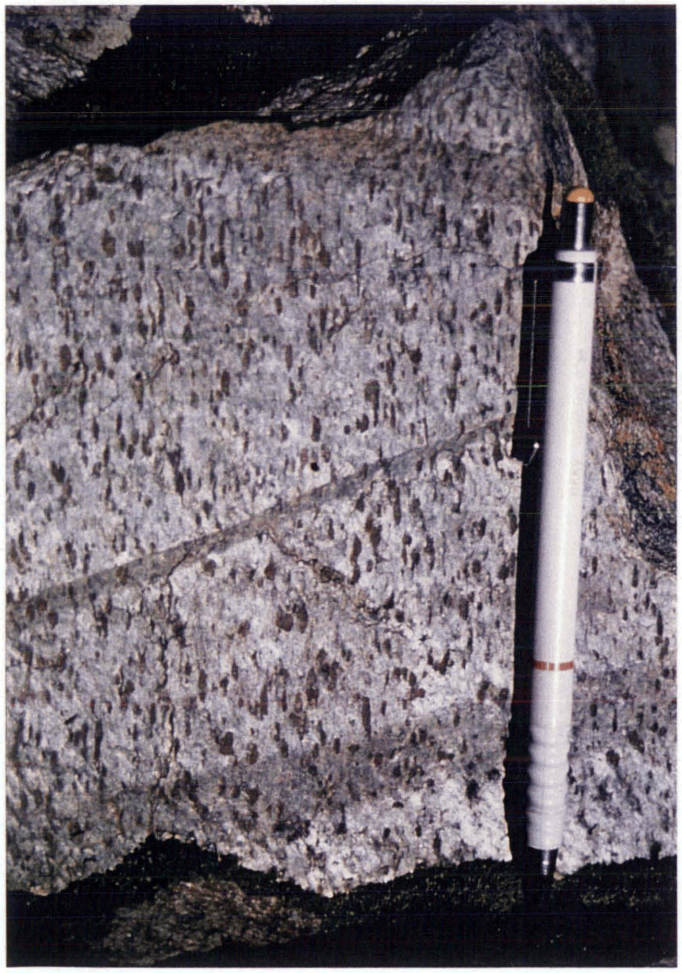

Figure 3.41B

Figure 3.41A

Unlike rocks outside the zone of D_2 deformation, rocks within this zone are heavily charged with ankerite porphyroblasts. On weathered surfaces, ankerites appear as orange spots; the texturally finer the beds, the larger the spots. The ankerite porphyroblasts are frequently elongate (Fig. 3.42), and together with elongate clasts, streaky micas, and elongate strain shadows adjacent to pyrite crystals, define a stretching lineation on S_2 planes. In the North domain, the stretching lineation is subhorizontal, trending generally N-NNE or S-SSW (Fig. 3.40A). In the South domain, the orientation is similar, but with a slightly higher northeasterly-southwesterly component (Fig. 3.40B).

A very important conglomerate horizon (1-2m thick), located in eastern lakeshore creeks north of Portia Creek, possesses a mylonitic texture. Several samples were extracted from Staircase Creek (informal name) for polishing and determination of shear-senses (Fig. 3.43). Clasts are stretched and boudinaged parallel to the predominant stretching lineation determined elsewhere. Winged porphyroclasts with σ-type and δ-type geometries (Hanmer and Passchier 1991), asymmetric strain shadows, and extensional shear bands (Hanmer and Passchier 1991) all show internally consistent senses of shear (Fig. 3.44). Domino structure (Simpson and Schmid 1993) displays either synthetic or antithetic shear with respect to the shear-sense indicated by other structures (Fig. 3.44). Domino structure is therefore not a reliable shear-sense indicator, a conclusion also reached by Hanmer and Passchier (1991). Given the predominant stretching lineation trend, the shear-sense indicators found in the mylonitic conglomerate indicate a dextral strike-slip shear with top to the S-SSW on an east dipping foliation.

Other shear-sense indicators found in the field are rare. Only one asymmetrically boudinaged quartz vein was found, the asymmetry of which is compatible with dextral strike-slip shear with top to the S-SSW on an east dipping foliation. Within a marble horizon immediately adjacent to the Anatoki Fault are quartz veins which outline southerly verging intrafolial folds, again compatible with dextral strike-slip shear with top to the S on an east dipping foliation.

As mentioned previously, within 200m of the Anatoki Fault, Haupiri rocks possess a pervasive S_2 foliation parallel to bedding. Outside this zone of 200m, S_2 rapidly decreases in intensity and is no longer parallel to bedding. The foliation surface then becomes difficult to differentiate between S_1 and S_2 because of the interference of the S_3

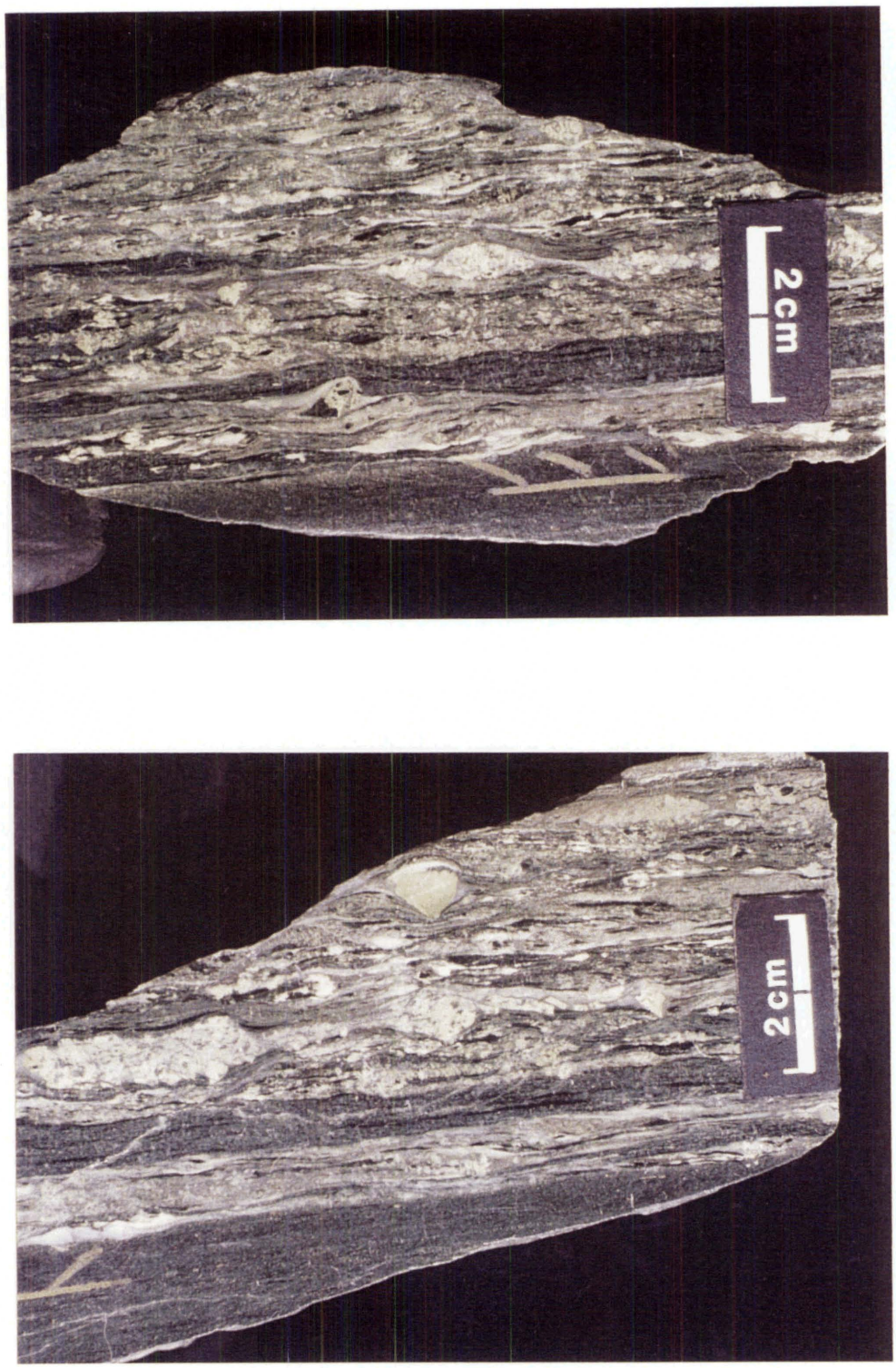

Figure 3.43: Polished rock slabs of undifferentiated Haupiri Group conglomerate from Staircase Creek (M26/ 749347). The conglomerate possesses a mylonitic structure related to D_2 deformation. Rock slabs are cut parallel to the S_2 stretching lineation. RJ2.

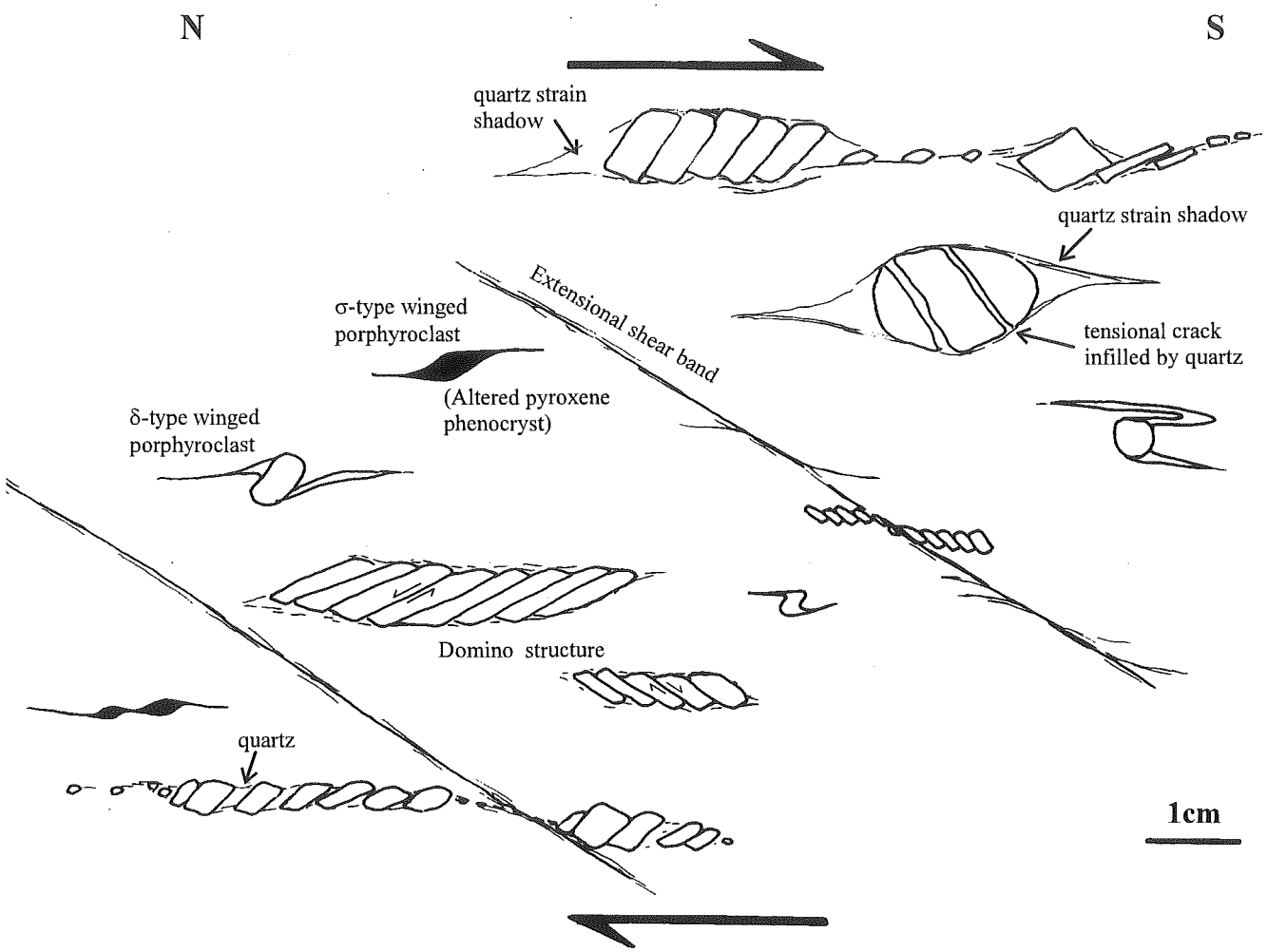

Figure 3.44: Sketch of volcanic clast shear-sense indicators derived from polished rock slabs of undifferentiated Haupiri Group conglomerate from Staircase Creek, Boulder Lake domain.

crenulation cleavage overprint. However, between 200-500m from the Anatoki Fault, the effects of D_2 are still observable, as evidenced by strained conglomerates with stretching lineations parallel to those within the zone of penetrative S_2 (see Section 3.8).

3.7.6 D_2 microscale structures

S_2 is a penetrative foliation defined principally by phyllosilicates, especially white mica and chlorite. In the texturally finest of rocks, the mineralogy is almost completely recrystallised to a low grade metamorphic assemblage consisting of:

- quartz + albite + muscovite + chlorite ± ankerite ± calcite ± rare biotite (in non-volcanic derived sediments).
- albite + quartz + chlorite + muscovite + epidote/clinozoisite + actinolitic hornblende + ilmenite + calcite + ankerite ± biotite ± tremolitic hornblende (in basic/intermediate volcanic derived sediments).
- accessory tourmaline and pyrite is found in both types of sediments.

It is difficult to constrain the precise facies of metamorphism. The presence of biotite does not indicate mid-greenschist facies because in basic volcanic derived sediments, biotite appears at lower temperatures than in pelites (Miyashiro 1973). Rare biotite is also observed in non-volcanic derived sediments but these sediments are not true pelites (i.e. they are not rich in Al nor poor in Ca). The abundance of calcite and ankerite suggests the introduction of a CO_2-rich fluid phase. CO_2-rich fluids can suppress the development of hydrous Ca-Al silicates such as prehnite and pumpellyite (Zen 1961). Thus it is concluded that the facies of metamorphism associated with D_2 is best termed low grade. A similar conclusion can be reached for D_1 metamorphism.

Ankerite comes in two forms; firstly as inclusion-rich porphyroblasts slightly elongate to the stretching lineation and secondly as inclusion-free porphyroblasts that are highly elongate parallel to the stretching lineation. The highly elongate inclusion-free ankerites, up to 4mm long, occur either as fibres in the shadow of inclusion-rich ankerites (Fig. 3.45, 3.46, 3.76), or alternatively, on their own (Fig. 3.78). Often, those attached to inclusion-rich ankerites grow in crystallographic continuity with them (Fig. 3.76).

Figure 3.45: Inclusion-rich ankerite porphyroblast with inclusion-free ankerite asymmetric strain fringes. Asymmetry of strain fringes indicates top to the left sense of shear. S_2 XZ section, RJ126, undifferentiated Haupiri Group. (A) CPL. (B) PPL.

Figure 3.46: Inclusion-rich ankerite porphyroblast with inclusion-free ankerite asymmetric strain fringes. Inclusion trails in the porphyroblast are oblique to the external foliation (S_2) and the inclusions are finer grained than S_2. Note how S_2 micas and solution seams wrap around the more rigid ankerite. S_3 crenulation cleavage can also be seen. RJ280, undifferentiated Haupiri Group.

0.5mm

Figure 3.46

0.5mm

Figure 3.45B

0.5mm

Figure 3.45A

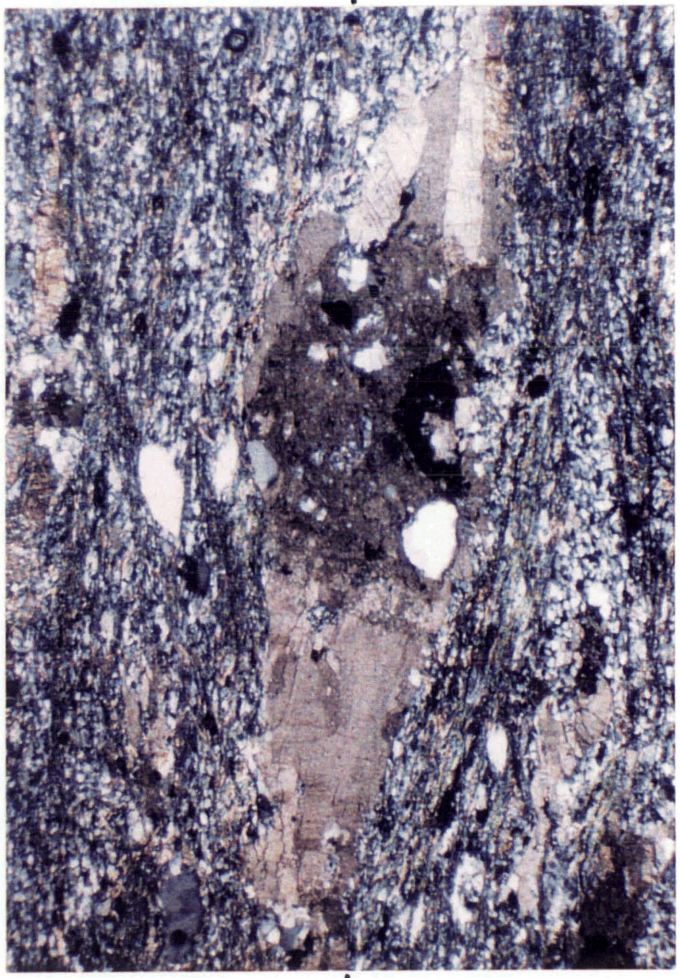

Although the inclusion-free ankerites are clearly related to D_2 associated metamorphism, the origin of the inclusion-rich ankerites is not so clear. Occasionally, the inclusion-rich ankerites display inclusion trails which are always oblique to, and finer grained than, the external foliation (Fig. 3.46). Given that the inclusion-rich ankerites appear to have grown prior to their attached inclusion-free ankerite strain fibres, the occurrence of oblique inclusion trails suggests these ankerites grew either in the early stages of D_2 related metamorphism, or represent ankerite metasomatism prior to D_2. The latter option is favoured because very similar ankerite porphyroblasts are found in more southern domains that are syn-D_1 in age. (see Section 5.5.2). The slightly elongate nature of inclusion-rich ankerites parallel to S_2 is explained by the presence of solution seams on porphyroblasts margins, evidence of solution transfer induced shape modification. The highly elongate nature of inclusion-free ankerites is a result of growth parallel to the extension direction (see Section 3.10.3).

As well as inclusion-rich ankerites, relict detrital quartz, feldspar, and rock fragment grains of coarse silt size or larger, provide visible sites for strain fringe developments (Fig. 3.47). The strain fringes usually consist of a mixture of ankerite, calcite, and quartz, and less commonly muscovite, chlorite, biotite, feldspar, and ilmenite. The strain fringes in samples are commonly symmetrically disposed about the rigid grain but many samples also possess asymmetric strain fringes indicative of non-coaxial strain. Ankerite fibre growth on relict detrital grains and inclusion-rich ankerite porphyroblasts show spectacular asymmetry (Fig. 3.45, 3.47). The fibres furthest from the centre of the fringe are the most elongate corresponding to the zone of greatest extension in the domain surrounding the rigid grain. All but one of the 18 thin-sections which displayed convincing asymmetric strain fringes parallel to the stretching lineation, indicate a dextral strike-slip shear with top to the S-SSW on an east dipping foliation.

Strain fringes adjacent to rigid pyrite crystals consist predominantly of calcite and quartz fibres (Fig. 3.48, 3.49). The fibres are both displacement- and face-controlled depending on the relative smoothness of pyrite faces. The strain fringes show increasing amounts of recrystallisation further from the pyrite faces indicative of antitaxial growth (Durney and Ramsay 1973). Longitudinal strains (e) of between 3 and 8 are indicated by the strain fringe dimensions. In many cases, strain fringes are totally recrystallised but elongate fibre outlines are most recognisable adjacent to the pyrite face. Given the complex

Figure 3.47: Detrital grains with asymmetric strain fringes. In all four photomicrographs, asymmetry indicates top to the left shear-sense. (A and B): Detrital feldspars with strain fringes of ankerite (A) and ankerite and quartz (B), S_2 XZ section, RJ103, CPL. (C): Detrital rock fragment with ankerite strain fringes, S_2 XZ section, RJ126, CPL. (D): Detrital subhedral feldspar with a chloritic strain fringe, S_2 XZ section, RJ104, PPL. All samples are undifferentiated Haupiri Group.

A
1mm
S_2
B
0.5mm
C
0.5mm
S_2
D
0.5mm

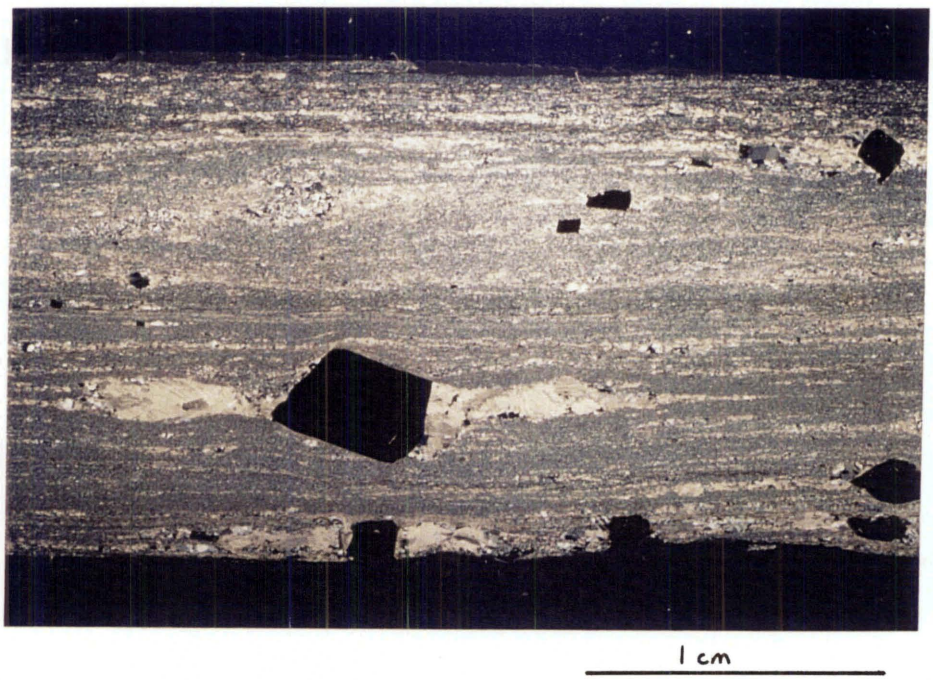

Figure 3.48: Pyrite with strain fringes of calcite and quartz parallel to S_2. S_2 XZ section, RJ1, undifferentiated Haupiri Group. CPL.

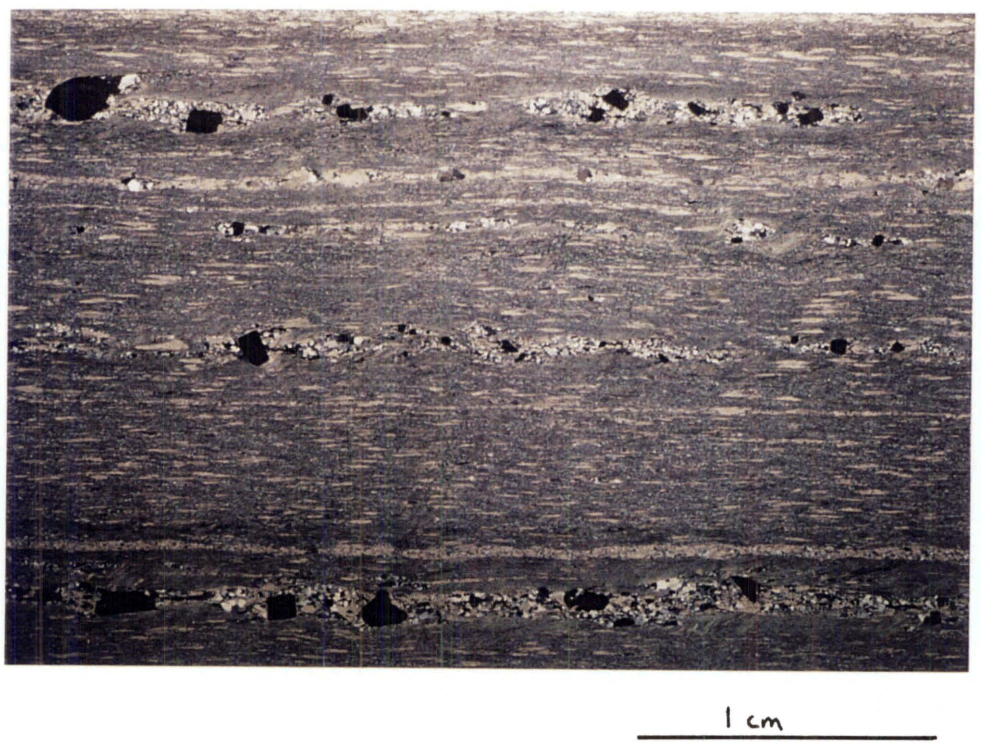

Figure 3.49: Pyrite occurring in discrete layers. Where this occurs, the adjacent strain shadows of calcite and quartz coalesce to form a secondary layering. Note the abundance of elongate inclusion-free ankerite porphyroblasts. S_2 XZ section, RJ108, undifferentiated Haupiri Group. CPL.

shapes of the pyrite crystals, most strain fringes appear symmetrically disposed. Hints of asymmetry occur but are often ambiguous. None of the strain fringes could confidently be related to the asymmetric strain fringe patterns of Etchecopar and Malavielle (1987) that are used for determining shear-sense.

The development of Q and M domains parallel to S_2 is common and often represents an enhancement of original compositional contrasts parallel to bedding. Secondary layering can also develop from the coalescence of strain shadows adjacent to multiple pyrite crystals that grew in discrete layers. (Fig. 3.49).

Quartz/calcite veins on the microscale show differing amounts of D_2 deformation depending on their relative age of formation. The oldest quartz veins are represented by trains of isolated boudins (Fig. 3.50), whereas younger oblique cutting veins are in various stages of boudinage and rotation towards the S_2 foliation (Fig. 3.51, 3.52). Boudins, linked by strain fringes, are occasionally stair-stepped indicating a sense of shear consistent with other shear-sense indicators (Fig. 3.53). A spectacular example of a cross-cutting vein which has been isoclinally folded and sheared is shown in Figure 3.54. Such examples also give a sense of shear consistent with other shear-sense indicators.

Thin-sections of mylonitic conglomerate confirm observations of shear-sense on polished rock slabs including asymmetric strain shadow/fringes, extensional cracks in clasts, and σ-type porphyroclasts. Many σ-type porphyroclasts consist of chlorite and actinolitic hornblende, that were originally clinopyroxene phenocrysts, and resemble mica-fish (Fig. 3.55).

Rocks from the zone of D_2 deformation are either L- or LS-tectonites but never S-tectonites. The tectonites suggest predominantly a plane or constrictional state of strain. Nevertheless, there are some LS-tectonites which show significant growth of ankerites and boudinage in sections perpendicular to the stretching lineations. These features suggest at least some LS-tectonites experienced a strain state that was in the field of flattening. Some thin-sections perpendicular to the stretching lineation show a kink-like crenulation indicative of a late stage compression along the Y strain axis.

Figure 3.50: Trains of isolated quartz/calcite boudins parallel to S_2. The boudins represent early generation veins. S_2 XZ section, RJ84, undifferentiated Haupiri Group. CPL.

Figure 3.51: Late stage oblique cutting quartz/calcite vein is boudinaged and rotated towards S_2. Note the presence of isolated quartz/calcite boudins which represent early generation veins. S_2 XZ section, RJ84, undifferentiated Haupiri Group. CPL.

Figure 3.52: Quartz/calcite vein boudinaged and rotated towards S_2. S_2 XZ section, RJ29, undifferentiated Haupiri Group. PPL.

Figure 3.53: Isolated quartz vein boudins are linked by a calcite stair-step indicating top to the right shear-sense. S_2 XZ section, RJ10, undifferentiated Haupiri Group. CPL.

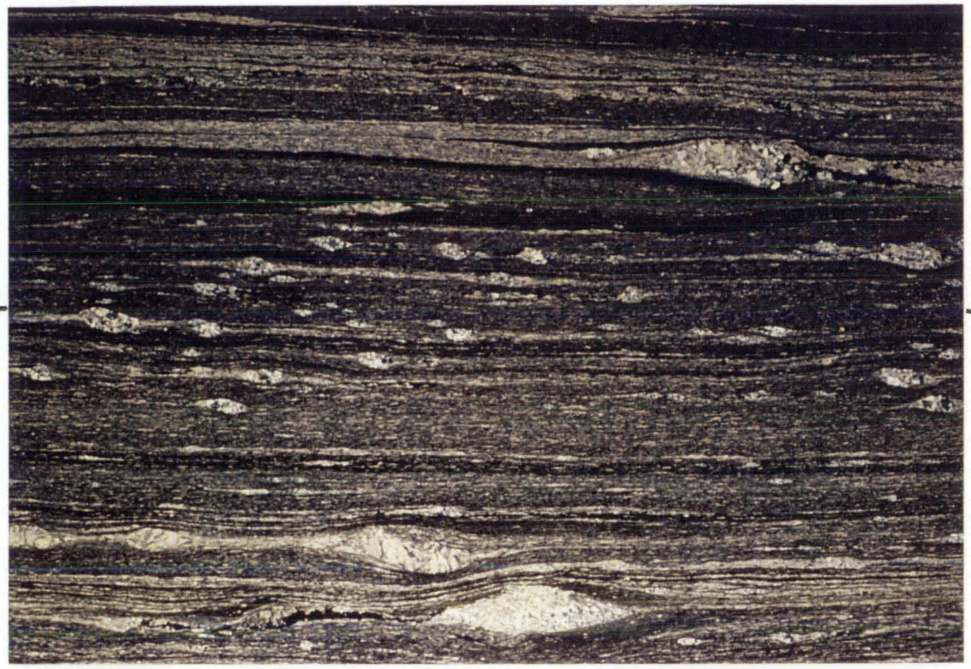

Figure 3.50

1cm

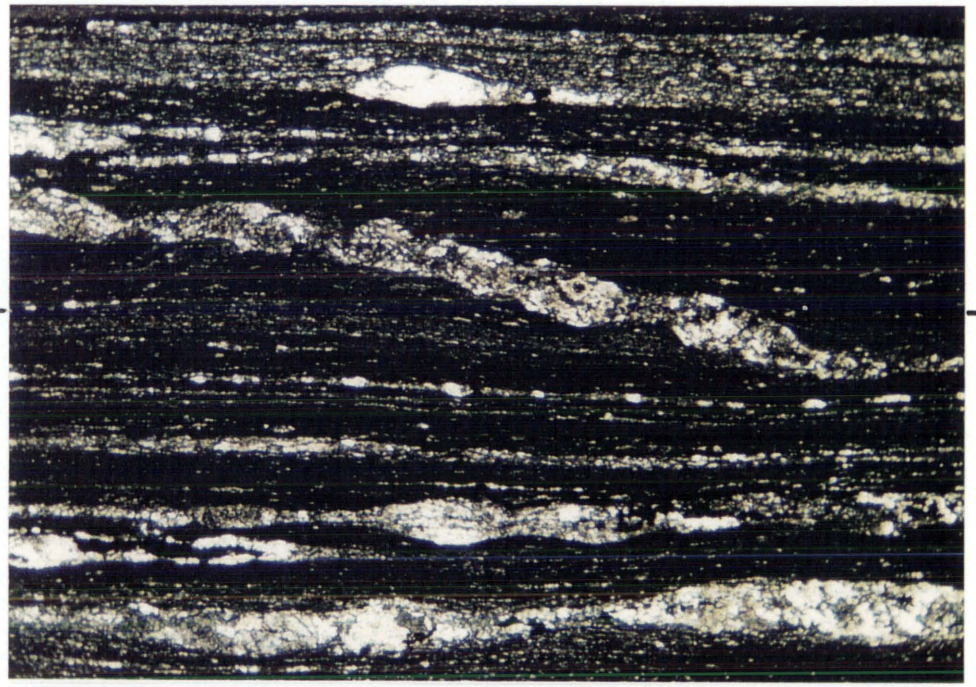

Figure 3.51

1mm

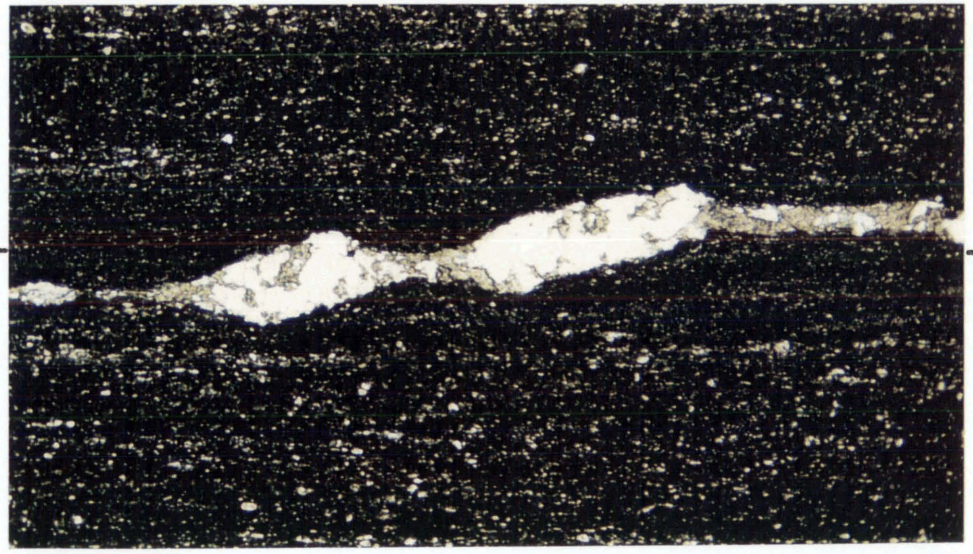

Figure 3.52

1mm

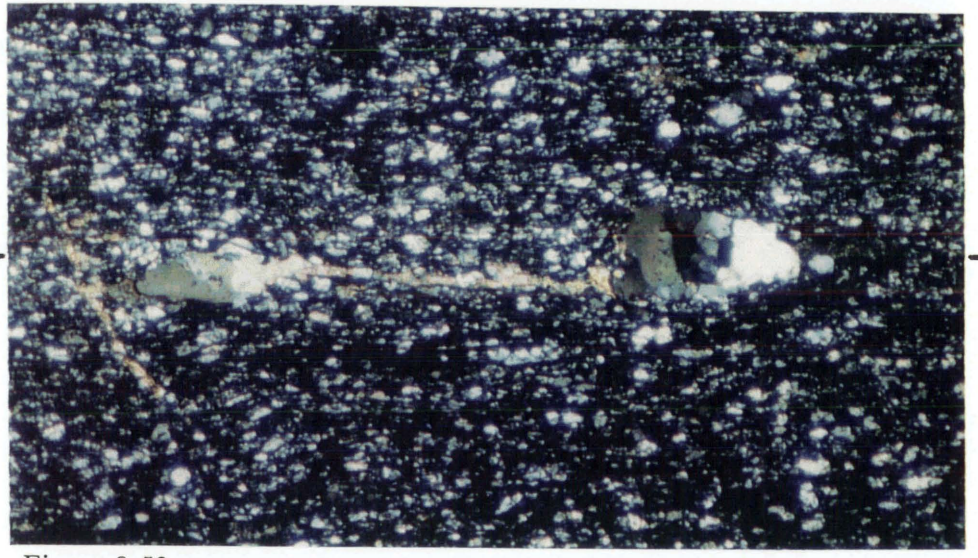

Figure 3.53

0.5mm

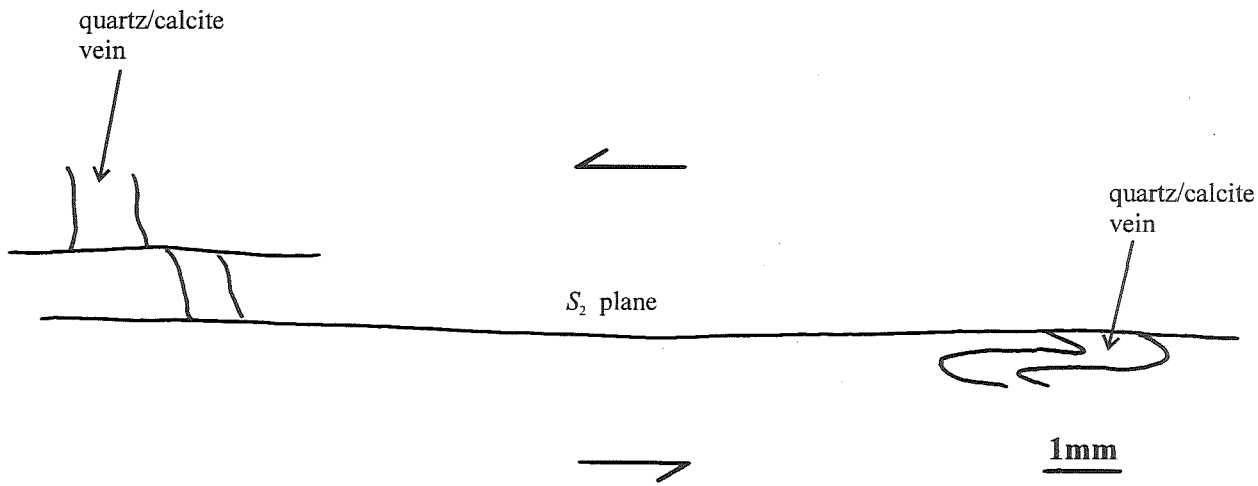

Figure 3.54: Line drawing of a cross-cutting quartz/calcite vein in thin-section view which has been isoclinally folded and sheared along S_2 planes. S_2 XZ section, RJ84, undifferentiated Haupiri Group.

Figure 3.55: σ-type porphyroclast from the mylonitic conglomerate, Staircase Creek. The porphyroclast consists of actinolitic hornblende (blue grains) and chlorite, and resembles a mica-fish geometry. Top to the left shear-sense is indicated. S_2 XZ section, RJ78, undifferentiated Haupiri Group. (A) CPL, (B) PPL.

Figure 3.56: Unusually large muscovite aggregates (centre and top left) parallel to S_2 are possibly of slickenfibre origin. S_2 XZ section, RJ314, undifferentiated Haupiri Group. CPL.

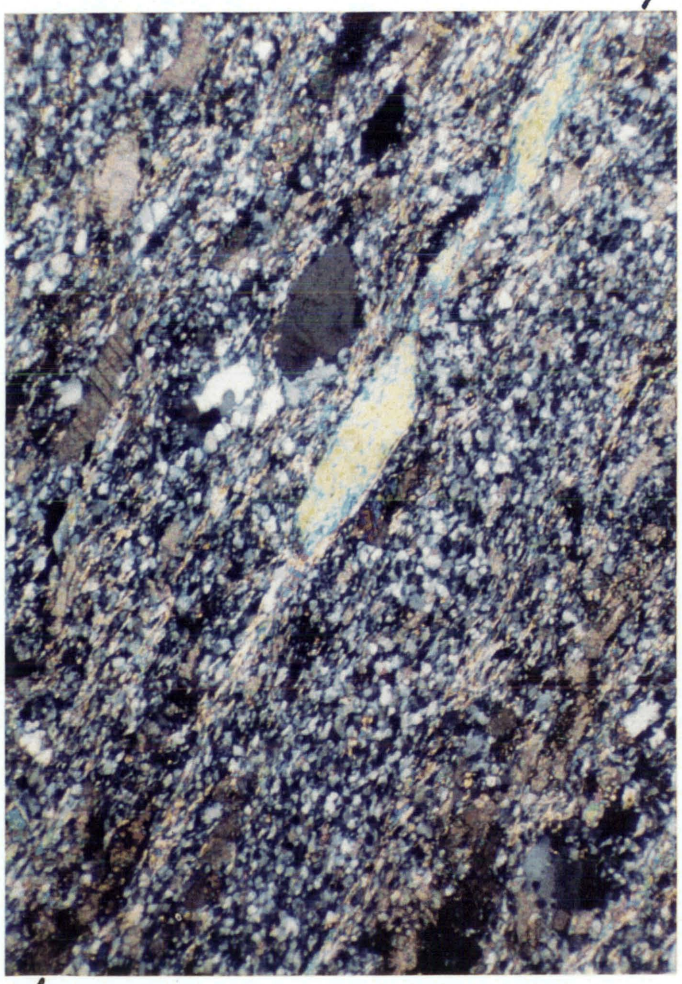

Figure 3.56

Figure 3.55B

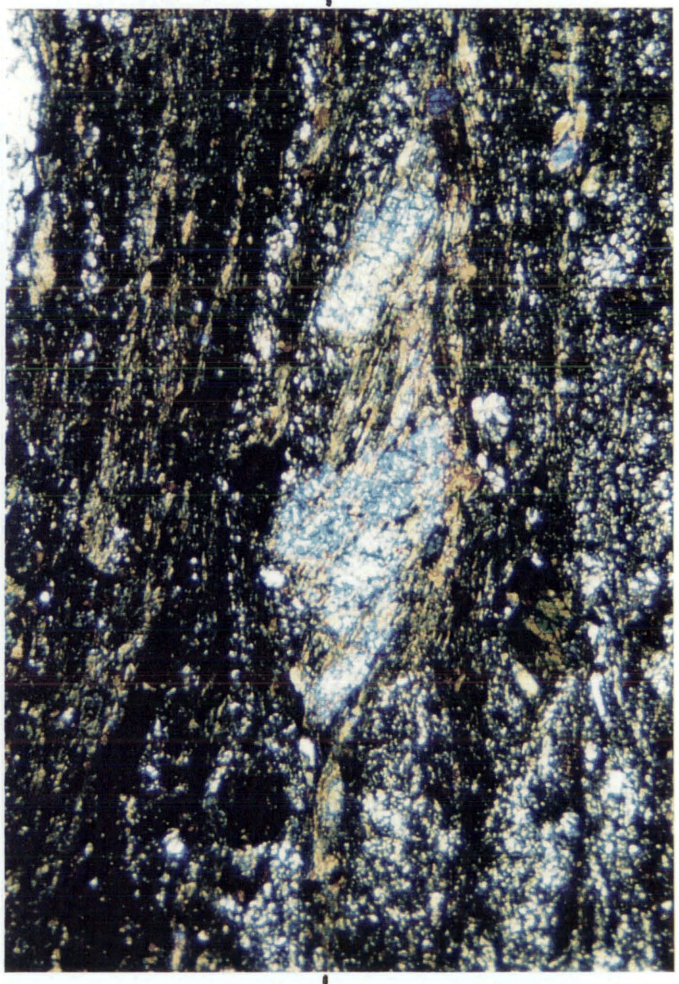

Figure 3.55A

The presence of Q and M domains, strain shadows, and the ubiquitous presence of solution seaming in specimens, implies solution transfer was a major component of D_2 strain accommodation. Plastic creep has played a minor strain accommodation role evidenced by the development of undulatory extinction and deformation bands in both detrital and vein quartz grains, and twinning in ankerite (Section 3.10). Unusually large muscovite aggregates parallel to S_2 are possibly of slickenfibre origin (Fig. 3.56). The muscovites may have formed in the steps of shear planes.

3.7.7 D_2 geochronology

Two samples (RJ81 and RJ280) were selected from undifferentiated Haupiri Group rocks affected by D_2 deformation for muscovite-whole rock Rb-Sr dating. RJ81 and RJ280 were chosen because they show the maximum development of S_2 related minerals including a high percentage of muscovite. Both samples are phyllites consisting of muscovite, chlorite, quartz, feldspar, ankerite, and opaque metamorphic minerals. The phyllosilicates and elongate inclusion-free ankerites define S_2 and it appears petrographically that both samples are fully recrystallised. However, RJ280 also contains inclusion-rich ankerite porphyroblasts with inclusion trails oblique to S_2 (Fig. 3.46) and make up 5-10% of the rock. As mentioned in Section 3.7.6, these inclusion-rich ankerite porphyroblasts are thought to have formed in the early stages of D_2 related metamorphism, or alternatively, represent ankerite metasomatism prior to D_2, in which case, they are probably syn-D_1 in age (thought to be Paleozoic, see Chapter 9). Both samples have been affected by D_3 deformation with variably developed discrete S_3 solution seams, and in RJ81 there are indications that new muscovite growth has occurred parallel to S_3.

The analytical methods and results of the muscovite-whole rock Rb-Sr dating are given in Appendix 2. RJ81 gives an age of 108 ± 12Ma whereas RJ280 gives an age of 173 ± 15Ma. The difference in age between the two samples needs to be explained given that both appear to have been penetratively deformed by D_2. If radiogenic isotope homogenisation of minerals in a rock sample is incomplete, the time of metamorphism cannot be accurately determined (Faure, 1986). On petrographic grounds, inclusion-rich ankerite porphyroblasts in RJ280 are suspected to be of pre-D_2 age (see above). If the porphyroblasts are of pre-D_2 age, then complete homogenisation in RJ280 during D_2

metamorphism may not have been achieved, and muscovite $^{87}Sr/^{86}Sr$ ratios would not be reset to whole rock values. This incomplete resetting of muscovite $^{87}Sr/^{86}Sr$ ratios would result in a geological meaningless age that is older than D_2 metamorphism. The Rb-Sr age of RJ280 is indeed older than RJ81 and thus supports the suggestion that the inclusion-rich ankerite porphyroblasts are of pre-D_2 age. If the ankerite porphyroblasts are of pre-D_2, then so too are the inclusions. The inclusions cannot be positively identified but there are indications that some are very fine grained micas. If this is the case then $^{87}Sr/^{86}Sr$ values for the muscovite separate will become higher and thereby increase the calculated age for RJ280. It follows from the above argument that the Rb-Sr age from RJ81 is the more meaningful age with respect to D_2 related metamorphism. On the other hand, RJ81 has a minor component of new muscovite growth related to D_3 and if D_3 is significantly younger than D_2, the Rb-Sr age of RJ81 may be too young.

It will be shown in Section 3.9 that, based on structural grounds, D_2 in both the Buller terrane and Takaka terrane are one and the same, and so too is D_3. D_2 in the Buller terrane is almost certainly Early Cretaceous in age (Section 3.9.1), and D_3 is mid-Cretaceous in age (Section 9.5.3). It would thus appear that the Rb-Sr age of RJ81 (108 ± 12Ma) is the most representative of D_2 and any new muscovite growth related to D_3 had only a minor effect on the D_2 Rb-Sr isotopic clock. Clearly, more Rb-Sr dating is required to confirm a D_2 Cretaceous age. It should be noted, however, that despite the petrographically visible uncertainties associated with RJ81 and RJ280, they were the best recrystallised and least multiply deformed samples that I could find for dating Haupiri Group D_2 tectonites.

3.7.8 D_3 macroscale and mesoscale structures

A widespread crenulation cleavage (S_3) affects both S_2 and S_1 (Fig. 3.57). The intensity of S_3 varies considerably over short distances so that in one locality it is strongly developed but 20m away, S_3 can only be observed in thin-section. The orientation of S_3 is essentially the same in both the North and South domains, striking generally between NNE and ENE, and dipping gently to moderately towards the SE (Fig. 3.58). Although the orientations of S_3 overlap with both S_1 and S_2 orientations, when S_3 is seen together with S_1 or S_2, it has always a more easterly strike.

Figure 3.57: S_3 crenulation cleavage. (A and B): S_3 crenulates an S_1 surface subparallel to bedding. (C): S_3 crenulates an S_2 surface subparallel to bedding . Note how S_3 refracts adjacent to the quartz vein in the bottom right hand corner of the photograph. (D): S_3 crenulates a volcanic-derived conglomerate clast that has been deformed by S_2. S_3 is marked by white coloured cleavage domains. (A) M26/ 749362, (B) M26/ 734321, (C) M26/ 746339, lens cap for scale. (D) Polished rock slab of sample RJ92.


A
Canon
ULTRASONIC

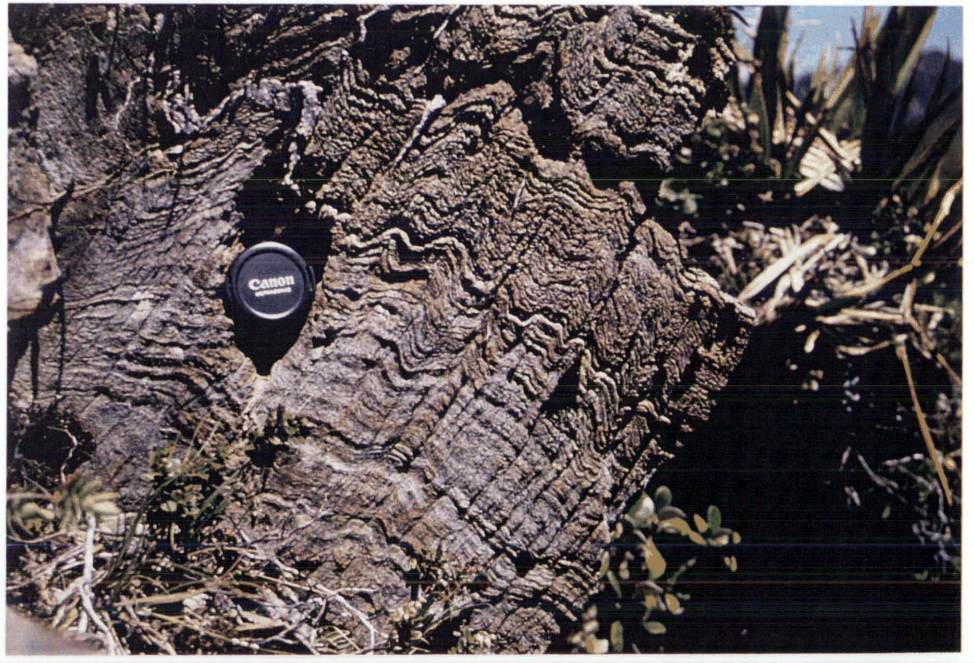
B
Canon

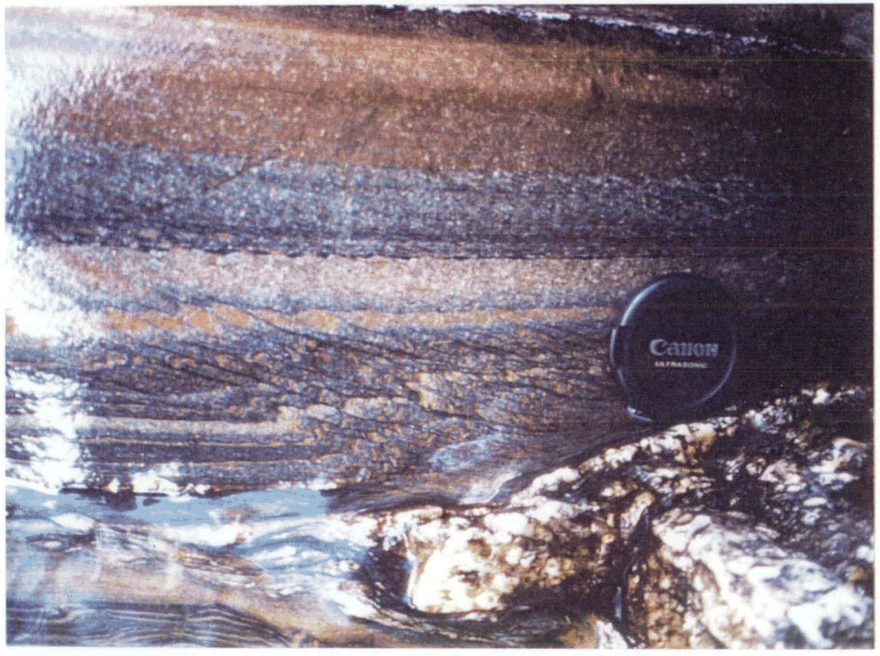
C
Canon

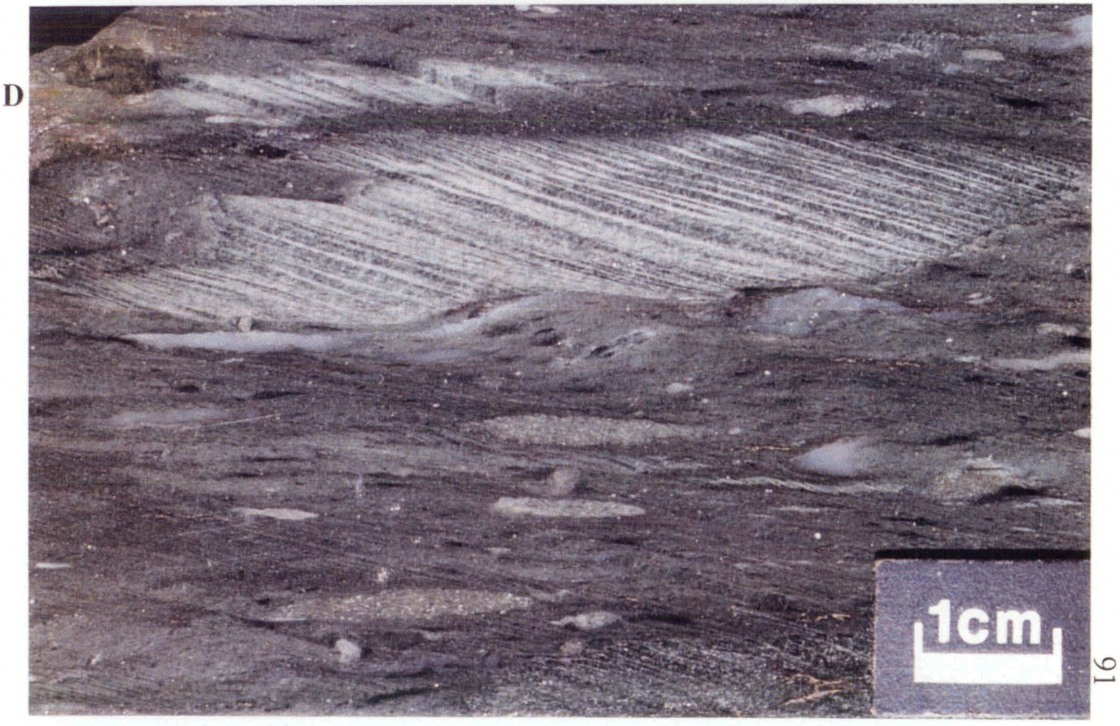
D
1cm

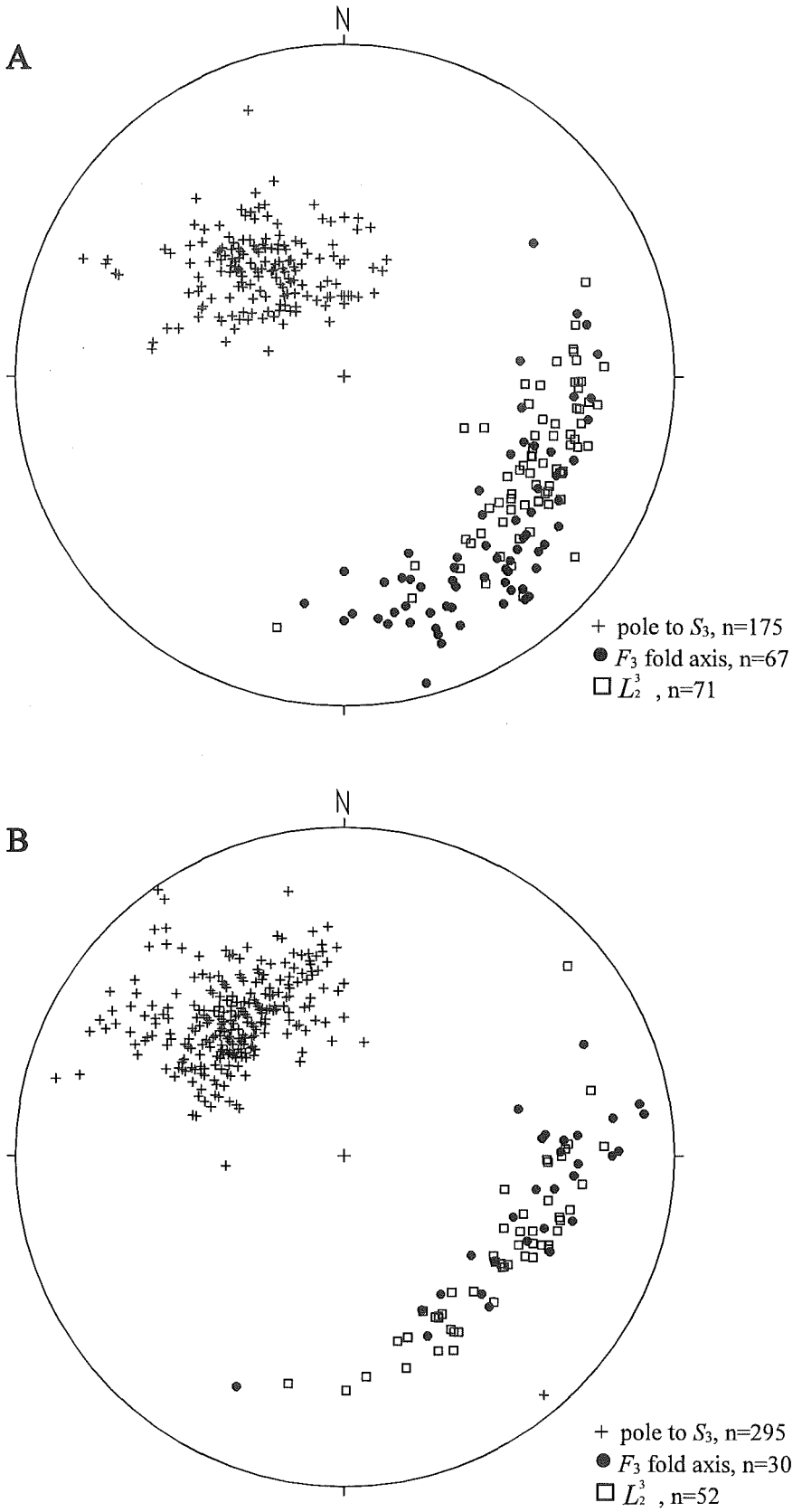

Figure 3.58: S_3, F_3, and L_2^3 orientations in the undifferentiated Haupiri Group rocks of the North (A) and South (B) domains. Note that F_3 and L_2^3 measurements are from the western limb of the Brown Cow syncline only whereas S_3 measurements are from all of the domain area.

S_3 is axial planar to mesoscale folds (F_3) which plunge gently or moderately towards the SE and ESE quadrants in the North and South domains respectively (Fig. 3.58). While S_3 is seen throughout the domain, F_3 folds are only observed when bedding is dipping towards the E or SE. In Figure 3.58, F_3 orientations are based on bedding as the folded reference surface and come exclusively from the western limb of the Brown Cow syncline. As would be expected, L_2^3 intersection lineations show a similar distribution to that of F_3 (Fig. 3.58). F_3 folds both D_2 and D_1 related structures (Fig. 3.59, 3.60) and varies in wavelength from large crenulations to ~50m. Most observed F_3 folds are of the order of 40-100cm wavelength. The folds are close to open with fold shapes ranging from D2 to D3 or E2 to E4 (see Appendix 3 for fold shape classification). Most mesoscale F_3 folds are asymmetric and verge northeastwards. At M26/ 750361, an F_3 fold of ~50m wavelength can be traced with characteristic S, M, and Z shaped parasitic folds.

Some confusion exists in the South domain where it is not always easy to tell if the observed NE striking cleavage is S_1 or S_3. Because S_1 is weakly developed in places, S_3 can appear slaty in outcrop when the rock is fine grained. However, the problem of designation is usually resolved when the cleavage is seen to be axial planar to F_3 folds. This is particularly clear on the eastern limb of the Brown Cow F_1 syncline where the F_3 fold vergence and orientation, taken in conjunction with bedding attitude, is incompatible with the cleavage designated as S_1.

In general, S_3 is well-developed in the finer and more mica-rich lithologies. S_3 typically refracts from coarse to fine layers and is perturbed around quartz veins (Fig. 3.57C, 3.61). Crenulations are widely spaced in sandy/gritty layers, and finely spaced, almost slaty in appearance, in silty layers. Quartz veins, including D_2 boudinaged veins, are crenulated/ folded by D_3 structures. Quite commonly, S_3 crenulations can migrate upwards into an F_3 fold. S_3 always intensifies in the hinge zone of an F_3 fold.

Figure 3.59: F_3 folding S_0 and S_1 (A), and S_0 and S_2 (B, C) in the undifferentiated Haupiri Group, Boulder Lake domain. (A) M26/ 750362, sledgehammer for scale. (B) M26/ 740326, lens cap for scale. (C) M26/ 737324, length of photo is ~6m.

A

B

C

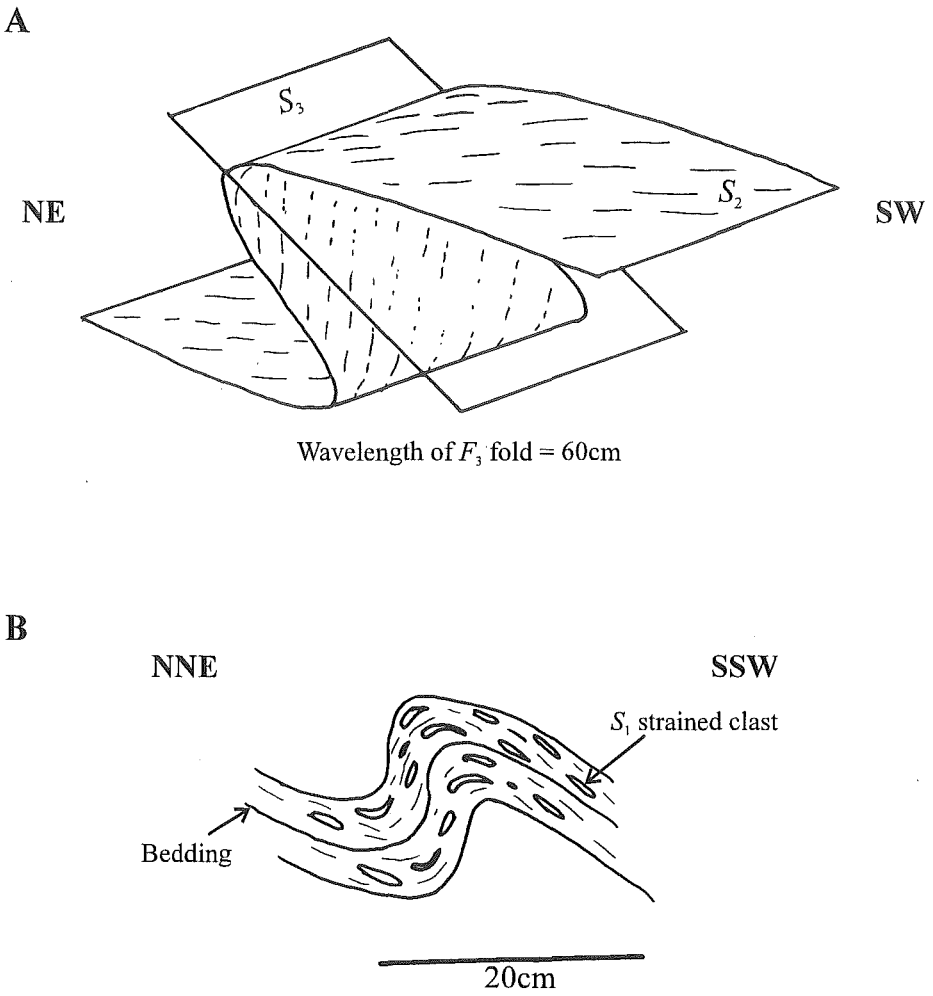

Figure 3.60: Field sketches of F_3 folding an S_2 surface and S_2 stretching lineation (A), and folding S_1 strained conglomerate clasts (B). In (B) S_1 is slightly oblique to bedding. Undifferentiated Haupiri Group, Boulder Lake domain. (A) M26/ 747358, (B) M26/ 735318.

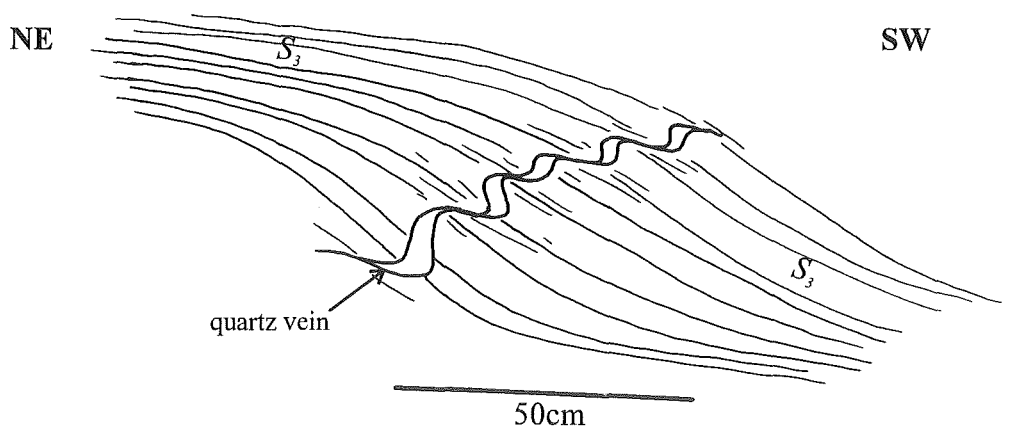

Figure 3.61: Field sketch of S_3 refracting around quartz veins, undifferentiated Haupiri Group, Boulder Lake domain. M26/ 748360.

3.7.9 D_3 microscale structures

In mica-rich lithologies, S_3 is best described as a zonal crenulation cleavage with either sharp or gradational boundaries (Fig. 3.62, 3.63). Q and M domains are sometimes developed (Fig. 3.63). M domains consist of fine grained muscovite + chlorite + opaques ± carbonates ± actinolitic/tremolitic hornblende, aligned parallel to S_3. This mineralogy indicates a low grade syn-D_3 metamorphism. When the pre-existing anisotropy is weakly developed, or the rock is coarser grained, S_3 can be represented by discrete pressure solution seams. Strain fringes are often seen to have grown parallel to S_3 (Fig. 3.64, 3.69).

(Text of Section 3.7.9 continues on page 100)

Figure 3.62: (A), (B), and (C) show S_3 as a spaced zonal crenulation cleavage with sharp or gradational boundaries. In (A), S_3 crenulates S_1 slaty cleavage. In (B), S_3 crenulates S_2 foliation. In (C), S_3 crenulates S_2 foliation immediately adjacent to an ankerite porphyroblast with strain fringes. (A) RJ282, PPL. (B) RJ68, PPL. (C) RJ65, CPL. Undifferentiated Haupiri Group.

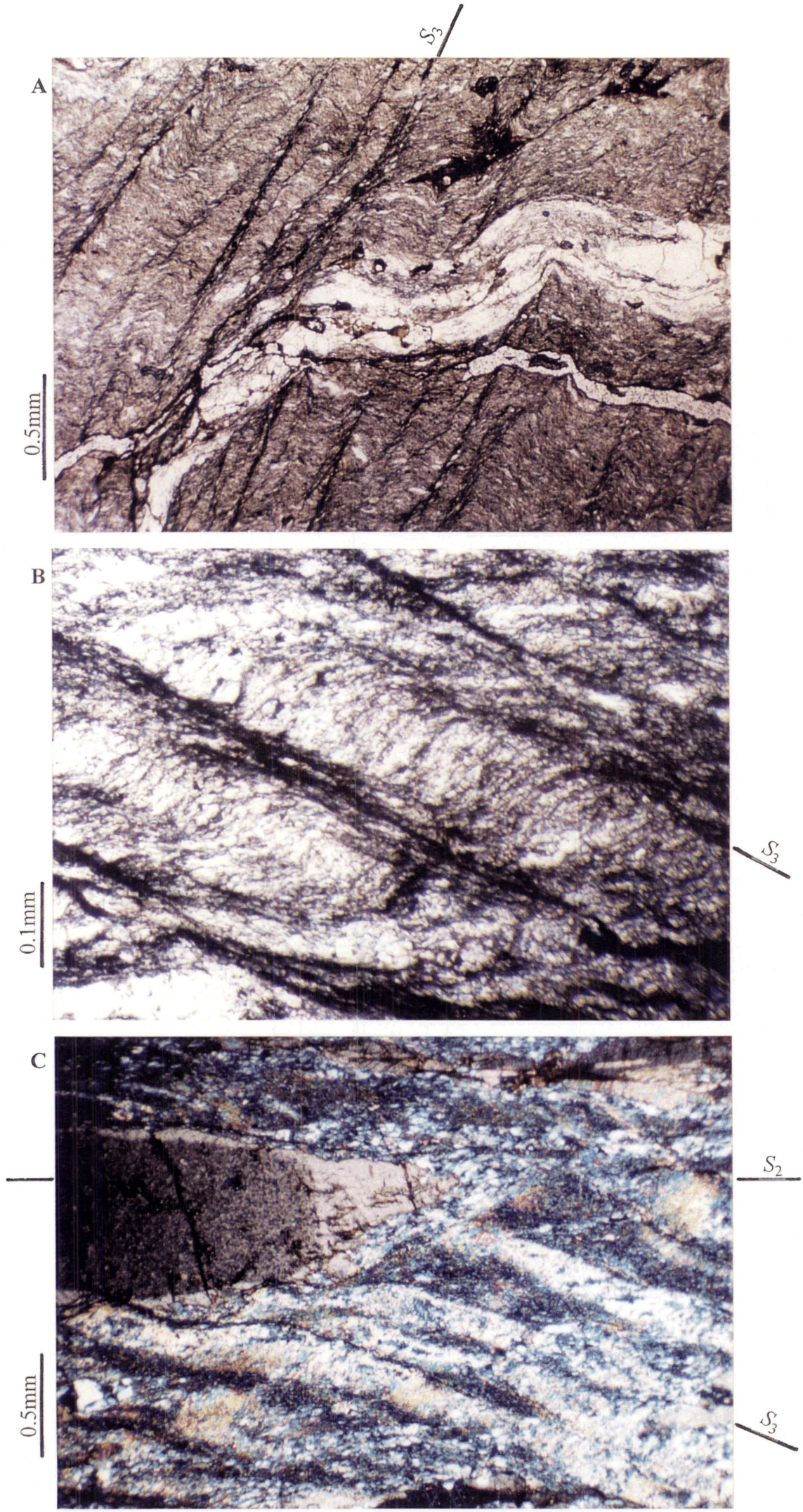
A
S_3
0.5mm
B
0.1mm
S_3
C
S_2
0.5mm
S_3

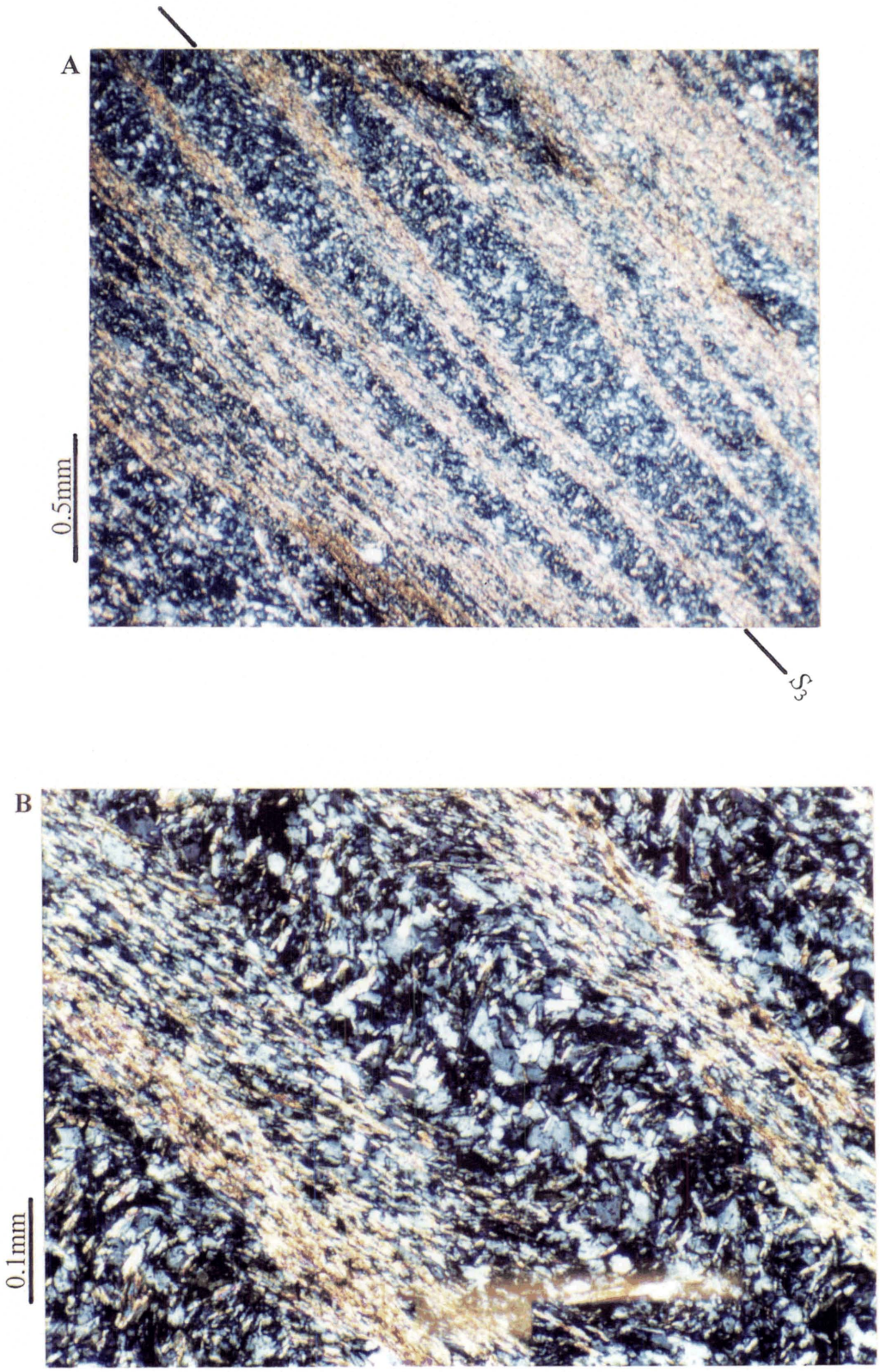

Figure 3.63: S_3 spaced zonal crenulation cleavage with sharp boundaries. In these photomicrographs, S_3 crenulates S_2 foliation, and good Q and M domains have developed. (B) is a close-up view of (A). The M domains consist of muscovite, tremolitic hornblende, and opaque minerals. RJ87, undifferentiated Haupiri Group. CPL.

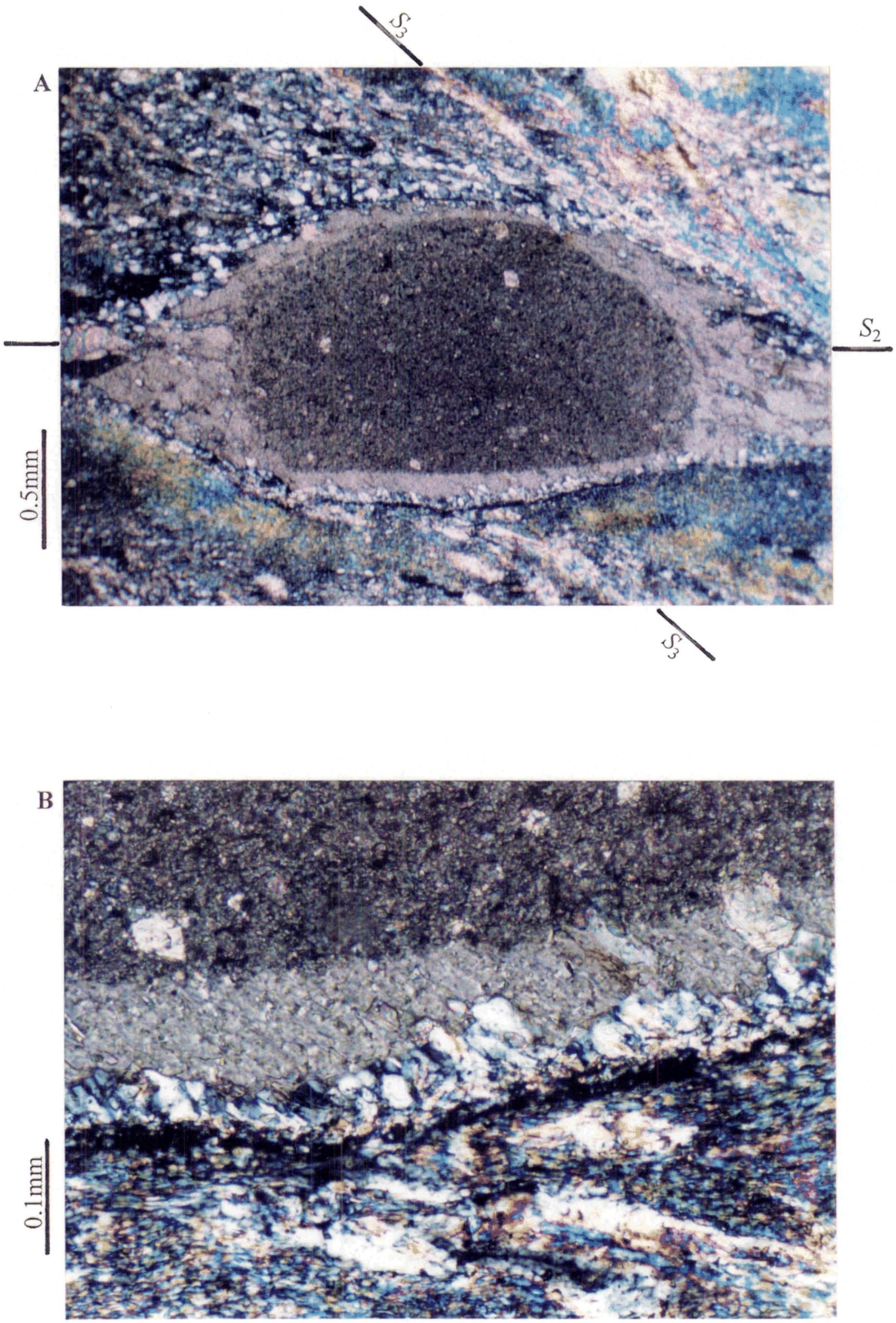

Figure 3.64: Inclusion-rich ankerite porphyroblast with long ankerite strain fringes parallel to S_2 and short ankerite/ quartz strain fringes growing parallel to S_3. Note how opaque solution seams, parallel to S_2 and wrapping around the ankerite, have been displaced by S_3 strain fringe growth. (B) is a close-up view of (A) showing S_3 strain fringe development. RJ65, undifferentiated Haupiri Group, CPL.

In D_2 tectonites, S_3 wraps and intensifies around margins of rigid objects such as quartz boudins (Fig. 3.65) and ankerite porphyroblasts. Quartz veins in D_2 deformed rocks are microfolded by S_3 (Fig. 3.66). The quartz grains in these veins, especially the thicker ones, exhibit features of plastic deformation and dynamic recrystallisation associated with S_3. Such features include deformation bands, subgrains, serrated grain boundaries, strong SPO parallel to S_3 (Fig. 3.67), and a moderate LPO with *c*-axes perpendicular to S_3. Where interbedded marble and slate occur, calcite layers on the microscale also display a strong SPO parallel to S_3. Calcite layers parallel to S_2 are sometimes folded by F_3. Where these folds occur, the orientation of S_3 in the adjacent mica-rich layers is perturbed, and the SPO in calcite layers reflects this perturbation (Fig. 3.68). Thus D_3 must be responsible for the calcite SPO.

In sections parallel to the D_2 stretching lineation, S_3 typically makes an angle with S_2 of 35° or less. When S_3 refracts around rigid objects, its orientation approaches that of S_2 (Fig. 3.65). In some D_2 tectonites, evidence of D_3 deformation is apparently absent and one suspects D_3 strain was not strong. However, if pyrite crystals are present, late stage fibre growths are observed consistently growing in the orientation of where S_3 would normally be (Fig. 3.69). On closer inspection, S_3 is observed within the low strain zones of S_2, adjacent to pyrite margins (Fig. 3.70). In these low strain zones, S_3 is quite clearly crenulating S_2. When S_3 is traced from the low strain zones into the D_2 M-domain high strain zones that wrap around the pyrite, the crenulations progressively open up and eventually disappear (Fig. 3.70). S_2 effectively decrenulates itself from the low strain zone into the high strain zone. Following from a similar case study described by Aerden (1996), the features described above suggest that D_3 has reactivated S_2 surfaces within the high strain M-domains. D_3 strain has effectively been taken up by induced shearing and/or solutioning along S_2. This reactivation suggests that in some D_2 tectonites at least, the local principal stress orientations responsible for S_3 became such that it was easier to reactivate a pre-existing anisotropy (S_2) than to crenulate it.

Figure 3.65: Photomicrograph showing how S_3 refracts and intensifies as it approaches rigid objects. In this photomicrograph, S_3 cleavage progressively becomes subparallel and more intense as it approaches a boudinaged quartz/ calcite vein. RJ100, undifferentiated Haupiri Group. PPL.

Figure 3.66: Quartz vein cutting obliquely to S_2 is microfolded by S_3. RJ68, undifferentiated Haupiri Group, PPL.

Figure 3.67: Partial view of a quartz vein folded by S_3. The quartz grains in the vein exhibit deformation bands, subgrains, serrated grain boundaries, and a strong SPO which is parallel to S_3. RJ68, undifferentiated Haupiri Group, CPL.

Figure 3.65

Figure 3.66

Figure 3.67

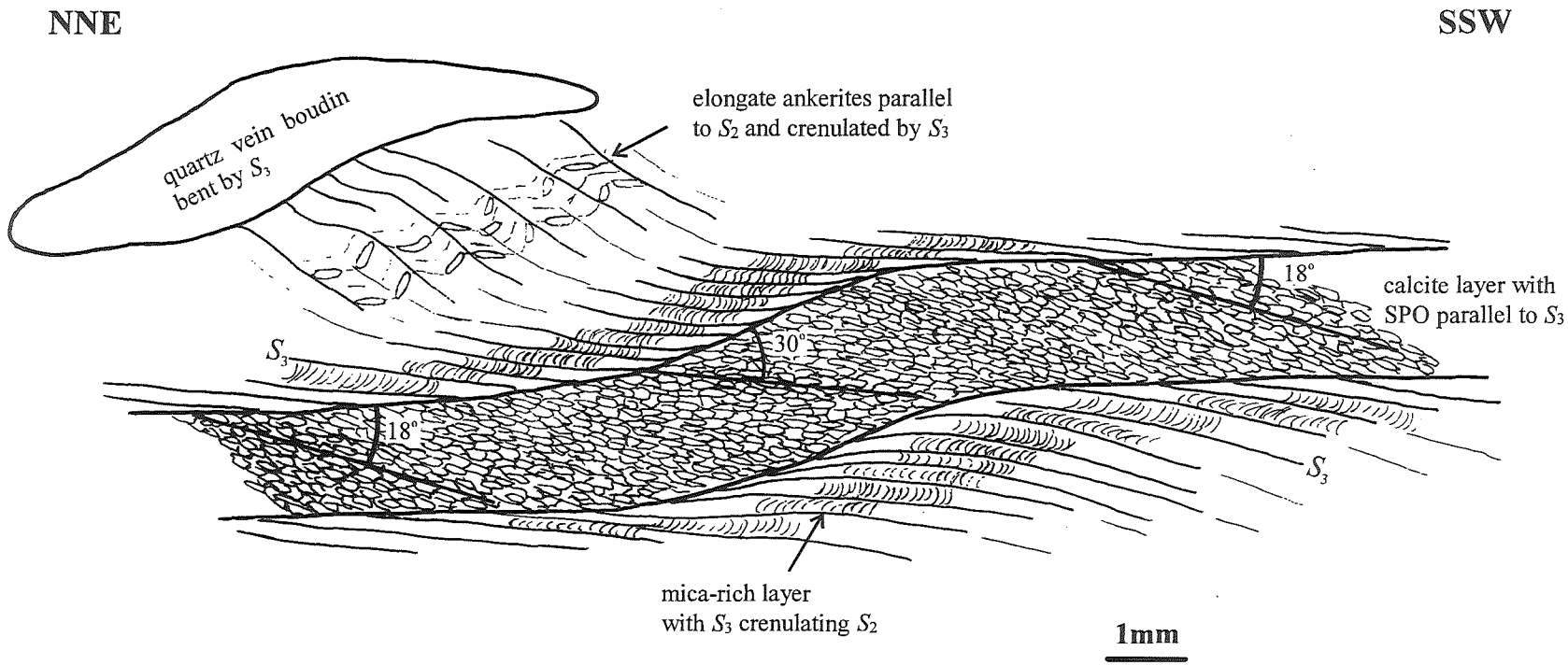

Figure 3.68: Sketch of thin-section (RJ100) showing S_3 perturbation around a gently folded (F_3) calcite layer. The calcite SPO within the calcite layer reflects the S_3 perturbation indicating that D_3 must be responsible for the calcite SPO. Sketch is parallel to the S_2 stretching lineation. S_2 is parallel to the compositional layering. Note how elongate ankerites, parallel to S_2, have been crenulated by S_3.

Figure 3.69: S_2 tectonite with long strain shadows adjacent to a pyrite cube. S_3 is not observed but late stage quartz strain fringes immediately adjacent to the pyrite grow in the direction of where S_3 is ought to be. S_2 XZ section, RJ1, undifferentiated Haupiri Group. CPL.

Figure 3.70: S_2 tectonite where S_3 is observed only within the low strain zone of S_2, immediately adjacent to a pyrite margin (see text for discussion). (B) is a close-up view of (A). RJ108, undifferentiated Haupiri Group. CPL.

0.1mm

Figure 3.70B

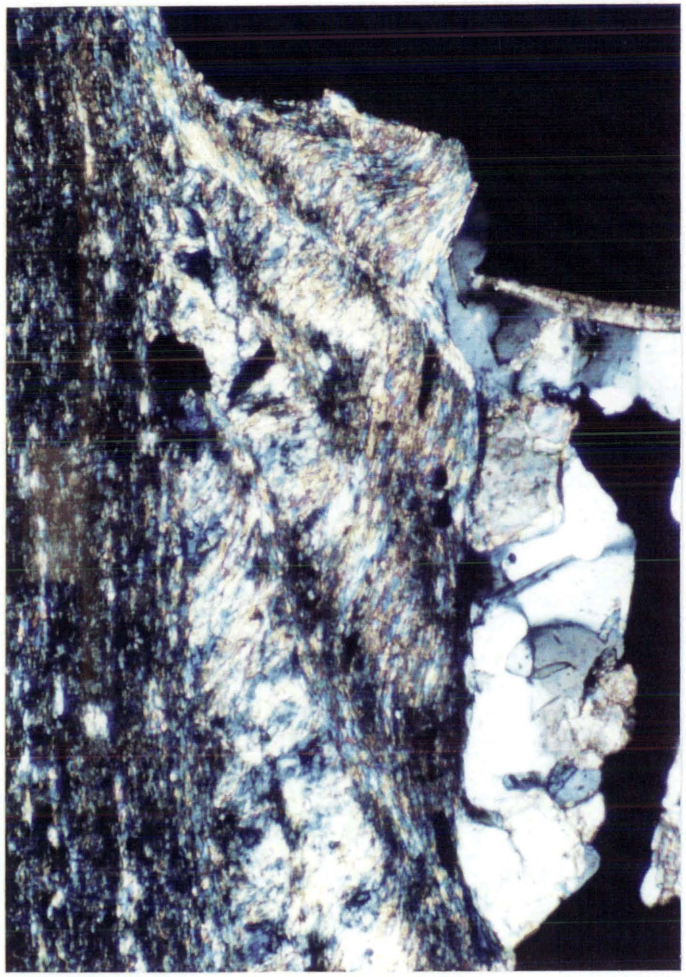

0.5mm

Figure 3.70A

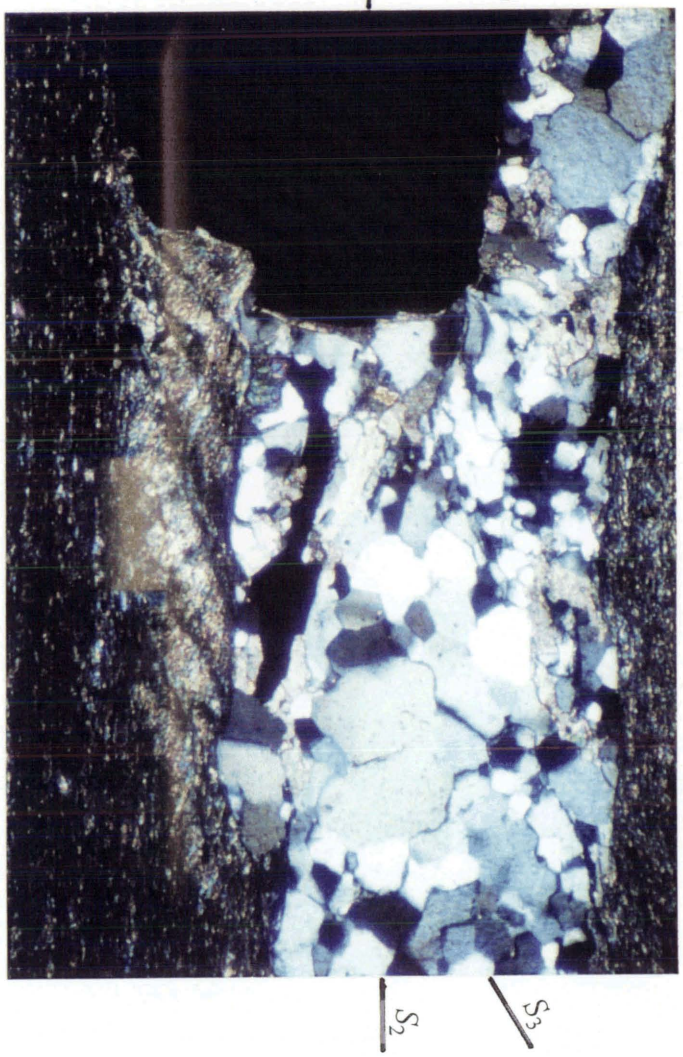

0.5mm

Figure 3.69

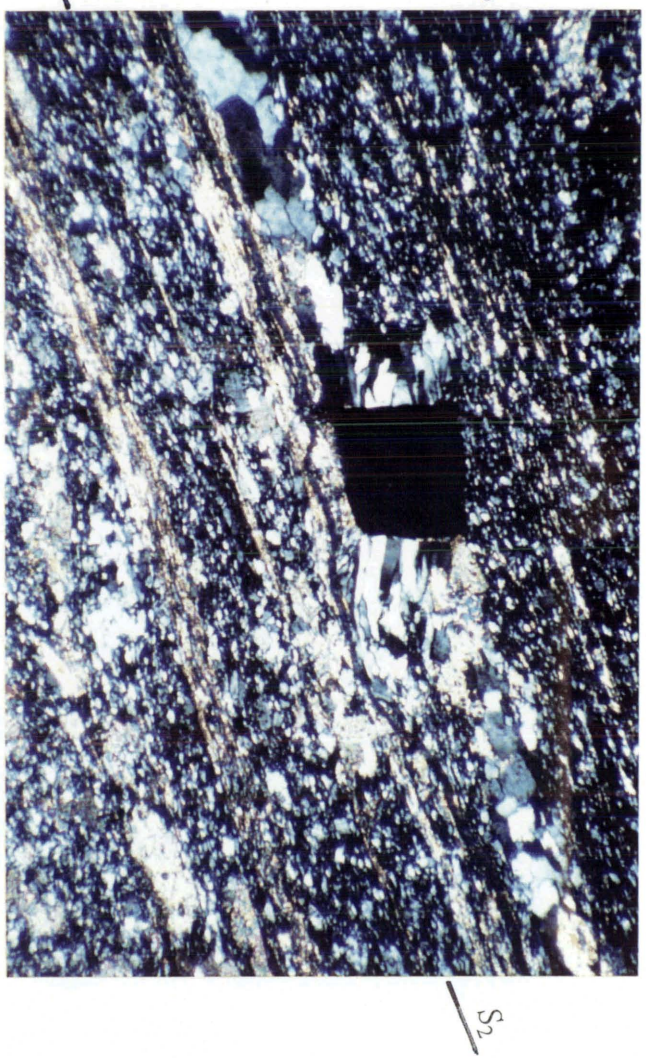

3.7.10 Other structures

Apart from D_1, D_2, and D_3 related structures, there are structures, particularly cleavages, that are of very restricted occurrence and cannot be positively correlated with any major deformational event. Worthy of mention is a mesoscale folding and associated axial planar cleavage observed primarily in Minaret Creek (informal name) at the northeast extremity of the Boulder Lake domain. Here, open folds plunge gently towards the S-SE, and the associated axial plane cleavage strikes NW, dipping moderately to the SW. The cleavage crenulates S_1.

A similar oriented crenulation cleavage is observed sporadically within the muddy matrix of the Balloon Mélange in the southeast of the Boulder Lake domain. This crenulation cleavage crenulates probable S_3 observed in the mélange (Section 8.4.1).

3.7.11 Cenozoic deformation

Numerous brittle faults are observed throughout the Takaka terrane of the Boulder Lake domain and clearly offset the D_1, D_2, and D_3 structures. The brittle faults range from discrete fault planes to 25m wide fault zones. The fault zones consist of up to 4m wide fault breccia and gouge anastomosing around packets of slightly or moderately disrupted rock (Fig. 3.71). Riedel shears are common, providing senses of shear. Most faults are reverse. Kink banding of slaty rock often occurs in close association with brittle faults. The major brittle faults are shown on Map 1 and these strike between north and east. Some of the faults continue into the Buller terrane rocks and offset the Anatoki Fault. The brittle faults are assumed to be related to Late Cenozoic uplift.

3.8 Quantitative strain in conglomerates

Conglomerate lenses occur throughout the Haupiri rocks of the Boulder Lake domain. The conglomerate clasts show varying degrees of deformation and are elongate in varying directions. An attempt was made to semi-quantify the strain pattern in the Haupiri conglomerates and to relate this pattern to the deformation events that the Haupiri rocks have experienced.

A

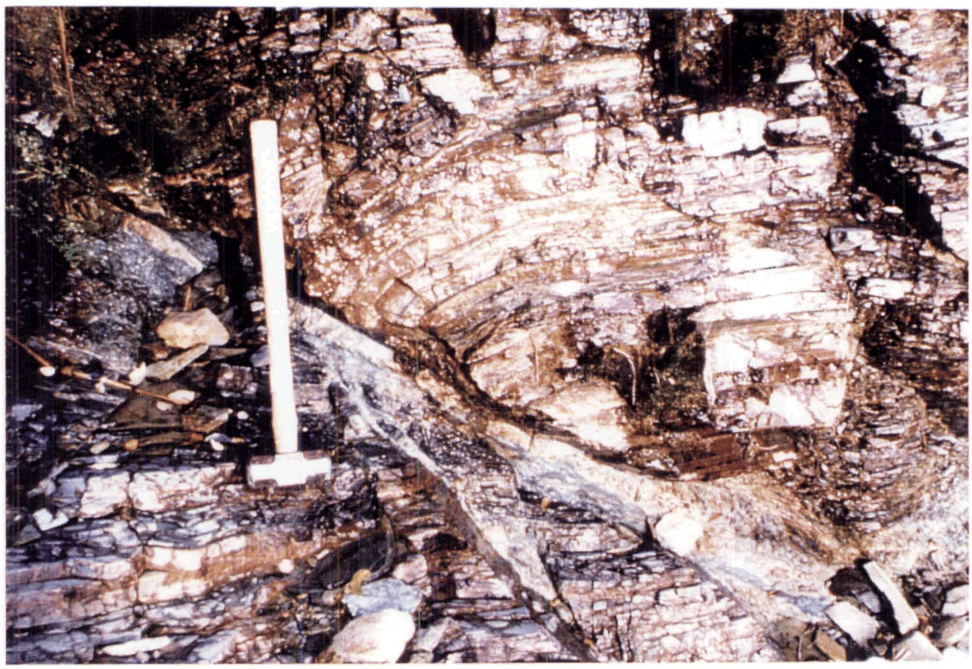

B

Figure 3.71: (A): Reverse brittle fault marked by 15cm thick pug zone. A hanging wall drag fold is observed. M26/ 748350. Sledgehammer for scale. (B): 25m wide brittle fault zone consisting of fault breccia and gouge anastomosing around packets of disrupted rock. Calphurnia Peak in background. M26/ 760342.

The conglomerates are generally matrix supported and consist of either lithic or quartzose clasts. Lithic clasts clearly show a higher degree of deformation than quartz clasts and, in many cases, are deformed by impinging quartz clasts. Because the lithic clasts show a higher degree of deformation, and therefore a truer reflection of total strain, only these were measured for strain analysis in handspecimens (see below).

Two methods were employed to estimate strain in conglomerate clasts. The first method was a visual estimate of the clast axial ratio (R_f) arithmetic mean parallel to the XZ strain axes (if known). Clearly this method is of low accuracy and is always an over-estimate of the true strain ellipse value (R_s) (Ramsay and Huber 1983). Nevertheless, the method did provide valuable information on recognition of strain patterns. The second method employed involved accurate measurements of R_f and calculation of the harmonic mean (Lisle 1977) to estimate R_s. Eight samples were collected for this method (Table 3.1). Each sample was sawn to produce three orthogonal faces, one parallel to the foliation (XY plane), one perpendicular to the foliation and maximum clast elongation direction (YZ plane), and the other perpendicular to the foliation but parallel to the maximum clast elongation direction (XZ plane). On each face, between 30 and 50 measurements of R_f were made and the harmonic mean calculated (Table 3.1).

Sample number	Location	Grid reference (M26)	XY	YZ	XZ	*k*-value
RJ92	Portia Creek	752343	2.31	2.79	6.51	0.73
RJ328	Eastern lakeshore creek	749351		4.27	15.21	0.78
RJ337	Upper Snow River	764326	2.10	2.89	6.34	0.58
RJ342	Gladiator Peak	736323	1.97	2.65	5.78	0.72
RJ355	Minaret Creek	767367	1.94		4.35	0.76
RJ356	Lower Snow River	768365	1.48		4.02	
RJ361	Lower Snow River	770351	3.33	3.49	11.18	0.93
RJ362	Lower Snow River	770351	3.07	3.48	10.4	0.83

Table 3.1: Harmonic means of R_f values in the XY, YZ, and XZ planes of eight conglomerate samples, undifferentiated Haupiri Group, Boulder Lake domain. No harmonic mean is recorded in the XY plane of RJ328, or in the YZ plane of RJ355 and RJ 356 because of difficulties experience in measuring a sufficient amount of R_f values. *k*-values are also given.

The harmonic mean has been shown by Lisle (1977) to be a good approximation of R_s (within 10%) as long as the true R_s is higher than 2.5 and assuming homogeneous strain and lack of a pre-deformational preferred orientation. In Table 3.1, five estimates of XY ratios fall below 2.5 and can be regarded as significantly higher than the true R_s value. It should be noted that some samples, particularly RJ92 (Fig. 3.57D), have been crenulated

by S_3 and clast shapes are modified. This modification should be taken into account when determining the accuracy of the strain estimates. However, because of the regional objective in this research, the accuracy determination is not regarded as important here.

The strain ratios for the XY, YZ, and XZ sections were combined to give the three dimensional constant volume strain ellipsoid, represented by the parameter k (Flinn 1962). k values shown in Table 3.1 were calculated using XY and YZ ratios where possible. To provide a check on the accuracy of the k value, k values were also calculated using XZ with XY, and XZ with YZ. These k values fall within 10% of the calculated k value shown in Table 3.1 and demonstrate that measurements are internally consistent. A k value was not calculated in RJ356 because the harmonic mean of 1.48 for XY was considered too low to be a reliable estimate of R_s.

The results of the two methods of strain quantification, together with maximum elongation directions, are shown geographically in Figure 3.72. Elongation directions have also been plotted stereographically in Figure 3.73. Two strain patterns are recognised. Firstly, conglomerate clasts in close proximity of the Anatoki Fault are elongate parallel to the S_2 stretching lineation (i.e. subhorizontal and trending N-S). In the field, these conglomerates are deformed parallel to the S_2 foliation. XZ estimates range between 5 and 15 and k values lie within the field of flattening. Secondly, conglomerate clasts in the remainder of the Boulder Lake domain, particularly those in the Snow River catchment area, plunge mainly steeply east. In the field, these conglomerates invariably possess a flattening plane that is slightly oblique to bedding in an orientation consistent with S_1. XZ strain estimates range between 2 and 11, the higher values occurring within the Snow River. k values lie in the field of flattening with one sample (RJ361) approximating plane strain. A considerable number of conglomerates between the Snow River and Anatoki Fault display a lack of deformation with R_f values of 1 or 1.5.

In summary, there is a clear correlation between quantitative strain patterns recorded in deformed conglomerates and deformation events recorded by other structures. Conglomerates in close proximity to the Anatoki Fault have been deformed by D_2, whereas the other conglomerates appear to have been deformed only by D_1.

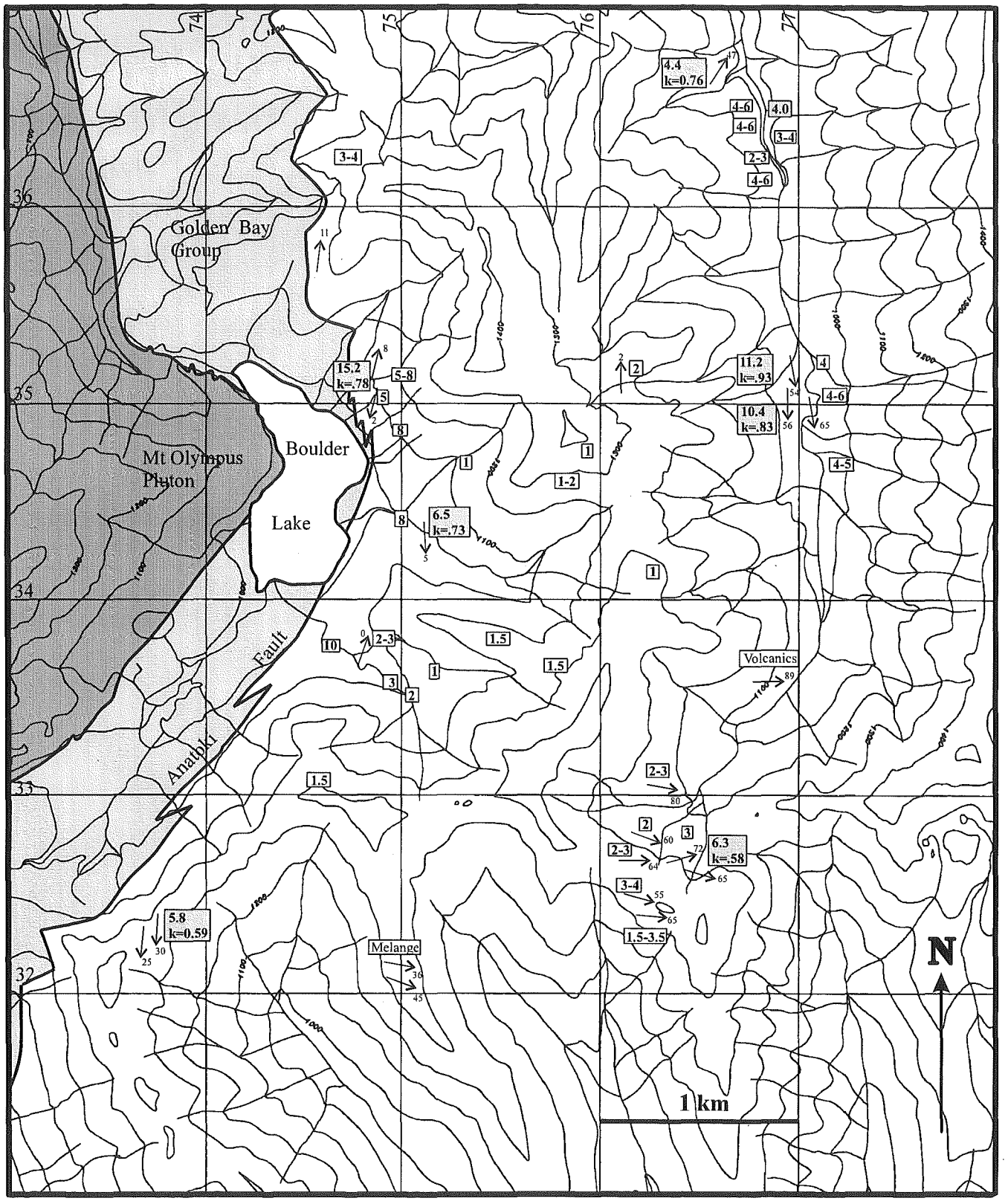

Figure 3.72: Quantitative strain analysis derived from conglomerate, undifferentiated Haupiri Group, Boulder Lake domain. White square values are visual estimates of the clast axial ratio (R_f) arithmetic mean, parallel to the X/Z strain axes (where known). Grey square values are harmonic means of R_f in the X/Z direction. Included in the grey squares are k values. Maximum elongation directions of clasts (trend and plunge) are also plotted.

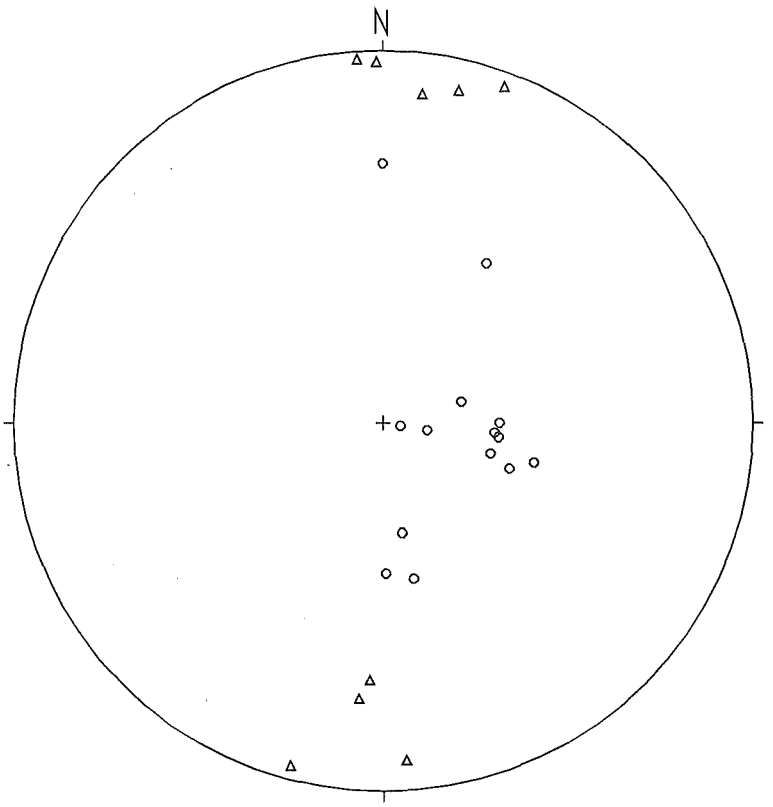

Δ conglomerate elongation direction close to Anatoki Fault, n=9
O conglomerate elongation direction away from the Anatoki Fault (mostly Snow River area), n=13

Figure 3.73: Conglomerate elongation directions in undifferentiated Haupiri Group, Boulder Lake domain.

3.9 Discussion

In this section, the structure in rocks both east and west of the Anatoki Fault are reviewed. This is followed by a comparison and discussion of structures east and west of the Anatoki Fault.

3.9.1 Structure in rocks west of the Anatoki Fault

The following points are pertinent for a discussion on the structure of the Boulder Lake domain:

1. A tectonic foliation occurs within, and is concordant with, the eastern margin of the Mt Olympus Pluton. This foliation is a result of a high temperature solid-state deformation (Rennison 1992). Stretching lineations associated with the foliation trend between NE and E.

2. A penetrative foliation (S_2), subparallel to the eastern margin of the Mt Olympus Pluton and the Anatoki Fault trace, occurs within the Golden Bay Group sediments between the Mt Olympus Pluton and Anatoki Fault. S_2 stretching lineations trend between NE and E.

3. Late stage magmatic differentiates (aplites) of the Mt Olympus Pluton are deformed by S_2.

4. No foliation is observed along the western margin of the Mt Olympus Pluton and adjacent country rock (Brathwaite 1968b; Rennison 1992).

5. Metamorphism, associated with S_2, increases from biotite grade (mid-greenschist facies) in rocks next to the Anatoki Fault to sillimanite grade (upper amphibolite facies) in rocks immediately adjacent to the eastern margin of the Mt Olympus Pluton. The presence of andalusite and cordierite indicate low pressures.

6. LS- and S-tectonites occur in rocks adjacent to the Mt Olympus Pluton (Orator Creek and Lake Outlet domains) whereas S-tectonites predominate in rocks furthest from the Mt Olympus Pluton (Arena Creek and Beak Creek domains).

7. Almost all shear-sense indicators in tectonites immediately adjacent to Mt Olympus Pluton suggest top to the SW-W sense of shear (Fig. 3.74).

8. A crenulation (S_{cren}) is observed in rocks immediately adjacent to the Mt Olympus Pluton (Orator Creek and Lake Outlet domains).

9. A crenulation cleavage (S_3) is strongly developed in graphitic slate immediately adjacent to the Anatoki Fault but weakly developed or absent in phyllites to the west (Beak Creek and Arena Creek domains).

Adjacent to the Mt Olympus Pluton, Golden Bay Group sediments are thermally metamorphosed, as evidenced by the presence of andalusite and cordierite. S_2, the penetrative foliation within the Golden Bay Group sediments, wraps around these porphyroblasts and thus must postdate pluton emplacement. Deformation post-pluton emplacement is supported by the fact that last stage magmatic differentiates of the Mt Olympus Pluton are deformed by S_2. Given that the syn-S_2 metamorphic assemblage increases from biotite grade to sillimanite grade towards the pluton contact, and that strain shadows associated with S_2 contain sillimanite, S_2 and the associated stretching lineation must have formed while the pluton was still very hot. A similar conclusion is reached for the tectonic foliation developed within the eastern margin of the Mt Olympus Pluton (Rennison 1992). Since both S_2 in the country rock and the tectonic foliation within the granite are of similar orientations and with similar stretching lineations (Map 1), it is concluded that the two foliations are an expression of a ductile deformation event that is confined to the eastern side of the Mt Olympus Pluton, and occurred soon after the eastern margin of the pluton had solidified at around ~111Ma. The deformation event is referred to as D_2.

According to Grindley (1971), both the Leslie and Douglas Formations thicken appreciably north and south of the Boulder Lake domain. If it is accepted that both the Leslie and Douglas Formations are represented in the Boulder Lake domain, then it

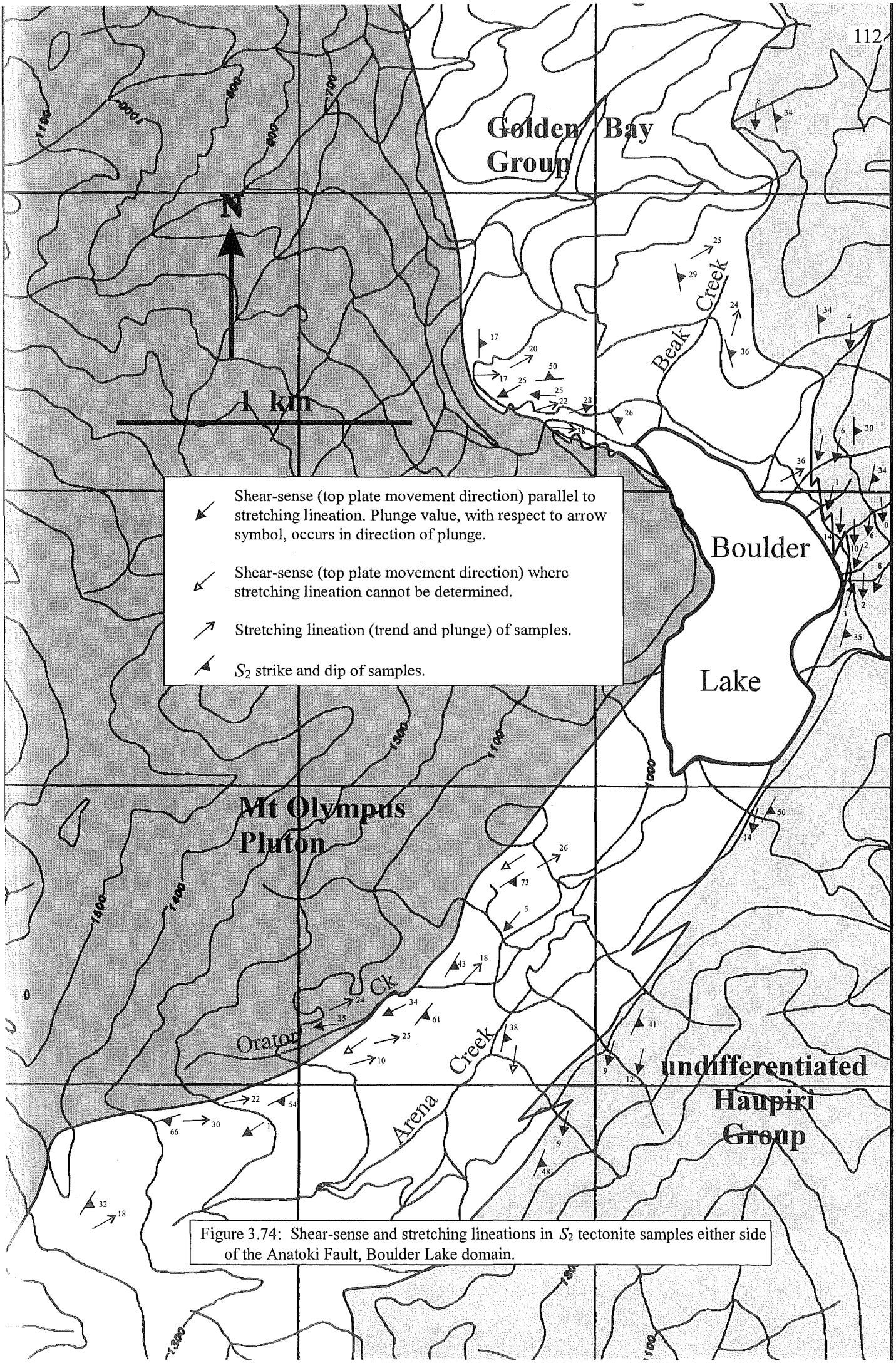

Figure 3.74: Shear-sense and stretching lineations in S_2 tectonite samples either side of the Anatoki Fault, Boulder Lake domain.

appears they have been tectonically thinned within the vicinity of the Mt Olympus Pluton. The thinning is best attributed to D_2.

The relationship between S_{cren} and S_3 is not well-understood. The fact that the orientation of S_{cren} in the Orator Creek domain is at 90° to S_3 in the eastern parts of the Arena Creek domain, and that there is no progressive change in orientation recorded between them, suggests that the two crenulations are unrelated. The recrystallisation of biotite in S_{cren} suggests the crenulation formed soon after S_2, when temperatures were still at least within the mid-greenschist facies.

D_1 mesoscale structures, clearly expressed in more southern domains and thought to be Paleozoic in age (see Section 9.3.1), are not observed in the Golden Bay Group rocks of the Boulder Lake domain. Microscale candidates for S_1 include a remnant slaty cleavage folded by F_2 (Orator Creek domain), a slaty cleavage preserved in strain shadows of quartz/graphite spots (Lake Outlet domain), and as inclusion trails in porphyroblasts of the thermal aureole. However, as previously pointed out, these features may alternatively be of early S_2 generation.

3.9.2 Structure in rocks east of the Anatoki Fault

Three major deformation events are recognised east of the Boulder Lake domain: D_1, D_2, and D_3.

D_1 is represented by macroscale folding (F_1) of Haupiri Group rocks with axes plunging gently or moderately towards N-NE. A weakly developed slaty cleavage (S_1) is axial planar to the folds. The maximum extension direction associated with D_1 is not certain but appears to be perpendicular to F_1 fold hinges, and parallel to F_1 axial planes, as suggested by strained conglomerate studies. Metamorphism associated with D_1 is of low grade.

Close to the Anatoki Fault, S_1 and bedding become rotated into S_2, a penetrative phyllitic foliation that is parallel to the Anatoki Fault and represents D_2 deformation. The D_2 zone of deformation is a zone of high non-coaxial ductile strain with subhorizontal stretching lineations trending subparallel to the Anatoki Fault trace. S_2 tectonites are either L or LS

in character. Shear-sense indicators give a dextral strike-slip shear with top to the S-SW on an east dipping foliation (Fig. 3.74). Syn-D_2 metamorphism is of low grade and associated with extensive carbonate (ankerite and calcite) metasomatism.

D_3, represented by mesoscale folding (F_3) and a crenulation cleavage (S_3), overprints all D_1 and D_2 related structures. Syn-D_3 metamorphism is low grade.

3.9.3 Comparison of structures east and west of the Anatoki Fault

S_2 east of the Anatoki Fault is of exactly the same orientation as S_2 west of the Anatoki Fault. Both foliations are parallel to the Anatoki Fault and both share stretching lineation and shear-sense orientations that are more alike than unlike (see below). In addition, both foliations appear to share a similar age of formation if the Rb-Sr ages acquired in the Takaka terrane are accepted. The most simplest conclusion is that S_2, either side of the Anatoki Fault, are the same structure and therefore represent the same deformation event, D_2, immediately postdating the Mt Olympus Pluton emplacement.

If the above conclusion is correct, then D_2 strain varies in character as seen by the changing nature of S_2 tectonites: L- and LS-tectonites immediately east of the Anatoki Fault, S-tectonites immediately west of the Anatoki Fault, and LS- and S-tectonites adjacent to the Mt Olympus Pluton. Non-coaxial D_2 strain is observed within the Haupiri rocks adjacent to the Anatoki Fault, and within the Golden Bay Group rocks immediately adjacent to the pluton.

The Mt Olympus Pluton, as a whole, is elliptical in outcrop shape (Brathwaite 1968b). At Boulder Lake, the eastern margin of the pluton is shaped in such a way as to appear as a protrusion extending from the main elliptical body (Map 1). Since D_2 occurred soon after the eastern margin of the Mt Olympus Pluton had solidified, D_2 deformation would be perturbed by the highly competent protrusion. Evidence of the perturbation is demonstrated in the Lake Outlet domain where S_2 changes dramatically in orientation to remain concordant with the pluton margin, but the deflection of S_2 weakens with increasing distance from the pluton margin. S_2 orientations in Haupiri rocks east of the Anatoki Fault are least deflected, and therefore their stretching lineations and shear-sense

orientations are most representative if D_2 is a regionally related deformation i.e. dextral strike-slip with top to the S-SW on an east dipping foliation.

Brathwaite (1968b, p.121) concluded that the foliation in the Mt Olympus Pluton was a result of "protoclastic deformation" of an already solidified pluton margin "caused by pressure from addition of magma below", the implication being that D_2 may be of local extent and related solely to forceful intrusion of the pluton. However, the increasing component of strike-slip shear with increasing distance from the pluton's eastern margin, together with the strong asymmetric development of foliation from west to east across the pluton and adjacent rocks (Rennison 1992), is inconsistent with forceful intrusion or expansion and rather suggests D_2 is related to a regional stress field. In addition, late stage magmatic differentiates (aplites) are deformed by S_2, indicating that D_2 must at least partly postdate complete pluton solidification.

It has been shown that under regional deformation, foliations in country rock are bent around plutons if there is a competency contrast between the two (Paterson *et al.* 1991; this study). Associated with this bending, stretching lineations close to the pluton margin can be expected to change orientation, the amount of change depending on the three dimensional shape of the pluton and the strain field it sets up when being deformed (Guglielmo 1993). Thus it seems likely that the stretching lineations observed along the eastern margin of the Mt Olympus Pluton, which differ in orientation from those in the Haupiri Rocks, are controlled by the three dimensional shape of the pluton. In the Lake Outlet domain, F_2 folding occurs, and fold axes are parallel to stretching lineations suggesting constriction perpendicular to the stretching lineations. It would appear that this constriction is also a result of the three dimensional shape of the pluton, where country rock was strained around the eastern margin protrusion but confined to the west by the eastern margin of the main pluton body.

Rennison (1992) found shear-sense indicators in two samples within close proximity of the Anatoki Fault. According to Rennison, these indicators give a normal sense of shear parallel to the eastward dip of the fault, and they are therefore in disagreement with all shear-sense indicators found close to the Anatoki Fault of this study. Given that the shear-sense indicators identified by Rennison are approximately perpendicular to the shear-sense indicators close to the Anatoki Fault of this study, and that no stretching

lineations were identified on the samples by Rennison, it may be that the shear-sense indicators identified by Rennison were not parallel to actual stretching lineations. The result is a shear-sense indicator that is not a valid indication of tectonic transport direction.

S_3, seen well-developed in graphitic slate west of the Anatoki Fault, is of exactly the same orientation as S_3 observed in rocks immediately east of the Anatoki Fault. Thus it appears D_3 deformation affects rocks both east and west of the Anatoki Fault; this is not unexpected since D_2 does the same. F_3 folds verge NE and the origin of this vergence is discussed in Section 9.6.3.

If we accept S_{cren} is unrelated to S_3 (see Section 3.9.1), than the absence of S_3 immediately adjacent to the Mt Olympus Pluton needs to be explained. It is possible that S_3 postdates S_{cren} given that S_{cren} formed soon after S_2 (Section 3.9.1). If S_3 does indeed postdate S_{cren}, then the absence can be explained by the fact that it is often difficult to crenulate a crenulation.

D_1 deformation observed in the Haupiri rocks is not observed in the Golden Bay Group rocks of the Boulder Lake domain and therefore cannot be compared. The D_1 structures in the Haupiri rocks will be discussed in a regional context in Section 9.5.1.

3.9.4 What is the Anatoki Fault in relation to D_2 deformation?

Although the Anatoki Fault shown on Map 1 technically marks the change in lithology from Golden Bay Group to undifferentiated Haupiri Group rocks, displacement on the fault is represented by a zone of ductile deformation either side of the fault, as evidenced by various rocks displaying non-coaxial strain. This zone of ductile deformation is expressed by Early Cretaceous D_2 related structures which have recorded dextral strike-slip strain. It follows that movement on the Anatoki Fault in the Boulder Lake domain was dextral strike-slip and Early Cretaceous in age. Because the Mt Olympus Pluton is part of the Separation Point Suite which intrudes both terranes, the post-Mt Olympus Pluton D_2 related movement represents reactivation of the terrane boundary. Although displacement is not necessarily concentrated on the Anatoki Fault trace, rheologically

weak marble does occur along the fault trace for part of the way, suggesting that very high strain may have been locally attained.

Much has been made of biotite observed in the Haupiri rocks as contact metamorphic in origin (Brathwaite 1968b), with the implication that no movement has occurred on the Anatoki Fault since pluton emplacement (Cooper 1989). This study, however, shows that biotite is associated with D_2 deformation soon after pluton emplacement. The D_2 metamorphic assemblage is low grade, but given the D_2 metamorphic gradient observed in the Golden Bay Group rocks, was probably just within the outer limits of the Mt Olympus Pluton thermal aureole.

Given the relationship of the Anatoki Fault trace with topography, together with the fact that the trace does not cut across the projected strike of S_2 immediately adjacent to it, the overall attitude of the fault plane geometry is subparallel to the average S_2 attitude in the four adjacent structural domains (Table 3.2), i.e. dipping moderately E north of Boulder Lake, and dipping moderately ESE south of Boulder Lake.

North of Boulder Lake	Beak Creek domain 338/ 31°E	North domain 006/ 36°E
South of Boulder Lake	Arena Creek domain 031/ 35°E	South domain 027/ 42°E

Table 3.2: average S_2 attitudes in the four structural domains adjacent to the Anatoki Fault

There is some evidence that the Anatoki Fault has been reactivated brittlely since D_2 as seen by brittle deformation features observed in graphitic slate immediately adjacent to the fault trace (Section 3.5.4 and Brathwaite 1968a).

3.9.5 Cause of the curved nature of the Anatoki Fault trace

From the previous discussion it is concluded that the curving of the Anatoki Fault trace in the Boulder Lake domain is a result of strain perturbations around the already solidified, but still hot, eastern margin of the Mt Olympus Pluton, a conclusion similarly reached by Rennison (1992) and initially suggested by Tulloch (1988). As mentioned earlier, evidence such as strike-slip shear, asymmetry of foliation from west to east across the pluton and adjacent country rocks, and deformation of late stage magmatic differentiates

is inconsistent with forceful intrusion of the Mt Olympus Pluton. Thus the hypothesis that the curving of the Anatoki Fault trace is solely a result of forceful emplacement of the Mt Olympus Pluton, as proposed by Grindley (1971), is rejected.

3.10 Ankerite twinning as a paleostress indicator

3.10.1 Introduction

Where S_2 is well-developed adjacent to the Anatoki Fault, elongate inclusion-free ankerite porphyroblasts frequently display deformation twinning. This deformation mechanism presents a unique opportunity to investigate the twin laws of ankerite, which has received little attention in the literature, and to investigate whether ankerite twinning can be used as a paleostress indicator. This section firstly gives an introduction to twinning in carbonates, followed by a description of ankerite *c*-axis and twin lamella preferred orientations, and the derivation of paleostress orientations. At the end of this section is a discussion of the paleostress orientations in terms of how they may relate to Takaka terrane deformation and also strain accommodation on the microscale.

3.10.2 Twinning in carbonates

Most carbonates are rhombohedral, and three possible rhombohedral forms are known by the letters *r*, *f*, and *e* (*r* is the rhombohedral cleavage). Calcite and dolomite are the two most common carbonates and their twin laws have been extensively studied. At room temperature, calcite twins easily on *e* at a minimal critical resolved shear stress (Turner *et al.* 1954). In fact, twin-gliding in calcite is so easy that it takes preference over all other plastic deformation mechanisms, such as slip, given that the individual grains are suitably oriented (Turner *et al.* 1954). This last proviso is given because *e*-twin gliding operates with a unique sense of shear and will only occur when σ_1 is at a high angle to the *c*-axis on individual grains (ideally 71°, Fig. 3.75) (Turner 1953). The effect of twin-gliding is to instantaneously rotate the c-axis by 52.5° towards σ_1 (Handin and Griggs 1951). *e*-twin gliding is therefore an effective mechanism for producing a *c*-axis preferred orientation subparallel to σ_1. Once a grain is completely twinned, it cannot continue to

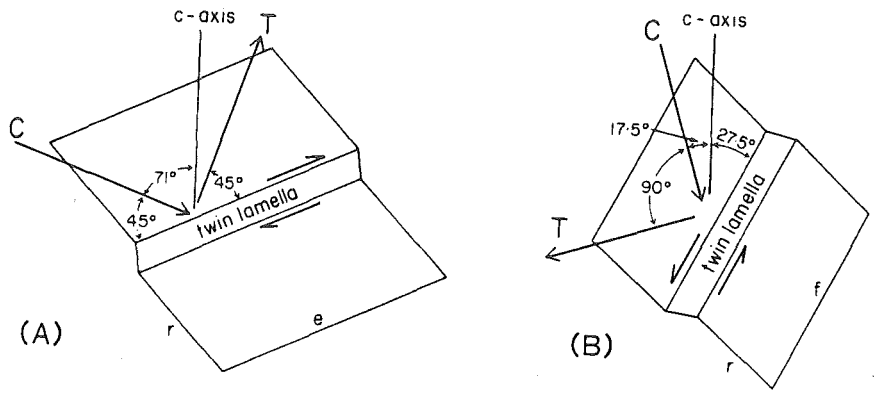

Figure 3.75: Crystal sections which show the angular relationships between twin lamellae, *c*-axes, and ideal compression (**C**) and tension (**T**) directions for calcite (A) and for dolomite (B) (from Shelley 1993).

twin unless σ_1 changes orientation. Further strain is accommodated by *r* or *f* slip (Turner and Weiss 1963).

The amount of strain that twin-gliding accommodates is relatively small and because of the susceptibility of individual grains to complete twinning, any visible twins in highly deformed and recrystallised calcite tectonites are likely to be related to a late minor deformation (Turner and Weiss 1963). Turner (1953), having noted that *e*-twin gliding operates with a unique sense of shear along a unique direction, proposed that ideal compression and tension directions exist for any set of twin lamellae (Fig. 3.75). If one plots the ideal compression and tension directions for all grains containing twin lamellae in a calcite tectonite, the mean orientation should equate to σ_1 and σ_3 respectively of the late minor deformation. This method is known as the "Turner method". In weakly deformed rocks the Turner method has been used successfully to determine geologically meaningful paleostress directions (e.g. Friedman and Conger 1964; Nissen 1964; Laurent 1987).

The twin law in dolomite is different from that in calcite. In dolomite, twin-gliding occurs on *f* planes and causes an instantaneous rotation of the *c*-axis away from σ_1 by 54°, and it will only be activated when the *c*-axis is at a low angle to σ_1 (17.5° on individual grains, Fig. 3.75) (Handin and Fairbairn 1955; Turner and Weiss 1963). Dolomite is much less plastic than calcite, and twinning is no exception. Twins are not commonly observed in dolomite because they are only activated at elevated temperatures and require a high critical resolved shear stress (Higgs and Handin 1959; Barber *et al.* 1981). Experimental works by Handin and Fairbairn (1955) and Barber *et al.* (1981) suggest *f*-twinning is common only at temperatures above 300°C, but Higgs and Handin (1959) suggest even higher temperatures (>400°C). *f*-twinning has been reported to occur in natural fault zones at temperatures as low as 270°C (Newman and Mitra 1994). *f*-twinning in dolomite operates with a unique sense of shear along a unique direction so that the Turner method of σ_1 and σ_3 determination in calcite can be applied equally as well to dolomite (Turner and Weiss 1963).

Ankerite forms a solid solution series with dolomite by partial substitution of Mg atoms with Fe (Deer *et al.* 1962). Crystallographically, ankerite is the same as dolomite except for very small changes in lengths and angles of the structure brought about by the

presence of the larger Fe ion (Deer *et al.* 1962). I have only found one paper, by Barber and Wenk (1979), that mentions ankerite twinning in passing. These authors report that ankerite, like dolomite, twin on the *f* plane. If Barber and Wenk (1979) are correct, then the Turner method of paleostress determination can be applied to twinned ankerites in samples from the Boulder Lake domain.

3.10.3 Samples

12 ankerite bearing samples, from the zone of D_2 deformation in the Takaka terrane, were selected for the Turner method analysis of paleostress directions. The samples came from Kiwi Creek in the north, to streams draining into Arena Creek in the south. The majority, however, were from streams immediately adjacent to the Boulder Lake eastern lakeshore (Table 3.3).

Samples chosen were ones where inclusion-free ankerites occur as porphyroblasts within a matrix of fine grained micas, quartz, and feldspar, or as large strain fringes to detrital porphyroclasts and inclusion-rich ankerites. Some samples (RJ103, 107, 126, 279, 325) show asymmetric strain shadows (Fig. 3.45, 3.47), and these are consistent with the overall D_2 sense of shear. The ankerites are elongate parallel to the D_2 stretching lineation.

Some samples (RJ99, 107, 108, 126, 279) contain early generation inclusion-rich ankerite porphyroblasts (Fig. 3.45). The orientations of these were not measured because they represent a different population of ankerites (Section 3.7.6). However, inclusion-free ankerite strain fringes attached to inclusion-rich ankerite porphyroblasts of exactly the same crystallographic orientation were measured (Fig. 3.76). Twinning in these strain fringe ankerites does not always extend into the inclusion-rich ankerites presumably because of the obstacles for twin-gliding brought about by the inclusions (Fig. 3.76). The majority of ankerites show sharp extinction and straight lamellae (Fig. 3.76).

The elongate nature of inclusion-free ankerites appear to be a result of growth parallel to the extension direction. Evidence for growth includes the frequent occurrence of ankerites as strain fringes, and the frequent occurrence of near euhedral terminations. In addition, inclusion-free ankerites contain multiple planes of minute fluid inclusions

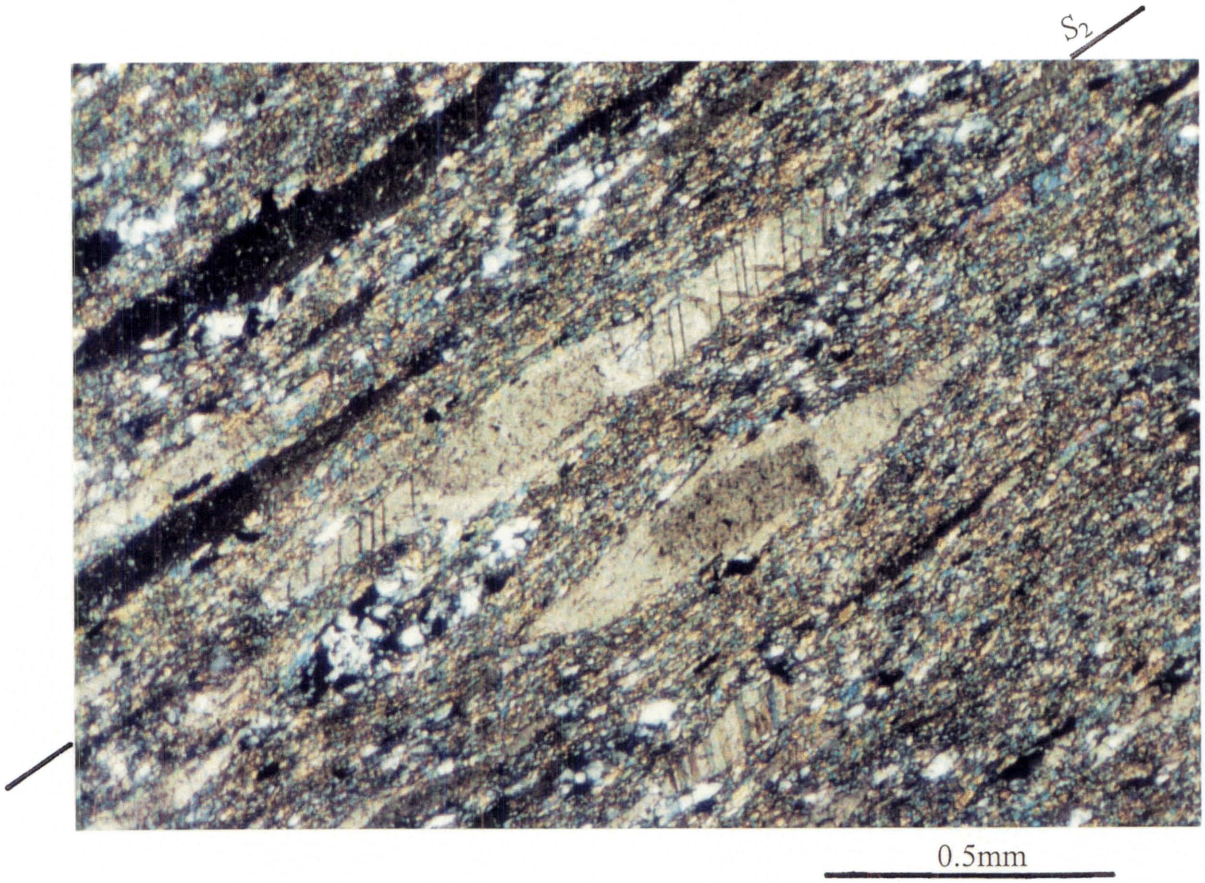

Figure 3.76: Inclusion-free ankerite strain fringe attached to inclusion-rich ankerite porphyroblast with the same crystallographic orientation. Extinction is sharp and twin lamallae are straight. Twin lamallae in the inclusion-free strain fringe are not present in the inclusion-rich porphyroblast. RJ107. CPL.

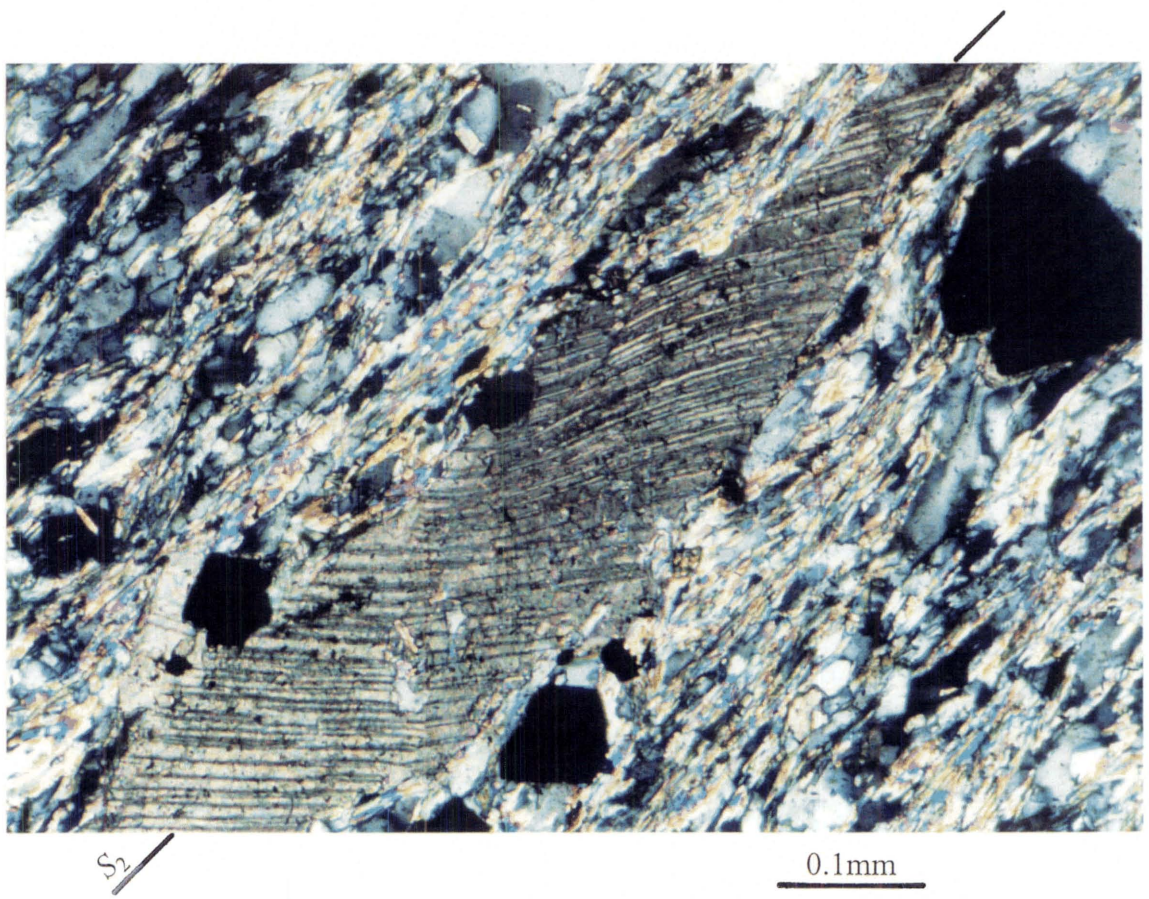

Figure 3.77: Ankerite in RJ327 displaying undulatory extinction and curved twin lamallae indicative of plastic slip. CPL.

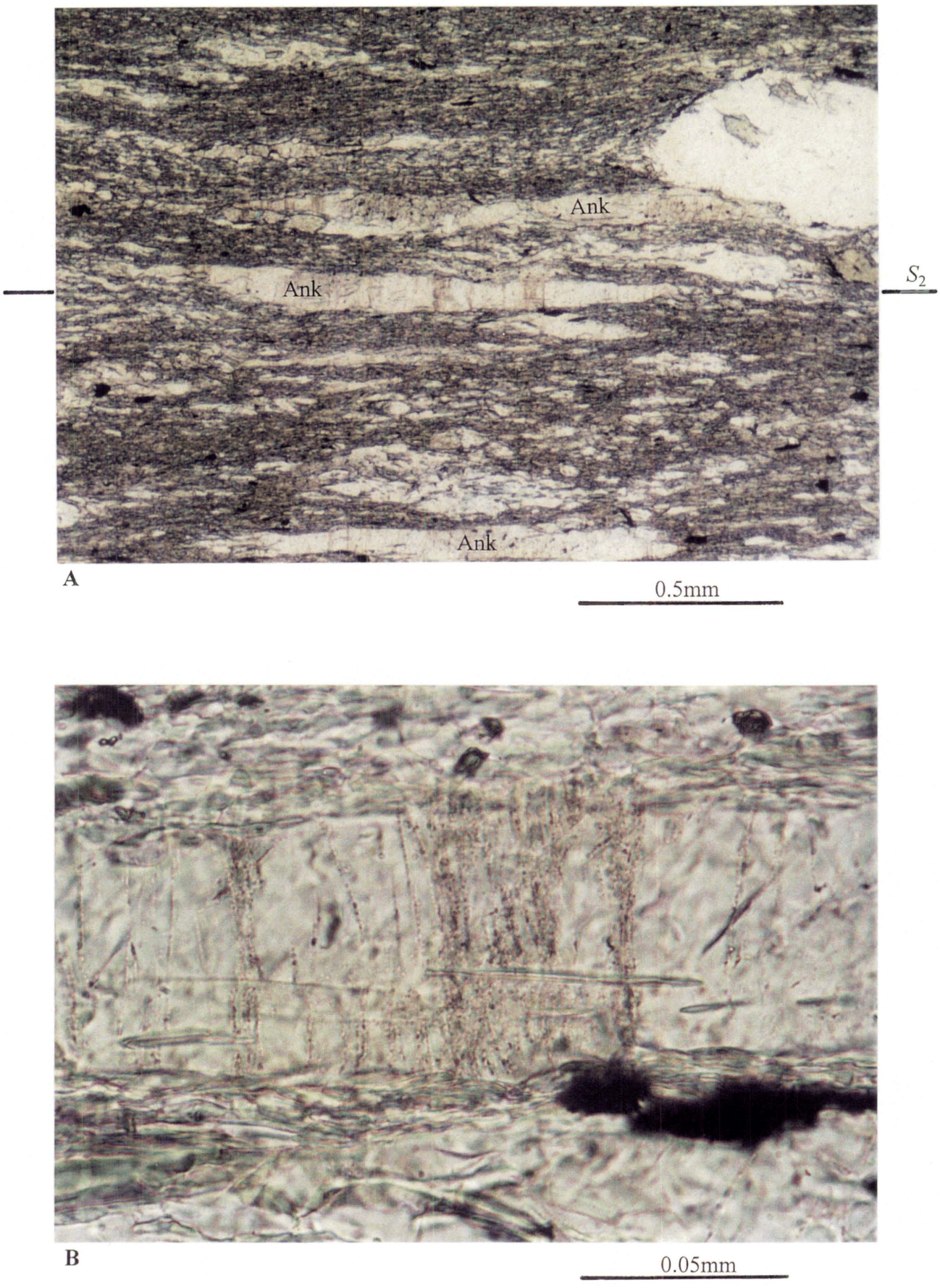

Figure 3.78: Inclusion-free ankerite (Ank) with multiple planes of minute fluid inclusions perpendicular to the grain elongation direction. (B) is a close-up view of ankerite in (A) showing the detail of fluid inclusion planes. RJ108. PPL.

perpendicular to the grain elongation direction (Fig. 3.78). These planes are very similar to that seen in "stretched" vein crystals of Durney and Ramsay (1973). According to these authors, the planes of fluid inclusions represent repeated microfracturing of individual crystals, as they were stretched, with the subsequent healing by overgrowth of each fracture. Although some ankerites, particularly in RJ327, display undulatory extinction and slight curvature of twin lamellae (Fig. 3.77), there is no convincing petrographic evidence to suggest that elongation of ankerites is a result of plastic deformation. Thus it would appear that whilst the inclusion-rich ankerites have acted rigidly, the inclusion-free ankerites are elongate as a result of growth during strain.

The ankerite twin lamellae are narrow and make no more than 10% of crystals, except in RJ327, where they may be as high as 15%. On average, about 39% of ankerites are twinned and 13% of those possess two or, very rarely, three sets of lamellae. The percentage of ankerites twinned, particularly those that contain two or more sets, is probably higher in reality because of a "blind spot" that exists in measuring planar features on the U-stage (Shelley 1993, p.323). In RJ327, 67% of the ankerites are twinned, and 25% of the ankerites possess two or more twins.

Sample number	Location	Grid reference (M26)	mean angle (*c*-to-twin pole)	standard deviation (*c*-to-twin pole) and population
RJ99	1st Ck. north of Staircase Ck.	749348	63.2	3.7 n=92
RJ103	2nd Ck. north of Staircase Ck.	748348	63.1	4.5 n=154
RJ107	2nd Ck. north of Staircase Ck.	749349	63.6	4.5 n=125
RJ108	2nd Ck. north of Staircase Ck.	749349	63.9	5.1 n=130
RJ117	Kiwi Creek	749355	63.0	4.7 n=97
RJ126	Arena Creek Catchment	740331	63.2	4.3 n=131
RJ279	3rd Ck. north of Staircase Ck.	748350	63.5	4.4 n=114
RJ309	Suspicion Creek	745339	63.0	4.2 n=117
RJ314	Arena Creek Catchment	739329	64.6	4.1 n=100
RJ322	4th Ck. north of Staircase Ck.	747351	63.6	4.1 n=140
RJ325	4th Ck. north of Staircase Ck.	748351	62.9	4.5 n=86
RJ327	4th Ck. north of Staircase Ck.	748351	62.5	3.8 n=234

Table 3.3: A listing of the 12 ankerite bearing samples giving location details and also *c*-to-twin pole mean angle and standard deviation.

3.10.4 Analytical procedure

In each sample, two thin-sections were made, one parallel to the stretching lineation and perpendicular to the foliation, the other perpendicular to both the stretching lineations and foliation. Using the U-stage, at least 140 measurements of the *c*-axis were made on

ankerites encountered on traverses across each thin-section. Where ankerites contained twin lamellae, these were also recorded. The measurements were then entered on to a computer. Utilising a modified version of CALCSTRESS (Shelley 1989), called ANKSTRESS, which is a computerised version of the Turner method, ideal compression and tension directions were calculated.

3.10.5 Results

Contoured stereographic projections of ankerite *c*-axes, twinned ankerite *c*-axes, poles to *f* lamellae, compression directions, and tension directions are presented in Figures 3.79 to 3.83. The mean angle and standard deviation between the twin lamella pole and the *c*-axis for each sample is given in Table 3.3.

Ankerite *c*-axis plots show near random distributions (e.g. RJ108, RJ126, RJ314 in Fig. 3.79) although many show a weak maximum perpendicular to the foliation (e.g. RJ309 and RJ327). Twinned ankerite *c*-axis plots consistently show a preferred orientation of *c*-axes at a high angle to foliation (Fig. 3.80), with some showing a girdle in which the axis is the stretching lineation (e.g. RJ103, RJ108).

In all samples the mean angle between the twin lamella pole and the *c*-axis (Table 3.3) is almost the same as the ideal interfacial angle between the *f*-twin pole and *c*-axis in dolomite (62.5°, Turner and Weiss 1963). This similarity indicates that ankerite has the same geometric twin law as dolomite. In RJ327, where slightly curved lamellae occur more frequently than any other sample, the angles between twin lamellae poles and *c*-axes show a normal distribution with a mean of 62.5° and a standard deviation of 3.8° (Fig. 3.84). Allowing for operator error in determining the exact orientation of *c*-axes and lamella poles, coupled with the fact that the mean interfacial angle matches exactly the ideal interfacial angle, the possibility of internally rotated lamellae resulting from plastic slip postdating twin formation, is thought to be relatively minor in RJ327. It is therefore believed that constructed compression and tension direction plots for all samples, based on the Turner method for dolomite, can be confidently treated at face value.

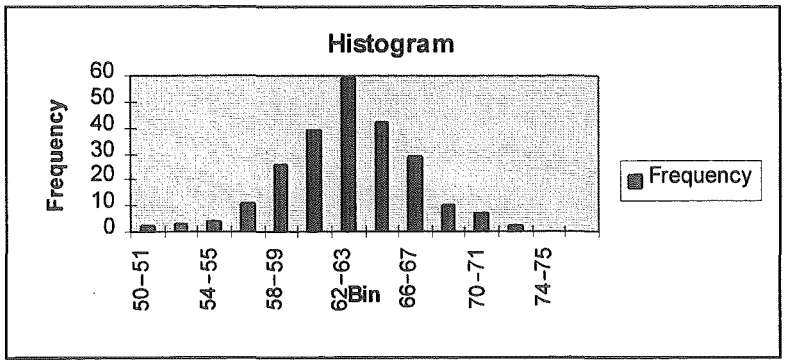

Figure 3.84: Histogram of c-to-twin pole angles in RJ327, n=234.

Compression direction (σ_1) plots show a very strong maximum subperpendicular to the foliation (Fig. 3.82). Some maxima have an associated girdle with axis subparallel to the stretching lineations (e.g. RJ103, RJ117, RJ325). Tension direction (σ_3) plots also show a very strong maximum subparallel to the stretching lineation (Fig. 3.83). Based on the orientations of σ_1 and σ_3, the intermediate stress axis (σ_2) is parallel to the foliation but perpendicular to the stretching lineation. Although compression and tension directions plot more or less perpendicular to the foliation and parallel to the lineation respectively, it is noticeable in the compression and tension direction plots of RJ117, RJ279, RJ309, RJ314, and RJ327 (Fig. 3.82 and 3.83) that there is a slight asymmetric distribution. In these samples, compression directions plot about 6° to 18° from the perpendicular to the foliation.

Clearly the distribution of compression directions and the *c*-axes of twinned ankerite are related. This comes as no surprise because the ideal compression direction for *f*-twinning in dolomite is 17.5° from the *c*-axis (Fig. 3.75). It cannot be argued that the strong maximum of compression directions is intimately related to a pre-existing *c*-axis preferred orientation (e.g. RJ309, RJ327 in Fig. 3.79 and 3.82) because samples which show a random *c*-axis distribution show an equally strong preferred orientation of compression directions (e.g. RJ108, RJ126, RJ314 in Fig. 3.79 and 3.82).

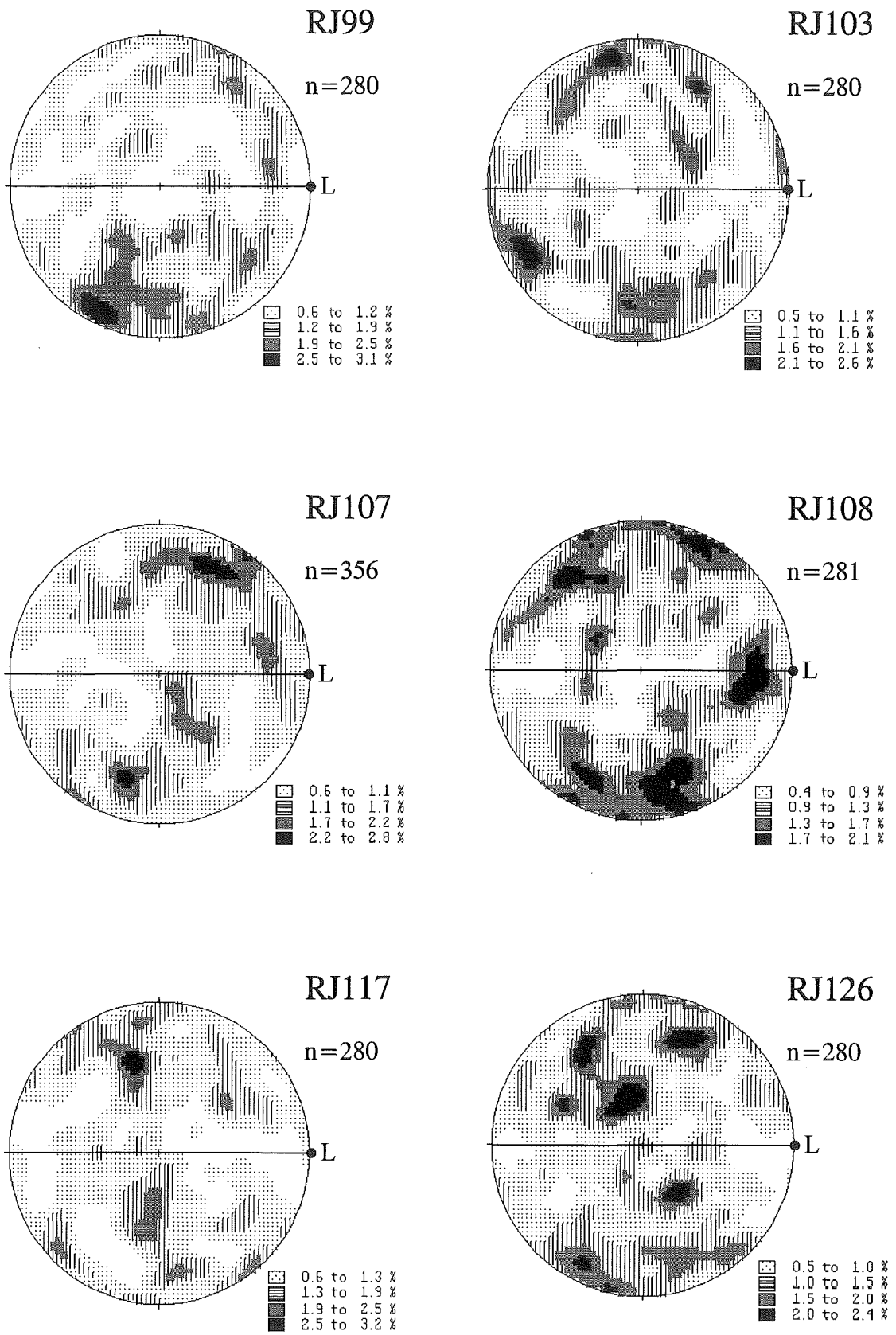

Figure 3.79: Contoured stereographic projections of ankerite *c*-axes from 12 D_2 tectonite samples, undifferentiated Haupiri Group, Boulder Lake domain. Horizontal line represents S_2 foliation. L= S_2 stretching lineation.

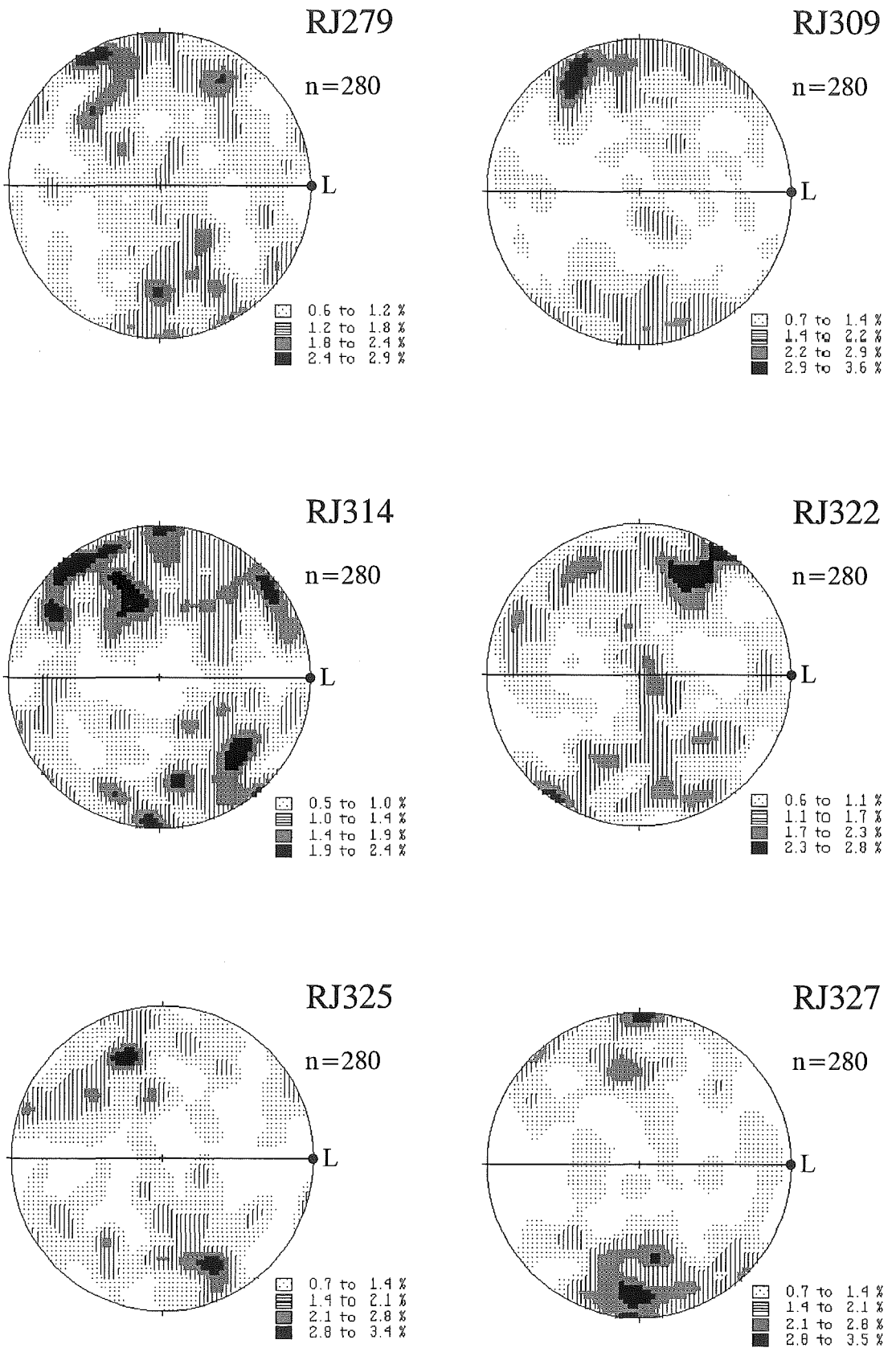

Figure 3.79 continued

Twinned ankerite *c*-axes

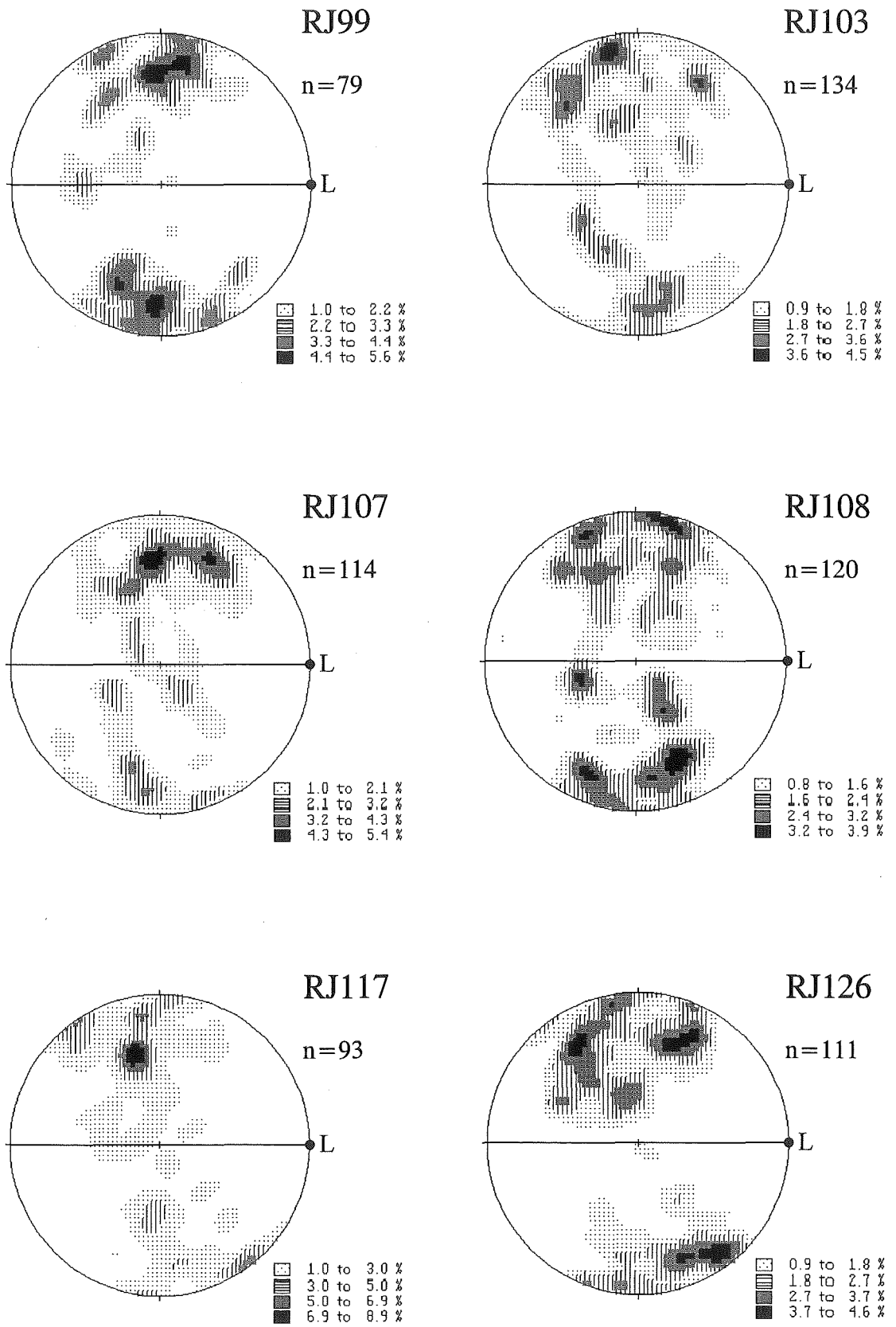

Figure 3.80: Contoured stereographic projections of twinned ankerite *c*-axes from 12 D_2 tectonite samples, undifferentiated Haupiri Group, Boulder Lake domain. Horizontal line represents S_2 foliation. L= S_2 stretching lineation.

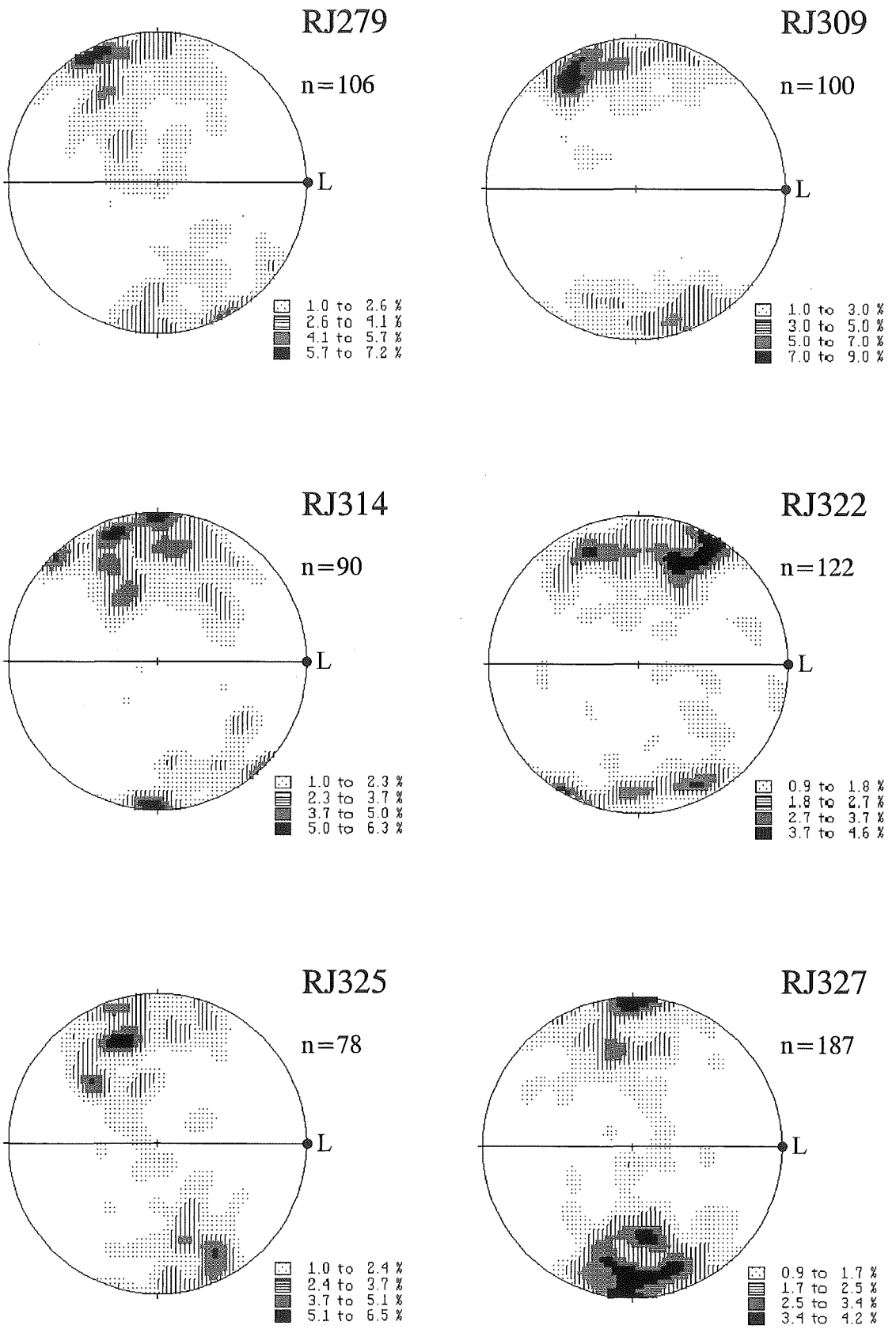

Figure 3.80 continued

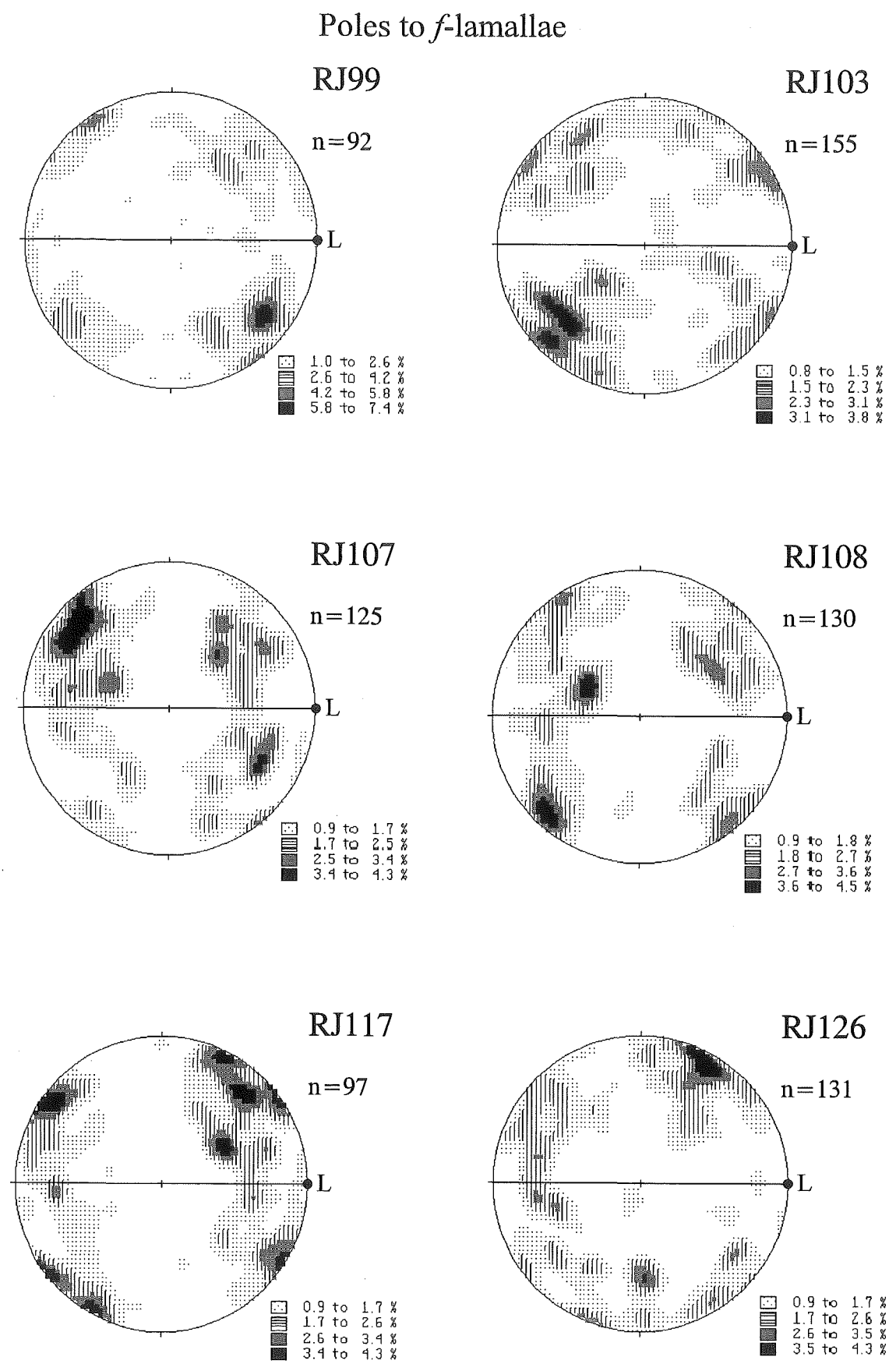

Figure 3.81: Contoured stereographic projections of poles to *f* lamallae from 12 D_2 tectonite samples, undifferentiated Haupiri Group, Boulder Lake domain. Horizontal line represents S_2 foliation. L= S_2 stretching lineation.

Poles to *f*-lamallae

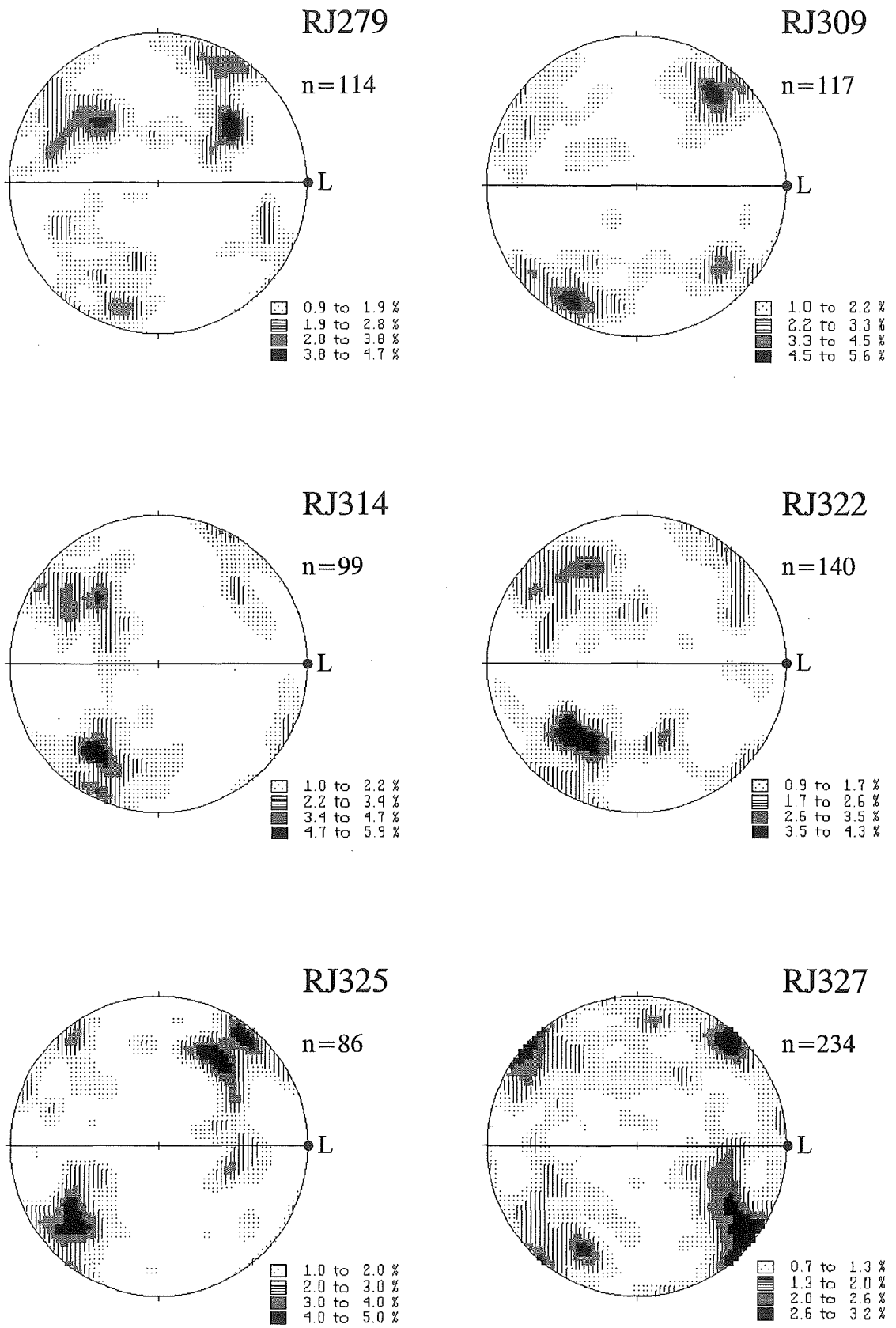

Figure 3.81 continued

Compression directions

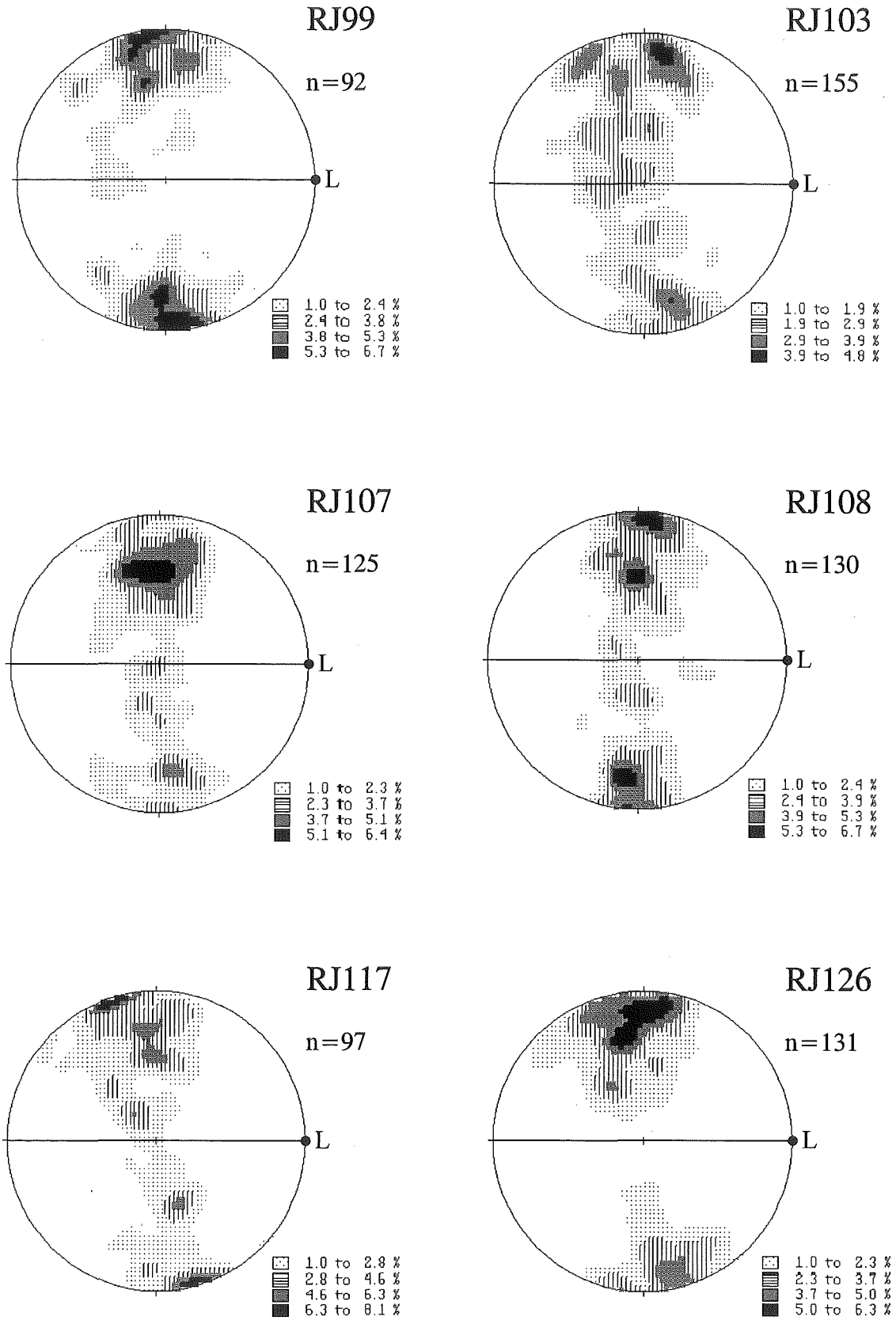

Figure 3.82: Contoured stereographic projections of compression directions from 12 D_2 tectonite samples, undifferentiated Haupiri Group, Boulder Lake domain. Horizontal line represents S_2 foliation. L= S_2 stretching lineation.

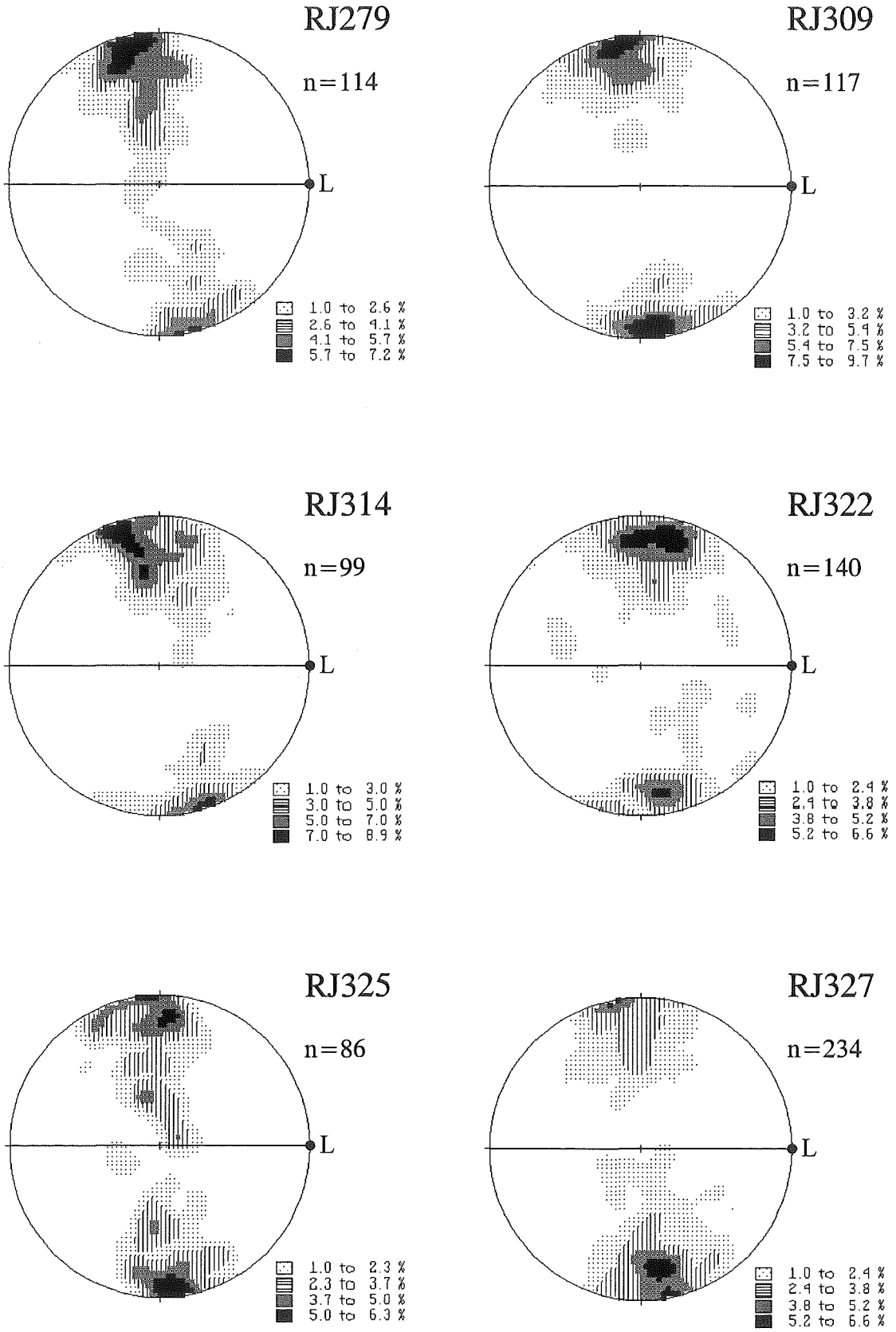

Figure 3.82 continued

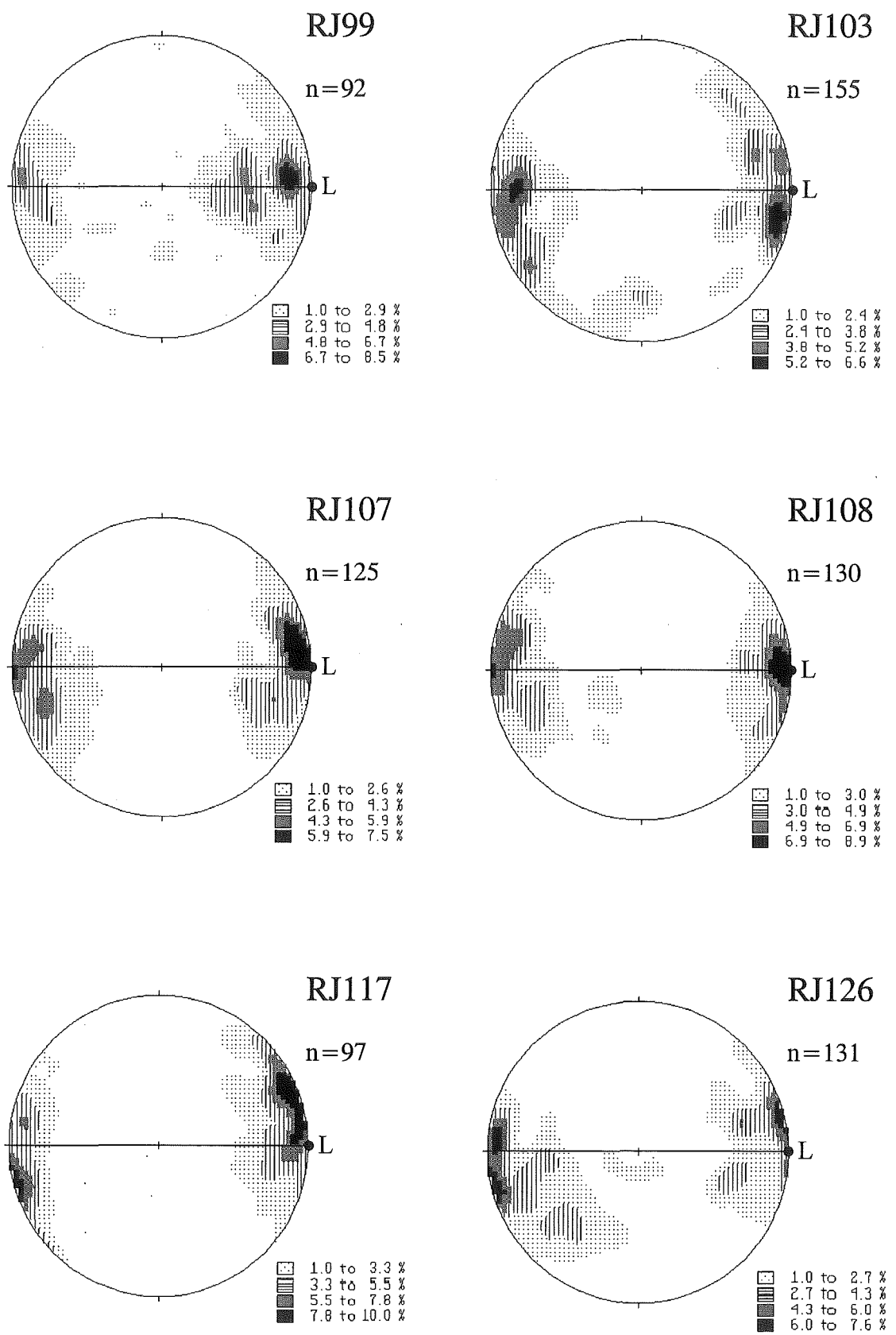

Figure 3.83: Contoured stereographic projections of tension directions from 12 D_2 tectonite samples, undifferentiated Haupiri Group, Boulder Lake domain. Horizontal line represents S_2 foliation. L= S_2 stretching lineation.

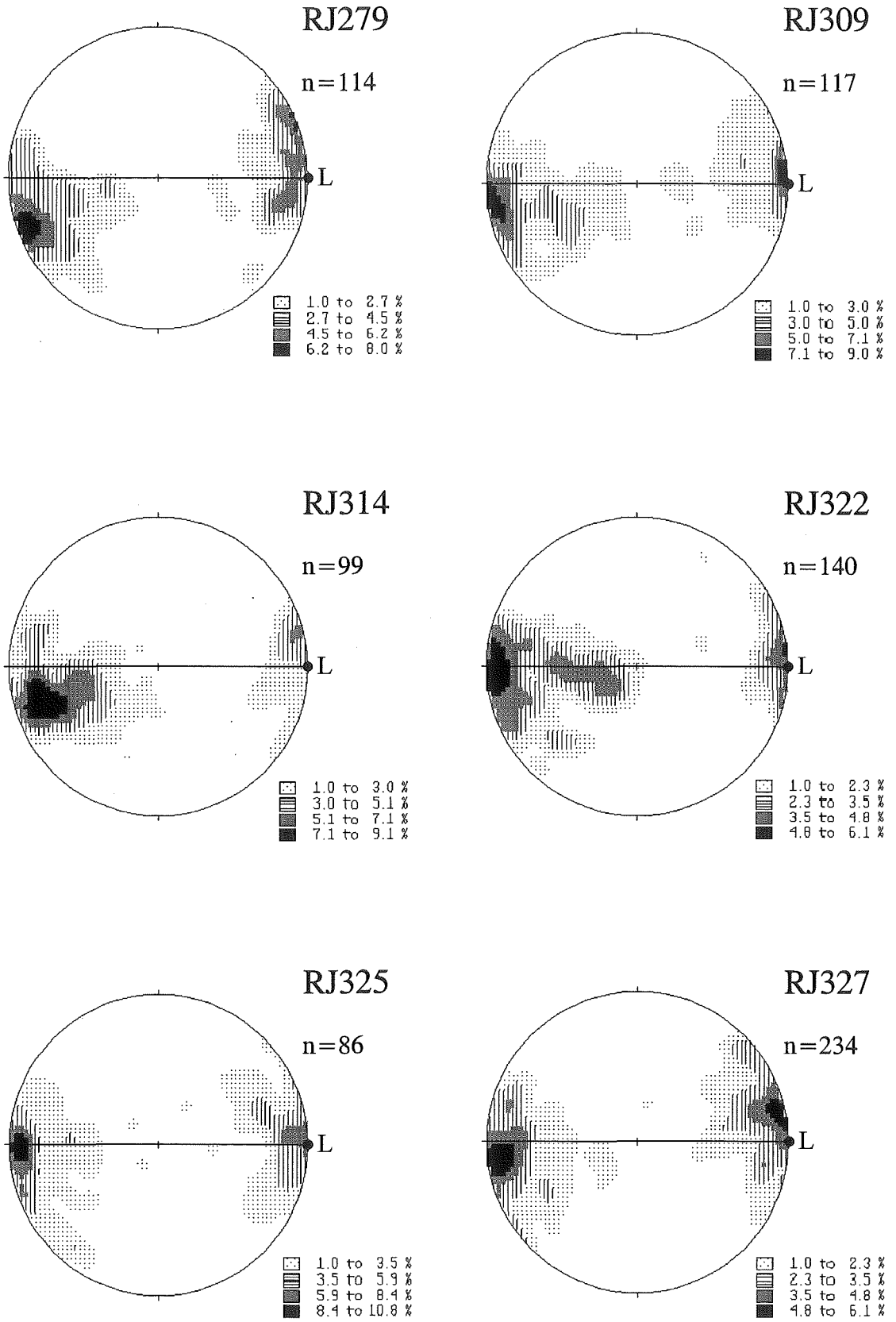

Figure 3.83 continued

3.10.6 Discussion

We know that in most calcite tectonites, the visible twin lamellae are related to a late minor deformation event (Turner and Weiss 1963). In calcite bearing samples from the zone of D_2 deformation, calcite grains are well-twinned. The twinning is probably related to D_3 deformation, or a later deformation, given that the calcite SPO is related to D_3 (Section 3.7.9). In contrast, ankerites show very little twinning in exactly the same samples. In the Snow River and in more southern areal domains, where the metamorphic facies and strain is lower (e.g. Lonely Lake and Kakapo Peak), ankerite porphyroblasts are very rarely twinned. These observations suggest ankerite does not twin easily, and any twinning is probably related to a relatively major strain event. Ankerite twinning almost exclusively occurs within the zone of D_2 deformation implying that twinning is related to D_2. Twinning related to D_3 is highly unlikely because it is difficult to envisage a scenario where ankerite did not twin under the high strain event of D_2, but did under the lesser strain event of D_3. Further evidence to suggest that twinning is related to D_2 is that the orientation of σ_2, which is orthogonal to σ_1 and σ_3, is the same orientation as Y of the D_2 finite strain axes.

Since twinning is most likely to be related to D_2, then it appears that the temperature for twin-gliding to be operative requires temperatures of at least low grade metamorphism (greater than ~250°) based on D_2 metamorphic mineralogy. This requirement is somewhat similar to dolomite.

From Section 3.9.2, it was concluded that strain associated with D_2 is non-coaxial. Where determined paleostress directions are orthogonal to S_2, these suggest that ankerite twinning accommodated a predominantly pure shear component of D_2 non-coaxial strain. A pure shear is supported by the frequent occurrence of doubly twinned ankerites, which in calcite at least, is commonly observed in coaxial deformation experiments but not in simple shear experiments (Schmid *et al.* 1987).

It was noted earlier that the results of five samples show an asymmetry of paleostress directions with respect to the foliation plane. When looking down the dip of the foliation (i.e. towards the E or ESE), the orientation of σ_1 in all four samples equates to 6°-18° clockwise rotation from the perpendicular to the foliation. This orientation is not

compatible with non-coaxial strain associated with top to the south sense of shear. The orientation of the σ_1 asymmetry is difficult to explain.

If twinning makes up only about 10% or less for most twinned ankerites, then it cannot account for much strain (Turner and Weiss 1963). Is there any other evidence that ankerite has accommodated D_2 plastic strain? Slightly curved lamellae and undulatory extinction proves that some plastic slip has been operative, presumably on {0001} by analogy with dolomite slip systems (Higgs and Handin 1959), but as discussed in Section 3.10.5, slip has been relatively minor since twin formation. In some samples, a weak *c*-axis maximum perpendicular to the foliation occurs. This maximum is consistent with basal slip but all evidence suggests the elongation of ankerites is a result of growth (Section 3.10.3). It is more likely that the *c*-axis maximum results from a growth preferred orientation of ankerite. To summarise, D_2 plastic strain accommodation in the ankerites is small and this is supported by evidence of micas and solution seams wrapping around them like that of a rigid object (Fig. 3.46 and 3.64). Experimental work by Higgs and Handin (1959) and Barber *et al.* (1981) show that dolomite, and presumably ankerite, is quite strong and considerably less plastic than calcite at low temperature. Thus it is concluded that early ankerite has essentially acted rigidly, and strain shadow development has been accommodated by ankerite growth. This is beautifully illustrated by the inclusion-rich ankerite porphyroblasts and inclusion-free ankerite strain shadows shown in Figure 3.45.

To conclude this section, the study of ankerite twinning finds good evidence that D_2 non-coaxial strain has been extremely partitioned in ankerite bearing tectonites. Phyllosilicates have accommodated the simple shear component, whereas ankerite porphyroblasts have accommodated pure shear. Pure shear strain in the ankerite porphyroblasts was small and was accommodated plastically by way of twin-gliding and slip, and brittlely by repeated microfracturing (Section 3.10.3). The conclusion concurs with the model of strain partitioning forwarded by Bell (1985).

CHAPTER 4

ADELAIDE TARN and LONELY LAKE DOMAINS

Chapter frontispiece: View of Lonely Lake domain looking towards the NNE. Drunken Sailors (centre right peak) is in Takaka terrane. Pt. 1630 (centre left peak) is in Buller terrane. At the low point in the ridge between Drunken Sailors and Pt. 1630 is the Anatoki Fault. Lonely Lake resides in the centre of a cirque basin immediately below the low point in the ridge. Dragons Teeth is in the far left background.

4.1 Introduction

This chapter combines two areal domains, Adelaide Tarn and Lonely Lake (Map 2), which are located to the south of Boulder Lake domain (Fig. 1.2). The two domains have been combined into one chapter because of the strong structural similarities between them.

Given that a significant amount of outcrop occurs above the bushline, exposure of mesoscale structures is excellent, making it possible to confidently construct a detailed structural history of Buller and Takaka terrane rocks in the Adelaide Tarn and Lonely Lake domains.

In this chapter the Buller terrane lithology and structure will be described first, followed by that of the Takaka terrane. The geometry of the Anatoki Fault will be described. Finally, the structures in both the Buller and Takaka terranes will be compared and discussed briefly.

4.2 Buller terrane: Lithology

The Adelaide Tarn and Lonely Lake domains, west of the Anatoki Fault, is dominated by rock that is best termed Douglas Formation (Golden Bay Group). The Douglas Formation in these domains is typically a grey, well-laminated, slaty siltstone. Light grey quartz-rich laminae (silt to very fine sand size) alternate with dark grey mica-rich laminae, and the quartz-rich laminae are frequently lensoidal. Individual laminae usually have a thickness in the range 0.5-5mm, and sets of laminae often form quartzitic- or pelitic-rich beds, typically 5-10cm thick. Within the Douglas Formation of the two domains there are areas where quartz sandstone beds are prominent (very fine to fine sand size, 1-10cm thick), and are interbedded with typical well-laminated siltstones (referred to here as sandy bedded Douglas Formation). Groups of quartz sandstone beds, up to 3m thick, can occur.

To the west of the Douglas Formation are rocks equated with the Leslie Formation (Golden Bay Group). These rocks consist of black, well-bedded, graphitic shale/slate and

occasional beds of quartz sandstone up to 60cm thick. The black shale often splits along bedding planes to reveal graptolites. Along the western margin of the Adelaide Tarn domain, two very thick quartz sandstone horizons (at least 50m thick) are mapped and equate with the Leslie quartzites of the Fenella Fault Zone (Cooper 1989).

Between typical Douglas and Leslie Formations lithologies is a transitional zone, approximately 150m thick, where lithologies are intermediate in character.

Immediately adjacent to the Anatoki Fault, north of The Needle and south of Drunken Sailors (Map 2), are slivers of dark grey to black graphitic slaty shale interbedded with thick beds, up to 1m, of quartz sandstone. In most places the slaty shale predominates over quartz sandstone but occasionally the opposite is true. Groups of quartz sandstone beds, up to 15m thick, can occur. The slaty shale commonly contains quartz-rich siltstone laminae and ankerite porphyroblasts.

4.3 Buller terrane: Structure

Two major deformation events are recognised within the Buller terrane rocks of the Adelaide Tarn and Lonely Lake domains: D_1 and D_3. (D_2 is not developed. See Section 2.1 for explanation of notation).

4.3.1 D_1 mesoscale structures

The first deformation event to affect Buller terrane rocks of the Adelaide Tarn and Lonely Lake domains is represented by mesoscale folding (F_1) and an associated axial planar slaty cleavage (S_1). F_1 and S_1 appear to be extensively developed throughout the two domains but are best preserved and outlined in sandy bedded Douglas Formation (Fig. 4.1 and 4.2). Areas of sandy bedded Douglas Formation include those near Pt.1450 (northernmost part of the Adelaide Tarn domain), the Adelaide Tarn hut area, the Anatoki Peak area, and the area immediately west of Lonely Lake (see Map 2). All D_1 structural measurements in the Adelaide Tarn domain come from near Pt. 1450 whereas in the Lonely Lake domain, measurements come mostly from the area west of Lonely Lake. In these two areas, D_3 mesoscale folding is negligible and therefore the orientations of D_1 structures may possibly be close to original.

Figure 4.1 (A): Tight F_1 fold hinge in sandy bedded Douglas Formation near Pt. 1450, Adelaide Tarn domain. Purple backpack for scale. (B): Close-up view of (A) showing S_1 axial planar cleavage at fold hinge. S_1 cleavage runs from bottom left to top right. S_3 crenulation cleavage is seen orthogonal to S_1 running from top left to bottom right. Hammer for scale. M26/ 723318.

Figure 4.2: S_1 axial planar cleavage and F_1 fold hinge in sandy bedded Douglas Formation near Pt. 1450, Adelaide Tarn domain. Fold shape is E4. Photo is taken at an odd angle giving an impression that the fold is recumbent but in reality is gently inclined (axial plane dips 23°SE) Hammer for scale. M26/ 722318.

Figure 4.2

Figure 4.1B

Figure 4.1A

F_1 axial planes strike between N and NE, dipping moderately or gently ESE, in the Adelaide Tarn domain, and strike mainly between NW and NNW, dipping moderately NE, in the Lonely Lake domain (Fig. 4.3). Fold axes are subhorizontal to gently plunging towards the S in the Adelaide Tarn domain, and subhorizontal to gently plunging towards either the NNW or SE-SSE in the Lonely Lake domain (Fig. 4.3). L_0^1 lineations are subparallel to F_1 (Fig. 4.3). F_1 mesoscale folds are tight to isoclinal with western limbs inverted and wavelengths ranging from 20cm to >5m. Fold shapes (see Appendix 3) are mainly D4 to F4, with E4 being the most common (Fig. 4.2).

S_1 slaty cleavage is axial planar to F_1 folds (Fig. 4.3). In F_1 hinge zones, and where laminated horizons occur, transposition of laminae may occur resulting in an incipient layering parallel to S_1. When laminated horizons are traced into F_1 limbs, laminae become subparallel to S_1, and quartz-rich laminae become lensoidal in shape with mica-rich laminae anastomosing around them.

F_1 fold hinges are rarely observed in typical well-laminated Douglas Formation. When observed, F_1 is isoclinal and S_1 is subparallel to bedding, explaining the lensoidal character of quartz-rich laminae. In slaty shale, ankerite porphyroblasts often appear elongate parallel to laminae. No thin-section work was undertaken but the elongation is probably due to ankerite strain fringe development, and suggests S_1 is also subparallel to bedding in the slaty shale.

Bedding orientations in sandy bedded Douglas Formation overlap with that of S_1 cleavage, and plot along a π-girdle in which the axis is approximately subparallel to measured F_1 fold axes (Fig. 4.4).

4.3.2 D_1 microscale structures

S_1 is a penetrative slaty cleavage defined predominantly by aligned muscovite and sericite ± chlorite (Fig. 4.5, 4.18, and 4.19). Quartz and rare feldspar grains are clastic and exhibit strain shadows parallel to S_1. The strain shadows consist of white mica and quartz. In mica-rich laminae, quartz grains display a good SPO parallel to S_1 (Fig. 4.5). Overgrowths parallel to S_1 suggest the SPO is a result of pressure solution.

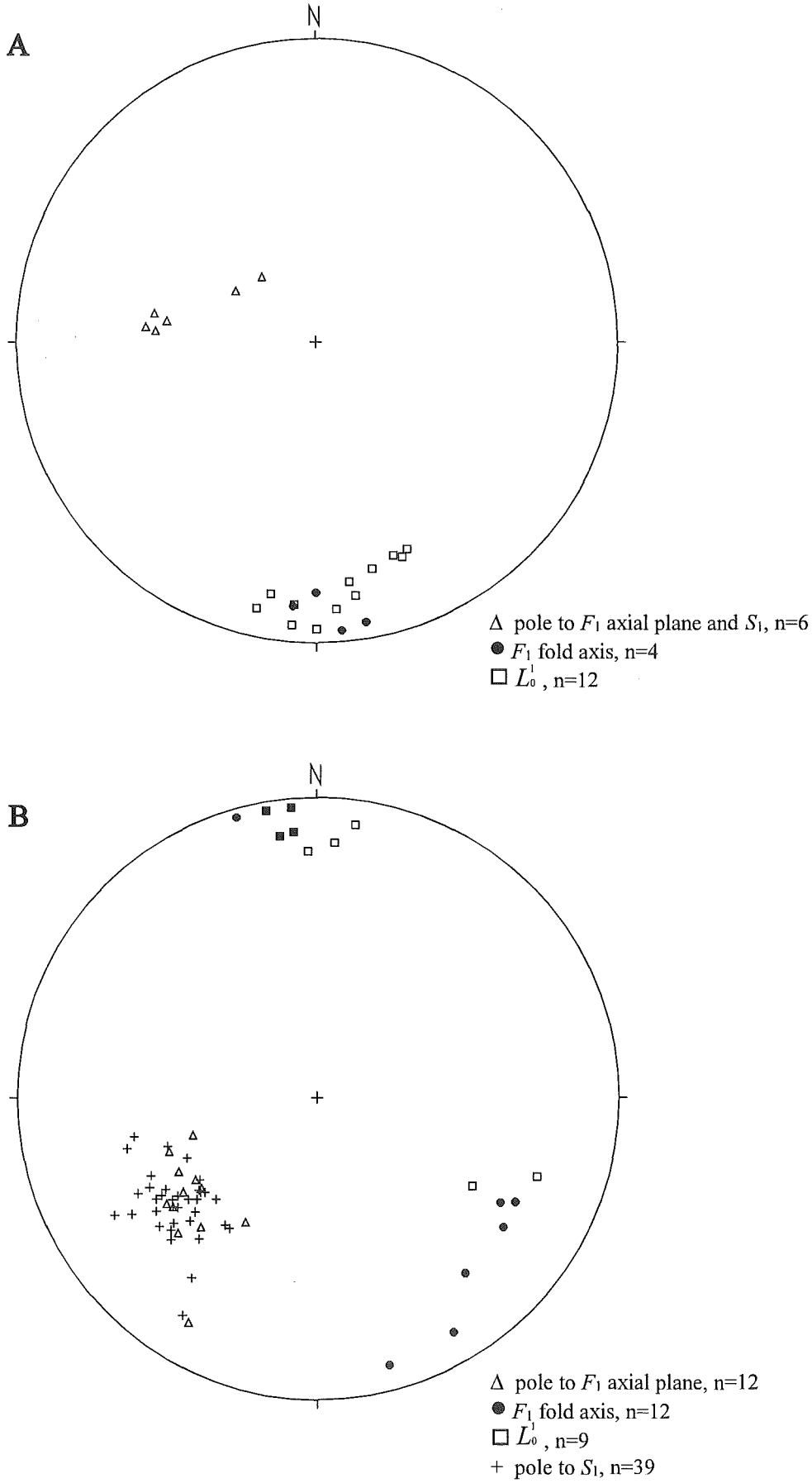

Figure 4.3 (A): F_1, L_0^1, and S_1 orientations in Buller terrane rocks of the Adelaide Tarn domain. All measurements come from sandy bedded Douglas Formation near Pt. 1450. (B): F_1, L_0^1, and S_1 orientations in Buller terrane rocks of the Lonely Lake domain. Most measurements come from sandy bedded Douglas Formation west of Lonely Lake. Note that filled squares are where filled circle symbols overlap with open squares symbols.

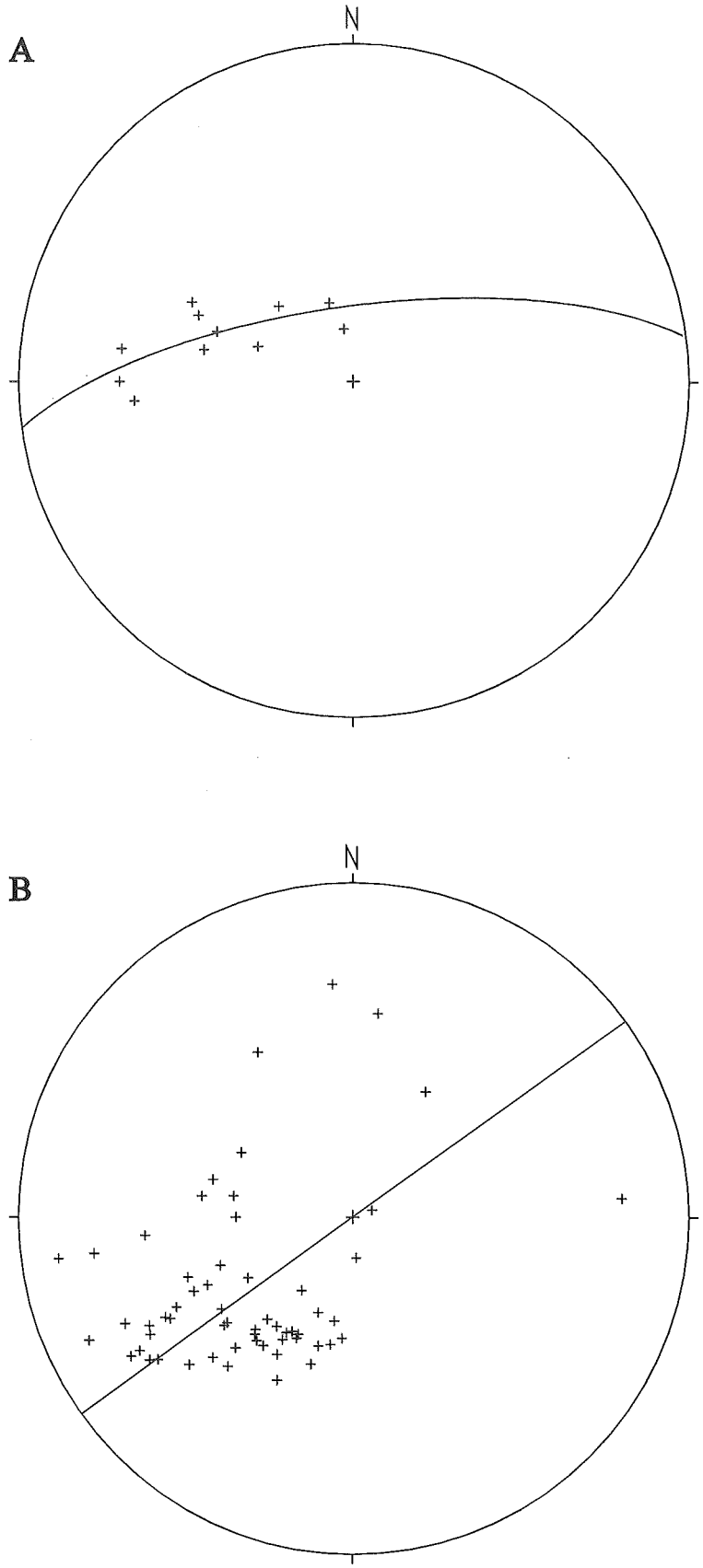

Figure 4.4 (A): Poles to bedding (+) in sandy bedded Douglas Formation, Adelaide Tarn domain, plot on a best fit π-girdle in which the axis (172/18°) is subparallel to measured F_1 fold axes. All measurements come from near Pt. 1450. n=11. (B): Poles to bedding (+) in sandy bedded Douglas Formation, Lonely Lake domain, plot on a best fit π-girdle in which the axis (324/01°) is approximately subparallel to measured F_1 fold axes. n=59

Figure 4.5: S_1 slaty cleavage defined principally by phyllosilicates. This picture is taken within a mica-rich laminae. The isolated quartz grains have undergone pressure solutioning which gives them a SPO parallel to S_1. S_3 zonal crenulation cleavage is seen in the top left corner. RJ43a, Douglas Formation. CPL.

Figure 4.6: Early generation quartz vein showing features of dynamic recrystallisation. RJ203, Douglas Formation. CPL.

Figure 4.7: F_3 open folding of well-laminated Douglas Formation, Lonely Lake domain. Wavelength of fold shown is ~4m. M26/ 714271.

Figure 4.5

Figure 4.6

Figure 4.7

The presence of muscovite, sericite, and chlorite but the absence of biotite suggest D_1 metamorphism was either subgreenschist or lowest greenschist facies.

Away from F_1 hinge zones, S_1 generally appears parallel to bedding on the scale of a thin-section. Occasionally, however, opaque solution seams parallel to S_1, may sometimes be observed at a small angle to bedding (less than 5°). In some samples, quartz-rich laminae are lensoidal and S_1 mica-rich domains wrap around them.

Early generation quartz veins show evidence of plastic deformation and incipient dynamic recrystallisation such as undulatory extinction, deformation bands, and newly developed small strain free grains along vein-quartz grain boundaries (Fig. 4.6).

Clastic quartz c-axes preferred orientation parallel to S_1

In all the Golden Bay Group lithologies of the Adelaide Tarn and Lonely Lake domains, it is a general observation that *c*-axes of clastic quartz grains are preferentially parallel to S_1.

In a recent study on clastic quartz grains in Golden Bay Group equivalents outcropping north of the Boulder Lake domain (Bay Schist of Grindley 1971), Stallard and Shelley (1995) found strong evidence that *c*-axes were preferentially oriented parallel to the stretching lineation within the first developed foliation. Orienting mechanisms considered by the authors included prism <c> slip, static recrystallisation, competitive anisotropic growth, competitive anisotropic solution, and mechanical rotation. Stallard and Shelley (1995) found no evidence for the first four mechanisms and concluded that mechanical rotation was the most likely cause of the LPO parallel to the stretching lineation. In this orientation mechanism, clastic quartz grains are known to be naturally elongate parallel to the *c*-axis (see Stallard and Shelley 1995 for references), and during deformation will mechanically rotate so that the long axes become parallel to the stretching direction. Stallard and Shelley advocate that grain boundary sliding is an essential part of the mechanical rotation orienting process.

The Golden Bay Group samples of the Adelaide Tarn and Lonely Lake domains show similar textures to those investigated by Stallard and Shelley (1995), and thus it is

suggested that mechanical rotation of naturally elongate quartz grains is the most likely cause of producing the observed preferred orientation of *c*-axes parallel to the foliation. It follows that although solution transfer was a major D_1 strain accommodating mechanism, so too was mechanical rotation and associated grain boundary sliding.

4.3.3 D_3 macroscale and mesoscale structures

D_3 is represented by mesoscale and small macroscale folds (F_3) with an associated axial planar crenulation cleavage (S_3). D_3 structures are best displayed in well-laminated Douglas Formation where spectacular "text-book" like folding can be observed (Fig. 4.7). In this section, F_3 folds are described using bedding as the folded reference surface.

In both the Adelaide Tarn and Lonely Lake domains, F_3 axial planes strike generally NE and are moderately dipping towards the SE (Fig. 4.8). F_3 fold axes plunge moderately towards the E or SE with L_0^3 lineations subparallel to them (Fig. 4.8). A plot of poles to bedding in well-laminated Douglas Formation shows a π-girdle distribution in which the axis plots closely to measured F_3 fold axes (Fig. 4.9). It should be remembered that a plot of poles to bedding in well-laminated Douglas Formation is effectively a plot of poles to S_1 as well, since S_1 is subparallel to S_0 in well-laminated rock (Section 4.3.1).

F_3 mesoscale folds are generally close to open although there is a tendency for folds in the Lonely Lake domain to be have larger interlimb angles compared with those of the Adelaide Tarn domain. Wavelengths range from large crenulations (~5cm) up to 10m. Fold shapes are quite variable (Fig. 4.10) but mainly range between D2 to D4, and E2 to E4. In mica-rich rock, folds may be chevron in shape. In many cases it can be demonstrated that mesoscale folds are parasitic to mappable macroscale folds. Macroscale folds have wavelengths of 30-40m. Many of the E to SE trending spurs that descend from the ridge-line that includes Anatoki Peak and Dragons Teeth (best seen on airphotos), are controlled primarily by the orientation of F_3 fold axes (Fig. 4.12, 4.13). Throughout the two domains the N/NE limbs of F_3 antiforms are often inverted, and particularly so in the Adelaide Tarn domain (Fig. 4.11).

Many mesoscale folds observed in the two domains show N/NE vergence (Fig. 4.14) and are parasitic to S/SW limbs of large mesoscale F_3 antiforms (Fig. 4.10). S/SW limbs

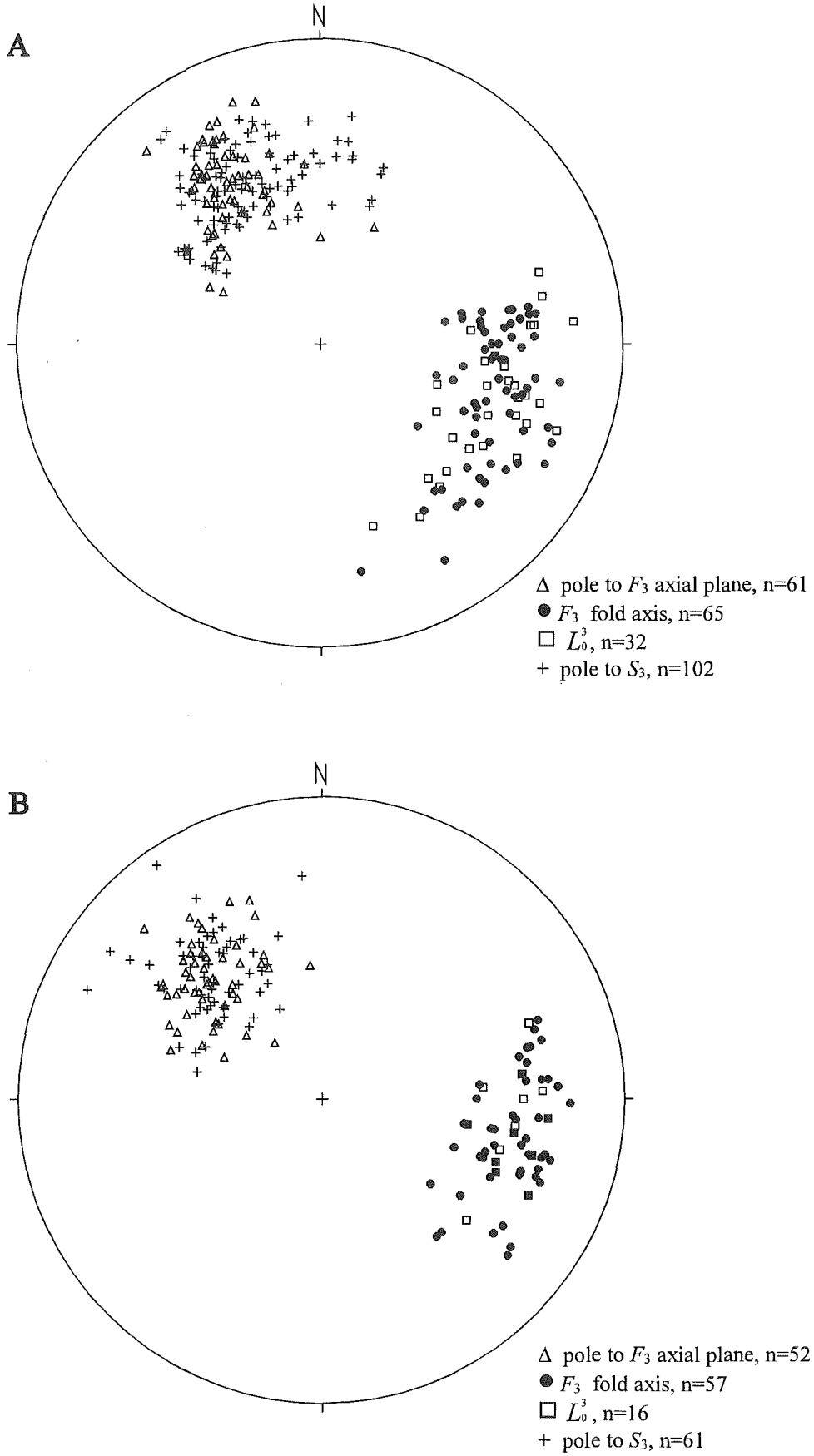

Figure 4.8: F_3, L_0^3, and S_3 orientations in Buller terrane rocks of the Adelaide Tarn (A) and Lonely Lake (B) domains. Note that filled squares are where filled circle symbols overlap with open squares symbols.

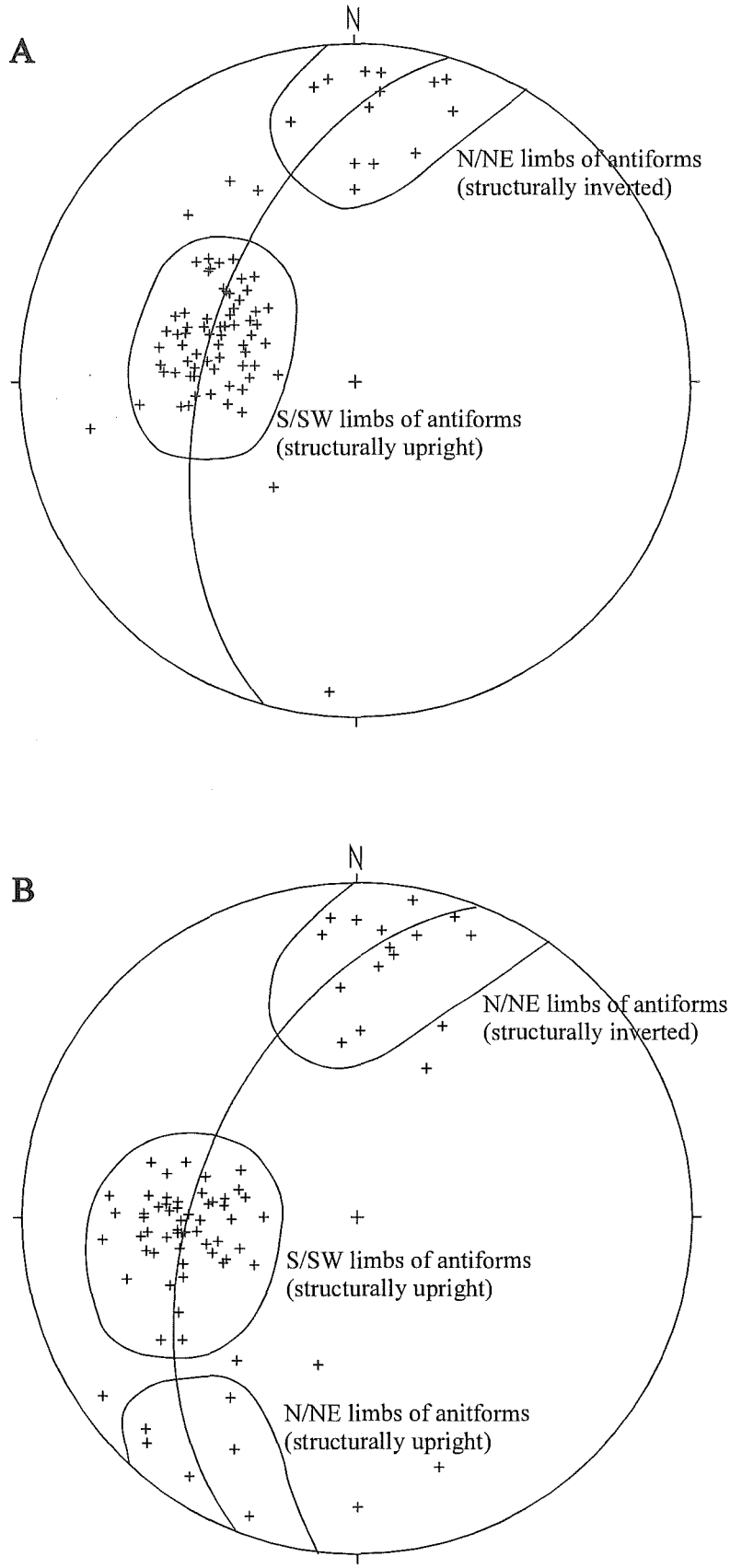

Figure 4.9 (A): Poles to bedding (+) in typical well-laminated Douglas Formation, Adelaide Tarn domain, plot on a best fit π-girdle in which the axis (106/38°) is subparallel to measured F_3 fold axes. n=85. (B): Poles to bedding (+) in typical well-laminated Douglas Formation, Lonely Lake domain, plot on a best fit π-girdle in which the axis (111/44°) is subparallel to measured F_3 fold axes. n=86.

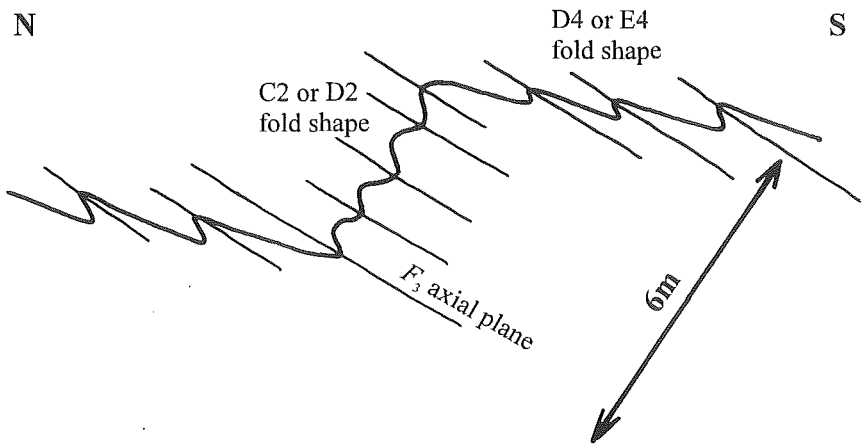

Figure 4.10: Field sketch of N/NE verging F_3 folds in profile just north of Dragons Teeth, Douglas Formation, Adelaide Tarn domain. M26/ 709281.

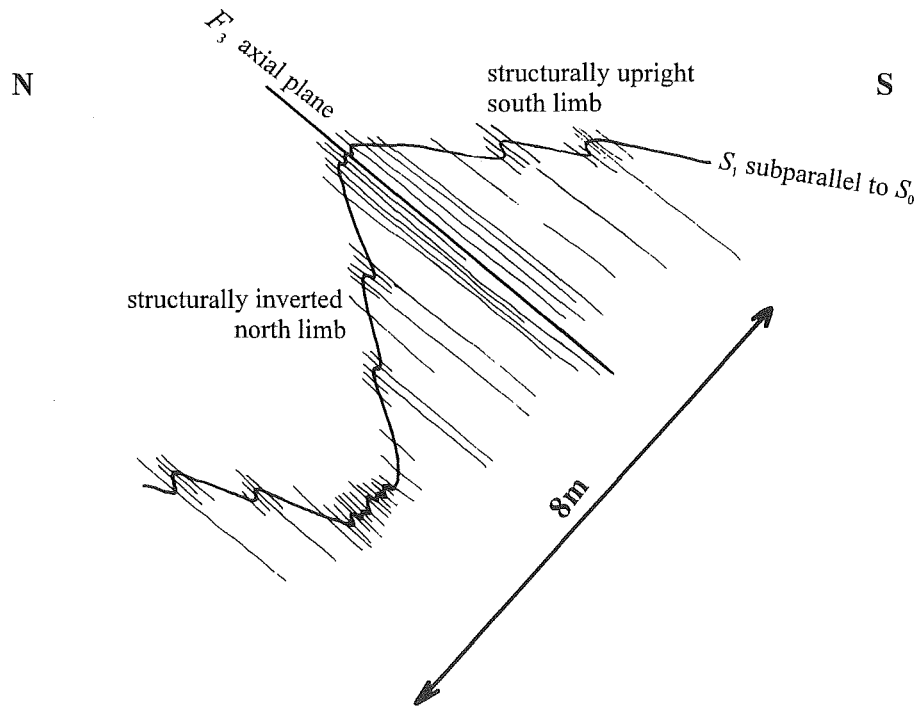

Figure 4.11: Field sketch of typical F_3 fold profile (antiform) in Douglas Formation, Adelaide Tarn domain. M26/ 716292.

Figure 4.12: E to SE trending spurs descending from the ridge-line that includes Anatoki Peak (left) and Dragons Teeth (centre right), are controlled by F_3 fold axes in Douglas Formation. Photo taken from near Yuletide looking SW.

Figure 4.13: Closer view of an east trending spur controlled by a F_3 mesoscale fold axis in Douglas Formation. Photo taken on east face of "The Needle".

tend to dominate the outcrop thus giving the impression that macroscale F_3 folds also verge towards the N-NE. Having said this, there are however, many large mesoscale examples of symmetrically shaped F_3 folds (Fig. 4.11). In the course of mapping, I did not detect any spatial pattern of areas where asymmetrical or symmetrical folding dominated.

F_3 is poorly developed in sandy bedded Douglas Formation and the folds have gentle wavelengths. Very occasionally F_3 is observed to have refolded F_1. In the Adelaide Tarn hut area, "type 3" fold interference patterns are observed (Fig. 4.15), and suggest the F_3 fold axes, which plunge SE, are approximately coaxial with F_1 at that locality (unfortunately, the outcrop did not permit accurate measurement of F_1).

S_3 crenulation cleavage (Fig. 4.16) is axial planar to F_3 folds (Fig. 4.8), and tends to be strongly developed at F_3 hinge zones and around competent units such as quartz veins. Where the rock is very micaeous, S_3 is often slaty in character. In contrast to F_3, S_3 tends to be well-developed in sandy bedded Douglas Formation but only where mica-rich laminae occur. In sandy bedded Douglas Formation, S_3 is clearly associated with the crenulation of both S_0 and S_1 surfaces (Fig. 4.1, 4.15).

On S_3 surfaces there is often a very fine lineation that trends subhorizontally NE-SW (Fig. 4.17). These lineations are approximately perpendicular to F_3 fold axes and L_0^3 lineations, and are thought to represent stretching lineations at the time of F_3 development.

In the one east-west traverse of Leslie Formation, west of Adelaide Tarn, D_3 structures are poorly developed, or absent, in black shale immediately adjacent to the thick quartz sandstone horizon of the Fenella Fault Zone, but become increasingly well-developed in an eastward direction. D_3 structures are well-developed in slaty shale immediately adjacent to the Anatoki Fault.

Figure 4.14: N/NE verging F_3 fold in Douglas Formation, Adelaide Tarn domain. An axial planar crenulation cleavage can be seen. M26/ 722302. Lens cap for scale.

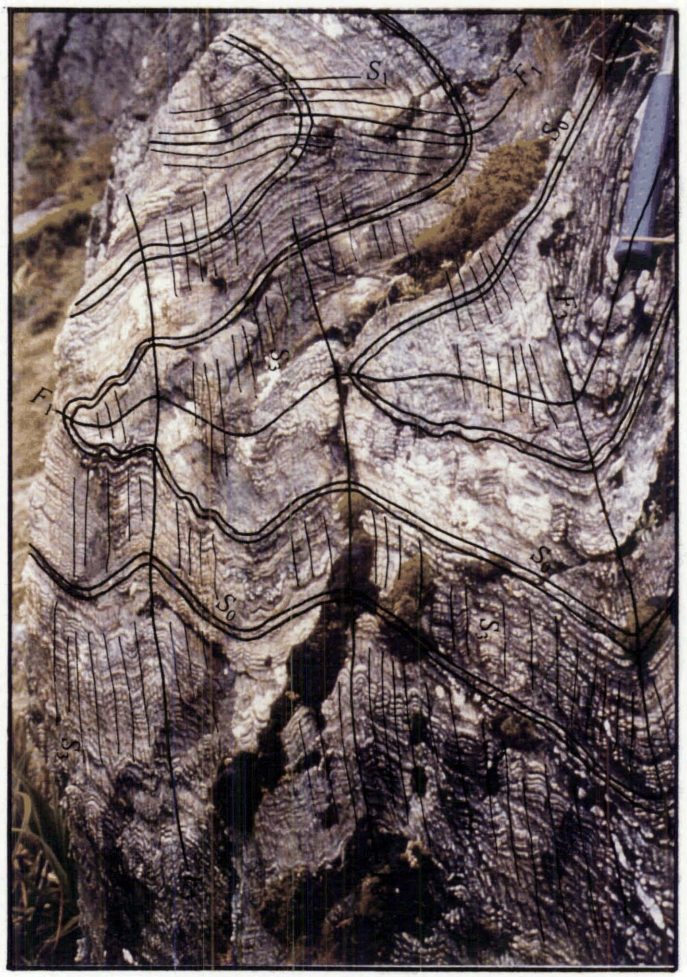

Figure 4.15: Type 3 fold interference pattern of F_1 and F_3 producing a birds head-like structure, sandy bedded Douglas Formation, Adelaide Tarn hut area. M26/ 715291. Blue hammer handle (top right) for scale.

A

B

Figure 4.16 (A): S_3 crenulation cleavage along a F_3 fold hinge, Douglas Formation. Photo taken in vicinity of Adelaide Tarn. Lens cap for scale. (B): S_3 crenulation cleavage, Douglas Formation, Lonely Lake domain. M26/ 717264. Lens cap for scale.

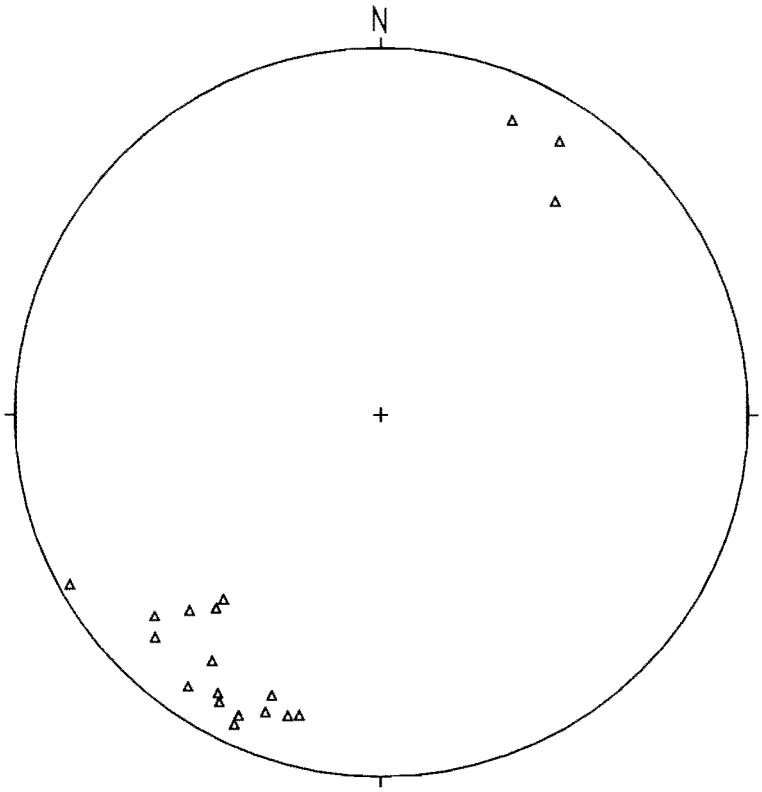

Figure 4.17: Elongation lineations (Δ) on S_3 cleavage surfaces, Buller terrane rocks in Adelaide Tarn domain, n=19.

4.3.4 D_3 microscale structures

In mica-rich laminae, S_3 is associated with the crenulation of S_1 slaty cleavage and can be represented either by a zonal crenulation cleavage with gradational or sharp boundaries (Fig. 4.18), or by a discrete crenulation cleavage (Fig. 4.19). When S_3 is zonal, cleavage domains are characterised by newly crystallised muscovite and sericite oriented subparallel to S_3. Cleavage domains show extreme preferential solutioning of quartz (Fig. 4.18). Typically, S_3 zones have a spacing between 0.1 and 0.3mm. In quartz-rich laminae, S_3 is always a discrete crenulation cleavage.

4.4 Takaka terrane: Lithology

In the Adelaide Tarn and Lonely Lake domains, rocks east of the Anatoki Fault consist of undifferentiated Haupiri Group, volumetrically insignificant Devil River Volcanics Group, and Balloon Mélange. In a north to south direction, undifferentiated Haupiri Group narrows in outcrop width whereas the Balloon Mélange widens (Map 2). A description of the Balloon Mélange, as well as the nature of the contact with undifferentiated Haupiri Group, is given in Chapter 8.

The undifferentiated Haupiri Group rocks in the Adelaide Tarn and Lonely Lake domains consist of conglomerates, grits, sandstones, shales, and minor tuffs/reworked tuffs, and share very similar bedding and compositional characteristics to those observed in the Boulder Lake domain (Section 3.6). Numerous younging directions are provided by graded beds ranging from 3cm to 1m, load casts, flame structures, scour structures, and rare cross-bedding.

Minor intrusives, thought to be part of the Devil River Volcanics Group, are usually green in colour, 3-10m thick, and often concordant with bedding. All intrusives show a metadolerite texture and composition. In the Lonely Lake domain, and within 150m of the Anatoki Fault, are minor intrusive or volcanic units, concordant with bedding, that have been extensively replaced by carbonate and quartz. In the field, these units may be mistaken for grey or orange coloured massive sandstones. Just west of Drunken Sailors is a 7m thick volcanic unit that displays pillow lava structure and small amounts of

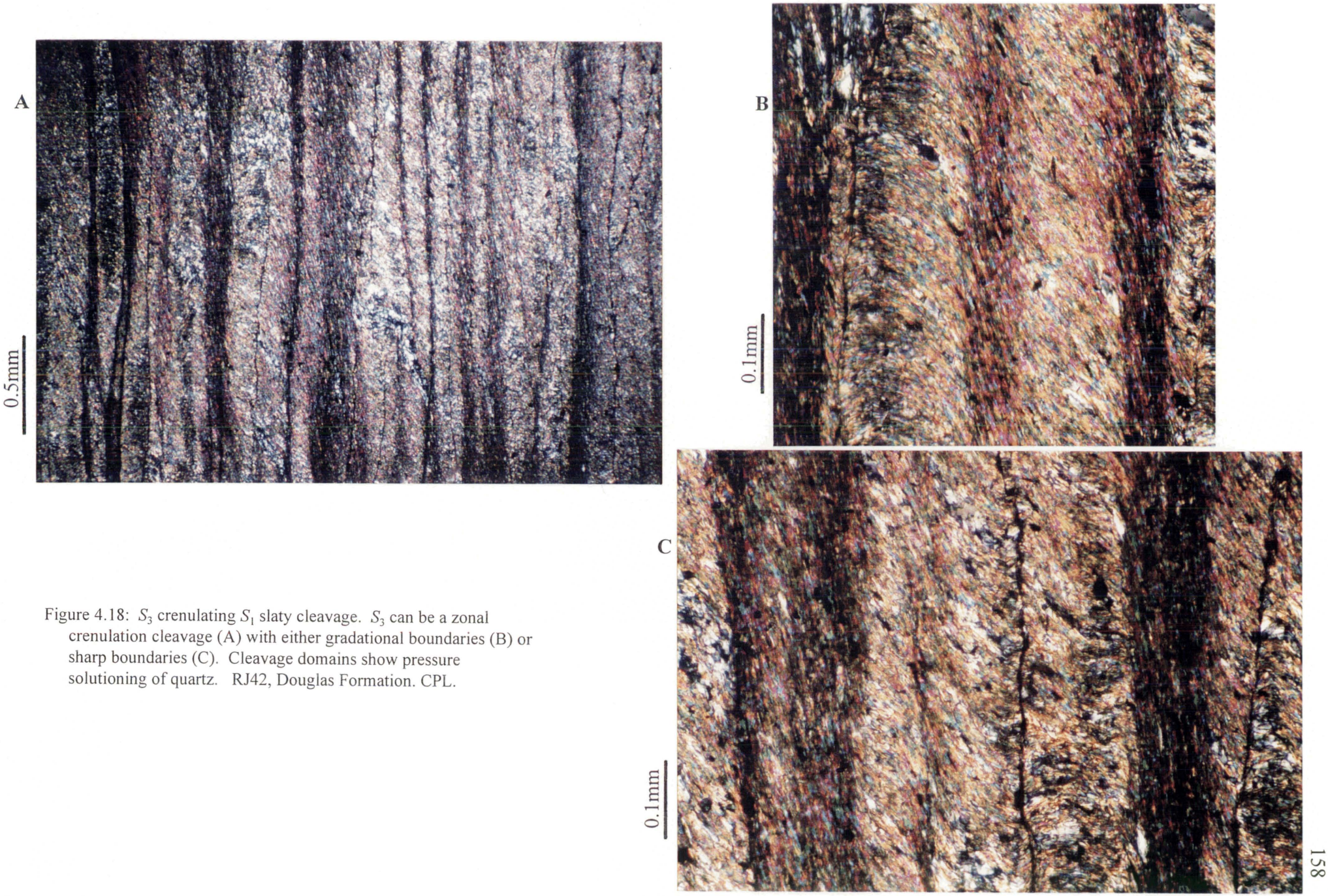

Figure 4.18: S_3 crenulating S_1 slaty cleavage. S_3 can be a zonal crenulation cleavage (A) with either gradational boundaries (B) or sharp boundaries (C). Cleavage domains show pressure solutioning of quartz. RJ42, Douglas Formation. CPL.

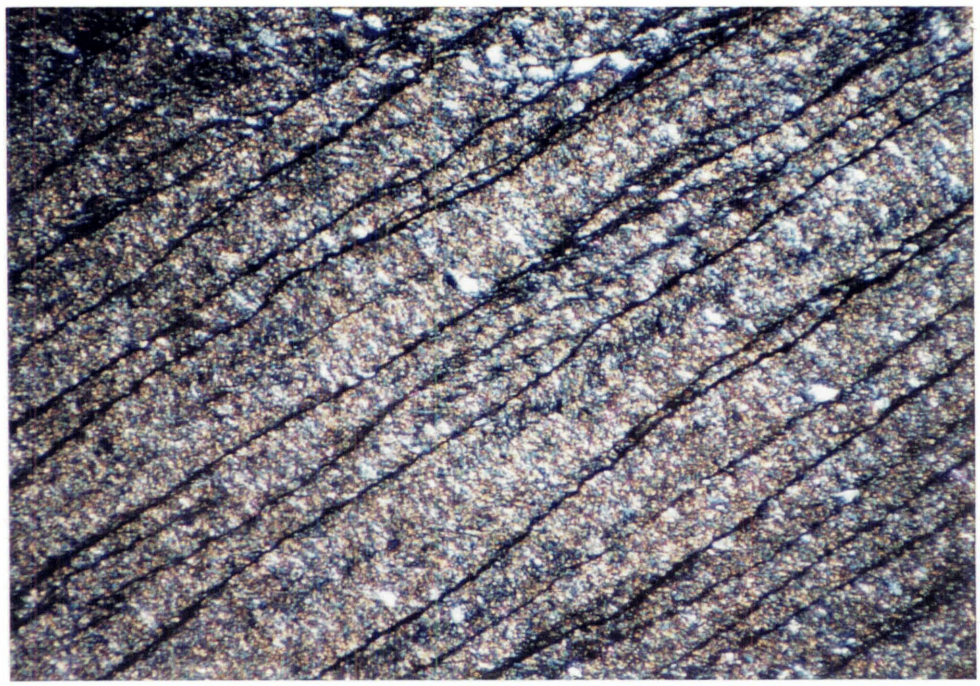

A

0.5mm

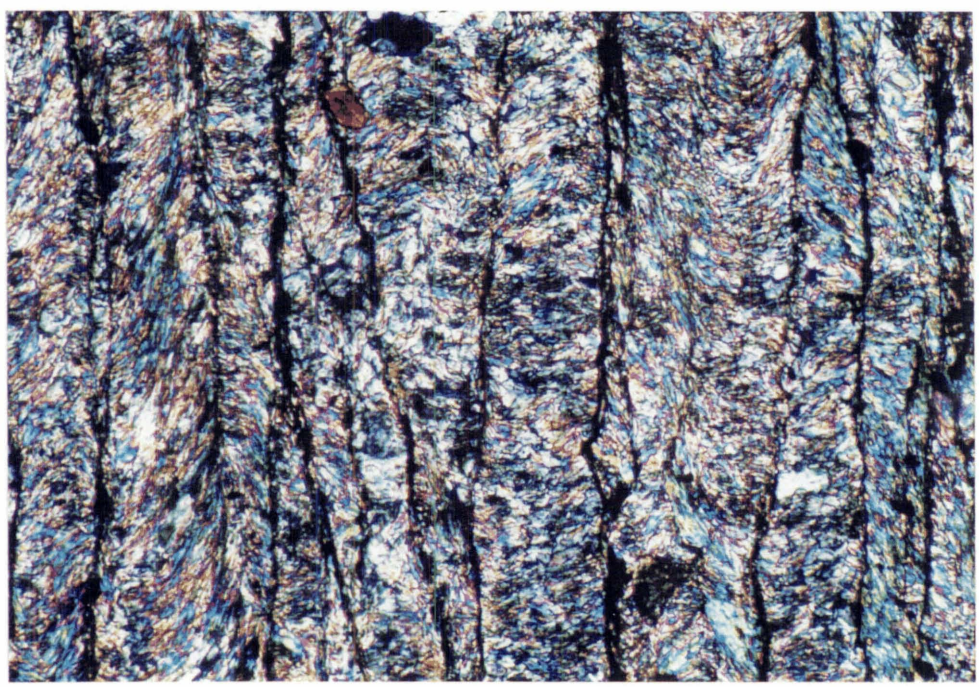

B

0.1mm

Figure 4.19: S_3 discrete crenulation cleavage crenulating S_1 slaty cleavage in sample RJ211 (A) and sample RJ203 (B), Douglas Formation. CPL.

interstitial calcareous sediment. In the north of the Adelaide Tarn domain, a deformed dolerite outcrops immediately east of the Anatoki Fault.

In contrast to the Boulder Lake domain, no interbedded black marble and graphitic slate is observed immediately adjacent to the Anatoki Fault.

In the Adelaide Tarn domain and east of the Balloon Mélange, are sediments very similar to undifferentiated Haupiri Group sediments west of the Balloon Mélange, and they have been designated as such. In the Lonely Lake domain, sediments east of the Balloon Mélange are siltstone and fine sandstone and their assignment is less certain. No analysis of the siltstones and fine sandstones was undertaken but they may be related to Junction Formation (see Section 8.5). On the eastern boundary of the Adelaide Tarn domain is a thick pile (up to 300m thick) of Devil River Volcanics Group basic intrusives and volcanics.

Ankerite metasomatism occurs sporadically throughout the two domains. However, within 60m of the Anatoki Fault, and exclusively within the Lonely Lake domain, undifferentiated Haupiri Group rocks are strongly ankeritic.

4.5 Takaka terrane: Structure

Two major deformation events are recognised in the undifferentiated Haupiri Group rocks of the Adelaide Tarn and Lonely Lake domains: D_1 and D_3. Deformation associated with the Balloon Mélange is described in Chapter 8. As in the Boulder Lake domain, evidence of synsedimentary deformation such as slump folds and disrupted bedding, is occasionally observed.

4.5.1 D_1 macroscale and mesoscale structures

Most bedding in the undifferentiated Haupiri Group rocks, west of the Balloon Mélange, is overturned and W-SW facing. The predominance of overturned bedding implies major deformation that is thought, for the reasons given below, to be related to an overturned western limb of an extremely large D_1 anticline.

In the field, D_1 is represented by mesoscale to mappable macroscale folds (F_1) and an associated axial planar cleavage (S_1). Both S_1 and mesoscale F_1 are mainly observed in areas where F_3 folding is gentle or non-existent. As a consequence, D_1 structural measurements come exclusively from areas where D_1 structures have experienced minor or no refolding. In the Adelaide Tarn domain, areas displaying little or no refolding are mainly from east of Yuletide Peak (Map 2) whereas in Lonely Lake domain such areas occur throughout.

F_1 axial planes and S_1 axial planar cleavage share similar orientations in both the Adelaide Tarn and Lonely Lake domains, striking between N and NW and dipping gently or moderately towards the east (Fig. 4.20). In contrast, F_1 fold axis and L_0^1 orientations in the Adelaide Tarn and Lonely Lake domains differ significantly. In the Adelaide Tarn domain, F_1 and L_0^1 are subhorizontal to gently plunging towards the N-NW or SE, whereas in the Lonely Lake domain, F_1 and L_0^1 have a spread of orientations trending between NW and SE (via the NE quarter) (Fig. 4.20). The large number of NNE to ENE trending lineations at Lonely Lake originate from a zone within 200m of the Anatoki Fault whereas the NW or SE trending lineations come from outside this zone and mainly from the ridge east of Drunken Sailors.

Apart from the F_1 folds within 200m of the Anatoki Fault in the Lonely Lake domain (see a description of these below), F_1 mesoscale folds face in a W-SW direction, are highly asymmetric with the NE-E dipping overturned limb dominating, and consistently verge to the NE-E (Fig. 4.21). Mesoscale wavelengths range from 40cm to several metres. Mappable macroscale folds show similar fold characteristics to those observed in outcrop and are particularly well-demonstrated in the Adelaide Tarn domain (Map 2). Interlimb angles range from close to gentle, and in the Adelaide Tarn domain interlimb angles become increasingly tighter towards the west.

East of Yuletide Peak, and surrounding a small tarn, outcrop is very good and clearly shows the non-cylindrical nature of mesoscale and macroscale F_1 folds. Some F_1 folds are observed to die out when traced along the fold axis, and one F_1 fold was observed to die out in profile. There is a suggestion that F_1 folds in the vicinity of the small tarn display an en-echelon arrangement with one macroscale open overturned anticline dying

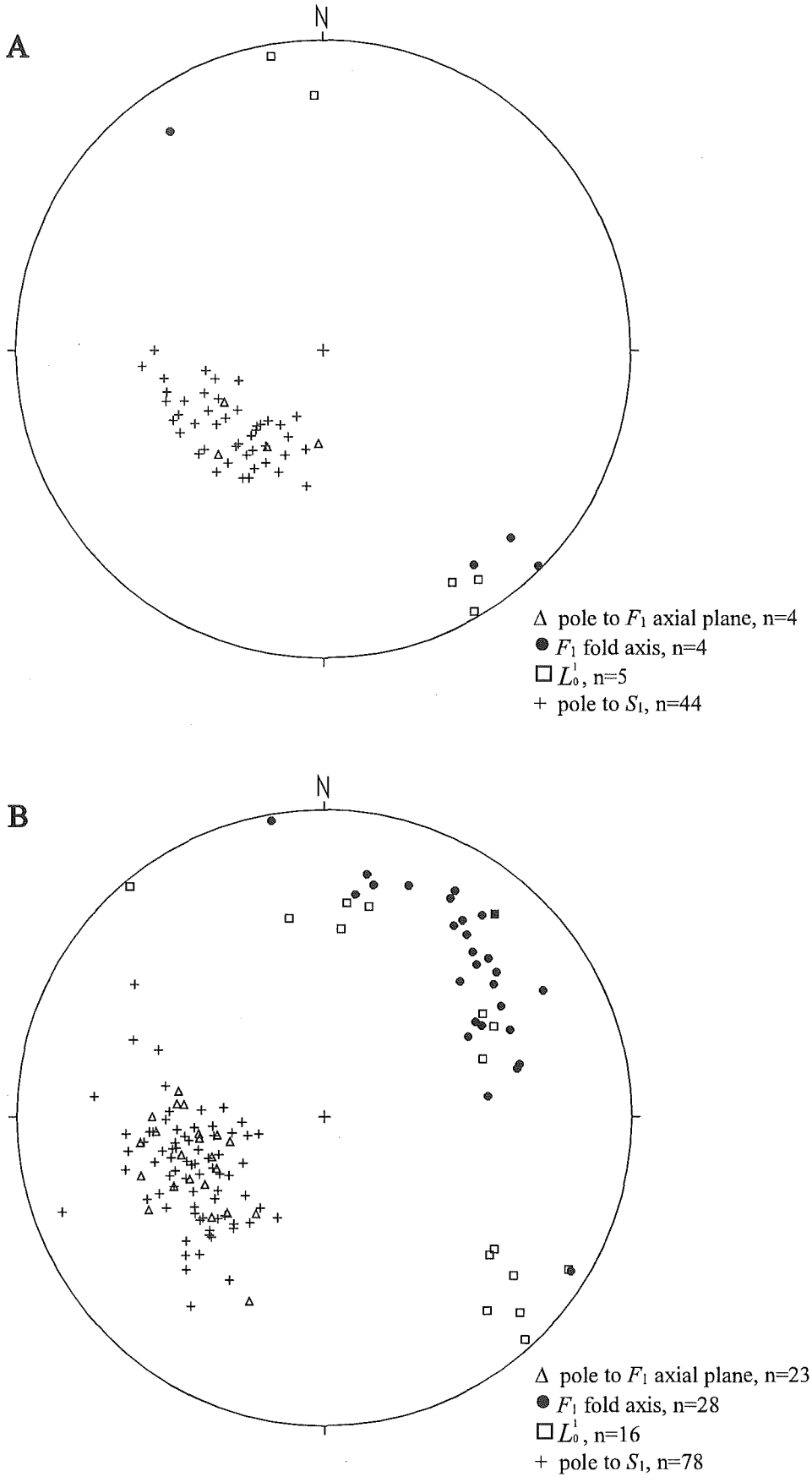

Figure 4.20: F_1, L_0^1, and S_1 orientations in undifferentiated Haupiri Group rocks of the Adelaide Tarn (A) and Lonely Lake (B) domains.

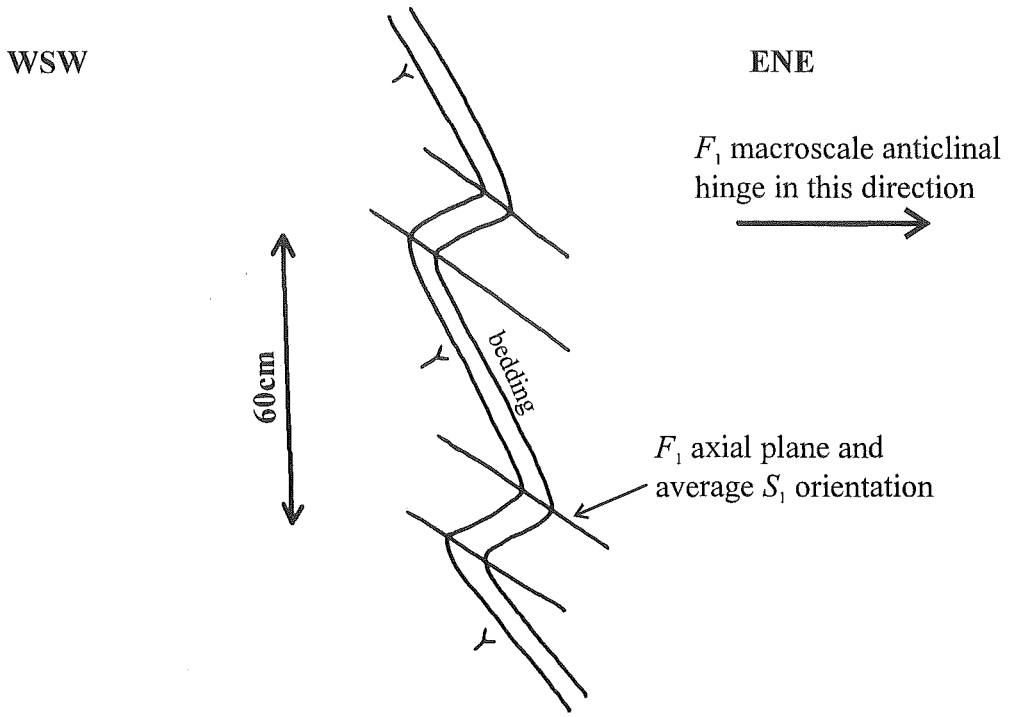

Figure 4.21: Field sketch of mesoscopic open overturned F_1 folding in profile, undifferentiated Haupiri Group, Adelaide Tarn domain. M26/ 734289.

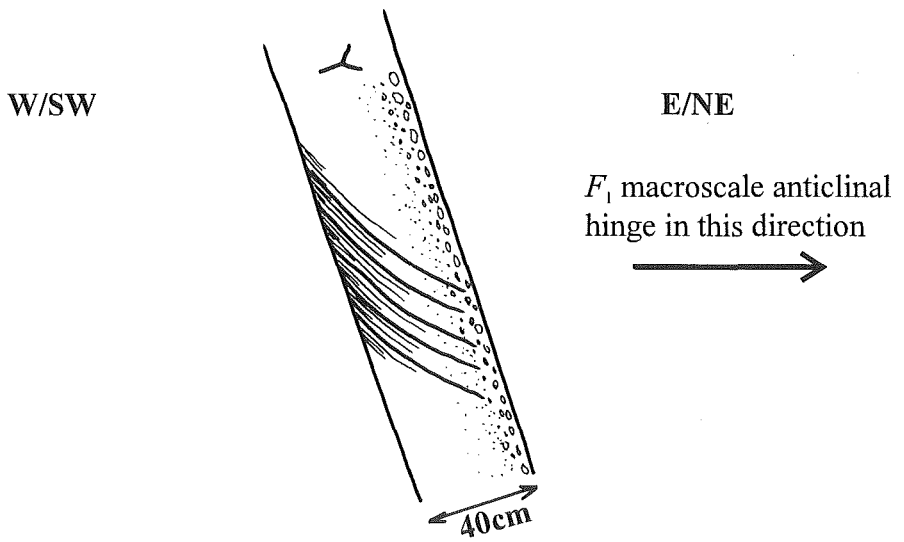

Figure 4.22: General relationship of S_1 refraction in overturned graded beds, undifferentiated Haupiri Group, Adelaide Tarn and Lonely Lake domains.

out southeastwards, and another open overturned anticline, about 100m to the SW of the previously mentioned one, dying out northwestwards (Map 2).

Regardless of non-cylindrical fold observations, poles to bedding measured in the area east of Yuletide Peak (Fig. 4.23A), and along the ridge east of Drunken Sailors (Fig. 4.23B), outline approximate π-girdle distributions in which the axes plot in near-similar orientation to measured F_1 fold axes and L_0^1.

S_1 is a penetrative slaty cleavage in muddy rocks and a closely spaced cleavage in coarser lithologies. S_1 is axial planar to asymmetric mesoscale F_1 folds (Fig. 4.21). When bedding is overturned and dipping NE-E, S_1 always has a lesser dip than bedding. In overturned graded beds, S_1 is refracted so that it is steeper in the direction of fining (Fig. 4.22), indicative of an anticlinal hinge towards the NE-E.

Stretching lineations on S_1 are provided by elongate conglomerate clasts, elongate chloritised phenocrysts, and ankeritic porphyroblast strain fringes. The elongate conglomerate clasts typically show X/Z ratios of 2:1. The stretching lineations plunge moderately towards the NE or E in both the Adelaide Tarn and Lonely Lake domains (Fig. 4.24), and are approximately perpendicular to most F_1 fold axes. Note that the stretching lineations in Haupiri Group rocks east of the Balloon Mélange plunge steeply to the E (Fig. 4.24).

As mentioned earlier, in the Lonely Lake domain and within 200m of the Anatoki Fault, F_1 fold axes plunge gently or moderately towards the NE quadrant and overlap with S_1 stretching lineations. These folds are also asymmetric, and in most cases, show a vergence towards the SE. NE trending fold axes have typically close to open interlimb angles with wavelengths between 20 to 60cm, and exclusively occur in thinly bedded fine sediments (Fig. 4.25). Small faults commonly occur within the hinge zone and are oriented parallel to the S_1 axial planar cleavage (Fig. 4.25).

Why the NE trending fold axes differ from F_1 fold axis orientations elsewhere is not well-understood given that their axial planes are of a similar orientation. Fold axes are known to rotate into parallelism with extension directions when they have a very high shear strain imposed upon them (Ramsay and Huber 1987). However, there is no

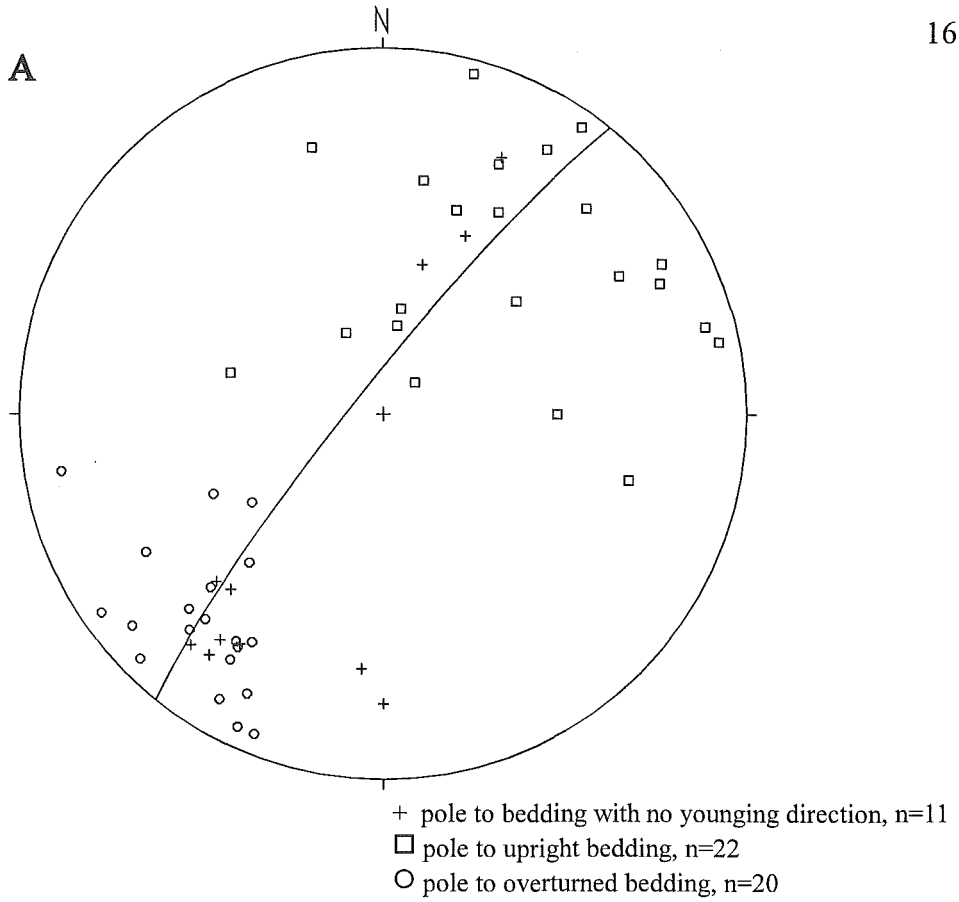

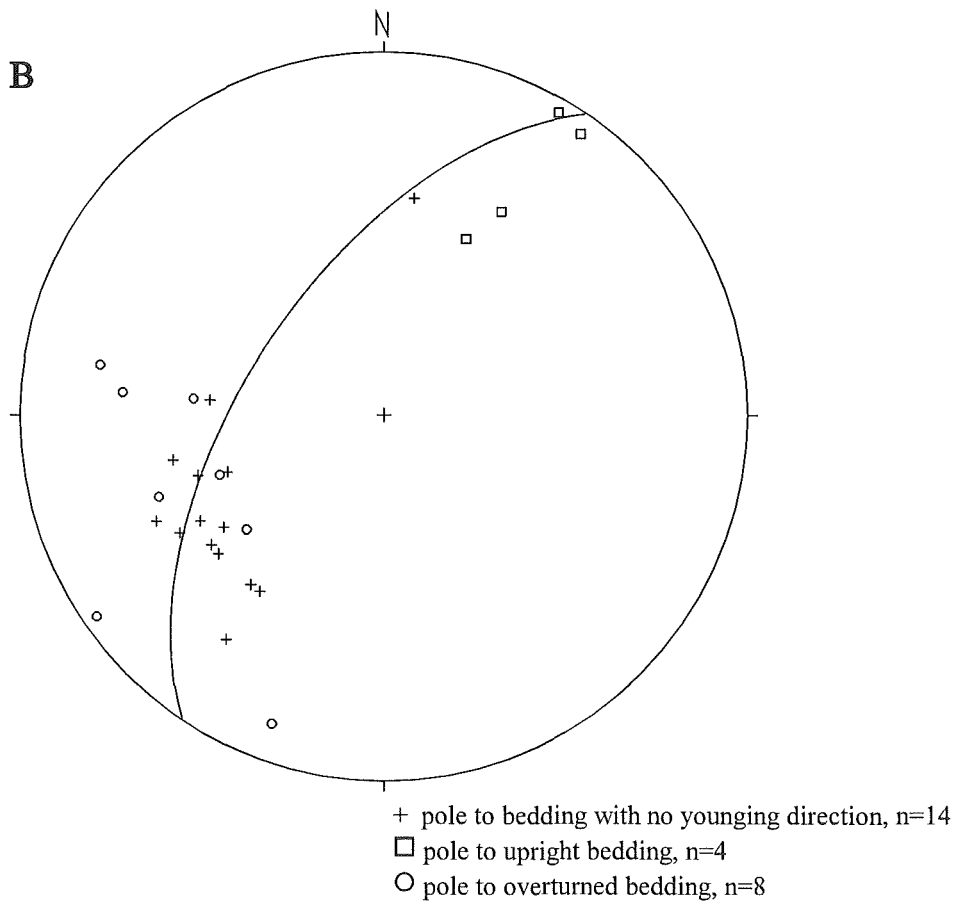

Figure 4.23 (A): Poles to bedding in undifferentiated Haupiri Group rocks in the vicinity of the small tarn east of Yuletide, Adelaide Tarn domain. The best fit π-girdle has an axis of 129/07°. (B): Poles to bedding in undifferentiated Haupiri Group rocks along the ridge east of Drunken Sailors, Lonely Lake domain. The best fit π-girdle has an axis of 124/30 °.

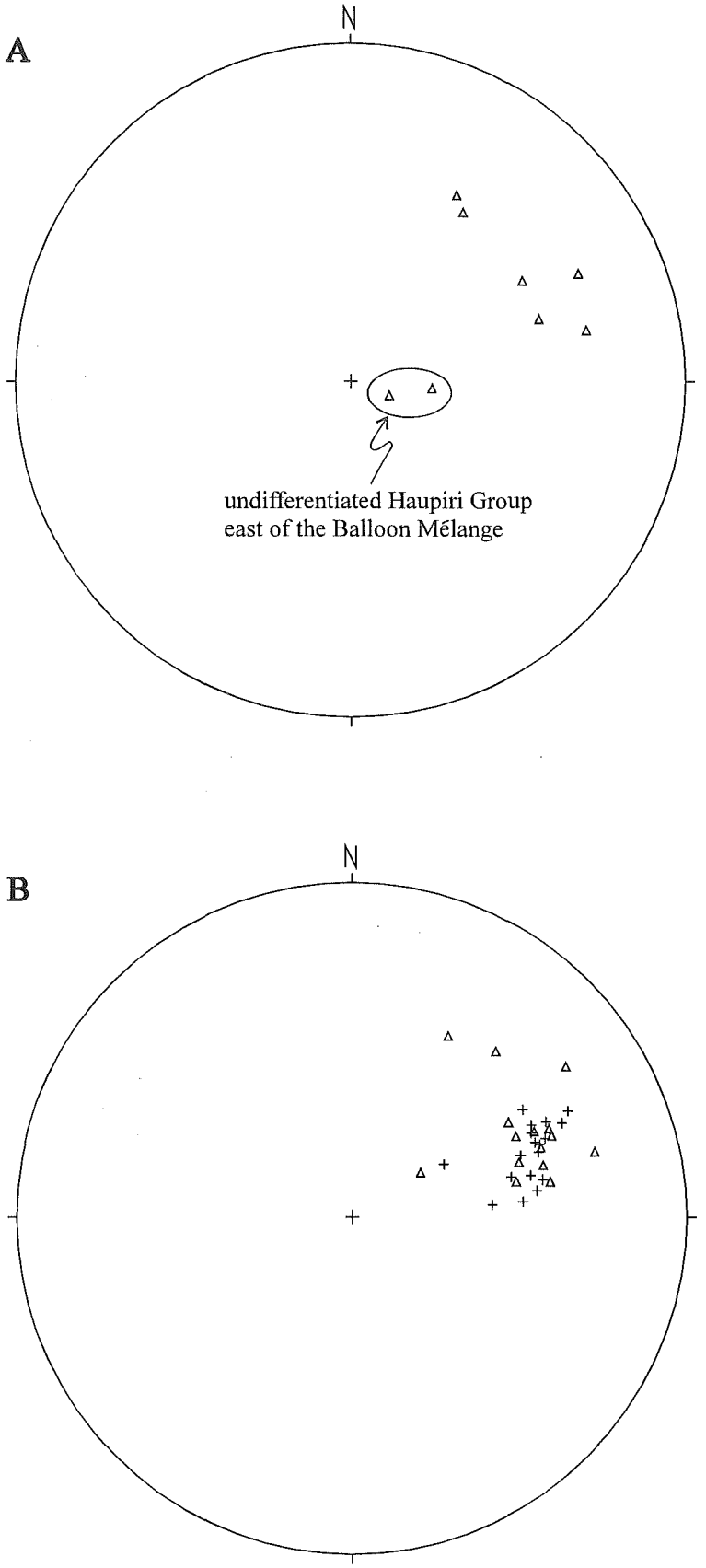

Figure 4.24: Stretching lineations (Δ) in undifferentiated Haupiri Group rocks, Adelaide Tarn (A) and Lonely Lake (B) domains. (A) n=8 (B) n=15.

evidence that axial planar S_1 in the NE trending folds is more intensely developed compared to axial planar S_1 elsewhere. In fact, S_1 in association with these folds is often quite weakly developed. There are a number of possibilities to explain the F_1 NE trending orientations:

1. The folds formed early in the D_1 deformation event when extension directions were differently oriented.
2. The folds formed with axes parallel to the extension directions because of strong shortening in the Y-axis direction.
3. Bedding in the area may have been already been tilted prior to F_1 development. The tilting may represent an early stage of D_1 deformation particular to that area.

Further work is required to differentiate between these possibilities.

4.5.2 D_1 microscale structures

S_1 is a penetrative slaty cleavage defined by aligned muscovite/sericite, chlorite, actinolitic hornblende, and opaque solution seams (Fig. 4.36). Detrital clasts of quartz or feldspar, and pyrite cubes, display good strain shadow and fringe development parallel to S_1 (Fig. 4.26).

Granule size sedimentary and volcanic rock fragments are flattened parallel to S_1 and possess their own internal S_1 penetrative cleavage (Fig. 4.27). Syn-S_1 metamorphic mineralogy consists of muscovite/sericite + chlorite ± ankerite ± actinolitic hornblende ± epidote and is indicative of sub-greenschist or low greenschist facies metamorphism. Detrital calcic feldspar grains are saussuritised.

Ankerite forms large spheroid or ovoid porphyroblasts (up to 3mm) in mudstone, whereas in sandstone, ankerite is mostly fine grained and disseminated. Weathered sandstone is usually orange coloured because of the disseminated nature of the ankerite. Similar to those seen in the field, large ankerite porphyroblasts in thin-section display strain fringes and shadows parallel to S_1 (Fig. 4.28). The strain fringes are made up of ankerite and sometimes asymmetric (Fig. 4.29). The asymmetry of the fringes together with the stretching lineation indicates a top to the SW-W sense of shear where bedding is overturned and steeper dipping than S_1. This sense of shear is to be expected for overturned limbs of SW facing anticlines. The ankerite porphyroblasts contain inclusion

Figure 4.25: NE trending F_1 folds in thinly bedded fine sediments of the undifferentiated Haupiri Group, Lonely Lake domain. Small faults occur within hinge zones parallel to the S_1 axial planar cleavage. M26/ 728254. Pencil for scale.

Figure 4.26: Large quartz grain with a recrystallised strain fringe of quartz parallel to S_1 cleavage. S_1 has subsequently been crenulated by S_3. RJ205, undifferentiated Haupiri Group. (A) CPL (B) PPL.

Figure 4.27: A sedimentary clast (centre) is flattened parallel to S_1 and subsequently crenulated by S_3. Note that the clast possesses an internal S_1 penetrative cleavage. S_3 is a zonal crenulation cleavage with gradational boundaries. RJ205, undifferentiated Haupiri Group. CPL.

0.5mm

Figure 4.27

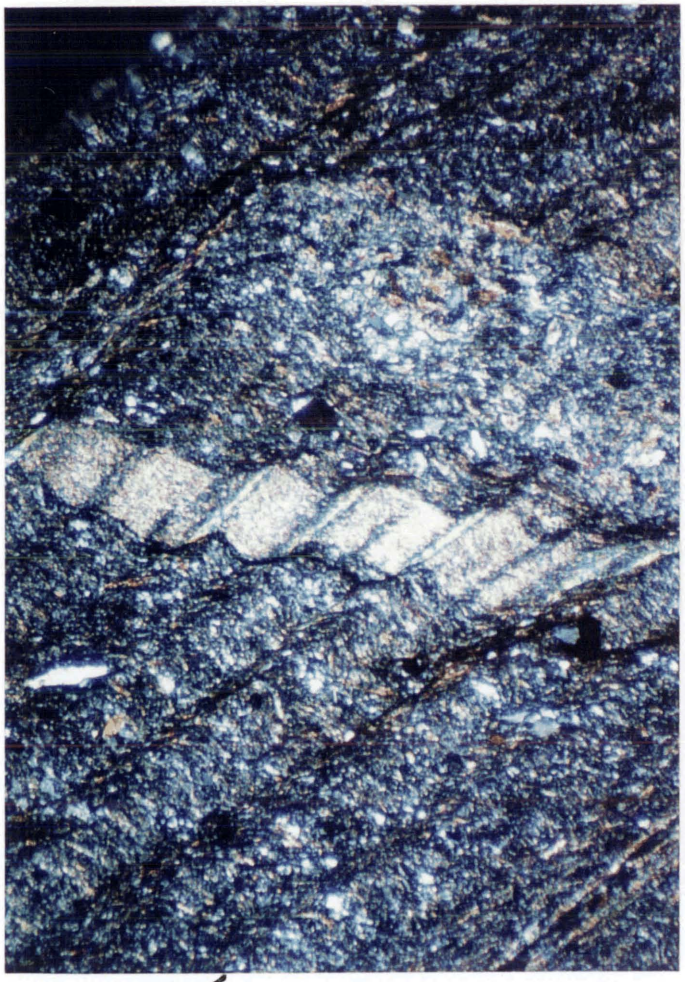

0.5mm

Figure 4.26

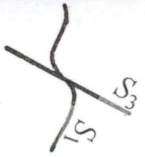

Figure 4.25

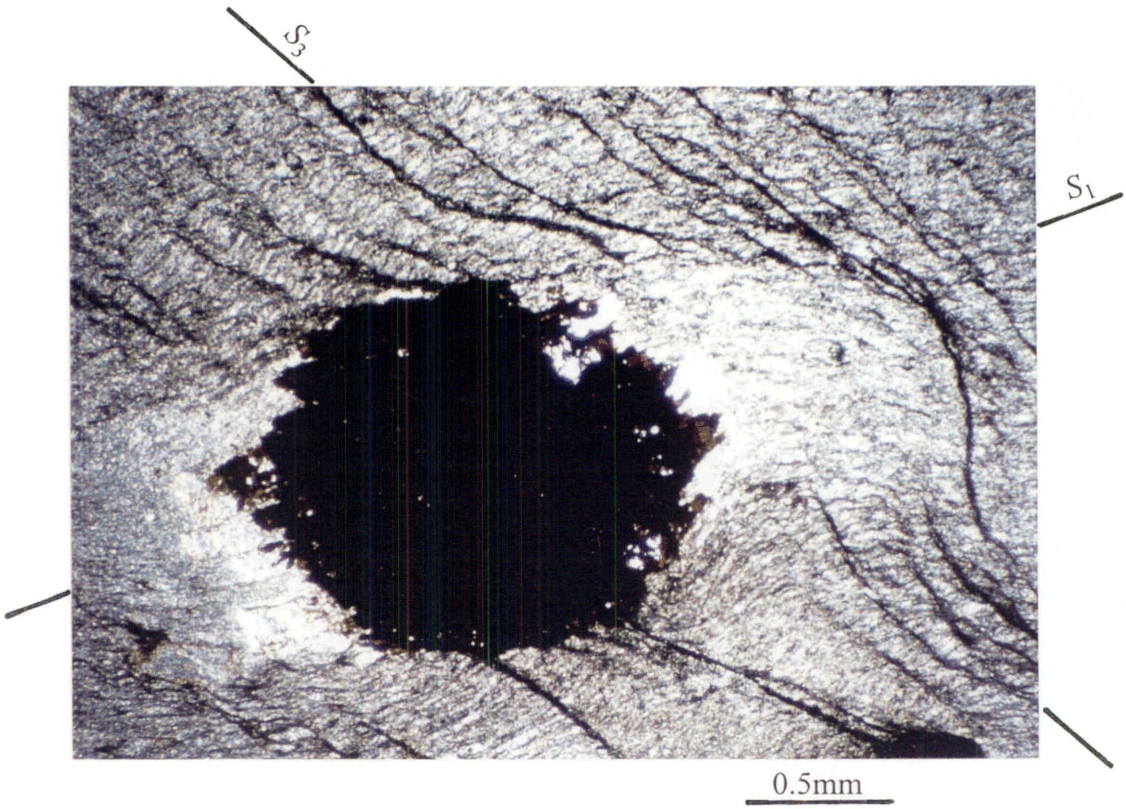

Figure 4.28: Ankerite porphyroblast with a strain shadow and ankerite strain fringe parallel to S_1. S_3 discrete crenulation cleavage wraps around the ankerite and shadow. Away from the ankerite porphyroblast (outside the field of view in this photomicrograph), S_3 is much less intense. RJ467, undifferentiated Haupiri Group. PPL.

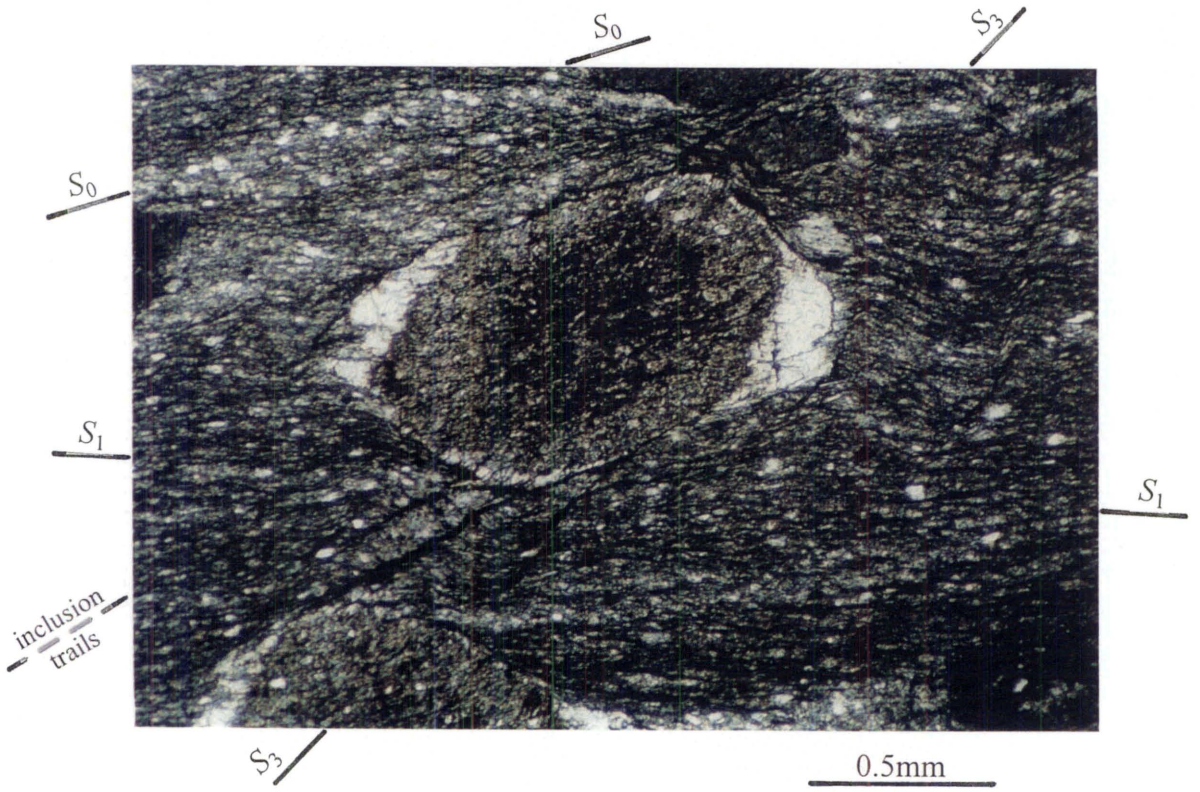

Figure 4.29: Ankerite porphyroblast with asymmetric ankerite strain fringes parallel to S_1. S_3 is also observed. The porphyroblasts contains inclusion trails (not well observed in this photo) which are oblique to bedding. RJ466, undifferentiated Haupiri Group. PPL.

trails which are consistently oriented oblique to bedding and S_1 (Fig. 4.29). The significance of the inclusion trails and orientation will be discussed in Section 5.5.2.

Given that the inclusion trails represent an early expression of D_1, and that S_1 wraps around the ankerite porphyroblasts, the timing of ankerite porphyroblast metasomatism must be syn-D_1.

4.5.3 D_3 mesoscale structures

D_3 is represented by mesoscale folds (F_3) (Fig. 4.30) and a crenulation cleavage (S_3) which is axial planar to these folds. S_3 is observed throughout the two domains but is best developed in shales (Fig. 4.31). F_3 folds have a more restrictive occurrence and are not observed east of Yuletide Peak in the Adelaide Tarn domain, or east of Drunken Sailors in the Lonely Lake domain. The lack of F_3 folds in these areas is thought to be related to the presence of generally coarser and thicker bedded sediments.

F_3 axial planes are generally NE striking, dipping moderately to the SE, in the Adelaide Tarn domain, and NE to ENE striking, dipping moderately or steeply to the SE, in the Lonely Lake domain (Fig. 4.32). Using bedding as a reference surface, F_3 fold axes and L_0^3 generally plunge gently to moderately towards the E in the Adelaide Tarn domain, and moderately towards the ESE in the Lonely Lake domain (Fig. 4.32). Although bedding has been folded by F_1, the majority of F_3 mesoscale folds were observed on overturned NE-E dipping limbs of F_1 macroscale folds, thus giving fairly consistent F_3 fold axis measurements. It should be noted however, that in the Adelaide Tarn domain some of the F_3 fold axis and L_0^3 measurements come from an upright F_1 macroscale limb that dips to the NE (located between Yuletide Peak and the Anatoki Fault, see Map 2). At this locality the macroscale F_1 interlimb angles must be relatively tight (probably close) because of the minimal scatter of F_3 fold axis measurements on Figure 4.32A. The more gently plunging fold axis shown in Figure 4.32A originates from this upright F_1 limb.

F_3 fold interlimb angles range considerably from close to gentle. In general, F_3 folds are more gentle in the Lonely Lake domain compared with those in the Adelaide Tarn domain. Wavelengths of mesoscale folds range from large crenulations (~5cm) to over

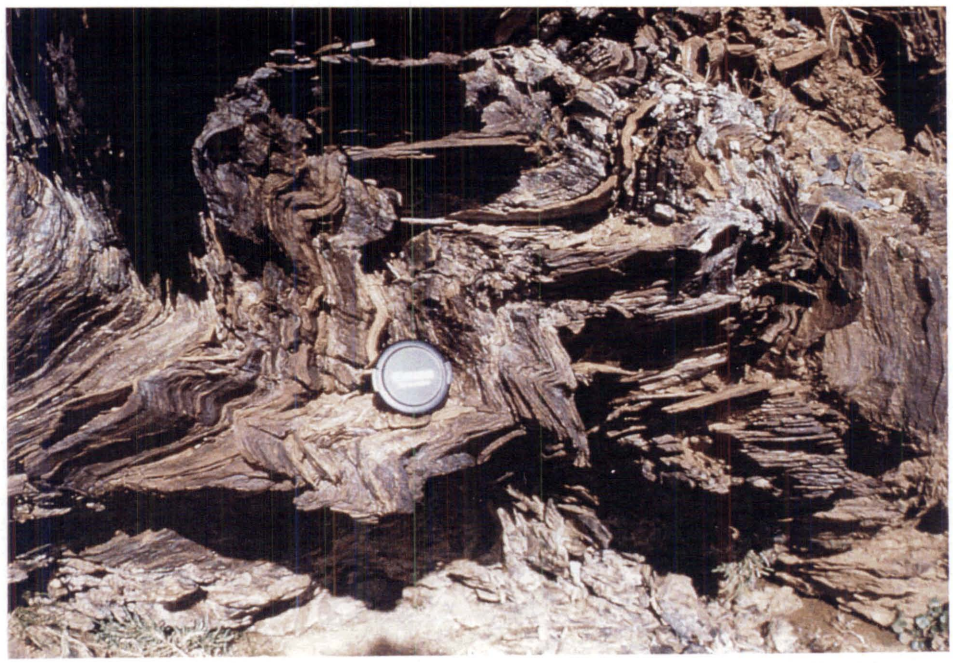

Figure 4.30: F_3 folding in ankeritic undifferentiated Haupiri Group sandstone and siltstone, Lonely Lake domain. M26/ 727255.

Figure 4.31: S_0, S_1, and S_3, all observed in the one outcrop. Bottom of lens cap lies on a bedding plane that separates a fine sandstone bed (top) from a dark-grey shale bed (bottom). S_1 is observed in the sandstone, whereas S_3 crenulation cleavage is observed in the shale. Undifferentiated Haupiri Group, Lonely Lake domain. M26/ 741259.

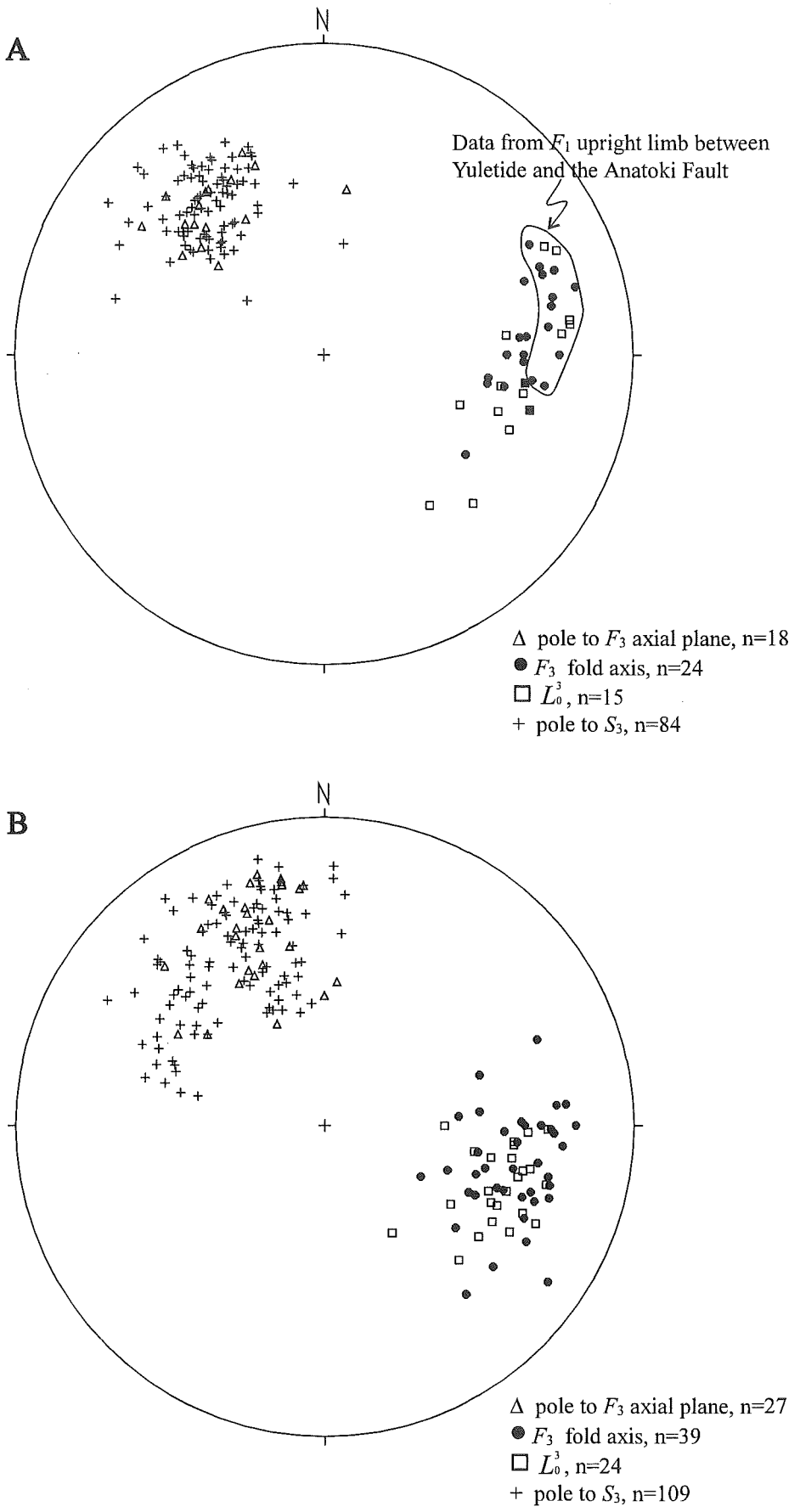

Figure 4.32: F_3, L_0^3, and S_3 orientations in undifferentiated Haupiri Group of the Adelaide Tarn (A) and Lonely Lake (B) domains. Note that filled squares are where filled circle symbols overlap with open squares symbols.

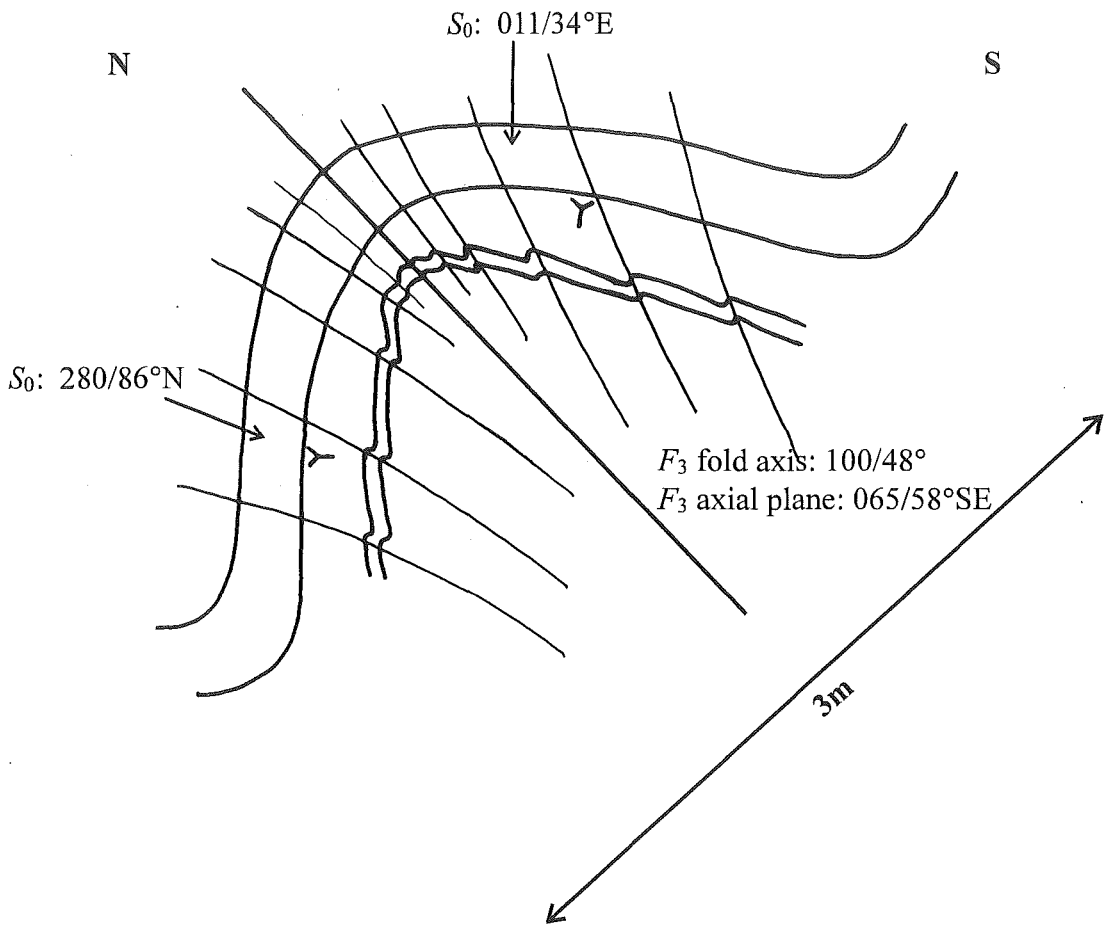

Figure 4.33: Field sketch of F_3 mesoscale antiform in profile, undifferentiated Haupiri Group, Lonely Lake domain. Fold wavelength decreases with decreasing thickness of bedding. S_3 fans around F_3 fold hinge. M26/ 727254.

3m depending partly on thickness of bedding (Fig. 4.33). Fold shapes are typically D1 to D3 or E1 to E3. In the Lonely Lake domain, and in areas where F_3 mesoscale folds are absent, very gentle macroscale F_3 folds with wavelengths of >10m have been identified on the basis of systematic changes in bedding and S_1 attitudes.

Bedding orientation in both the Adelaide Tarn and Lonely Lake domains display a considerable scatter due to F_3 folding of upright and overturned F_1 fold limbs (Fig. 4.34). Where interlimb angles are tighter, the northern limb of F_3 antiforms are often structurally inverted causing overturned bedding of F_1 fold limbs to become upright (Fig. 4.35A), and upright bedding of F_1 fold limbs to become overturned (Fig. 4.35B). Many F_3 folds are symmetrical but there are several examples of north verging folds in which the southern limbs of antiforms are longest.

S_3 crenulation cleavage crenulates both bedding and S_1 (Fig. 4.31), and in some cases is observed to crenulate D_1 strained conglomerate clasts. S_3 is subparallel to F_3 axial planes (Fig. 4.32), and is often strongly developed along F_3 fold hinge zones. Commonly, S_3 is so intensely developed in areas of F_3 folding that S_1 cannot be identified. Sometimes S_3 cleavage is fanned considerably on either side of F_3 fold hinges (Fig. 4.33) and displays refraction across graded beds.

4.5.4 D_3 microscale structures

In shales, S_3 can be either a zonal crenulation cleavage with sharp (Fig. 4.36) and gradational (Fig. 4.27) boundaries, or a discrete crenulation cleavage (Fig. 4.28). In zonal crenulation cleavage, white mica, actinolitic hornblende, and chlorite have grown parallel to S_3 (Fig. 4.36). S_3 is often absent in sandstones, or is represented by a more widely spaced discrete crenulation cleavage. Granule size sedimentary or volcanic rock fragments, flattened parallel to S_1, are also crenulated by S_3 (Fig. 4.27). S_3 is typically wrapped and intensified around ankerite porphyroblasts (Fig. 4.28).

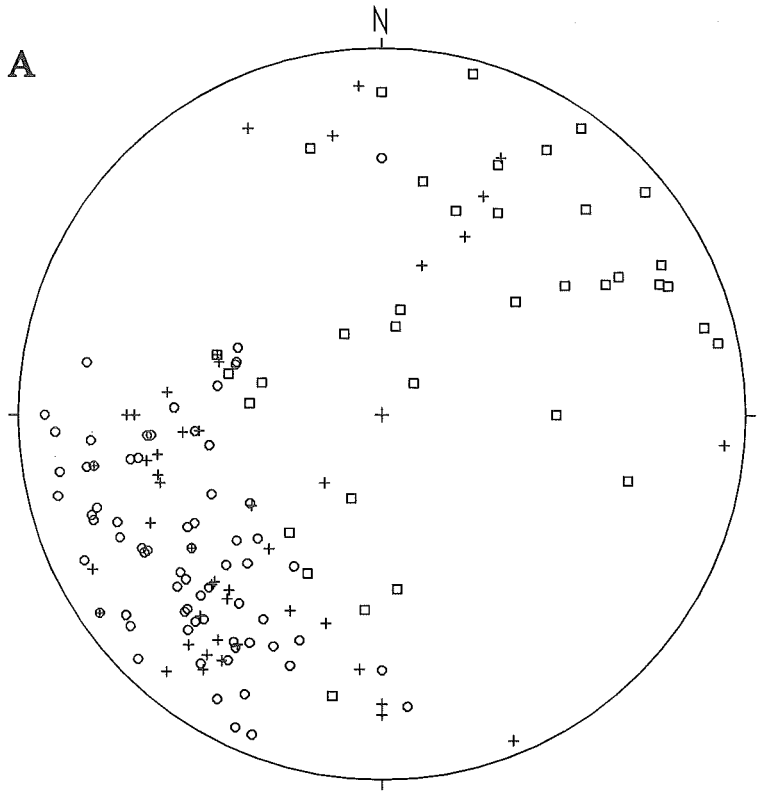

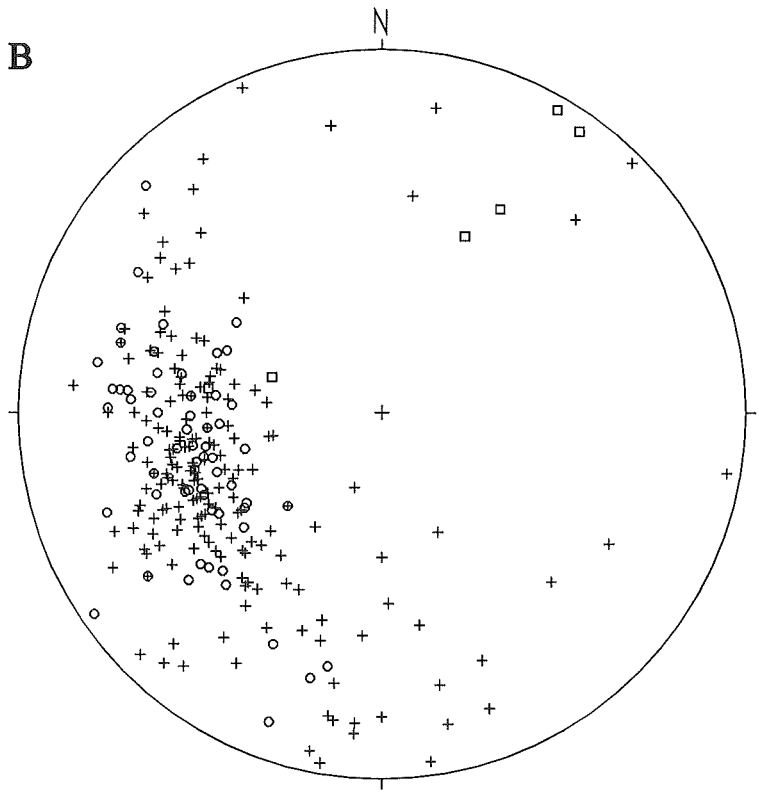

Figure 4.34: Poles to bedding in undifferentiated Haupiri Group of the Adelaide Tarn (west of the Balloon Mélange) (A) and Lonely Lake (B) domains.

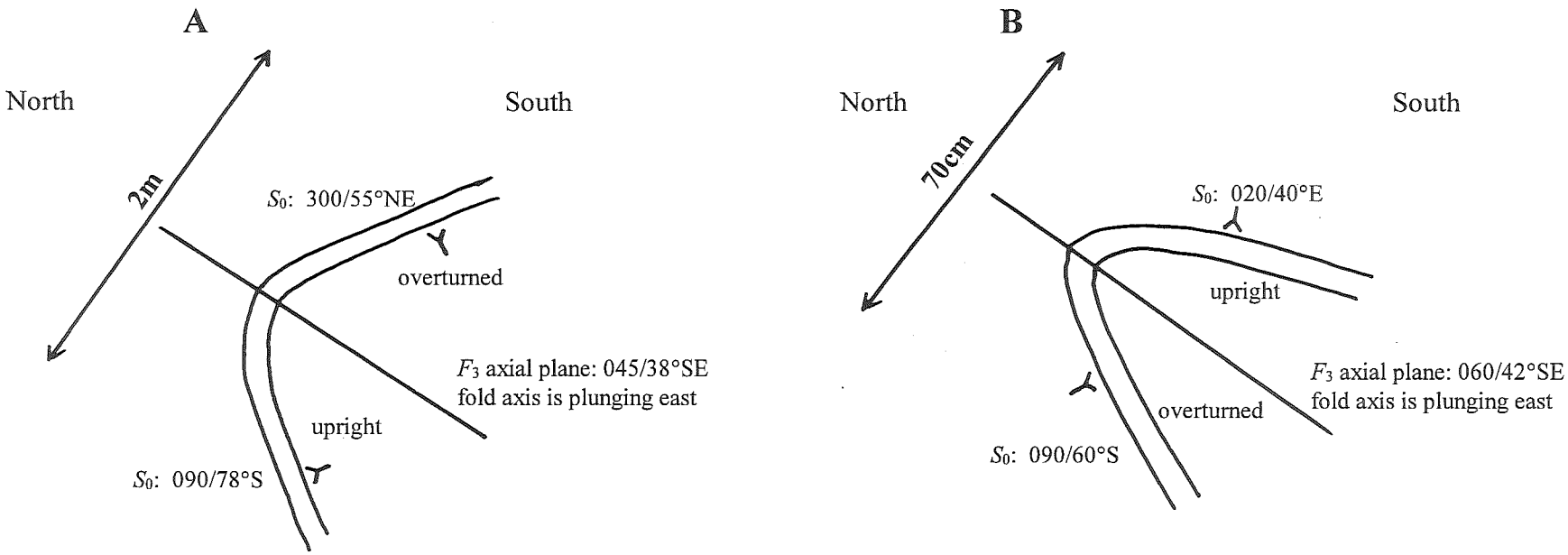

Figure 4.35 (A): Field sketch profile of an F_3 antiform on the overturned limb of an F_1 anticline. Here the F_3 fold is relatively tight and the northern limb is structurally inverted causing overturned bedding to become upright. Undifferentiated Haupiri Group, Adelaide Tarn domain. M26/ 731290. (B): Field sketch profile of an F_3 antiform on the upright limb of an F_1 anticline. Here the F_3 fold is relatively tight and the northern limb is structurally inverted causing upright bedding to become overturned. Undifferentiated Haupiri Group, Adelaide Tarn domain. M26/ 727291

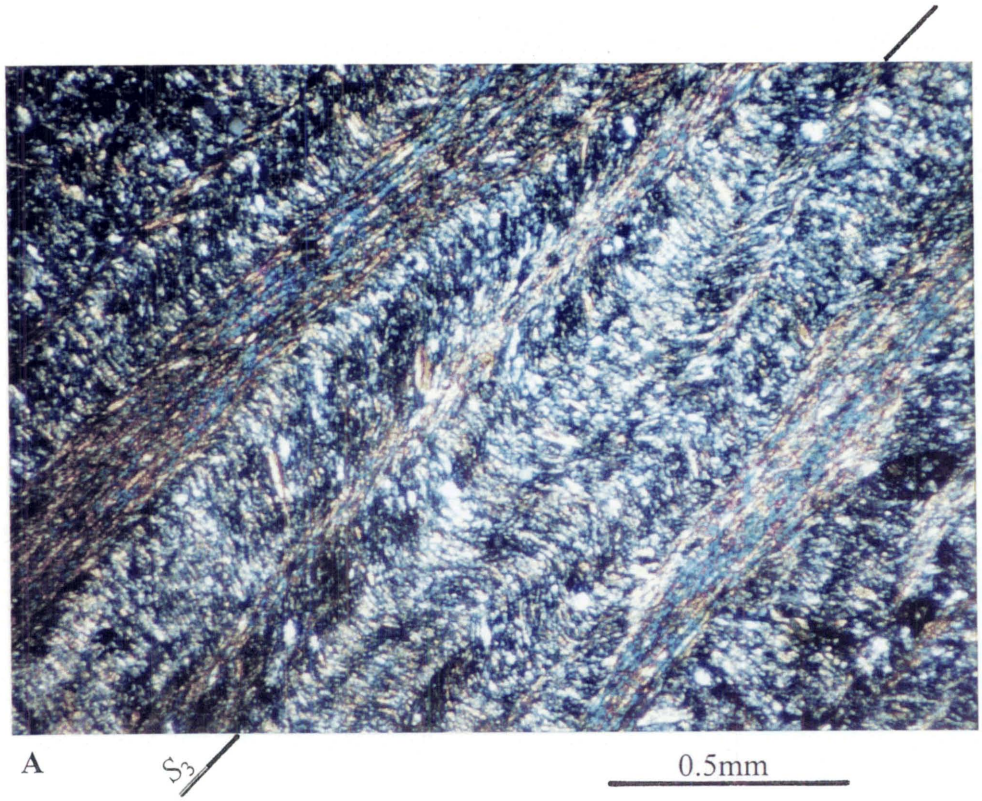

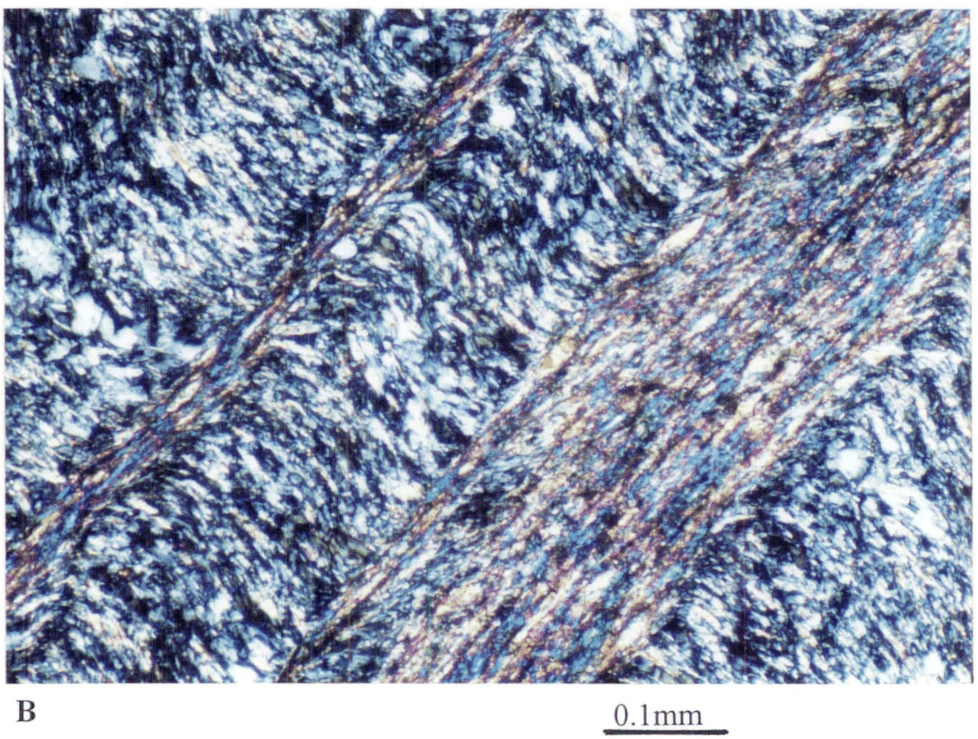

Figure 4.36 (A): S_3 zonal crenulation cleavage with sharp boundaries crenulating S_1. (B): Close-up view of (A). S_1 is a penetrative cleavage defined by aligned white mica, chlorite, and actinolitic hornblende. S_3 cleavage domains are defined by the same minerals, growing parallel to S_3, but devoid of quartz and feldspar. RJ205, undifferentiated Haupiri Group. CPL.

4.5.5 Other structures

In the lower reaches of the northern branch of the Anatoki River, undifferentiated Haupiri Group like rocks outcrop east of the Balloon Mélange. Here, bedding youngs eastward. S_3 is well-developed and has been crenulated by a cleavage which strikes NNE and dips moderately to the NNW. This NNE striking cleavage is associated with isolated open style mesoscale folds that gently plunge towards the north. The cleavage and folding is very similar in style and orientation to that observed in both the northeast and southeast extremities of the Boulder Lake domain (Section 3.7.10).

At Drunken Sailors in the Lonely Lake domain, a well-exposed shear zone up to 1.5m thick is exposed (Fig. 4.37). The shear zone walls are sharp yet the shear zone rock possesses a strong internal foliation that microscopically consists of mica-rich seams, opaque solution seams, and a carbonate SPO. Sharply defined shear zone walls and internal foliation are consistent with a semi-brittle shear zone. The shear zone has a north-south strike and dips to the east. The internal foliation shows a "S-C like" asymmetry that suggests movement was towards the west. Interestingly, S_3 crenulates the foliation indicating the shear zone is a relatively early structure. Given its similar attitude (see next section) and close proximity to the Anatoki Fault, the shear zone may be related to early movement on the Anatoki Fault. Two similarly oriented but thinner and less well-exposed shear zones have been identified within close proximity to the Anatoki Fault in the Lonely Lake domain.

The dolerite immediately adjacent to the Anatoki Fault in the Adelaide Tarn domain has been completely recrystallised to a greenschist facies metamorphic mineralogy of tremolitic and actinolitic hornblende + chlorite + saussuritised feldspar + epidote + opaques. Relic pyroxene shapes are preserved in places. The metadolerite has undergone ductile deformation and possesses a foliation (Fig. 4.38). Unfortunately, the dolerite exposed is not *in situ* and, therefore, it cannot be determined if the foliation is parallel to S_1 or related to D_1.

Figure 4.37: A shear zone on the north face of Drunken Sailors, undifferentiated Haupiri Group, Lonely Lake domain. The shear zone is picked out by the brown/ orange weathering of ankerite. Purple backpack for scale on right side of photograph. M26/ 728255.

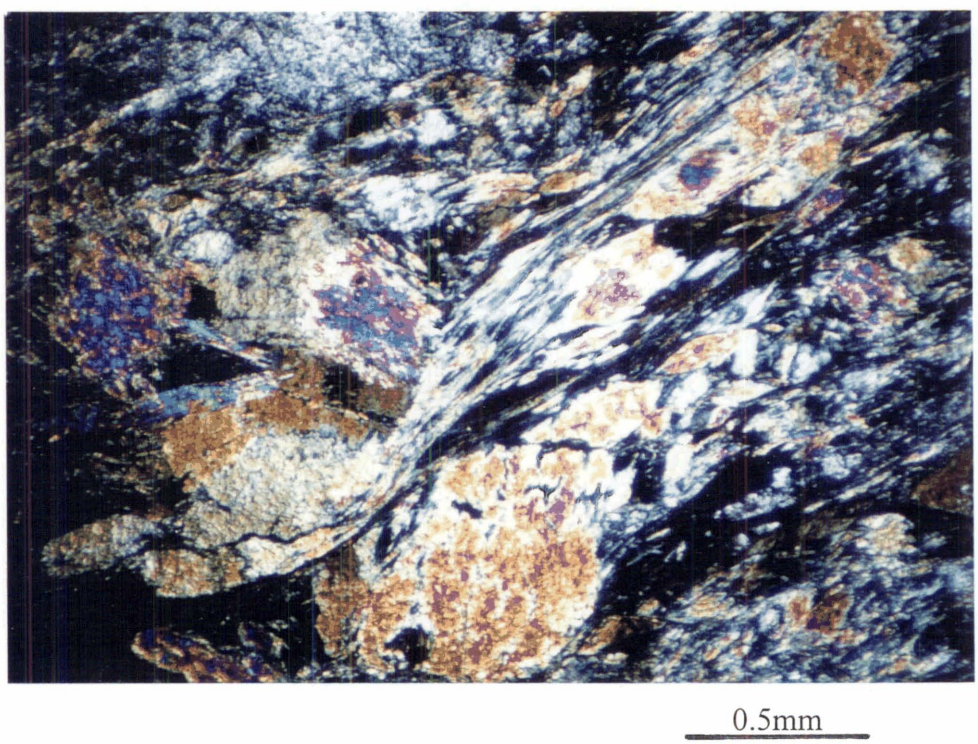

Figure 4.38: Deformed metadolerite with a foliation defined by chlorite and actinolitic hornblende. The large high birefringent grains are tremolitic and actinolitic hornblende. Sample RJ221.

4.6 Anatoki Fault attitude

In the Adelaide Tarn and Lonely Lake domains, the position of the Anatoki Fault trace is well-constrained and indicates an approximately north-south strike. Given the strong topographic relief in the headwaters of the Anatoki River south branch, a good approximation of the dip of the fault plane can also be determined. The position of the Anatoki Fault is known west of Yuletide Peak in the Adelaide Tarn domain, and west of Drunken Sailors in the Lonely Lake domain (see chapter frontispiece). It is also known that Douglas Formation outcrops all along the east dipping slope that descends from Anatoki Peak to Pt. 744. in the Anatoki River (Map 2). No outcrop occurs in the Anatoki River east of Pt. 744 but given the above contraints, and assuming north-south striking structure contours, a dip no steeper than 40° is calculated (Fig. 4.39). Based on the distribution of Douglas Formation and undifferentiated Haupiri Group near the ridge-lines north and south of the Anatoki River south branch, the Anatoki Fault trace on Map 2 is drawn approximately 250m downstream from Pt. 744. Structure contour construction of the interpreted Anatoki Fault trace in the headwaters of the Anatoki River suggests the Anatoki Fault attitude is ~350/35°E.

It is important to note that previous mapping in this area by Grindley (1961, 1971) shows the range between Dragons Teeth and Lonely Lake to be of Takaka terrane lithology ("Anatoki Formation"). As a result, a right angle bend in the Anatoki Fault trace, near Adelaide Tarn, was drawn on Grindley's map. My mapping shows that the range between Dragons Teeth and Lonely Lake is made of Buller terrane lithologies and the right angle bend of the Anatoki Fault proposed by Grindley does not exist.

4.7 Discussion

In the Adelaide Tarn and Lonely Lake domains, two major deformation events (D_1 and D_3) are recognised in both the Buller and Takaka terranes. A comparison of D_1 and D_3 structures in the two terranes is given below.

In the Takaka terrane, the first deformation event is represented by folding and an axial planar slaty cleavage. Younging directions, bedding-cleavage relationships, and

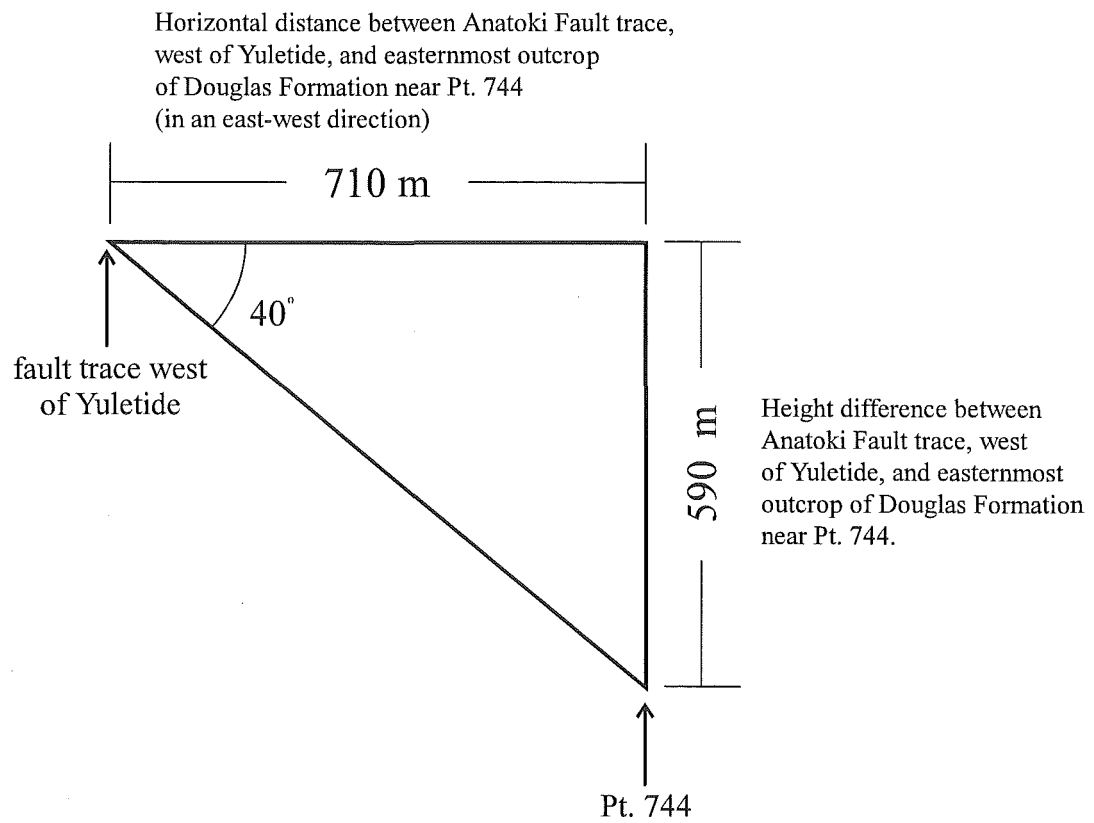

Figure 4.39: Dip calculation of the Anatoki Fault plane in the headwaters of the Anatoki River south branch.

mesoscale fold vergence suggest that the undifferentiated Haupiri Group rocks, west of the Balloon Mélange, are related to an overturned western limb of a large macroscale W to SW facing anticline. In the Buller terrane, the first deformation event is also related to folding and an axial planar slaty cleavage. However, because of the lack of younging directions in Buller terrane rocks, the large macroscale fold structure is uncertain. What is known is that, in general, rocks must young from west to east because Douglas Formation is stratigraphically younger than Leslie Formation (Cooper 1989).

An overlap of D_1 related structural orientations in both Buller and Takaka terrane is observed in the Lonely Lake domain, excluding the anomalous NE trending fold axes. Although D_1 structural orientations either side of the Anatoki Fault do not overlap in the Adelaide Tarn domain, the orientations are clearly not dissimilar. The overall similarity of D_1 structural orientations either side of the Anatoki Fault suggest they may be related to each other. This possibility is discussed further in Chapter 9 and 10.

The second deformation event (D_3) recognised in the Buller terrane is represented by mesoscale to macroscale folds and an axial planar crenulation cleavage. The D_3 structures and their orientations are almost identically matched in Takaka terrane rocks and this is especially so in rocks within close proximity of the Anatoki Fault. Thus it is confidently concluded that D_3 in the Buller terrane and D_3 in the Takaka terrane are one and the same. Slight differences in fold characteristics (e.g. fold shapes) between the two terranes are attributed to differences in bedding thicknesses with generally thicker bedded sequences in the Takaka terrane and generally laminated sequences in the Buller terrane.

Apart from a deformed dolerite and minor shear zones (Section 4.5.5), there is no evidence that deformation is significantly stronger in the rocks close to the Anatoki Fault compared to elsewhere. The Anatoki Fault cannot be observed directly but its position can be constrained to within about 20m. Thus it would appear the Anatoki Fault in the Adelaide Tarn and Lonely Lake domains is more likely to be represented by a discrete shear rather than a zone of ductile deformation. Ankerite metasomatism, especially in the Takaka terrane rocks, is intense close to the Anatoki Fault, and suggests CO_2-rich fluids were channelled along the fault.

CHAPTER 5

PEAK 1610
and
KAKAPO PEAK DOMAINS

Chapter frontispiece: Near vertical dipping volcanically derived epiclastics on the southwest side of Kakapo Peak. In the far distance, a near vertical limestone sliver (light grey unit amongst the bush covered slope) marks the Anatoki Fault of the Mt Benson domain. View looking south.

5.1 Introduction

The description of two areal domains, Peak 1610 and Kakapo Peak (Map 3), have been combined in one chapter because of their similarity in structure. The two domains occur south of the Lonely Lake domain and north of the Mt Benson domain (Fig. 1.2). All exposure in the two domains is above the bushline. Along the ridge-line from Kakapo Peak to Mt Snowden, there is excellent exposure of the Balloon Mélange.

As in previous chapters, the Buller terrane lithology and structure is described first before that of the Takaka terrane.

5.2 Buller terrane: Lithology

In the Buller terrane rocks of the Peak 1610 and Kakapo Peak domains, two distinctive lithologies are recognised. In the westernmost part of the domain, and making up most of the Buller terrane, are rocks that are best ascribed to Douglas Formation. These rocks are typically grey laminated siltstones. Laminae characteristics are similar to those described for laminae in Douglas Formation in the Adelaide Tarn and Lonely Lake domains (Section 4.2) but here the laminae are generally thicker. Beds of predominantly pelitic-rich siltstone or, more commonly, quartz-rich fine or very fine sandstone occur frequently and are generally 1-5cm thick but sometimes up to 20cm thick. Rare thick (~1m) quartz sandstone beds are also observed. Very occasionally, beds may display grading from quartzose sandstone to pelitic siltstone, providing valuable way-up indicators.

East of Douglas Formation and immediately west of the Anatoki Fault are dark grey slaty shales interbedded with quartz sandstone. In most places the dark grey shale predominates over quartz sandstone. The shale commonly contains siltsize quartz-rich laminae and ankerite porphyroblasts (altered to iron oxides). Quartz sandstone beds are usually 20cm to 2m thick. Immediately adjacent to Douglas Formation is a prominent quartz sandstone bed that ranges in thickness from 4 to 15m and can be traced along strike for over 1.5km (Map 3).

The contact between Douglas Formation and the slaty shale unit is marked by a 1-1.5m thick brittle fault zone consisting of a well-cemented foliated fault breccia riddled with boudinaged quartz veins. The fault zone appears to be approximately concordant with adjacent bedding attitudes.

5.3 Buller terrane: Structure

Buller terrane rocks in the Peak 1610 domain are very limited in outcrop, and as a consequence, this section concentrates on structures seen in the Kakapo Peak domain. Structure in the Peak 1610 domain is described briefly at the end of this section.

In contrast to the Adelaide Tarn and Lonely Lake domains, the Buller terrane rocks of the Kakapo Peak domain have been affected by only one major deformation (D_1). Subsequent minor deformation including a crenulation cleavage (S_{ii}) and cross-folding is recognised.

5.3.1 D_1 macroscale and mesoscale structures in Kakapo Peak domain

D_1 structures differ in style between Douglas Formation and the slaty shale unit, and therefore will be described separately.

Douglas Formation

D_1 deformation in the Douglas Formation is recognised by mesoscale folds (F_1) and an axial planar slaty cleavage (S_1). F_1 axial planes strike N-NNW, dipping steeply east or subvertical (Fig. 5.1). F_1 fold axes and L_0^1 plunge anywhere between subhorizontal to moderately towards the N-NNW or S-SSE (Fig. 5.1). The variation in plunge appears to be due to cross-folding (see Section 5.3.3). Fold interlimb angles range from tight to open with wavelengths in the order of 2-10m. Where folds are tight, the rock is a laminated siltstone. Quartz-rich laminae on fold limbs become lensoidal in form with mica-rich laminae anastomosing around them. As a result, bedding appears almost parallel to cleavage.

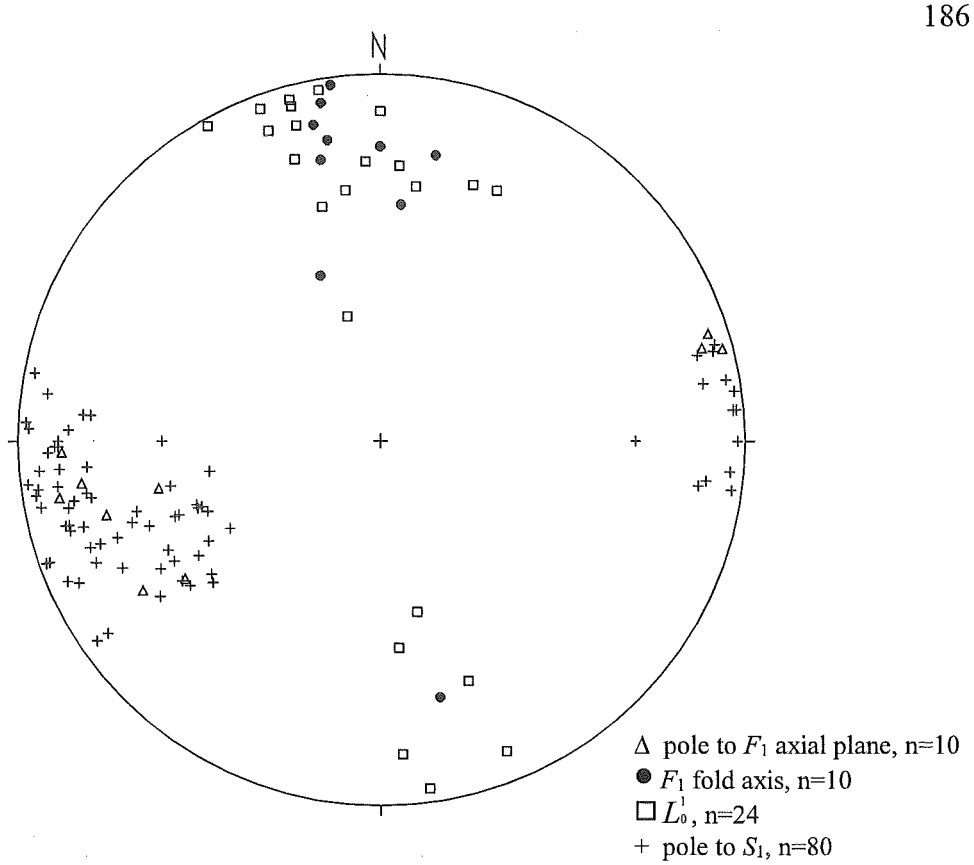

Figure 5.1: F_1, L_0^1, and S_1 orientations in the Douglas Formation, Kakapo Peak domain.

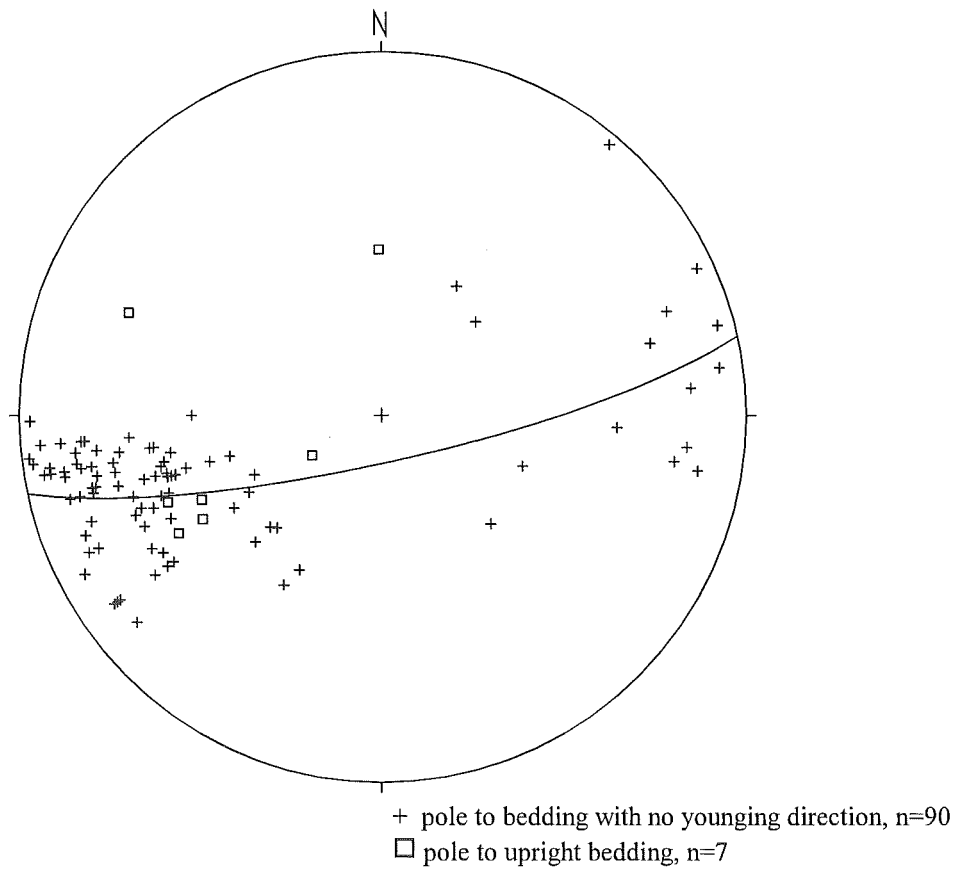

Figure 5.2: Poles to bedding in Douglas Formation, Kakapo Peak domain, plot on a best fit π-girdle distribution in which the axis (348/11 °) is subparallel to the average F_1 fold axes / L_0^1 measurements.

S_1 slaty cleavage is axial planar to F_1 (Fig. 5.1), and can be refracted quite markedly between pelitic-rich siltstone and quartz-rich sandstone beds. Rare graded beds can be picked out because of cleavage refraction (Fig. 5.3). Fanning cleavage around F_1 fold hinges is a common phenomena. S_1 is always penetrative and slaty in pelitic-rich beds, and spaced in sandy beds (Fig. 5.3). In laminated rock, S_1 can be domainal as illustrated by good M domain development in Figure 5.4.

Poles to bedding show a π-girdle distribution in which the axis is subparallel to the average of F_1/L_0^1 lineations (Fig. 5.2). Rare younging direction indicators show F_1 faces upright. In general, F_1 folds are asymmetric with eastern limbs of anticlines longer than western limbs, thus giving a westerly vergence. Occasionally, western limbs of anticlines are overturned. The vergence of F_1 folds is consistent with an eastern limb of a N-S trending macroscale anticline.

Slaty shale unit

The main expression of D_1 deformation in the slaty shale unit is a penetrative slaty cleavage in shale and spaced in quartz sandstone (S_1). S_1 is NNE to NW striking, dipping moderately or steeply eastwards (Fig. 5.6). S_1 refracts strongly between shale and quartz sandstone, and at any particular outcrop, S_1 in quartz sandstone is always dipping more gently towards the east than in shale.

Bedding generally strikes between N and NNW, dipping steeply east or subvertical, but sometimes steeply west (Fig. 5.7). In any particular outcrop, S_1 is always dipping more gently towards the east than bedding.

Unlike the systematic and regular folding in the Douglas Formation, isolated F_1 mesoscale folds hinges occur sporadically within the shale. These folds are always tight or isoclinal, and when the entire fold can be observed, they are seen to have wavelengths of less than 1m. Fold axes and L_0^1 plunge in various orientations along the S_1 plane (Fig. 5.6). The distribution of fold axes and L_0^1 is difficult to explain but may be partially explained by cross-folding (see Section 5.3.3).

Figure 5.3: S_1 cleavage refraction in rare graded beds, Douglas Formation, Kakapo Peak domain. S_1 is slaty in muddy layers and spaced in sandy layers. Note pencil for scale which is subparallel to S_1 in muddy layer. M26/ 723201.

Figure 5.4: S_1 cleavage with good M domain development, Douglas Formation, Kakapo Peak domain. M26/ 724201. Lens cap for scale.

Figure 5.5: S_1 slaty cleavage (pressure solution seams) which wrap around elongate ankerite porphyroblasts. Strain fringes occur on the margins of the porphyroblast parallel to S_1. Note that the ankerite has been oxidised to iron oxides. RJ433, slaty shale unit, PPL.

Figure 5.3

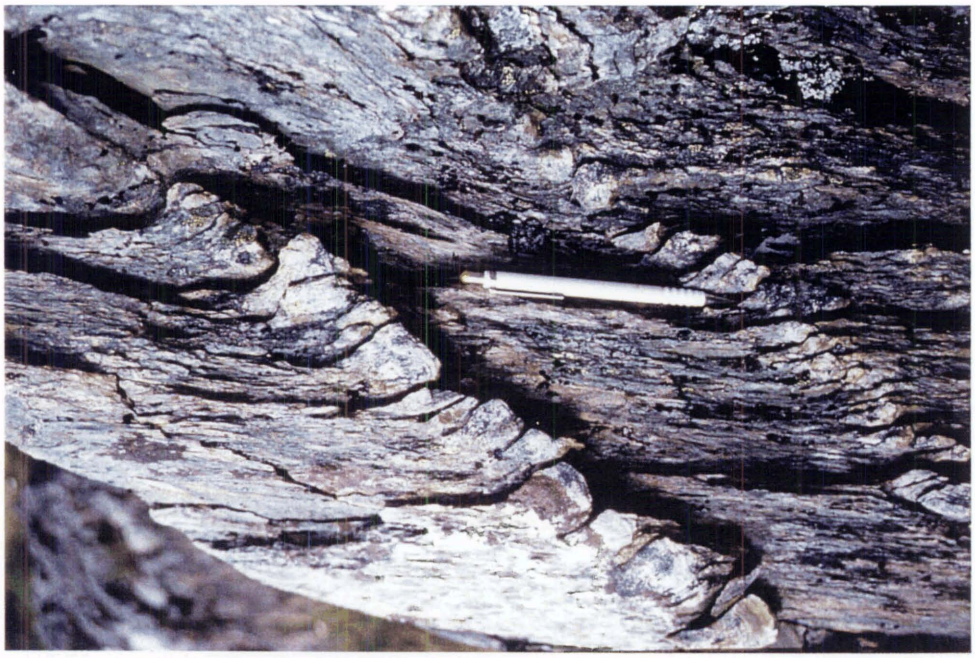

Figure 5.4

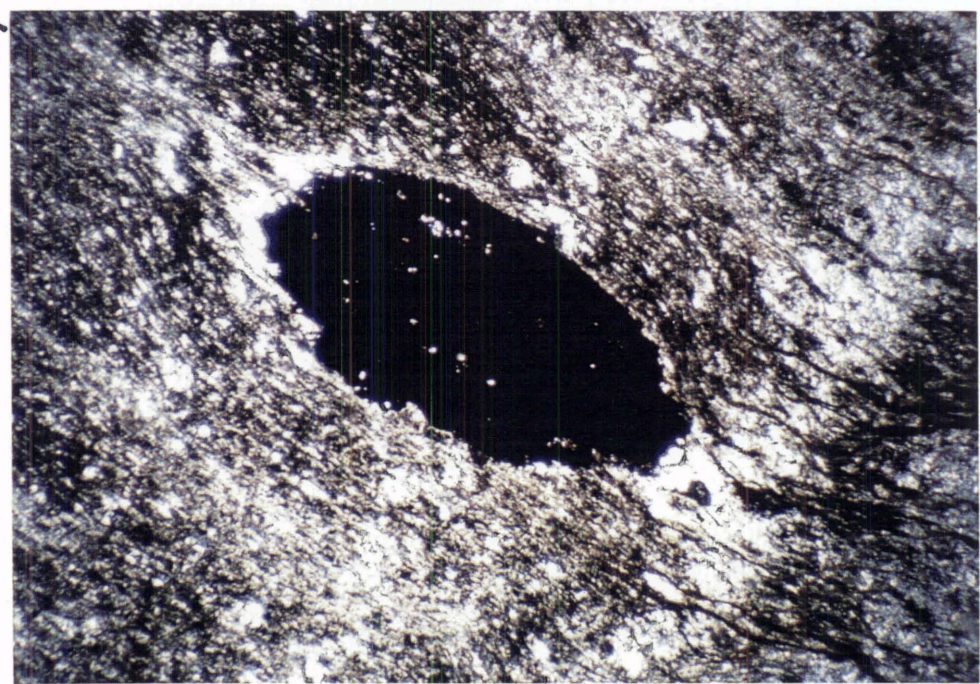

Figure 5.5

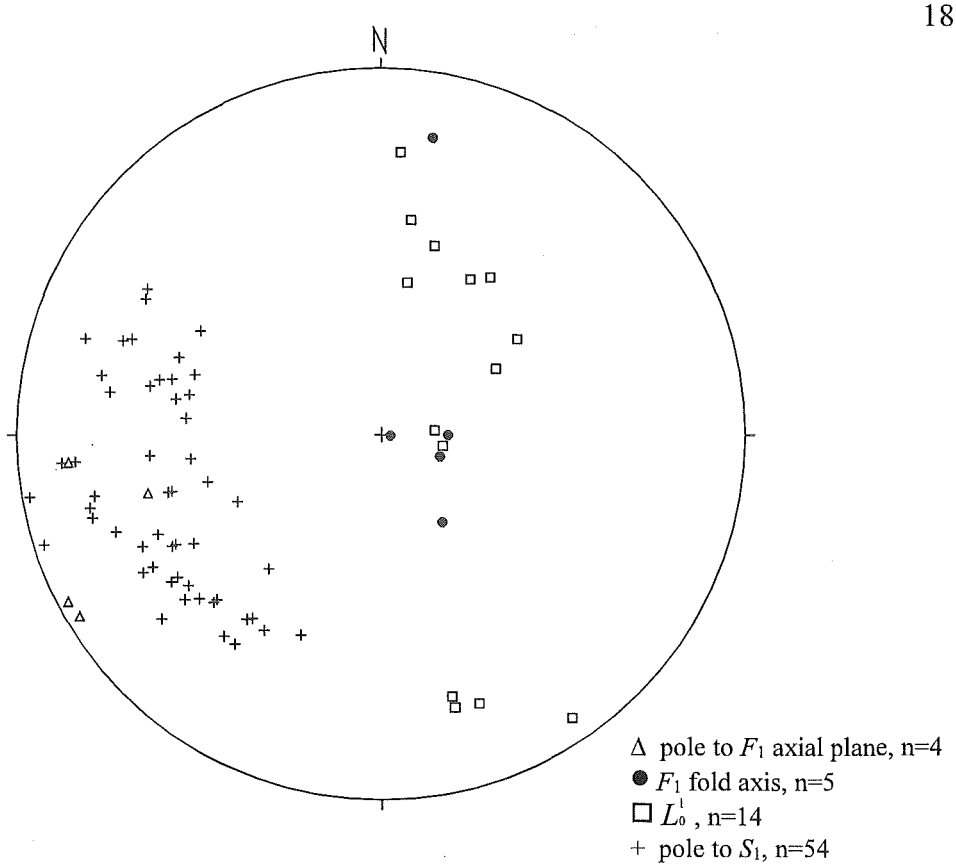

Figure 5.6: F_1, L_0^1, and S_1 orientations in the slaty shale and quartz sandstone unit, Kakapo Peak domain.

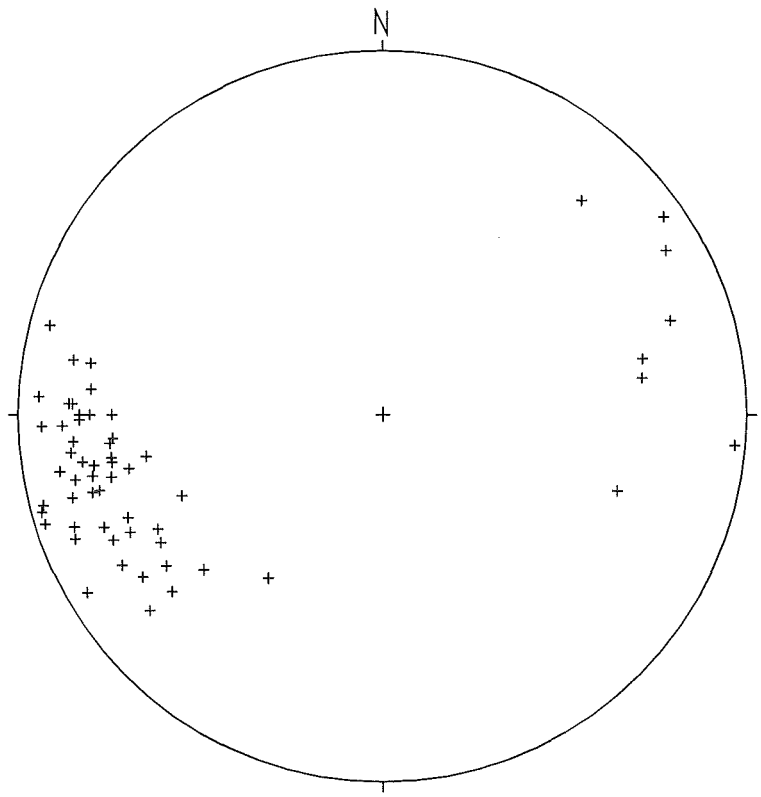

Figure 5.7: Poles to bedding (+) in slaty shale and quartz sandstone unit, Kakapo Peak domain. n=63

Given the orientation of fold structures in the Douglas Formation, the overall bedding/ cleavage relationship and cleavage refraction in the slaty shale unit is consistent with a structurally inverted eastern limb of a N-S trending macroscale synform.

5.3.2 D_1 microscale structures in Kakapo Peak domain

S_1 is a penetrative slaty cleavage that is defined by a combination of aligned white micas and pressure solution seams in pelitic-rich Douglas Formation, and mainly pressure solution seams in the shale unit (Fig. 5.5). Metamorphism appears to be very low grade. Quartz grains retain their clastic shapes and show a preferred orientation of *c*-axes subparallel to S_1 (see Section 4.3.2 for discussion of this).

Ankerite porphyroblasts are widely developed in slaty shale but less so in Douglas Formation. S_1 wraps around the ankerites accompanied by the development of strain fringes (Fig. 5.5).

5.3.3 Other deformation in Kakapo Peak domain

In Douglas Formation and slaty shale, there is sporadic development of a crenulation cleavage (S_{ii}) which strikes generally E-W and dips moderately or steeply N or subvertical (Fig. 5.8). The crenulation spacing can vary from 1mm to 3cm. Occasionally associated with S_{ii}, but only observed in the Douglas Formation, are open to gentle folds (F_{ii}) in which the wavelengths range between large crenulations (~5cm) to no more than 20cm. F_{ii} axes and intersection lineations, observed on steeply dipping or subvertical S_0 and S_1 planes, plunge moderately to steeply north (Fig. 5.8).

In the Douglas Formation, L_0^1 and F_1 fold axes show considerable plunge variation to the north or south (Fig. 5.1). Spatially, there is a systematic pattern to plunge variation in a north-south direction, suggesting either an earlier or later phase of folding in an approximately east-west orientation. The systematic spatial pattern, together with a π-girdle distribution of bedding, suggests it is unlikely that the plunge variation is due to non-cylindrical F_1 folding.

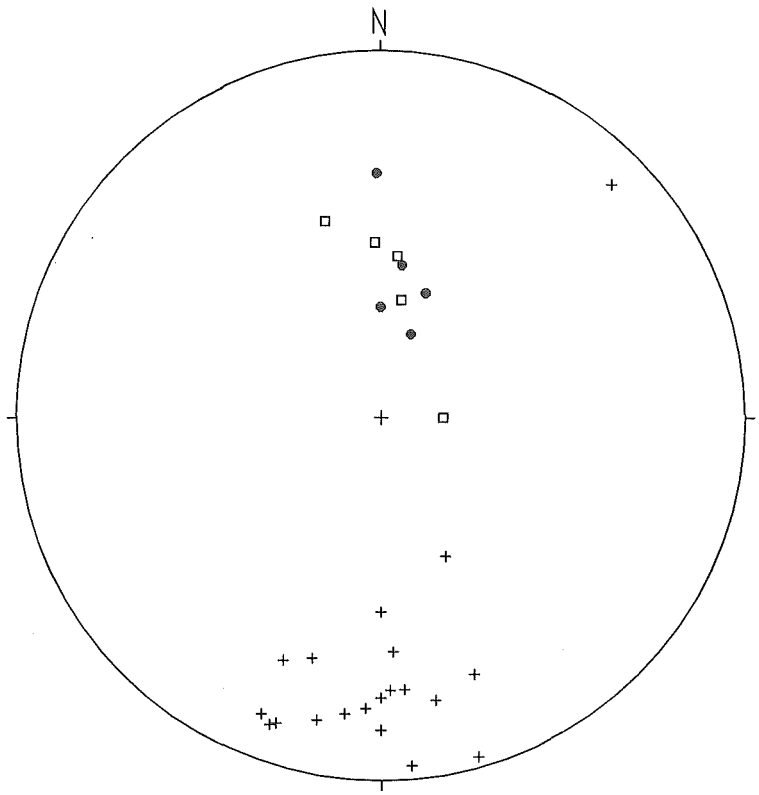

+ pole to S_{ii} in both Douglas Formation and shale/ quartz sandstone unit, n=20

● F_{ii} fold axis in Douglas Formation only (steeply dipping bedding or S_1 are the reference surfaces), n=5

□ L_0^{ii} / L_1^{ii} in Douglas Formation only, n=5

Figure 5.8: S_{ii}, F_{ii}, and L_0^{ii} / L_1^{ii} orientations in Buller terrane rocks of the Kakapo Peak domain.

In the slaty shale unit, a systematic spatial pattern of S_1 strike variation with respect to S_0 is observed. There are areas where S_1 has a more westerly component of strike with respect to S_0, and other areas where S_1 has a more easterly component of strike with respect to S_0. In addition, the variation of S_1 orientations overall are greater than that of S_0 (compare Fig. 5.6 with Fig. 5.7). Although data are sparse, the contrasting areas of S_1 strike variation seem to alternate in a north-south direction and suggests the existence of cross-folding in an east-west direction. It follows that the plunge variation of L_0^1 and F_1 in the Douglas Formation is also probably due to a later phase of folding rather than an earlier phase.

Any such cross-folding may be intimately linked with the crenulation cleavage and associated mesoscale folding.

5.3.4 Structure in the Peak 1610 domain

In limited and non-continuous exposure of Douglas Formation, bedding strikes approximately N-S, dipping moderately E. Quartz-rich laminae are typically lensoidal and a slaty cleavage is sometimes seen slightly oblique to bedding. These observations suggests a cleavage is subparallel to bedding.

In limited exposure of the slaty shale unit, bedding and slaty cleavage strike N-NW, dipping moderately or steeply E. In any particular outcrop, bedding is always more steeper dipping than cleavage.

Given that the cleavage orientation and character resembles that of S_1 at Kakapo Peak and Lonely Lake, the cleavage is therefore designated as such.

5.4 Takaka terrane: Lithology

In the Peak 1610 and Kakapo Peak domains, Takaka terrane rocks consist of, from west to east, a sliver of limestone (up to ~18m thick), a narrow belt of undifferentiated Haupiri Group and Devil River Volcanics Group rocks (200-1000m wide), and Balloon Mélange (Map 3). The Balloon Mélange is described in Chapter 8.

The dark grey limestone is deformed and variably recrystallised. Nevertheless, various allochems are still recognisable including organic plates, fossil fragments, intraclasts, and pellets (Fig. 5.18A). Dolomite/ankeritic rhombs are observed in some samples. In addition, detrital clasts of quartz and chert, and recrystallised micas occur in discrete layers. Layers of primary chert have been observed in one limestone sample (RJ147). The age of the limestone is thought to be Early Ordovician, based on conodont identification in the same limestone sliver of the Mt Benson domain (Section 6.4), and is correlated with Summit Limestone.

The eastern contact of the limestone is marked by interbedded limestone and ankeritic shales, with the limestone beds discontinuous and lensoidal in shape. The shales are highly strained and mineralised by pyrite. Given that the shales probably represent part of the undifferentiated Haupiri Group that occurs east of the limestone sliver, the contact described above suggests a sedimentary contact between undifferentiated Haupiri Group and Summit Limestone. However, it is known that the contact is highly strained (see Section 5.5.4), and together with the lensoidal character of limestone beds and narrowness of the sliver outcrop (Map 3), suggests a ductile faulted contact is more probable.

As in domains further north, the undifferentiated Haupiri Group rocks contain a mixture of conglomerates, grits, sandstones, shales, and minor tuffs/reworked tuffs. Bedding and compositional characteristics are very similar to those described in the Boulder Lake domain (Section 3.6). Again, graded beds (10cm to 1m thick), flame structures, and scour channels provide excellent way-up indicators.

A topographically prominent horizon of basic volcanics and volcanically-derived epiclastics (Fig. 5.9, 5.10), up to 60m thick, can be mapped almost continuously from the

A

B

Figure 5.9 (A): Undeformed lava pillows with the interstices between pillows consisting of carbonate (orange stained in this photo). (B): Deformed lava pillows with well-foliated interstitial limestone anastomosing around them. Note the extension veins orthogonal to the elongate pillows (best seen in the pillow on which the sledge hammer handle rests on). Both (A) and (B) are from a Devil River Volcanics Group horizon which interfingers with undifferentiated Haupiri Group, Peak 1610 domain. (A) M26/ 722227 (B) M26/ 722226. For scale, sledgehammer is 58cm long.

north of the Peak 1610 domain to the south of the Kakapo Peak domain (Map 3). The basic volcanics in this horizon are made up of lava flows, lava pillows (Fig. 5.9), and tuffs. The volcanics are petrologically similar to the Benson Volcanics (C. Münker pers. comm. 1996) and are therefore designated as part of the Devil River Volcanics Group. A prominent lava flow is observed to the west of Kakapo Peak and is up to 20m thick. Lava pillows are well-displayed between Peak 1610 and 1512, and the lava pile there is up to 15m thick. The lavas consist of phenocrysts of clinopyroxene and olivine, which may be either fresh or as pseudomorphs, and a matrix of fine grained actinolitic hornblende needles, saussuritised feldspar, epidote, chlorite, and opaques. Large pseudomorphs of pyroxene, up to 1cm in length, also occur in tuffs (Fig. 5.11). The epiclastics are made up of breccias (up to 20m thick), sandstones and siltstones, and are derived mainly from reworked tuffs. In addition to this prominent horizon, there are isolated tuff and reworked tuff beds, up to 3m thick, that also contain large pseudomorphs of pyroxene.

Rare impure limestone beds are observed interbedded with the volcanically-derived epiclastics, and carbonate also makes up a significant part of the coarse epiclastic matrix. In addition, the interstices between lava pillows commonly consists of a creamy limestone (Fig. 5.9). These occurrences of limestone indicate a carbonate background sedimentation during eruption.

Minor intrusives, up to 20m thick and concordant with bedding in Haupiri rocks, are observed in both the Peak 1610 and Kakapo Peak domains. The intrusives in the Peak 1610 domain are green in colour, and thin-sections show them to be metadolerites. The intrusives recognised in the Kakapo Peak domain are grey in colour due to extensive carbonate and quartz replacement. Microscopic texture suggests the intrusives at Kakapo Peak are also dolerites. The intrusives have been provisionally designated as part of the Devil River Volcanics Group.

Ankeritic metasomatism is variable in the undifferentiated Haupiri Group rocks but most intense within ~100m of the Anatoki Fault. Ankerite porphyroblasts are up to 3mm in size. Pyrite mineralisation is also common in sediments immediately adjacent to the limestone sliver.

Figure 5.10: Volcanic breccia in Devil River Volcanics Group, near Kakapo Peak. Carbonate in the matrix has been dissolved out, due to weathering, causing the volcanic clasts to stand out in outcrop. The clasts are strained parallel to S_1, and their elongate shapes define the stretching lineation. Bedding is subparallel to S_1 in (B). (A) M26/ 726205, (B) M26/ 726204. For scale, sledgehammer head is 13cm long.

Figure 5.11: Pseudomorphs of pyroxene phenocrysts (now chlorite) in tuff/ reworked tuff. The pseudomorphs are deformed and define S_1. The white minerals are carbonate. RJ162, volcanically-derived epiclastic bed in Devil River Volcanics Group near Peak 1610.

Figure 5.10A

Figure 5.10B

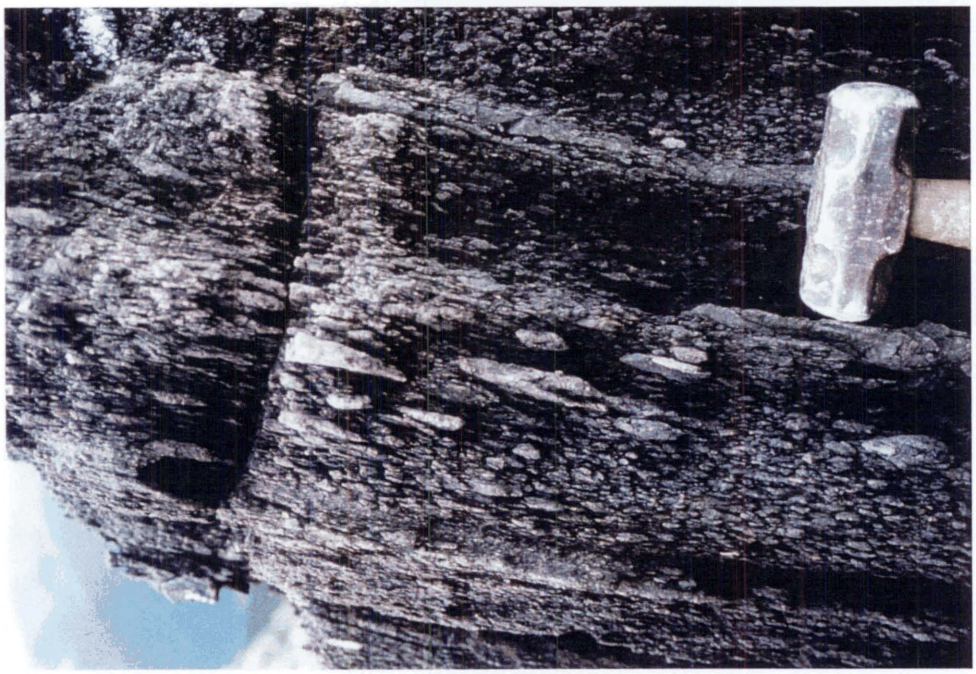

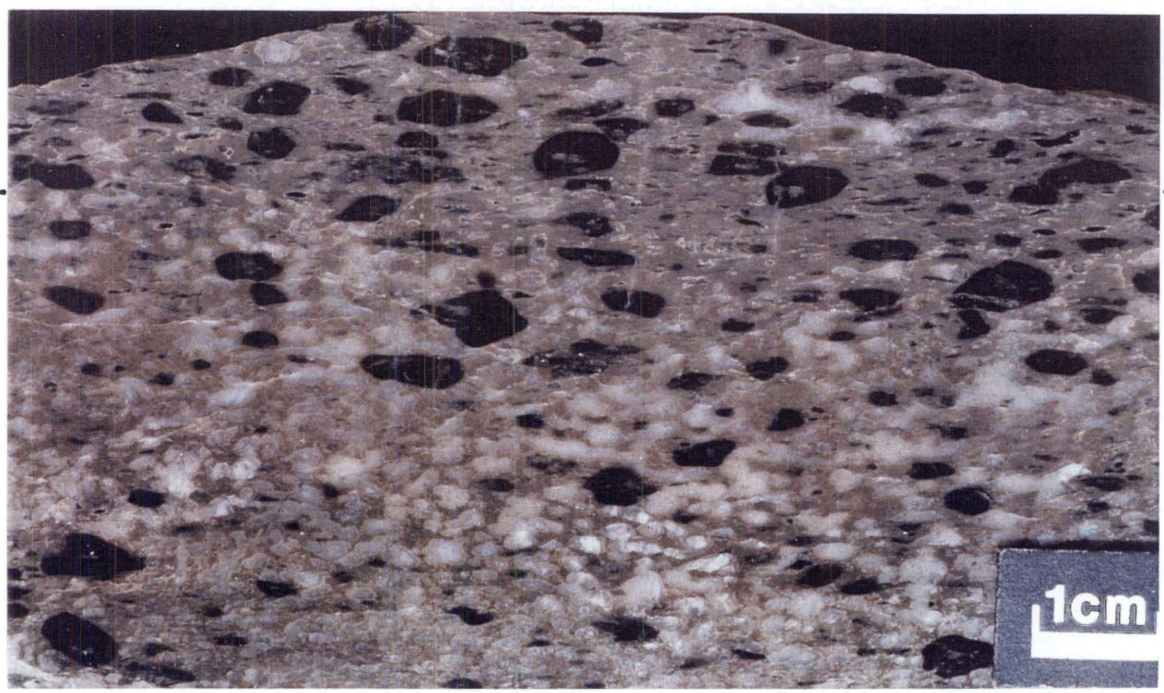

Figure 5.11

5.5 Takaka terrane: Structure

In the undifferentiated Haupiri and Devil River Volcanics Groups, only one major deformation event is recognised (D_1). Deformation in the limestone sliver is also thought to be related to D_1. The structure in the Balloon Mélange is described in Chapter 8.

5.5.1 D_1 mesoscale structures

D_1 is represented primarily by a cleavage (S_1) with an associated and prominent stretching lineation. In addition, there are rare isolated folds with S_1 axial planar to them. S_1 is slaty in shale and spaced in sandstone. S_1 is also defined by deformed clasts in volcanic breccias (Fig. 5.10), and deformed pseudomorphs of pyroxene crystals in tuffs/ reworked tuffs (Fig. 5.11). In many alternating sandstone/shale horizons, S_1 is only observed in the shales.

In both domains, S_1 strikes generally between N and NNW, dipping moderately or steeply to the east, or subvertical (Kakapo Peak domain only) (Fig. 5.12). Associated with S_1 is a prominent stretching lineation that is defined in the field by:

- the elongation direction of ankerite and pyrite strain fringes
- elongate chloritised pyroxene crystals in tuffs and reworked tuffs (Fig. 5.11)
- elongate volcanic breccia clasts (Fig. 5.10)
- elongate lava pillows (Fig. 5.9B)

In the latter stretching lineation indicator, the pillows have become elongate by a combination of brittle deformation, as evidenced by many extensional veins orthogonal to the elongation direction (Fig. 5.9B), and ductile deformation, as microscopically evidenced by strained phenocrysts and groundmass (Section 5.5.2). Foliated limestone anastomosing around the pillows provides an excellent example of strain partitioning (Fig. 5.9B). In the Kakapo Peak domain, volcanic breccia clasts have X/Z ratios of about 2-3:1. In contrast, conglomerates containing a mixture of quartz, sedimentary, and volcanic clasts display very little evidence of strain.

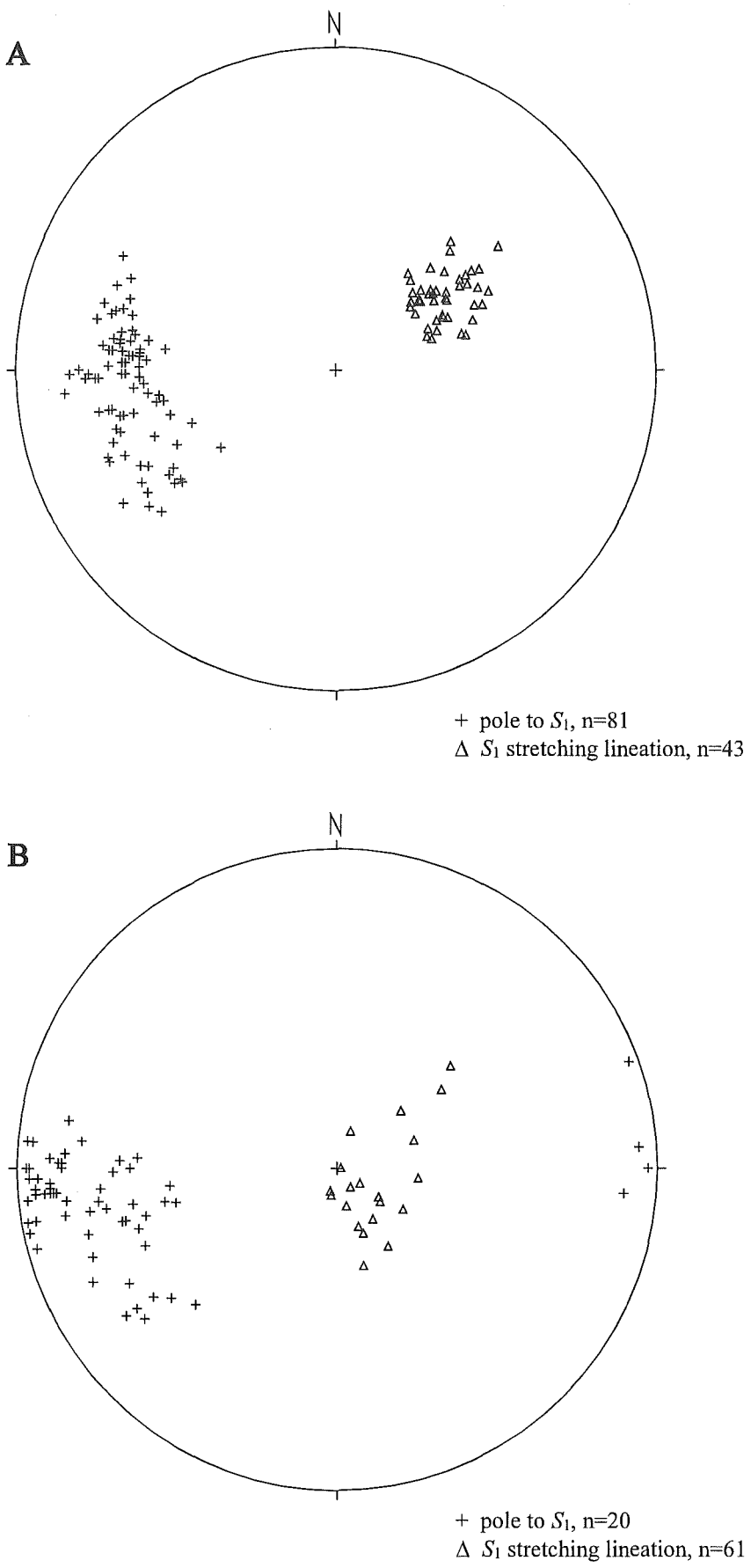

Figure 5.12: S_1 and S_1 stretching lineations in the undifferentiated Haupiri Group and Devil River Volcanics Group of the Peak 1610 (A) and Kakapo Peak (B) domains.

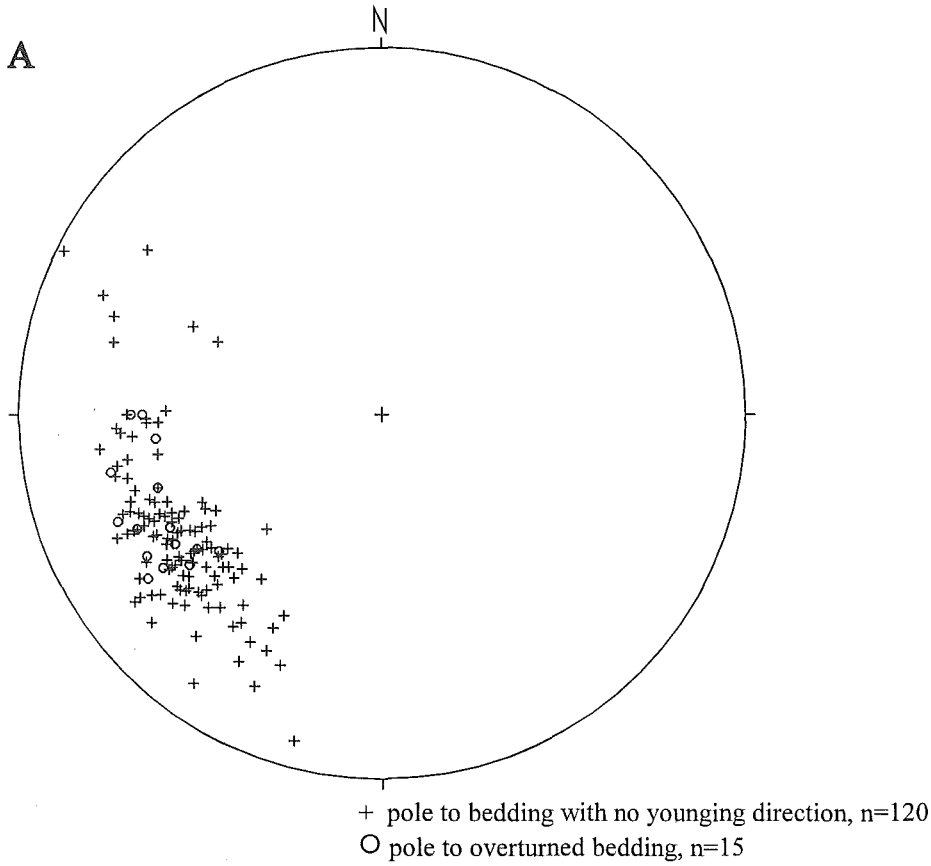

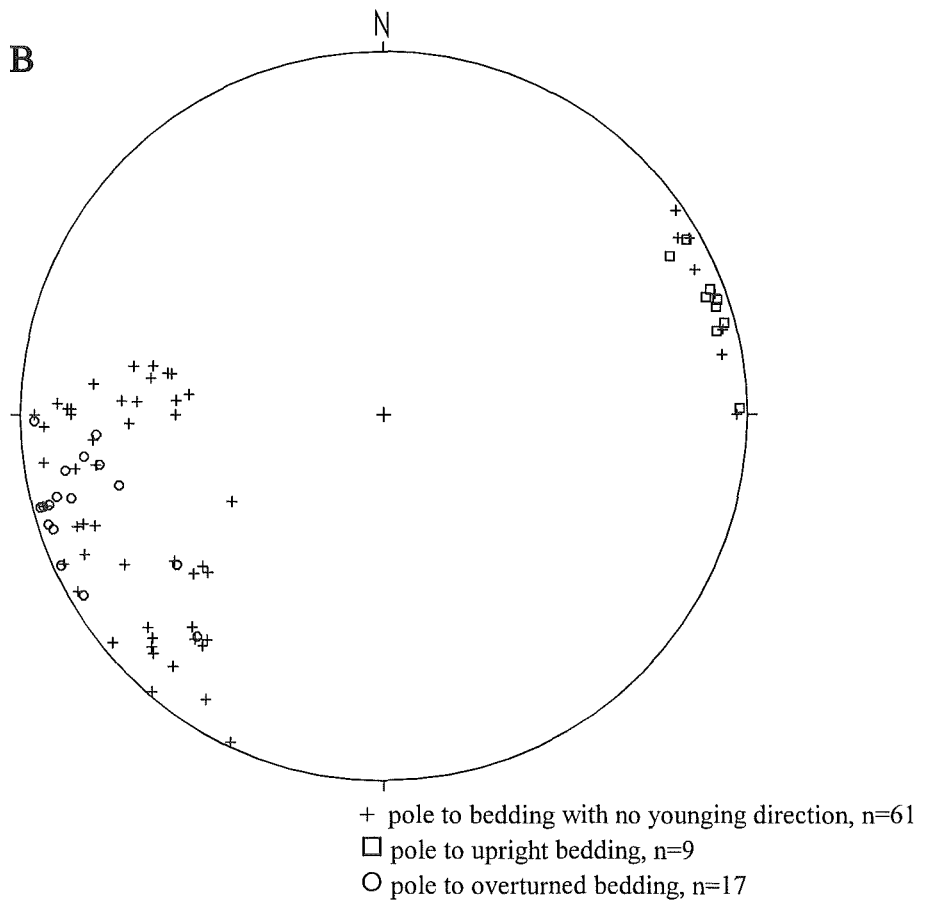

Figure 5.13: Poles to bedding in the undifferentiated Haupiri Group and Devil River Volcanics Group of the Peak 1610 (A) and Kakapo Peak (B) domains.

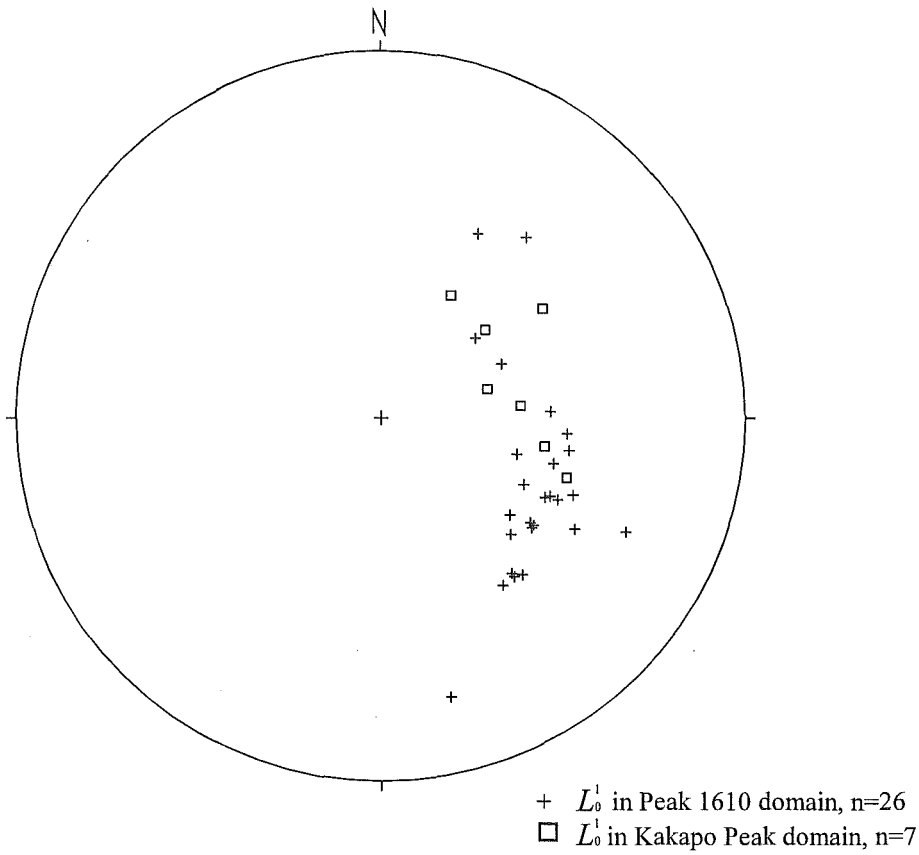

Figure 5.14: L_0^1 orientations in the undifferentiated Haupiri Group of the Peak 1610 and Kakapo Peak domains.

The stretching lineations plunge moderately or steeply NE-ENE in the Peak 1610 domain (Fig. 5.12A), and plunge steeply towards the eastern quadrant or subvertical in the Kakapo Peak domain (Fig. 5.12B).

Bedding in both domains strikes generally between N and NW, dipping moderately or steeply to the NE, or subvertical (Kakapo Peak domain only) (Fig. 5.13). All bedding is either overturned or subvertical. At any particular outcrop, bedding is generally found to have a more westerly component of strike with respect to S_1 strike, but there is no obvious pattern as to which plane is steeper dipping than the other. As a result, L_0^1 plunges moderately or steeply between NE and SE, although in the Peak 1610 domain, L_0^1 is generally plunging SE (Fig. 5.14).

Very rare and isolated close folds, with wavelengths of less than 30cm and to which S_1 is the axial plane, are observed in both domains. Unfortunately the orientation of fold axes were difficult to measure due to the nature of the outcrop, but they plunge approximately towards the easterly quadrant.

5.5.2 D_1 microscale structures

In shale, S_1 is a penetrative slaty cleavage defined by aligned fine grained white micas, chlorite, and opaque solution seams. In ankerite porphyroblast bearing dark-grey shale horizons that occur within ~150m of the Anatoki Fault, mesoscale S_1 (i.e. that measured in the field) is the latest of several foliation surfaces recognised microscopically. Using two typical ankerite porphyroblast bearing shale thin-sections for illustrative purposes (RJ176 and RJ155), one can see that these foliation surfaces seem related to one deformation event as a result of non-coaxial progressive deformation.

In RJ176, three foliation surfaces are recognised (refer to Figure 5.15). Mesoscale S_1 wraps around the porphyroblasts, and strain shadows and ankerite/quartz strain fringes are developed. The shadows and fringes are most elongate and asymmetric parallel to the stretching lineation, and provide a sense of shear. In the strain shadow, there is a preserved foliation (S_{shad}), oblique to S_1, which clearly curves into S_1 at the margins of the shadow. In the ankerite porphyroblasts themselves, straight inclusion trails define a foliation (S_{incl}), which is oblique to both S_{shad} and S_1. In some cases, the porphyroblasts

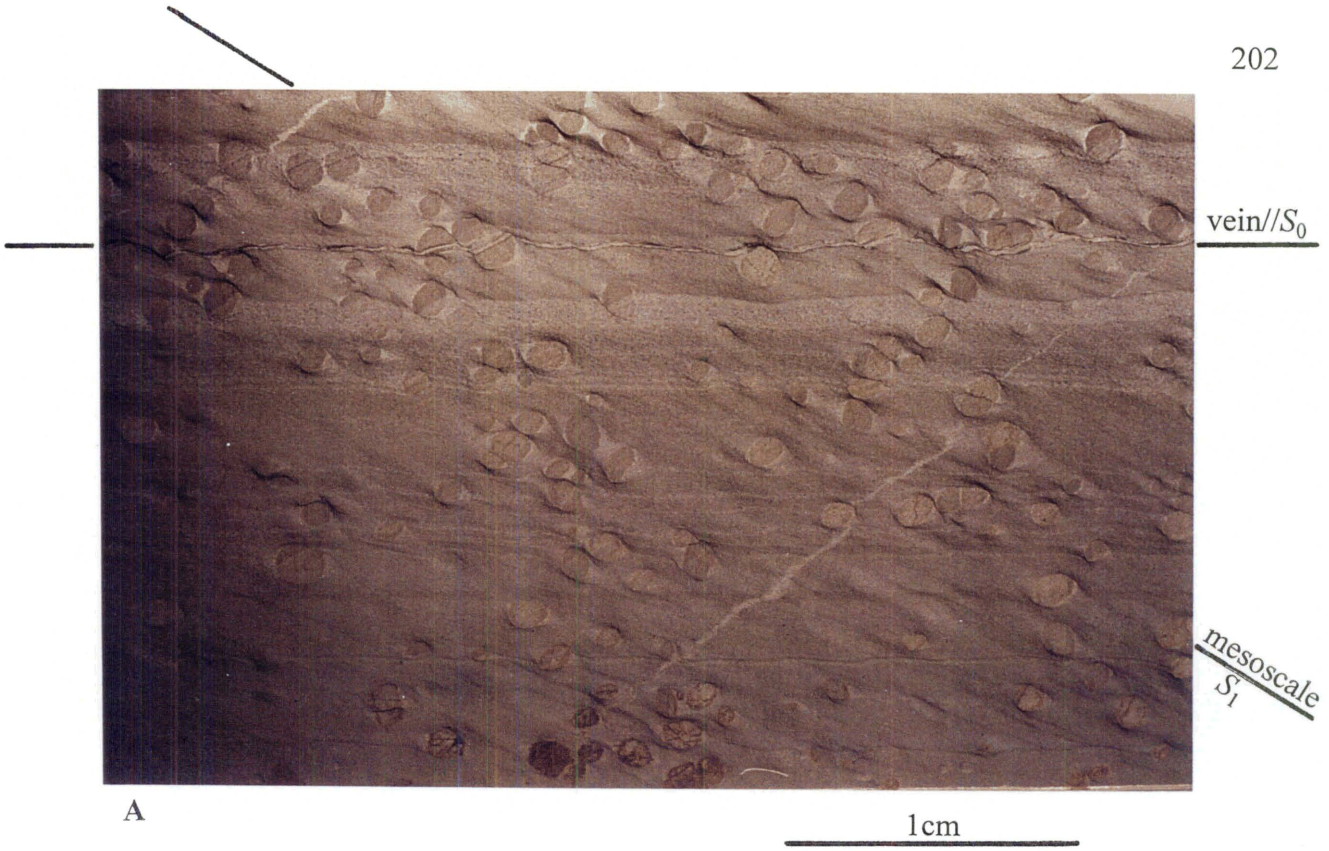

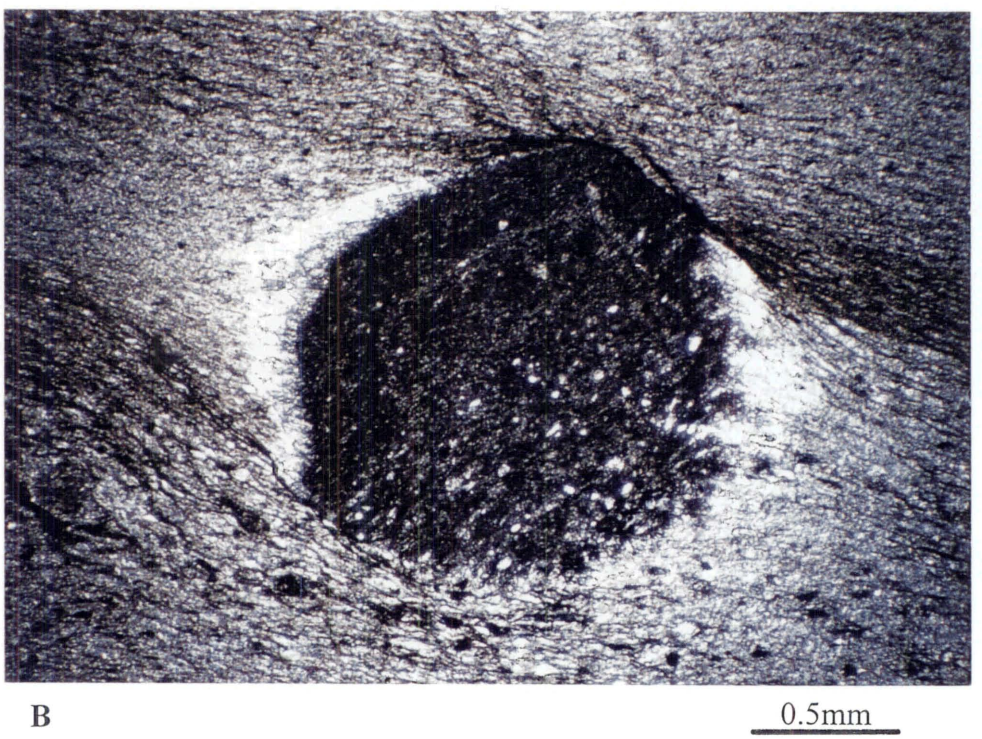

Figure 5.15 (A): Photograph of RJ176 S_1 XZ thin-section. PPL. Note the thin vein, parallel to bedding, which has been overgrown by ankerite porphyroblasts prior to mesoscale S_1 development. (B): Photomicrograph of an ankerite porphyroblast in RJ176 with inclusion trails parallel to the included bedding plane. Note the asymmetry of the strain fringe and shadow. S_1 XZ section. PPL. A line drawing of this photomicrograph is given in (C) (next page).

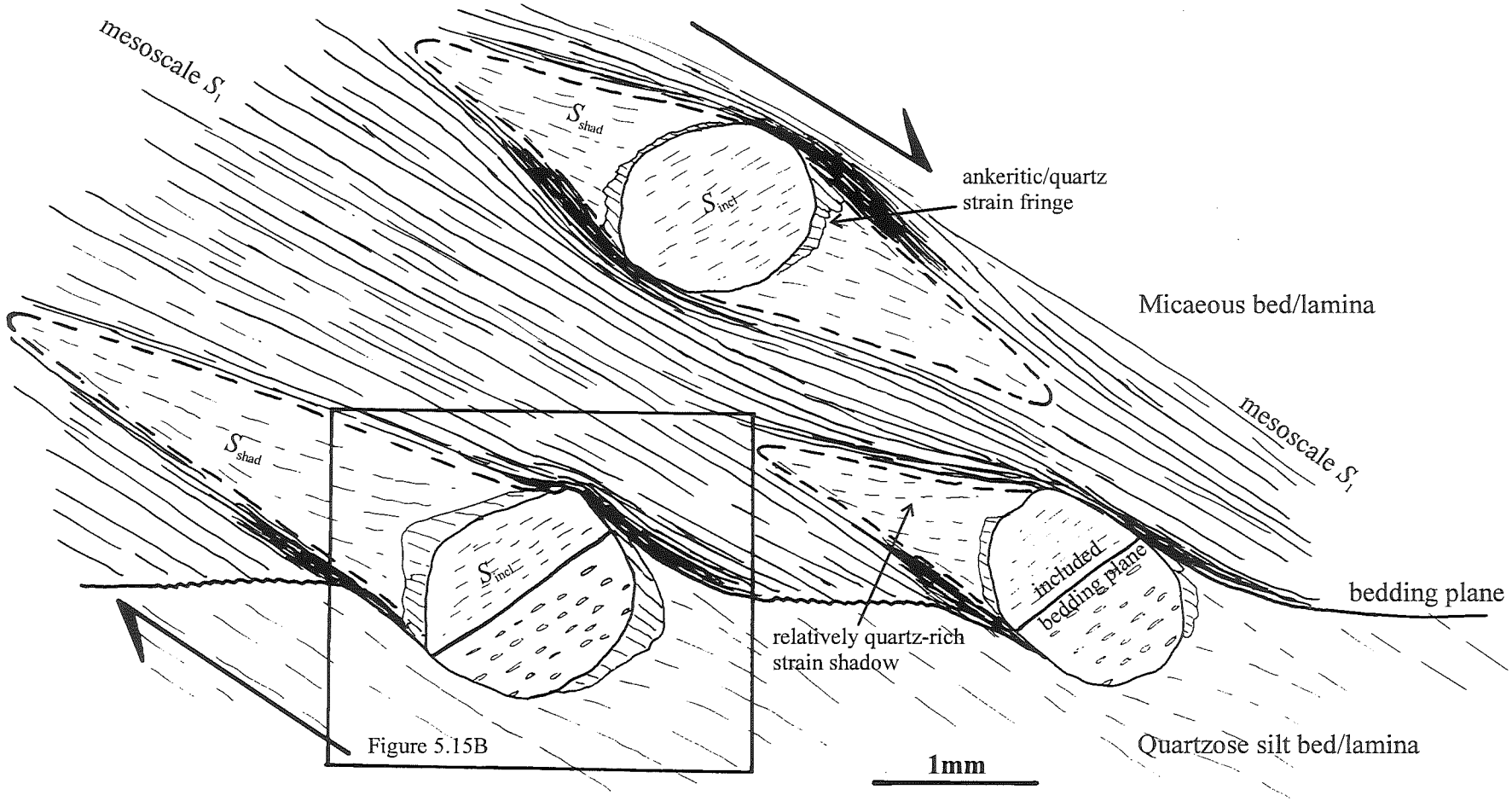

Figure 5.15 continued (C): Line drawing of RJ176 S_1 XZ section. The drawing depicts the microstructure observed in ankerite porphyroblast bearing shale, undifferentiated Haupiri Group (see text for description). Rectangle outlines a line drawing of (B) (previous page).

have overgrown bedding planes and clearly show that S_{incl} is subparallel to included bedding planes (Fig. 5.15). The included bedding planes are themselves oblique to external bedding.

Most importantly, S_{incl} and included bedding planes in all ankerite porphyroblasts of the RJ176 thin-section are consistently oriented, suggesting that the porphyroblasts have not rotated (Bell 1985). In this model, it is the external bedding and foliation surfaces that have been rotated in a clockwise direction in Figure 5.15. The clockwise direction is deduced by the progressive rotation from S_{incl} to S_{shad} to S_1 which is consistent with the top to the right shear-sense given by the asymmetry of strain shadows and fringes (Fig. 5.15). The foliation surfaces have probably rotated by a combination of mechanical rotation, recrystallisation, and growth processes. Bedding has rotated passively with the progressive development of the foliation surfaces.

One could instead argue that it is the ankerite porphyroblasts that have rotated and not the matrix (Zwart 1962). However, if porphyroblast rotation is advocated, the porphyroblasts would have had to rotate anticlockwise, as indicated by internal-external bedding relationships (Fig. 5.15), and this is inconsistent with the sense of shear provided by the asymmetry of strain shadows and fringes. Another reason why ankerite porphyroblast rotation seems improbable is because one would have to advocate a fortuitous coincidence of exactly the same angle of rotation in all porphyroblasts, given that inclusion trails are consistently oriented.

Occasionally, strain fringes immediately adjacent to the porphyroblasts are elongate parallel to S_{shad}, but toward the margins of the porphyroblast, the fringes are more parallel to S_1 (Fig. 5.15). Presuming the fringes all formed at the same time, the change in elongation direction is thought to be an expression of non-coaxial strain partitioning in which the central fringes reflect dominantly progressive shortening strain and the marginal fringes reflect dominantly progressive shearing strain (Bell 1985). In the same light, S_{shad}, which is parallel to the elongate strain fringes, is a preserved foliation that has accommodated progressive shortening strain. S_{shad} curves into S_1 along the margins because of increasing progressive shearing strain towards the margins (Bell and Johnson 1992).

In RJ155, four foliation surfaces are recognised (refer to Figure 5.16). Mesoscale S_1 is only incipiently developed in thin-section view and postdates an earlier external foliation in which strain shadows are parallel to. Both foliations appear to be intimately related, and in RJ155, it is best to refer to the earlier foliation as S_{1a}, and mesoscale S_1 as S_{1b}. S_{shad} and S_{incl} in RJ155 are observed in the same relative orientations as similarly seen in RJ176. Along the margins of most porphyroblasts, S_{incl} can be traced to curve in a clockwise direction into S_{shad}, which subsequently curves into S_{1a}, and which finally curves into the developing S_{1b}. The clockwise curving of progressively younger S surfaces is consistent with the top to the right shear-sense indicated by asymmetric strain shadows (Fig. 5.16).

The ankerites in RJ155 show multiple stages of growth, so that in some cases, millipede microstructure (Bell and Rubenach 1980) of inclusion trails is observed (Fig. 5.16). Millipede microstructure was initially interpreted as indicating a deformation path that involved bulk heterogeneous shortening which was near coaxial at the scale of a microlithon (Bell and Rubenach 1980). More recently, millipede microstructure and associated opposite concave microfolds (Johnson and Moore 1996) have been reviewed by Johnson and Bell (1996). It is the conclusion of these authors that the microstructure can form in any deformation path between bulk coaxial shortening and bulk simple shearing.

In summary, and excluding the uncertainty of millipede microstructure, I believe the consistent curving of progressively younger S surfaces, as seen in RJ155 and RJ176, is the result of a single non-coaxial deformation event (D_1). It follows that ankerite metasomatism is syn-D_1.

Six ankerite porphyroblast bearing shale samples were collected in the Peak 1610 domain (RJ155, 168, 169, 171, 176, 177), one in the Kakapo Peak domain (RJ440), and also one in the Lonely Lake domain (RJ466: Fig. 4.29). In geographical coordinates, S_{incl} in all eight ankerite porphyroblast bearing shale samples is always of an orientation that is near vertical or at least steeper dipping to the east than S_1. Shear-sense in the shales is provided by strain shadow/fringe asymmetry and tracking the curvature of S_{shad} (the old foliation preserved in a zone of low strain), into S_1 (the new foliation in a zone of high strain) (Bell and Johnson 1992). The shear-sense indicators in all eight samples is

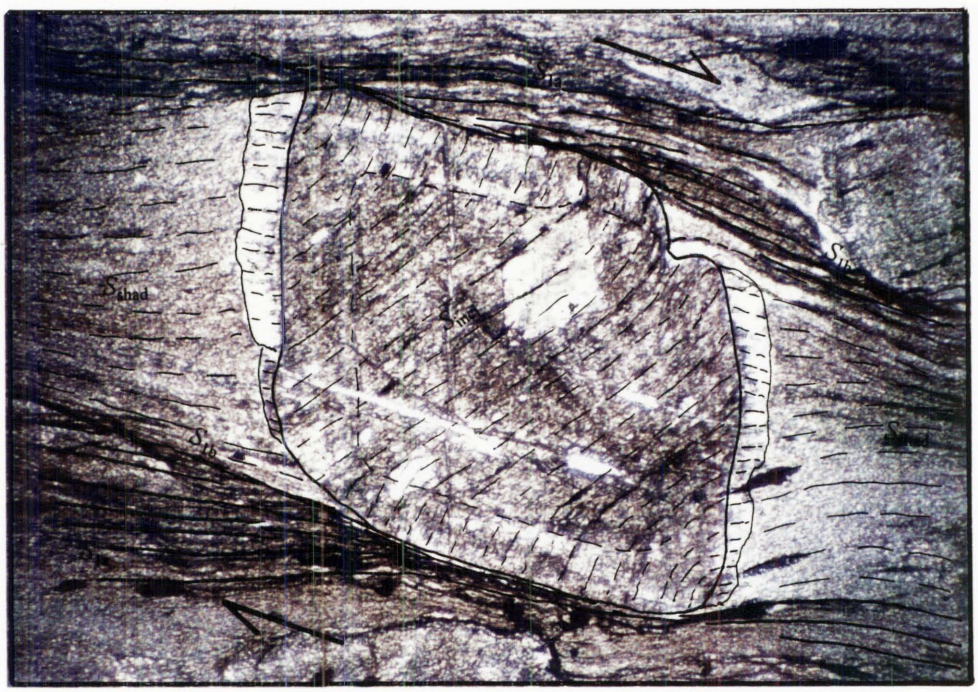

A

0.5mm

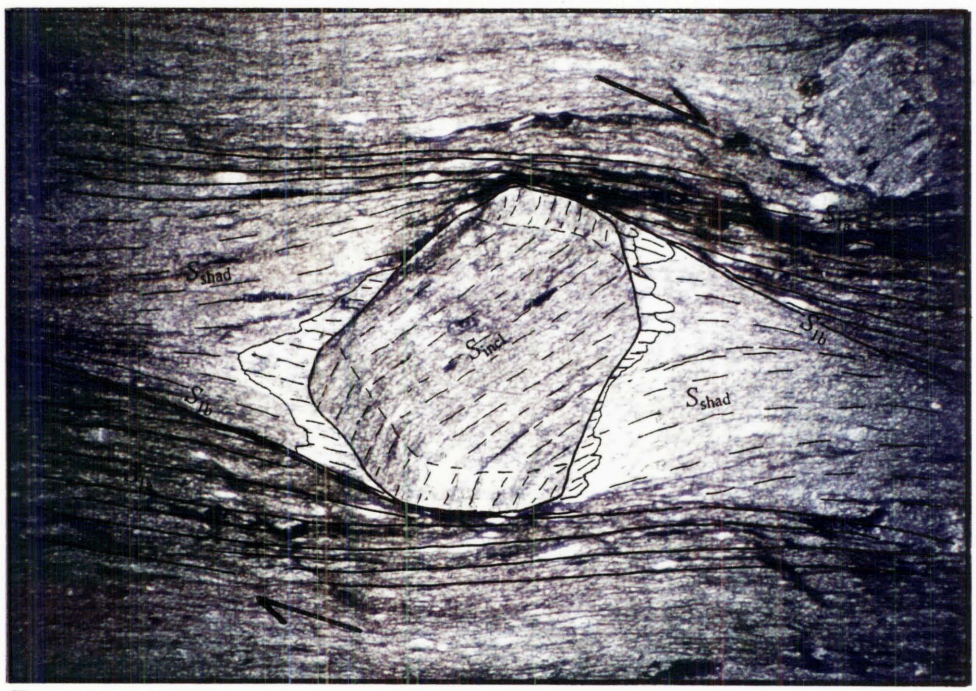

B

0.5mm

Figure 5.16: (A and B) Microstructure in the S_1 XZ section of RJ155, an ankerite porphyroblast bearing shale sample, undifferentiated Haupiri Group (see text for description). Note the ankerite zonation and millipede microstructure. PPL.

consistent and gives a top to the SW/W sense of shear when observed parallel to the stretching lineation. The significance of these observations is discussed in Chapter 9.

The intrusives show negligible or no ductile deformation microscopically. The volcanics, however, do show some evidence of ductile deformation. In the groundmass, actinolitic hornblende prisms show a weak to moderate SPO and defines S_1. Pseudomorphs of olivine and pyroxene phenocrysts show strained crystal shapes in a plane that is parallel to S_1. The phenocrysts must have been altered prior to deformation since it is not possible to deform olivine and pyroxene plastically except at very high temperatures.

Limestone anastomosing around lava pillows is finely recrystallised. Calcite grains possess an SPO which defines local S_1.

The syn-D_1 metamorphic mineralogy in non-volcanic derived shales (quartz + white mica + carbonate ± chlorite) and in volcaniclastics (chlorite + actinolitic/tremolitic hornblende + carbonate ± epidote) is indicative of a very low grade metamorphism.

5.5.3 D_1 discussion

Based on the observations described in the previous section, the orientation of inclusion trails in ankerite porphyroblasts are thought to represent an early orientation of mesoscale S_1, assuming that the porphyroblasts have not rotated with respect to geographical coordinates. That all eight samples from different localities show the same approximate orientation of inclusion trails, both within the sample and between samples, is strong evidence for non-rotation. Nevertheless, it is possible that the entire rock pile of the domains has undergone a bulk rotation but this seems unlikely.

Assuming no bulk rotation, S_{incl} appears to have formed in a subvertical orientation which was subparallel to included bedding (Fig. 5.17A). Thus bedding was already deformed, probably by folding, prior to ankerite porphyroblast growth and mesoscale S_1 formation. Subsequent to the deformation, S_1 development and top to the SW/W sense of shear led to the overturning of bedding from an originally subvertical orientation (Fig. 5.17B). Development of mesoscale S_1 appears not to have been symmetrically oriented

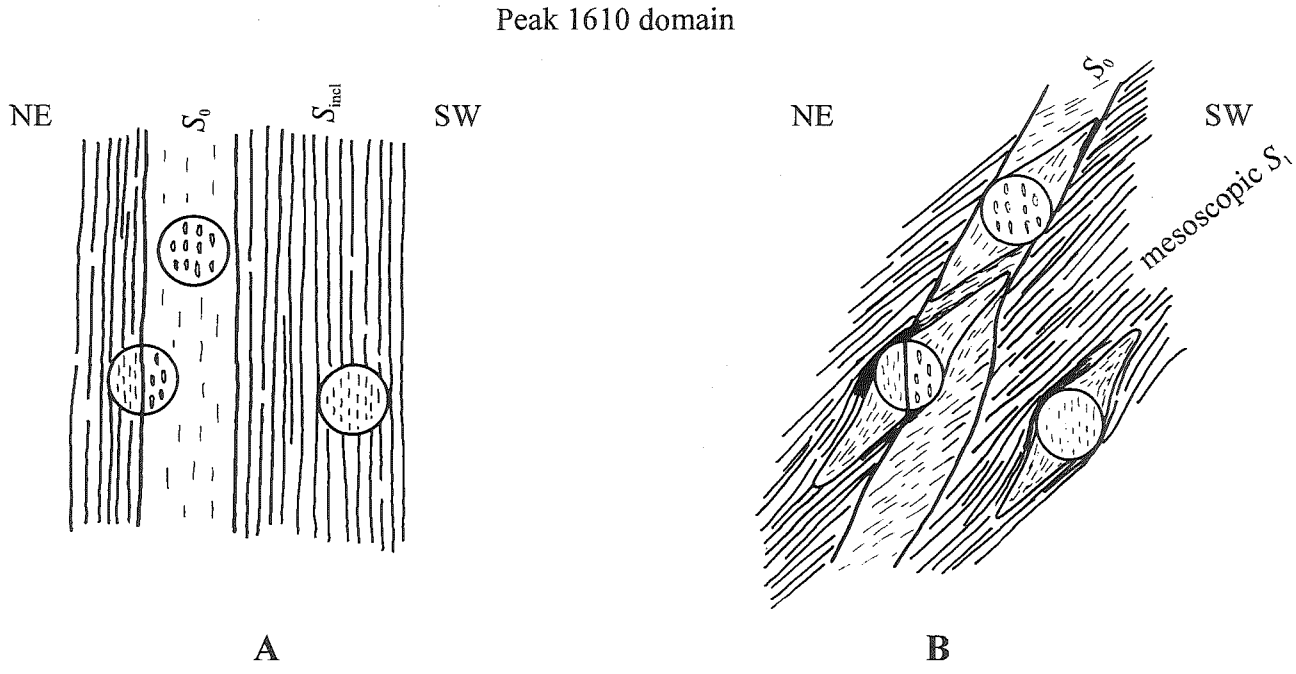

Figure 5.17: Diagram to illustrate original orientation of bedding at time of ankerite porphyroblast growth, assuming the porphyroblasts have not rotated with respect to geographical coordinates (A). S_1 development and top to the WSW shear-sense led to the overturning of bedding (B). See text for further discussion. Both (A) and (B) are parallel to stretching lineation and perpendicular to bedding. (A) and (B) are not perpendicular to S_1 thereby giving an apparent dip less than S_0.

with respect to bedding as evidenced by the fact that L_0^1 lineations are oblique rather than orthogonal to S_1 stretching lineations (as seen in domains further north). The relationship of overturned bedding with mesoscale S_1 suggest the undifferentiated Haupiri Group rocks in the Peak 1610 and Kakapo Peak domains represent an overturned western limb of large macroscale anticline, the S_1 stretching lineations being perpendicular to the anticlinal fold axes. Shear-sense indicators are consistent with an overturned western limb of an anticline.

Mesoscale S_1 is not considered as S_3 observed in the adjacent Lonely Lake domain mainly because the orientation of S_1 is orthogonal to S_3 in the Lonely Lake domain. In addition, breccia clasts in the Peak 1610 and Kakapo Peak domain are flattened parallel to S_1, and this is in accord with conglomerate clasts at Lonely Lake and Adelaide Tarn, where they are always flattened parallel to S_1 and never to S_3. In some ankerite porphyroblast bearing shales of the Peak 1610 domain, a discontinuous pressure solution crenulation cleavage is seen in thin-section and occurs in the immediate vicinity of ankerite porphyroblasts. Oriented thin-sections suggest the crenulation cleavage is consistent with S_3 in the Lonely Lake domain.

5.5.4 Deformation in the limestone sliver and adjacent rocks

From mapping in the Stanley River catchment between the Peak 1610 and Kakapo Peak domain, the limestone sliver strikes approximately 350°, dipping 60°E. However, south of Kakapo Peak the dip appears to steepen up to ~80°E.

The limestone sliver is variably deformed so that it consists now of rocks ranging from weakly deformed limestone to calc-mylonite. Most of the limestone is weakly to moderately deformed and a cleavage is variably developed. The cleavage is subparallel to the margins of the limestone sliver and to S_1 in adjacent Haupiri Group and Devil River Volcanics Group rocks (i.e. N-NNW striking, dipping moderately or steeply east, or subvertical). On cleavage planes there is a weak stretching lineation that is subparallel to stretching lineations in adjacent Haupiri Group and Devil River Volcanics Group rocks. Bedding, where recognised, is subparallel to the cleavage but often shows evidence of pinch and swell structure and boudinage. There is scattered evidence of isoclinal folds of bedding. In thin-section, allochems are in various stages of

Figure 5.18 (A): Fossil fragments and plates in weakly deformed limestone. Plates display multiple twinning. Rough solution seams and incipient recrystallisation along grain boundaries can be observed. RJ188, Limestone sliver, CPL. (B): Large allochem in which over 50% is recrystallised to fine grains. RJ191, limestone sliver, CPL.

Figure 5.19: Asymmetric calcite strain fringes around detrital quartz grains in limestone sliver. Shear-sense is top to the right. XZ section, RJ408. CPL.

0.5mm

Figure 5.19

0.5mm

Figure 5.18B

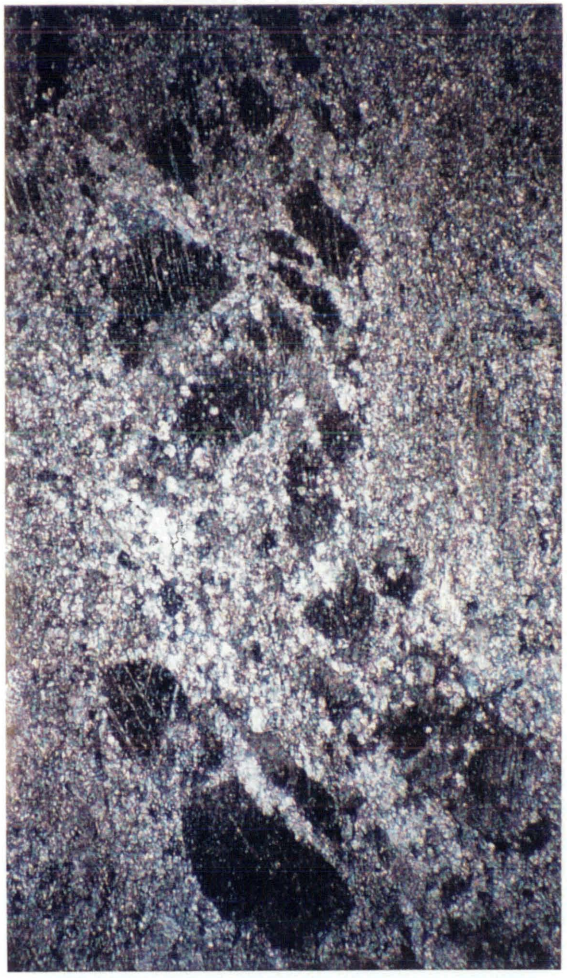

0.5mm

Figure 5.18A

recrystallisation to a fine grain size (Fig. 5.18). Fossil plates display multiple twinning and undulatory extinction. Allochems show a SPO that is subparallel to solution seams, and together these define the mesoscale cleavage. Where detrital grains of quartz occur, there are elongate strain fringes of calcite parallel to the lineation seen on cleavage planes (Fig. 5.19), thus establishing the lineation as a stretching lineation. These elongate fringes are consistently asymmetric (Fig. 5.19), and indicate a top to the west sense of shear on a steep east dipping plane i.e. reverse movement (Kakapo Peak domain).

Only two occurrences of calc-mylonite were seen. At M26/ 722221 in the Peak 1610 domain, a distinctive 5-12cm calc-mylonite layer is observed directly along the western margin of the limestone sliver (Fig. 5.20). At M26/ 725201 in the Kakapo Peak domain, calc-mylonite was observed in the middle of the limestone sliver. In calc-mylonite, the cleavage develops into a layering (Fig. 5.21), and a strong lineation is observed. Both the layering and lineation are subparallel to S_1 and the stretching lineation in adjacent Haupiri Group and Devil River Volcanics Group rocks respectively. The grain size in the calc-mylonites is less than 8μm. Quartz veins are extremely boudinaged, and intrafolial folds are observed (Fig. 5.21). A weak SPO of calcite grains oblique to layering is observed similar to that in calcite tectonites of the Crow River domain. As shown for that domain, the asymmetry of calcite SPO with respect to layering provides a sense of shear (Section 7.4.3). Both the vergence of intrafolial folds and calcite SPO asymmetry indicate a top to the southwest (Peak 1610 domain) or west (Kakapo Peak domain) sense of shear on an east dipping plane (i.e. reverse movement).

Immediately west of the limestone sliver is a ~1m thick Buller terrane derived (semi-) brittle shear zone (Fig. 5.20). The shear zone is well-indurated, intensely foliated, and riddled with boudinaged quartz and calcite veins. The shear zone foliation is concordant with the margin of the limestone sliver.

Within 20m of the eastern margin of the limestone sliver, bedding in the undifferentiated Haupiri Group rocks becomes subparallel to S_1 (i.e. N-NNW striking, dipping moderately to steeply east, or subvertical). S_1 becomes intensely developed as compared to its development in undifferentiated Haupiri Group rocks further east. It is in this zone that I have found one sample in which ankerite porphyroblasts show a few twin lamallae. Presuming twinning occurred during S_1 development, the twinning indicates temperatures

Figure 5.20: The Anatoki Fault with the Buller terrane derived (semi-) brittle shear zone on the left side, and Takaka terrane derived calc-mylonite on the right side. M26/ 722221½. Lens cap for scale.

Figure 5.21: Calc-mylonite displaying layering and remnant intrafolial folds. Average grain size is less than 8μm. XZ section, RJ149. CPL.

Figure 5.22: Asymmetric strain fringes around pyrite in undifferentiated Haupiri Group shale close to the Anatoki Fault. Shear-sense is top to the left. Note that quartz fibres are displacement-controlled on the pyrite's left margin, but both face- and displacement-controlled on the right margin. XZ section RJ413. CPL.

0.5mm

Figure 5.22

S1

0.5mm

Figure 5.21

Figure 5.20

at the time of deformation approached ~250°C (see Section 3.10.6). Interestingly, there is no evidence of ankerite twinning elsewhere and one could argue that the restricted occurrence of twinning is due to other factors such as a higher strain or the presence of fluids. Where pyrite occurs, very elongate strain fringes are observed and define the stretching lineation. In thin-section, the strain fringes are made of quartz fibres. The fringes are both displacement-controlled and face-controlled and show a consistent asymmetry (Fig. 5.22). The asymmetric patterns observed in sections parallel to the stretching lineation indicate a sense of shear (Etchecopar and Malavieille 1987) that is top to the west on a steep east dipping plane (i.e. reverse movement).

In summary, the limestone sliver shares a similar cleavage, stretching lineation, and sense of shear not only in undifferentiated Haupiri Group in close proximity to the sliver but also elsewhere in the domain. This suggests that deformation in the limestone sliver may be intimately related to D_1 in the Haupiri Group and Devil River Volcanics Group rocks. This suggestion will be developed upon in Chapter 9.

CHAPTER 6

MT BENSON DOMAIN

Chapter frontispiece: The Anatoki Fault in the Mt Benson domain is marked by a prominent steeply dipping limestone sliver (foreground). In the far background is Waingaro Peak (left) and Kakapo Peak (right). View is towards the north.

6.1 Introduction

The Mt Benson areal domain (Map 4) incorporates a topographic ridge that extends in a northwesterly direction from Mt Benson, and lies approximately 4km south of the Kakapo Peak domain (Fig. 1.2). The primary objective of studying the Mt Benson domain is to investigate the structure in Buller terrane rocks adjacent to the Anatoki Fault. A secondary objective is to look at the microstructure in the prominent limestone sliver immediately east of the Anatoki Fault. Takaka terrane rocks east of the limestone sliver were not investigated.

6.2 Buller terrane: Lithology

Three major bodies of rock are recognised in the Buller terrane rocks of the Mt Benson domain. Along the western extremity of the domain is black to dark grey slaty shale with thick beds of quartz sandstone. The slaty shale contains graptolites, and the rock is identified as Leslie Formation (Grindley 1980). To the east of Leslie Formation, the shale grades into a well-laminated grey slaty siltstone, identified as typical Douglas Formation (Grindley 1980). The eastern margin of the Douglas Formation becomes increasingly rich in quartz sandstone beds, and laminated siltstone darkens in colour. Eventually the rock becomes a dark grey to black slaty shale with thick isolated beds of quartz sandstone, up to ~1m thick, and looks remarkably like Leslie Formation in the west of the domain. This slaty shale outcrops from M26/ 727156 eastwards to the Anatoki Fault.

6.3 Buller terrane: Structure

One major deformation event (D_1) is recognised in both the Douglas Formation and the slaty shale east of it. In addition, an S_{ii} and F_{ii} is recognised solely within the Douglas Formation and is possibly related to D_3 recognised in domains further north. Insufficient structural information was obtained in the Leslie Formation for detailed description here.

6.3.1 D_1 mesoscale structures

In the shale between Douglas Formation and the Anatoki Fault, D_1 is represented solely by a slaty cleavage (S_1). S_1 strikes between N and NW, dipping moderately towards the NE (Fig. 6.1). Bedding strikes approximately N-S, dipping steeply east, or subvertical (Fig. 6.2). S_1 is therefore always gentler in dip than bedding. In addition, S_1 always has a more westerly component of strike relative to bedding.

Bedding in the Douglas Formation itself is similar to that in the slaty shale striking approximately N-S and steeply dipping to the east or west, or subvertical (Fig. 6.2). The lensoidal character of quartz-rich laminae suggests a cleavage occurs subparallel to bedding. The suggestion is given weight by domains further north, where the lensoidal character of quartz-rich laminae in Douglas Formation is the result of strain associated with S_1 subparallel to bedding (Section 4.3.1 and 5.3.1). Thus it is highly likely that D_1 in the Douglas Formation of the Mt Benson domain is represented by a cleavage, S_1, subparallel to bedding.

No cleavage related folds are observed in either lithology but measured L_0^1 intersection lineations in the slaty shale plunge gently or moderately N-NE (Fig. 6.1).

6.3.2 D_1 microscale structure

In the shale between Douglas Formation and the Anatoki Fault, S_1 slaty cleavage is defined primarily by finely spaced opaque solution seams (Fig. 6.3). In addition, fine grained white micas grow along and parallel to the solution seams. Ankerite porphyroblasts are slightly elongate parallel to S_1, and S_1 is slightly wrapped around the porphyroblasts (Fig. 6.3). The wrapping of S_1 around porphyroblasts might suggest that the porphyroblasts predate S_1. However, given that the wrapping is not strong, and solution seams are developed within the adjacent strain shadows, the ankerites are more likely to have grown syn-S_1 and therefore syn-D_1. All slaty shale samples from between Douglas Formation and the Anatoki Fault contain thin quartz-rich laminae in which S_1 is refracted (Fig. 6.4). The refraction of S_1 in quartz-rich laminae is such that it has a gentler dip towards the east relative to the muddy laminae.

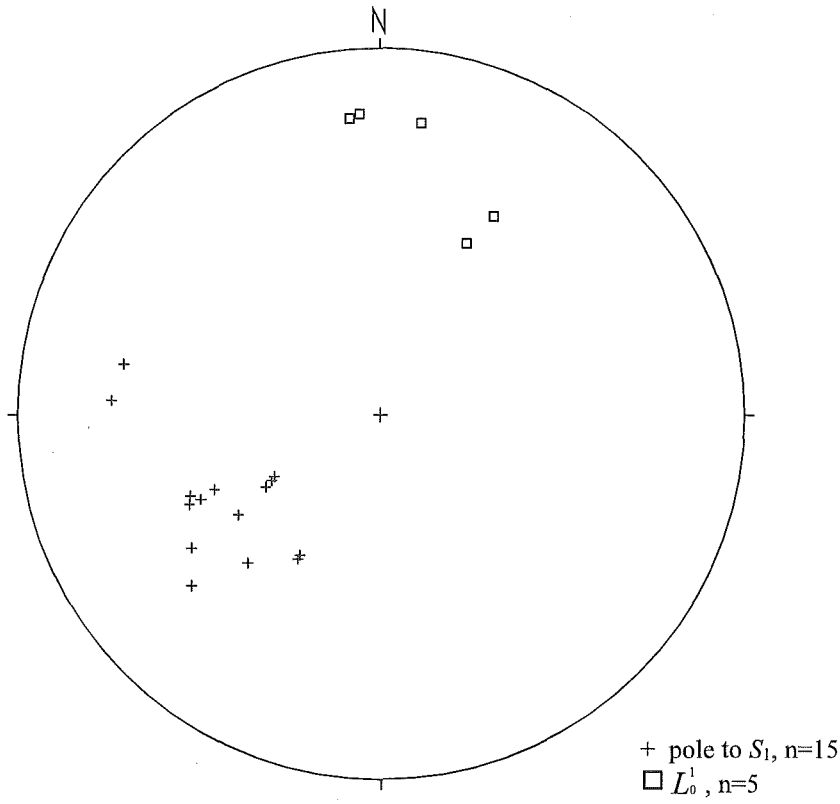

Figure 6.1: S_1 and L_0^1 orientations in slaty shale unit between Douglas Formation and the Anatoki Fault, Mt Benson domain.

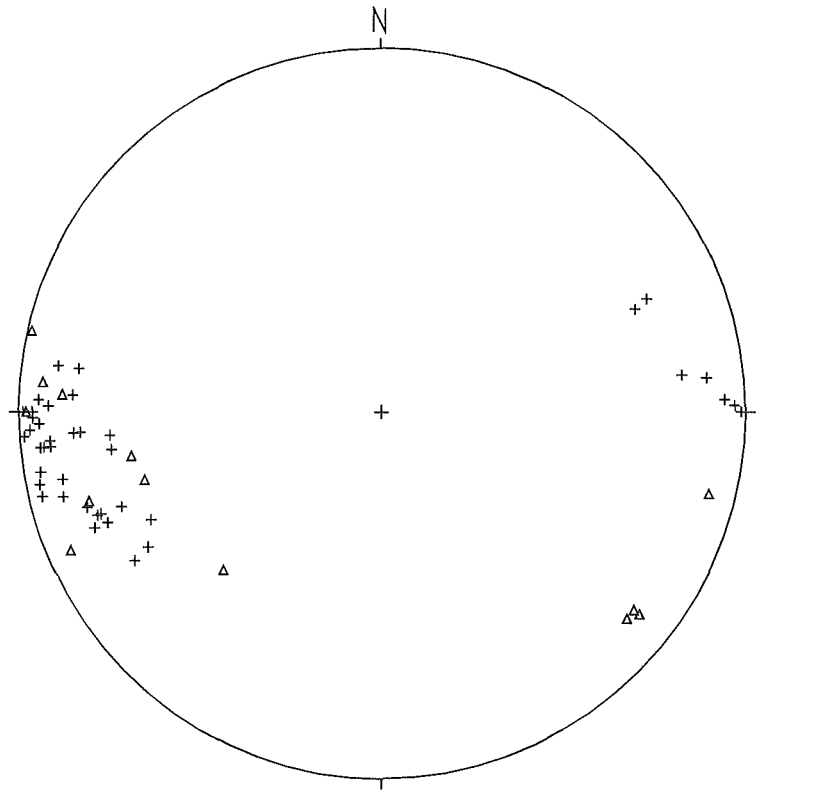

Figure 6.2: Poles to bedding in Douglas Formation and slaty shale unit, Mt Benson domain.

Figure 6.3: Finely spaced opaque solution seams (S_1) anastomosing around an oxidised, slightly elongate, ankerite porphyroblast. Note that S_1 is oblique to quartz-rich laminae. RJ131, slaty shale unit between Douglas Formation and the Anatoki Fault. PPL.

Figure 6.4: S_1 refracting between quartz-rich and muddy laminae in the slaty shale unit between Douglas Formation and the Anatoki Fault. RJ130. PPL.

Figure 6.5: S_{ii} crenulations and small F_{ii} folds in Douglas Formation, Mt Benson domain. For scale, most wavelengths of crenulations are 3-4mm. M26/ 720159.

Figure 6.3

Figure 6.4

Figure 6.5

6.3.3 F_{ii} and S_{ii} structure

In Douglas Formation, there is a mesoscale folding (F_{ii}) and a prominent axial planar crenulation or crenulation cleavage (S_{ii}). F_{ii} folds have NNE-NE striking axial planes which are subvertical, or dipping steeply to the SE or NW (Fig. 6.6). The majority of F_{ii} fold axes plunge moderately or steeply to the north (Fig. 6.6). F_{ii} folds are open to gentle with wavelengths ranging from large crenulations (~5cm) to 3m.

S_{ii} orientations are axial planar to F_{ii} folds (Fig. 6.6). Spacing of crenulations and crenulation cleavage planes range from 1mm to 5cm (Fig. 6.5). Occasionally a conjugate kink-like S_{ii} cleavage is observed. S_{ii} is most strongly developed in F_{ii} hinge zones where thin mica cleavage domains may develop.

Oddly, F_{ii} and S_{ii} are not observed in the slaty shale between the Douglas Formation and the Anatoki Fault but are observed in Leslie Formation.

6.3.4 Discussion

The slaty shale between Douglas Formation and the Anatoki Fault has been mapped by Grindley (1980) as Peel Formation. In domains further north, dark grey shale and slate immediately west of the Anatoki Fault are also mapped by Grindley (1971) as Peel Formation. Peel Formation is thought by Grindley (1980) to be younger than Douglas Formation based on the presence of graptolites that occur in lithologically similar rocks occurring east of the Anatoki Fault, the implication being that Buller terrane rocks occur on both sides of the Anatoki Fault. However, an investigation of the graptolite bearing rocks east of the Anatoki Fault by Cooper (1989), concludes that they are in fact part of the Takaka terrane (known as Baldy Formation) and unrelated to the slaty shale that occurs immediately west of the Anatoki Fault. Thus the link between graptolite bearing rocks east of the Anatoki Fault and slaty shale immediately west of the Anatoki Fault is severed, and the age of the slaty shale is unknown. Cooper and Tulloch (Fig. 3, 1992) infer that the slaty shale west of the Anatoki Fault (at Mt Benson) is not Peel Formation but actually Leslie Formation, and the reason why Leslie Formation occurs both west and east of the younger Douglas Formation is because of the existence of a large macroscale west-facing syncline (see Figure 2.4). The inference of a macroscale syncline is based on

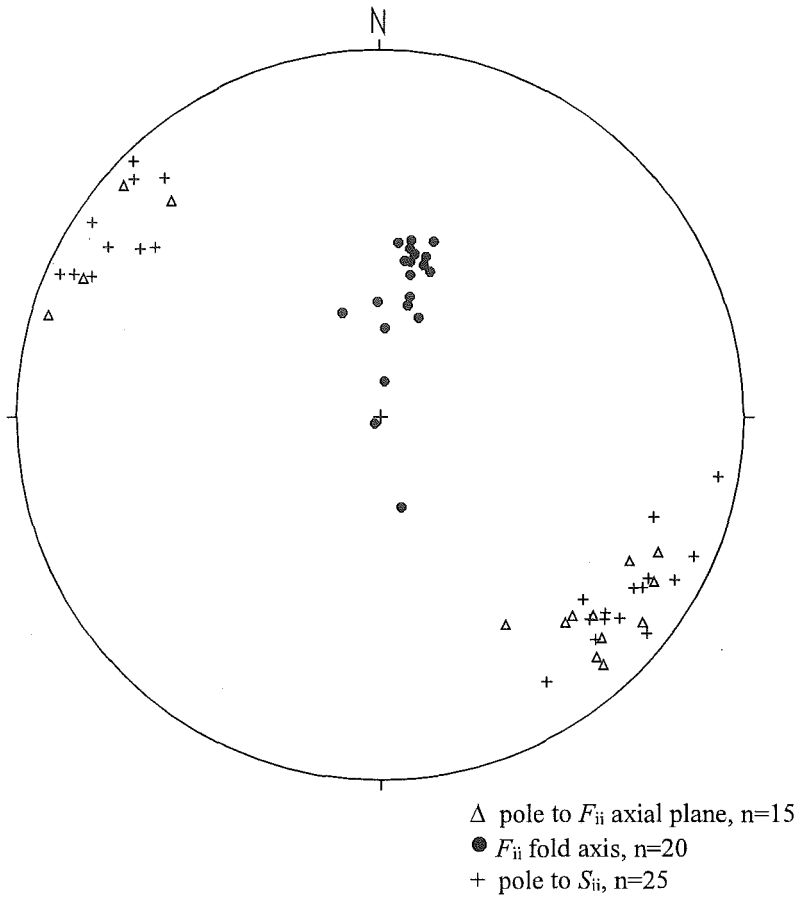

Figure 6.6: F_{ii} and S_{ii} orientations in Douglas Formation, Mt Benson domain.

the lithological similarity of the slaty shale with that of the Leslie Formation, and rare graded beds in the slaty shale indicating a westward younging direction (R. A. Cooper, pers. comm. 1997).

The study of structures in the Mt Benson domain supports the proposition that a macroscale syncline exists because the bedding/cleavage relationships and cleavage refraction in the slaty shale, immediately west of the Anatoki Fault, is consistent with that of an overturned or subvertical eastern limb of such a syncline. L_0^1 in the slaty shale indicates that the syncline plunges to the north. Bedding orientations in both the Douglas Formation and slaty shale (Fig. 6.2) suggest the syncline is tight with a N-S striking axial plane that is subvertical or steeply inclined to the east. The slaty shale and isolated quartz sandstone beds are lithologically similar to that of the Leslie Formation, and thus should be designated as such, as suggested by Cooper and Tulloch (1992). The question then raised is whether all dark grey shales and slates, immediately west of the Anatoki Fault, in domains further north could also be designated as Leslie Formation? The question and structural implications will be addressed in Chapter 9. Figure 6.7 is an E-W cross-section of the Mt Benson domain depicting the interpreted macroscale syncline.

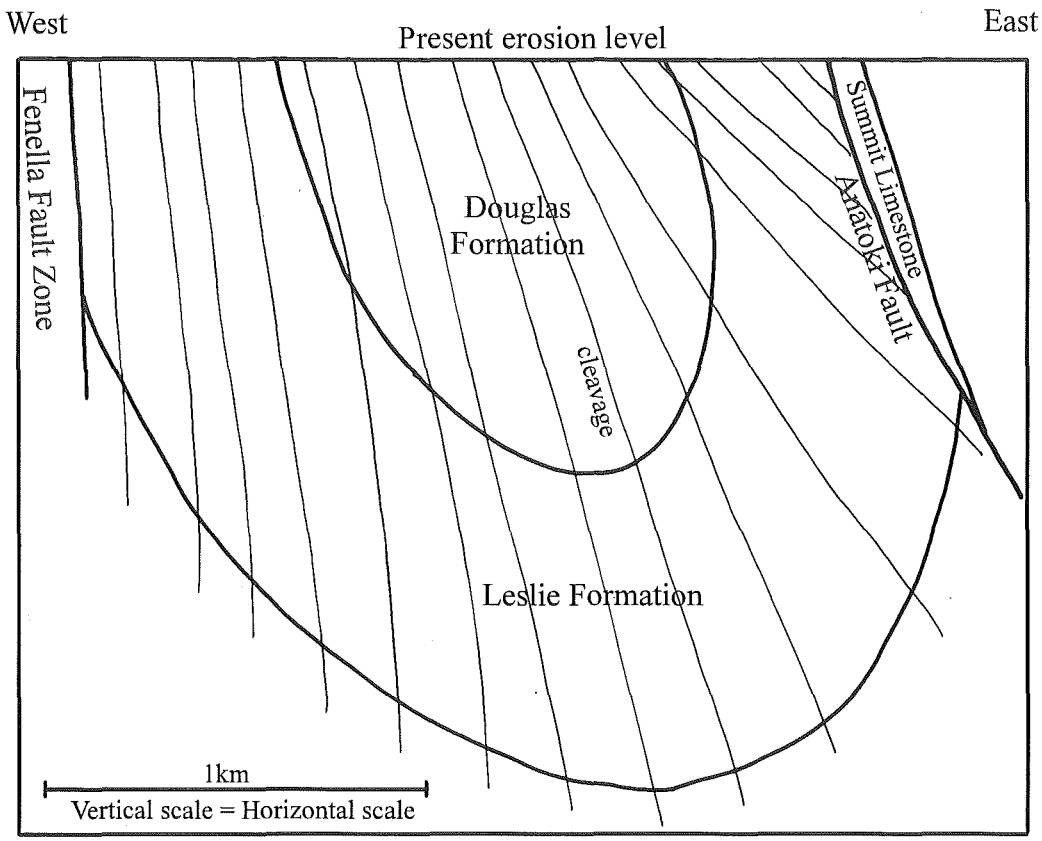

Figure 6.7: East-West cross-section of the Mt Benson domain depicting the interpreted macroscale syncline in the Buller terrane. The cross-section was constructed along Grid Northing 15.75 of Map 4.

6.4 Takaka terrane: Lithology

In the Mt Benson domain, the only Takaka terrane rock studied was the limestone sliver immediately east of the Anatoki Fault, and bedded calcareous shales and sandstones that occur within 10m of the limestone.

Lithologically, the limestone sliver (between 40 and 130m thick) is similar to that described for the Peak 1610 and Kakapo Peak domains. The limestone in the Mt Benson domain contains Early Ordovician conodonts (J. Simes, pers. comm.), and thus appears to correlate with Summit Limestone.

The contact between the limestone sliver and adjacent calcareous shales, sandstones and rare grit appears gradational, with interbedding of the limestone and calcareous clastics (Fig. 6.8). Where interbedding occurs, the limestone beds are sometimes lensoidal. The contact appears to be sedimentary but it is not known whether the calcareous sediments belong to a separate formation or represents a facies within the Summit Limestone. Unfortunately, outcrop to the east is covered in scree.

6.5 Takaka terrane: Structure

6.5.1 Mesoscale structures

The limestone sliver is a marked topographic feature, not only along the ridge-line of the Mt Benson domain (see chapter frontispiece), but also north into the Waingaro River catchment. From the topographic expression, the sliver appears to strike approximately 350°, dipping between 70°E and subvertical.

A cleavage is developed in both the limestone sliver and adjacent calcareous sediments, and it strikes between N and NNW and dips steeply east (Fig. 6.10). Rare impure limestone beds within the sliver are transposed and boudinaged parallel to cleavage. Bedding in the calcareous sediments is subparallel to cleavage although occasionally it is gently warped and steeper dipping than cleavage (Fig. 6.8). Interestingly, the cleavage is only weakly developed along the western margin of the limestone sliver which marks the

Figure 6.8: Interbedding of calcareous clastics with limestone, eastern margin of limestone sliver, Mt Benson domain. Bedding is gently warped (near sledge hammer) but the cleavage remains constant in orientation. M26/ 732½154.

Figure 6.9: Elongate framboidal pyrite grains (orange brown), with quartz/calcite (white) strain fringes, occurring in calcareous sediment immediately adjacent to the limestone sliver. The elongation direction is parallel to a prominent lineation observed along the eastern margin of the limestone sliver. The rock face in this photograph is approximately parallel to cleavage and bedding. M26/ 732½154. Lens cap for scale.

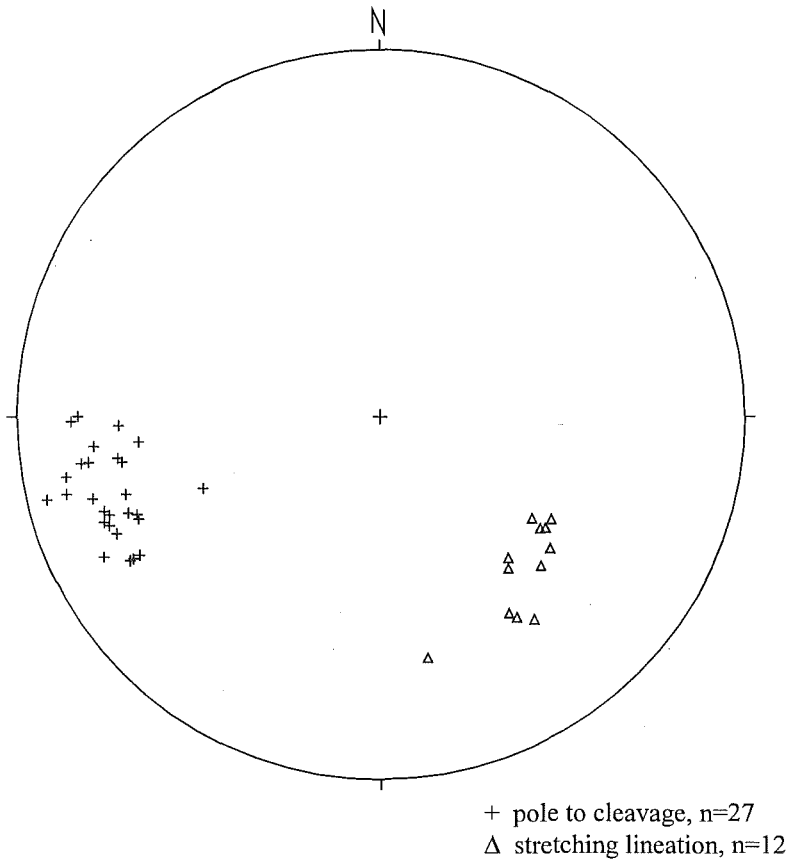

Figure 6.10: Cleavage and stretching lineation orientations in the limestone sliver and adjacent calcareous sediments, Takaka terrane, Mt Benson domain.

Anatoki Fault; it is actually more strongly developed along the eastern margin of the limestone sliver and within the adjacent calcareous sediments. Calc-mylonite was observed at M26/ 732155 where limestone is interbedded with calcareous sediment. Calc-mylonite was not observed anywhere within the main limestone sliver itself.

A prominent lineation is observed on cleavage planes along the eastern margin of the sliver and in adjacent calcareous sediments. The lineation plunges moderately towards the SE (Fig. 6.10) and is clearly a stretching lineation because elongate framboidal pyrite grains with quartz/calcite strain fringes are parallel to it (Fig. 6.9).

6.5.2 Microscale structures

Cleavage is defined principally by solution seams and a SPO of deformed allochems in limestone, and by solution seams and aligned white micas in calcareous sediments. Along the eastern margin of the limestone sliver and adjacent calcareous sediments, strain fringes around pyrite crystals and detrital quartz clasts are highly elongate and asymmetric parallel to the stretching lineation. Excellent asymmetric face-controlled and displacement-controlled strain fringes provide a consistent top to the SE sense of shear i.e. dextral-normal slip (Fig. 6.11).

No reliable evidence of the sense of shear was provided in the calc-mylonite. The calc-mylonite does, however, exhibit strong boudinaging and folding of quartz veins (Fig. 6.12). Calcite grains are equidimensional and thus provide no evidence for determining the shear-sense by way of an asymmetric SPO. The layering in the calc-mylonite wraps around isolated rhombic dolomitic grains which display isolated twin lamellae.

Figure 6.11 (A): Asymmetric displacement-controlled calcite strain fringe around a pyrite porphyroblast. (B): Asymmetric displacement- and face-controlled calcite strain fringe around a pyrite porphyroblast. In both (A) and (B) shear-sense is top to the right. XZ section, RJ142, interbedded limestone and calcareous shale unit. CPL.

Figure 6.12: Folded and boudinaged quartz vein in calc-mylonite. RJ137 CPL.

Figure 6.11A
0.5mm
cleavage

Figure 6.11B
0.5mm
cleavage

Figure 6.12
0.5mm
cleavage

CHAPTER 7

CROW RIVER DOMAIN

Chapter frontispiece: View of Mt Olive looking towards the WNW. Garibaldi Ridge occurs in the left background. Mt Olive is made up of Summit Limestone and is the only exposure above the bushline in the Crow River domain. The Anatoki Fault occurs just to the left of Mt Olive, directly above the bushline.

7.1 Introduction

The Crow River domain (Map 5) is centred on a segment of the Anatoki Fault, bounded north and south by the Cenozoic NE striking Karamea and Skeet Faults respectively (Fig. 1.2). The primary objective of mapping the Crow River domain was to investigate the Crow Granite, a north-south trending elongate pluton (6 x 1.5km), and its contact relationships with Buller and Takaka terrane rocks. Coleman (1977, 1981) shows Buller terrane lithologies (Douglas Formation) west, north, and south of the Crow Granite, and Takaka terrane lithologies (Baldy Formation and Summit Limestone) east of it. Coleman (1977, 1981) shows the eastern margin of the granite as faulted and thus this margin effectively marks the position of the Anatoki Fault.

Outcrop in the Crow River domain is limited to Mt Olive Stream (informal name), Mt Olive tops, Little Crow River, and the middle reaches of the Crow River. The outcrop differs from previous domains in that there is very little exposure above the bushline.

Much time was spent in the field sampling Crow Granite for geochemical and geochronological analysis by Dr. Roddy Muir. The results are presented in Muir *et al.* (in press) and only the geochronology is noted in the following section to help constrain movement history on the Anatoki Fault.

7.2 Description of units

7.2.1 Crow Granite

The Crow Granite is best observed in Mt Olive Stream and in the vicinity of the Crow River-Little Crow River confluence. The granite is relatively coarse grained with pink megacrysts of K-feldspar up to 9cm long (Fig. 7.1). Other minerals identifiable in the field include quartz, green tinged plagioclase, biotite, and hornblende. Enclaves are common and consist of fine to medium grained melano-mesocratic biotite/hornblende-rich rock. Phenocrysts of white and pink feldspar occur within and across margins of enclaves (Fig. 7.2).

Figure 7.1: Typical texture of Crow Granite with pink megacrysts of K feldspar. Float, Crow River. For scale, sledgehammer head is 13cm long.

Figure 7.2: A mafic enclave within Crow Granite. Note how a pink megacryst has grown across the margin of the enclave. Float, Crow River. For scale, lens cap is 56mm in diameter.

Figure 7.3: A brittle shear and associated slickenfibres cut and displace altered cordierite spots (Co) in hornfelsed sediment east of the Crow Granite. RJ238. PPL.

Figure 7.3

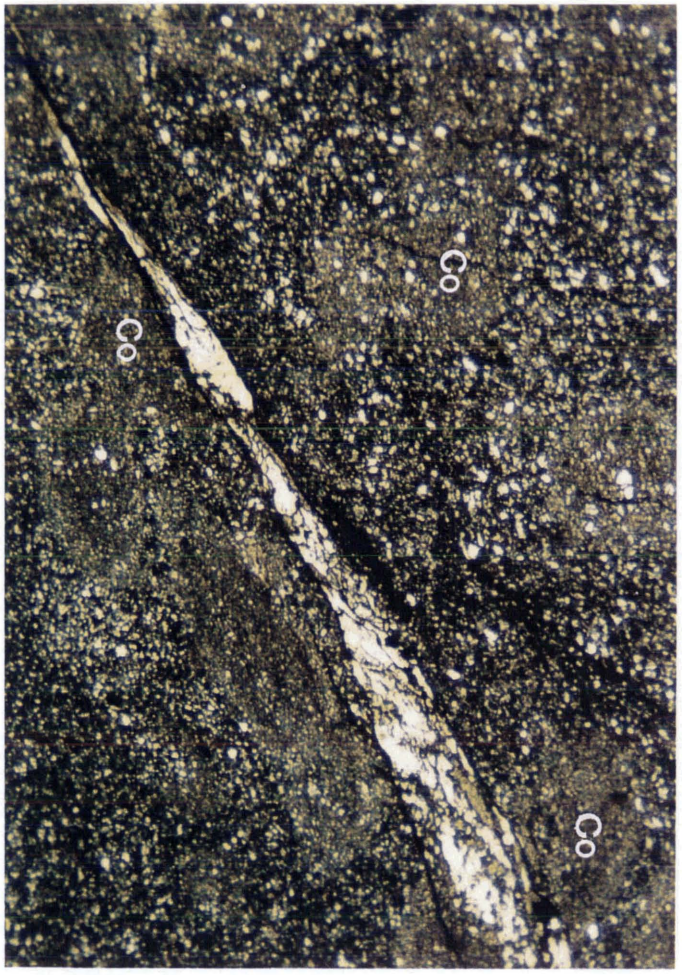

Figure 7.2

Figure 7.1

Throughout the mapped area there is very little variation to the above mineralogical and textural description except for the following: at M27/ 704893, white rather then pink K-feldspar phenocrysts, up to 3cm, and the presence of muscovite is characteristic for about 150m downstream; at M27/ 704875, altered granitoid is riddled with quartz-rich veins which are molybdenite bearing; isolated float in Mt Olive Stream displays an alternating layering of leucocratic and hornblende-rich melanocratic rock.

Structurally, no magmatic or tectonic foliation is observed either in outcrop or in float. The granite is well-jointed, and discrete brittle faults occur here and there. Brittle shear zones become conspicuous close to the pluton's eastern margin (Section 7.3.2).

U-Pb SHRIMP dating of zircons from a specimen of Crow Granite (RJ8G) gave an age of 137.3±2.5Ma (earliest Cretaceous) (Muir *et al.* in press). This date is unusual in that it suggests the Crow Granite is unrelated to the nearby Karamea Suite granitoids (~375Ma) or Separation Point Suite granitoids (~118Ma). The nearest correlatives are the Cable Granodiorite (142Ma, Kimbrough *et al.* 1993), the western Buller Diorite pluton (142Ma, Kimbrough in Johnston 1990), and the Rotoroa Complex (156-130Ma, Kimbrough *et al.* 1993). These intrusives form part of the Median Tectonic Zone (Bradshaw 1993) (Fig. 1.1).

7.2.2 Douglas Formation (Buller terrane)

A limited area of Douglas Formation was studied within 800m of the western margin of the Crow Granite in the Crow River. The area studied corresponds to the "middle unit" of Douglas Formation (Coleman 1981, p. 20) described as "dark grey siliceous siltstone and fine sandstone with interbedded black carbonaceous pyritic shale, quartzite, and highly siliceous sandstone and quartzite." Based on known stratigraphy further north, the age of Douglas Formation in this domain is assumed to be Late Ordovician (Cooper 1979a).

Outside the thermal aureole of the Crow Granite, graphitic shale contains a penetrative cleavage and ankerite porphyroblasts. The relationship between the ankerite porphyroblasts and cleavage is similar to that with S_1 in the slaty shale of the Mt Benson domain (Section 6.3.2), and suggests the porphyroblasts are syn-cleavage formation.

Within 200m of the Crow Granite, pelitic and semi-pelitic cordierite and andalusite bearing hornfels is interbedded with impure quartzite. The pre-existing cleavage has been either obliterated in the hornfels or is represented by a very weak SPO of micas. Thermal spots are randomly oriented and show no evidence of strain.

Structural data collected in the Douglas Formation for this domain is very limited (less than 15 measurements) because of the non-continuous exposure. No folds were observed but bedding is consistently steeply dipping and striking NW. Penetrative cleavage observed at M27/ 690887 is near vertical and NNW striking. The limited data correlates well with data from Coleman (1977) for Douglas Formation immediately west of the domain. Coleman recognises a predominance of steep bedding attitudes as a result of upright, tight to isoclinal mesoscale folding. The fold axes plunge between 0° and 50° to the north and south, and are most likely to be related to F_1 in areal domains further north.

7.2.3 Hornfelsed sediment east of the Crow Granite (Baldy Formation of Coleman 1977, 1981)

Hornfelsed sediment east of the Crow Granite is observed only in two places: in the Little Crow River (M27/ 713878) and at Mt Olive (M27/ 702909). It consists of bedded shale and very fine quartzose sandstone which has a hornfels overprint. In the Little Crow River, hornfelsed sediment shows a weak biotite foliation in the matrix which is oblique to very weak non-biotite inclusion trails in the altered cordierite spots. The lack of strain shadow development and other strain related features imply that the weak biotite foliation is related to only minor strain, probably in association with the nearby Crow Granite intrusion.

A characteristic of the hornfelsed sediment is the high density of brittle shears and related solution seams cutting through the rock. The shears cut and displace altered cordierite spots (Fig. 7.3). All shear surfaces have slickensides and/or slickenfibres of quartz and chlorite.

Coleman (1977) originally assigned the hornfelsed sediment to Baldy Formation at Mt Baldy, based on its lithological similarity. At Mt Baldy, the Baldy Formation conformably overlies Summit Limestone and is thought to be Ordovician in age. In my

opinion, the hornfelsed sediment of the Crow River domain looks petrologically similar to hornfels of the Douglas Formation, and assignment to Baldy Formation is questioned.

7.2.4 Summit Limestone (Takaka terrane)

A 300-400m wide continuous band of Summit Limestone outcrops from along the top of Mt Olive south-southeastwards to the Little Crow River. The Summit Limestone is predominantly a dark grey fine grained limestone often containing thin graphitic laminae and a variable clastic component. Black to dark grey carbonaceous mudstone interbedded with limestone is widespread and defines bedding. Occasionally the carbonaceous mudstone may dominate the outcrop, and although I regard it as a facies variant, Coleman (1977, 1981) has mapped it as a separate unit (Patriarch Formation). Coleman (1981) reports conodonts in the limestone that indicate an Early Ordovician age.

The internal structure of the limestone is complex, with many outcrops displaying noncylindrical and disharmonic close to isoclinal folding of bedding. Some fold hinges vary in attitude by more than 60° within a single outcrop. A stereoplot of fold axes displays no systematic pattern and indicates that the limestone has deformed in a rather inhomogeneous ductile fashion (Fig. 7.4). The western half of the limestone band can be very well-foliated. This is particularly so in the headwaters of Mt Olive Stream and the Mt Olive tops, where the limestone is well-exposed and shows evidence of strong non-coaxial strain. The western half of the limestone band is referred to as the Summit Limestone shear zone, and is described in Section 7.4.

7.2.5 Anatoki Formation (Takaka terrane)

The structure of the Anatoki Formation was studied in a 1.5km section of the Little Crow River east of the Summit Limestone band. In the Little Crow River, the formation consists mainly of grey-green and orange coloured laminated siltstones, sandstones, and the occasional granule or fine pebble conglomerate. Beds are commonly graded and can be up to 1m in thickness. Along with graded beds, some excellent load casts, flame structures, and rare cross-bedding provides good way-up indicators. Synsedimentary deformation is evident in places with such structures as synsedimentary faults, slump

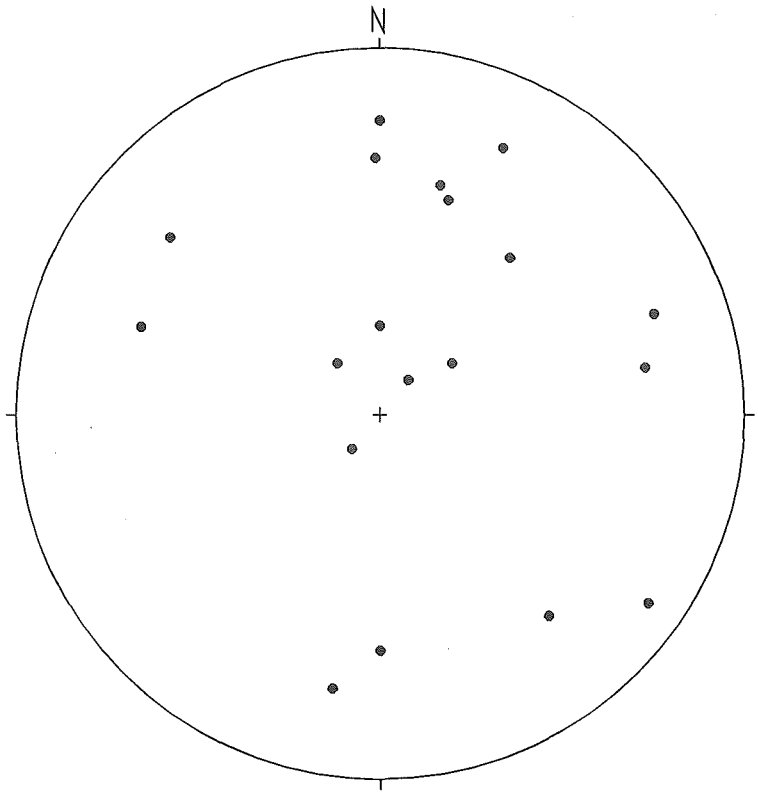

Figure 7.4: Summit Limestone fold axis orientations (●) excluding the Mt Olive Stream area, Crow River domain.

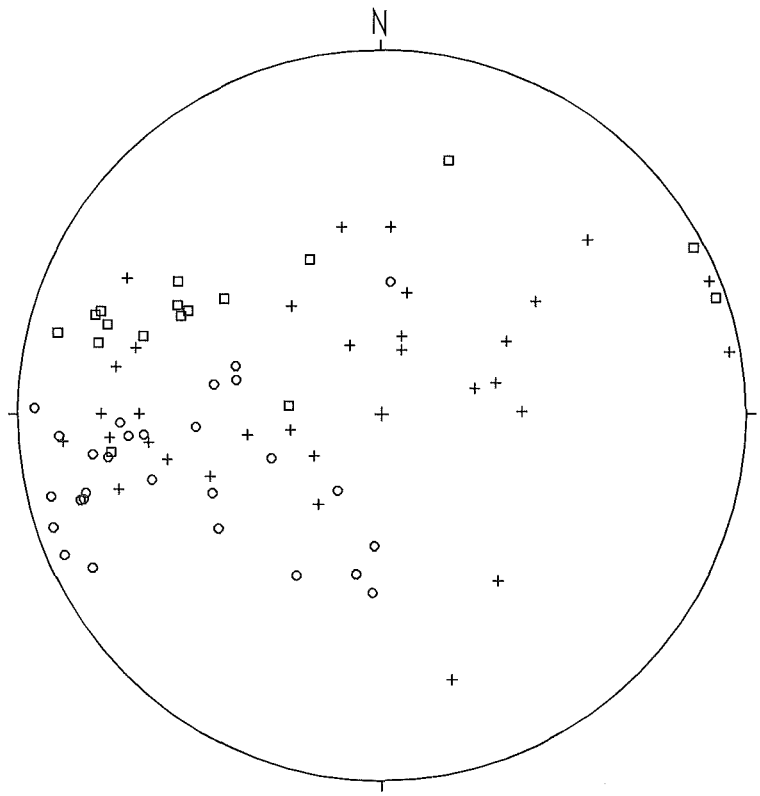

Figure 7.5: Bedding orientations in the Anatoki Formation, Little Crow River, Crow River domain.

folds, and convolute laminations observed. Trilobite fauna in lithologically and stratigraphically similar rock, located at nearby Mt Patriarch (Coleman 1977; Wright *et al.* 1994), suggests a Late Cambrian age.

Because the orientation of structures in river polished outcrop is never as easily observed as in weathered surfaces on ridge tops, a complete analysis of structures in the Anatoki Formation was not made. Most bedding is moderately to steeply dipping towards the eastern quarter and often overturned (Fig. 7.5). Only one cleavage is observed (S_{ii}) and visible only in siltstone horizons. In places, S_{ii} appears to be crenulating a pre-existing foliation but the foliation surface is difficult to measure. S_{ii} dips predominantly to the west at a moderate to steep angle (Fig. 7.6), and is axial planar to close-gentle mesoscale folds (F_{ii}) that plunge from gently north to moderately south (Fig. 7.7). Intersection lineations (L_0^{ii}) show a similar trend (Fig. 7.7).

F_{ii} and S_{ii} must postdate an earlier phase of folding because:

- several outcrops reveal an S_{ii} cleavage relationship with overturned bedding that suggests it is incompatible with a first phase of folding (Fig. 7.8).
- Poles to overturned and upright bedding overlap, and are found within a broad cluster (Fig. 7.5). This overlapping cluster must represent both limbs of a relatively tight fold phase yet S_{ii} poles (Fig. 7.6) plot outside the main cluster. If S_{ii} was related to this tight fold phase, its poles would plot amongst the main cluster of bedding.

The attitude of the earlier phase of folding (F_i), implied from the above points, is difficult to ascertain. On outcrop scale, no mesoscale folds or cleavage appears to be related to the folding. However, there are distinct areas in the Little Crow River which are either predominantly upright or predominantly overturned, and therefore indicate the approximate positions of macroscale F_i axial plane traces (see Map 5). The overlapping cluster of overturned and upright bedding which dip east suggests the F_i axial plane also dips eastward and the F_i fold axis lies along this plane. Although the majority of overturned and upright beds dip east, there is a weak spread of data defining a very broad π-girdle in which the axis is similar to the mean of L_0^{ii} and F_{ii} fold axes (i.e. subhorizontal or gently plunging south). The π-girdle orientation either represents an inherited feature of F_i, in which case coaxiality between F_i and F_{ii} fold axes is suggested, or alternatively, represents F_{ii} folding of a tight F_i fold phase, in which case the F_i fold

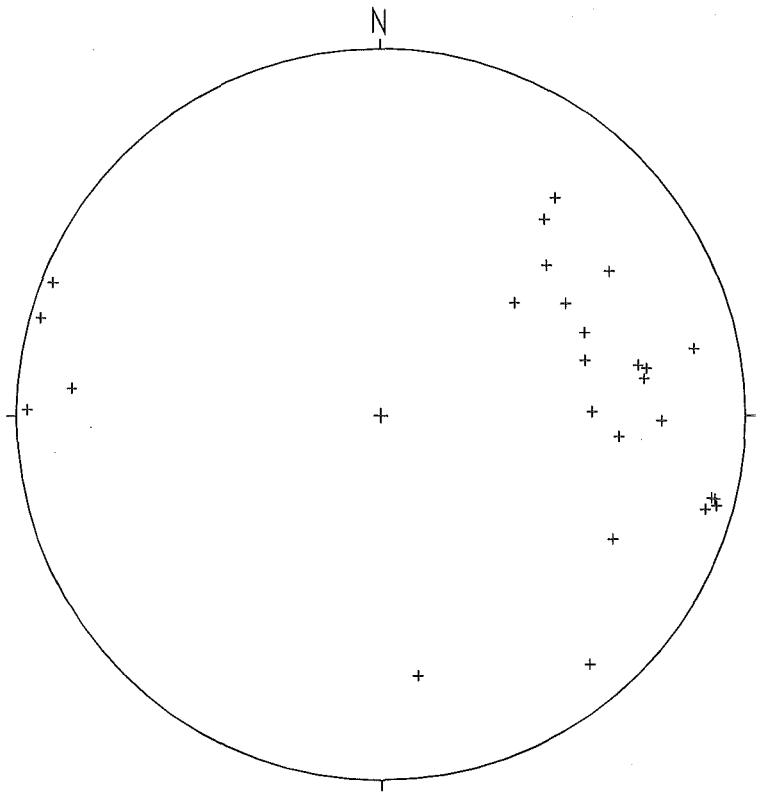

Figure 7.6: Poles to S_{ii} (+) in the Anatoki Formation, Little Crow River, Crow River domain. n=26 .

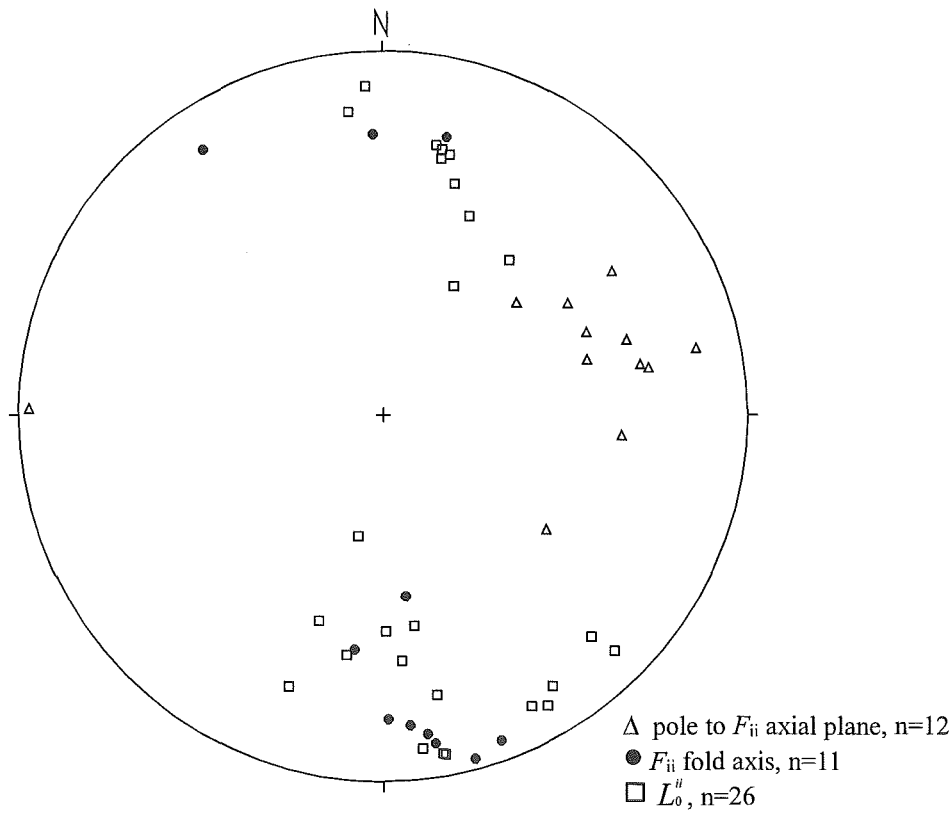

Figure 7.7: F_{ii} and L_o^{ii} orientations in the Anatoki Formation, Little Crow River, Crow River domain.

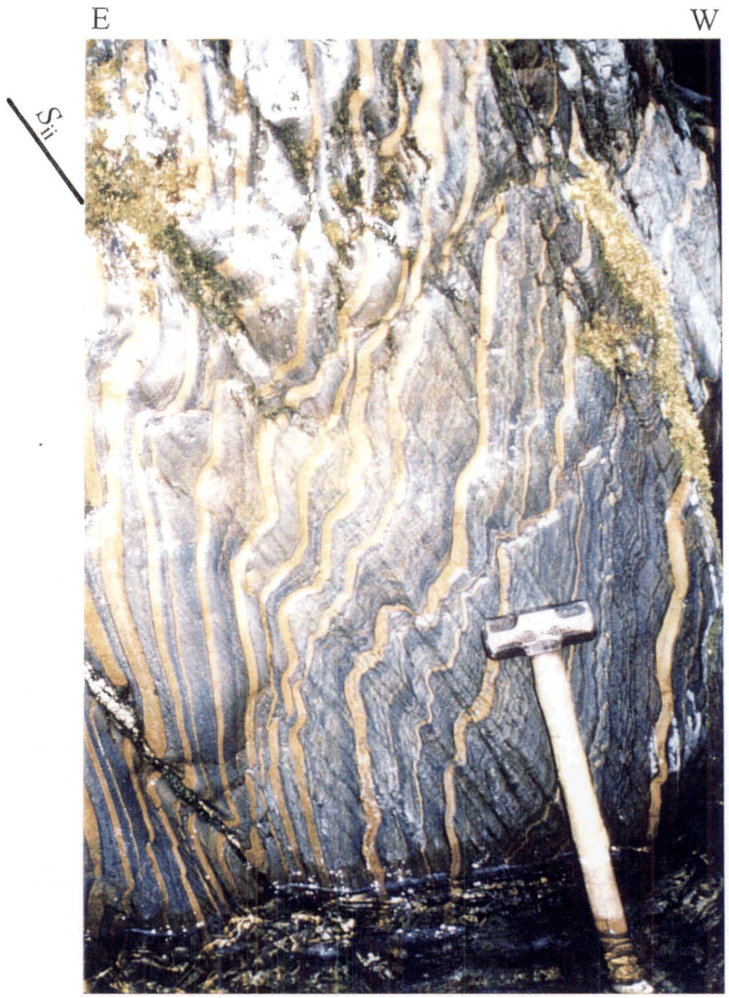

Figure 7.8: S_{ii} crenulates steeply dipping overturned bedding that youngs to the west. The cleavage relationship with bedding suggests that S_{ii} is incompatible with a first phase of folding. Anatoki Formation, Crow River domain. M27/ 724890. Sledgehammer for scale.

axis orientation cannot be determined (except to say that it lies along an east dipping plane).

7.3 Description of contacts

7.3.1 Douglas Formation / Crow Granite contact

The clearly intrusive contact between Crow Granite and Douglas Formation can be observed at M27/ 698872. No evidence of ductile strain or significant brittle faulting is observed along the western margin of the Crow Granite or in hornfelsed Douglas Formation anywhere within the Crow River domain.

7.3.2 Crow Granite / Hornfelsed sediment east of the Crow Granite contact

Excellent exposure of the contact between Crow Granite and hornfelsed sediment is seen in the Little Crow River at M27/ 713878. 50 to 100m west of the contact, Crow Granite becomes noticeably fractured. Within 50m of the contact, brittle shear zones up to 1m thick occur. These shear zones are marked by crush microbreccia, protocataclasite, and cataclasite (Fig. 7.9) which have thin seams (<5cm) of slickensided weakly-cemented fault breccia and gouge cutting through.

Immediately adjacent to the contact, the granite is moderately fractured with clay-rich shears. The contact is marked by 1.5-2cm thick well-cemented fault pug. Clay seams in the adjacent crushed granite and hornfelsed metasediment curve into and become parallel with the pug zone. The sigmoidal form of the clay seams demonstrate that the granite has moved up relative to the hornfels metasediment. Immediately east of the contact, the hornfelsed metasediment has been broken up and now forms a cemented fault breccia. East of the breccia, the hornfelsed metasediment is highly sheared and, as shown earlier in Section 7.2.3, the shearing postdates hornfelsing.

From the description of the contact between Crow Granite and hornfelsed sediment, it is clear the contact represents a brittle fault, with movement taking place after the pluton solidification and hornfelsing. It can be reasonably assumed that the hornfelsed sediment

Figure 7.9

Protocataclasite in granite: Deformation in quartz is represented by widely space dilation fractures, kinking along basal planes, internal cracking, undulatory extinction, and subgrain development (A). On many of the internal cracks are fine quartz grains, which are thought to have formed as a result of dynamic recrystallisation. Although broken up, much of the quartz in the protocataclasite retain their original grain outlines. Feldspar grains display much higher effects of cataclasis, being weaker than quartz in the low temperature regime because of its susceptibility to fracturing along cleavage planes (Tullis and Yund 1977; Evans 1988). The original feldspar grains have been severely fractured along both cleavage and twin planes. Alteration, particularly along cleavage planes, together with infilling of fractures by fine phyllosilicates, has allowed slip (microfaulting) to readily occur (B). As a result, the original feldspar grain outline is now commonly elongate in shape.

Cataclasite in granite: Cataclasite bands cut through protocataclasite. Outlines of original grains are no longer recognised, and quartz and feldspar have been dimutised to angular fragments of various sizes (C). Because feldspar has been almost completely altered to fine phyllosilicates and calcite during cataclasis, it has undergone greater grain size reduction than quartz. Phyllosilicates and calcite have reprecipitated along a dense network of intergranular microshears which, as a result, define a rough foliation.

Sample RJ247, Crow Granite, (A) and (C) CPL, (B) PPL.

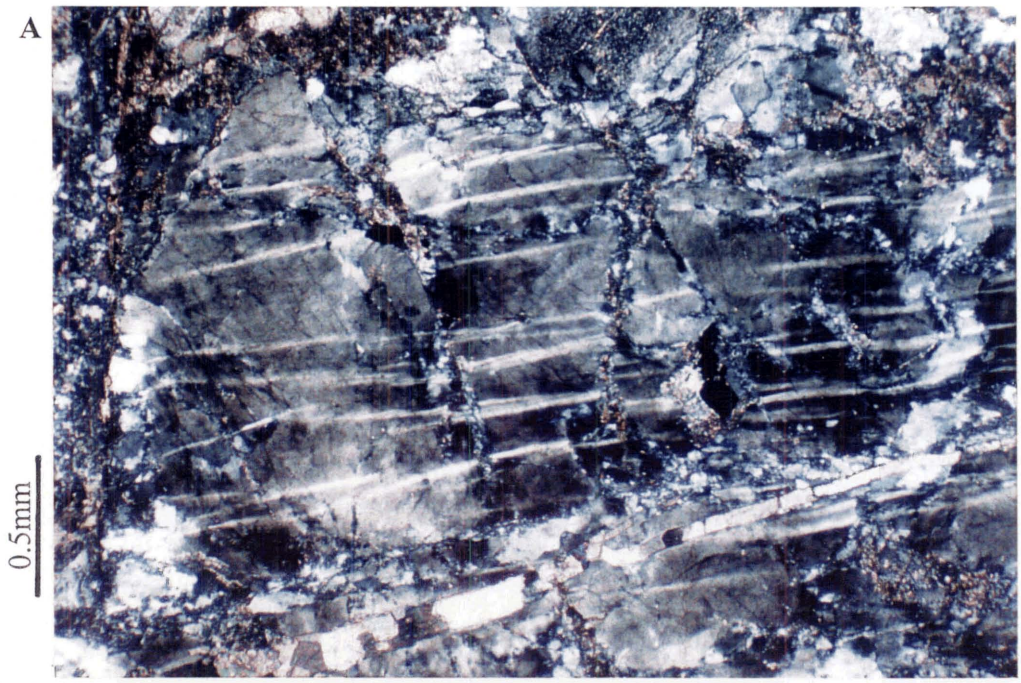
A
0.5mm

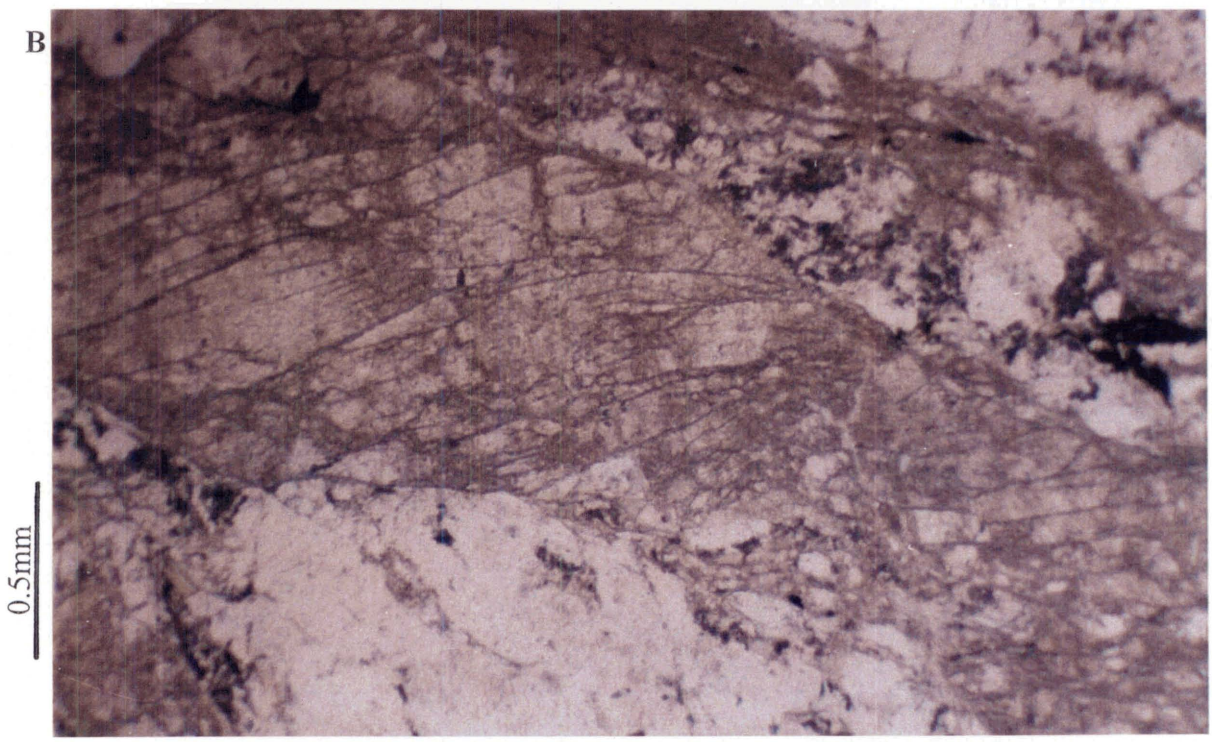
B
0.5mm

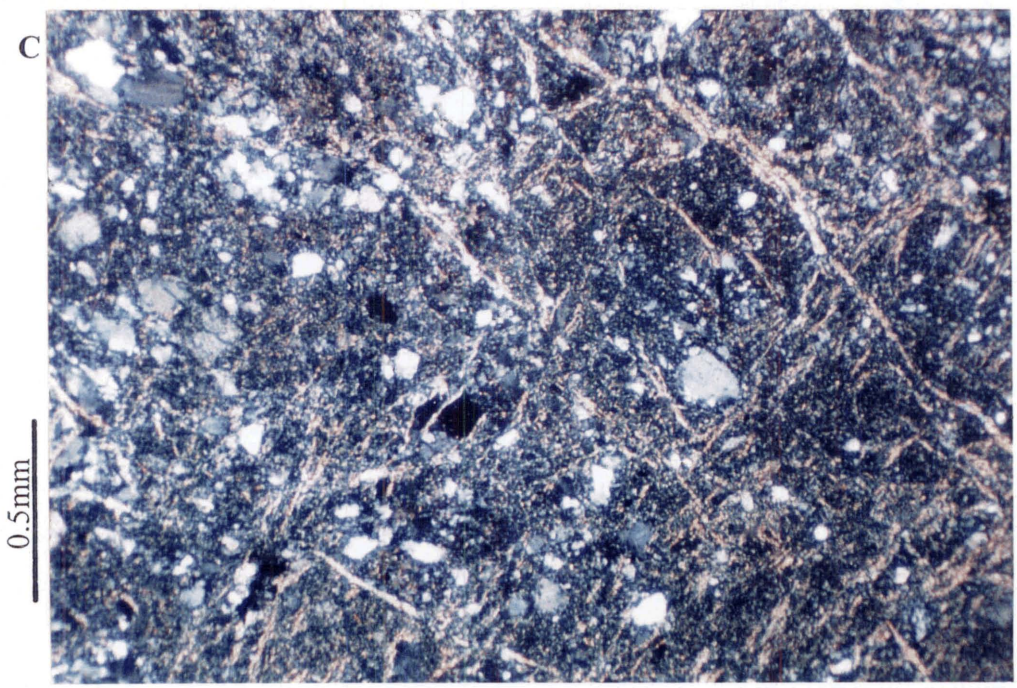
C
0.5mm

was a result of the intruding Crow Granite, and therefore displacement on the fault has not been on a regional scale.

7.3.3 Crow Granite / Summit Limestone contact

At M27/ 708904, a contact between the Crow Granite and Summit Limestone is hidden within a waterfall/bluff section of Mt Olive Stream. The nature of the contact is unknown but is repeated by a later cross-cutting moderate to steeply east dipping reverse brittle fault. The fault is marked by 60cm of granite derived cohesionless fault breccia with fractured granite on its eastern side and well-foliated limestone on its western side. Slickensides indicate dip-slip movement.

In a tributary of the Little Crow River (M27/ 711870), the contact between Crow Granite and Summit Limestone can be located within three metres, but is not exposed. Sediment derived well-cemented and foliated fault breccia float, originating from near this locality, is made up of clasts similar to the hornfelsed sediment of the Little Crow River. The fault breccia shows evidence of extreme pressure solutioning. The granite is fractured whereas the limestone is well-foliated.

7.3.4 Hornfelsed sediment east of the Crow Granite / Summit Limestone contact

This contact is not exposed. However, towards its eastern margin, the hornfelsed sediment contains quartz veins and displays numerous post-hornfels shear planes that anastomose around more competent lozenges. Being highly sheared throughout, the narrow mapped strips of hornfelsed sediment in the Little Crow River and west of Mt Olive are likely to be fault bounded on both sides.

7.3.5 Summit Limestone / Anatoki Formation contact

In the Little Crow River, at M27/ 716883, the Summit Limestone is in fault contact with Anatoki Formation. The fault is marked by a 3m brittle shear zone of carbonaceous mudstone and lenses of thin limestone. The zone is riddled with calcite veins, slickensides, and pug parallel to shear surfaces. In thin-section, the limestone lenses reveal high strain due to pressure solutioning.

7.4 Summit Limestone shear zone

A distinctive intensely foliated tectonite forms the western half of the Summit Limestone band, and is well-exposed in the headwaters of Mt Olive Stream and the Mt Olive tops. From structural and microstructural observations made mainly from the exposure and sample collections in the Mt Olive Stream headwaters, it can be confidently shown that the intensely foliated tectonite is associated with a ductile shear zone. Petrographically, the tectonite is best termed a fine grained marble, although where dynamic recrystallisation has not occurred, metalimestone is a more appropriate term. Fine grained marbles show the highest amount of strain whereas metalimestone display the least.

7.4.1 Field structures

Up to 200m east from the western margin of Summit Limestone, well-layered marble dominates the outcrop. The layering strikes NW-NNW, dipping moderately to steeply towards the NE, and an associated lineation plunges moderately to steeply towards the E or ESE (Fig. 7.10). The layering appears to represent highly attenuated bedding parallel to cleavage, and this has been confirmed microscopically. The lineation has a streaky appearance and elongate strain fringes around pyrite cubes are parallel to it, indicating the lineation is of stretching origin. Within the shear zone there are zones of metalimestone where bedding appears less strained. The metalimestone contains a cleavage that is oblique to bedding, and is shallower dipping.

Quartz and calcite veins of several generations cut obliquely across, or are subparallel to, the layering. The older veins are useful in delineating fold structures such as a sheath fold (Fig. 7.11), and several intrafolial folds (Fig. 7.12) with fold axes subparallel to the stretching lineation (Fig. 7.10). A mesoscale δ-type porphyroclast indicates a sense of shear that was top to the E-ESE i.e. dextral-normal movement.

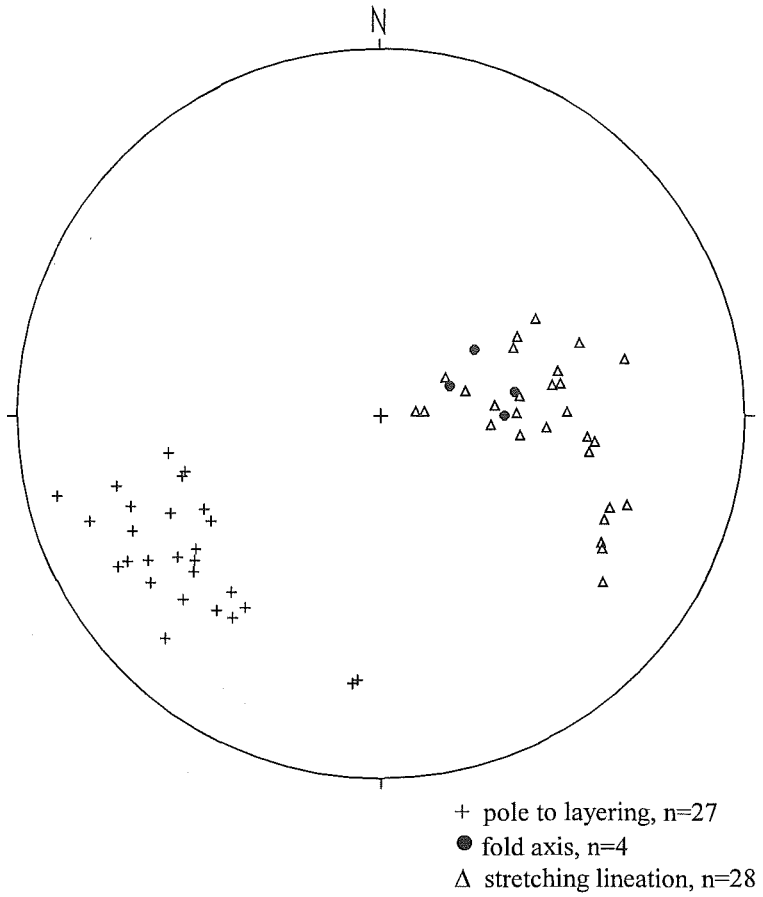

Figure 7.10: Layering, fold axes, and stretching lineation orientations in the Summit Limestone shear zone, Mt Olive Stream and Mt Olive tops area, Crow River domain.

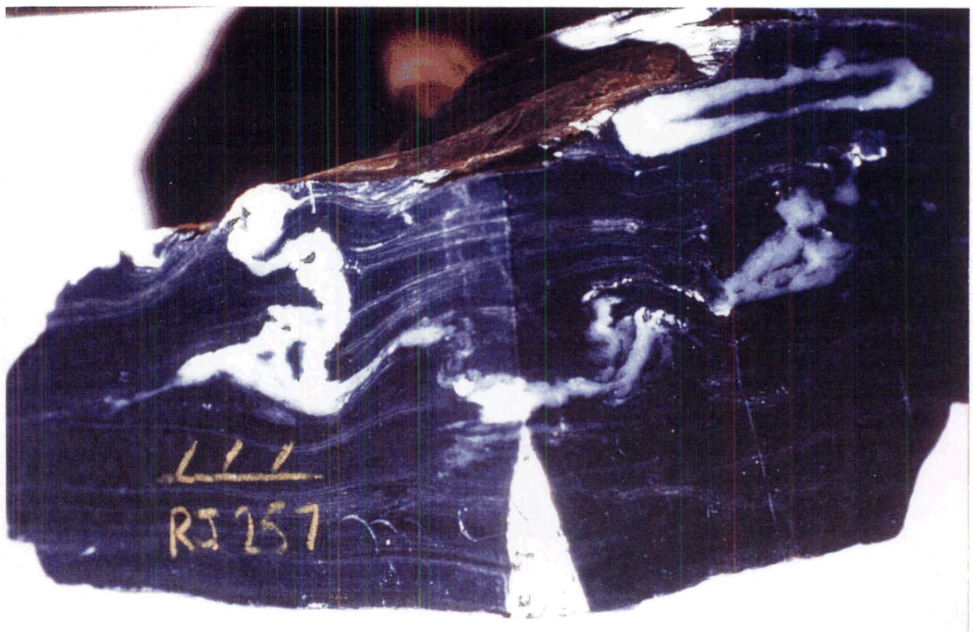

Figure 7.11: Hand specimen of a calcite tectonite from the Summit Limestone shear zone, Crow River domain. The hand specimen has been cut perpendicular to the foliation and perpendicular (right side) and parallel (left side) to the stretching lineation. The "eye" of a sheath fold is outlined by an early generation calcite vein in the section cut perpendicular to the stretching lineation. Sample RJ257 collected from M26/ 708905. For scale, the orientation mark is 2.5cm long.

Figure 7.12: An intrafolial fold outlined by a quartz vein within the Summit Limestone shear zone. The fold axis is subparallel to the stretching lineation. Crow River domain. M27/ 708905. Lens cap for scale.

7.4.2 Microscale structures

The following is a description of microstructures observed in a traverse across the 200m shear zone. The description goes into some detail because various deformation microstructures can be observed which provide information on the state of strain. Metalimestone displaying the least strain is described first followed by fine grained marble showing increasing amounts of strain. Finally, a sample (RJ252) located immediately adjacent to the Crow Granite is described to help constrain the timing of shear zone movement.

Description

Under the microscope, bedding is represented by variable amounts of clastic quartz grains and/or graphite content. Metalimestone showing the least strain possesses discontinuous irregular opaque solution seams and symmetrical strain fringes around porphyroclasts of quartz and pyrite. The solution seams and strain fringes are oblique to bedding, and it is the solution seams which equate with cleavage observed in the field. Early generation calcite veins are truncated by the solution seams (Fig. 7.13). The calcite grain size in metalimestones is highly variable but always very fine grained (3-25μm). Grain shapes are irregular. Occasionally, large calcite single crystals occur (up to 500μm) and these probably represent remnants of organic plates such as crinoid ossicles. The larger grains and strain fringe grains frequently display both thick and thin twins, some of which are curved and associated with undulatory extinction.

With increasing strain, the angle between bedding and solution seams becomes increasing acute, and solution seams become more smooth and continuous. Symmetrical strain fringes adjacent to pyrite crystals indicate a longitudinal strain (e) of up to 2.2 parallel to the lineation. Calcite grains become less variable in size and develop a weak to moderate SPO parallel to the solution seams.

Within the zone of high strain, composition layering observed under the microscope can be seen to represent highly attenuated bedding. Remnants of isoclinally folded bedding and early generation veins are still preserved, particularly in sections perpendicular to the lineation. Parallel to the layering are boudinaged early generation veins (Fig. 7.14), thin continuous solution seams, elongate porphyroclasts, and strain fringes. Trains of drawn out fine opaques suggest attenuation of early generation solution seams.

Figure 7.13: Early generation calcite vein is truncated by a solution seam in least strained rocks of the Summit Limestone shear zone. RJ253. PPL.

Figure 7.14: Boudinaged quartz vein in calcite tectonite, Summit Limestone shear zone. XZ ultrathin-section, RJ259. CPL.

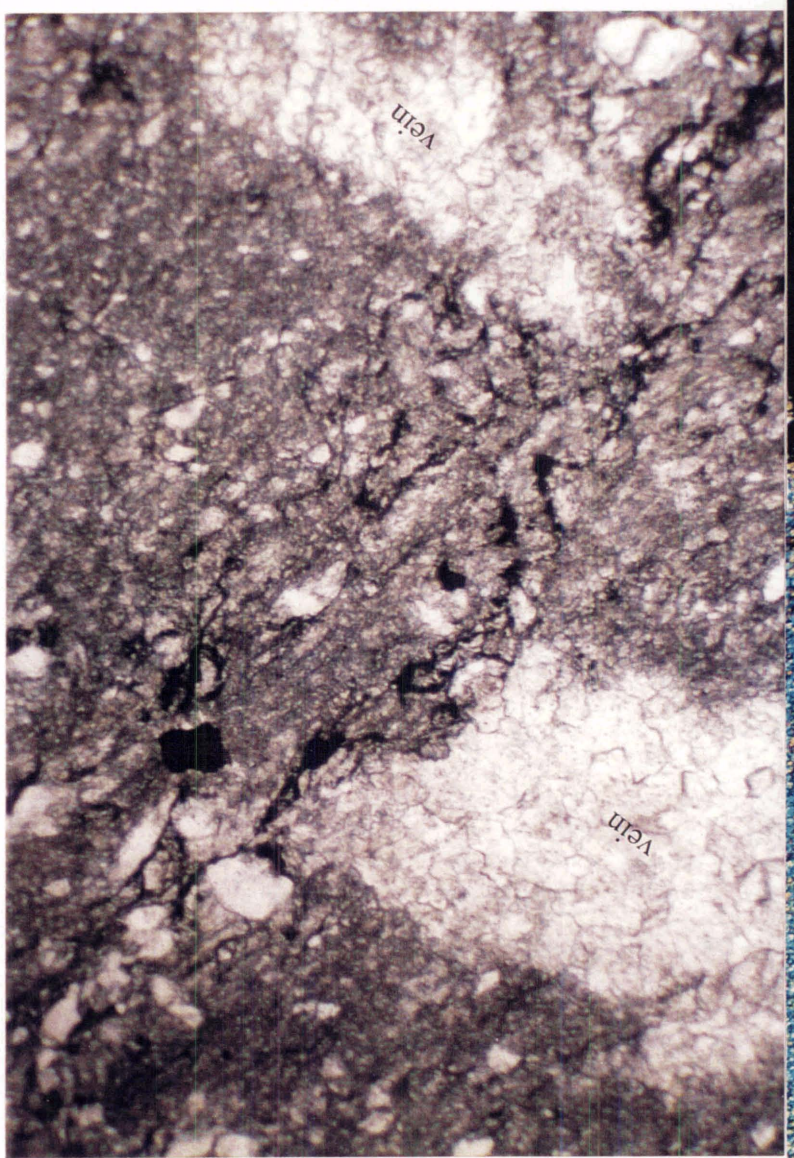

Figure 7.13

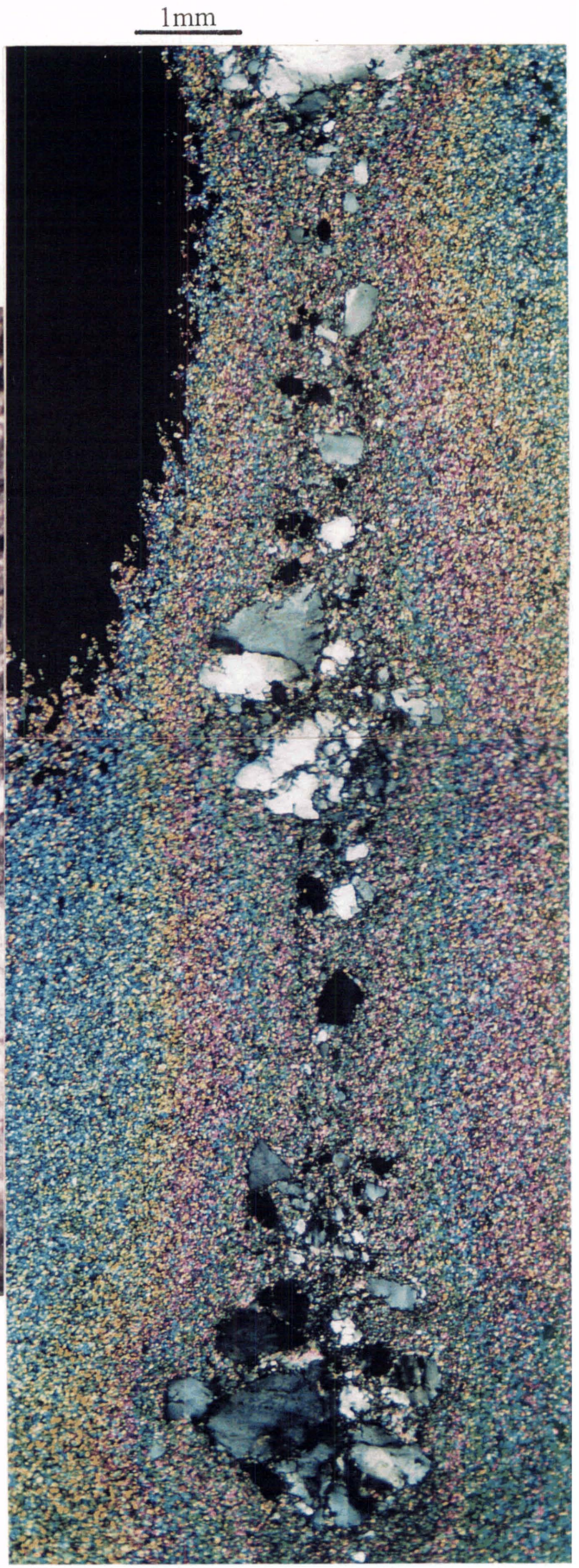

Figure 7.14

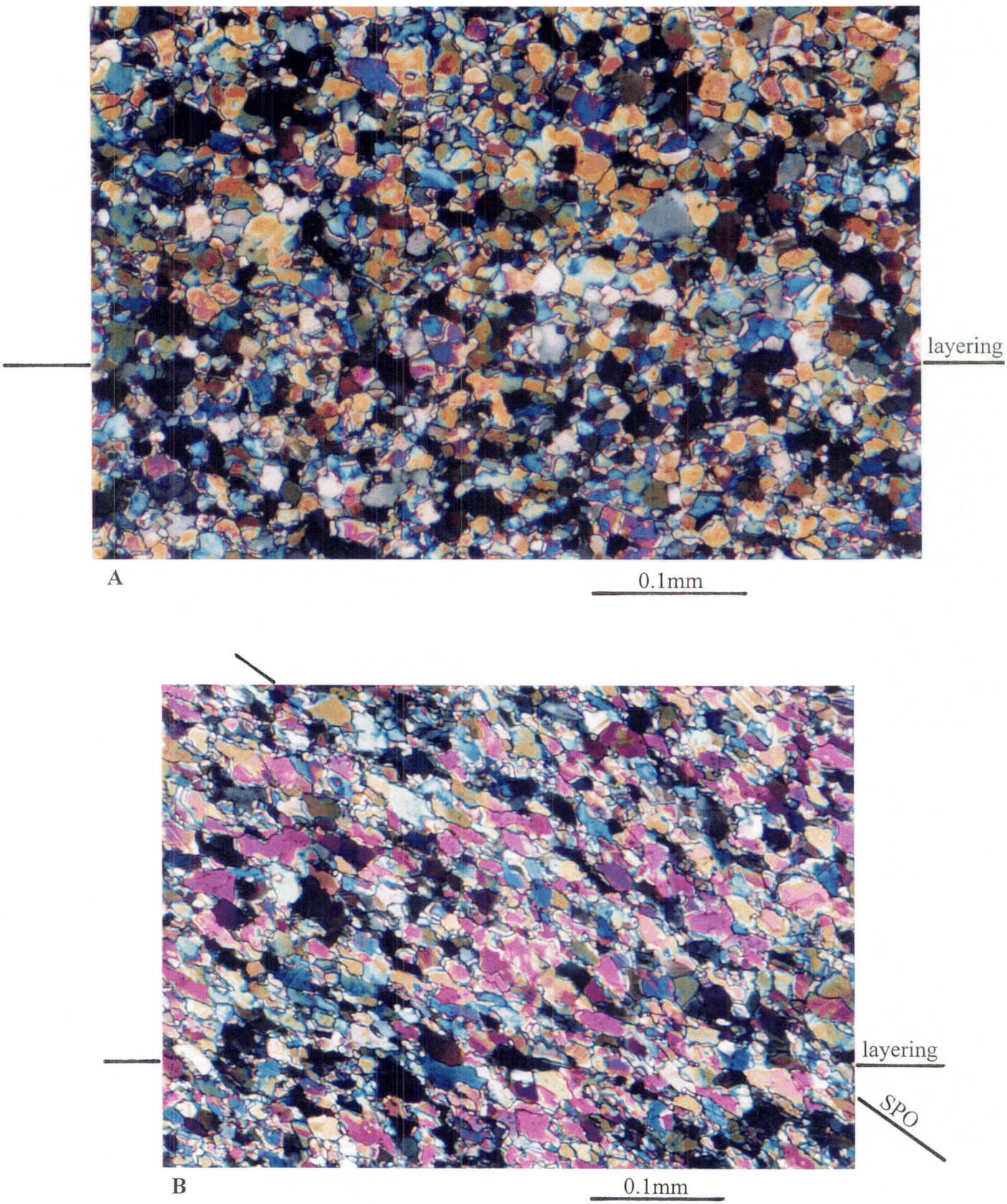

Figure 7.15: Calcite tectonite showing equidimensional calcite grains in sections perpendicular to the layering and stretching lineation (A), and a calcite grain SPO oblique to the layering in sections perpendicular to the layering and parallel to the stretching lineation (B). Ultrathin-section of RJ258, Summit Limestone shear zone. CPL.

The calcite grains in sections perpendicular to the lineation are equidimensional in aspect with straight boundaries and 120° dihedral angles (Fig. 7.15A, 7.22C). In contrast to the lesser strained rocks, there is very little variability of grain size within layers, and grain size is coarser on average (~20μ). There is a strong negative correlation between grain size and graphite/opaque content. Such a relationship accentuates the layering in thin-section view. Few or no strain fringes around detrital quartz grains occur in the sections perpendicular to lineation.

In sections parallel to the lineation, a foliation defined by calcite grain shapes occurs oblique to the layering by about 25-40° (Fig. 7.15B, 7.22A, 7.22B). Aspect ratios of 2-3:1 for calcite grains are common. The more elongate grains show undulatory extinction, deformation bands, and subgrain development (Fig. 7.16). Grains boundaries are both smooth and curved, some with 120° dihedral angles, whereas others are mildly serrate or bulging. Twins are sparse, but where observed, are thin or thick and always straight. The SPO of calcite grains is seen only in sections parallel to the lineation thereby confirming that the lineation is of mineral stretching origin. It follows that the highly strained marbles are best termed L-tectonites because they lack a SPO and strain shadow development in sections perpendicular to the stretching lineation.

Large single crystal calcite porphyroclasts also display a SPO, but in contrast to matrix grains, they are most elongate parallel to the layering (Fig. 7.17). Calcite porphyroclasts commonly show thick curved twins with some displaying twin-boundary migration.

Stair-stepping of cataclased single calcite porphyroclasts and numerous "in plane" δ-type fossil fragment porphyroclasts (Fig. 7.18), with appendages parallel to the layering, all show consistent dextral-normal sense of shear. Quartz and calcite strain fringes around detrital quartz grains, commonly show subgrain development and recrystallisation towards their distal ends indicative of antitaxial growth. The strain fringe orientation is oblique to the layering but parallel to the matrix calcite SPO. The more elongate ones, with longitudinal strains of at least 4 are asymmetrical and curve into the layering, providing a sense of shear. Distal ends of calcite strain fringes are so recrystallised that they are often difficult to differentiate from matrix calcite grains. A summary of the microscopic stretching lineations and shear-sense indicators is presented in Figure 7.19.

Figure 7.16 (A): Undulatory extinction and subgrain development in very elongate calcite grain (centre green grain). XZ ultrathin-section, RJ258, Summit Limestone shear zone. CPL. (B): Elongate calcite grain with subgrain boundary (centre cream-grey grain). XZ ultrathin-section, RJ252, CPL.

Figure 7.17: Single crystal calcite porphyroclast with a SPO parallel to the layering and oblique to the calcite matrix SPO. XZ ultrathin-section of RJ258, Summit Limestone shear zone, CPL.

Figure 7.16A

Figure 7.16B

Figure 7.17

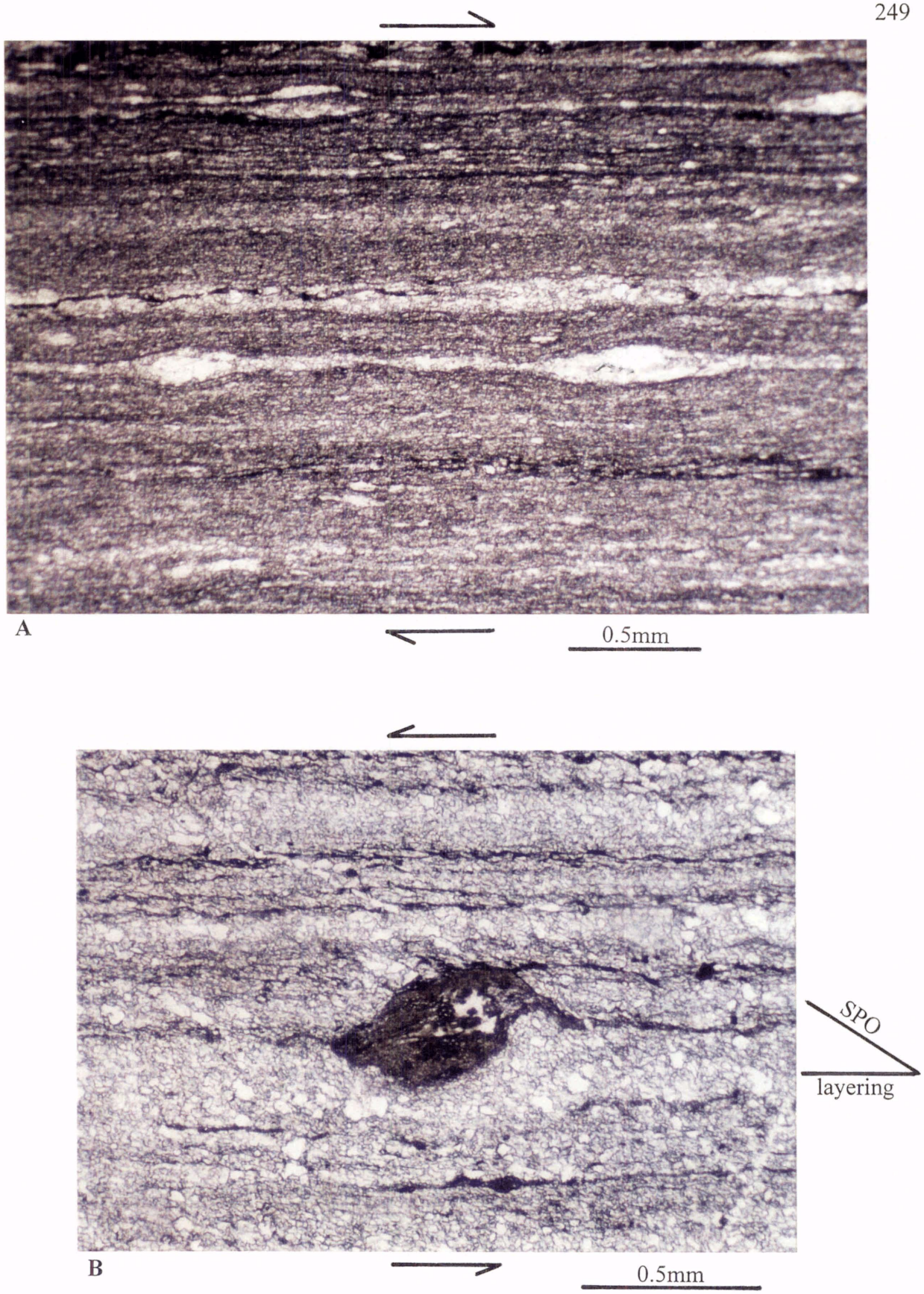

Figure 7.18 (A): Stair-stepping of calcite porphyroclast. Shear-sense is top to the right. XZ section, RJ255, Summit Limestone shear zone. PPL. (B): "In-plane" δ-type porphyroclast (fossil fragment). Shear-sense is top to the left. XZ section, RJ257, Summit Limestone shear zone. PPL.

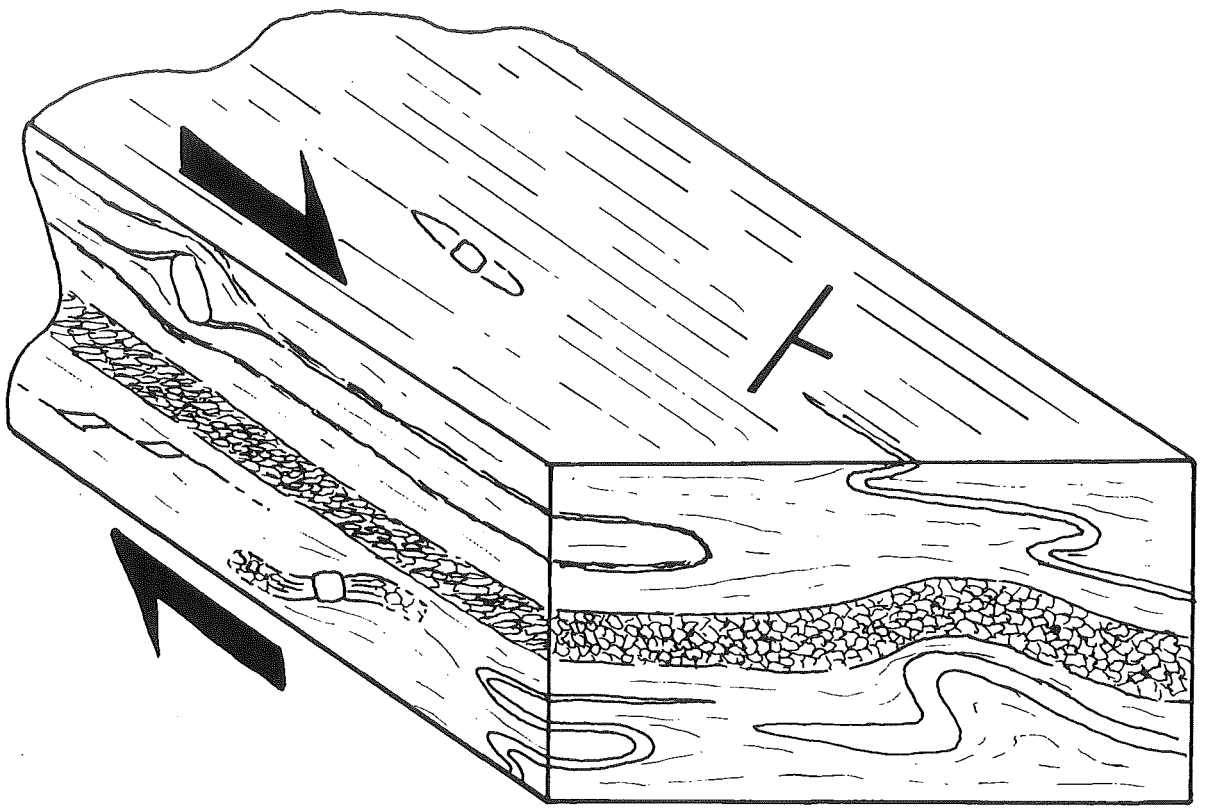

Figure 7.19: Schematic handspecimen revealing the microscopic stretching lineation and shear-sense indicators (stair-stepping, δ-type porphyroclasts, calcite SPO, and asymmetric strain shadows). Note how fold axes are typically parallel to the stretching lineation and some folds are sheath folds. Typical hand specimen orientation is 330/70 °NE; lineation plunges eastwards; shear-sense is top to the east (dextral-normal shear).

Early generation veins in the high stain rocks display a "core and mantle" structural geometry (Fig. 7.20). The cores (usually >200μm), which represent the remnants of large vein crystals, display strong undulatory extinction and equiaxed or elongate subgrain development near their perimeters. The convoluted cores are surrounded by a mantle of finer (~20μm average) recrystallised equiaxed grains. Many of these grains have crystallographic orientations closely related to that of the core. Cores are heavily twinned displaying complex twin-in-twin relationships and conjugate sets (Fig. 7.21). These twins are thick and curved, and many show evidence of twin-boundary migration (Fig. 7.21). In contrast, mantle grains display a few thin or thick straight twins (Fig. 7.20). New grains sometimes form internally within cores. They are sited primarily along twin or fracture sites (Fig. 7.21). Similar core and mantle structures are observed where isolated large single calcite porphyroclasts occur amongst the finer grained matrix.

An important sample (RJ252) collected closer to the Crow Granite contact (within 15m) shows very similar microstructures to that described for rocks in the high strain zone further away from the granite (Fig. 7.22), but differs in that it is coarser grained (~35μm average) and contains phlogopite porphyroblasts (Fig. 7.23). In some domains of the thin-section, phlogopite plates are subparallel to the layering but in others it is randomly oriented with well-developed strain fringes. The strain fringes about the phlogopites are consistently oblique to the layering but sub-parallel to the strong SPO of calcite grains and strain fringes adjacent to detrital quartz grains (Fig. 7.23).

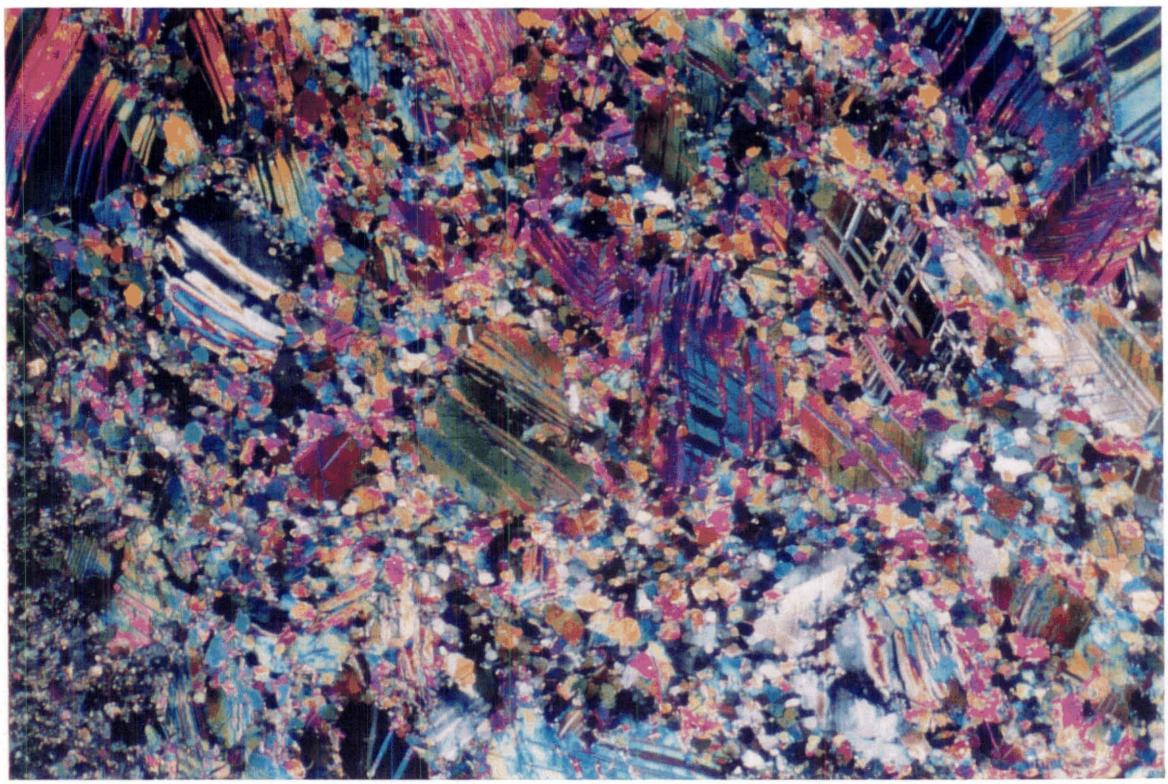

A

0.5mm

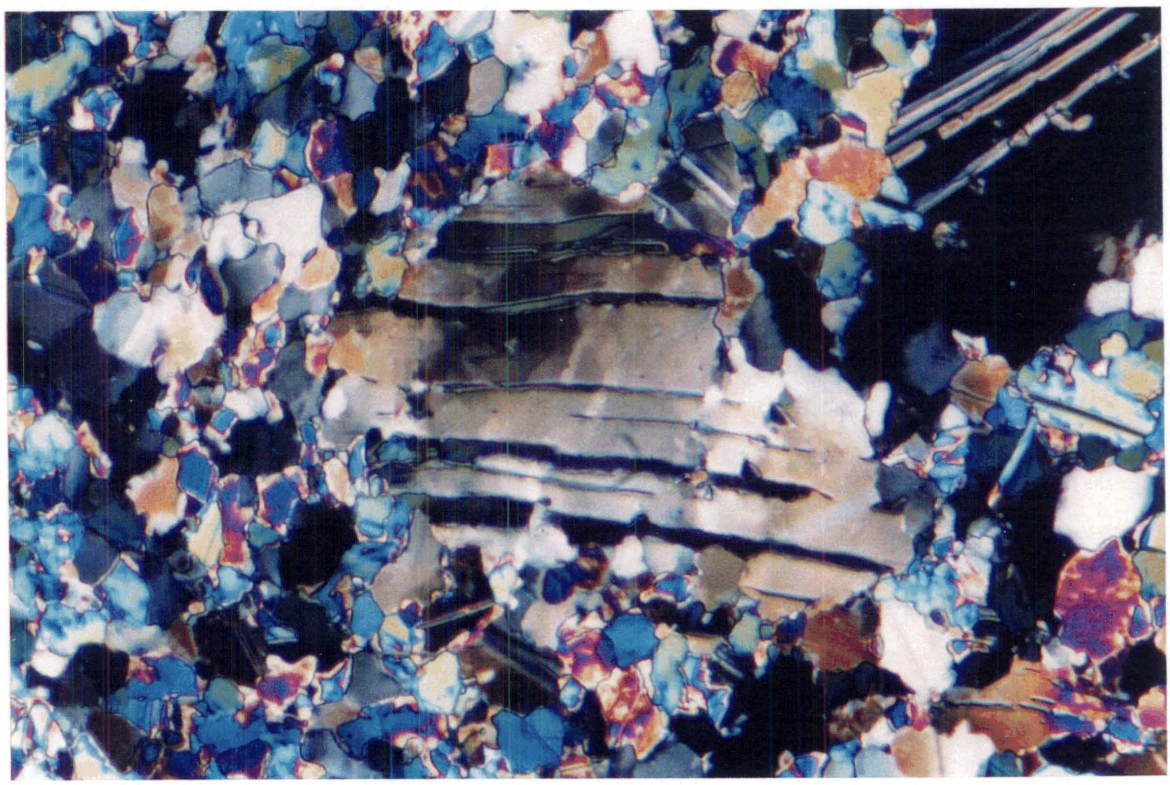

B

0.1mm

Figure 7.20 (A): "Core and mantle" structure in early generation calcite veins (see text for description). (B): Detail of "core and mantle" structure. Note the strong plastic deformation of the core (deformation bands and subgrains) and rotation recrystallisation of equiaxed grains at the core's perimeter. Both (A) and (B) are ultrathin-sections of RJ257, Summit Limestone shear zone. CPL.

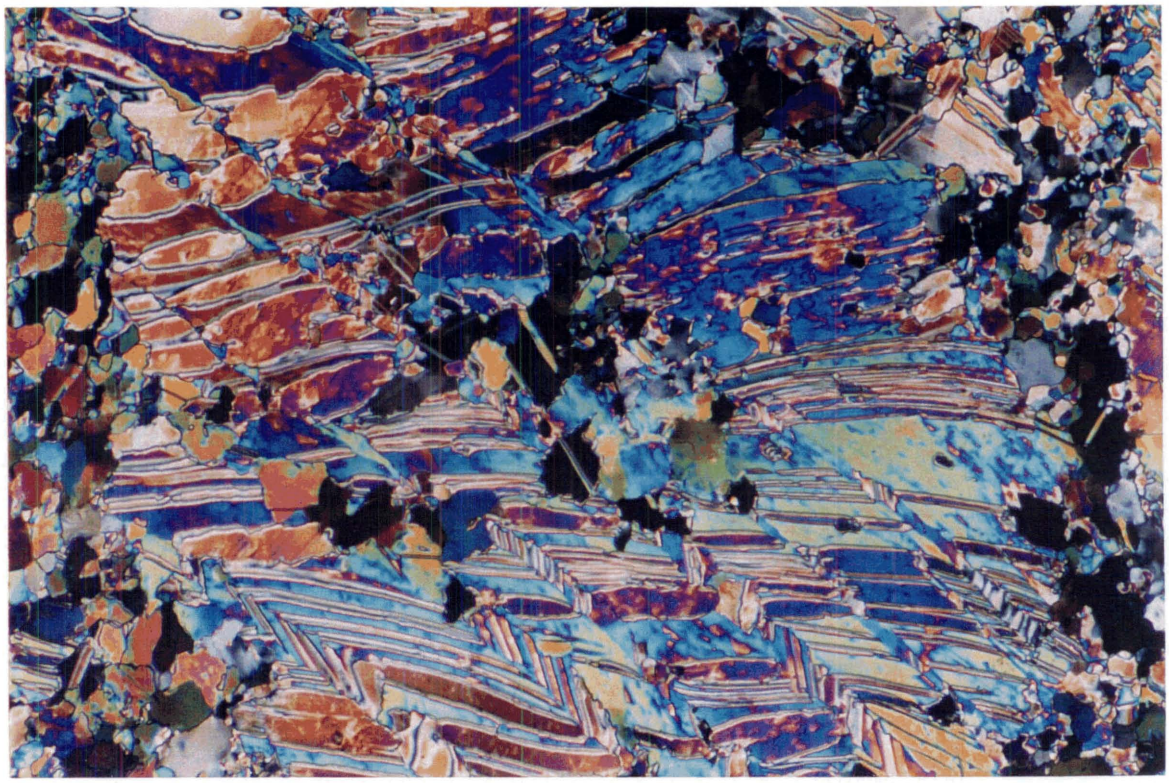

A

0.1mm

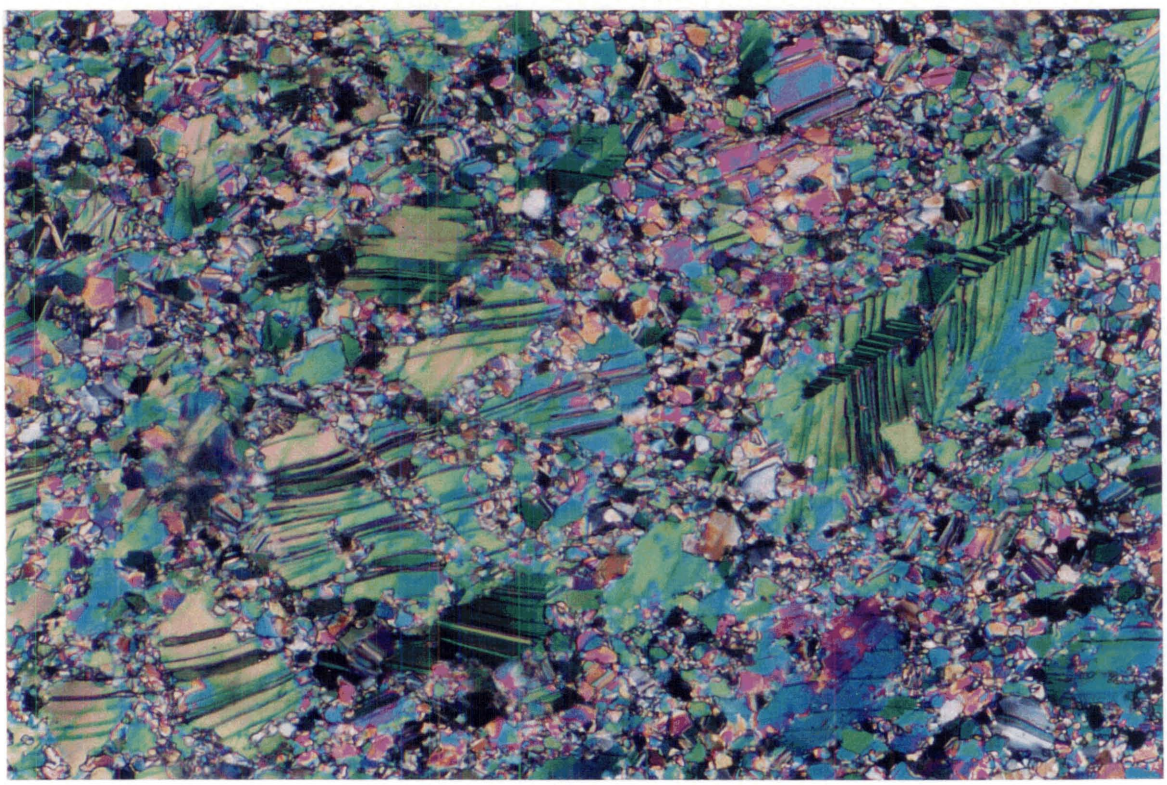

B

0.1mm

Figure 7.21 (A): A large "core" calcite grain displaying complex twin-in-twin relationships, twin-boundary migration (top left), and internal recrystallised finer grains. Ultrathin-section of RJ257,. Summit Limestone shear zone. CPL. (B): A large "core" calcite grain displaying twin-boundary migration (right side) and a network of recrystallised fine grains that were former twin or fracture sites. Ultrathin-section of RJ259, Summit Limestone shear zone. CPL.

Figure 7.22: Ultrathin-sections of RJ252, Summit Limestone shear zone. (A): The section perpendicular to the layering and parallel to the stretching lineation consists of a strong calcite SPO oblique to the layering. CPL. (B): Same as (A) but in PPL. (C): The section perpendicular to the layering and stretching lineation consists of equidimensional calcite grains. CPL.

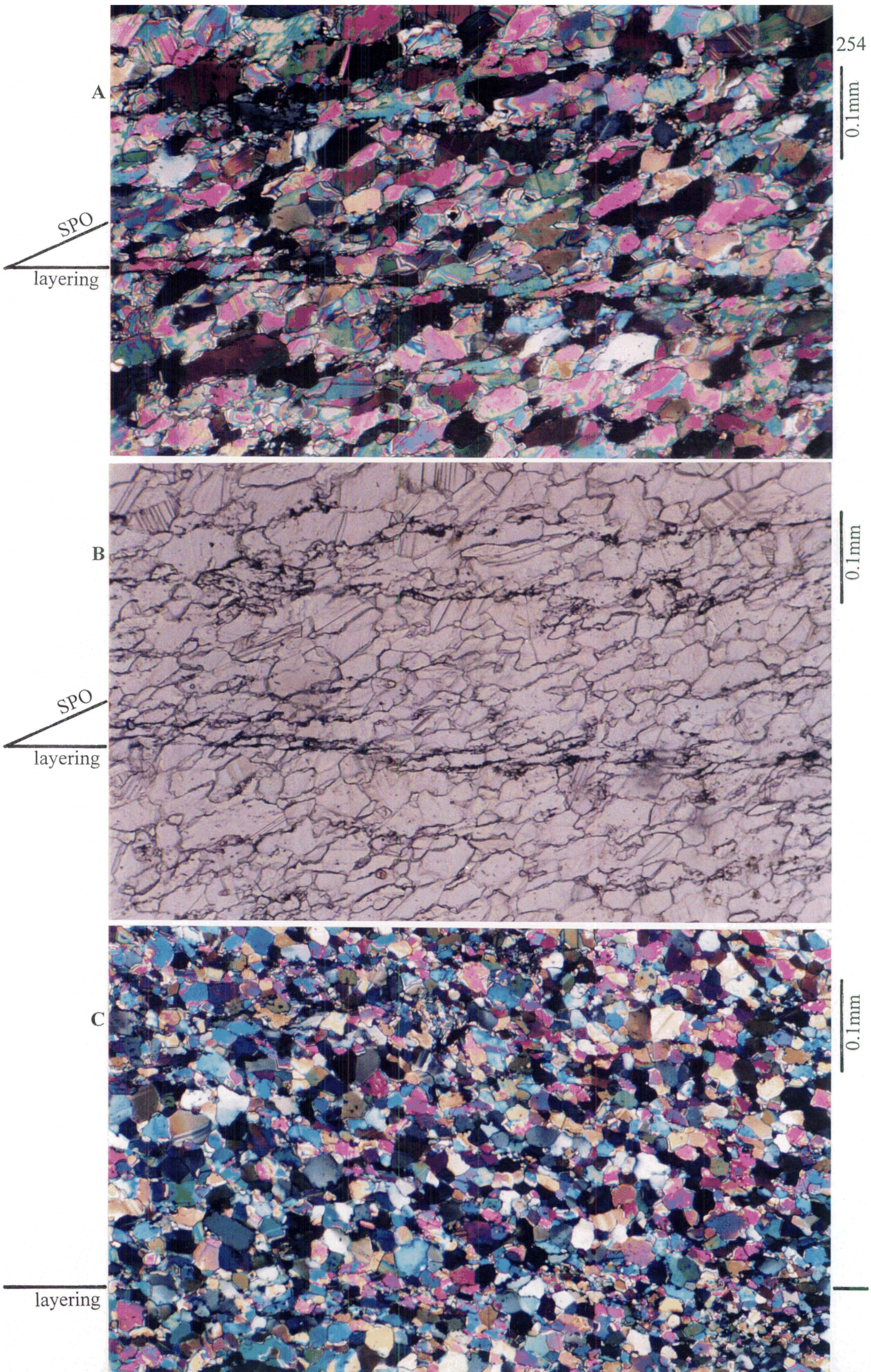
A
254
0.1mm
SPO
layering
B
0.1mm
SPO
layering
C
0.1mm
layering

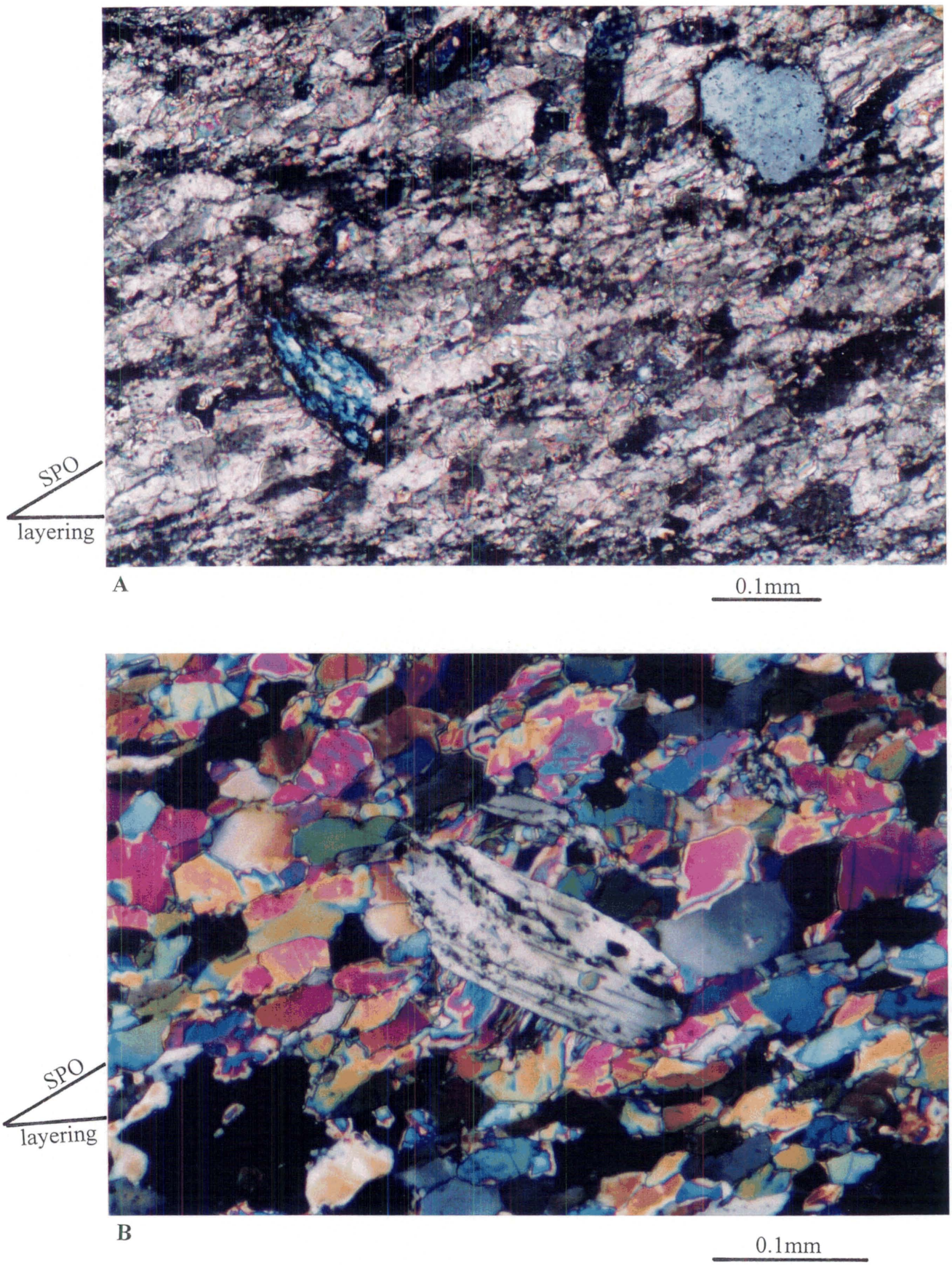

Figure 7.23: (A): Phlogopite porphyroblast (blue grain) in RJ252 with strain fringe subparallel to the calcite SPO and strain fringes adjacent to the detrital quartz grain (grey grain). XZ standard thin-section, CPL. (B): Phlogopite porphyroblast (centre grain) in RJ252 with proximal end of face-controlled strain fringe slightly oblique to the calcite SPO and ≈50° to the layering. The distal end of the strain fringe has rotated into parallelism with the calcite SPO and recrystallised. XZ ultrathin-section, CPL.

7.4.3 Discussion

The microstructural description of rocks in the shear zone indicates that a number of strain accommodating mechanisms on the grain scale as well as recrystallisation have been operative.

In the least strained rocks, the predominance of strain fringes and solution seams suggests solution transfer was a major strain accommodating mechanism. Nevertheless, twinning and the presence of curved twins and undulatory extinction indicates plastic deformation also played a role. The matrix grain size appears to show little modification prior to deformation. The grain size distribution reflects the protolith which probably had a microspar and sparry texture. This texture could have originated in the original limestone through diagenetic neomorphism (Folk 1965).

In the highly strained rocks, undulatory extinction and subgrain development suggests dislocation creep, aided by dynamic recrystallisation, was the dominant deformation mechanism. Urai *et al.* (1986) state that core and mantle structure is the main evidence for dislocation creep and rotation recrystallisation. Good examples of core and mantle structure involving calcite in the literature are: van der Pluijm (1991), Schmid *et al.* (1981), and Schmid *et al.* (1980). These examples display exactly the same features as seen in the early generation veins. As a result of rotation recrystallisation, >50% of the vein crystals have experienced grain size reduction, and can therefore be defined as a calc-mylonite. Urai *et al.* (1986) suggests limited grain-boundary migration plays a significant role in rotation recrystallisation. Indeed, the presence of 120° dihedral angles amongst the recrystallised grains coupled with the presence of twin-boundary migration in the cores suggest grain-boundary migration has been operative in the calc-mylonite veins.

It was noted that matrix calcite grains of highly strained marble is coarser grained, and more restricted in size, compared to the matrix of least strained metalimestone. Unless the high strain domain coincided with an originally coarser grained rock, I conclude that the coarser grain size can only be explained by grain-boundary migration. This is supported by the presence of mildly serrate and bulging grain boundaries. The

coarsening appears not to be related to the nearby Crow Granite because coarser higher strained rocks can occur further away from the granite than lesser strained counterparts.

From the least strained rocks to the most strained rocks, bedding becomes progressively attenuated, and becomes subparallel to cleavage (solution seams). It follows that in the highest strained rocks, the compositional layering, which is highly attenuated bedding and solution seams, is representative of the finite strain ellipse. This conclusion is supported by the fact that the distal ends of strain fringes, and SPO of calcite porphyroclasts, which track the finite strain ellipse, is subparallel to the layering. It is known that in highly strained rocks, the X axis of the finite strain ellipse approaches, and becomes subparallel to, the shear zone wall (Ramsay 1980). It follows that any marker, such as bedding, will also rotate into parallelism with the shear plane (Fig. 7.24) and thus it is concluded that the observed layering in the Summit Limestone shear zone approximates the shear plane.

The above conclusion is supported by the fact that stair-steps and δ-type porphyroclast appendages tend to be subparallel to the shear plane (Hanmer and Passchier 1991), and in the Summit Limestone shear zone examples, they are parallel to the layering. Stair-stepping, δ-type porphyroclasts, and sheath folds are indicative of high shear strain and non-coaxial flow, and in the case of "in-plane" δ-type porphyroclasts are indicative of non-ideal simple shear (Hanmer 1990; Hanmer and Passchier 1991).

In the high strain rocks, the matrix calcite SPO defines a foliation oblique to the layering. The most elongate grains show undulatory extinction, deformation bands, and equiaxed subgrain development indicating that dislocation creep is responsible for grain elongation and subsequent subgrain development. Since the layering represents the finite strain ellipse, it follows that the matrix calcite SPO must represent the last increments of strain. This is supported by the fact that proximal ends of antitaxial strain fringes are sub-parallel to the matrix calcite SPO. The calcite SPO is up to 42° oblique to the layering, indicating non-coaxial strain approached simple shear.

The asymmetry of the matrix calcite SPO foliation with respect to the layering is remarkably similar to that seen in quartz mylonites and referred to as either Type II S-C mylonites (Lister and Snoke 1984), or in terms of S_A and S_B foliations (Law *et al.* 1984).

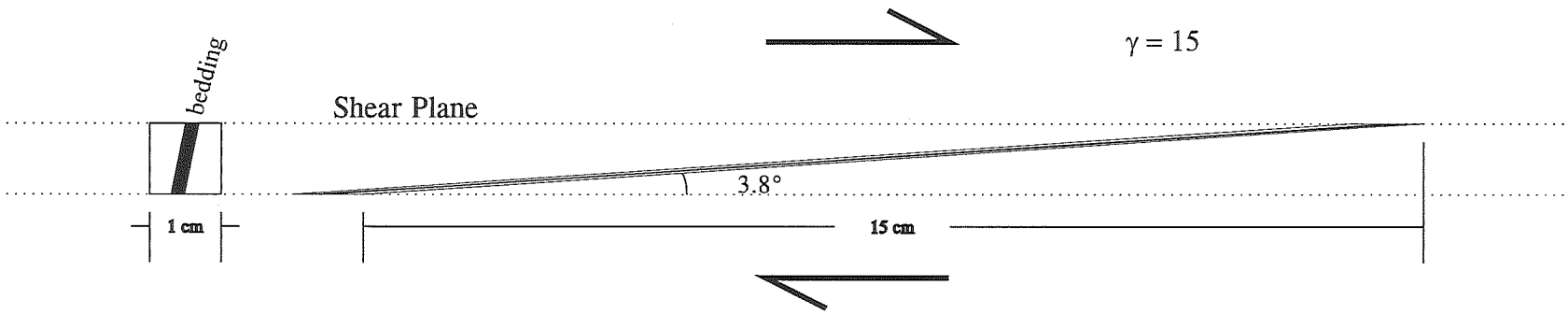

Figure 7.24: Diagram that demonstrates how a passive marker, such as bedding, will rotate into parallelism with the shear plane when a high shear strain is applied. In this diagram, a shear strain of 15 is applied to bedding that is at a high angle to the shear plane. After the shear strain is applied, bedding becomes <4° to the shear plane.

Similar microstructure has also been observed in calc-mylonite (van der Pluijm 1991; Lafrance *et al.* 1993) and described in terms of S-C planes. The authors describe the S planes or S_B foliation, equivalent to the matrix calcite SPO foliation, as representing dynamic recrystallisation which "periodically resets the finite strain clock" (Lister and Snoke 1984. p.631). The asymmetry of the matrix calcite SPO with respect to the layering therefore provides a sense of shear. The shear-sense indicated is dextral-normal shear in agreement with all other shear-sense indicators (Fig. 7.19).

Strain fringes around detrital quartz porphyroclasts indicate that solution transfer played a minor but significant part in the plastic dominated non-coaxial deformation of high strain rocks.

Phlogopite in RJ252 is significant in that it is a mineral of restricted occurrence most commonly found in regionally or thermally metamorphosed impure carbonate rocks (Deer *et al.* 1962). The phlogopite was only found in a sample very close to the Crow Granite (within ~15m) but not in any others further away (12 samples in all). I suggest the phlogopite, together with calcite grain coarsening in RJ252, is logically due to the thermal effect of granite intrusion. This suggestion implies that the Crow Granite was intruded in the vicinity of Summit Limestone.

Strong strain fringe development around the phlogopite is parallel to the matrix calcite SPO foliation in RJ252, and implies that the last increment of strain postdates pluton emplacement. Given that calcite is very susceptible to annealing (Griggs *et al.* 1960), the complete absence of annealing texture in RJ252 modifying the dynamically recrystallised matrix calcite SPO foliation, suggests that ductile shear was not synchronous with Crow Granite intrusion but instead must postdate it. Furthermore, the microstructure in RJ252 displays the same sense of shear as all other samples of the 200m shear zone.

Interestingly, the least strained rocks within the Summit Limestone shear zone, which are rocks that have not experienced a dynamic recrystallisation overprint, show no evidence of thermal metamorphism. These rocks occur some 50m from the Crow Granite, yet the thermal aureole on the western margin of the Crow Granite is up to 200m. The difference in thermal aureole extent either side of the Crow Granite will be explored in Section 7.6.

In summary, the Summit Limestone shear zone is principally made up of highly strained rocks where non-coaxial deformation has been plastically accommodated. Shear-sense indicators are consistent and give a dextral-normal sense of shear. Within the Summit Limestone shear zone are zones where the rocks are less strained and the strain appears coaxial. Solution transfer played a major role in accommodating strain in these less strained rocks. The variable distribution and accommodation of strain in the shear zone is indicative of strain partitioning (Fig. 7.28). The westernmost rock of the Summit Limestone shear zone reveals evidence that the shear zone postdates Crow Granite emplacement.

7.4.4 Deformation temperature

Twinning morphology and the presence of recrystallisation may help determine temperature during the formation of the shear zone.

Two types of twins are observed in the shear zone:

A. Thick curved twins which occur in "cores" and porphyroclasts of highly strained rocks, some of which display twin-boundary migration. Thick curved twins also are displayed in strain fringe grains of lesser deformed rock.

B. Thin or thick straight twins in grains of least strained rocks and the recrystallised grains of the high strain rocks. Thin straight twins are also found in late stage cross-cutting veins.

Based on a very well-constrained study of natural twinning, Burkhard (1993) suggests thick curved twins (Type III of Burkhard) are indicative of >200°C and the presence of twin-boundary migration (Type IV) is indicative of >250°C. Burkhard interprets Type III and IV twins to be related to major deformation. Straight twins are interpreted to indicate temperatures <300°C (thick twins: type II) and <200°C (thin twins: type I) and are usually associated with late stage or minor deformation. My observations of twinning characteristics and occurrence (A and B above) appear to be in agreement with the deformation interpretations of Burkhard and thus his temperature classification may be applicable to this study.

Most experimental work has shown that both rotation recrystallisation and grain-boundary migration of calcite occurs at temperatures above at least 400°C (e.g. Turner *et*

al. 1956; Wenk *et al.* 1973; Schmid *et al.* 1987). Unfortunately these experiments were performed under geologically unrealistic strain rates. Heard (1963) successfully demonstrated that a decrease in strain rate lowered the temperature required for recrystallisation to be effective. Well-developed "intragranular" and "intergranular" recrystallisation, found to be common at 600-800°C at strain rates* near $10^{-3}sec^{-1}$, are also observed at 350-500°C at $10^{-7}sec^{-1}$. From this relationship, Heard suggests recrystallisation could occur as low as 200°C with strain rates that are more geologically realistic ($10^{-14}sec^{-1}$). Naturally deformed calcite tectonite examples where both rotation recrystallisation and grain-boundary migration have occurred at low temperatures are described by:

- Schmid *et al.* (1981): <400°C
- Behrmann (1983): ~300°C
- Groshong *et al.* (1984): >270°C
- Heitzmann (1987): ~300°C
- de Bresser (1989): ~200°C
- Burkhard (1993): ~330°C.
- Lafrance *et al.* (1994): <350°C

I have not found any description in the literature of the preservation of dynamic recrystallisation microstructure in marbles naturally deformed at temperatures above 400°C. Griggs *et al.* (1960) showed, in experimental work, that calcite aggregates anneal at temperatures above 500°C. Thus annealing probably explains the apparent absence of dynamic recrystallisation microstructure provided temperatures were greater than 400-500°C after deformation ceased.

In summary, based on twin characteristics and dynamic recrystallisation effects, temperatures above ~250°C but not higher than 400°C are suggested. However, the lack of ductile deformation in the nearby Crow Granite and lack of ribbon development in clastic quartz grains, within the marble, suggest temperatures did not exceed ~300°C.

* Strain rate is a constant rate of percentage shortening or elongation. The figures quoted by Heard (1963) refer to percentage elongation.

7.4.5 Differential stress

It is well-known that dynamically recrystallised grain-size decreases with increased differential stress (e.g. Chester 1989). In naturally deformed rocks, differential stress may be quantified, based on grain size, if the mechanism of recrystallisation is known (Poirier 1985). Schmid *et al.* (1980) obtained a stress versus grain-size relationship from experiments on Carrara marble where the dominant recrystallisation mechanism was rotational recrystallisation.

In the early generation veins of Summit Limestone tectonites, there is good evidence that dynamically recrystallised grains are a result of rotational recrystallisation and thus an opportunity is presented to estimate differential stress. The empirically derived equation of Schmid *et al.* (1980) is:

$$\sigma = 10^{3.67}\, d^{-1.01} \text{ where d = grain size (}\mu\text{m) and } \sigma \text{ = differential stress (bars)}$$

The recrystallised grain-size in early generation veins is 20μm, giving a differential stress estimate of 227bars (22.7MPa). Caution is needed in interpreting this estimate as it is likely that differential stress varies between early generation veins and the matrix.

7.5 Fabric analysis of calcite tectonites

7.5.1 Introduction

In low temperature simple-shear experiments it has been demonstrated that the *c*-axis preferred orientation is deflected from the pole to the flattening plane towards σ_1 (Schmid *et al.* 1987; Wenk *et al.* 1987). Extensive twinning is the dominant orienting mechanism and rapidly rotates the *c*-axes of calcite into near parallelism with σ_1 (Schmid *et al.* 1987). It follows that an obliquity of *c*-axis girdles, with respect to the flattening plane in natural low temperature shear zones, can be used to determine the sense of shear and the approximate orientation of the shear plane (Fig. 7.25) (Shelley 1993). Unfortunately it is often difficult to know if extensive twinning has been operative because grains easily become completely twinned (Turner and Weiss 1963; Schmid *et al.* 1987), thereby masking any evidence of earlier extensive twinning. Observed twin lamallae are, in most

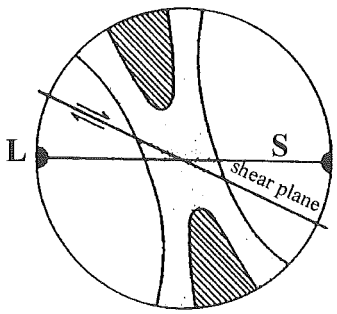

Figure 7.25: Relationship of a *c*-axis girdle to the foliation/flattening plane (S) and shear plane in natural shear zones (simple shear) where twinning is the dominant orienting mechanism. σ_1 is 45° to the shear plane, and the finite extension direction (L) rotates towards the shear plane with increasing strain. Sense of shear is dextral (from Shelley 1993).

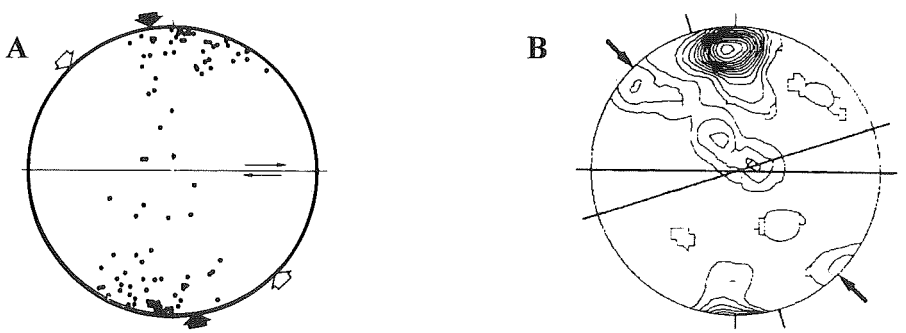

Figure 7.26: *c*-axis preferred orientation for calcite rock deformed in the grain-boundary migration microfabric regime of simple shear experiments where the shear sense is dextral. (A) Freidman and Higgs (1981). (B) Schmid *et al.* (1987). In (A), horizontal line represents the shear plane, open broad arrows represent σ_1 oriented at 45° to the shear plane, and filled broad arrows represent the axis of finite shortening i.e. Z. In (B), horizontal line represents the shear plane, arrows represent σ_1 oriented at 45° to the shear plane, and inclined line represents the plane of finite flattening.

cases, the consequence of an unrelated late stage minor deformation (Turner and Weiss 1963).

The microstructures in high strain calcite tectonites of the low temperature Summit Limestone shear zone demonstrate non-coaxial strain, and a dextral-normal sense of shear. An analysis of *c*-axis preferred orientations in the tectonites was therefore undertaken to see if it supports the microstructurally determined sense of shear.

7.5.2 Samples and results

Three high strain samples (RJ257, RJ258, RJ259) were selected for measurements of *c*-axis orientations. In addition, RJ252, located immediately adjacent to the Crow Granite was also selected. Due to the fine grained nature of the tectonites, ultrathin-sections of the samples were made.

The results of the analyses are shown in Figure 7.27. In the three high strain samples, the *c*-axes preferred orientation is at a high angle to the layering. In RJ258 and RJ259, the maximum is perpendicular to the layering whereas in RJ257, the maximum is deflected from the perpendicular towards the matrix calcite SPO and away from the microstructural shear-sense inferred σ_1 orientation. In contrast, RJ252 shows a very diffuse girdle of *c*-axes that shows no orthogonal relationship to the layering. When elongate grains are measured separately, the *c*-axes plot at low angles to the layering (Fig. 7.27E).

7.5.3 Discussion

The results from the high strain samples are surprising, given that they show no deflection away from the normal to the plane of flattening towards the microstructural shear-sense inferred σ_1 orientation, as would be expected in extensively twinned shear zone tectonites. On the other hand, there is no evidence that extensive twinning has occurred because the calcite grains are dynamically recrystallised. The possibility is then raised that the *c*-axis preferred orientation is a result of other deformation mechanisms.

From the microstructural discussion it was concluded that the layering in high strain rocks is subparallel to the shear plane. Therefore, the *c*-axis preferred orientation in

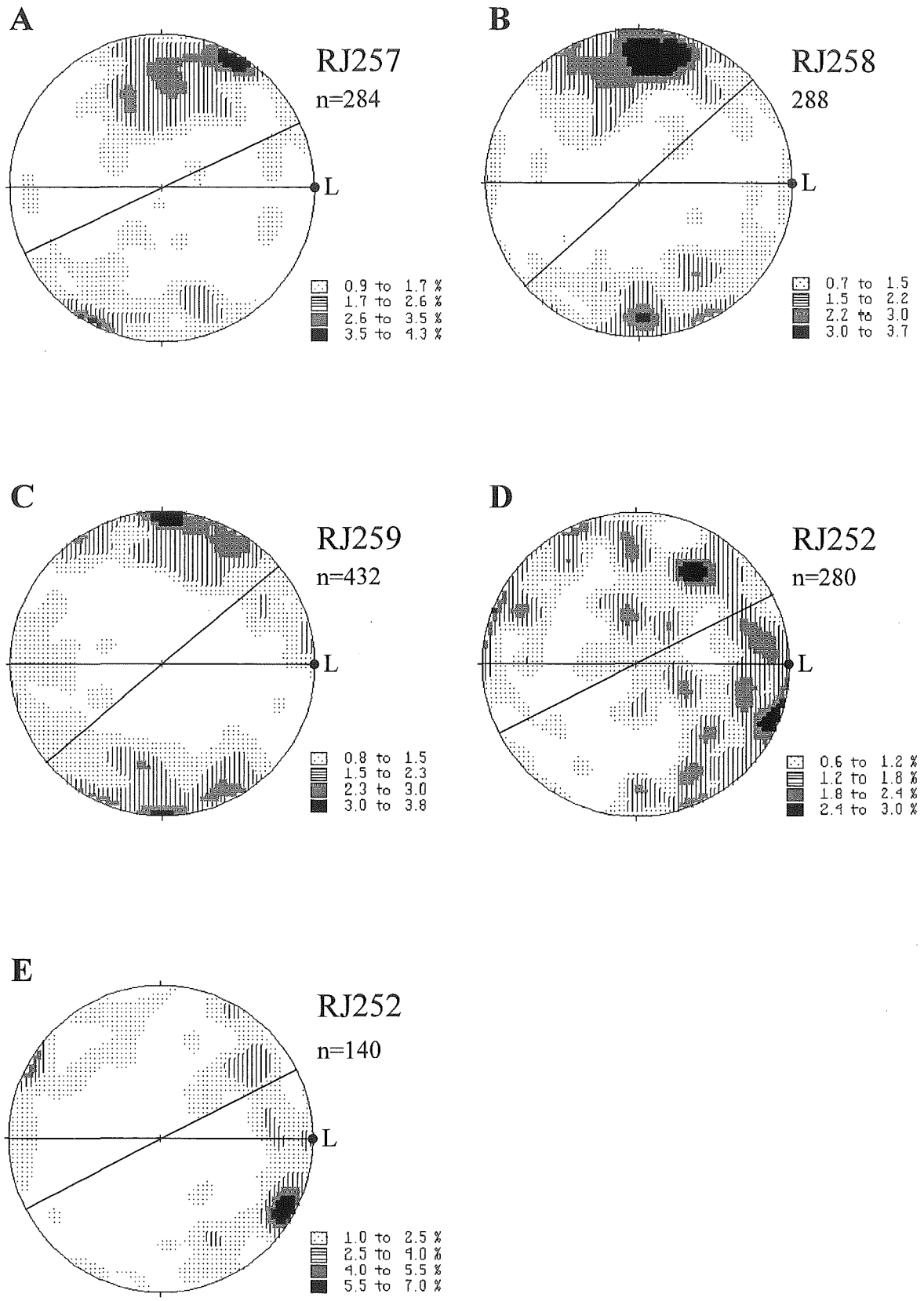

Figure 7.27: Contoured stereographic projections of *c*-axis measurements for all calcite grains in RJ257 (A), RJ258 (B), RJ259 (C), RJ252 (D), and elongate grains in RJ252 (E). Horizontal line represents layering. The line oblique to layering represents the calcite SPO foliation. L = stretching lineation.

RJ257, RJ258, and to a lesser extent RJ259, are subperpendicular to the shear plane. Given this information, a direct comparison of the natural LPO in this study can be made with that observed in all simple-shear deformation experiments of calcite rocks, because the shear plane orientation is the common reference surface. The *c*-axis preferred orientation of RJ257, RJ258, and RJ259 most closely matches that in which calcite rock was experimentally deformed under high temperature conditions (800-900°C) and shear strains of $10^{-2}s^{-1}$ and $10^{-4}s^{-1}$ (Freidman and Higgs 1981; Schmid *et al.* 1987). In these experiments, the original grains are completely dynamically recrystallised and display a SPO oblique to the shear plane. The *c*-axis maximum is perpendicular to the shear plane in the case of Schmid *et al.* (1987), and slightly deflected from the perpendicular away from σ_1 in the case of Freidman and Higgs (1981) (Fig. 7.26). This microstructure and fabric is referred to as the "grain-boundary migration microfabric regime" by Schmid *et al.* (1987). The *c*-axis maximum perpendicular to the shear plane indicates basal slip and is thought to be achieved by migration recrystallisation selectively consuming unfavourably oriented grains for easy slip (Schmid and Casey 1986; Schmid *et al.* 1987).

Similar microstructure and fabric from low temperature shear zones (200°-450°C) have been reported in the literature (e.g. Busch and van der Pluijm 1995; Lafrance *et al.* 1993), and have been compared with the high temperature experimental grain-boundary migration regime. Lafrance *et al.* (1993) show that the obliquity of many natural low temperature *c*-axis preferred orientations reported in the literature are not consistent for a given sense of shear, and that their microstructures are more consistent with dynamic recrystallisation and intracrystalline slip.

It is concluded that the *c*-axis preferred orientations and microstructures from the high strain rocks of the Summit Limestone shear zone are consistent with the grain-boundary migration regime of Schmid *et al.* (1987), and therefore any obliquity observed (e.g. RJ257) cannot be used to indicate the sense of shear. This conclusion can be extended to any natural calcite shear zones where complete dynamic recrystallisation has occurred, because it cannot be confidently shown that the preferred orientation is a result of extensive twinning. The results of this study may be a good example of where natural low temperature deformation mechanisms are duplicated by higher temperature and faster strain rate laboratory experiments (see Paterson 1976).

The fabric of RJ252 is enigmatic and much more difficult to explain than the other samples. The microstructure of elongate grains display undulatory extinction and subgrain development, and implies that dislocation creep has been operative. Thus the reasonably strong maximum, observed at a low angle to the layering in the most elongate grains (Fig. 7.27E), may be of plastic deformation origin. Interestingly, the *c*-axis preferred orientation maximum corresponds to a r-slip maximum produced in the experimental simple shear intracrystalline regime of Schmid *et al.* (1987). It is speculated that the *c*-axis preferred orientation for the most elongate grains may reflect an easy-slip preferred orientation on *r*.

The most elongate grain *c*-axes appear to significantly contribute to the girdle makeup for all grains in RJ252 (compare Fig. 7.27E with Fig. 7.27D). Nevertheless, even if a plastic deformation origin for the elongate grain *c*-axis maximum is accepted, the girdle for all grains is very diffuse and needs to be explained. Griggs *et al.* (1960) showed that annealing tends to randomise any pre-existing LPO in calcite. Given the closeness of the Crow Granite, and the presence of phlogopite porphyroblasts, the very diffuse *c*-axis girdle for all grains in RJ252 (Fig. 7.27D) suggests annealing may have initially randomised the fabric, but plastic deformation processes, such as that suggested for the most elongate grains, has modified the random fabric to the present girdle distribution.

I have attempted to explain the origin of the *c*-axis preferred orientation in RJ252 in terms of plastic deformation. However, the *c*-axis preferred orientation shows no similarity with that of RJ257, RJ258, and RJ259 even though their microstructures are similar. The lack of fabric similarity implies either that different plastic deformation mechanisms have been active, or alternatively, other orienting mechanisms have been operative (e.g. growth).

7.6 Anatoki Fault movement in the Crow River domain

From the previous description of units and contacts, the following points are relevant to the history of the Anatoki Fault:

1. The Crow Granite pluton intruded Buller terrane sandstone and shale on its western side (Sections 7.2.2 and 7.3.1), and in the vicinity of Takaka terrane limestone on its eastern side (Section 7.4.3) at ~137Ma.

2. Petrologically, the hornfelsed sediment on the eastern side of the pluton is similar to Douglas Formation (Section 7.2.3), and may therefore represent pendants of Buller terrane rock on the eastern margin of the pluton.
3. Based on the western margin of the Summit Limestone with respect to topography, the general attitude of the Anatoki Fault in the Crow River domain dips steeply E-NE.
4. The western half of the Summit Limestone band has undergone non-coaxial ductile shear with top to the E-ESE sense of shear (dextral-normal movement) (Section 7.4).
5. Movement on the Summit Limestone ductile shear zone postdates Crow Granite emplacement (Section 7.4.3) and took place at temperatures around 250-300°C (Section 7.4.4).
6. Numerous unit contacts in the vicinity of the Anatoki Fault are faults (Section 7.3). Apart from the Summit Limestone ductile shear zone, the fault zones are always brittle but display features that are indicative of some depth during fault movement (quartz veining, slickenfibres, cemented fault breccia and pug, cataclasites, pressure solutioning). In addition, some of these brittle fault zones show evidence of reactivation (cross cutting non-cemented pug seams, non- or weakly-cemented fault breccia and gouge, slickensides).
7. The thermal effects of the Crow Granite can be detected up to 200m in the Douglas Formation, west of the Crow Granite (Section 7.2.2), but between ~15m and 50m in Summit Limestone, east of the Crow Granite (Section 7.4.3). The differences in the extent of thermal effects may be due to either the three dimensional shape of the pluton, or alternatively, due to tectonic shortening between Summit Limestone and Crow Granite. The latter is considered more probable since a <50m thermal aureole seems too small, given the size of the pluton.

Point 1 implies the Buller and Takaka terranes had amalgamated prior to ~137Ma, and that the Crow Granite intruded almost directly along the pre-137Ma position of the Anatoki Fault, hornfelsing the surrounding sediments of both terranes. Because of the intrusion and subsequent deformation (point 5), very little can be determined about Anatoki Fault movement in the Crow River domain prior to ~137Ma.

Limestones represent rheologically weak zones in the crust because of their susceptibility to plastic deformation at any temperature. In a scenario where limestone is in close proximity to granite, it is extremely likely that in any deformation event involving both

lithologies, strain will be strongly partitioned with limestone taking up most of the strain. Thus any crustal movement between the Buller terrane and Takaka terrane post ~137Ma will be concentrated in the Summit Limestone. Such a scenario has indeed happened (points 4 and 5) and thus the position of the Anatoki Fault is now located at the contact between Summit Limestone and Crow Granite/hornfelsed sediment (point 2) (Fig. 7.28).

Movement on the Summit Limestone ductile shear zone took place at temperatures of around 250-300°C which implies a depth of about 8-10km if an average geothermal gradient of 30°C/km is assumed. Nearby faults, which separate units, have similar strikes as the Summit Limestone shear zone. Given that movement on these brittle faults occurred at some depth (point 6) it is suggested that they are related to Summit Limestone shear zone movement when temperatures were around 250-300°C. Movement in the Summit Limestone shear zone was ductile, whereas movement in adjacent rocks was brittle and concentrated near contacts (Fig. 7.28); together this movement effectively represents Anatoki Fault movement. Given that the movement postdates the Crow Granite, which has thermally affected both terranes, Anatoki Fault movement recorded in the Crow River domain must represent reactivation.

Because the major Late Cenozoic Karamea and Skeet faults occur nearby, the late stage cross-cutting pug seams, non- or weakly-cemented fault breccia and gouge, and slickensides are most likely to be related to Late Cenozoic uplift. N to NE striking faults offsetting contacts along the Mt Olive tops, including the fault which is responsible for repeating the Crow Granite and Summit Limestone contact in Mt Olive Stream (Section 7.3.3), are also probably related to Late Cenozoic deformation.

The probable tectonic shortening that has occurred along the eastern margin of the Crow Granite (point 7) can be accounted for by either ductile shear in the Summit Limestone shear zone, and/or brittle faulting that was synchronous or postdating Summit Limestone shear zone movement.

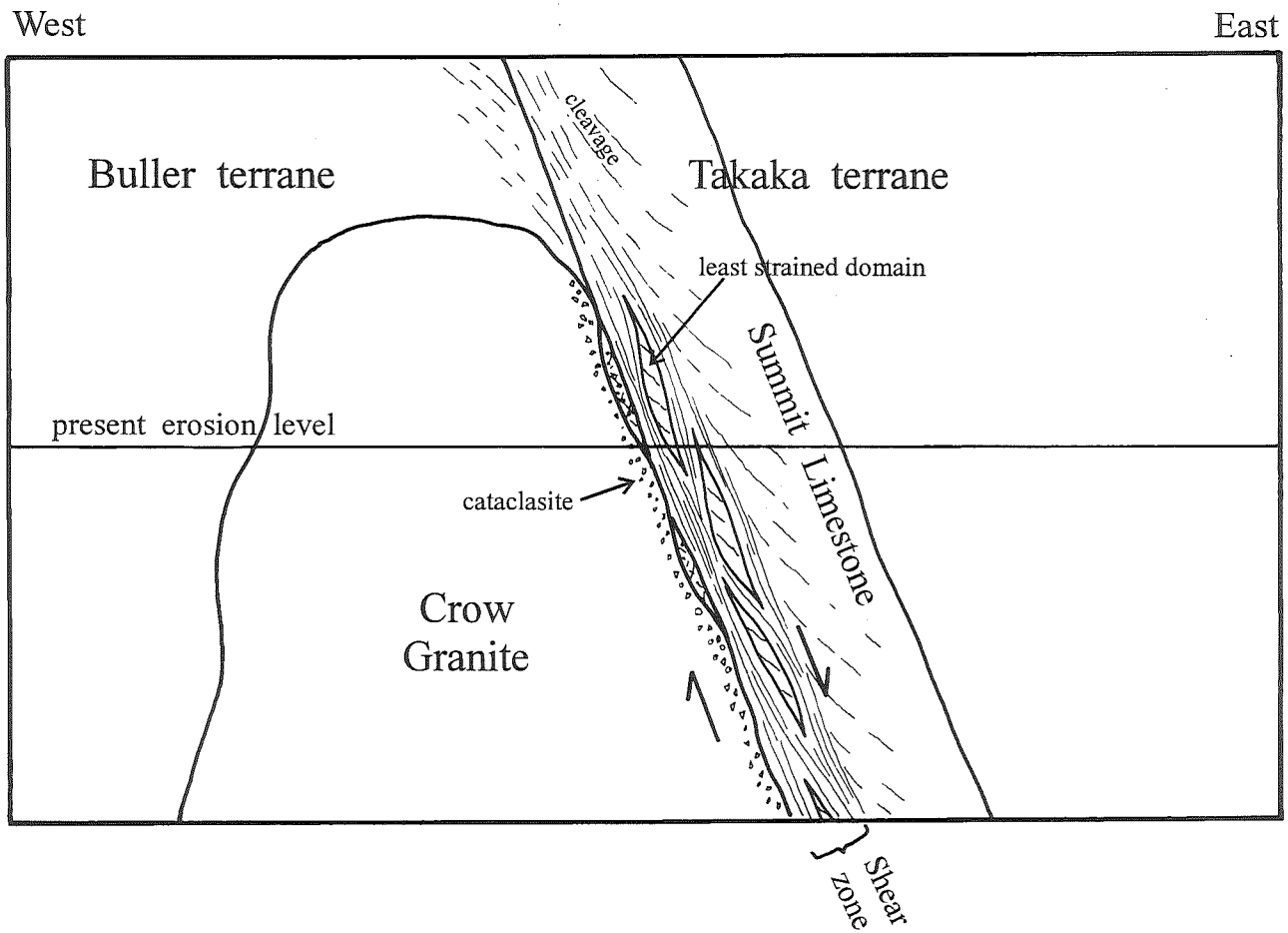

Figure 7.28: Schematic cross-section of the Crow River domain. Post 137Ma movement on the Anatoki Fault has been partitioned with Summit Limestone taking up the majority of the strain. Within the Summit Limestone there is further strain partitioning with least strained domains (coaxial strain) and high strain (non-coaxial strain) domains (see Section 7.4.3). Movement in the Summit Limestone shear zone was ductile whereas movement in adjacent rocks was brittle.

CHAPTER 8

BALLOON MÉLANGE

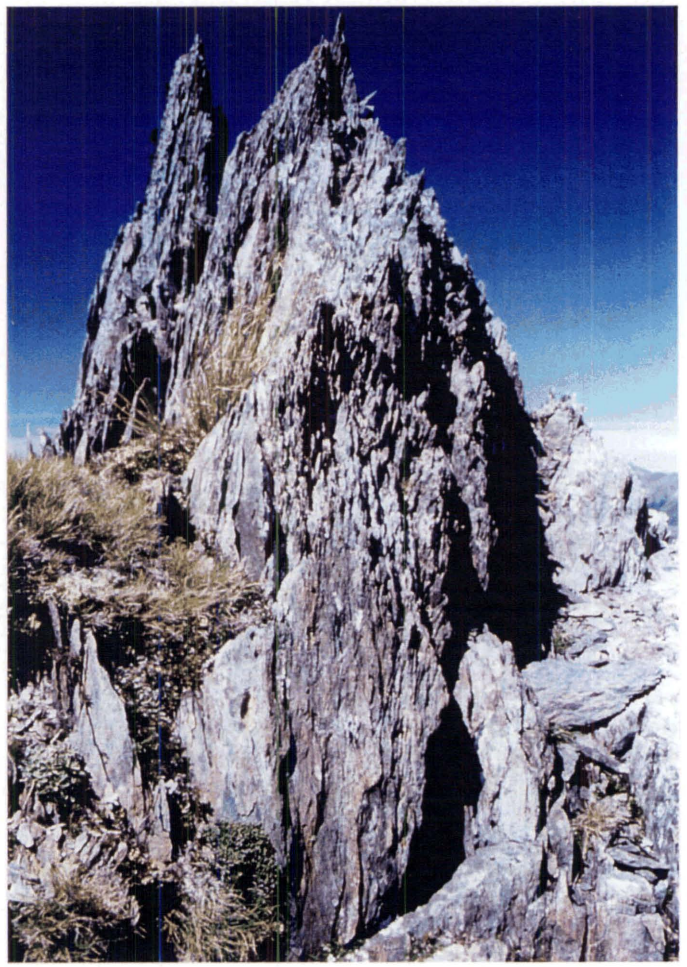

Chapter frontispiece: Balloon Mélange near Kakapo Peak possesses a strong near vertical slaty fabric. M26/ 735205.

8.1 Introduction

From the southeast corner of the Boulder Lake domain all the way south to the Kakapo Peak domain there is a north-south trending belt of rock, up to 2.5km wide, with characteristics that best fit the definition of a mélange (Maps 1 to 3). As will be shown in this chapter, the mélange shows characteristics and age of formation which are very similar to the sandstone/mudstone derived mélange that forms most of the Balloon Mélange mapping unit in the Cobb Reservoir area (Cooper 1993; Pound 1993). The name Balloon Mélange is therefore extended to include the mélange in the study area.

This section describes the characteristics of the Balloon Mélange, including composition, structure, and its contact relationships with adjacent rock units. The description is based mainly on observations from the Kakapo Peak and Lonely Lake domains, where exposure is best.

8.2 Description of Balloon Mélange

The Balloon Mélange investigated in the study area consists predominantly of sandstone inclusions set in a matrix of mudstone, here termed as "full mélange" (Fig. 8.1). In some places, the rock type more resembles that of "broken formation" (Raymond 1984) in which internal continuity of strata can be observed despite the disrupted nature of the rock (Fig. 8.2). Sandstone beds in broken formation are partially dismembered by brittle normal faults oblique to bedding. Broken formation is always surrounded by full mélange and therefore can be regarded as a type of inclusion itself. Broken Formation can grade into full mélange over the space of a few metres. In areas of broken formation, one may occasionally find intact bedding on the outcrop scale. Thus there is a complete spectrum of textures ranging from intact bedding, to broken formation, to full mélange, and it follows that the Balloon Mélange was derived from what was once a bedded sediment protolith (Fig. 8.3).

In addition to the sandstone/mudstone derived mélange, there are isolated but mappable bodies of chert. The Balloon Mélange in this study therefore fits the established definition of a mélange given by Raymond (p. 18, 1984) as "a body of rock mappable at a

Figure 8.1: Sandstone-rich full mélange (A) and sandstone-poor full mélange (B). The orange coloured rock is sandstone whereas the dark grey or black rock is the muddy matrix. Float, south branch of Stanley River. Lens cap for scale.

Figure 8.2: Broken Formation. Continuity of strata can be observed despite the disrupted nature of the rock. Float, south branch of Stanley River. Hammer for scale.

Figure 8.1A

Figure 8.1B

Figure 8.2

scale of 1:24 000 or smaller and characterised both by the lack of internal continuity of contacts or strata and by the inclusion of fragments and blocks of all sizes, both exotic and native, embedded in a fragmented matrix of finer-grained material". Very thin (<20cm) lenses of dark grey limestone were observed near Kakapo Peak at M26/ 730205.

Full mélange is either sandstone-rich or sandstone-poor (Fig. 8.1). Where full mélange is sandstone-rich, there is a widely spaced anastomosing network of thin mudstone seams, and the protolith was probably a thick-bedded sandstone (Fig. 8.3). Where full mélange is sandstone-poor, discrete sandstone inclusions are scattered widely within a matrix of mudstone, and the protolith was probably a bedded mudstone (Fig. 8.3). Sandstone inclusions range in size from <1cm in the sandstone-poor mélange to the metre-scale in the sandstone-rich mélange. Inclusions which display internal bedding are sporadically found. Texturally, the mélange occasionally varies so that it is possible to find sandstone inclusions set in a finer sandstone matrix, or alternatively, a mudstone inclusion set in a more muddy matrix. Sometimes the rock is a massive mudstone or sandstone over several metres with no apparent disruption.

Occasionally in full mélange, families of inclusions occur and can be pieced back together into one large inclusion, similarly to that of a jigsaw puzzle (Fig. 8.4). Very rarely, there is field evidence to suggest the matrix was unlithified when inclusions broke up (see Fig. 8.4), and the significance of this will be discussed in Section 8.4.3.

Similar characteristics to that described above are observed in the sandstone/mudstone derived mélange of the Cobb Valley (Stewart 1988; Cooper 1993). Excellent illustrations of mélange texture and structure in the Cobb Valley are given in Stewart (1988)*.

* Stewart (1988) refers to the sandstone/ mudstone derived mélange as "block-in-matrix" tectonites in the Balloon Formation of Grindley (1980).

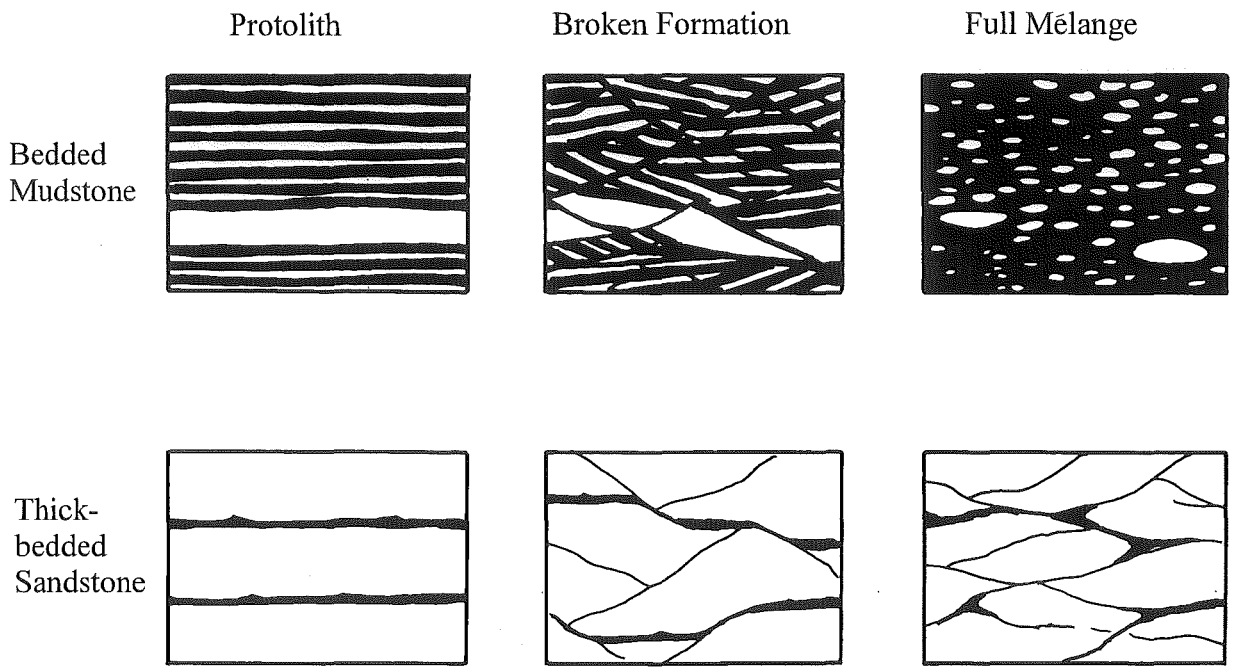

Figure 8.3: Stages in the Balloon Mélange development. Modified after Cooper (1993).

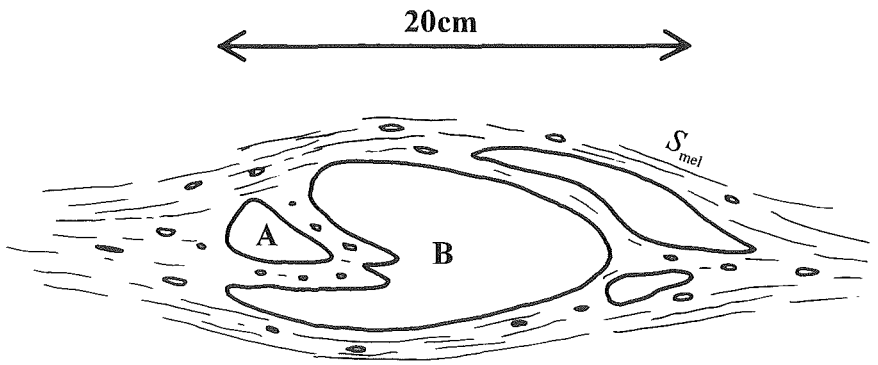

Figure 8.4: Field sketch of a sandstone inclusion family which probably originates from the break-up of one large inclusion. Note that if inclusion **A** was originally part of inclusion **B**, which seems likely, then the matrix inbetween was probably unlithified at time of break-up. M26/ 731206.

8.3 Composition of full mélange

The most common sandstone inclusion is a poorly sorted feldspathic arenite or wacke* (Fig. 8.5). Grain size varies from coarse to very fine sand. Detrital components are monocrystalline and polycrystalline quartz, plagioclase, microcline, chlorite, muscovite, and rocks fragments. Rock fragments include metamudstone, chert, and rare metamorphic and acid igneous clasts. Accessory heavy minerals include zircon, hornblende, and tourmaline. Other sandstone inclusions identified are moderately to well-sorted feldspathic arenites and rare calcarenites. The overall composition and texture of the sandstone inclusions are similar to those in the sandstone/mudstone derived mélange of the Cobb Valley (Stewart 1988; Pound 1993). In the Cobb Valley, the sandstone/mudstone derived mélange protolith is thought to be Junction Formation (Pound 1993; Cooper 1993).

The mélange matrix is composed of a very poorly sorted sandy mudstone (Fig. 8.6) with sand grain sizes and composition matching that of the sandstone inclusions. Some sand grains are of very coarse size. Composition of the muddy material is a mixture of chlorite and fine grained white mica. The matrix texture is not typical of common sediments. Similarity in maximum sand grain size and composition with that of the inclusions, together with the poorly sorted nature, may indicate that the matrix was derived by mixing of mudstone with grains derived from the sandstones. This suggestion is supported by the fact that many boundaries between sandstone inclusions and matrix are gradational rather than sharp in thin-section (Fig. 8.7), and the fact that it is often difficult to distinguish inclusion from clast. If a mixing of mudstone and sandstone origin of the matrix is accepted then the mudstone was probably unlithified, and the sandstone poorly lithified, at time of mixing.

Ankerite metasomatism affects the Balloon Mélange to varying degrees. Some areas of Balloon Mélange are highly ankeritic and others much less so. Ankerite texture is fine grained and disseminated in the sandstone inclusions but porphyroblastic in the matrix (Fig. 8.8). In the field, sandstone inclusions typically weather to an orange colour and stand out from the matrix (Fig. 8.1).

---

* Classification of sandstones is based on Williams *et al.* (1982).

Figure 8.5: A poorly sorted feldspathic arenite typical of sandstone inclusion composition in the Balloon Mélange. Note the large muscovite (Ms) grains present which are characteristic of the composition. RJ388. CPL.

Figure 8.6: A very poorly sorted sandy mudstone is typical of the matrix in the Balloon Mélange. Note the strain shadow development around quartz grains and solution seams. $S_{mél}$ XZ section, RJ390. PPL.

Figure 8.7: A gradational boundary between muddy matrix and a sandstone inclusion in the Balloon Mélange. The sandstone inclusion is at the bottom left tapering out towards the centre. Note the similarity in maximum grain size. $S_{mél}$ XZ section, RJ390. PPL.

Figure 8.8: Ankerite porphyroblasts (dark brown and circular) in muddy matrix of full mélange. $S_{mél}$ solution seams anastomose around the porphyroblasts and sandstone inclusions (light brown lenses). $S_{mél}$ XZ section RJ446. PPL.

Figure 8.6 $S_{mél}$ 0.5mm

Figure 8.8 $S_{mél}$ 1cm

Figure 8.5 0.5mm

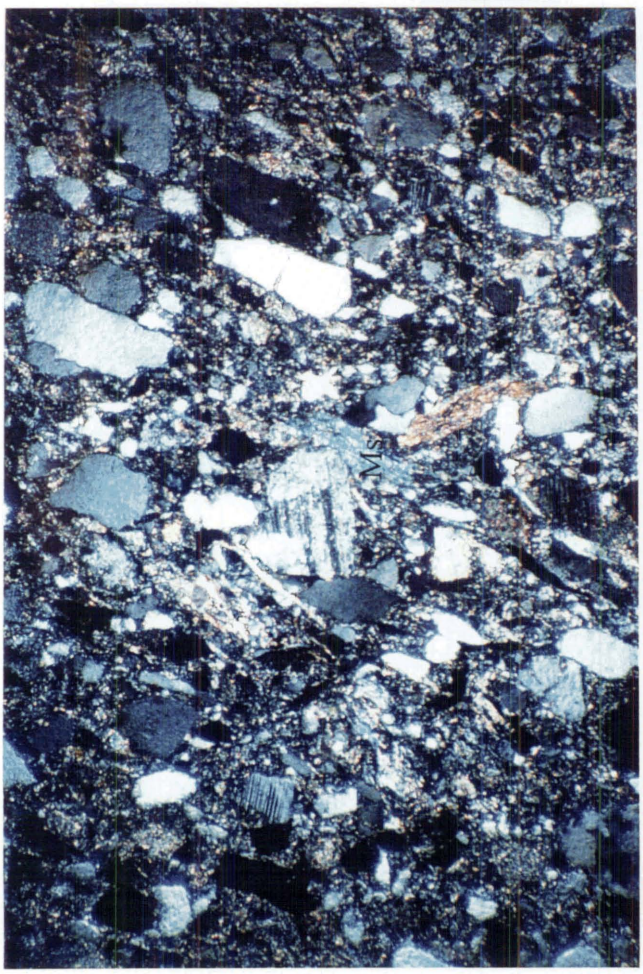

Figure 8.7 $S_{mél}$ 0.5mm

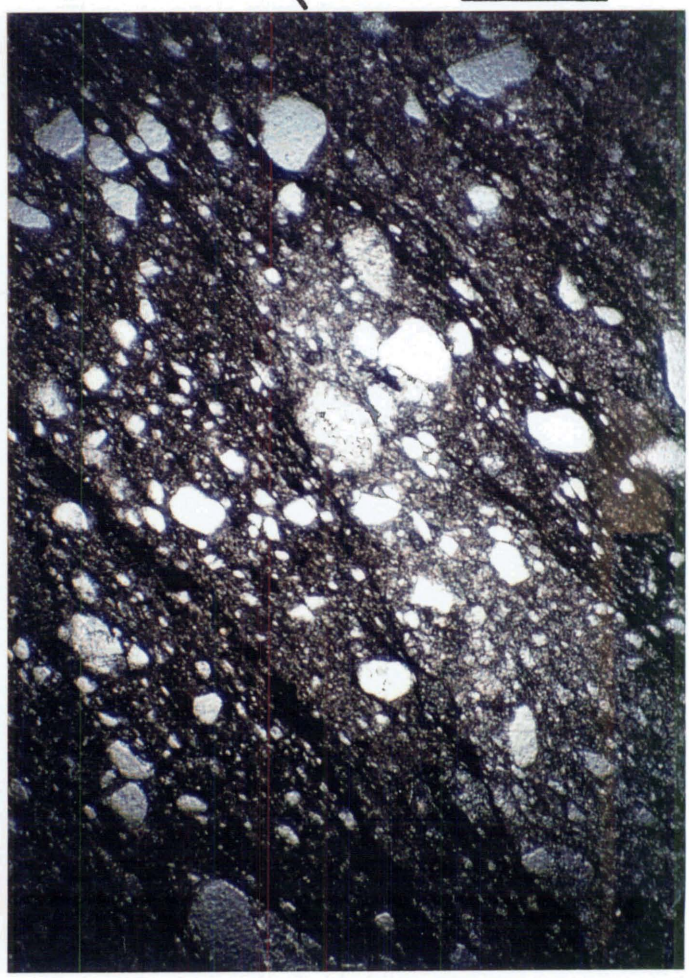

8.4 Structure of full mélange

8.4.1 Mesoscale structures

Throughout the mélange there is a penetrative slaty cleavage ($S_{mél}$) best expressed in the muddy matrix (see chapter frontispiece). Sandstone inclusions are aligned parallel to $S_{mél}$, with the muddy matrix and $S_{mél}$ anastomosing around them (Fig. 8.4). In the Boulder Lake, Adelaide Tarn, Lonely Lake, Peak 1610, and Kakapo Peak domains, $S_{mél}$ strikes NNW-NNE, dipping moderately or steeply E (Fig. 8.9). In the Kakapo Peak domain, $S_{mél}$ can also be subvertical. Sandstone inclusions are often elongate in the plane of $S_{mél}$ and plunge approximately down dip towards the east (Fig. 8.9). Elongation ratios are typically 2:1.

Within the sandstone inclusions, quartz or calcite veins are sometimes observed and are always at a high angle to the elongation axis of clasts. This observation suggests the elongation axis represents the extension direction.

In the Lonely Lake, Adelaide Tarn, and Boulder Lake domains, $S_{mél}$ in mélange is crenulated by a cleavage that is of exactly the same orientation as S_3 in nearby Haupiri Group rocks. It is suggested that the crenulation cleavage correlates with S_3 and therefore $S_{mél}$ is pre-D_3.

8.4.2 Microscale structures

$S_{mél}$ in the muddy matrix is defined by a SPO of white mica and chlorite, together with intense smooth pressure solution seaming. Solution seams anastomose around sandstone inclusions, sand-size grains in the matrix, and ankerite porphyroblasts (Figs. 8.6, 8.8, 8.10, 8.11, 8.12). Strain shadows are developed in the plane of $S_{mél}$ (Figs. 8.6, 8.8, 8.10, 8.11). Very occasionally, overgrowth and limited strain fringe development are also developed adjacent to inclusions, detrital grains, and ankerite porphyroblasts (Fig. 8.12), and consist of ankerite, quartz, and phyllosilicates. Some samples show very intense solution seaming, and quartz grain shapes have been modified by pressure solution (Fig. 8.11). All of the above features indicate that $S_{mél}$ formed when the matrix was lithified.

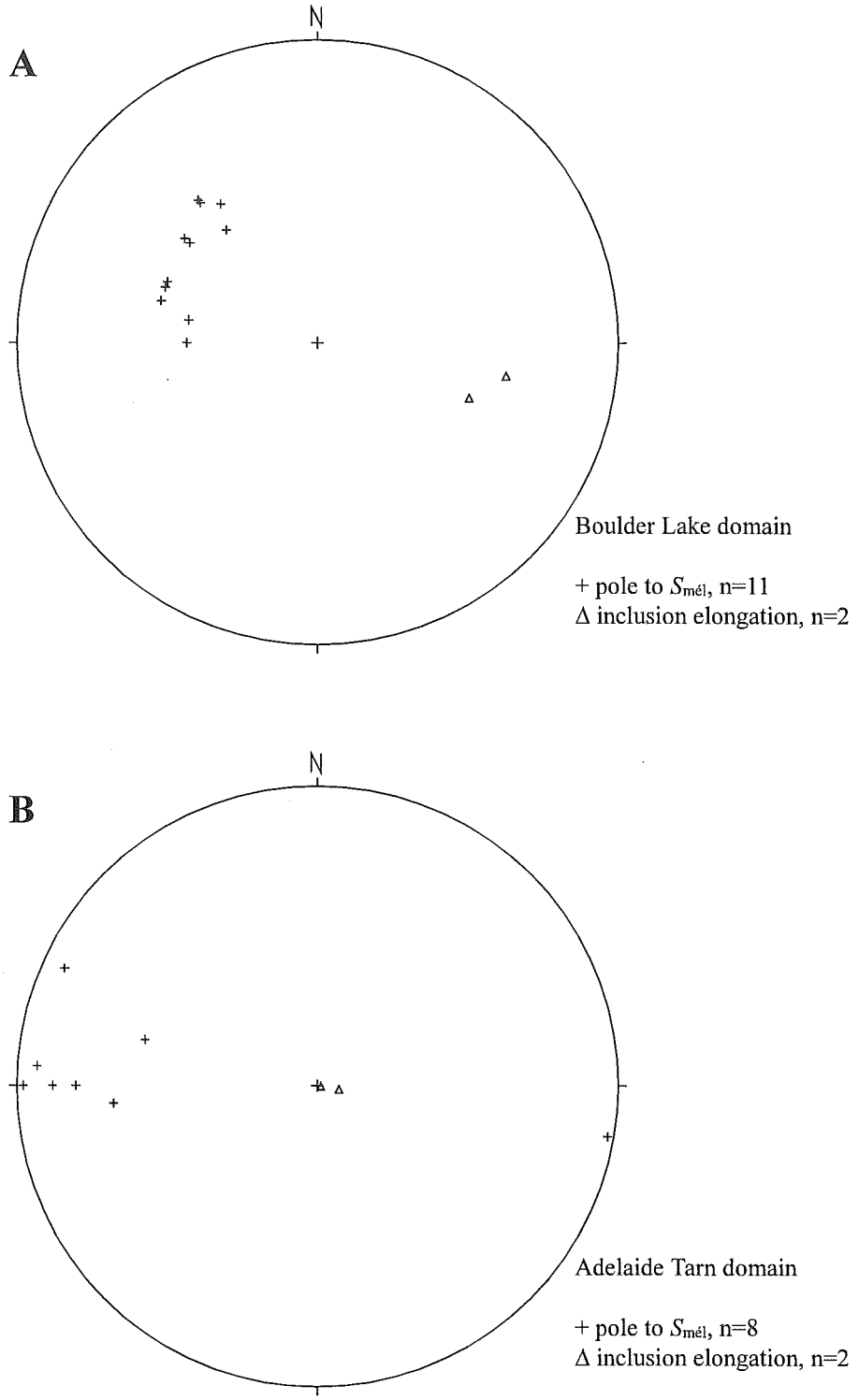

Figure 8.9: $S_{mél}$ and sandstone inclusion elongation orientations in Balloon Mélange of the Boulder Lake domain (A), Adelaide Tarn domain (B), Lonely Lake domain (C), Peak 1610 domain (D), and Kakapo Peak domain (E). (Figure 8.9 continues on next page)

Figure 8.9 continued

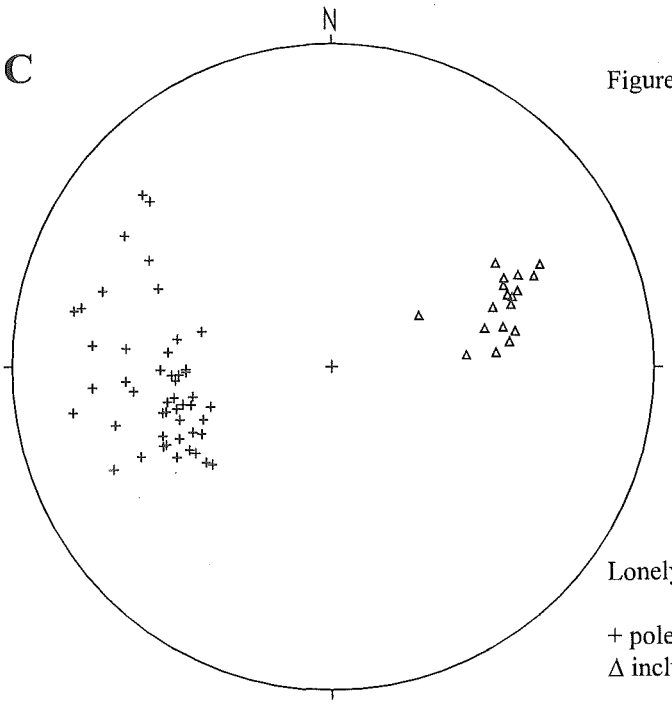

Lonely Lake domain

+ pole to $S_{mél}$, n=49
Δ inclusion elongation, n=18

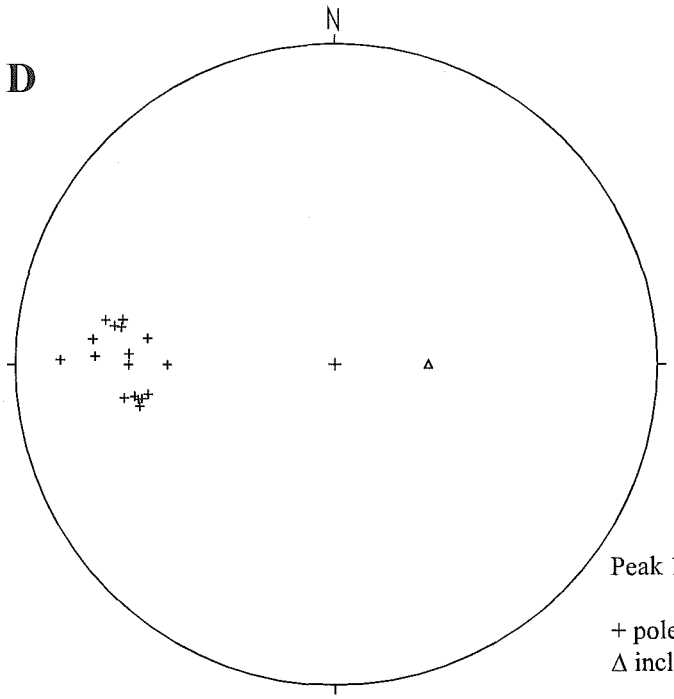

Peak 1610 domain

+ pole to $S_{mél}$, n=17
Δ inclusion elongation, n=1

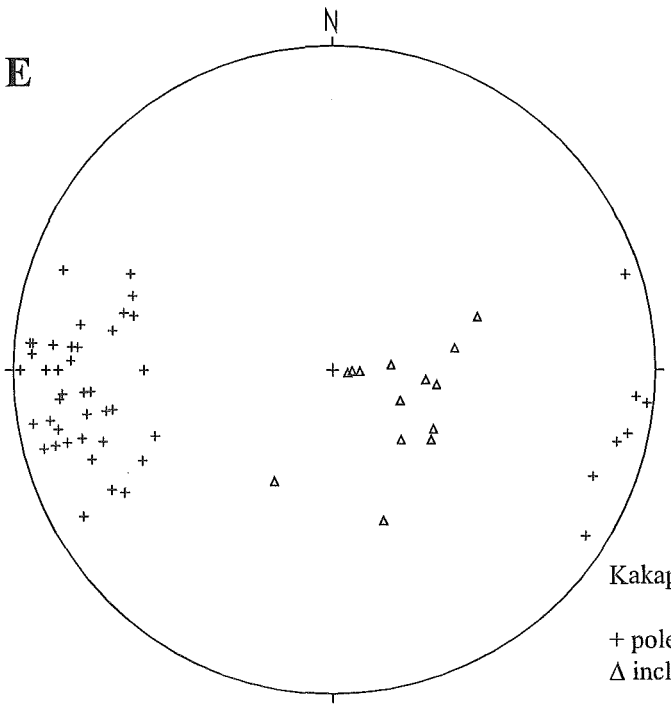

Kakapo Peak domain

+ pole to $S_{mél}$, n=52
Δ inclusion elongation, n=14

Figure 8.10: $S_{mél}$ solution seams anastomose around quartz sand grains in the muddy matrix of Balloon Mélange. The quartz grains have well-developed strain shadows. Note that the top left of the photomicrograph is occupied by a sandstone inclusion where solution seams and strain shadows are almost non-existent. $S_{mél}$ XZ section, RJ446. PPL.

Figure 8.11: Contrasts in strain between inclusion and matrix. Intense $S_{mél}$ solution seaming is observed in the sandy mudstone matrix (bottom right) but relatively little strain is observed in the sandstone inclusion (top left). Quartz grain shapes in the matrix have been modified by pressure solutioning. $S_{mél}$ XZ section, RJ446. PPL.

Figure 8.12: Quartz grains modified by pressure solutioning in muddy matrix. The large quartz grain (Qtz) has an overgrowth on the left margin and a phyllosilicate/ quartz strain fringe on the right margin. $S_{mél}$ XZ section, RJ446. PPL.

Figure 8.10

Figure 8.11

Figure 8.12

$S_{mél}$ solution seams in sandstone inclusions are not always conspicuous but when present are rough and more widely spaced than those in the matrix (Fig. 8.10, 8.11). Strain shadows/fringes are only weakly developed in sandstone inclusions, and there is no evidence of pressure solutioning of quartz grains (Fig. 8.10, 8.11).

The white mica, chlorite, and strain shadows in the mélange are all elongate in the same direction as the elongate sandstone inclusions. This parallelism of elongation suggests that the elongate inclusions indicate a tectonic stretching lineation, not just a flow direction in say a mass sedimentary flow.

Similar to those observed in the field, some sandstone inclusions in thin-section view appear to be related to each other, in that they can be joined together as one. In Figure 8.13, a sandstone inclusion has clearly broken apart, and the space created has been infilled by the sandy mudstone matrix; there is relatively little evidence of pressure solution. At first sight, the inclusion appears to have broken up by a process of boudinage related to $S_{mél}$ deformation. However, if the break-up was related to $S_{mél}$, one would expect the $S_{mél}$ solution seams to wrap around the broken margins of the inclusion, and the area between the broken margins and the solution seams to be infilled by strain fringes, not sandy mudstone. Instead the pressure solution seams appear relatively undeflected across the sandy mudstone that lies in between the broken margins of the inclusion. A possible explanation of the microstructure observed in Figure 8.13 is that at the time of inclusion break-up, the matrix was unlithified and was injected into the space created.

In general, all sandstone inclusions in thin-section view have sandy mudstone strain shadows devoid of any significant pressure solution seams. Since sandstone inclusions most probably originate from once continuous beds (Section 8.2), then as suggested for the microstructure seen in Figure 8.13, the entire matrix in thin-section view may have been in an unlithified state at the time of mélange formation. Given that the sandstone inclusions represent broken up fragments of once continuous beds, the sandstone is suggested to have been at least semi-lithified at the time of mélange formation. Nevertheless, the sandstone had to be sufficiently friable to shed grains into the developing matrix (see Section 8.3).

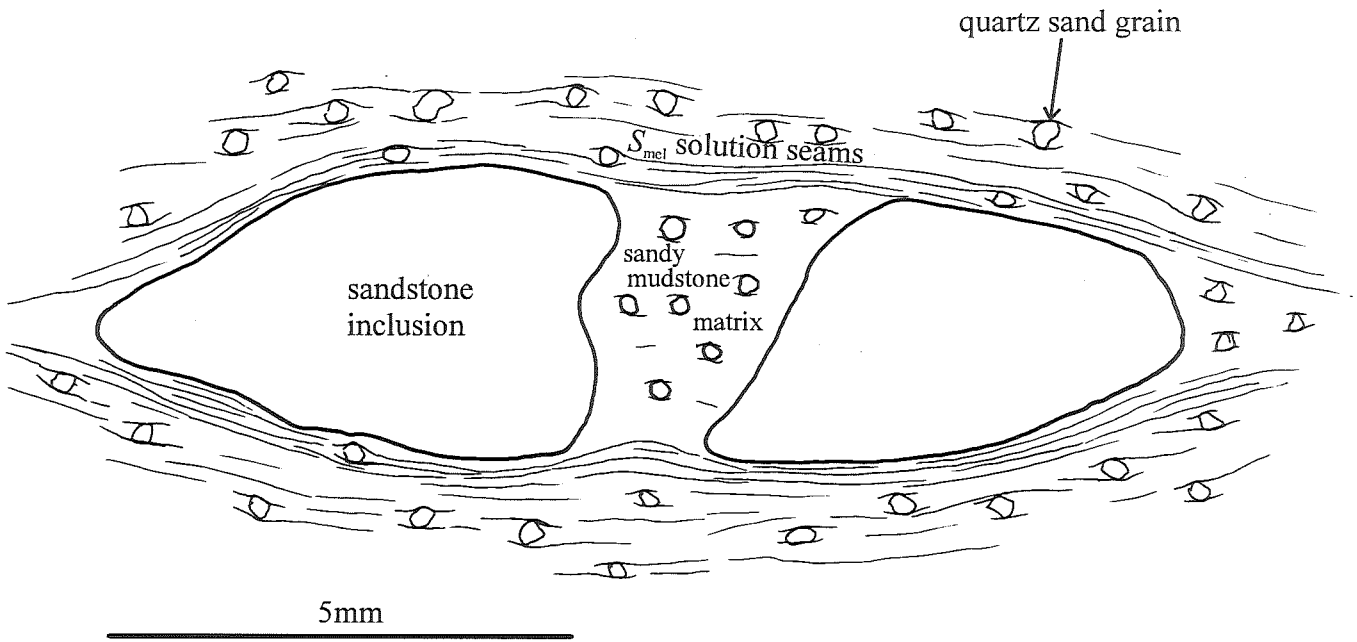

Figure 8.13: Line drawing of a sandstone inclusion, in thin-section view, which has broken apart (see text for discussion). RJ390, Balloon Mélange.

8.4.3 Discussion of deformation and mélanging

There is strong evidence, particularly microscopic evidence, that indicate two deformations occurred when the Balloon Mélange unit was in two different states of lithification. The two deformations recognised are:

- an early deformation in which the muddy matrix was in an unlithified state (see previous section for microscopic evidence, and Figure 8.4). As discussed in the previous section, this deformation is responsible for the microscopic mélange texture, and it follows that the mélange texture observed on the mesoscale also formed at this time. Given that the mélange was derived from what was once a bedded sediment protolith (Section 8.2), the complete spectrum of textures, ranging from intact bedding, to broken formation, to full mélange, is attributed to layer-parallel extension (Cowan 1985).
- $S_{mél}$ related deformation in which both the matrix and inclusions were in a lithified state, as evidenced by strain shadows, strain fringes, solution seams, and quartz/calcite extensional veins in inclusions. $S_{mél}$ deformation represents a tectonic overprint of the already formed mélange texture.

The sandstone inclusions are elongate parallel to $S_{mél}$ related extension directions (strain shadows/fringes) and therefore $S_{mél}$ deformation must, at least in part, be responsible for the present clast elongation and orientation. However, microstructures suggest that $S_{mél}$ strain in sandstone inclusions is small (Section 8.4.2), and this rather suggests that at least some of the present elongation dimensions can be accounted for prior to $S_{mél}$. In addition, if the inclusions were elongate in an orientation that differed greatly to its present orientation prior to $S_{mél}$ deformation, high $S_{mél}$ strain in the X direction in the matrix would need to be invoked for mechanical rotation of inclusions that are only being slightly strained themselves (Fig. 8.14). Microstructures suggest that $S_{mél}$ strain in the matrix was not sufficient for mechanical rotation. Thus prior to $S_{mél}$ deformation, the inclusions were already elongate to some degree and sub-parallel to the $S_{mél}$ extension direction. It follows that the early unlithified layer-parallel extension deformation had an extension direction near-coaxial to $S_{mél}$ extension. This near-coaxialism of extension directions suggests that the early unlithified deformation may represent an earlier stage of the $S_{mél}$ related deformation, or alternatively, the coaxiality could be coincidental and the two deformations unrelated.

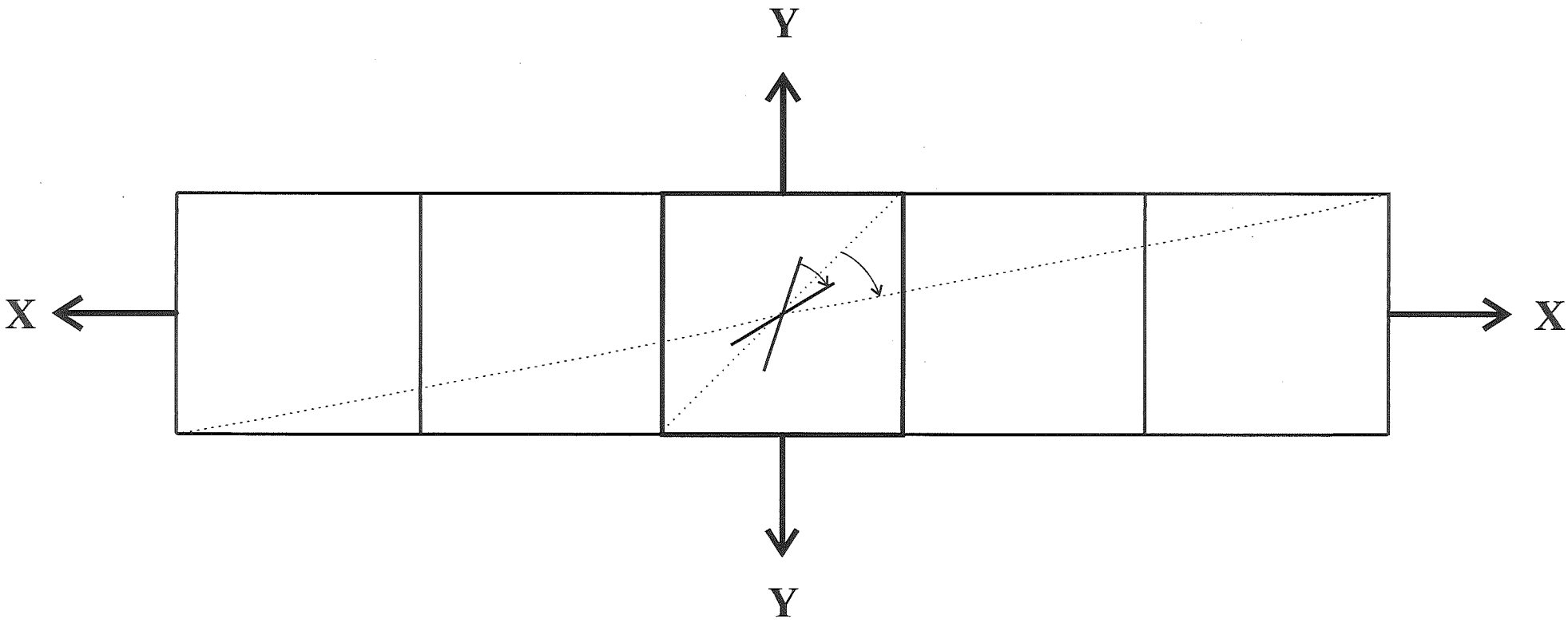

Figure 8.14: This diagram demonstrates how a high strain in the X direction is required to rotate an inclusion, that isn't undergoing strain itself, by a significant amount. In this diagram a unit square has undergone a longitudinal (e) plane strain of 4. The inclusion (represented by the black line) is initially oriented at 72° to X, and becomes oriented at 31° to X after the strain is applied. If strain is constrictional, less strain is required for the same amount of rotation whereas a flattening would require more strain.

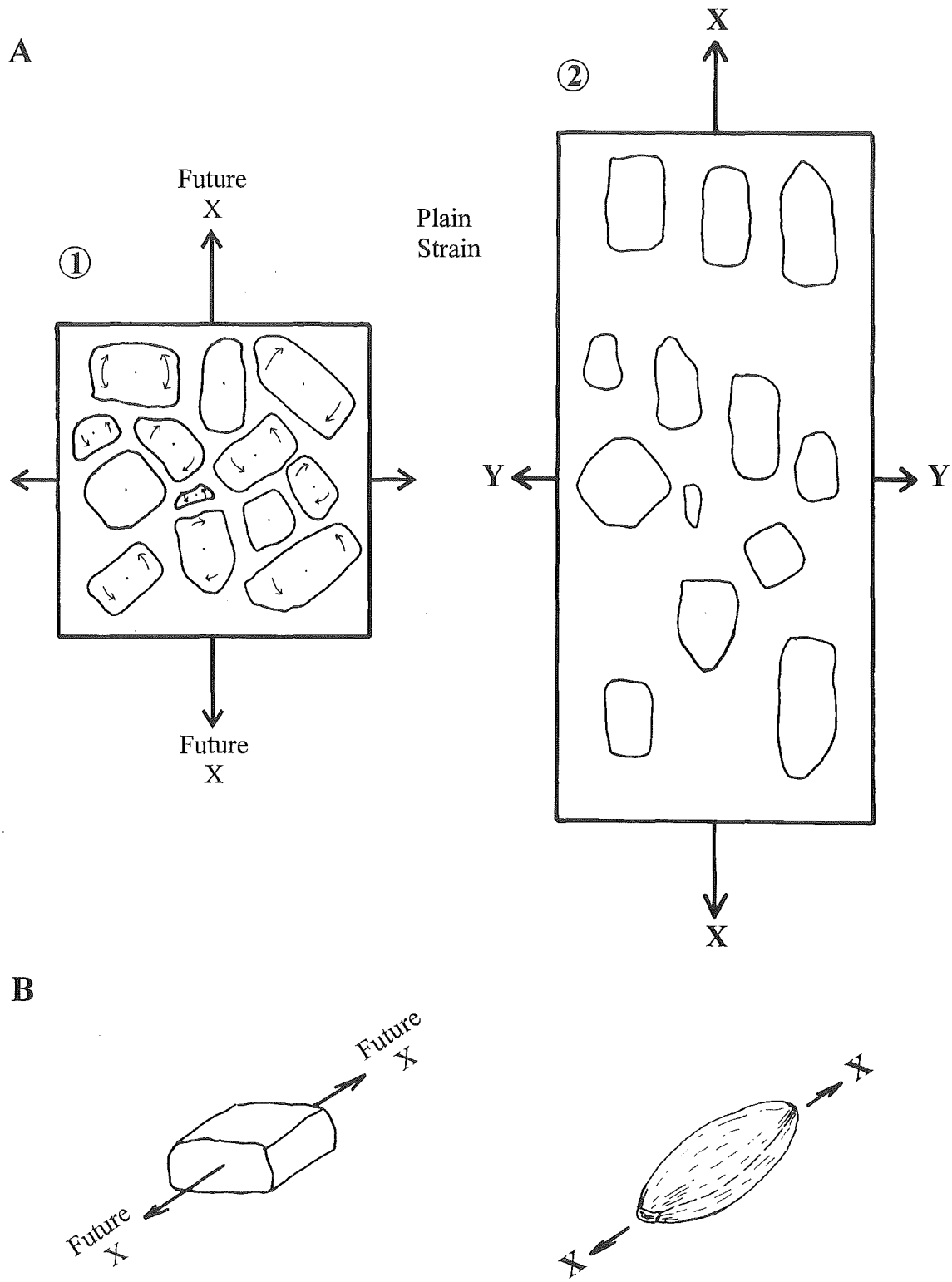

Figure 8.15: (A) and (B) represent two possible alternatives for the origin of the sandstone elongation preferred orientation. In (A), the semi-lithified or lithified sandstone inclusions were randomly oriented and elongate during the initial stages of sandstone bed break-up in an unlithified matrix (A1). As mélanging proceeded, a preferred extension direction developed, and sandstone inclusions were rotated towards that direction (A2). In (B), semi-lithified sandstone inclusions were "plastically" strained with long axis parallel to the extension direction.

The above paragraph suggests that elongation and preferred orientation of sandstone inclusions were achieved during the unlithified mélanging related deformation. Two possible alternatives for the origin of the sandstone inclusion elongation and preferred orientation are presented in Figure 8.15. Sandstone inclusions were either randomly elongate during the initial stages of sandstone bed break-up, and then later aligned by mechanical rotation in an unlithified matrix towards the extension direction (Fig. 8.15A), or alternatively, and especially if the sandstone inclusions were semi-lithified rather than completely lithified, were "plastically" strained with long axis parallel to the extension direction (Fig. 8.15B). The inclusions which contain internal bedding (rarely found) display less deformation than others, suggesting they were more lithified during the mélanging event.

8.5 Balloon Mélange contact relationships with adjacent rock units

Excluding the isolated bodies of chert, the Balloon Mélange lithology is monotonous, consisting of only sandstone and mudstone, with little variation in composition. It is bounded to the west by undifferentiated Haupiri and Devil River Volcanics Groups which, in contrast to the mélange, are lithologically diverse (conglomerates to siltstones, volcanics, shallow intrusives). If indeed the Balloon Mélange of this study is the same as the sandstone/mudstone derived component of the Balloon Mélange mapping unit in the Cobb Valley, which is considered most likely, then its protolith is probably Junction Formation (Pound 1993; Cooper 1993). The Junction Formation is thought to have been deposited at a passive continental margin (Pound 1993). In contrast, the undifferentiated Haupiri and Devil River Volcanics Groups lithology are more characteristic of an island arc sequence. Thus it appears the Balloon Mélange described in this thesis is unrelated to the undifferentiated Haupiri Group; the contact between them discordant and could be either unconformable, tectonic, or intrusive.

At M26/ 730247 and the immediate vicinity (Lonely Lake domain), the contact between the Balloon Mélange and undifferentiated Haupiri Group can be well-constrained and is seen to be far from simple. Within ~10m of the mélange, undifferentiated Haupiri Group sediments are disrupted, and in places, bedding is chaotically folded and faulted. At one outcrop, mélange appears to intrude the sediments. The distribution of mélange ESE of Lonely Lake suggests it interfingers with undifferentiated Haupiri Group sediments (Map

2 and cross-section D-D'). Given that the undifferentiated Haupiri Group lithology here is distinctly different to that of the mélange (mélange interfingering with conglomerate and coarse graded beds), and in light of the intrusion evidence, the interfingering pattern is better explained by intrusion rather than by sedimentary or tectonic processes.

In the northern part of the Adelaide Tarn domain and southern part of the Boulder Lake domain, the Balloon Mélange noticeably wedges out. In this area, the mélange is surrounded by undifferentiated Haupiri Group rocks and appears to cut across the general strike of bedding. These features are suggestive of an intrusive relationship, but it should be noted that the mapped distribution of mélange in this area is highly interpretative because of limited field data.

In summary, the western margin of the Balloon Mélange appears to be discordant and there is evidence that at least some of the margin is intrusive.

The eastern margin of the mélange and rocks east of it were not studied in any detail for this project. However, it can be noted that in the Boulder Lake domain and most of the Adelaide Tarn domain, the mélange is bounded by undifferentiated Haupiri Group sediments, but in the Kakapo Peak domain it is bounded by the Devil River Volcanics Group. Both the undifferentiated Haupiri Group and Devil River Volcanics Group east of the mélange are lithologically quite distinct from the Balloon Mélange. Therefore, the contact is probably discordant. In the southern part of the Adelaide Tarn domain, and in the Lonely Lake and Peak 1610 domains, the eastern margin is bounded by sandstone and siltstone. The sandstone and siltstone may represent undisrupted protolith because these lithologies are very similar to that in the mélange. The sandstone and siltstone are provisionally designated Junction Formation.

Along the Kakapo Peak-Mt Snowden ridge, a 1.1km wide body of massive or thick-bedded sandstone with rare mudstone beds is compositionally the same as that of the sandstone inclusions in the mélange. The contact between the sandstone body and mélange is gradational based on the fact the mélange becomes increasingly richer in metre scale sandstone inclusions towards the sandstone body. The sandstone body is thought to represent part of the mélange protolith (Junction Formation) that was not disrupted due to its massive or thick-bedded nature. Because the sandstone body is

bounded to the east, west, and north by mélange (south of Kakapo Peak domain was not mapped), it may possibly represent a "mega-inclusion" rather than the parent rock *in situ*.

Also along the Kakapo Peak-Mt Snowden ridge, but west of the sandstone body, are several outcrops of dolerite which wedge out rapidly towards the north. Based primarily on the prominent topographic expression that the doleritic rock makes south of the ridge-line, the outcrops are inferred to represent the northern extremity of a ~200m wide igneous body. Microscopically, some dolerites are relatively fresh containing unaltered clinopyroxene, saussuritised and sericitised feldspar laths with inclusions of apatite needles, skeletal ilmenite, and pseudomorphs of olivine (the pseudomorphs consisting of chlorite/actinolitic-hornblende/serpentine). Other dolerites have been extensively replaced by carbonates. Unfortunately, the contact between dolerite and mélange was not investigated but the outcrop pattern suggests the dolerite is an intrusion, rather than an inclusion. Similar dolerite bodies with similar microtextures are observed near Mt Benson where they intrude Benson Formation sediments (Münker 1993).

8.6 General discussion

$S_{mél}$ attitude and its associated stretching lineation from all domains are remarkably similar to S_1 and its stretching lineation in undifferentiated Haupiri Group (compare Fig. 8.9A-E with Figs. 3.38B, 3.73, 4.20, 4.24, 5.12). The similarity strongly suggests $S_{mél}$ is equivalent to S_1, and that the Balloon Mélange body was alongside the Haupiri Group rocks during D_1 deformation.

The early mélange forming deformation which involved unlithified sediments can be attributed to either intrusive (commonly diapiric), tectonic, sedimentary/gravity driven processes, or a combination of these (Raymond 1984; Cowan 1985).

In the Cobb Valley, the sandstone/mudstone derived mélange is thought to originate primarily by a tectonic process* (Stewart 1988; Pound 1993; Cooper 1997), and in an

* The sandstone/mudstone derived mélange should not be confused with the diamictite that outcrops around Lake Sylvester, Deep Creek, and Cobb Reservoir. This diamictite, noted for its great range in clast types and roundness, is part of the Balloon Mélange mapping unit (R. A. Cooper, pers. comm. 1997) but appears to be of sedimentary origin (Grindley 1980; Stewart 1988; Pound 1993). None of the Balloon Mélange in my study area looked remotely like that of the diamictite in the Cobb area.

accretionary wedge setting (Cooper and Tulloch 1992; Pound 1993). The main evidence for a tectonic process is that the sandstone/mudstone derived mélange incorporates mappable inclusions of Haupiri and Devil River Volcanics Group rocks. Stewart (1988) states the presence of a phyllosilicate matrix anastomosing around inclusions, strain shadows and fringes, and extensional quartz veins is evidence for a tectonic origin. However, my study shows these strain features are related to D_1 and are not attributable to the mélanging process.

The evidence of intrusive contacts suggests that the entire body of Balloon Mélange may be of intrusive origin. However, in contrast to the Balloon Mélange of this study, mélanges that are thought to be of intrusive origin are generally known to contain inclusions of diverse shape, size, and composition that are chaotically disposed (Cowan 1985; Barber *et al.* 1986). Most importantly, intrusive mélanges show no evidence that they were derived by the progressive layer-parallel disruption of sediments (Cowan 1985).

The Balloon Mélange in this study does show evidence of progressive layer-parallel disruption. The complete spectrum of original interbedded sandstone and mudstone, to broken formation, to full mélange, is thought to be the result of two possible processes, layer-parallel extension driven by gravitationally induced spreading, or alternatively, layer-parallel shear in imbricate faulting of accretionary wedges (Cowan 1985 and references therein). Considering the thickness of the mélange, the contrast of lithology with that of the adjacent Haupiri Group, and the incorporation of "exotic" inclusions documented in the Cobb Valley, I believe the latter option is the most applicable to the Balloon Mélange of this study. In this case, the intrusive contacts would be only of local extent, representing small intrusive mélange bodies extending from the tectonic mélange (sill-like in the case of cross-section D-D'). A local intrusive origin is supported by the fact that broken formation or intact bedding is not observed in close proximity to the interpreted intrusive contacts. The intrusive origin probably reflects fluid overpressuring in the accretionary wedge of Cooper and Tulloch (1992) and Pound (1993). Such an association of intrusive mélanges (commonly diapiric) and accretionary wedges is documented in the literature (e.g. Barber *et al.* 1986; Brown and Westbrook 1988; Pickering *et al.* 1988; Brown and Orange 1993).

In summary, I believe the main component of Balloon Mélange of this study is a result of layer-parallel shear associated with imbricate faulting in an accretionary wedge. The western margin of the Balloon Mélange is a tectonic contact that is locally intrusive, the implication being that the contact is not a reactivated structure of later regional tectonic deformation (see Chapter 9).

8.7 Age of mélange development

Given that the mélange intrudes the undifferentiated Haupiri Group, thought to be Middle Cambrian to early Late Cambrian in age, the Balloon Mélange of this thesis must be younger than the maximum age of the Group. If the age of the Balloon Mélange protolith is true (Junction Formation: early Middle Cambrian), then the mélange is probably not much younger than Late Cambrian because it is thought to have formed while the matrix was still unlithified. Based on the fact that the mélange incorporates Haupiri Group units but not Patriarch Group units or younger, Cooper (1997) suggests the main period of Balloon Mélange development in the Cobb Reservoir area formed in the mid Late Cambrian. Pound (1993) suggests Balloon Mélange development started to form as early as Middle Cambrian. In summary, the age of Balloon Mélange development in the study area is thought to be Late Cambrian.

CHAPTER 9

STRUCTURAL SYNTHESIS

9.1 Introduction

This chapter reviews the various structures observed in each areal domain and integrates them into deformation events. A timing of deformation events is then established. However, in order to better constrain the timing of deformation events it is necessary to firstly review structures and deformation events recognised outside the study area and then compare them with those recognised in the study area. Buller terrane structure and deformation events, outside and within the study area, are reviewed first followed by that in the Takaka terrane. Structures and deformation events on either side of the Anatoki Fault are then compared and discussed.

Tectonites directly related to Anatoki Fault movement are reviewed and followed by a discussion of how they may be related to the deformation events recognised.

In the review of structures and deformation events outside the study area, various localities are mentioned. Please refer to Figure 1.1 and 1.2 for location reference. Please note that the chronological notation of structures and deformation events (e.g. F_1, S_1, D_1) refer only to the study area.

9.2 A review of Buller terrane deformation outside the study area

The first penetrative deformation recognised in the Buller terrane, is a regional single folding event. The folds are simple, upright or steeply inclined, and with fold axes subhorizontal to moderately plunging in an approximate N-S direction (Grindley 1971, 1980; Laird 1972; Coleman 1977, 1981; Nathan 1978a; Cooper 1979b; Roder and Suggate 1990; Harrison 1993; Rattenbury 1996). Near the Anatoki Fault in the Aorere River, the folds are more gently inclined, with axial planes dipping towards the E-NE

(Stallard 1994). From the Paparoa Range (Fig. 1.1) southwards, folds appear to swing in trend towards the WNW-ESE direction (Laird 1972), although Nathan (1978b) suggests the WNW-ESE folds are superimposed on earlier N trending folds. Associated with the folding is a low grade regional metamorphism (Nathan 1978b; Shelley 1975b; Roder and Suggate 1990; Harrison 1993; Stallard 1996) and an ubiquitous axial planar slaty cleavage (Grindley 1971, 1980; Laird and Shelley 1974; Shelley 1975b; Coleman 1977, 1981; Nathan 1978b; Cooper 1979b; Roder and Suggate 1990; Harrison 1993; Stallard 1994; Rattenbury 1996).

Timing of the regional folding event can be constrained both stratigraphically and geochronologically. A maximum age is provided by the folding of Late Ordovician Golden Bay Group sediments (Cooper 1979b). A minimum age is provided by contact metamorphic minerals, associated with the Middle to Late Devonian Karamea Batholith, which overprint the axial planar slaty cleavage (Roder and Suggate 1990). In addition, a lack of internal deformation in the Karamea Batholith suggests that major Buller terrane deformation predated the intrusion (Rattenbury 1996). The folding event can be further constrained if it is accepted that the style of deformation and lower grade of metamorphism in the Early Devonian Reefton Group is unrelated (Cooper 1989). However, the Reefton Group is completely fault bounded (Bradshaw 1995) and may represent a higher structural level, thus making differences in deformation style and metamorphism an unreliable constraint. Sedimentology of the Reefton Group (shallow marine), in comparison to the Greenland Group (turbiditic deep water), is suggestive of an unconformity between the two groups. Geochronologically, K-Ar whole rock dates of pelitic Greenland Group rocks, west of the Karamea Batholith, give ages of 438-395Ma (Silurian to Early Devonian) that are interpreted as post-regional low grade metamorphic closure ages, and provides a minimum age of slaty cleavage formation (Adams *et al.* 1975). Laird and Shelley (1972) and Shelley (1975b) have demonstrated that the slaty cleavage in Greenland Group rocks around Reefton and Greymouth (Fig. 1.1) formed in wet sediments during water expulsion, suggesting deformation soon after deposition. In summary, the regional folding event appears to have occurred between the Late Ordovician and Middle Devonian but most evidence suggests it occurred towards the earlier end of this age range i.e. Late Ordovician-Silurian. The folding event is referred to by Cooper (1989) as the "Greenland Tectonic Event".

Folding that either predates the regional folding described above (Coleman 1977; Cooper 1979b), or is different in style (Bishop 1968), has been recognised in some parts of the Buller terrane. These occurrences of folding appear to be of local extent and probably represent either synsedimentary deformation, or early stages of the deformation event responsible for the regional folding.

Localised occurrences of folding and crenulation cleavage development postdating the regional folding event have also been recognised (Roder and Suggate 1990; Harrison 1993; Stallard 1994). The folding and crenulation cleavage of Stallard (1994) is thought to have developed prior to Early Cretaceous movement along a hypothesised zone of dextral shear in the Aorere Valley (Fig. 1.2). This east-west trending zone of dextral shear apparently displaces the Anatoki Fault (Stallard 1994).

The Fenella Fault Zone, near the eastern margin of the Buller terrane, is a major zone of faulting and folding which contains a highly attenuated Aorangi Mine succession (Cooper 1989). The zone is 0.5km to 2km in width and is parallel to the Anatoki Fault from Boulder Lake to the Wangapeka valley (Cooper 1989). Cooper suggests the movement predates the Mt Olympus Pluton but no evidence is given.

No ductile deformation is observed in the latest Cretaceous Pakawau Group cover (Bishop 1971; Grindley 1971, 1980). Therefore, it is concluded that the Fenella Fault Zone, and the folding and crenulation cleavage that postdates the regional folding event, must predate the latest Cretaceous.

Brittle deformation structures occur throughout the Buller terrane and these mainly relate to Cretaceous-Tertiary extension and Late Cenozoic oblique compression.

9.3 Buller terrane deformation in the study area

9.3.1 D_1 deformation event

In the Adelaide Tarn, Lonely Lake, Kakapo Peak, and Mt Benson domains, the first set of structures recognised are N-S trending folds with east dipping or upright axial planes and an associated axial planar slaty cleavage (Table 9.1). Folds are typically tight, and western limbs of antiforms are commonly overturned. The similarity in orientation suggests the first set of structures recognised in these four domains formed in the same deformation event (D_1), and are therefore designated F_1 and S_1 respectively. Metamorphism associated with S_1 appears to be either subgreenschist or lowest greenschist facies. Limited data of bedding and cleavage attitudes in the Crow River Domain also suggest the occurrence of N-S trending folds that are of probable D_1 generation (Section 7.2.2).

	F_1 Axial Plane and fold tightness	F_1 Fold Axis	S_1
Boulder Lake domain	Not present	Not present	Not present
Adelaide Tarn domain	-mesoscale folds -tight to isoclinal -N-NE strike -mod. or gentle E dip	-subhorizontal to gentle S plunge	-axial planar
Lonely Lake domain	-mesoscale folds -tight to isoclinal -NW-NNW strike -moderate NE dip	-subhorizontal to gentle NNW or SE-SSE plunge	-axial planar
Peak 1610 domain	Poor outcrop exposure	Poor outcrop exposure	-N-NW strike -mod. or steep E dip
Kakapo Peak domain	-mesoscale folds Douglas Formation -N-NNW strike -steep E or subvertical dip. -tight to open Slaty shale unit -sporadic folding -axial plane approximates S_1 -tight to isoclinal	Douglas Formation -subhorizontal to moderate N-NNW or S-SSE plunge Slaty shale unit -various orientations along S_1 plane	Douglas Formation -axial planar Slaty shale unit -NNE-NW strike -mod. or steep E dip
Mt Benson domain	-inferred tight macroscale syncline -N strike -steep E or subvertically inclined	-N plunge	Douglas Formation -N strike - subvertical or steep E or W dip Slaty shale unit -N-NW strike -moderate E-NE dip
Crow River domain	Not observed	Not observed	-NNW strike -subvertical dip

Table 9.1 Buller terrane D_1 structural orientations

F_1 and S_1 orientations most closely resemble those associated with the regional folding event recognised outside the study area. It follows that D_1 can probably be correlated with the regional folding event and thus is thought to be Paleozoic in age (Late Ordovician - Late Devonian). It should be noted that folds documented in the near vicinity of the study area, and correlated with the regional folding event, also have overturned western limbs (Harrison 1993; Stallard 1994).

F_1 folds in the Adelaide Tarn, Lonely Lake, and Kakapo Peak domains are generally tight and observed only on the mesoscale, whereas in the Mt Benson domain the only F_1 folding recognised is observed on the macroscale. The inference of the large macroscale syncline in the Mt Benson domain is based mainly on the conclusion that the dark grey slaty shale unit immediately adjacent to the Anatoki Fault is Leslie Formation (Section 6.3.4), and the synclinal limbs are outlined by Leslie Formation on either side of Douglas Formation.

In Section 6.3.4, the question was raised as to whether all dark-grey/black shales and slates in the more northern domains, immediately west of the Anatoki Fault, are Leslie Formation rocks. In the Kakapo Peak domain it was concluded the structure in the slaty shale unit is indicative of an eastern limb of a N-S trending macroscale synform whereas the structure in the adjacent Douglas Formation is indicative of an eastern limb of a N-S trending macroscale anticline. The contrasting limbs of fold structures suggests the brittle fault zone between the Douglas Formation and slaty shale unit (Section 5.2) is a significant one. Given the structure of the nearby Mt Benson domain, I suggest the slaty shale in the Kakapo Peak domain is Leslie Formation and represents a fault bounded eastern limb of a large N-S trending macroscale syncline juxtaposed against the western limb of the same syncline; the intervening hinge zone is interpreted to be faulted out (see cross-section E-E'). Dark-grey/black shales and slates, immediately adjacent to the Anatoki Fault, also occur in the northern part of the Adelaide Tarn domain and in the Boulder Lake domain. Nothing is known about macroscale D_1 structures in those domains but it is speculated that the shales and slates are Leslie Formation, the implication being that faulting or D_1 folding would have to be invoked for the existence of Leslie Formation occurring east of the Douglas Formation.

9.3.2 D_2 deformation event

As discussed in Chapter 3, the foliation surface which curves around the eastern margin of the Mt Olympus Pluton in the Boulder Lake domain is Early Cretaceous in age and intimately related to movement on the Anatoki Fault. The foliation surface appears to be co-planar with S_1 at the Adelaide Tarn and Boulder Lake domain boundary but given that it formed at a much later time, is designated S_2. Locally developed folds associated with S_2 are referred to as F_2, and S_2 and F_2 together represent D_2 deformation. Non-coaxial deformation associated with D_2 related movement on the Anatoki Fault (Chapter 3) must continue south of the Boulder Lake domain. Possible expressions of this deformation in more southern domains will be explored in Section 9.7.3.

9.3.3 D_3 deformation event

Mesoscale to small macroscale folds with an associated axial planar crenulation cleavage are superimposed on D_1 structures in the Adelaide Tarn and Lonely Lake domains. The fold axial planes and crenulation cleavage are NE striking and dip moderately to the SE (Table 9.2). Fold axes plunge to the E or SE, are close to open, and many are asymmetric with a N/NE vergence. In the Beak Creek and Arena Creek structural domains of the Boulder Lake areal domain, similarly oriented crenulation cleavage and rare folds (Table 9.2) are superimposed on the Early Cretaceous S_2 foliation. The crenulation cleavage can be traced from the Boulder Lake domain into the Adelaide Tarn domain with no change in orientation (see Maps 1 and 2), and thus it is concluded that the superimposed folding and crenulation cleavage in all three domains are one and the same.

Given that the crenulation cleavage and folding are superimposed on S_2 in the Boulder Lake domain, the folding and crenulation cleavage are designated F_3 and S_3 respectively. The deformation event associated with F_3 and S_3 must postdate the Early Cretaceous S_2 foliation surface but predate the undeformed latest Cretaceous Pakawau Group cover sequence. D_3 is consequently considered to be mid-Cretaceous. The slight variation of F_3 and S_3 orientations observed between the Beak Creek and Arena Creek structural domains, and between these two structural domains and the Adelaide Tarn areal domain (Table 9.2), reflects the deflection of strain axes around the more competent Mt Olympus Pluton.

	F_3 Axial Plane and fold tightness	F_3 Fold Axis	S_3
Boulder Lake domain	-rare open folds. -axial plane approximates S_3	Beak Creek domain -gentle or moderate NE-SE plunge Arena Creek domain -gentle or moderate ESE plunge	Beak Creek domain -NNE-ENE strike -mod. or steep SE dip Arena Creek domain -ENE-E strike -moderate S dip
Adelaide Tarn domain	-close to open -NE strike -moderate SE dip	-moderate E-SE plunge	-axial planar
Lonely Lake domain	-close to open -NE strike -moderate SE dip	-moderate E-SE plunge	-axial planar
Peak 1610 domain	Poor outcrop exposure	Poor outcrop exposure	Poor outcrop exposure
	F_{ii} Axial plane	F_{ii} Fold Axis	S_{ii}
Kakapo Peak domain	-axial plane approximates S_{ii}	-mod. or steep N plunge	-E strike -mod./steep N or subvertical dip
Mt Benson domain	-open to gentle -NNE-NE strike -subvertical or steep SE or NW dip	-mod. or steep N plunge	-axial planar
Crow River domain	Not observed	Not observed	Not observed

Table 9.2 Buller terrane D_3 and F_{ii}/S_{ii} structural orientations. Bedding is the fold axis reference surface which is in general subparallel to S_1 or S_2 (Boulder Lake domain only).

In the Kakapo Peak and Mt Benson domains, folding (F_{ii}) and an axial planar crenulation cleavage (S_{ii}) are also observed superimposed on D_1 structures. S_{ii} and F_{ii} are sporadically developed in the Kakapo Peak domain and well-developed in the Mt Benson domain. F_{ii} folds are open to gentle and show no vergence. S_{ii} orientation differs from S_3 but the difference is not great (Table 9.2). It is suggested here that S_{ii} and F_{ii} may be related to D_3; the difference in orientation from F_3 and S_3 in more northern domains may reflect a changing strain axis orientation between the Lonely Lake and Kakapo Peak domains. Unfortunately, the lack of outcrop in the intervening Peak 1610 domain makes the connection difficult to prove.

In a study of structure in Golden Bay Group lithologies immediately west of the Mt Benson and Kakapo Peak domains, Harrison (1993) recognises a superimposed cleavage (his GBS_3) in which the orientation matches that of S_{ii} in the Mt Benson domain. In addition, superimposed ESE-SE plunging folds recognised in Roaring Lion Formation by Harrison (his RLF_2) may also be related to D_3 deformation recognised in this study.

A SE dipping crenulation cleavage superimposed on D_1 structures is also observed in the Aorere Valley (Stallard 1994) north of Boulder Lake. It is suggested that this cleavage (Stallard's S3) can be correlated with S_3 of this study. Note, however, that Stallard interprets the crenulation cleavage as predating Early Cretaceous movement of a hypothesised zone of dextral shear in the Aorere Valley (Fig. 1.2), thus conflicting with a mid-Cretaceous age suggested in this thesis.

The mesoscale "reclined or recumbent folds with axes plunging steeply down-dip to the east and overturned northward" recognised in Douglas Formation by Grindley (p. 5, 1971) were believed to correlate with the first phase folds in his allochthonous Central Belt model (see Section 2.4). I confidently believe that these folds are the same as the F_3 folds recognised in this study. Therefore, I suggest they cannot be related to a first phase of deformation as proposed by Grindley (1971).

9.4 A review of Takaka terrane deformation outside the study area

9.4.1 Folding and cleavages

In contrast to the Buller terrane, deformation in the Takaka terrane is somewhat more complex with most areas having undergone multiple deformation. As mentioned in Chapter 2, the latest Cambrian-Silurian passive margin assemblage is possibly allochthonous with respect to the Cambrian island arc assemblage. In view of this possibility, I believe it is wise to discuss early folding and cleavage development in the two assemblages separately.

Cambrian island arc assemblage

The first set of structures in the Cambrian assemblage consists of regionally developed mesoscale to macroscale N-S trending tight folds that are generally upright to overturned with west facing anticlines and synclines; fold axes are subhorizontal or gently plunge towards the north or south (Grindley 1971, 1980; Torrey 1984; Maclean 1994). In muddy lithologies, a slaty cleavage is observed axial planar to the folds (Grindley 1980; Maclean 1994). Where fold structures are not observed, a N-S striking cleavage is observed nonetheless (Stewart 1988; Münker 1993). Stretching lineations associated

with the N-S striking cleavage are generally trending in an E-W orientation (Grindley, 1980; Stewart 1988). Metamorphism associated with the N-S trending folds and axial planar cleavage development appears to have been no greater than lowest greenschist facies (Powell 1986; Stewart 1988).

Earlier macroscale recumbent folds with E-W axes, refolded by the regional N-S folding, are described by Grindley (1971, 1978, 1980). Many of these folds, including the two best examples quoted by Grindley (Lindsay Syncline, Brown Cow Syncline), have since been reinterpreted as being originally N-S trending and inclined (Maclean 1994; this study). Other folds, thought by Grindley to be originally recumbent with E-W axes (e.g. Little Devil Syncline, Grindley 1971), appear to be inferred purely on the basis of a simple invariant stratigraphic succession of the time. Given that the Cambrian stratigraphy has since undergone major revision (see Section 2.4), the existence of these folds is questioned. In addition, it is difficult to find evidence that the recumbent folds of Grindley were originally E-W trending; they could just as easily be interpreted as inclined folds with N-S trending subhorizontal fold axes. Elongate conglomerate pebbles plunging E-W cannot be used as supporting evidence of E-W trending folds (Grindley 1980) because it is well-known that elongation directions are equally, if not mostly, perpendicular or at a high angle to fold axes in rocks that have not been subjected to very high strain (e.g. Cloos 1947).

Timing of the N-S trending folds is not well-established. At Mt Snowden, located immediately east of the Kakapo Peak domain, a major synclinal structure which folds Cambrian sediments, is cut by a 485 ± 35Ma (Late Cambrian to Middle Ordovician) doleritic dike (Ar-Ar date, C. Münker pers. comm. 1997). The cross-cutting relationship of the dike to the fold suggests N-S folding is Middle Ordovician or older.

Latest Cambrian-Silurian passive margin assemblage

The first set of folds recognised are recumbent folds observed primarily in Summit Limestone and Arthur Marble (Fig. 5 in Johnston 1974; Coleman 1977, 1981; Grindley 1980; Newman 1979; Shelley 1991) as well as in the Wangapeka Formation (Grindley 1980; Shelley 1984), Hailes Quartzite (Shelley 1984) and Pikikiruna Schist on the Pikikiruna Range (Shelley 1981, 1991). Included in this set of folds are the F_1 folds

recognised by Hickey (1986) in the Wangapeka Formation of the Upper Takaka area. The recumbent folds tend to be isoclinal, and axes trend either N-S (Coleman 1977; Shelley 1981, 1984, 1991) or within the NE-SE quadrant (Grindley 1980; Coleman 1981). The folds are sometimes observed to be separated by low angle thrusts (Coleman 1977, 1981; Newman 1979), or postulated to be (Shelley 1991). There are some indications that the earliest recumbent folding in the Arthur Marble formed while it was still unlithified (Newman 1979; Shelley 1991), but later folds were related to metamorphism that reached upper greenschist facies (Pikikiruna Schist: Shelley 1981, 1991). In the Wangapeka Formation, a slaty cleavage is developed axial planar to the folds (Shelley 1984; Hickey 1986), and associated metamorphism is subgreenschist or low greenschist facies (Hickey 1986; Windle and Craw 1991). Based on stretching lineations and various movement indicators, Shelley (1991) suggests the recumbent folds observed on the Pikikiruna Range are a result of tectonic movement with a shear-sense of top to the east.

The recumbent folds affect the Silurian Hailes Quartzite in Shelley's (1984) model of structures. On the Pikikiruna Range, N-S trending recumbent folds are cut by the Rameka Gabbro (Grindley 1971; Shelley 1981) dated at 367Ma (Late Devonian) by Harrison and McDougall (1980). Excluding the possibility of synsedimentary folds, it appears that the recumbent folding can be constrained to sometime in the Early to Middle Devonian.

Many of the recumbent folds have been refolded by a second phase of N-S trending folds (Coleman 1981; Shelley 1984; Hickey 1986) which appear to be widely developed throughout the passive margin assemblage. The mesoscale to macroscale N-S trending second phase folds are generally tight with subhorizontal or gently plunging axes. The folds may be upright to overturned towards the west (Coleman 1977, 1981; Wright *et al.* 1994), or upright to overturned towards the east (Bishop 1967; Johnston 1974; Grindley 1980; Coleman 1981). Where recumbent folding is not documented, the N-S trending upright/inclined folds appear to face upwards (e.g. Coleman 1977, 1981; Grindley 1980). In the Upper Takaka area, Hickey (1986) interprets the second phase of folds as inclined and westerly verging whereas Shelley (1984) interprets the same phase as easterly verging and recumbent; in either interpretation the folds are coaxial to the earlier

recumbent folds. Both authors suggest the second phase of folds and the earlier recumbent folds are related to the same progressive sequence of events.

In muddy lithologies, a slaty cleavage is observed to be axial planar to the second phase of folds (Bishop 1967; Grindley 1980; Coleman 1977, 1981). However, where second phase folding refolds earlier recumbent folds, a crenulation cleavage results instead (Shelley 1984; Hickey 1986). Metamorphism associated with the second phase of N-S trending folds and axial planar cleavage is subgreenschist or low greenschist facies (Hickey 1986; Windle and Craw 1991).

The Baton Formation basal conglomerate has previously been thought to indicate a significant unconformity, and it has been suggested that major deformation, including all N-S trending fold structures, occurred prior to its deposition in the Early Devonian (the pre-Baton Event of Cooper 1989; Cooper and Tulloch 1992). The conglomerate, which rests on top of the passive margin assemblage, contains some clasts that are similar to the rocks of the Cambrian island arc assemblage (Willis 1965; Grindley 1978). Although the clast composition indicates the two assemblages were in close proximity of each other by at least the Early Devonian, it does not necessarily indicate that N-S trending folds had formed prior to the Early Devonian. In fact, much of the Baton Formation appears to be folded with a strongly developed slaty cleavage (Grindley 1980; Coleman 1981; M. A. Bradshaw pers. comm. 1996) despite suggestions to the contrary (Powell 1986). The folds trend subhorizontally between the NW (Coleman 1981) and NNE (Willis 1965), and thus it appears they may be related to the widely developed N-S trending folds seen throughout the passive margin assemblage. In addition, recent work suggests the basal conglomerate is a mass-flow type conglomerate and it may not indicate a break in sedimentation at this level (M. A. Bradshaw pers. comm. 1996).

In the Upper Takaka area, where two phases of N-S trending coaxial folding are reported by Shelley (1984) and Hickey (1986), a riebeckite granite dike intrudes Ordovician-Silurian sediments. The dike is deformed, and a crenulation cleavage, presumably related to the second fold phase, postdates the intrusion (Windle and Craw 1991), although Hickey (1986) suggests it does not. The granite is younger than the Silurian sediments it cuts, and both Rb-Sr model age and K-Ar geochronology suggests a Late Triassic age (Tulloch 1992). If the conclusions of Windle and Craw (1991) and the isotopic age of the

granite is accepted, then this has important age constraint implications for the N-S trending folds. It is possible that the second coaxial fold phase is much younger and quite unrelated to the first. Clearly a reinvestigation of the structures around the granite, and geochronology of the granite is required.

In summary, it appears that the passive margin assemblage was firstly deformed by recumbent folding that probably occurred in the Early or Middle Devonian. The assemblage was subsequently deformed by widely developed N-S trending upright or inclined folds which are probably younger than the Early Devonian Baton Formation and possibly as young as the Mesozoic. However, both Shelley (1984) and Hickey (1986) suggest the two fold phases are related to the same deformation event in the Devonian, and the coaxiality of fold phases in several places supports this suggestion.

Folding and cleavage common to both the island arc and passive margin assemblages

Throughout the Takaka terrane, a fold phase that postdates and is oblique to the N-S trending fold structures has been recognised (Grindley 1971, 1980; Coleman 1981; Shelley 1984, 1991; Torrey 1984; Hickey 1986; Stewart 1988). Orientation of fold axes vary but they mainly plunge towards the NE to SE quadrants (Grindley 1971, 1980; Torrey 1984; Hickey 1986; Stewart 1988) and this suggests they occur preferably on east dipping limbs of N-S trending macroscale folds. In the Wangapeka area, mesoscale folds that trend mainly E-SE, but sometimes W-SW, occur on the limbs of N-S trending upright or overturned to the west macroscale folds (Coleman 1977). Coleman (1977) interpreted them as predating the N-S trending folds but as has been demonstrated in this study (F_3 mesoscale folds superimposed on F_1 macroscale folds, Fig.4.35), the mesoscale folds are better interpreted as superimposed on the N-S trending macroscale folds.

Often associated with the NE to SE plunging folds is an axial planar crenulation cleavage (Grindley 1971, 1980; Coleman 1981; Torrey 1984; Stewart 1988). In many parts of the Takaka terrane, a crenulation cleavage is observed on its own (Ghent 1968; Grapes and Stedman 1993; Münker 1993; Maclean 1994; Challis *et al.* 1995). Orientations of the crenulation cleavage near my study area are generally within the NE quadrant with steep dips (Torrey 1984; Stewart 1988; Münker 1993; Maclean 1994) but unfortunately there is a lack of detailed description of these.

The NE to SE plunging folds and crenulation cleavages are, in most cases, difficult to constrain in time, and given their variable development (they are often absent), they are difficult to correlate on a regional scale. It is known, however, that the crenulation cleavages in the north of the Eastern Belt probably postdate the Early Cretaceous given that they crenulate a distinctive Early Cretaceous chromian muscovite fabric (Grapes and Stedman 1993; Challis *et al.* 1995), as well as contact metamorphic minerals of the Early Cretaceous Separation Point Batholith (Ghent 1968). In addition, my reconnaissance petrology at Parapara Peak shows a crenulation cleavage that postdates contact metamorphic garnets in schist (Bay Schist of Grindley 1971). At Parapara Peak, the contact metamorphism is thought to be related to the nearby Onahau Granite, which is Early Cretaceous in age (Grindley 1971; Challis *et al.* 1995), thus making the crenulation cleavage post-Early Cretaceous in age. NE to SE plunging folds and crenulation cleavages must predate the latest Cretaceous-Tertiary cover rocks, given that the cover rocks show only flexural-slip type folds related to major NE striking Cenozoic faults.

Based on K-Ar, Ar-Ar, and Rb-Sr geochronology of schistosity forming metamorphic minerals, Challis *et al.* (1995) advocate an Early Cretaceous amphibolite grade metamorphism and deformation of Onekaka Schist in the north of the Eastern Belt. The metamorphism and deformation are thought to be intimately related to the nearby intrusion of the Separation Point Suite (Challis *et al.* 1995). Note that this is in direct contrast to the Pikikiruna Schist, some 15km to the SE, which is thought to be mid-Paleozoic in age (Shelley 1981, 1991).

The Permian Parapara Group rocks have experienced two phases of deformation. The first deformation predates Early Cretaceous contact metamorphic minerals and was associated with slaty cleavage development (Hoke and Grapes 1996; my reconnaissance geology of Flowers Formation), and possible large-scale folding (Hoke and Grapes 1996). The second deformation postdates Early Cretaceous intrusions and folds the entire Permian sequence into a north plunging syncline (Hoke and Grapes 1996). This fold possesses an axial planar crenulation cleavage (L. Hoke pers. comm. 1997).

To summarise, there is widespread evidence of variably developed Mesozoic deformation expressed by folding and/or cleavage and schistosity. At least some of this deformation

was post-Early Cretaceous and pre-latest Cretaceous. Other deformation appears to be pre-Early Cretaceous (deformation of Parapara Group).

9.4.2 Faults and shear zones

As mentioned in the introduction, the Takaka terrane and in particular, the Central Belt, comprises several fault-bounded slices, each with an internally consistent stratigraphy that differs somewhat to that of its neighbours (Cooper and Tulloch, 1992). Unfortunately, there is very little age constraint on movement of the bounding faults. Their similarity in orientation to the N-S trending folds suggest they were probably initiated during folding related deformation which in the arc assemblage could be as early as Cambrian but elsewhere probably Devonian or younger. Based on extensive sedimentary petrography, Pound (1993) suggests the N-S faults in the arc assemblage were active in the Cambrian in order to bring differing source rocks within close proximity of each other, and thus explain the varied source rock composition in some of the stratigraphically younger Haupiri Group rocks (e.g. Lockett Conglomerate). Many of the mapped N-S striking faults of Grindley (1971, 1980) and Coleman (1981) appear to truncate the N-S trending folds. These truncations suggest the movement on the faults, at least in part, postdates the folding (Cooper 1989). Minor E-W striking faults offset the earlier N-S striking faults (Cooper 1989) but these are of unknown age. Coleman (1977, 1981) has shown that some of the N-S striking faults in the Wangapeka area have been reactivated in the Cenozoic. Others, like those in the Cobb area, appear not to have displaced Tertiary sediments (see Grindley's 1980 map). The N-S striking faults in the north of the terrane must have been active in the Early Cretaceous in order to explain the localisation of Early Cretaceous Separation Point Suite related chromian metasomatism adjacent to these faults (Challis *et al.* 1995).

Major NE striking faults, including the Karamea and Wakamarama Faults (Fig. 1.2), displace Tertiary cover rocks and offset earlier N-S striking faults (Bishop 1971; Grindley 1971, 1980; Coleman 1981). They are marked by strong topographic expressions, and clearly the most recent movement on them is Late Cenozoic in age.

The N-S striking Devil River Fault and its associated zone of ductile deformation, the Waingaro Schist zone (up to 1.5km wide), separates the Central and Eastern Belts (Fig.

1.2) (Powell 1993, 1994, 1995). Greenschist facies metamorphism is associated with the deformation, and mylonitic fabrics are common (Powell 1984). North of the Karamea Fault, the Devil River Fault zone is almost vertical. Shear-sense indicators and a steep east plunging stretching lineation indicate the Central Belt has moved up relative to the Eastern Belt (Powell 1984, 1985). South of the Karamea Fault, the Devil River Fault zone dips moderately west (see Grindley's 1980 map) suggesting the fault has rotated along strike. Powell (1984) suggests the fault zone has rotated from an originally subhorizontal orientation displacing the Central Belt eastward over the Eastern Belt. Brittle faults bound the Devil River Fault zone (Powell 1984) that appear to predate mid-Tertiary sediments (see Grindley's 1980 map). Thus the present day attitude of the Devil River Fault zone is thought by Powell (1984) to be accounted for by pre-middle Tertiary brittle fault rotation. In the Wangapeka Valley there is evidence that the Devil River Fault has reactivated in the Late Cenozoic (Coleman 1977, 1981).

According to Powell (1984, 1985), the ductile deformation of the Devil River Fault zone truncates at least one phase of N-S trending folds, and predates a thermal metamorphic event in the north of the terrane (probably related to Early Cretaceous plutonism). Powell (1986) assigns an Early Devonian age of deformation based on the assumption of major deformation prior to deposition of the Baton Formation.

Some Early Cretaceous granitoids in the Takaka terrane possess tectonic foliations. These include the Knuckle Hill and Pakawau stocks (Tulloch 1988, my reconnaissance fieldwork), and the western margin (up to 1km wide) of the Separation Point Batholith (the "Wainui Shear zone" of Grindley 1971; Hutton 1995). Thin-section analysis of the tectonic foliation in the Separation Point Batholith indicates it formed at least in amphibolite grade temperatures (Hutton 1995), and in the Knuckle Hill and Pakawau stocks, at least mid-greenschist facies. Since no metamorphic event has been documented after the Early Cretaceous in Northwest Nelson, it appears the foliations probably formed syn- or soon after granitoid emplacement. In the case of the Separation Point Batholith, the tectonic foliation is thought to be related to emplacement of the batholith along a major N-S oblique shear zone with dextral strike-slip and top to the west thrusting (Hutton 1995).

9.5 Takaka terrane deformation in the study area

9.5.1 D_1 deformation event

In the Boulder Lake, Adelaide Tarn, Lonely Lake, Peak 1610, and Kakapo Peak domains, the first set of structures recognised is a penetrative slaty cleavage, that in the three northern domains at least, is axial planar to folds. The slaty cleavage strikes between N-NW (also NNE in the Boulder Lake domain) and dips east or subvertical (Table 9.3). Metamorphism associated with S_1 appears to be either subgreenschist or lowest greenschist facies. In all five domains, a stretching lineation associated with the cleavage plunges towards the easterly quadrant (Table 9.3).

	F_1 Axial Plane and fold tightness	F_1 Fold Axis	S_1	Stretching Lineation
Boulder Lake domain	North domain -N strike -mod. E to subvertical dip South domain -NNE-NE strike -mod. SE to subvertical dip	North domain -gentle N-NNE plunge South domain -gentle/moderate NE plunge	North domain -NNW-NNE strike -mod. E to subvertical dip South domain -NNE strike -mod. ESE to subvertical dip	steep E plunge
Adelaide Tarn domain	-close to gentle (tightness increases towards the west) -N-NW strike -mod. or gentle E dip	-subhorizontal to gentle N-NW or SE plunge	-axial planar	-mod. NE-E plunge -steep E plunge (east of Balloon mélange)
Lonely Lake domain	-close to gentle -N-NW strike -mod. or gentle E dip	-spread from NW to SE via NE. -NNE-ENE fold plunges come from within 200m of the Anatoki Fault.	-axial planar	-mod. NE-E plunge
Peak 1610 domain	Rare isolated close folds plunge towards the easterly quadrant with S_1 axial planar		-N-NNW strike -mod. or steep E dip	mod. or steep NE-ENE plunge
Kakapo Peak domain	Rare isolated close folds plunge towards the easterly quadrant with S_1 axial planar		-N-NNW strike -subvertical or mod./steep E dip	-steep E or subvertical plunge
Mt Benson domain	Not investigated	Not investigated	Not investigated	Not investigated
Crow River domain	F_i axial plane inferred to dip east	Unknown	Not observed	Not observed
Balloon Mélange	Not observed	Not observed	-NNW-NNE strike -subvertical or mod./steep E dip	- subvertical or mod./steep ENE-ESE plunge

Table 9.3 Takaka terrane D_1 and F_i (Crow River domain only) structural orientations

Two large macroscale folds are recognised in the Boulder Lake domain, the Brown Cow syncline which is NW-W facing, and the No Man anticline which is upright. These two fold structures plunge gentle to moderately towards the N-NE. Younging directions, bedding-cleavage relationships, and fold vergence suggest the undifferentiated Haupiri Group rocks, west of the Balloon Mélange in the Adelaide Tarn and Lonely Lake domains, are related to an overturned western limb of a large macroscale W to SW facing anticline (Section 4.5.1). Younging directions, bedding-cleavage relationships, and shear-sense indicators in the undifferentiated Haupiri Group rocks of the Peak 1610 and Kakapo Peak domains (Section 5.5) suggest they, too, are related to an overturned western limb of a large macroscale west facing anticline. Intersection lineations, mesoscale folds and π-girdle distributions of bedding in the Adelaide Tarn and Lonely Lake domains (Section 4.5.1) indicate the orientation of the large macroscale fold axis there is subhorizontal to gently plunging towards the N-NW or SE. The orientation of the stretching lineations in the five domains appears to be subperpendicular to the large macroscale fold axis.

The overall similarity in orientation of slaty cleavages, fold axial planes, fold facing directions, and stretching lineations in the Boulder Lake, Adelaide Tarn, Lonely Lake, Peak 1610, and Kakapo Peak domains, suggests they are all related to one deformation event. Given that they are the first set of structures recognised, they are designated S_1 and F_1 accordingly, and the deformation event recognised is D_1. In addition, $S_{mél}$ and stretching lineations in the Balloon Mélange are correlated with D_1 structures (Section 8.6). All D_1 structural orientations, including stretching lineations and fold facing directions, resemble those associated with the N-S trending folds recognised elsewhere in the Cambrian arc assemblage. It thus seems likely that F_1 folds are correlated with the N-S trending folds developed elsewhere.

Despite the portrayal of similarity in D_1 structural orientations given above, there is a significant difference in F_1 and S_1 orientations, especially fold axes, between the Boulder Lake and Adelaide Tarn domains (see Table 9.3). I believe the difference in structural orientations between these two domains can at least partly be accounted for by reorientation of structures as a consequence of subsequent deformation (D_3) (see Section 9.5.3 for further discussion).

The Summit Limestone sliver along the Anatoki Fault is thought to be Early Ordovician in age (Section 6.4), and bounded by Late Cambrian undifferentiated Haupiri Group rocks to the east and Buller terrane rocks to the west. In all domains where the limestone sliver occurs, the western contact is a fault (Anatoki Fault). In the Peak 1610 and Kakapo Peak domains, the eastern contact is also probably tectonic (Section 5.4). Given that undifferentiated Haupiri Group rocks in the Peak 1610 and Kakapo Peak domains probably represent the overturned western limb of a large-scale F_1 west facing anticline, the limestone sliver may represent a remnant of the stratigraphic sequence above the undifferentiated Haupiri Group rocks. The narrowness of the limestone sliver suggests it represents a sheared outer margin of the overturned western limb of the large-scale F_1 anticline. A similarity in stretching lineations and cleavage supports the proposition that the limestone was involved in the same fold structure as that of the adjacent undifferentiated Haupiri Group (Section 5.5.4). In addition, shear-sense indicators in the limestone sliver and adjacent undifferentiated Haupiri Group rocks are compatible with an overturned western limb of an F_1 anticline (Section 5.5.4). It is difficult to explain the origin of the limestone sliver in any other way without invoking a complex fault movement history on either side of it.

Folds on an interdomainal scale are thought to be non-cylindrical based on correlations made between the Boulder Lake and Adelaide Tarn domains. The Brown Cow syncline in the Boulder Lake domain is correlated with a syncline east of Yuletide in the Adelaide Tarn domain (Map 2). The syncline wavelength decreases southwards indicative of dying out in that direction. In fact, the syncline in the Adelaide Tarn domain becomes parasitic to a large anticline located to the east. In the Adelaide Tarn, Lonely Lake, Peak 1610, and Kakapo Peak domains, the observed western limb of a large-scale W facing anticline is correlated with the western limb of the No Man anticline in the Boulder Lake domain. Thus it appears the wavelength of the anticline increases southward. In the Adelaide Tarn domain, at least, the hinge of the anticline is thought to be located in the Balloon Mélange, given that undifferentiated Haupiri Group rocks east of the Balloon Mélange young eastwards (Map 2: axial plane trace shown with "?" marks). If the interpretation of an anticlinal hinge in Balloon Mélange of the Adelaide Tarn domain is correct, then the large scale fold axis is N-S trending (see bedding orientation on either limb on Map 2), as opposed to indications that it is NW-SE trending closer to the Anatoki Fault (see above discussion).

The interpreted F_i axial plane in the Anatoki Formation of the Crow River domain shares a similar orientation to F_1 axial planes in domains further north, and to axial planes of N-S trending folds recognised by Coleman (1977, 1981) immediately to the east and south of the domain. It is therefore speculated that F_i in the Crow River domain is related to the D_1 deformation event.

Age of the D_1 deformation event

Since it is thought the Summit Limestone sliver originated from the sheared western limb of an overturned F_1 anticline, then this suggests the latest Cambrian-Silurian passive margin assemblage lay above the Cambrian arc assemblage prior to the formation of F_1. Given that no tectonic break is recorded in the passive margin assemblage, D_1 is suggested to be younger than the Silurian. This age constraint also applies to the upright/ inclined folding and cleavage in the passive margin assemblage throughout the Takaka terrane (Section 9.4.1), all of which are similar in orientation to that of D_1 structures. It is therefore suggested here that F_1 is related to the widely developed N-S trending upright/ inclined folding observed in the passive margin assemblage as well as those observed in the Cambrian arc assemblage. It is interesting to note that a N-S trending syncline within Late Ordovician Baldy Formation is observed immediately to the south of the Mt Benson domain (Mt Mytton: Cooper unpublished).

If D_1 structures are Devonian or younger it conflicts with the Middle Ordovician or older age of a N-S trending fold in the Cambrian arc assemblage located at Mt Snowden (C. Münker pers. comm. 1997). I suggest that two phases of essentially coaxial folding occur in the Cambrian arc assemblage based on indirect evidence from the Balloon Mélange outlined below; the first occurring in the Late Cambrian and the second simultaneously with the Devonian or younger N-S trending folds recorded in the passive margin assemblage.

In Chapter 8 it was concluded that the Balloon Mélange records two deformation events with similar extension directions. The first deformation (considered to be pre-D_1) occurred when the rock was essentially unlithified producing the mélange texture, and the other when the rock was lithified producing the $S_{mél}$ slaty cleavage (considered to be D_1). The Balloon Mélange may be the only formation that displays clearly the structural

evidence for two deformations (with similar extension directions) which correspond to the proposed two phases of coaxial folding. I suggest that the mélanging, which is thought to have occurred in the Late Cambrian (Section 8.7), occurred synchronously with the first phase of upright facing folds. The lack of an axial planar cleavage associated with the first fold phase presumably results from turbulent flow during the strain and dewatering of unlithified rocks, probably corresponding to an accretionary prism/fore-arc setting in which the mélange formed. $S_{mél}$ formed synchronously with the second fold phase (i.e. Devonian or younger), and it is at this time that a penetrative axial planar cleavage (S_1) developed with similar orientations to $S_{mél}$. The reason for a lack of structural evidence for two fold phases of folding in undifferentiated Haupiri Group rocks may be because the second fold phase underwent coaxial Type 0 superimposition (Ramsay and Huber, 1987) in which the second fold phase wavelength was controlled by that of the first.

9.5.2 D_2 deformation event

As described in Chapter 3, a foliation surface is recognised in the Boulder Lake domain which parallels and occurs within 200m of the Anatoki Fault. It is distinguished from S_1 based on differing stretching lineation orientations and age of formation (Section 3.9.2), and thus is designated as S_2. S_2 exclusively represents D_2 deformation in the Takaka terrane, an Early Cretaceous deformation event intimately related to movement on the Anatoki Fault, and affecting both terranes in the Boulder Lake domain (Section 3.9). Since D_2 is thought to be related to a regional stress field (Section 3.9.3), it probably correlates with other Early Cretaceous deformation recognised outside the study area, particularly that of faulting and shear zone movement in the north of the Takaka terrane (Challis *et al.* 1995, Hutton 1995), tectonic foliations in granitoids, and perhaps the deformation and metamorphism represented by Onekaka Schist (Challis *et al.* 1995). Since all of these deformations are closely associated to Early Cretaceous magmatism, it suggests regional deformation was occurring simultaneously with magmatism; ductile deformation was localised immediately adjacent to plutons and stocks whereas only brittle deformation occurred elsewhere.

9.5.3 D_3 deformation event

Folds, which are mainly mesoscale, and an associated axial planar crenulation cleavage are superimposed on D_1 and D_2 structures in the Boulder Lake domain, and on D_1 structures in the Adelaide Tarn and Lonely Lake domains. The fold axial planes and crenulation cleavages in all three domains are generally NE striking and dipping SE with dips increasing from Boulder Lake to Lonely Lake domain (Table 9.4). Fold axes generally plunge towards the E to SE sector (Table 9.4). A crenulation cleavage that crenulates $S_{mél}$ is also observed in the Balloon Mélange of these three domains. The crenulation cleavage is exactly the same orientation as that seen in the undifferentiated Haupiri Group rocks. The strong similarity in orientation of structures between the three domains suggests they are all related to a single deformation event. Given that they are superimposed on S_2 in the Boulder Lake domains, the folds and crenulation cleavage are designated as F_3 and S_3 respectively. The deformation event associated with F_3 and S_3 must postdate the Early Cretaceous S_2 foliation surface but predate the undeformed latest Cretaceous Pakawau Group cover sequence. Thus D_3 is considered to be mid-Cretaceous. D_3 may correlate with other post-Early Cretaceous pre-latest Cretaceous folds and crenulation cleavages recognised in the Takaka terrane outside the study area, particularly those recognised in the north of the terrane.

F_3 interlimb angles vary from close to gentle and, on average, are more gentle in the Lonely Lake domain compared with those to the north. D_3 structures are not observed in the Peak 1610 and Kakapo Peak domains except possibly as a crenulation cleavage observed in thin-section only. It appears, therefore, that D_3 deformation affected only the northern domains of this study. Reconnaissance fieldwork in the Rocky River, located halfway between the Boulder Lake domain and the Aorere River (Fig. 1.2), revealed excellent examples of mesoscale folds and axial planar crenulation cleavage in which the orientations match those of F_3 and S_3. This suggests the effects of D_3 deformation continues to the north of the study area. F_3 folds that display vergence, including those in the Rocky River, are almost always verging towards the N-NE.

F_{ii} and S_{ii} in the Anatoki Formation of the Crow River domain have an orientation that differs somewhat from F_3 and S_3 (Table 9.4) and therefore their relationship to D_3 is unknown.

	F_3 Axial Plane and fold tightness	F_3 Fold Axis	S_3
Boulder Lake domain	-close to open -axial plane approximates S_3	North domain -gentle or mod. plunge towards the SE quadrant South domain -gentle or mod. plunge towards the ESE quadrant	-NNE-ENE strike -gentle or moderate SE dip
Adelaide Tarn domain	-close to gentle -NE strike -moderate SE dip	-gentle or moderate E plunge	-axial planar
Lonely Lake domain	-close to gentle -NE-ENE strike -mod. or steep SE dip	-moderate ESE plunge	-axial planar
Peak 1610 domain	Not observed	Not observed	-crenulation in thin-section possibly S_3
Kakapo Peak domain	Not observed	Not observed	Not observed
Mt Benson domain	Not investigated	Not investigated	Not investigated
Crow River domain	F_{ii} axial plane approximates S_{ii}	F_{ii}: gently N to moderately S plunging (via horizontal)	S_{ii}: moderate or steep W dip
Balloon Mélange	Not observed	Not observed	Crenulation cleavage that has same orientation as S_3

Table 9.4 Takaka terrane D_3 and F_{ii}/S_{ii} (Crow River domain only) structural orientations. Bedding is the fold axis reference surface.

The change in orientation of D_1 structures between the North and South structural domains of the Boulder Lake areal domain, and between these two structural domains and the Adelaide Tarn areal domain (Table 9.1), is believed to be at least partly a result of, and is consistent with, the superimposition of D_3 strain around the competent Mt Olympus Pluton. This is well-illustrated by the curved nature of the Brown Cow syncline axial plane trace (see Map 1). The significant change in fold axis orientation between the Boulder Lake domain and Adelaide Tarn domain (from NE to NW) may have been as an original feature, due to non-cylindrical folding, which has been amplified by the superimposition of D_3 strain.

9.6 Comparison of study area deformation events either side of the Anatoki Fault.

9.6.1 D_1 deformation event

In the Adelaide Tarn and Lonely Lake domains, and as discussed in Section 4.7, D_1 mesoscale structures either side of the Anatoki Fault show a similarity in orientation. From the structural synthesis so far discussed, D_1 macroscale structures throughout the

study area on either side of the Anatoki Fault share a common orientation. Both terranes show D_1 structures that indicate shortening in an approximate east-west direction, and both show fold structures with overturned western limbs. In the Takaka terrane, D_1 extension appears to be subperpendicular to macroscale fold axes. Based on structural grounds alone, I suggest that D_1 on either side of the Anatoki Fault represents the same deformation event.

Based on the previous reviews of this chapter, D_1 in the Buller terrane rocks of the study area is thought to have occurred anywhere between the Late Ordovician and Middle Devonian but probably towards the older end of this age range (Late Ordovician-Silurian). D_1 in the Takaka terrane rocks of the study area is thought to be Devonian or younger. The age constraints for D_1 on either side of the Anatoki Fault overlap but an age correlation cannot be convincingly demonstrated and shall be further discussed below.

Evidence that D_1 in the Buller terrane occurred in the Late Ordovician-Silurian comes from areas west of the Karamea Batholith and at least 40km from the terrane boundary. Could perhaps deformation east of the Karamea Batholith be younger in age and match that of the maximum age for D_1 in the Takaka terrane? It is known that diachronous deformation occurs in terranes of Antarctica and southeastern Australia which have been correlated with the Buller terrane (see a review of these in Chapter 10). In the Robertson Bay terrane of northern Victoria Land (Antarctica) there is a progressive younging of axial planar slaty cleavage formation from 500Ma to 460Ma, across the generally trend of folds, based on extensive K-Ar and Ar-Ar dating (Adams and Kreuzer 1984; Dallmeyer and Wright 1992). In the Ballarat-Bendigo belt of southeastern Australia, there is a progressive younging of deformation of around 30-35Ma in the Devonian, across the general trend of folds, based on constraints of granite intrusion (Gray and Willman 1991). Based on these examples, it is conceivable that the Buller terrane N-S trending fold event is diachronous, and that folding in the east may overlap in age with the maximum age of D_1 structures in the Takaka terrane. However, the regional N-S folding in the Buller terrane cannot be younger than the Middle to Late Devonian Karamea Batholith (Section 9.2). In the Takaka terrane it was suggested that the upright/ inclined N-S trending folds (thought to include F_1) are related to Early-Middle Devonian recumbent folds (Section 9.4.1). Given the coaxiality of regional fold structures in both

terranes and the known age constraints, I suggest that D_1 in the Buller terrane rocks of the study area can conceivably be of the same age as D_1 in the Takaka terrane rocks of the study area, that is, Early-Middle Devonian.

9.6.2 D_2 deformation event

It has been shown in Chapter 3 that D_2 on either side of the Anatoki Fault are one and the same, and occurred immediately postdating the Early Cretaceous Mt Olympus Pluton emplacement. D_2 is intimately related to movement on the Anatoki Fault (Section 3.9.4).

9.6.3 D_3 deformation event

D_3 structures on either side of the Anatoki Fault are almost identical in orientation and this is particularly well-demonstrated in the Adelaide Tarn and Lonely Lake domains. In addition, D_3 on either side is thought to be mid-Cretaceous and thus it follows that D_3 in the Buller terrane and Takaka terrane are one and the same.

F_3 mesoscale folds in both terranes commonly display vergence towards the N-NE. Vergence of mesoscale folds is often used to indicate their position on major fold limbs (Bell 1981), and has been used for indicating large macroscale F_1 structures in this thesis. However, F_3 mesoscale folds throughout the study area are consistently N-NE verging, indicating the vergence is unrelated to major F_3 folds. Instead, I believe the vergence is simply a product of D_3 strain (with Z perpendicular to S_3) superimposed on D_1 tilted east dipping bedding surfaces that make up the majority of the study area (Fig. 9.1). The orientation of S_3 indicates D_3 shortening was NW-SE directed, and based on probable stretching lineations on Buller terrane S_3 surfaces (Fig. 4.17), D_3 extension is thought to be subhorizontally NE-SW directed.

Apart from S_2 related metamorphism, and dealt with in Chapter 3, metamorphism associated with all other cleavage surfaces indicate subgreenschist or lowest greenschist facies. Thus metamorphism cannot be used to help support correlation of various structures.

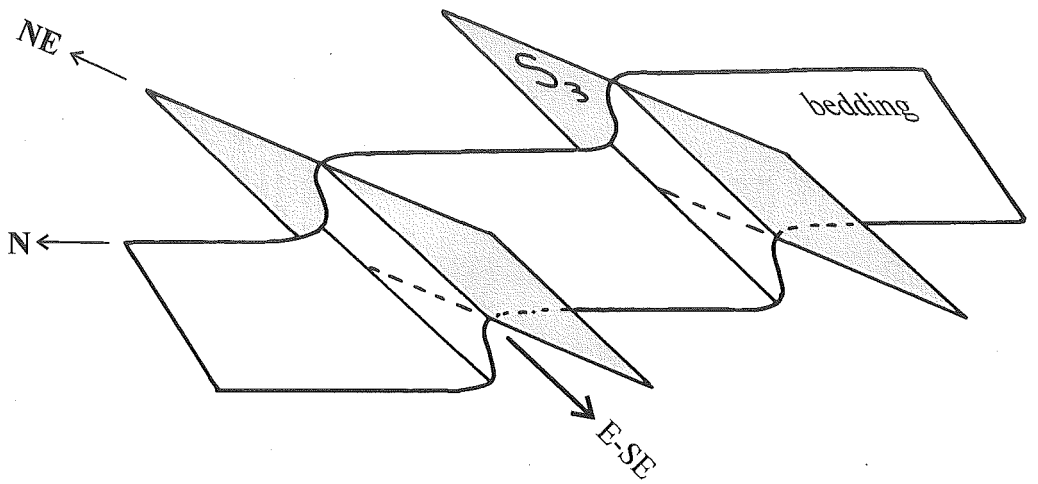

Figure 9.1: Diagram showing how D_3 strain (represented by S_3), superimposed on an east dipping bedding surface, will result in E-SE plunging F_3 folds with N-NE vergence.

9.7 Anatoki Fault

9.7.1 Attitude

From the previous areal domain chapters it is known that the Anatoki Fault dips between 30-45°E in the Boulder Lake, Adelaide Tarn, and Lonely Lake domains, ~60°E in the Peak 1610 and Kakapo Peak domains (~80°E south of Kakapo Peak), between 70°E-90° in the Mt Benson domain, and steeply E-NE in the Crow River domain. To the north of the study area, the Anatoki Fault dips between 28-45°E in the Aorere River (Stallard 1994), and to the south of the study area, the Anatoki Fault appears to be subvertical (see Coleman's map 1981). Overall, the Anatoki Fault is a N-S striking, E dipping fault that steepens southwards.

9.7.2 Style, direction, and history of movement

The style and direction of movement on the Anatoki Fault varies considerably along strike.

In the Boulder Lake domain, ductile dextral strike-slip movement is recorded in the Early Cretaceous and is related to D_2 (Section 3.9.4). Movement occurred over a relatively wide zone of shear that incorporates both Buller and Takaka terrane rocks. There is some evidence of brittle reactivation, and thin pug seams (Section 3.5.4) suggest that at least some of this movement was Late Cenozoic in age.

In the Adelaide Tarn and Lonely Lake domains, movement probably occurred along a discrete shear rather than a zone of deformation (Section 4.7). A ductilely deformed dolerite and narrow semi-brittle shear zones nearby (Section 4.5.5) suggest movement occurred at depth. Evidence from one of the semi-brittle shear zones suggests that movement of the Anatoki Fault was reverse-slip at one stage in its history. Unfortunately there is no evidence of when that movement occurred.

In the Peak 1610 and Kakapo Peak domains, movement on the Anatoki Fault was both brittle and ductile. Ductile movement occurred within the limestone sliver and adjacent highly strained undifferentiated Haupiri Group rocks, whereas brittle movement is

recorded in the adjacent Buller terrane (semi-) brittle shear zone (Section 5.5.4). Ductile movement in the limestone sliver is reverse-slip and thought to be related to D_1 deformation in the Takaka terrane (Section 5.5.4), in other words representing a relatively early stage in its history of movement. Previous work on shear-sense indicators in the limestone sliver at Kakapo Peak also indicate ductile reverse-slip movement (Powell 1985).

In the Mt Benson domain, ductile deformation in the limestone sliver and adjacent highly strained calcareous sediments records dextral normal-slip (Section 6.5.2). Timing of movement in the Mt Benson domain is unknown.

In the Crow River domain, ductile dextral normal-slip movement is recorded in the Summit Limestone shear zone immediately adjacent to the Anatoki Fault trace. This particular movement occurred post-earliest Cretaceous (Section 7.6). Brittle fault movement in adjacent Buller terrane rocks and Crow Granite give evidence that faulting occurred at depth probably at the same time as movement in the Summit Limestone shear zone (Section 7.6). Late Cenozoic pug seams, fault breccia and gouge cross-cut the brittle faults.

In the Upper Crow River and Wangapeka valley areas, located south of the Crow River domain (Fig. 1.2), reconnaissance fieldwork shows that the Anatoki Fault is a near vertical (semi-) brittle shear zone up to 8m wide. The shear zone consists of well-indurated intensely foliated rock which is cut by numerous quartz veins, and in places, indurated fault breccia. Evidence of extreme pressure solutioning indicates the shear zone formed at depth but there is no evidence of time of movement. Cross-cutting the shear zone are thin zones of soft fault gouge indicative of Late Cenozoic reactivation.

In the mid to late Tertiary Murchison Basin, directly south of the Wangapeka valley, Lihou (1993) suggests the Late Cenozoic Tainui Fault is a southern extension of the Anatoki Fault. If this is the case, significant Late Cenozoic reactivation of the Anatoki Fault, at least in the south of Northwest Nelson, is indicated. Nevertheless, I believe much of the movement and shortening that is accommodated by Late Cenozoic faults in the Murchison Basin is, in the Paleozoic rocks of Northwest Nelson, accommodated by the major NE striking Cenozoic faults in preference to the N-S striking faults.

9.7.3 Discussion of movement history

In the Peak 1610 and Kakapo Peak domains, D_1 related movement in the Takaka terrane is thought to be preserved (Section 5.5.4). The east over west reverse movement recorded in the Peak 1610 and Kakapo Peak domains is compatible with east-west shortening implied by D_1 structures in the Takaka terrane. It will be suggested in Chapter 10 that D_1 in both terranes is related to terrane amalgamation, and thus the Anatoki Fault movement recorded in the Peak 1610 and Kakapo Peak domains is important because it provides the only evidence of movement that may relate to terrane amalgamation.

Many segments of the Anatoki Fault have reactivated including that of the Boulder Lake (Section 3.9.4) and Crow River domains (Section 7.6) Although most segments record brittle movement (except in the rheologically weak limestone slivers), the Boulder Lake domain segment was ductile during reactivation because of the thermal effects of the nearby Mt Olympus Pluton. Given that significant Early Cretaceous D_2 ductile strain is recorded in the Boulder Lake domain, and that D_2 is thought to relate to a regional stress-field (Section 3.9.3), one would expect an expression of that ductile strain to be accommodated in a brittle fashion along more southern segments of the Anatoki Fault. In the Crow River domain, post-earliest Cretaceous dextral normal-slip movement recorded is consistent with dextral strike-slip and overlaps in time of movement with D_2. Dextral normal-slip is also recorded in the Mt Benson domain. It is therefore suggested that Anatoki Fault tectonites in the Mt Benson and Crow River domains are related to Early Cretaceous D_2 movement observed in the Boulder Lake domain.

If the above suggestion is accepted then one must explain why the intervening Peak 1610 and Kakapo Peak domains record reverse-slip in the limestone sliver which is thought to be related to D_1 movement. It could be argued that Early Cretaceous movement in the Peak 1610 and Kakapo Peak domains is indeed expressed, but instead of being accommodated in the limestone sliver, it is accommodated in the brittle shear zone adjacent to it. D_1 related movement would therefore be preserved in the limestone sliver. Little is known about the postulated brittle shear zone that represents the Anatoki Fault in the Adelaide Tarn and Lonely Lake domains but it is conceivable that Early Cretaceous movement was also accommodated there.

If the suggestion that the entire Anatoki Fault in the study area underwent Early Cretaceous movement is accepted, one must further explain why Early Cretaceous movement was accommodated preferably in the limestone sliver at Mt Benson but not in the limestone sliver at Peak 1610 and Kakapo Peak domains. This is a problem that is difficult to resolve and indicates that maybe Early Cretaceous movement was not actually accommodated in the brittle shear zone of the Adelaide Tarn, Lonely Lake, Peak 1610, and Kakapo Peak domains but, instead, transferred to other nearby N-S striking faults. It is known that other N-S striking faults in Northwest Nelson have been active in the Early Cretaceous (Challis *et al.* 1995, Hutton 1995). An obvious candidate for accommodating movement south of the Boulder Lake domain would be the Fenella Fault Zone which, interestingly, only makes its appearance south of Boulder Lake. It is possible that movement occurred on the Fenella Fault Zone synchronously with that on the Anatoki Fault, or alternatively, preferential accommodation of movement stepped from one fault to the other several times along strike. One may argue that the movement at Mt Benson and Crow River domains is quite unrelated to that seen at the Boulder Lake domain, in which case Early Cretaceous movement at the Boulder Lake domain had to be transferred to other faults further south.

In summary, several segments of the Anatoki Fault are known to have reactivated over time. These segments include the Boulder Lake domain in the Early Cretaceous, the Crow River domain in the post-earliest Cretaceous, and the Boulder Lake, Crow River, Upper Crow River, and Wangapeka valley areas in the Late Cenozoic. Early Cretaceous D_2 related ductile movement on the Anatoki Fault in the Boulder Lake domain, was either accommodated brittlely by the same fault and/or transferred to other nearby N-S striking faults further south. Nevertheless, I suggest that movement recorded in the Crow River and Mt Benson domains is probably related to D_2 movements. In the Peak 1610 and Kakapo Peak domains, D_1 movement is thought to be preserved and may relate to original movements of the Anatoki Fault.

Comment on fault plane attitude

The curving of the Anatoki Fault trace in the Boulder Lake domain is a result of D_2 strain perturbations around the Mt Olympus Pluton (Section 3.9.3). It follows that the attitude of the fault plane in the Boulder Lake domain has been modified during reactivation. In

the Crow River domain, deformation on the Anatoki Fault has been partitioned between the Summit Limestone and the Crow Granite (Section 7.6), and thus it seems the attitude of the fault plane in this domain has also been modified during reactivation.

In the intervening segments of the Anatoki Fault it is difficult to know if the attitude has been modified. The decreasing dip of the fault plane from the Kakapo Peak domain northwards coincides with a decreasing dip of F_1 axial planes in the Buller terrane (Table 9.1). The decrease in dip northwards may reflect an original feature, or alternatively, may be linked to deformation that has occurred in the Cretaceous. The N-S trending Granity Creek pluton extends for 6km south of the Mt Olympus Pluton (Fig. 1.2). The pluton is undated but is correlated with the Olympus Granite (Grindley 1971). Based on its close proximity to the Mt Olympus Pluton, the two plutons probably join up at depth and it is speculated that the granitic body may extend at depth into the Lonely Lake and Adelaide Tarn domains (the domains are ~5km east of the Granity Creek Pluton). If the speculation is correct, and assuming the Anatoki Fault was originally steeper dipping, Cretaceous deformation (D_2 and/or D_3 strain) around the more competent granitic body may have modified the Anatoki Fault attitude to gentler dips.

Given that movement in the Peak 1610 and Kakapo Peak domains is thought to relate to D_1 in the Takaka terrane, and that D_1 structures indicate east-west shortening, the Anatoki Fault could not have been an originally west dipping fault plane during D_1 deformation because normal movement would be implied.

9.8 Ankerite metasomatism

Ankerite metasomatism (i.e. ankerite porphyroblast growth) in both the Buller and Takaka terranes is variably developed but most intense immediately adjacent to the Anatoki Fault. The intensity of ankerite metasomatism adjacent to the Anatoki Fault suggests the fault acted as a channelway for CO_2-rich fluids, and was probably active at the time of metasomatism. Two distinct periods of ankerite metasomatism are recognised in the study area.

1. Microstructural relationships between mesoscale S_1 and ankerite porphyroblasts in almost all domains and both terranes suggest the first period of ankerite metasomatism was either pre- or syn-mesoscale S_1 but in most cases syn-D_1 (Sections 4.5.2, 5.5.2 and

6.3.2). If it is accepted that ankerite metasomatism occurred at the same time in both terranes, as seems likely, then the microstructural relationships are consistent with the suggestion presented earlier that D_1 in both terranes are one and the same.

2. In the Boulder Lake domain, ankerite porphyroblast growth grew parallel to S_2 (Section 3.7.6). Thus, the second period of ankerite metasomatism was syn-D_2.

Ankerite strain fringes also grew subsequently to ankerite porphyroblast growth during D_1 and D_2 deformation and metamorphism.

CHAPTER 10

GENERAL DISCUSSION and CONCLUSIONS

10.1 Introduction

This chapter is primarily a discussion of how the deformation events recognised in the study area relate to the geological history of the Western Province. To put the Early Paleozoic history of the Western Province in context, a review of the southwest Pacific margin of Gondwanaland is presented first. A new plate tectonic model is then presented to explain the Early Paleozoic deformational history of the Buller and Takaka terranes. The latter part of the chapter reviews and discusses tectonics in the Cretaceous. The major conclusions of the thesis are presented at the end of the chapter.

10.2 Terrane correlation in Gondwanaland

Plate reconstructions of the southwest Pacific in the late Mesozoic show the New Zealand continent in close proximity to western Marie Byrd, northern Victoria Land, Tasmania, and southeast Australia (e.g. Fig. 10.1; Fig. 5 of Lawver and Gahagan 1994). It has long been recognised that these five areas share a similar Paleozoic history (e.g. Cooper and Grindley 1982), and together are thought to make up part of the Paleozoic Pacific margin of Gondwanaland (Coney *et al.* 1990). The purpose of this section is to briefly review the correlatives of the Buller and Takaka terranes along the Paleozoic Pacific margin so as to put the two terranes in context with regard to a proposed plate tectonic model presented in Section 10.3.

A

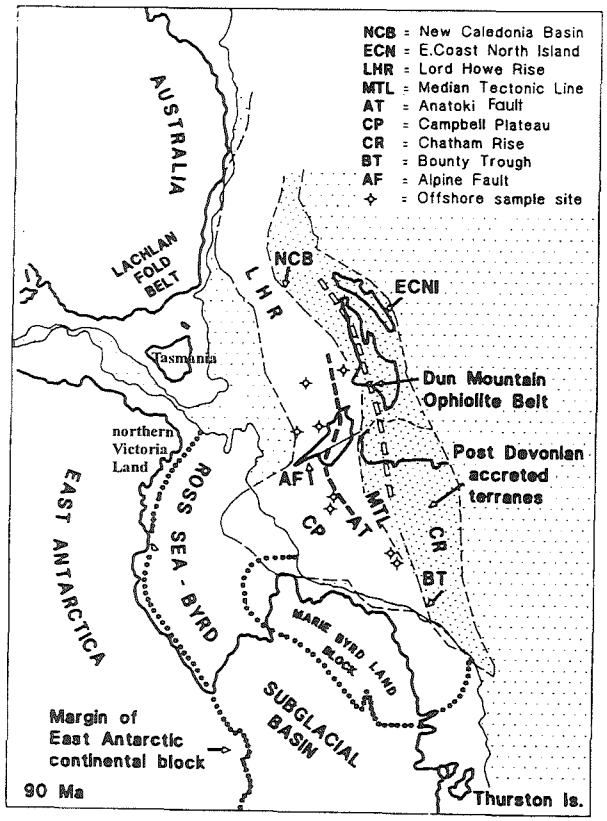

B

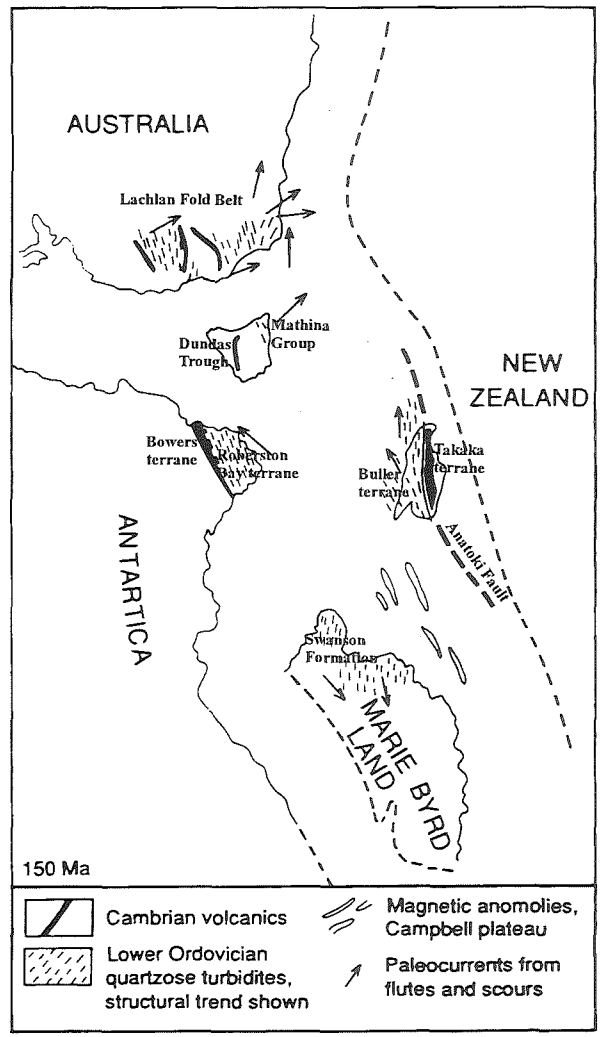

Figure 10.1 (A): Plate reconstruction for the southwest Pacific margin of Gondwanaland at 90Ma. (B): Reconstruction for the southwest Pacific margin of Gondwanaland at 150Ma. Both (A) and (B) from Cooper and Tulloch (1992).

10.2.1 Western Marie Byrd Land

The Ford Ranges of Western Marie Byrd Land is mostly made up of quartz-rich turbidites of the Swanson Formation (Bradshaw *et al.* 1983). The formation is deformed by large upright folds (Bradshaw *et al.* 1983), and K-Ar and Rb-Sr geochronology (Adams 1986; Adams *et al.* 1995) suggest cleavage formation associated with the deformation occurred between 450-410Ma. Similarity in sedimentology, composition, and age and style of deformation, has prompted Bradshaw *et al.* (in press) to suggest the Swanson Formation is a correlative of the Greenland Group in the Buller terrane. Like the Greenland Group, the Swanson Formation is cut by Devonian, Carboniferous, and Cretaceous granitoids thereby reinforcing such a correlation (Bradshaw *et al.* in press).

10.2.2 Northern Victoria Land

Northern Victoria Land is made up of three terranes; from west to east they are, Wilson terrane, Bowers terrane, and Roberston Bay terrane (Fig. 10.2).

The quartz-rich turbidites of the Cambrian to Early Ordovician Robertson Bay Group, the major unit of the Roberston Bay terrane, closely resembles the Greenland Group of the Buller terrane in both lithology and deformation style (Bradshaw *et al.* in press). It, too, is folded by a regionally extensive episode of upright folding (Stump 1995) but cleavage formation associated with the deformation appears to be somewhat older at around 500-460Ma (Adams and Kreuzer 1984; Dallmeyer and Wright 1992). In fact, deformation appears to have been diachronous from about 500Ma in the west to 460Ma in the east. Latest Cambrian-earliest Ordovician body fossils in the uppermost stratigraphic levels of the group suggest deformation was occurring simultaneously with deposition (Stump 1995).

The Bowers terrane consists of Cambrian volcanics and a varied assemblage of Cambrian to Ordovician sedimentary rocks. The volcanics are interpreted to be of island arc affinity (Weaver *et al.* 1984) and most of the interfingering and overlying sedimentary units are thought to have formed in a shallow marine and fluvial environment (summarised in Stump 1995). The Cambrian volcanic and sedimentary units show strong similarity to the Cambrian of the Takaka terrane (Münker and Cooper 1995; Bradshaw *et*

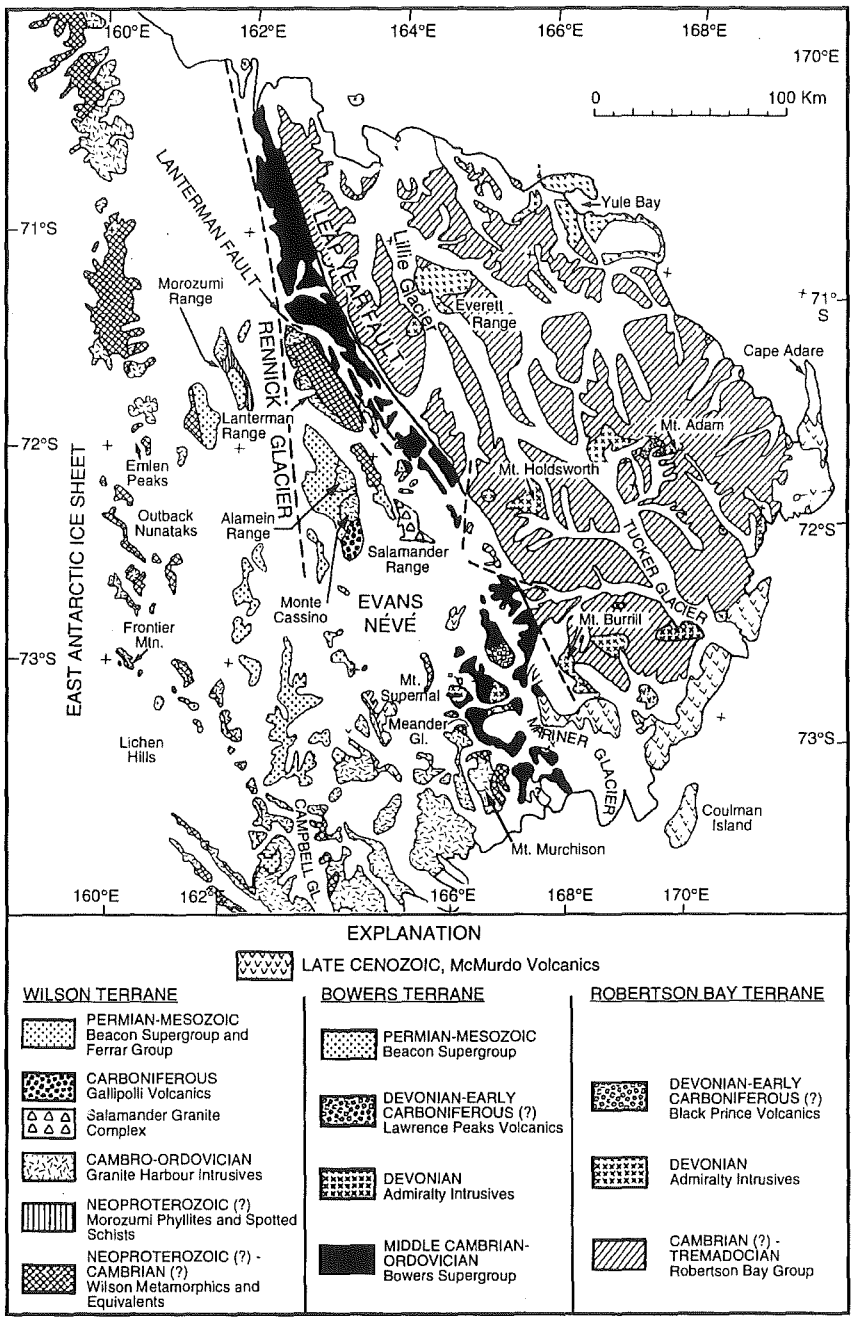

Figure 10.2 Geological map of northern Victoria Land (from Stump 1995)

al. in press). The Bowers terrane is deformed by upright folding (Stump 1995), but timing of deformation is uncertain.

Both the Roberston Bay and Bowers terranes are cut by Devonian granitoids (Admiralty Intrusives) (Stump 1995) supporting a link with the Buller and Takaka terranes.

10.2.3 Tasmania

Tasmania can be split into the Western and Eastern Tasmania terranes (Powell and Ballie 1992) (Fig. 10.3).

The Dundas Trough of the Western Tasmania terrane consists of Early-Middle Cambrian ultramafic-mafic complexes, Middle-Late Cambrian "arc-like" volcanics and associated flanking marine sediments, overlain by an Ordovician to Early Devonian shallow marine sequence of limestone, sandstone, and siltstones (Cooper and Grindley 1982). The stratigraphy of the Dundas Trough shows a strong similarity to that of the Takaka terrane particularly in the Ordovician to Silurian sedimentary sequence (Cooper and Tulloch 1992). However, the Middle-Late Cambrian Tasmanian volcanics are dominated by intermediate to acidic volcanics reflecting continental crust involvement (Crawford and Berry 1992), and this contrasts with the mafic dominated Devil River Volcanics Group (Münker and Cooper 1997). In the Western Tasmania terrane, a complicated plate tectonic setting occurred in the Cambrian, including obduction of the ultramafic-mafic complexes on to Precambrian basement (Crawford and Berry 1992). Subsequent folding related deformation is constrained stratigraphically to the Early-Middle Devonian (see Powell and Baillie 1992).

The Eastern Tasmania terrane wholly consists of the quartz-rich turbiditic Mathinna Group. The Mathinna Group is Ordovician to Early Devonian in age, and based on stratigraphic constraints, was deformed by upright folds in the Early Devonian (Powell and Ballie 1992). The Ordovician part of the Mathinna Group may possibly be a correlative of the Buller terrane (Cooper 1991). Powell and Ballie (1992) suggest that the Western and Eastern Tasmania terranes were simultaneously deformed by further folding and faulting in the Middle Devonian. Both terranes are intruded by Middle to Late

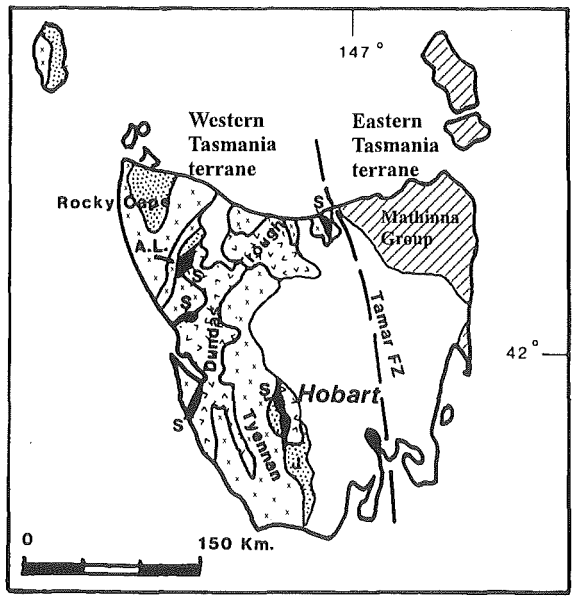

Figure 10.3 Precambrian and Lower Paleozoic geological map of Tasmania. The Tamar "fracture zone" separates the Western Tasmania terrane from the Eastern Tasmania terrane. The Dundas and related troughs are shown by the "v" pattern. The Mathinna Group is shown by diagonal lines. "s"= ultramafic bodies; "x" = Precambrian basement; stipple = Late Precambrian to Middle Cambrian sedimentary rocks. (from Coney *et al.* 1990)

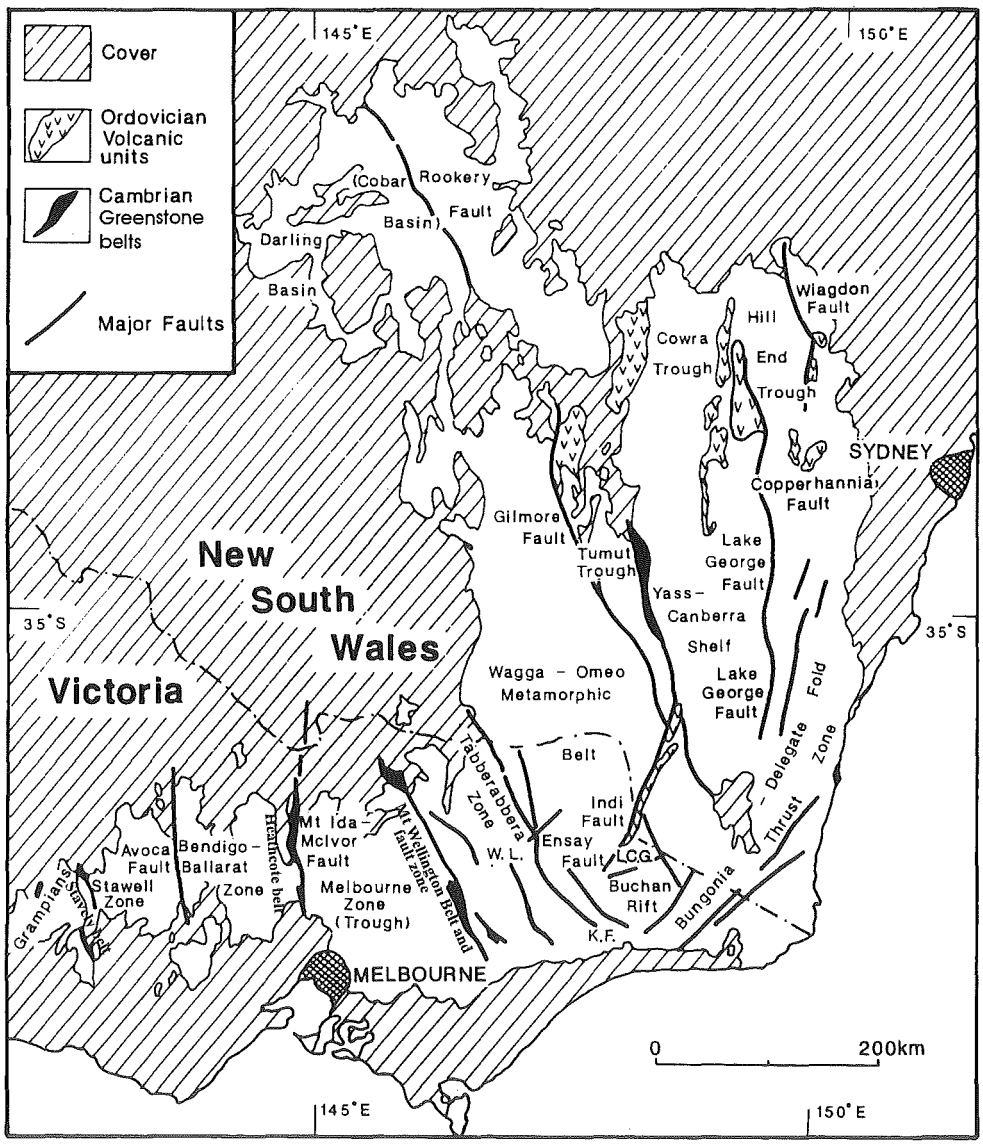

Figure 10.4 Geological map of the Lachlan Fold Belt, southeastern Australia (from Fergusson and Coney 1992).

Devonian granites (Powell and Ballie 1992) supporting a link with the New Zealand terranes.

10.2.4 Southeastern Australia

The Paleozoic rocks of southeastern Australia form the Lachlan Fold Belt (Fig. 10.4), and are characterised by Cambrian greenstones, a widespread Ordovician turbidite and pelagic black shale succession, and a deep-marine to continental Silurian to Early Carboniferous succession with volcanics and abundant plutonic rocks (Fergusson and Coney 1992).

In the west of the Lachlan Fold Belt are three narrow N-S trending fault-bounded Early to Middle Cambrian greenstone belts (Fig. 10.4). From west to east they are the Stavely, Heathcote, and Mt Wellington greenstone belts. Composition of volcanics in the Stavely belt suggest a continental margin affinity (Crawford 1984) whereas the majority of the Heathcote and Mt Wellington belts suggest they represent back-arc basin tholeiites associated with an island arc (Crawford and Keays 1987). The Heathcote and Mt Wellington belts also contain some orogenic andesites (Crawford and Keays 1978; Crawford 1984). The volcanics and associated volcaniclastics in all three belts have contrasting post-Cambrian successions. The Stavely belt is unconformably overlain by Silurian shallow water sandstones; the Heathcote belt is comformably overlain by Ordovician turbidites; the majority of the Mt Wellington Belt is unconformably overlain by Ordovician shales; the Waratah Bay section of the Mt Wellington Belt is unconformably overlain by Early Ordovician limestone (Cooper and Grindley 1982). Stump *et al.* (1986) have correlated the Stavely Belt and Silurian sandstones with the Bowers terrane. All three Cambrian greenstone belts have elements that suggest a possible link with the Takaka terrane. However, the Heathcote belt and the majority of the Mt Wellington belt appear to represent the underlying base of the Ordovician turbidite succession in the southwest Lachlan Fold Belt (see Cooper and Grindley 1982), and thus it seems unlikely they are correlatives of the Takaka terrane.

The widespread Ordovician and locally Silurian quartz-rich turbidites, pelagic pelites, and cherts, that make up a large part of the Lachlan Fold Belt (Cooper and Grindley 1982), are possible correlatives of the Buller terrane. The turbidites are all deformed by

upright folds and steep contractional faults that flatten with depth (Glen 1992). Timing of deformation varies irregularly across the belt from Silurian to Middle Devonian, and the Early Carboniferous (Fergusson and Coney 1992). Abundant granitoids of mostly Silurian to Devonian age intrude the turbidites and are generally syn- or post-tectonic (Fergusson and Coney 1992). It has been suggested that the sediments of the Ballarat-Bendigo zone of Victoria match most closely to that of the Buller terrane (Cooper and Tulloch 1992). The Ballarat-Bendigo zone is deformed by upright folding which occurred diachronously in the Early to Middle Devonian, and mainly predate Early to Middle Devonian granitoids (Fergusson *et al.* 1986; Gray and Willman 1991).

10.2.5 The New Zealand problem

It was stated above that extensive mainly Ordovician quartz-rich turbidites, pelagic pelites, and cherts make up a large part of the Lachlan Fold Belt (Cooper and Grindley 1982). The environmental setting of these sediments is thought to be a large deep water turbidite fan complex (Powell 1983). The Lachlan Fold Belt extends for about 700km in an E-W direction and 500km in a N-S direction. Structural analysis of the belt suggests a minimum of 50%-60% shortening in an east-west direction (Coney *et al.* 1990; Fergusson and Coney 1992), and size estimates of the original turbidite fan has been thought to be as large as 2000km across and 2-5km thick (Coney 1992). The large Bengal fan in the eastern Indian Ocean is the closest modern day analogue to this Lower Paleozoic fan, and even this is small in comparison.

Based on plate tectonic reconstructions for the Cretaceous, it seems likely that western Marie Byrd Land, Robertson Bay terrane, Eastern Tasmania terrane, and the Buller terrane were part of the extremely large Early Paleozoic fan. The source of the sediments which fed the fan appears to be Gondwanaland and more specifically the Ross-Delamerian Orogen of East Antarctica and southeastern Australia (Coney *et al.* 1990). What the fan was deposited on is somewhat controversial but in southeastern Australia it has been suggested to be either oceanic crust and/or thin continental crust (cf. Collins and Vernon 1992 with Fergusson and Coney 1992). Inboard (relative to Gondwanaland) from this turbidite fan there appears to be a Cambrian arc assemblage based on the present geographical relationships of the Bowers terrane, Western Tasmania terrane, and the greenstone belts of southeastern Australia (particularly the Stavely belt) with that of the

turbiditic terranes. Overlying shallow marine or fluvial sediments in the Antarctic and Tasmanian arc assemblages support the proposition that they were inboard relative to the deep water turbidite fan.

In the above review it was suggested the Takaka terrane can be correlated to the other Cambrian arcs. However, reconstructions of Late Mesozoic Gondwanaland which have removed the effects of New Zealand oroclinal bending* suggest that the Takaka terrane was outboard from the future turbidite fan complex (e.g. Fig. 10.1B; Grindley and Davey 1982). Herein lies the New Zealand problem, and there appear to be four possible solutions:

1. The Takaka terrane originated from the inboard Cambrian arc and was brought to its present relative position by being thrust over the turbidite fan in a west to east direction.
2. The Takaka terrane originated from the inboard Cambrian arc and was brought to its present relative position by strike-slip movement.
3. The Takaka terrane was never part of the inboard Cambrian arc but instead originated along another segment of the Gondwanaland margin that was some distance from the northern Victoria Land-Tasmania-southeastern Australia arc. Its present relative position is brought about by strike-slip movement.
4. The Takaka terrane was never part of the inboard Cambrian arc but instead originated in its present relative position, outboard from the future turbidite fan complex.

Structural data on terrane boundaries between the Wilson, Bowers, and Roberston Bay terranes suggest west over east thrusting (summarised in Stump 1995; Flöttmann and Kleinschmidt 1991), and plate tectonic models suggest the upper levels of the Bowers terrane was emplaced over the Roberston Bay terrane (Flöttmann and Kleinschmidt 1991, Dallmeyer and Wright 1992). These models certainly support solution 1 above. However, taking the width of the Roberston Bay terrane and the width of the offshore New Zealand continent west of the Anatoki Fault* into account, solution 1 would require at least 500km of thrust related tectonic transport, an amount that seems rather unrealistic

*for a discussion of the timing of oroclinal bending see Bradshaw *et al.* (1996).
*offshore well data suggests the existence of Buller terrane west of the South Island (Cooper and Tulloch 1992).

considering there is no evidence in the Cambrian of the Takaka terrane to suggest it had been transported over the Buller terrane (e.g. east verging folds). Cooper (1991, p. 51) speculates that the Takaka terrane "represents a bit of western Tasmania thrust over a bit of Victoria". Again, a distance of at least 400km of thrust related tectonic transport would be required.

In an east-west transect across the Central Belt of the Takaka terrane, there are Cambrian rock units that have been interpreted to represent an accretionary prism (Balloon Mélange: Cooper and Tulloch 1992; Pound 1993), island arc volcanics (Benson Volcanics: Münker and Cooper 1995), and a back-arc basin (Mataki [Salisbury] Volcanics: Pound 1993; Münker and Cooper 1997). The range of plate tectonic environments is remarkable when it is considered that the Central Belt is only 15km wide in an east-west direction. Given that modern day arc assemblages are 200km wide or more (see Westbrook 1982), and after removing the effects of shortening, the present extent of the Cambrian arc assemblage appears to represent only a small fragment of its former self. Although structural evidence for strike-slip movement is lacking, a reasonable way of reducing the arc width is by way of large scale strike-slip movement. Large scale strike-slip movement has been advocated in northern Victoria Land to explain missing rock (Bradshaw *et al.* 1985), and in the Lachlan Fold Belt to explain duplication of rock (Glen *et al.* 1992). In addition, there is good structural evidence for strike-slip movement in the Lachlan Fold Belt (Fergusson *et al.* 1986, Glen 1992). Solutions 2 and 3 require strike-slip movement and therefore warrant consideration.

Solution 2 requires the Takaka terrane to be displaced by strike-slip from an inboard to outboard position across the turbidite fan. However, as can be seen in Figure 10.5, to achieve solution 2 necessitates the accompanying baggage of Ross-Delamerian Orogen rocks and the duplication of turbidite fan rocks on the outboard margin of the Takaka terrane. There is no evidence that Ross-Delamerian Orogen rocks such as the Wilson terrane or the Adelaide fold belt exist east of the Antarctic-Tasmania-southeastern Australia Cambrian arc terranes, nor evidence of the Ordovician turbidite rocks east of New Zealand, thus suggesting solution 2 is unlikely.

Solution 3 is easier to envisage as there is no need for strike-slip faulting to transect across the turbidite fan complex nor displace Ross-Delamerian Orogen rocks (Fig. 10.5).

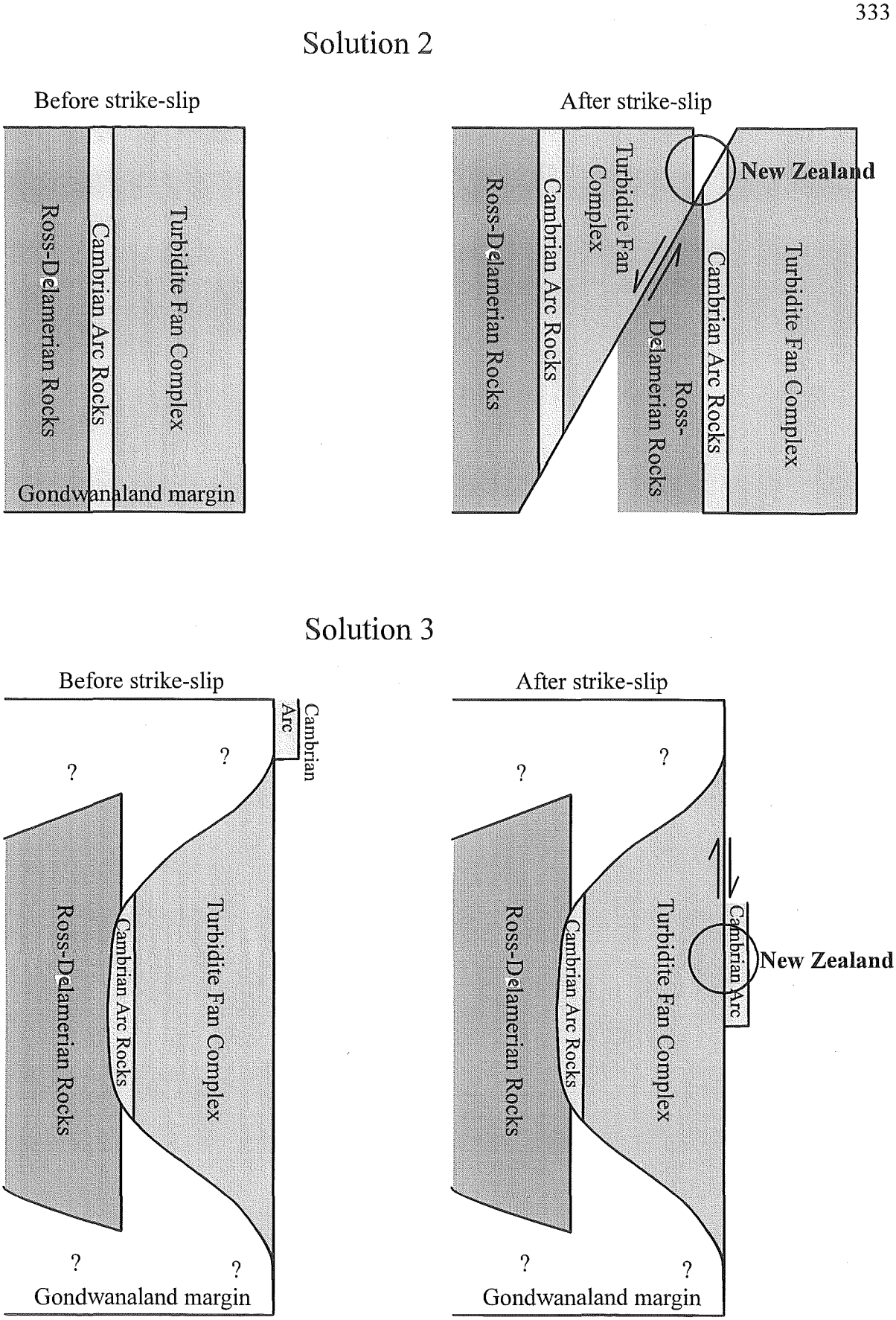

Figure 10.5: Diagrammatic representation of solution 2 and solution 3 of the New Zealand problem. See text for discussion.

I have not reviewed rocks outside the southwest Pacific margin of Gondwanaland but it is reasonable to assume that the Gondwanaland margin was not uniformly consisting of an inboard Cambrian arc and an outboard Ordovician turbidite fan complex. Somewhere there were irregularities, much like continental margins today, and these are postulated in Figure 10.5 in order to make solution 3 possible. Solution 3 requires a very large amount of strike-slip movement.

Solution 4 is the least complicated in terms of plate tectonic movements. Nevertheless, strike-slip movement probably still occurred in order to explain the present width of the Takaka terrane arc assemblage. Solution 4 does not provide an obvious source for continentally-derived clastics in the Takaka terrane, particularly that of the Silurian shallow marine Hailes Quartzite which implies a continental source very nearby. This is in contrast to solution 1, 2, and 3 in which the Gondwanaland margin is the obvious source. Perhaps deformation, granitic plutonism, and uplift in the Silurian, which occurs in parts of the Lachlan Fold Belt (Fergusson and Coney 1992), may be related to the deposition of Hailes Quartzite. Alternatively, there may have been a continent to the east.

The above review highlights the New Zealand problem, and all four basic solutions are not satisfactory. There is no doubt the plate tectonic setting in the Early Paleozoic is a great deal more complicated and far less linear than Figure 10.5 leads us to believe. This is all the more true when one views the variety of plate tectonic setting in the modern day western Pacific alone. Nevertheless, it is my opinion that solutions 3 and 4, where the Takaka terrane never originated inboard from the Buller terrane, are easiest to accept. The ideas of solution 3 and 4 are offered as alternative "Gondwanaland margin constraints" in a plate tectonic model that brings the Buller and Takaka terranes together (see next section).

10.3 Terrane amalgamation

According to Cooper (1989) the age constraints for the amalgamation of the Buller and Takaka terranes are post-Late Ordovician (the age of the youngest Greenland Group sediments) and pre-Early Cretaceous (the age of the Separation Point Suite which intrudes both terranes). I have shown that both Buller and Takaka terrane sediments were

thermally affected by the intrusion of the Crow Granite and thus terrane docking must predate ~137Ma. It has previously been suggested, as an option, that terrane docking postdates the Devonian, based on the differences in Middle-Late Devonian magmatic activity observed on either side of the terrane boundary; Karamea granitoids are restricted to the Buller terrane and Riwaka Complex ultramafic-mafic rocks are restricted to the Takaka terrane (Cooper 1989; Cooper and Tulloch 1992). However, recent research on the Karamea Suite and the Riwaka Complex suggest these two intrusives are fundamentally similar both in geochronology and geochemistry (Muir *et al.* 1996a, b). In particular, the mafic rocks of the Karamea Suite, the Zetland Diorite, bears a close resemblance geochemically to the Brooklyn Diorite of the Riwaka Complex (Muir *et al.* 1996b). Similar geochemistry and geochronology of the two intrusive suites gives strong evidence that terrane amalgamation had occurred prior to the Middle-Late Devonian magmatic activity (Muir *et al.* 1997). The more silicic dominated compositions of the Karamea Batholith is thought to reflect the contamination of mafic magmas by Greenland Group sediments (Muir *et al.* 1996b).

From the above discussion it appears that terrane amalgamation occurred between Late Ordovician and Middle Devonian. Discussion in Chapter 9 suggested that D_1, in both terranes, are of the same orientation and are possibly of the same age: Early-Middle Devonian. An Early-Middle Devonian D_1 event falls within the geochronological and stratigraphic constraints of terrane amalgamation outlined above. It is therefore suggested that D_1 in both terranes is related to terrane amalgamation, and since D_1 is thought to be Early-Middle Devonian in age, so too is terrane amalgamation.

A new plate tectonic model is presented for the Early Paleozoic rocks of Northwest Nelson (Fig. 10.6). The model attempts to integrate the various regional structures and stratigraphic constraints recognised in the two terranes, as well as Gondwanaland margin constraints (previous section). The terrane amalgamation section of the model is based on the coaxiality of fold phases and common strike of faults seen throughout the Early Paleozoic rocks of Northwest Nelson. The terrane amalgamation section also utilises the ideas relating to the uplifted Central Belt hypothesis of Cooper (1979). D_1 structural orientations in both terranes, and east-over-west reverse D_1 associated movement recorded on the Anatoki Fault (Peak 1610 and Kakapo Peak domain), are used to indicate

that east-west shortening was associated with final movements relating to terrane amalgamation.

Please note that when the words "Takaka terrane assemblage" and "Buller terrane assemblage" are mentioned in the model description, these refer to the upper crustal section only (i.e. most of the sediments and volcanics that are exposed today). The model differentiates between the upper and lower crust.

Figure 10.6A

An island arc subduction zone occurs in the Middle-Late Cambrian and forms the basis of the Takaka terrane Cambrian arc assemblage. The volcanic arc and fore-arc assemblages are represented by the Devil River Volcanics Group (represented mainly by the Benson Volcanics) and various formations of the Haupiri Group respectively. Overlying the down-going plate are Junction Formation turbidites of which the source is unknown but could be Gondwanaland if the subduction zone is eastward dipping. These turbidites are incorporated in an accretionary prism and subsequently mélanged (Balloon Mélange). Fore-arc sediments and volcanics may or may not be gently deformed at this stage. Subduction ceases in the mid Late Cambrian, perhaps as a result of ridge subduction (Münker and Cooper 1997), or perhaps as a result of an approaching thickened crust (oceanic or continental); subduction is transferred elsewhere. In both cases, and especially so for an approaching thickened crust, deformation strengthens during the final phase of subduction (not depicted in Figure 10.6A). The strengthening deformation results in fold development and further mélanging in which arc assemblage units are incorporated into the mélange.

The plate tectonic setting shown in Figure 10.6A has been developed to show the origin of pre-D_1 structures in the Cambrian arc assemblage. It is probable, however, that the plate tectonic setting is somewhat more complicated, with some formations of the assemblage indicating a back-arc basin (Pound 1993, Münker and Cooper 1997), and possibly a continental margin subduction system (Pound 1993). Figure 10.6A assumes the down-going plate of the subduction zone was dipping in an east or west direction (present coordinates). This assumption is based on the present lithological distribution of major rock units, particularly that of the Benson Volcanics (see Grindley 1971, 1980 maps), which suggests the island arc was approximately N-S striking. In addition, a N-S

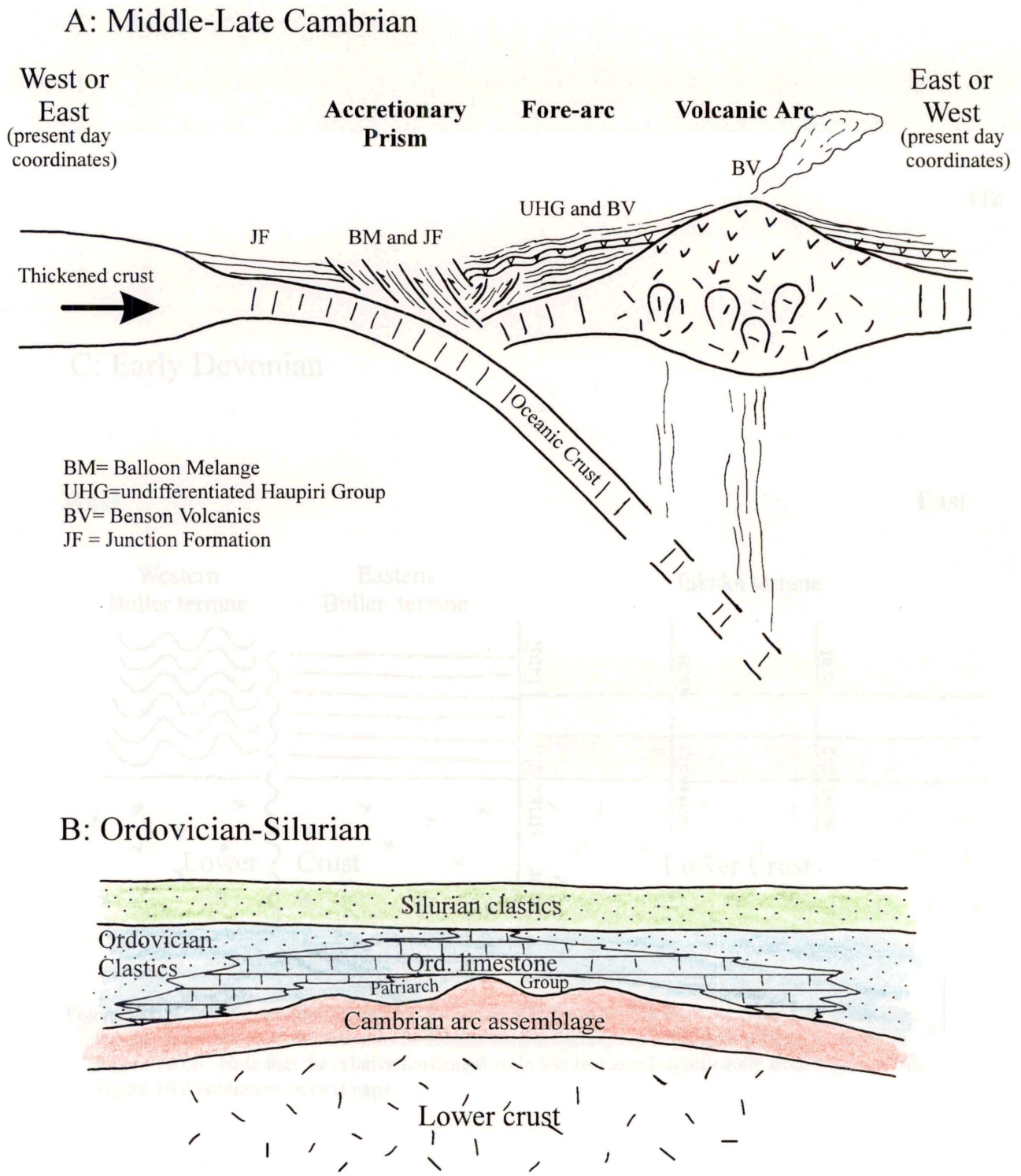

Figure 10.6 (A): Plate tectonic setting for the Takaka terrane in the Middle-Late Cambrian. See text for description. Note that the thickened crust depicted could alternatively be a spreading ridge. Strengthening deformation in the Late Cambrian, prior to the cessation of subduction, is not depicted. (B): Plate tectonic setting for the Takaka terrane in the Ordovician-Silurian. See text for description. Figure 10.6 continues on next page.

C: Early Devonian

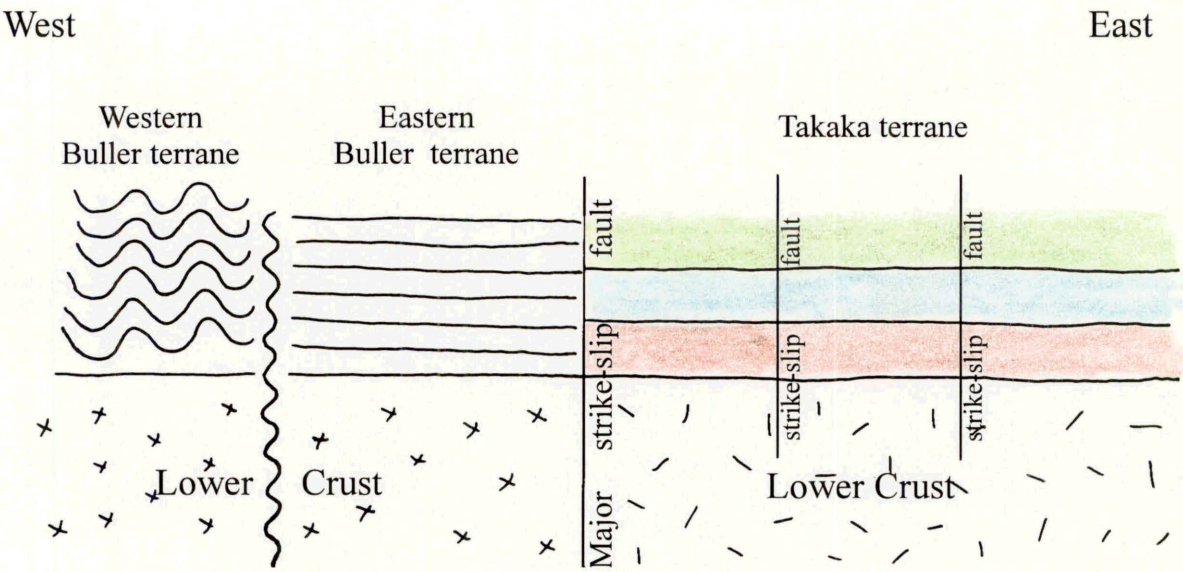

Figure 10.6 (C): Plate tectonic setting for the Buller and Takaka terranes in the Early Devonian. See text for description. Coloured units in Takaka terrane correspond to the coloured units shown in Figure 10.6b. Note that the relative horizontal scale has increased significantly from Figure 10.6b. Figure 10.6 continues on next page.

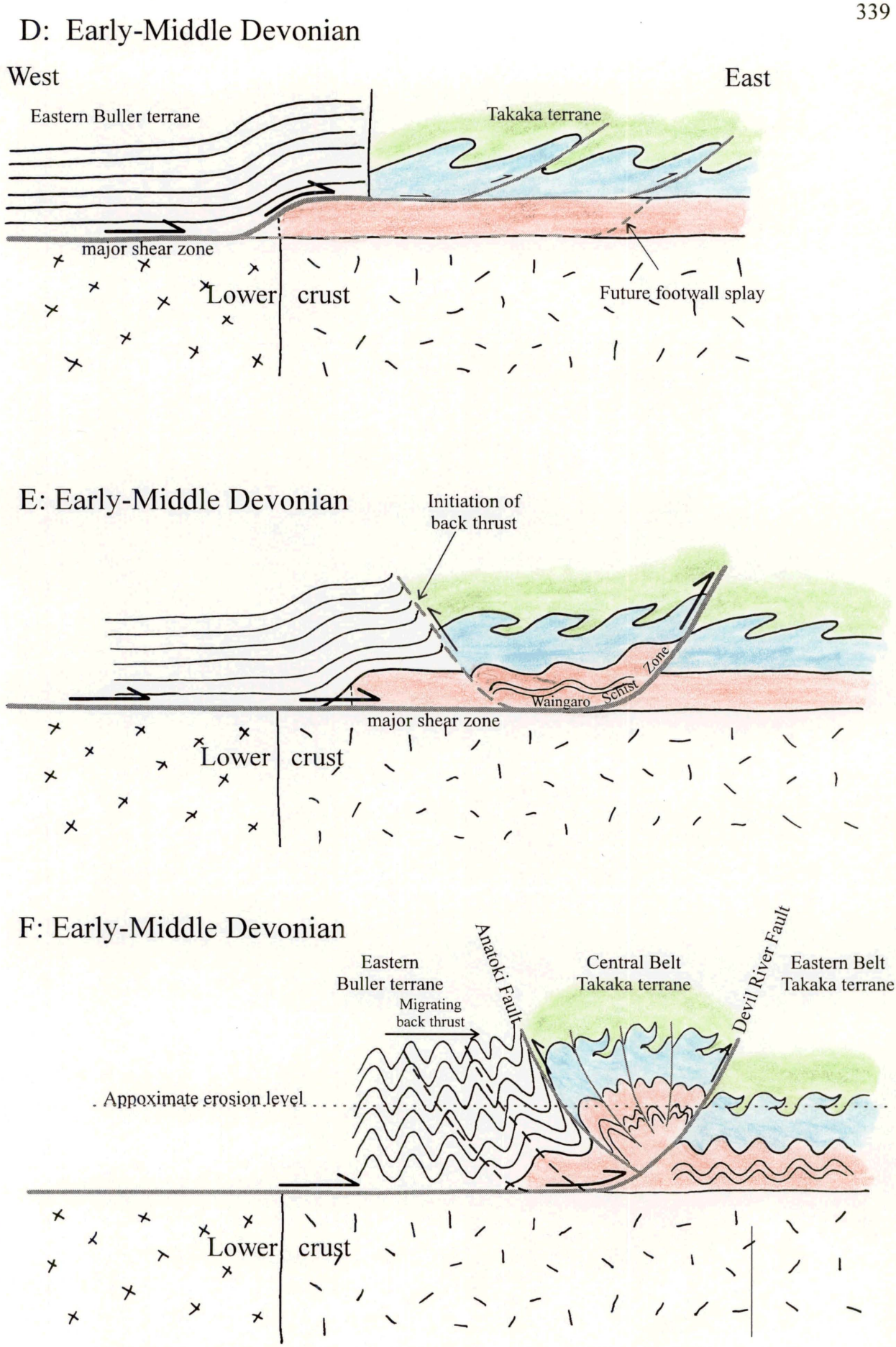

Figure 10.6 (D),(E) and (F): Plate tectonic setting for the Buller and Takaka terranes in the Early to Middle Devonian. Coloured units in Takaka terrane correspond to the coloured units shown in Figure 10.6b. See text for description.

strike of the island arc system is favoured because it explains the coaxiality between the Cambrian and Devonian structures. The lithological distribution does not indicate which way the subduction zone was dipping. For example, the Balloon Mélange, which is interpreted here to represent an accretionary prism, occurs both east and west of the arc-related Benson Volcanics. I suggest that large scale strike-slip movement and thrusting in the Devonian (see below) have rearranged and repeated portions of the Cambrian island arc assemblage, thus making reconstruction of the arc environment from the present arrangement of fault slices difficult.

Figure 10.6B

By the end of the Cambrian, the extinct arc, which now has a thickness comparable to thin continental crust, is within proximity of the Gondwanaland margin. It may have always been there, or it was brought there if the down-going plate of the island arc subduction zone was east dipping.

Following the shutdown of subduction, a latest Cambrian to Silurian passive margin assemblage is deposited above and around the eroded arc (Cooper 1979, 1989; Cooper and Tulloch 1992). Carbonate is preferentially developed along the flanks of the subsiding extinct arc. Clastic sediments probably have a source in Gondwanaland. Geochemistry of the Ordovician sediments in both the Buller and Takaka terranes suggest some slight differences between them (Roser *et al.* 1996). The differences led Roser *et al.* (1996) to speculate that different source regions of Gondwanaland may have been tapped. This speculation is in accord with the Gondwanaland constraints of solution 3. Alternatively, the slight geochemical differences could be viewed as insignificant, and the Takaka and Buller terrane clastics may have shared the same Gondwanaland source in accord with solution 4. The lithological similarity between the Late Ordovician Wangapeka/Baldy Formations (Takaka terrane) and the Golden Bay Group (Buller terrane) certainly supports a common source region. However, as mentioned in Section 10.2.5, the source of the shallow water Silurian Hailes Quartzite for solution 4 remains problematic.

In the Buller terrane, latest Cambrian to Ordovician passive margin sediments relating to a turbidite fan complex along the Gondwanaland margin, are deposited on oceanic crust and/or thin continental crust (Section 10.2.5). At this stage, the Buller terrane is some

distance from the Takaka terrane, and is either inboard (solution 4), or laterally distant (solution 3), from the Takaka terrane with respect to the Gondwanaland margin. In the Late Ordovician-Silurian (probably Silurian), deformation is experienced in the west of the Buller terrane (see Figure 10.6C), the cause of which I suggest is related to the overall plate tectonic regime that leads to final terrane amalgamation in the Early to Middle Devonian. The deformation in the Buller terrane may also be connected with Late Ordovician-Silurian deformation recognised in western Marie Byrd Land, and/or Silurian deformation in the Lachlan Fold Belt.

Figure 10.6C

In the Early Devonian, a convergent strike-slip plate tectonic environment is initiated which leads to eventual terrane amalgamation (D_1). Strike-slip movement, partitioned along N-S striking faults, is thought to almost exclusively dominate the early stages of deformation, and brings the two terranes in to close proximity. Strike-slip movements juxtapose different sections of the original Takaka terrane and lower crust. Convergence dominates the final stages of deformation, and amalgamates the two terranes.

Strike-slip is thought to be a necessary component of movement in order to explain the width of the Takaka terrane arc assemblage (see Section 10.2.5), and it is essential for the Gondwanaland constraints of solution 3. There is no direct evidence for strike-slip tectonics in the Buller and Takaka terranes, and the rocks only record evidence for east-west directed convergence thought to have formed in the final stages of deformation. A similar situation occurs in the modern-day convergent strike-slip plate boundary of New Zealand. The Alpine Fault initiated as a strike-slip fault at about 25Ma, and displacement has become increasingly oblique over the last 10Ma (Norris *et al.* 1990). Associated mylonites record only oblique to near dip-slip movement, and hide the fact that the Alpine Fault has had 480km of strike-slip movement (Norris *et al.* 1990). Similarly, tight folds in the mid to late Tertiary Murchison basin, which occurs almost adjacent to the Alpine Fault, relate to pure compression, rather than strike-slip movements (Lihou 1993). Thus, by comparison with Neogene tectonics, absence of evidence of strike-slip does not preclude an early major strike-slip phase.

Figure 10.6D

In the Early to Middle Devonian, a major shear zone is postulated at the base of the Buller terrane turbidite assemblage which detaches the turbidites from the lower crust and initiates major eastward convergence (D_1) with the Takaka terrane assemblage. The shear zone cuts across the terrane boundary and ramps up over the more competent Cambrian arc assemblage. The shear zone transfers much of its movement in to the rheologically weaker thick Ordovician limestones, and as a result, the entire passive margin assemblage is involved in extensive eastward-directed movement and recumbent folding; the assemblage is detached from the Cambrian arc rocks. Hanging wall splays from the shear zone cut into the passive margin assemblage.

To simplify the model, the contacts between the various major units of the Takaka terrane and the lower crust are shown to be horizontal. In reality, these contacts may be highly irregular as a result of previous strike-slip juxtaposition of Takaka terrane slices. The major shear zone postulated would therefore probably have a series of ramps and flats. In addition, Figure 10.6D shows the base of the Takaka terrane assemblage to be exactly at the same depth as that of the Buller terrane. However, if the depth to the lower crust in the Buller terrane is deeper than in the Takaka terrane, then the above model would suggest a deeper ramp structure at the terrane boundary. Note that if the depth to the lower crust in the Buller terrane is shallower than in the Takaka terrane, then the following model of thin-skinned tectonics does not work.

Figure 10.6E

At some stage, a footwall splay of the major shear zone propagates along the discontinuity which separates the Cambrian arc assemblage from the competent lower crust. The splay then propagates upward towards the surface because it either encounters highly competent rock in the Cambrian arc assemblage (e.g. the main body from which the Cobb Igneous Complex originates), or alternatively, underlying competent crust at a much higher structural level than shown in Figure 10.6E. Most movement is transferred to the footwall splay which becomes the major shear zone. Movement on the shear zone, at the base of the arc assemblage, is ductile, resulting in the formation of the Waingaro Schist Zone. The arc assemblage begins to be thrust upwards along this shear zone, and a back thrust is initiated along the terrane boundary.

Figure 10.6F

As the Buller terrane is pushed eastward, the segment between the eastward migrating back-thrust and the major shear zone is tectonically wedged up. This tectonically wedged segment is represented by the Central Belt; the back-thrust is the Anatoki Fault and the major shear zone is the Devil River Fault. The tectonic wedge resembles the "palm tree/pop-up" structure suggested by Stallard (1994), and the wedging is probably aided by a small component of strike-slip movement. Most N-S striking faults in the tectonic wedge will, however, be reverse in nature. Simultaneously with the onset of the tectonic wedging process, is the initiation of upright N-S trending folds (F_1) in both the Buller and Takaka terrane assemblages. Recumbent folds in the Takaka terrane Ordovician-Silurian rocks are coaxially refolded, and pre-existing Cambrian N-S trending folds are tightened. Axial planar cleavage (S_1) is developed. As wedging continues, the upright folds (F_1) in the majority of the wedge and the immediately adjacent Buller terrane, are tightened and overturned to the west.

Similar tectonic wedges to that portrayed in the model have been well-documented in the Rocky Mountain fold and thrust belt (Fig. 10.7; Price 1986). Back thrusts are common in the Lachlan Fold Belt (Glen 1992), and these are also related to tectonic wedges. In many respects the tectonic wedge of this model resembles the zone of maximum uplift along the modern-day New Zealand plate boundary. This zone of maximum uplift in New Zealand is bounded by the Alpine Fault and the Main Divide Fault. The Main Divide Fault represents a back-thrust off the Alpine Fault (Cox and Findlay 1995), and the Alpine Fault is thought to flatten with depth (Norris *et al.* 1990) . The Devil River Fault may be analogous to the Alpine Fault whereas the Anatoki Fault may be analogous to the Main Divide Fault.

Some of the N-S striking faults, other than the Anatoki and Devil River Faults, may have been inherited features relating to Cambrian subduction that formed the Balloon Mélange and initial phase of folding (pre-D_1). These faults most probably reactivated during terrane amalgamation given that they truncate N-S trending folds (Section 9.4.2). Note, however, the interpretive tectonic contact along the western margin of the Balloon Mélange in the study area appears not to have reactivated (Section 8.6).

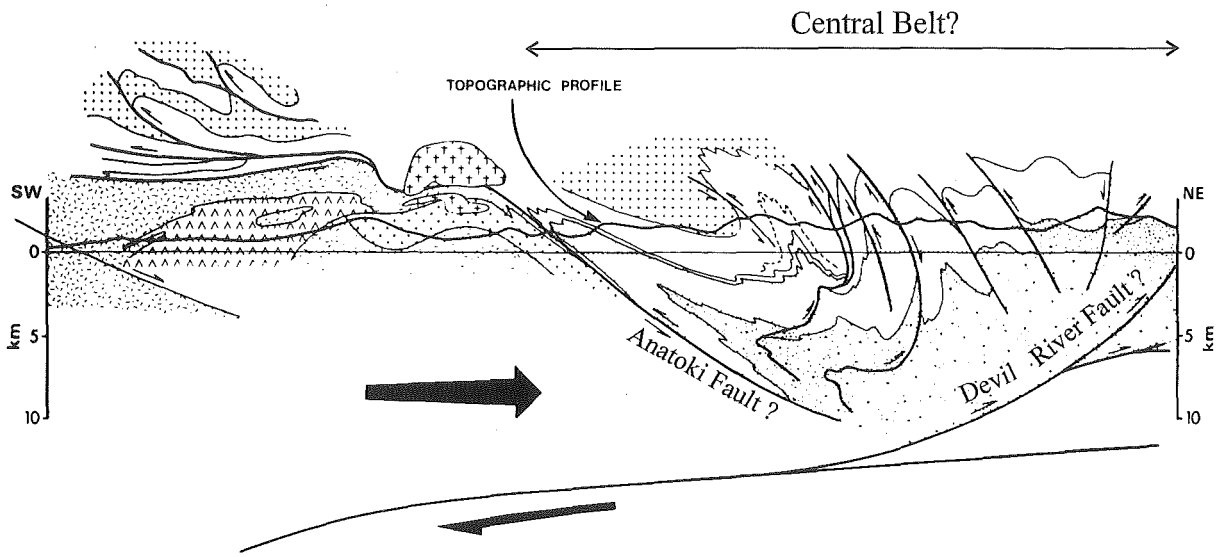

Figure 10.7: A tectonic wedge in the Canadian Cordillera. Note the scale which is comparable with the Central Belt of the Takaka terrane. Could the internal structure of the Central Belt be similar to this? (From Price 1986)

Discussion of model

The model above portrays thin-skinned tectonics where the listric reverse faults flatten with depth and accommodate shortening in the upper crust. The model does not consider the lower crust. Two alternatives for the lower crust are possible. The lower crust in the New Zealand region was not experiencing shortening i.e. the upper crust is completely detached from the lower crust and relate to lower crustal movements elsewhere. Alternatively, the lower crust was experiencing thickening but it is difficult to know what effect this would have on the upper crust. It is possible that lower crustal thickening led to the generation of melts near its base, and that when convergence ceased in the Middle Devonian, the melts were injected to higher levels forming the Karamea Batholith and Riwaka Complex in the Buller and Takaka terranes respectively. It is interesting to note that the Silurian to Devonian granitoids in the Lachlan Fold Belt, are also attributed to crustal thickening in the lower crust (Fergusson and Coney 1992). The Karamea Batholith is extremely elongate in a N-S direction and parallel to the Anatoki Fault (see Fig. 1.1), suggesting that its location is fundamentally controlled by pre-existing N-S striking structures associated with terrane amalgamation.

Strong Late Silurian to Middle Devonian deformation is well-known in the possible Buller and Takaka terrane correlatives of southeastern Australia (Bowning-Bindian and Tabberabberan Orogenies, Fergusson and Coney 1992) and Tasmania (Powell and Baillie 1992), and it is suggested that the events there probably relate to the Early-Middle Devonian terrane amalgamation in New Zealand. In addition, post-tectonic Devonian granitoids in the Ballarat-Bendigo zone and Tasmania overlap with those in New Zealand (Fergusson *et al.* 1986; Powell and Baillie 1992).

The model implies that the Takaka terrane passive margin assemblage is autochthonous with respect to the Cambrian arc assemblage because it requires the least amount of plate tectonic gymnastics in the Paleozoic. An autochthonous passive margin assemblage is supported by a geochemical link between the Patriarch Group and the Cambrian arc assemblage (Roser *et al.* 1996). If an allochthonous passive margin assemblage is assumed (i.e. a separate terrane), then the small pause in sedimentation between it and the Cambrian arc assemblage (mid Late Cambrian) must be considered fortuitous. Nevertheless, an allochthonous passive margin assemblage remains a possibility (see

Section 2.4) but a complex model of plate tectonics in the Lower Paleozoic would need to be invoked including the possibility, based on structural information, that the passive margin assemblage originated from entirely west of the arc, and tectonically displaced over it.

The fault-bounded slices now recognised in the Takaka terrane (Cooper and Tulloch 1992) are interpreted to result from a combination of both the early strike-slip movement and the tectonic wedging process.

The relationship of the Early Devonian Baton Formation to terrane amalgamation remains unresolved. If indeed the Baton Formation basal conglomerate contains some clasts derived from the Cambrian arc assemblage, as suggested by Willis (1965) and Grindley (1978) (no petrographic work has been reported to substantiate this claim), then the Cambrian arc assemblage was uplifted somewhat earlier than the above model suggests, and an unconformity at the base of the Baton Formation is implied. Nevertheless, deformation relating to terrane amalgamation is still considered to continue during, and after, deposition of the Baton Formation, because it is folded and penetratively cleaved. Alternatively, if a break in sedimentation is not recorded at the base of the Baton Formation, as suggested by M. A. Bradshaw (pers. comm. 1996), then the clasts may possibly originate from an unknown source; the timing of the uplifted Central Belt would consequently be unconstrained by the Baton Formation and may have occurred after its deposition.

The model does not account for the Pikikiruna Schist and its higher grade of metamorphism, and it is difficult to explain its occurrence. It may be that the schist formed early on in the Devonian deformation and was brought to higher structural levels by movement on hanging wall splays depicted in Figure 10.6D.

10.4 Cretaceous tectonics

The Buller terrane has marked Gondwanaland affinities with terranes in Antarctica and Australia, and given that the Takaka terrane probably amalgamated with the Buller terrane prior to the Late Devonian, suggests the Western Province had become an autochthonous part of Gondwanaland from the Carboniferous onwards (Bradshaw 1993).

The Median Tectonic Zone (Fig. 1.1 insert) is interpreted to be a disrupted remnant of magmatic arcs that developed along the Mesozoic Gondwanaland margin (Bradshaw 1994; Kimbrough *et al.* 1993). The fundamental orientation of the margin is thought to have been NW-SE trending (Bradshaw *et al.* 1996). The Eastern Province (Fig. 1.1 insert) consists of a series of Permian to Cretaceous accreted terranes.

The Cretaceous was an extremely active and changeable tectonic period in New Zealand (Bradshaw 1989). In the Early Cretaceous, the New Zealand continent was under the influence of oblique convergent margin tectonics when the Phoenix plate subducted obliquely, with a dextral component, below the accreted terranes and the Cretaceous New Zealand continent (Bradshaw 1989). It was around this time that the Western Province, Median Tectonic Zone, and Eastern Province achieved close proximity to each other (Bradshaw 1993). The Early Cretaceous Separation Point Batholith is thought to have developed as a result of the Median Tectonic Zone colliding with the Western Province (Muir *et al.* 1995). Oblique convergent margin tectonics continued in the Eastern Province until 105 ± 5Ma where the tectonic regime then changed to one of extension oriented in a NE-SW direction (Bradshaw 1989; Luyendyk 1995; Bradshaw *et al.* 1996). Extension led to the development of NW trending core complexes (Tulloch and Kimbrough 1989; Gibson *et al.* 1988), sedimentary basins (Laird 1993), and dike swarms (Bishop 1992) in the Western Province (recognised south of Northwest Nelson). Extension continued until at least 85Ma when at that time the Tasman Sea opened and a widespread marine transgression ensued (Bradshaw 1989). The ~118Ma Separation Point Batholith provides a maximum age for the cessation of convergence related tectonics in the Western Province. A minimum age of inception of extension related tectonics in the Western Province is provided by the ~101.5Ma Stitts tuff (Bradshaw *et al.* 1996), a unit at the base of a NW trending extensional sedimentary basin (Laird 1993). Waight *et al.* (1997) suggests the 114-109Ma plutonism in the Hohonu Batholith (southeast of Greymouth) is a result of crustal thinning and extension following overthickening during collision of the Median Tectonic Zone with the Western Province. If the plutonism model of Waight *et al.* (1997) is accepted, then regional extension in the Western Province could have begun as early as 114Ma. It is interesting to note that the Mt Olympus Pluton of the Separation Point Suite was emplaced contemporaneously with magmatism in the Hohonu Batholith.

A major Z shaped double bend in the basement terranes occurs in the New Zealand continent, and is best outlined by the Median Tectonic Zone (see Fig. 1.1 insert). Bradshaw *et al.* (1996) has put forward a strong case that the dextral Z bend developed between intrusion of the Separation Point Batholith and prior to deposition of extensional sedimentary basins i.e. between ~118Ma and ~101Ma. The case is based on the fact that the Gondwanaland margin becomes sharply reoriented by almost 90° as the Cenozoic plate boundary is approached, whereas Cretaceous extension indicators show no reorientation close to the plate boundary. In addition, it is unlikely that the Gondwanaland margin double bend is original because of the improbability that the elongate Separation Point Batholith was emplaced at a high angle to the regional NW trending orientation of the Gondwanaland margin (Bradshaw *et al.* 1996).

D_2 of this study is thought to have formed shortly after ~111Ma (Chapter 3). D_2 is a dextral non-coaxial strain along the reactivated Anatoki Fault zone in the Boulder Lake domain. D_2 may be possible supporting evidence for dextrally directed oroclinal bending in the mid-Cretaceous. Alternatively, D_2 may predate oroclinal bending, in which case the Anatoki Fault would be NW striking, and relate to dextral shear associated with the oblique dextrally directed subduction of the Phoenix plate (see Fig. 3 of Bradshaw 1989). Other N-S striking faults known to have been active in the Early Cretaceous (Section 9.4.2) may also relate to either oroclinal bending or oblique convergent margin tectonics.

D_3 of this study is thought to have occurred sometime between D_2 and the latest Cretaceous (Chapter 9). D_3, as well as other post-Early Cretaceous pre-latest Cretaceous folds and crenulation cleavages recognised elsewhere in the Takaka terrane, indicates compression in the mid-Cretaceous. The regional geology of the Western Province indicates a tectonic extensional regime occurred certainly since ~101Ma but possibly as early as 114Ma. D_3 may therefore indicate convergent margin related compressive forces were operating in Northwest Nelson until a minimum age of ~101Ma, implying a D_3 age between ~101 and ~111Ma. Alternatively, it may represent a previously unrecognised compressional event that occurred simultaneously with extension elsewhere in the Western Province. It is possible this compressional event may be intimately related to oroclinal bending.

10.5 Conclusions

In the study area, three major deformation events are recognised in both the Buller and Takaka terranes, and these can be correlated across the terrane boundary so that the three consecutive deformation events are the same in each terrane.

The first major deformation, D_1, is represented by N-S trending large scale folds and an axial planar slaty cleavage, as well as east-over-west reverse ductile movement recorded on the Anatoki Fault. D_1 structures relate to other N-S trending structures in both terranes, and based on constraints outside the study area, these structures indicate an Early to Middle Devonian, east-west compressional event. The second deformation, D_2, is represented by a well-developed foliation observed in the northernmost domain of the study area (Boulder Lake domain). The foliation expresses a zone of non-coaxial ductile deformation which is associated with Early Cretaceous dextral strike-slip reactivation of the Anatoki Fault soon after emplacement of the ~111Ma Mt Olympus Pluton. Reactivation on a southern segment of the Anatoki Fault, which postdates the intrusion of the ~137Ma Crow Granite, as well as ductile/brittle movement in other segments, is possibly related to D_2 movements. The third deformation, D_3, is represented mainly by mesoscale folds and an axial planar crenulation cleavage. D_3 is thought to be mid-Cretaceous in age, and the orientation of the structures suggests shortening in a NW-SE direction. The Anatoki Fault was further reactivated, brittlely, in the Late Cenozoic.

The Balloon Mélange, occurring exclusively in the Cambrian arc assemblage of the Takaka terrane, records two deformations. The first deformation predates D_1 and was associated with the mélanging when sediments were essentially unlithified; the deformation is thought to have occurred in the Late Cambrian. The second deformation formed when the mélange was lithified, and the orientation of associated structures suggests it can be correlated with D_1. The occurrence of the pre-D_1 deformation, together with new evidence of pre-D_1 folding from outside the study area (C. Münker pers. comm. 1997), suggests that some of the N-S trending folds in the arc assemblage developed initially in the Late Cambrian. The orientation of extension directions associated with the pre-D_1 and D_1 strain are more-or-less the same.

It is proposed here that the Takaka terrane was juxtaposed against the Buller terrane along a convergent strike-slip plate boundary in the Early to Middle Devonian. In this model, the passive margin assemblage of the Takaka terrane is considered autochthonous to the Cambrian arc assemblage, and much of the original terrane has been removed by strike-slip movement. D_1 structures represent the final expression of terrane amalgamation which was dominated by east-west convergence. This convergence involved thin-skinned tectonics in which the Central Belt of the Takaka terrane is interpreted as an uplifted tectonic wedge. The Anatoki Fault is a back-thrust related to a major shear zone represented by the Waingaro Schist/Devil River Fault. This model accounts for most of the mid-Paleozoic structures observed in both terranes.

Pre-D_1 structures in the Takaka terrane are thought to be related to compressional forces in the accretionary wedge and fore-arc setting associated with a Cambrian island arc subduction system. D_2 is thought to relate either to the oroclinal bending of New Zealand, or alternatively, to oblique convergent margin tectonics in the Early Cretaceous. The setting in which D_3 originated is less certain, but D_3 does indicate that Northwest Nelson was undergoing further shortening along NW-SE lines in the mid-Cretaceous.

Analyses of microscale structures, including shear-sense indicators, have provided important detailed information on the various deformation events recognised. Fabric analysis of ankerite and calcite has provided new information on microscale deformation. Twin laws in ankerite, which are the same as those in dolomite, have been used to determine paleostress axes. Twin analyses of ankerite porphyroblasts in D_2 non-coaxial tectonites provide good evidence of microscale strain partitioning during which the porphyroblasts accommodated pure shear. Twinning in ankerites relates to major deformation events and occurs at temperatures above ~250°C. Analyses of calcite tectonites suggest that other plastic deformation mechanisms, other than twinning, are responsible for *c*-axes preferred orientations in natural low temperature shear zones. In such cases, preferred orientations of calcite *c*-axes are not reliable shear-sense indicators.

ACKNOWLEDGEMENTS

Firstly I would like to thank my supervisors, David Shelley and John Bradshaw, for providing advice throughout the last four years and giving critical reviews of the drafts. David provided detailed insights into matters microscopic whereas John counter-balanced this by providing insights into matters relating to "the big picture". Particular thanks goes to David who provided stimulating arguments on various subject matters both geological and otherwise. Thanks to John who walked to Boulder Lake in lightning time! Other members of the academic staff at the University of Canterbury thanked are: Roddy Muir for encouraging me to chase the Crow Granite, Steve Weaver for giving me a room of my own, David Bell for providing social entertainment, and Jarg Pettinga for just being there.

Many thanks goes to Roger Cooper (IGNS) and Carsten Münker (Göttingen University) for sharing their valuable knowledge of Northwest Nelson geology. I really really thank Roger for his continued encouragement and interest in my work. Thanks also to Mark Rattenbury (IGNS) for exposing me to regional geological mapping in the Tasman Wilderness Area, an experience I will treasure for a long time. Tod Waight and Roland Maas (La Trobe University) are thanked for offering to do Rb-Sr dating.

A humungous thank you to Rob Spiers for fantastic and quickly made thin-sections. Rob encouraged and helped me make ultrathin-sections and Ar-Ar thick-sections (work in progress) and I really thank him for that. Thanks also to Kerry Swanson for photography and helping me overcome the many difficulties experienced with the outdated photomicrograph camera. Michael Finnemore is thanked for matters relating to that horrible computer program called AutoCAD, and computer assistance in general. Chris Chamberlain is thanked for help with drafting techniques "long live the drafting pen!". Cathy Knight, Arthur Nicholas, Stephen Brown, and Nigel Newman are thanked for various technical assistance.

The Mason Fund is gratefully acknowledged for providing valuable financial assistance towards thesis printing costs and field related expenses, in particularly, helicopter support. Without this assistance, this project could not have been possible. The Department of Conversation is thanked for the use of their huts, especially the new and luxurious Boulder Lake Hut, and for turning Northwest Nelson into a National Park (well done!).

An enormously large thank you to Jock and Bev Harrison who provided the spa pool, scallops, and luxury accommodation in Takaka between periods of wet weather in the field. A big thanks also to Ian Harrison and Helen Donaldson who helped in the field. Thanks to all you guys for your continued encouragement.

Thanks Mum, Dad, Michael and Tracey for your support and encouragement. Thanks for fixing the car Dad, washing the clothes Mum, arguing about politics Michael, and talking about life in general Tracey. Thanks Tracey for helping with the grammar.

I would like to give a big thank you to all my student friends who helped me get through the last four years: Tod Waight, thanks for being a room buddy early on in the piece; Steven Beresford, thanks for not being my room buddy later on in the piece; Alastair Ritchie, thanks for being someone to lecture to; Mark Armstrong, thanks for bringing the

crudity of the department to new lows; Helen Grant, thanks for keeping the "Retro" scene alive and well; Jeremy Webb, thanks for talking too much; Kay Cooper, thanks for matters political and encouraging me not to measure *c*-axes; Rod Burt, thanks for keeping the Star Wars trilogy alive and discussing aspects of geology I know nothing about (i.e. volcanics!); and Simon Ward, thanks for procrastinating and helping me with CorelDraw. Thanks also go to Nescafé.

Many thanks to Aaron Stallard and Don Maclean, who I joined forces with in 1993 to conquer Northwest Nelson geology (at least a bit of it!). Thanks also to undergraduate geology related friends that have left New Zealand a long time ago for greener pastures: Liz Kennedy, Mathew Perry, Ian Harrison, Alastair Syme, Carl Starks. "I'll join you soon!". For keeping me sane during my write-up period, thanks go to David Graham who took me into the hills every few weeks.

I would like to express my gratitude to Rod Burt and Chris Chamberlain for reviewing parts of the thesis, and to David Graham and Liz Martin (also Kim) for colouring in the maps. Brilliant work guys!

And now for a big serious hug. A very sincere thanks goes to Helen Donaldson, Liz Martin, Jen Autridge, Rob Spiers, Kim Rollison, Alastair Syme, Liz Kennedy, Nigel Robinson, Helen Grant, and Ingrid Hertel **for being true friends** and helping me get through a particularly difficult time in my life that occurred towards the end of the project.

Finally, a thank you to Fran Muckle; it's because of you that I am now a much stronger person. "The pain now is part of the happiness then.....thats the deal" (Shadowlands).

Alternative abstract for this thesis:

"Once upon a time there was some rocks in New Zealand; they got pushed against some other rocks in New Zealand, and got all squished up and crumbly and mangled. Then lots of German tourists walked all over them. The end." (from Tod Waight 1996) ☺

REFERENCES

Adams, C. J. 1986: Geochronological studies of the Swanson Formation of Marie Bryd Land, West Antarctica, and its correlation with northern Victoria Land, East Antarctica and South Island, New Zealand. *New Zealand Journal of Geology and Geophysics 29*: 345-358.

Adams, C. J.; Harper, C. T.; Laird, M. G. 1975: K-Ar ages of low grade metasediments of the Greenland and Waiuta Groups in Westland and Buller, New Zealand. *New Zealand Journal of Geology and Geophysics 18*: 39-48.

Adams, C. J.; Kruezer, H. 1984: Potassium-argon age studies of slates and phllites form the Bowers and Robertson Bay terranes, north Victoria Land, Antartica. *Geologishes Jahrbuch B60*: 265-288.

Adams, C. J.; Seward, D.; Weaver, S. D. 1995: Geochronology of Cretaceous granites and metasedimentary basement on Edward VII Peninsula, Marie Byrd Land, West Antarctica. *Antarctic Science 7*: 265-277.

Bal, A; Lewis, D.W. 1994: A Cretaceous-early Tertiary macrotidal estuarine-fluvial succession: Puponga Coal Measures in Whanganui Inlet, onshore Pakawau Sub-basin, Northwest Nelson, New Zealand. *New Zealand Journal of Geology and Geophysics 37*: 287-307.

Barber, A. J.; Tjokrosapoetro, S.; Charlton; T. R. 1986: Mud volcanoes, shale diapirs, wrench faults, and melanges in accretionary complexes, Eastern Indonesia. *American Association of Petroleum Geologists Bulletin 70*: 1729-1741.

Barber, D. J.; Wenk, H. R. 1979: Deformation twinning in calcite, dolomite, and other rhombohedral carbonates. *Physics and chemistry of minerals 5*: 141-165.

Barber, D. J.; Heard, H. C.; Wenk, H. R. 1981: Deformation of dolomite single crystals from 20-800°C. *Physics and chemistry of minerals 7*: 271-286.

Behrmann, J. H. 1983: Microstructure and fabric transitions in calcite tectonites from Sierra Alhamilla (Spain). *Geologische Rundschan 72*: 605-618.

Bell, A. M. 1981: Vergence: an evaluation. *Journal of Structural Geology 3*: 197-202.

Bell, J. M.; Webb, E. J. H.; Clarke, E. de C. 1907: The Geology of the Parapara Subdivision, Karamea, Nelson. *New Zealand Geological Survey Bulletin 3*.

Bell, T. H. 1985: Deformation partitioning and porphyroblast rotation in metamorphic rocks: a radical reinterpretation. *Journal of Metamorphic Geology 3*: 109-118.

Bell, T. H.; Rubenach, M. J. 1980: Crenulation cleavage development - evidence for progressive bulk inhomogeneous shortening from "millipede" microstructures in the Robertson River Metamorphics. *Tectonophysics 68*: T9-T15.

Bell, T. H.; Johnson, S. E. 1992: Shear sense: a new approach that resolves conflicts between criteria in metamorphic rocks. *Journal of Metamorphic Geology 10*: 99-124.

Benson, W. N. 1956: Cambrian Rocks and Fossils in New Zealand. *El Systema Cambrico, su Paleogeografia y et Problema de su Base 2 (2)*: 285-288. 20th International Geological Congress, Mexico.

Bishop, D. G. 1967: The structural geology of the Mount Burnett Dolomite deposit, Northwest Nelson. *New Zealand Journal of Geology and Geophysics 10*: 870-891.

Bishop, D. G. 1968: Reclined folds and coaxial refolding in the Paleozoic rocks of Northwest Nelson. *New Zealand Journal of Geology and Geophysics 11*: 593-607.

Bishop, D. G. 1971: Sheet S1, S3, and pt. S4 Farewell-Collingwood (1st ed.) Geological Map of New Zealand 1: 63 360. Map and notes (15 p.). Wellington, New Zealand. Department of Scientific and Industrial Research

Bishop, D. G. 1992: Extensional tectonism and magmatism during the middle Cretaceous to Paleocene, north Westland, New Zealand. *New Zealand Journal of Geology and Geophysics 35*: 81-91.

Bishop, D. G.; Bradshaw, J. D.; Landis, C. A. 1985: Provisional terrane map of South Island, New Zealand. *In*: Howell, D. G. *ed.* Tectonostratigraphic Terranes of the Circum-Pacific Region. *Circum Pacific Council for Energy and Mineral Resources earth science series 1*: 515-521.

Borradiale, G. J.; Bayle, M. B.; Powell, C. McA. 1982: Atlas of Deformational and Metamorphic Rock Fabrics, Springer-Verlag, Berlin, 551p.

Bradshaw, J.D. 1982: S13 - Cobb: a review of the new map and the structural interpretation of the Central Belt rocks of S13 and S8. *New Zealand Journal of Geology and Geophysics 25*: 371-375.

Bradshaw, J. D. 1989: Cretaceous geotectonic patterns in the New Zealand region. *Tectonics 8*: 803-820.

Bradshaw, J. D. 1993: A review of the Median Tectonic Zone: terrane boundaries and terrane amalgamation near the Median Tectonic Line. *New Zealand Journal of Geology and Geophysics 36*: 117-125.

Bradshaw, J. D.; Andrews, P. B.; Field, D. B. 1983: Swanson Formation and related rocks of Marie Byrd Land and comparison with the Robertson Bay Group of north Victoria Land. *In*: Oliver, R. L.; James, P. R.; Jago, J. B. *eds.* Antarctic Earth Science. Australia Academy of Science, Canberra. Pp. 274-279.

Bradshaw, J. D.; Weaver, S. D.; Laird, M. G. 1985: Suspect terranes and Cambrian tectonics in Northern Victoria Land, Antartica. *In*: Howell, D. G. *ed.* Tectonostratigraphic Terranes of the Circum-Pacific Region. *Circum Pacific Council for Energy and Mineral Resources earth science series 1*: 467-479.

Bradshaw, J. D.; Weaver, S. D.; Muir, R. J. 1996: Mid-Cretaceous oroclinal bending of New Zealand terranes. *New Zealand Journal of Geology and Geophysics 39*: 461-468.

Bradshaw, J. D.; Pankhurst, R. J.; Weaver, S. D.; Storey, B. C.; Muir, R. J.; Ireland, T. R. in press: New Zealand superterranes recognised in Marie Byrd Land and Thurston Island. *Terra Antartica.*

Bradshaw, M. A. 1995: Stratigraphy and structure of the Lower Devonian rocks of the the Waitahu and Orlando Outliers, near Reefton, New Zealand, and their relationship to the Inangahua Outlier. *New Zealand Journal of Geology and Geophysics 38*: 81-92.

Brathwaite, R.L. 1968a: The geology of the Boulder Lake area, Northwest Nelson. Part 1 - The Anatoki Formation. *New Zealand Journal of Geology and Geophysics 11*: 78-91.

Brathwaite, R.L. 1968b: The geology of the Boulder Lake area, Northwest Nelson. Part 2 - The Mount Olympus granite pluton. *New Zealand Journal of Geology and Geophysics 11*: 92-122.

Brown, K.; Westbrook, G. K. 1988: Mud diapirism and subcretion in the Barbados Ridge accretionary complex: The role of fluids in accretionary processes. *Tectonics 7*: 613-640.

Brown, K. M.; Orange, D. L. 1993: Structural aspects of diapiric melange emplacement; the Duck Creek diapir. *Journal of Structural Geology 15*: 831-847.

Burkhard, M. 1993: Calcite twins, their geometry, appearance and sgnificance as stress-strain markers and indicators of tectonic regime: a review. *Journal of Structural Geology 15*: 351-368.

Busch, J. P.; van der Pluijm; B. A. 1995: Calcite textures, microstructures and rheological properties of marble mylonites in the Bancroft shear zone, Ontario, Canada. *Journal of Structural Geology 17*: 677-688.

Campbell, H. J.; Smale, D.; Grapes, R.; Landis, C.; Hoke, L. 1996: Parapara Permian: sequence and history reconsidered. *Geological Society of New Zealand Miscellaneous Publication 91A*: 39

Challis, A.; Grapes, R.; Palmer, K. 1995: Chromian Muscovite, Uvarovite and Zincian Chromite: products of regional metasomatism in Northwest Nelson, New Zealand. *The Canadian Mineralogist 33*: 1263-1284.

Chester, F. M. 1989: Dynamic recrystallisation in semi-brittle faults. *Journal of Structural Geology 11*: 847-858.

Clark, R. H.; Vella, P.; Waterhouse, J. B. 1967: The Permain and Parapara Peak, Northwest Nelson. *New Zealand Journal of Geology and Geophysics 8*: 232-246.

Cloos, E. 1947: Oolite deformation in the South Mountain fold, Maryland. *Geological Society of America Bulletin 58*: 843-918.

Coleman, A. C. 1977: Structure and stratigraphy of Lower Paleozoic rocks of the Mount Patriarch-Crow River area, Northwest Nelson, New Zealand. *New Zealand Journal of Geology and Geophysics 20*: 401-424.

Coleman, A. C. 1981: Part sheets S18, S19, S25 and S26 Wangapeka. Geological Map of New Zealand 1: 63 360. Map and notes (39 p.). Department of Scientific and Industrial Research, Wellington, New Zealand.

Collins, W. J.; Vernon, R. H. 1992: Paleozoic arc growth, deformation and migration across the Lachlan Fold Belt, southeastern Australia. *Tectonophysics 214*: 381-400.

Coney, P. J. 1992: The Lachlan belt of eastern Australia and Circum-Pacific tectonic evolution. *Tectonophysics 214*: 1-25.

Coney, P. J.; Edwards, A.; Hine, R.; Morrison, F.; Windrim, D. 1990: The regional tectonics of the Tasman orogenic system, eastern Australia. *Journal of Structural Geology 12*: 519-543.

Cooper, R. A. 1979a: Lower Paleozoic rocks of New Zealand. *Journal of the Royal Society of New Zealand 9*: 29-84.

Cooper, R. A. 1979b: Ordovician geology and graptolite faunas of the Aorangi Mine area, Northwest Nelson, New Zealand. *New Zealand Geological Survey Paleontological Bulletin 47*. 127p.

Cooper, R. A. 1984: Lower Paleozoic Terranes. *Geological Society of New Zealand Miscellaneous Publication 31A*.

Cooper, R. A. 1986: Central Belt structure: an alternative interpretation. *Geological Society of New Zealand Miscellaneous Publication 34*: 11-13.

Cooper, R. A. 1989: Lower Paleozoic terranes of New Zealand. *Journal of the Royal Society of New Zealand 19*: 73-112.

Cooper, R. A. 1991: In the beginning.....The earliest history of East Australia and New Zealand. *Geological Society of New Zealand newsletter 92*: 47-52.

Cooper, R. A. 1993: Northwest Nelson - basement geology. Part 1: The Takaka Terrane - background and introduction. *Geological Society of New Zealand Miscellaneous Publication 79B*: 76-84.

Cooper, R. A. 1997: The Balloon Melange and Early Paleozoic history of the Takaka Terrane, New Zealand. *Terrane Dynamics - 97 conference extended abstract volume*: 46-49.

Cooper, R. A. *in prep*. Early Paleozoic geology *In* Rattenbury, M. (compiler), Nelson sheet. Geological map of New Zealand 1:250 000 (2nd ed.). Institute of Geological and Nuclear Sciences, Lower Hutt, N.Z.

Cooper, R. A.; Wright, A. J. 1972: Silurian rocks and fossils at Hailes Knob, Northwest Nelson, New Zealand. *New Zealand Journal of Geology and Geophysics 15*: 318-335.

Cooper, R. A.; Grindley, G. W. 1982. Late Proterozoic to Devonian sequences of southeastern Australia, Antarctica and New Zealand and their correlation. *Geological Society of Australia Special Publication 9*. 103p.

Cooper, R. A.; Tulloch, A. J. 1992: Early Paleozoic terranes in New Zealand and their relationship to the Lachlan Fold Belt. *Tectonophysics 214*: 129-144.

Cowan, D. S. 1985: Structural styles in Mesozoic and Cenozoic melanges in the western Cordillera of North America. *Geological Society of America Bulletin 96*: 451-462.

Cox, S. C.; Findlay, R. H. 1995: The Main Divide Fault Zone and its role in formation of the Southern Alps, New Zealand. *New Zealand Journal of Geology and Geophysics 38*: 489-499.

Cox, S. F.; Etheridge, M. A. 1983: Crack-seal fibre growth mechanisms and their significance in the development of oriented layer silicate microstructure. *Tectonophysics 92*: 147-170.

Crawford, A. J. 1984: Geochemistry of Cambrian volcanics in some dispersed fragments of East Gondwanaland foldbelts. Seventh Australian Geological Convention, Sydney. Geological Society of Australia, Abstracts 12.

Crawford, A. J.; Keays, R.R. 1978: Cambrian greenstone belts in Victoria; marginal seacrust slices in the Lachlan Fold Belt of southeastern Australia. *Earth and Planetary Science Letters 41*: 197-208.

Crawford, A. J.; Keays, R.R. 1987: Petrogenesis of Victorian Cambrian tholeiites and implications for the origin of associated boninites. *Journal of Petrology 28*: 1075-1109.

Crawford, A. J.; Berry, R. F. 1992: Tectonic implications of Late Proterozoic-Early Paleozoic igneous rock associations in western Tasmania. *Tectonophysics 214*: 37-56.

Crook, K. S. W.; Feary, D. 1982: Development of New Zealand according to the forearc model of crustal evolution. *Tectonophysics 87*: 65-107.

Dallmeyer, R. D.; Wright, T. O. 1992: Diachronous cleavage development in the Robertson Bay terrane, northern Victoria Land, Antarctica: Tectonic implications. *Tectonics 11*: 437-448.

de Bresser, B. H. P. 1989: Calcite c-axes tectures along the Gavernie thrust zone, central Pyrenees. *Geologie En Mijnbouw 68*: 367-375.

Deer, W. A.; Howie, R. A.; Zussman, J. 1962: Rock Forming Minerals, Vol. 3 (sheet silicates) and Vol. 5 (Non-silicates), Longman, London. Vol. 3: 270p., Vol 5: 371p.

Durney, D. W.; Ramsay, J. G. 1973: Incremental strains measured by syntectonic crystal growths. *In* De Jong, K. A.; Scholten, R. *eds.* Gravity and Tectonics, Wiley, New York, 67-95.

Etchecopar, A; Malavielle, J. 1987: Computer models of pressure shadows: a method for strain measurement and shear-sense determination. *Journal of Structural Geology 9*: 667-677.

Evans, J. P. 1988: Deformation mechanisms in granitic rocks at shallow crustal levels. *Journal of Structural Geology 10*: 437-443.

Faure, G. 1986: Principles of Isotope Geology (*2nd edition*). Wiley, New York. 589p.

Fergusson, C. L.; Gray, D. R.; Cas, R. A. F. 1986: Overthrust terranes in the Lachlan Fold Belt, southeastern Australia. *Geology 14*: 519-522.

Fergusson, C. L.; Coney, P. J. 1992: Convergence and intraplate deformation in the Lachlan Fold Belt of southeastern Australia. *Tectonophysics 214*: 417-439.

Fleuty, M. J. 1964: The description of folds. *Geological Association Proceedings 75*: 461-492.

Flinn, D. 1962: On folding during three dimensional progressive deformation. *Quarterly Journal of the Geological Society of London 118*: 385-428.

Flöttman, T.; Kleinschmidt, G. 1991: Kinematics of major structures of North Victoria and Oates Lands, Antarctica. *Memorie della Società Geologica Italiana 46*: 273-282.

Folk, R. L. 1965: Some aspects of recrystallisation in ancient limestones. *In*: Pray, L. C.; Murray, R. C. *eds*. Dolomitization and limestone diagenesis. *Society of Economic Paleontologists amd Mineralogists Special Publication 13*: 14-48.

Friedman, M.; Conger, F. G. 1964: Dynamic interpretation of calcite twin lamallae in a naturally deformed fossil. *Journal of Geology 72*: 361-368.

Freidman, M., Higgs, N. G. 1981: Calcite fabrics in experimental shear zones. *In*: Carter, N. L.; Freidman, M.; Logan, J. M.; Stearns, D. W. *eds*. Mechanical Behaviour of Crustal Rocks. The Handin Volume. American Geophysical Union. *Geophysical Monograph 24*: 11-27.

Ghent, E. D. 1968: Petrology of metamorphosed pelitic rocks and quartzites, Pikikiruna Range, Northwest Nelson, New Zealand. *Transactions of the Royal Society of New Zealand 5*: 193-213.

Gibson, G. M.; McDougall, I.; Ireland, T. R. 1988: Age constraints on metamorphism and the development of a metamorphic core complex in Fiordland, southern New Zealand. *Geology 16*: 405-408.

Glen, R. A. 1992: Thrust, extensional and strike-slip tectonics in an evolving Paleozoic orogen - a structural synthesis of the Lachlan Orogen of southeastern Australia. *Tectonophysics 214*: 341-380.

Glen, R. A.; Scheibner, E.; VandenBerg, A. H. M. 1992: Paleozoic intraplate escape tectonics in Gondwanaland and major strike-slip duplication in the Lachlan orogen of southeastern Australia. *Geology 20*: 795-798.

Grapes, R.; Stedman, H. 1993: Northwest Nelson - basement geology. Part 3: Cretaceous metasomatism of Onekaka Schist, Northwest Nelson. *Geological Society of New Zealand Miscellaneous Publication 79B*: 137-146.

Gray, D. R.; Willman, C. E. 1991: Deformation in the Ballarat Slate Belt, central Victoria, and implications for crustal structure across southeastern Australia. *Australian Journal of Earth Science 38*: 171-201.

Griggs, D. T.; Paterson, M. S.; Heard, H. C.; Turner, F. J. 1960: Annealing recrystallisation in calcite crystals and aggregates. *Geological Society of America Memoir 79*: 21-37.

Grindley, G. W. 1961: Sheet 13 - Golden Bay (1st ed.) Geological Map of New Zealand 1: 250 000. Department of Scientific and Industrial Research,Wellington, New Zealand.

Grindley, G. W. 1971: Sheet S8 - Takaka (1st ed.) Geological Map of New Zealand 1: 63 360. Map and notes (19 p.). Department of Scientific and Industrial Research, Wellington, New Zealand.

Grindley, G. W. 1978: *In*: R. P. Suggate, G. R. Stevens, Te Punga, M. T. *eds*. Geology of New Zealand. Vol. 1. Department of Scientific and Industrial Research, Wellington, New Zealand. Pp. 118-135.

Grindley, G. W. 1980: Sheet S13 - Cobb (1st ed.) Geological Map of New Zealand 1: 63 360. Map and notes (46 p.) Department of Scientific and Industrial Research, Wellington, New Zealand.

Grindley, G. W. 1986: Paleozoic tectonic history, Northwest Nelson. *Geological Society of New Zealand Miscellaneous Publication 34*: 20-22.

Grindley, G.W.; Davey, F. J. 1982: The reconstruction of New Zealand, Australia and Antarctica. *In*: Craddock, C. *ed.* Antarctic Geoscience. Unversity of Wisconsin Press, Madison. Pp. 15-29

Groshong, R. H.; Pfiffner, O. A.; Pringle, L. R. 1984: Strain partitioning in the Helvetic thrust belt of eastern Switzerland from the leading edge to the internal zone. *Journal of Structural Geology 6*: 5-18.

Guglielmo, G. 1993: Interference between pluton expansion and non-coaxial tectonic deformation: three dimensional computer model and field implications. *Journal of Structural Geology 15*: 593-608.

Handin, H.; Griggs, D. T. 1951: Deformation of Yule Marble (Part 2). *Geological Society of America Bulletin 62*: 863-886.

Handin, H.; Fairbairn, H. W. 1955: Experimental deformation of Hasmark dolomite. *Geological Society of America Bulletin 66*: 1257-1274.

Hanmer, S. 1990: Natural rotated inclusions in non-ideal shear. *Tectonophysics 176*: 245-255.

Hanmer, S.; Passchier, C. 1991: Shear-sense indicators: a review. *Geological Survey of Canada paper 90-17*: 72p.

Harrison, I. S. 1993: *The structure of the Buller Terrane west of the Anatoki Thrust, Upper Cobb Valley, Northwest Nelson, New Zealand.* Unpublished M.Sc. thesis, lodged in the library, University of Canterbury, New Zealand.

Harrison, M. T.; McDougall, I. 1980: Investigations of an intrusive contact, Northwest Nelson, New Zealand - 1. Thermal, chronological and isotopic contraints. *Geochimica et cosmochimica acta 44*: 1985-2003.

Heard, H. C. 1963: Effects of large changes in strain rate in the experimental deformation of Yule Marble. *Journal of Geology 71*: 162-195.

Heitzmann, P. 1987: Calcite mylonites in the Central Alps "rootzone". *Tectonophysics 135*: 207-215

Henderson, J.; Grange, L. I.; Macpherson, E. O. 1924: Motueka Subdivision. *New Zealand Geological Survey, 18th Annual Report* Pp. 4-6.

Henderson, J.; Grange, L. I.; Macpherson, E. O. 1925: Motueka Subdivision. *New Zealand Geological Survey, 19th Annual Report* Pp. 4-5.

Henderson, J.; Grange, L. I. 1926: Motueka Subdivision. *New Zealand Geological Survey, 20th Annual Report* Pp. 4-5.

Henderson, J.; Macpherson, E. O.; Grange, L. I. 1959: The Geology of Motueka Subdivision. *New Zealand Geological Survey Bulletin 35.* (compiled by G. Shaw)

Hickey, K. A. 1986: *Geology of Paleozoic and Tertiary rocks between Upper Takaka and the Waingaro River, Northwest Nelson.* Unpublished M.Sc. thesis, lodged in the library, University of Auckland, New Zealand.

Higgs, D. V.; Handin. J. W. 1959: Experimental deformation of dolomite single crystals. *Geological Society of America Bulletin 70*: 245-278.

Hippertt, J. F. M. 1994: Microstructures and *c*-axis fabrics indicative of quartz dissolution in sheared quartzites and phyllonites. *Tectonophysics 229*: 141-163.

Hoke, L; Grapes, R. 1996: Structural and metamorphic history of the Parapara Peak area, Northwest Nelson. *Geological Society of New Zealand Miscellaneous Publication 91A*: 89

Hudleston, P. J. 1973: Fold morphology and some geometrical implications of theories of fold development. *Tectonophysics 16*: 1-46.

Johnson, S. E.; Bell, T. H. 1996: How useful are "millipede" and other similar porphyroblast microstructures for determining synmetamorphic deformation histories? *Journal of Metamorphic Geology 14*: 15-28.

Johnson, S. E.; Moore, R. R. 1996: De-budding the "millipede" porphyroblast microstructure: a serial thin-section study and 3-D computer animation. *Journal of Metamorphic Geology 14*: 3-14.

Johnston, M. R. 1974: Geology of the Mount Arthur District, Northwest Nelson. *New Zealand Journal of Geology and Geophysics 17*: 75-92.

Johnston, M. R. 1990: Geology of the St Arnaud District, southeast Nelson (Sheet N29). *New Zealand Geological Survey bulletin 99*. 199 p. and map. Wellington, New Zealand. Department of Scientific and Industrial Research.

Keble, R.A.; Benson, W.N. 1929: Ordovician Graptolites of Northwest Nelson. *Transactions of the New Zealand Institute 59*: 840-863.

Kimbrough, D.L.; Tulloch, A.J.; Geary, E.; Coombs, D.S.; Landis, C.A. 1993: Isotopic ages from the Nelson region of South Island New Zealand: crustal structure and definition of the Median Tectonic Zone. *Tectonophysics 225*: 433-448.

Lafrance, B.; White, J. C.; Williams, P. F. 1994: Natural calcite c-axis fabrics: an alternative interpretation. *Tectonophysics 229*: 1-18.

Laird, M. G. 1972: Sedimentology of the Greenland Group in the Paparoa Range, West Coast, South Island. *New Zealand Journal of Geology and Geophysics 15*: 372-393.

Laird, M. G. 1993: Cretaceous continental rifts: New Zealand region. *In*: Ballance, P. F. *ed.* South Pacific sedimentary basins. Sedimentary basins of the world 2. Elsevier, Amsterdam. Pp. 37-49.

Laird, M. G.; Shelley, D. 1974: Sedimentation and early tectonic history of the Greenland Group, Reefton, New Zealand. *New Zealand Journal of Geology and Geophysics 17*: 839-854.

Landis, C. A.; Coombs, D. S. 1967: Metamorphic belts and orogenesis in southern New Zealand. *Tectonophysics 4*: 501-518.

Laurent, P. 1987: Shear-sense determination on striated faults from *e* twin lamellae in calcite. *Journal of Structural Geology 9*: 591-595.

Law, R. D.; Knipe, R. J.; Dayan, H. 1984: Strain path partitioning within thrust sheets: microstructural and petrofabric evidence from the Moine Thrust zone at Loch Eriboll, northwest Scotland. *Journal of Structural Geology 6*: 477-497.

Lawver, L. A.; Gahagan, L. M. 1994: Constraints on timing of extension in the Ross Sea region. *Terra Antartica 1(3)*: 545-552.

Lihou, J. C. 1993: The structure and deformation on the Murchison Basin, South Island, New Zealand. *New Zealand Journal of Geology and Geophysics 36*: 95-105.

Lisle, R. J. 1977: Estimation of the tectonic strain ratio from the mean shape of deformed elliptical markers. *Geologie en mijnbouw 56*: 140-144.

Lister, G. S.; Dornsiepen, U. F. 1982: Fabric transitions in the Saxony granulite. *Journal of Structural Geology 4*: 81-92.

Ludwig, K. R. 1990: ISOPLOT: A plotting and regression program for radiogenic isotope data, for IBM-PC compatible computers. *United States Geological Survery Openfile Report 88-557.*

Luyendyk, B. P. 1995: Hypothesis for Cretaceous rifting of east Gondwana caused by slab capture. *Geology 23*: 373-376.

Maclean, D. R. 1994: *The geology and geochemistry of the Cambrian Devil River Volcanics, Anatoki Range, Northwest Nelson.* Unpublished M.Sc. thesis, lodged in the library, University of Canterbury, New Zealand.

McClay, K. 1987: The Mapping of Geological Structures. *Geological Society of London Handbook.* Open University Press, England. 161p.

McKay, A. 1879: The Baton River and Wangapeka Districts and Mount Arthur Range. *New Zealand Geological Survey, reports of geological exploration, 1878-1979 12*: 97-121.

Mainprice, D.; Bouchez, J. L.; Blumenfeld, P.; Tubia, J. M.: 1986 Dominant *c* slip in naturally deformed quartz: implications for dramatic plastic softening at high temperature. *Geology 14*: 819-822.

Miyashiro, A. 1973: Metamorphism and Metamorphic Belts, George Allen and Unwin, London. 492p.

Muir, R. J.; Ireland, T. R.; Weaver, S. D.; Bradshaw, J. D. 1992: Ion microprobe (SHRIMP) U-Pb zircon dating of Western Province granitoids. *Geological Society of New Zealand Miscellaneous Pulication 63A*: 110.

Muir, R. J.; Ireland, T. R.; Weaver, S. D.; Bradshaw, J. D. 1994: Ion microprobe U-Pb zircon geochronology of granitic magmatism in the Western Province of the South Island, New Zealand. *Chemical Geology (Isotope Geoscience Section) 113*: 171-189.

Muir, R.J.; Weaver, S.D.; and Bradshaw, J.D.; Eby, G. N.; Evans, J. A. 1995: The Cretaceous Separation Point batholith, New Zealand: granitoid magmas formed by melting of mafic lithosphere. *Journal of the Geological Society, London 152*: 689-701.

Muir, R. J.; Ireland, T. R.; Weaver, S. D.; Bradshaw, J. D. 1996a: Ion microprobe dating of Paleozoic granitoids: Devonian magmatism in New Zealand and correlations with Australia and Antarctica. *Chemical Geology 127*: 191-210.

Muir, R.J.; Weaver, S.D.; and Bradshaw, J.D.; Eby, G. N.; Evans, J. A.; Ireland, T. R. 1996b: Geochemistry of the Karamea Batholith, New Zealand and comparisons with the Lachlan Fold Belt granites of SE Australia. *Lithos 39*: 1-20

Muir, R. J.; Bradshaw, J. D.; Ireland, T. R.; Jongens, R; Weaver, S. D. 1997: Terrane docking in western New Zealand. *Terrane Dynamics - 97 conference extended abstract volume*: 121-123.

Muir, R. J.; Ireland, T. R.; Weaver, S. D.; Bradshaw, J. D.; Waight, T. E.; Jongens, R; in press: SHRIMP U-Pb geochronology of Cretaceous magmatism in NW Nelson-Westland, South Island, New Zealand. *New Zealand Journal of Geology and Geophysics.*

Münker, C. 1993: *Geology and geochemistry of metavolcanic rocks west of Cobb Reservoir, Northwest Nelson, New Zealand.* Unpublished Diploma thesis, University of Göttingen, Germany.

Münker, C; Cooper, R. A. 1997: The early Paleozoic Takaka terrane, New Zealand, as part of the Australian/Antarctic Gondwana margin: new insights from the trace elements and isotope geochemistry of Cambrian volcanics. *Terrane Dynamics - 97 conference extended abstract volume*: 124-128.

Nathan, S. 1978a: Sheets S31 and pt S32 Buller-Lyell (1st ed.) Geological Map of New Zealand 1:63 360. Map and notes (32 p.) Department of Scientific and Industrial Research, Wellington.

Nathan, S. 1978b: Sheets S44 Greymouth (1st ed.) Geological Map of New Zealand 1:63 360. Map and notes (36 p.) Department of Scientific and Industrial Research, Wellington.

Newman, N. A. 1979: *Mineralization at Mount Owen, Central Nelson.* Unpublished M.Sc. thesis, lodged in the library, University of Canterbury, New Zealand.

Newman, J.; Mitra, G. 1994: Fluid-influenced deformation and recrystallisation of dolomite at low temperatures along a natural fault zone, Mountain City window, Tennessee. *Geological Society of America Bulletin 106*: 1267-1280.

Nissen, H. U. 1964: Dynamic and kinematic analysis of deformated crinoid stems in a quartz greywacke. *Journal of Geology 72*: 346-360.

Norris, R. J.; Koons, P. O.; Cooper, A. F. 1990: The obliquely-convergent plate boundary in the South Island of New Zealand: implications for ancient collision zones. *Journal of Structural Geology 12*: 715-725.

Ongley, M.; Macpherson, E. O. 1923: The Geology and Mineral Resources of the Collingwood Subdivision, Karamea Division. *New Zealand Geological Survey Bulletin 25.*

Park, J. 1890: On the Geology of Collingwood County, Nelson. *New Zealand Geological Survey, reports of geological exploration, 1888-1889, 20*: 186-243.

Paterson, M. S. 1976: Some current aspects of experimental rock deformation. *Philosophical Transactions of the Royal Society of London, Series A, 283*: 163-172.

Paterson, S. R.; Tobisch, O. T.; Vernon, R. H. 1991: Emplacement and deformation of granitoids during volcanic arc construction in the Foothills terrane, central Sierra Nevada, California. *Tectonophysics 191*: 89-110.

Pickering, K. T.; Agar, S. M.; Ogawa, Y. 1988: Genesis and deformation of mud injections containing chaotic basalt-limestone-chert associations: examples from the SW Japan forearc. *Geology 16*: 881-885.

Poirier, J. P. 1985: Creep of Crystals. Cambridge University Press, Cambridge. 260p.

Pound, K. S. 1993: *Geology of the Lower Paleozoic Haupiri Group Rocks, Cobb Valley area, Northwest Nelson, New Zealand (with a special emphasis on the provenance and sedimentology of the sedimentary rocks).* Unpublished Ph.D. thesis, lodged in the library, University of Otago, New Zealand.

Powell, C. McA. 1979: A morphological classification of rock cleavage. *Tectonophysics 58*: 21-34.

Powell, C. McA. 1983: Tectonic relationship between the Late Ordovician and Late Silurian paleogeographies of southeastern Australia. *Journal of the Geological Society of Australia 30*: 353-373.

Powell, C. McA., Ballie, P. W. 1992: Tectonic affinity of the Mathinna Group in the Lachlan Fold Belt. *Tectonophysics 214*: 193-209.

Powell, N.G. 1983: Waingaro Schist zone between the Anatoki and Takaka Rivers, Northwest Nelson. *Geological Society of New Zealand Miscellaneous Publication 30A*.

Powell, N.G. 1984: *Metamorphism within a part of the Waingaro schist zone, Northwest Nelson, New Zealand.* Unpublished M.Sc. thesis, lodged in the library, University of Auckland, New Zealand.

Powell, N.G. 1985: Devil River Fault and Anatoki Thrust: Their associated structures, mechanisms and senses of movement. *Geological Society of New Zealand Miscellaneous Publication 32A*: 70.

Powell, N. G. 1986: Timing of metamorphism and deformation in the Takaka Terrane, with notes on metamorphic zonation. *Geological Society of New Zealand Miscellaneous Publication 34*: 33-35.

Price, R. A. 1986: The southeastern Canadian Cordillera: thrust faulting, tectonic wedging, and delamination of the lithosphere. *Journal of Structural Geology 8*: 239-254.

Ramsay, J. G. 1980: Shear zone geometry: a review. *Journal of Structural Geology 2*: 83-99.

Ramsay, J. G.; Huber, M. I. 1983: The Techniques of Modern Structural Geology, (Vol. 1: Strain Analysis). Academic Press, London. 452p.

Ramsay, J. G.; Huber, M. I. 1987: The Techniques of Modern Structural Geology, (Vol. 2: Folds and Fractures). Academic Press, London. 452p.

Rattenbury, M. 1996: Buller Terrane deformation and granitic intrusion, Northwest Nelson. *Geological Society of New Zealand Miscellaneous Publication 91A*: 148

Raymond, L. A. 1984: Classification of melanges. *Geological Society of America, Special Paper 198*: 7-20.

Rennison, M. W. 1992: *The petrology, structure and geochemistry of the eastern margin of Mount Olympus Pluton, Northwest Nelson, New Zealand.* Unpublished B.Sc.(Hons) thesis, lodged in the library, University of Canterbury, New Zealand.

Roder, G. H.; Suggate, R. P. 1990: Sheet L29BD - Upper Buller Gorge. Geological Map of New Zealand 1:50 000. Map and notes (52 p.) Department of Scientific and Industrial Research, Wellington.

Roser, B. P.; Cooper, R. A.; Nathan, S.; Tulloch, A. J. 1996: Reconnaissance sandstone geochemistry, provenance, and tectonic setting of the lower Paleozoic terranes of the West Coast and Nelson, New Zealand. *New Zealand Journal of Geology and Geophysics 29*: 1-16.

Rutter, E. H.; Casey, M.; Burlini, L. 1994: Preferred crystallographic orientation development during the plastic and superplastic flow of calcite rocks. *Journal of Structural Geology 16*: 1431-1446.

Schmid, S. M.; Paterson, M. S.; Boland, J. N. 1980: High temperature flow and dynamic recrystallisation in Carrara Marble. *Tectonophysics 65*: 245-280.

Schmid, S. M.; Casey, M.; Starkey, J. 1981: The microfabric of calcite tectonites from the Helvetic nappes (Swiss Alps). *In*: McClay, K. R.; Price, N. J. *eds.* Thrust and Nappe Tectonics. *Geological Society of London. Special Publication 9*: 151-158

Schmid, S. M.; Casey, M. 1986: Complete fabric analysis of some commonly observed quartz c-axis patterns. *In*: Hobbs, B. E.; Heard, H. C. *eds*. Mineral and Rock Deformation: Laboratory Studies. The Paterson Volume. American Geophysical Union. *Geophysical Monograph 36*: 263-286.

Schmid, S. M.; Panozzo, R.; Bauer, S. 1987: Simple shear experiments on calcite rocks: rheology and microfabric. *Journal of Structural Geology 9*: 747-778.

Shelley, D. 1975a: Metamorphic belts and volcanic arc migration in New Zealand. *Nature 258*: 668-672.

Shelley, D. 1975b: Temperature and metamorphism during cleavage and fold formation of the Greenland Group, north of Greymouth. *Journal of the Royal Society of New Zealand 5*: 65-75.

Shelley, D. 1981: The Pikikiruna nappe, Northwest Nelson. *New Zealand Journal of Geology and Geophysics 24*: 593-602.

Shelley, D. 1984: Takaka River recumbent fold complex, Nelson, New Zealand. *New Zealand Journal of Geology and Geophysics 27*: 139-149.

Shelley, D. 1989: CALCSTRESS: a program that calculates compression and tension directions from calcite U-stage data. *Computers and Geosciences 15*: 269-273.

Shelley, D. 1991: Structure, fabric, and metamorphism of Arthur Marble, Pikikiruna Range, Nelson, New Zealand. *New Zealand Journal of Geology and Geophysics 34*: 385-396.

Shelley, D. 1993: Igneous and metamorphic rocks under the microscope: classifications, textures, and mineral preferred orientations. Chapman and Hall, London. 445p.

Sibson, R. H. 1977: Fault rocks and fault mechanisms. *Journal of the Geological Society of London 133*: 191-214.

Simpson, C.; Schmid, S. M. 1983: An evaluation of criteria to deduce the sense of movement in sheared rocks. *Geological Society of America Bulletin 94*: 1281-1288.

Stallard, A. R. 1994: *An investigation of the geology and tectonics of the Bay Schist in the context of the Buller Terrane - Takaka Terrane boundary.* Unpublished M.Sc. thesis, lodged in the library, University of Canterbury, New Zealand.

Stallard, A. R.; Shelley, D. 1995: Quartz *c*-axes parallel to stretching directions in low-grade metamorphic rocks. *Tectonophysics 249*: 31-40.

Stewart, M. 1988: *The geology of the Cobb Reservoir area, Northwest Nelson.* Unpublished M.Sc. thesis, lodged in the library, University of Canterbury, New Zealand.

Stump, E. 1995: The Ross Orogen of the Transantarctic Mountains. Cambridge University Press. 284p.

Stump, E.; White, A. J. R.; Borg, S. G. 1986: Reconstruction of Australia and Anatarctica: evidence from granites and recent mapping. *Earth and Planetary Science Letters 79*: 348-360.

Tobisch, O.T.; Paterson, S. R. 1988: Analysis and interpretation of composite foliations in areas of progressive deformation. *Journal of Structural Geology 10*: 745-754.

Torrey, C. E. 1984: *The geology and mineralisation of Mount Snowden, Northwest Nelson, New Zealand.* Unpublished manuscript, held by the Department of Geological Sciences, University of Canterbury, New Zealand.

Tullis, J.; Yund, R. A. 1977: Experimental deformation of dry Westerly granite. *Journal of Geophysical Research 82*: 5705-5718

Tulloch, A. J. 1988: The Anatoki Thrust and the Mount Olympus Pluton - Who pushed who? *Geological Society of New Zealand Newsletter 82*: 43-44.

Tulloch, A. J. 1992: Petrology of the Sams Creek peralkaline granite dike, Takaka, New Zealand. *New Zealand Journal of Geology and Geophysics 35*: 193-200.

Tulloch, A. J.; Brathwaite, R. L. 1986: C7: Granitoid rocks and mineralisation of Westland-West Nelson, New Zealand. *New Zealand Geological Survey Record 13*: 65-92.

Tulloch, A. J.; Kimbrough, D.L. 1989: The Paparoa metamorphic core complex, Westland, New Zealand, Cretaceous extension associated with fragmentation of the Pacific margin of Gondwana. *Tectonics 8*: 1217-1234.

Turner, F. J. 1953: Natural and dynamic interpretation of deformation lamallae in calcite of three marbles. *American Journal of Science 251*: 276-298.

Turner, F. J.; Grigg, D. T.; Heard, H. C. 1954: Experimental deformation of calcite crystals. *Geological Society of America Bulletin 65*: 883-934.

Turner, F. J.; Grigg, D. T.; Clark, R. H.; Dixon, R. H. 1956: Deformation of Yule Marble, Part VII: Development of oriented fabrics at 300°C-500°C. *Geological Society of America Bulletin 67*: 1259-1294.

Turner, F. J.; Weiss, L. E. 1963: Structural analysis of Metamorphic Tectonites, McGraw-Hill, New York. 545p.

Urai, J. L.; Means, W. D.; Lister; G. S. 1986: Dynamic recrystallisation of minerals. *In*: Hobbs, B. E.; Heard, H. C. *eds*. Mineral and Rock Deformation: Laboratory Studies. The Paterson Volume. American Geophysical Union. *Geophysical Monograph 36*: 161-199.

van der Pluijm, B. A. 1991: Marble mylonites in the Bancroft shear zone, Ontario, Canada: microstructure and deformation mechanisms. *Journal of Structural Geology 13*: 1125-1135.

Waight. T. E., Weaver, S.D.; Ireland, T. R.; Maas, R.; Muir, R. J.; Shelley, D. 1997: Field characteristics, petrography, and geochronology of the Hohonu Batholith and the adjacent Granite Hill Complex, North Westland, New Zealand. *New Zealand Journal of Geology and Geophysics 40*: 1-14.

Ward, C. M. 1984: *Geology of the Dusky Sound area, Fiordland, with emphasis on the structural-metamorphic development of some porphyroblastic staurolite pelites.* Unpublished Ph.D. thesis lodged in the library, University of Otago New Zealand.

Ward, C. M. 1986: The Fanny and Goodyear terranes of southern Fiordland and their relations with west Nelson. *Geological Society of New Zealand Miscellaneous Publication 34*: 46-48.

Weaver, S. D.; Bradshaw, J. D.; Laird, M. G. (1984): Geochemistry of Cambrian volcanics of the Bowers Supergroup and implications for the Early Paleozoic tectonic evolution of northern Victoria Land, Antarctica. *Earth and Planetary Science Letters 68*: 128-140.

Wenk, H. R.; Venkitasubramanyan, C. S.; Baker, D. W. 1973: Preferred orientations in experimentally deformed limestone. *Contributions to Mineralogy and Petrology 38*: 81-114.

Wenk, H. R.; Takeshita, T.; Bechler, E., Erskine, B. G.; Matthies, S. 1987: Pure shear and simple shear calcite textures. Comparison of experimental, theoretical and natural data. *Journal of Structural Geology 9*: 731-745.

Westbrook, G. K. 1982: The Barbados ridge complex: tectonics of a mature forearc system. *In*: Leggett, J. K. *ed.* Trench-forearc geology: sedimentation and tectonics on modern and ancient active plate margins. *Geological Society of London Special publication 10*: 275-290.

Williams, L. A.: Turner, F. J.; Gilbert, C. M. 1982: Petrography, an introduction to the study of rocks in thin sections. 2nd ed. W. H. Freeman, San Francisco, 626p.

Willis, I. 1965: Stratigraphy and structure of the Devonian strata at Baton River, New Zealand. *New Zealand Journal of Geology and Geophysics 8*: 35-48.

Windle, S. J.; Craw, D. 1991: Gold mineralisation in a syntectonic granite dike, Sams Creek, Northwest Nelson, New Zealand. *New Zealand Journal of Geology and Geophysics 34*: 429-440.

Wright, A. J.; Cooper, R. A.; Simes J. E. 1994: Cambrian and Ordovician faunas and stratigraphy, Mt. Patriarch, New Zealand. *New Zealand Journal of Geology and Geophysics 37*: 437-476.

Zen, E-an. 1961: The zeolite facies: an interpretation. *American Journal of Science 259*: 401-409.

Zwart, H.J. 1962: On the determination of polymetamorphic mineral associations and its application of the Bosost area (Central Pyrenees). *Geologische Rundschan 52*: 38-65.

APPENDIX 1: Definition of Anatoki Formation and undifferentiated Haupiri Group

As highlighted by Roser *et al.* (1996), there is currently debate on the definition of the Anatoki Formation and its type area. This appendix outlines the original definition of Anatoki Formation and suggests how the formation name should be used today. The appendix also justifies why I use the term "undifferentiated Haupiri Group" for rocks immediately east of the Anatoki Fault between the Boulder Lake and Kakapo Peak domains.

Original definition of the Anatoki Formation

In the Central Belt, Grindley (1961) mapped volcanic-rich sandstones, grits, and shales, with thick bands of conglomerates and volcanics, and named them Anatoki Formation. The three principal areas of Anatoki Formation were the Wangapeka Valley, Cobb Reservoir, and the area immediately east of the Anatoki Fault between Boulder Lake and Kakapo Peak. These areas were lithologically correlated and assumed to be of the same age. Brathwaite (1968a) described the Anatoki Formation at Boulder Lake in detail, and Grindley (1971) nominated this area as the type area. Unfortunately, the type area is completely fault bounded and unfossiliferous. As a result, Grindley (1961, 1971, 1980) assigned a Late Cambrian age for the type area based on stratigraphic relationships of lithologic correlatives seen elsewhere.

Recent work

Rocks lithologically correlated as Anatoki Formation by Grindley (1971, 1980) have been reinterpreted as Junction Formation in the Cobb Reservoir area (Stewart 1988; Pound 1993) and Buller terrane lithologies north of the Aorere River (Cooper in prep.). As a result, the only documented age constraints for remaining areas of Anatoki Formation are:

- a conformable contact with overlying fossiliferous latest Cambrian siltstone of the Patriarch Formation at Mt Patriarch in the Wangapeka Valley (~60km south of the type area) (Wright *et al.* 1994).

- The fossiliferous Late Cambrian Mytton beds, a possible facies variant of the Anatoki Formation, conformably underlying fossiliferous lowermost Ordovician Summit Limestone at Mt Mytton in the Cobb Valley (Cooper 1989; Roser *et al.* 1996).

In light of these documentations, Roser *et al.* (1996) made a distinction between Anatoki Formation rocks that are well-constrained stratigraphically but occur some distance from the type area (Mt Mytton and Mt Patriarch areas), and "Anatoki Formation" for rocks where the stratigraphic age and position is uncertain (i.e. the type area).

It is the opinion of R. A. Cooper (pers. comm. 1996) and myself that the sediments between Boulder Lake and Kakapo Peak may in fact be equivalents of the Tasman Formation and/or other formations of the Haupiri Group which interfinger with the Benson Volcanics. The main justification is that volcanics petrologically similar to the Benson Volcanics interfinger with the sediments at Kakapo Peak (C. Münker pers. comm. 1996). In addition, there are strong sedimentological similarities, for example in the presence of voluminous mass flow conglomerates. Given that the Patriarch Group does not contain volcanics, the presence of interfingering volcanics (and coarse volcanically-derived epiclastics) seen at Peak 1610 and Kakapo Peak domains link the sediments closely to the Haupiri Group. Thus, for the purposes of this thesis, I feel it is best to term the sediments between Boulder Lake and Kakapo Peak as undifferentiated Haupiri Group, and not Anatoki Formation. Future detailed stratigraphic and sedimentary petrographic work is necessary.

Suggested definition of Anatoki Formation

On the new 1:250 000 Nelson sheet, Cooper (in prep.) proposes a redefinition of the Anatoki Formation using the Mt Patriarch area as the type section which would conserve the name for use in its present stratigraphic position and age. The rocks there are chert-rich and volcanic-rich sandstone, siltstone, and granule conglomerate, and calcareous siltstones and sandstones. On the new Nelson sheet, the rocks between Boulder Lake and Kakapo Peak are to be designated undifferentiated Haupiri Group.

APPENDIX 2: Rb-Sr analytical methods and results

Two samples (RJ81 and RJ280) were selected for muscovite-whole rock Rb-Sr isotope dating. The samples selected come from the D_2 zone of deformation in undifferentiated Haupiri Group rocks of the Boulder Lake domain. Approximately 1kg of fresh rock from each sample was crushed using a hydraulic ram and sent to Dr. Tod Waight of La Trobe University, Melbourne, for further preparation and Rb-Sr isotope determination.

Analytical methods (T. E. Waight pers. comm. 1997)

Muscovite was separated using conventional heavy liquid and magnetic separation techniques, then hand-picked to ensure purity. The muscovite separate was ultrasonically washed in acetone and water to remove any heavy liquid contaminants. Whole rock and mineral separate samples were spiked with a $^{87}Rb/^{84}Sr$ tracer and analysed by isotope dilution. Samples were dissolved, and Rb and Sr separated using conventional HF-$HN0_3$-HCL dissolution and cation exchange column chemical techniques; whole rocks were dissolved in high pressure teflon bombs whereas micas were dissolved in open teflon beakers. Samples were analysed on a Finnigan MAT262 thermal ionisation mass spectrometer in multicollector mode at the School of Earth Sciences, La Trobe University. Sr was loaded in 4µl at H_3PO_4 onto single Ta filaments, and Rb was loaded in 1-2µl of 1M HCl onto double Re filaments. Spike stripping and isotope dilution calculations were performed off-line. Procedural blanks were negligible relative to sample sizes, and no blank corrections were applied to the data.

Analytical reproducibility errors are the same as that applied for Waight et. al. (1997), and are ±0.5% for $^{87}Rb/^{86}Sr$, and ±0.01% for $^{87}Sr/^{86}Sr$ based on repeated analyses of standard solutions. Both percentage errors are 2σ values of reproducibility that have been well-established at La Trobe University.

Isotope compositions for the muscovite separates, with respect to the whole rock compositions, resulted in a less than ideal separation between data points for two point isochron calculation, and consequently there are large errors in the calculated age. This was particularly so for RJ280 (see table) and thus leaching of the muscovite separate for RJ280 was undertaken by Dr. Roland Maas of La Trobe University. The leaching

process involved the washing of the bulk muscovite separate in 0.5-1.0M HCl which was then centrifuged, dried, and weighed. The muscovite was leached for one hour in 6M HCl in a closed beaker at 100°C. The sample was further centrifuged with the leachate, and using a pipette, transferred to a new beaker. This process was then repeated in Milli-Q water. The leachate and residue were dried and re-weighed for analysis.

Isochron ages and errors were calculated using the ISOPLOT program of Ludwig (1990). Two point isochrons are Model-1 fits (the only cause of scatter are the assigned errors i.e. analytical reproducibility), whereas the 4-point isochron for RJ280 is a Model-3 fit (scatter is due to a combination of assigned errors plus an unknown but normally distributed variation of initial $^{87}Sr/^{86}Sr$). Errors on all ages are 2σ.

Results (T. E. Waight pers. comm. 1997)

The results of the Rb-Sr isotope determination are given in the table below:

Sample	$^{87}Rb/^{86}Sr$	$^{87}Sr/^{86}Sr$	Rb (ppm)	Sr (ppm)
RJ81 whole rock	1.1466	0.71181±2	95.9	242.1
RJ81 muscovite.	1.7487	0.71273±3	59.6	98.7
RJ280 whole rock	1.1617	0.71507±2	85.6	213.3
RJ280 musc. (bulk)	1.3938	0.71565±2	111.0	230.5
RJ280 musc. (leach)	3.6482	0.72115±15	4.8	3.8
RJ280 musc. (residue)	1.5139	0.71577±10	109.6	209.5

Muscovite(bulk)-whole rock two point isochrons for the two samples give the following ages:

- RJ81 108 ± 12Ma (two point isochron)
- RJ280 176 ± 31Ma (two point isochron)

The error for RJ280 is large because of the lack of variability in $^{87}Rb/^{86}Sr$ and $^{87}Sr/^{86}Sr$ muscovite and whole rock values. Leaching on RJ280 helped to reduce these errors (see table). A four point isochron (whole rock, musc. bulk, musc. leach, musc. residue), using the same analytical percentage errors as mentioned previously, yielded an age of:

- RJ280 173 ± 15Ma (four point isochron).

APPENDIX 3: Classification schemes and terminology

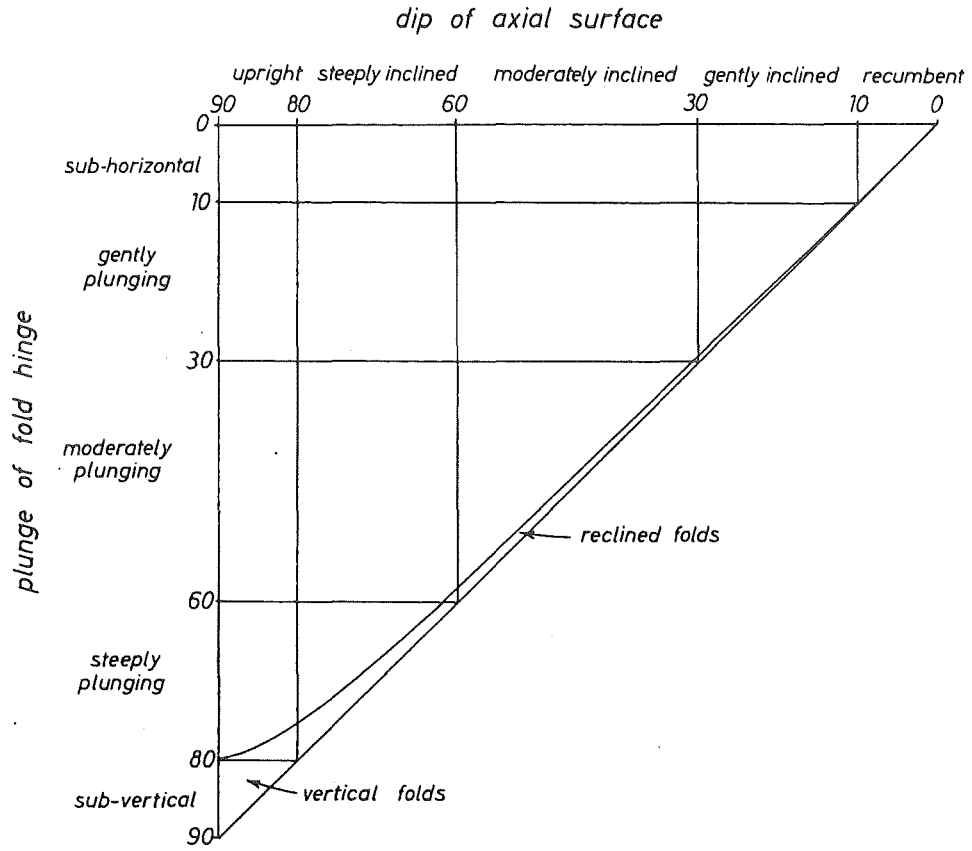

Classification of fold orientation (after Fleuty, 1964)

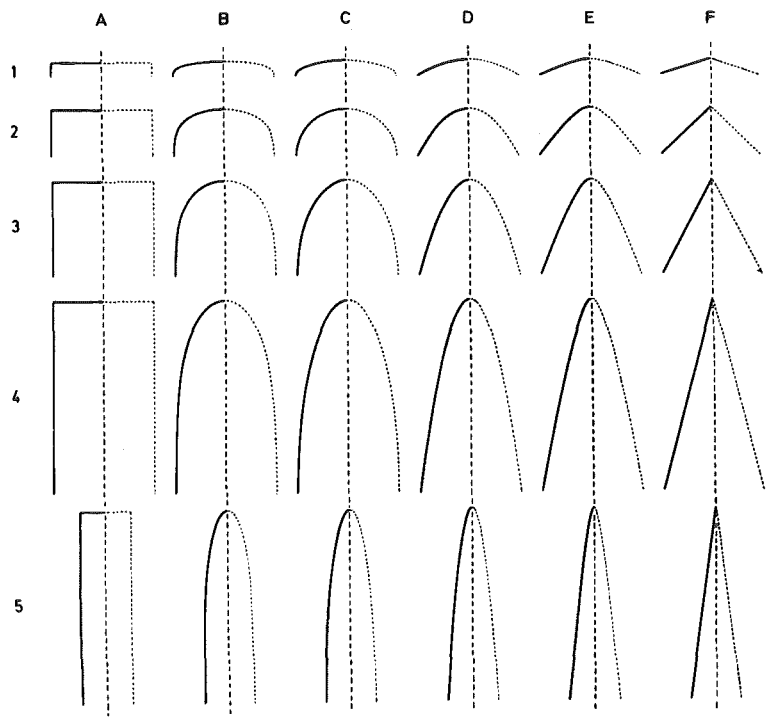

Classification of fold shape (after Hudleston, 1973).

Table 6.4 A classification of fault rocks (modified after Sibson, 1977).

		Random–fabric	Foliated	
Incohesive		*Fault breccia* (visible fragments > 30% of rock mass)	*Foliated fault breccia*	
		Fault gouge (visible fragments < 30% of rock mass)	*Foliated gouge*	
Cohesive	glass/devitrified glass	Pseudotachylite	*Foliated Pseudotachylite*	
	Nature of matrix: tectonic reduction in grain size dominates; grain growth by recrystallisation and neomineralisation	Crush breccia Fine crush breccia Crush microbreccia	(fragments > 0·5 cm) (0·1 cm < fragments < 0·5 cm) (fragments < 0·1 cm)	0–10%
		Protocataclasite	Protomylonite	10–50%
		Cataclasite	Mylonite	50–90%
		Ultracataclasite Flinty crush rock	Ultramylonite	90–100%
	grain growth pronounced	?	Blastomylonite	

cataclasite series; Phyllonite varieties; mylonite series; Proportion of matrix

Classification of fault rocks (after McClay, 1987 which is a modified version of Sibson, 1977).

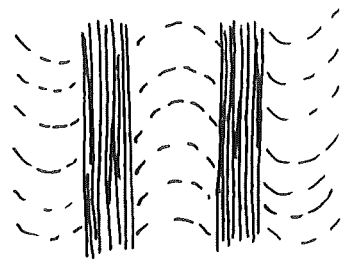

Zonal crenulation cleavage
with sharp boundaries

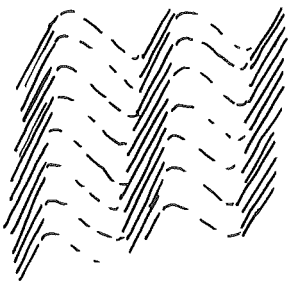

Zonal crenulation cleavage
with gradational boundaries

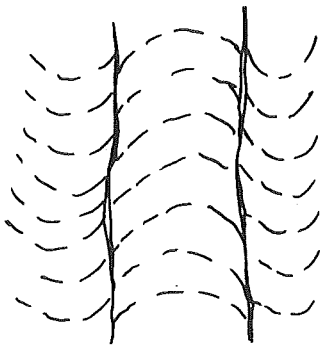

Discrete crenulation cleavage
(usually defined by opaque solution seams)

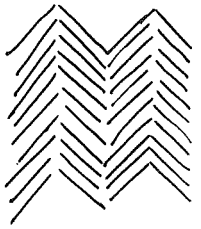

Crenulation only .
(no dissolution)

Terminology for crenulation cleavage (modified after Powell, 1979 and Borradaile *et al.*, 1982). Zonal crenulation cleavage occupies a volume of rock comparable to the volume of uncrenulated rock. In contrast, discrete cleavage occupies only a very small percentage volume of the rock.

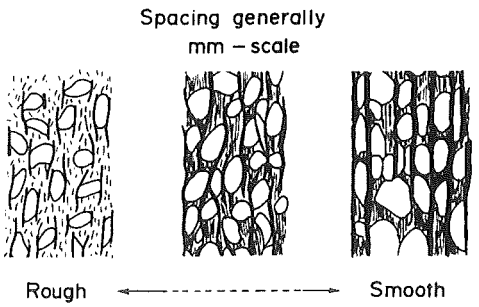

Pressure solution seam shape in sandy lithologies with no pre-existing planar anisotropy (after Powell, 1979).

APPENDIX 4: Sample Reference

A complete list of samples stored and catalogued in the Department of Geological Sciences, University of Canterbury, is given in the tables that follow. The samples listed include those mentioned in the thesis and all thin-sections made during the course of study. The tables are arranged in chapter order of areal domains and Balloon Mélange. The last table lists samples from reconnaissance fieldwork.

Key to tables

- "Field no." refers to the sample number used in the field.
- "UC no." refers to University of Canterbury collection catalogue number.
- "Grid reference" is based on the NZMS 260 topographic map series.
- "Main foliation/cleavage" refers to the main foliation/cleavage surface(s) observed in thin-section.
- "Handspecimen orientation" refers to the orientation of the dip and strike symbol given on the handspecimen. A hooked dip symbol on the specimen indicates the measurement was taken on the bottom surface. For storage space reasons, only samples referred to in the text have handspecimens catalogued. If a handspecimen orientation is not given in the tables then there is no handspecimen associated with the thin-section(s).
- "XZ section" refers to the thin-section that is parallel to the stretching lineation and perpendicular to the main cleavage/schistosity.
- "YZ section" refers to the thin-section that is perpendicular to both the stretching lineation and main cleavage/schistosity.
- "XY section" refers to the thin-section parallel to the main cleavage/schistosity.
- "Section ⊥ to intersect lin" refers to the thin-section (sub) perpendicular to the S_3 intersect lineation (unless otherwise indicated) and perpendicular to the main cleavage/schistosity. Two ticks in this column mean there is also a thin-section parallel to the intersect lineation.

Note: cleavage designations written on handspecimens and thin-section labels are local designations used during the research period and should not be compared to the regional cleavage chronological designation given in the thesis and appendix tables.

Boulder Lake domain: Buller terrane

Field no.	UC no.	Grid reference	Rock unit	Description	Main foliation/ cleavage	handspecimen orientation	XZ section	YZ section	Section ⊥ to intersect lin
RJ4	16054	M26/735330	Golden Bay Group	crenulated phyllite	S_2, S_{cren}				✓ S_{cren}
RJ112	16055	M26/746351	Golden Bay Group	phyllite	S_2		2 perpendicular thin-sections		
RJ114	16056	M26/747352	Golden Bay Group	graphitic phyllite	S_2, S_3				✓
RJ116	16057	M26/747353	Golden Bay Group	graphitic slate	S_2, S_3				✓
RJ120	16058	M26/740332	Golden Bay Group	phyllite	S_2, S_3				✓
RJ283	16059	M26/737338	Golden Bay Group	graphitic slate	S_2, S_{cren}				✓✓ S_{cren}
RJ286	16060	M26/737338	Golden Bay Group	slaty quartz sandstone	S_2				✓ S_{cren}
RJ287	16061	M26/737338	Golden Bay Group	crenulated phyllite	S_2, S_{cren}				✓✓ S_{cren}
RJ289	16062	M26/739337	Golden Bay Group	sandy schist	S_2				✓✓ S_{cren}
RJ290	16063	M26/737335	Golden Bay Group	sandy schist	S_2		✓ (approx.)		
RJ291	16064	M26/736333	Golden Bay Group	crenulated schist	S_2, S_{cren}	034/44°SE			✓ S_{cren}
RJ294	16065	M26/733333	Golden Bay Group	crenulated schist	S_2, S_{cren}	039/61°SE	✓	✓	
RJ297	16066	M26/732332	Olympus Granite	mylonitic granite	biotite foliation		✓		
RJ298	16067	M26/732332	Olympus Granite	mylonitic granite	biotite foliation		✓		
RJ299	16068	M26/731332	Olympus Granite	mylonitic granite	biotite foliation	346/36°E	✓	✓	
RJ317	16069	M26/737331	Golden Bay Group	phyllite	S_2	011/38°E			✓✓ S_{cren}
RJ319	16070	M26/747350	Golden Bay Group	phyllite	S_2, S_3				✓
RJ331	16071	M26/744355	Golden Bay Group	phyllite	S_2	342/40°E	✓	✓	
RJ332	16072	M26/745355	Golden Bay Group	crenulated graphitic slate	S_2, S_3				✓
RJ334	16073	M26/738353	Golden Bay Group	quartzite	S_2		✓ (approx.)		
RJ335	16074	M26/736354	Golden Bay Group	graphitic slate/ schist	S_2	360/17°E	✓	✓	
RJ363	16075	M26/728329	Golden Bay Group	schist	S_2		✓	✓	
RJ364	16076	M26/727329	Golden Bay Group	crenulated schist	S_2, S_{cren}	064/54°SE	✓	✓	
RJ365	16077	M26/726329	Golden Bay Group	slaty quartz sandstone	S_2, S_{cren}				✓✓ S_{cren}
RJ366	16078	M26/723325	Golden Bay Group	schist	S_2				✓✓ S_{cren}
RJ367	16079	M26/725323	Golden Bay Group	crenulated graphitic slate	S_2, S_3	108/48°S			✓
RJ370	16080	M26/724326	Golden Bay Group	crenulated schist	S_2, S_{cren}	065/60°SE			✓ S_{cren}
RJ479	16081	M26/739352	Golden Bay Group	quartzite	S_2	338/28°E	✓	✓	
RJ479	16082	M26/739352	Olympus Granite	aplite	muscovite foliation	338/28°E	✓	✓	
RJ481	16083	M26/738353	Golden Bay Group	slaty quartz sandstone	S_2		✓ (approx.)	✓ (approx.)	
RJ482	16084	M26/737353	Golden Bay Group	schist	S_2, S_{cren}	265/50°N	✓	✓	
RJ503	16085	M26/737337	Golden Bay Group	graphitic slate	S_1(?), S_2				✓ S_2

Boulder Lake domain: Takaka terrane

Field no.	UC no.	Grid reference	Rock unit	Description	Main foliation/ cleavage	handspecimen orientation	XZ section	YZ section	Section ⊥ to intersect lin
RJ1	16086	M26/749347	undiff. Haupiri Group	phyllitic siltstone	S_2	025/37°SE	✓		
RJ2	16087	M26/749347	undiff. Haupiri Group	mylonitic conglomerate	S_2	008/36°E	no thin-section		
RJ6	16088	M26/747338	undiff. Haupiri Group	volcanic derived sandstone	S_2		unoriented thin-section		
RJ7	16089	M26/746338	undiff. Haupiri Group	phyllite siltstone	S_2		✓		
RJ10	16090	M26/746339	undiff. Haupiri Group	slaty sandstone/ phyllitic siltstone	S_2, S_3	022/42°E	✓ (approx.)		
RJ29	16091	M26/750347	undiff. Haupiri Group	volcanic derived siltstone/ sandstone	S_2	360/61°E	✓		
RJ31	16092	M26/749347	undiff. Haupiri Group	phyllite	S_2		✓	✓ (approx.)	
RJ32	16093	M26/749347	undiff. Haupiri Group	phyllite	S_2		✓		
RJ33	16094	M26/749347	undiff. Haupiri Group	mylonitic conglomerate	S_2	017/38°E	no thin-section		
RJ34	16095	M26/749347	undiff. Haupiri Group	mylonitic conglomerate	S_2	355/37°W	✓		
RJ35	16096	M26/749347	undiff. Haupiri Group	volcanic derived siltstone/ sandstone	S_2		✓		
RJ64	16097	M26/745339	undiff. Haupiri Group	slaty sandstone	S_2		✓		
RJ65	16098	M26/746339	undiff. Haupiri Group	crenulated phyllitic siltstone	S_2, S_3	030/46°SE	✓		✓
RJ67	16099	M26/746339	undiff. Haupiri Group	volcanic derived siltstone/ sandstone	S_2		✓		
RJ68	16100	M26/746338	undiff. Haupiri Group	crenulated phyllite	S_2, S_3	unoriented			✓
RJ70	16101	M26/746338	undiff. Haupiri Group	crenulated slaty siltstone	S_2, S_3				✓
RJ73	16102	M26/747338	undiff. Haupiri Group	slaty siltstone/ sandstone	S_2 (oblique to S_0)		unoriented thin-section		
RJ74	16103	M26/747338	undiff. Haupiri Group	slaty siltstone	S_2 (oblique to S_0)		✓		
RJ76	16104	M26/749347	undiff. Haupiri Group	slaty siltstone	S_2		✓	✓	
RJ77	16105	M26/749347	undiff. Haupiri Group	tuff/ reworked tuff	S_2		✓	✓	
RJ78	16106	M26/749347	undiff. Haupiri Group	mylonitic conglomerate	S_2	014/32°E	✓	✓	
RJ78A	16107	M26/749347	undiff. Haupiri Group	crenulated phyllite	S_2, S_3				✓
RJ79	16108	M26/749347	undiff. Haupiri Group	crenulated phyllite	S_2, S_3				✓
RJ80	16109	M26/749347	undiff. Haupiri Group	crenulated slaty sandstone	S_2, S_3				✓
RJ81	16110	M26/749347	undiff. Haupiri Group	phyllite	S_2, S_3	used for dating	✓ (approx.)	✓ (approx.)	
RJ82	16111	M26/749347	undiff. Haupiri Group	phyllite	S_2		✓	✓	
RJ83	16112	M26/749347	undiff. Haupiri Group	mylonitic conglomerate	S_2	356/45°E			
RJ84	16113	M26/749347	undiff. Haupiri Group	phyllite/ phyllonite?	S_2	011/34°E	✓	✓ (approx.)	
RJ85	16114	M26/733322	undiff. Haupiri Group	slaty sandstone	S_2, S_3				✓
RJ87	16115	M26/735322	undiff. Haupiri Group	crenulated slaty siltstone	S_2, S_3	034/32°SE			✓
RJ88	16116	M26/734322	undiff. Haupiri Group	tuff/ reworked tuff	S_2		✓ (approx.)		
RJ92	16117	M26/752343	undiff. Haupiri Group	strained conglomerate	S_2	335/69°SW	no thin-section		
RJ95	16118	M26/750344	undiff. Haupiri Group	slaty siltstone	S_2, S_3				✓
RJ98	16119	M26/747342	undiff. Haupiri Group	tuff/ reworked tuff	S_2		✓		
RJ99	16120	M26/749348	undiff. Haupiri Group	phyllitic sandy siltstone	S_2, S_3	018/41°E	✓	✓	
RJ100	16121	M26/749348	undiff. Haupiri Group	phyllitic siltstone (with calcite layers)	S_2, S_3	030/34°SE	✓	✓	✓
RJ101	16122	M26/749348	undiff. Haupiri Group	crenulated phyllitic siltstone	S_2, S_3				✓
RJ103	16123	M26/748348	undiff. Haupiri Group	slaty sandstone	S_2	018/44°E	✓	✓	
RJ104	16124	M26/749349	undiff. Haupiri Group	tuff/ reworked tuff	S_2	016/32°E	✓		
RJ107	16125	M26/749349	undiff. Haupiri Group	phyllite	S_2	015/34°E	✓	✓	

Boulder Lake domain: Takaka terrane (continued)

Field no.	UC no.	Grid reference	Rock unit	Description	Main foliation/ cleavage	handspecimen orientation	XZ section	YZ section	Section ⊥ to intersect lin
RJ108	16126	M26/749349	undiff. Haupiri Group	phyllite	S_2	012/34°E	✓	✓	
RJ109	16127	M26/749349	undiff. Haupiri Group	volcanic derived siltstone/ sandstone	S_2		✓		
RJ110	16128	M26/750350	undiff. Haupiri Group	phyllitic siltstone	S_2 (oblique to S_0)		✓		
RJ117	16129	M26/749355	undiff. Haupiri Group	slaty sandstone	S_2	358/34°E	✓	✓	
RJ118	16130	M26/749355	undiff. Haupiri Group	slaty sandstone/ siltstone	S_2		✓	✓	
RJ123	16131	M26/740331	undiff. Haupiri Group	crenulated slaty siltstone	S_2, S_3				✓
RJ125	16132	M26/740331	undiff. Haupiri Group	metalimestone	S_2		✓	✓	
RJ126	16133	M26/740331	undiff. Haupiri Group	sandy phyllite	S_2, S_3	068/28°SE	✓	✓	
RJ127	16134	M26/741330	undiff. Haupiri Group	volcanic derived sandstone	S_2, S_3		✓		
RJ279	16135	M26/748350	undiff. Haupiri Group	phyllitic sandy siltstone	S_2	012/31°E	✓	✓	
RJ280	16136	M26/748350	undiff. Haupiri Group	phyllite	S_2, S_3	used for dating			✓
RJ282	16137	M26/750361	undiff. Haupiri Group	slaty siltstone	S_1, S_3	141/13°			✓
RJ307	16138	M26/745339	undiff. Haupiri Group	marble	S_2, S_3		2 perpendicular thin-sections		
RJ309	16139	M26/745339	undiff. Haupiri Group	phyllitic sandy siltstone	S_2	029/49°SE	✓	✓	
RJ310	16140	M26/745339	undiff. Haupiri Group	phyllitic sandy siltstone	S_2, S_3		✓	✓	
RJ312	16141	M26/734324	undiff. Haupiri Group	marble	S_3		unoriented thin-section		
RJ314	16142	M26/739329	undiff. Haupiri Group	phyllite sandy siltstone	S_2, S_3	022/48°E	✓	✓	
RJ322	16143	M26/747351	undiff. Haupiri Group	phyllite sandy siltstone	S_2, S_3	356/32°E	✓	✓	
RJ323	16144	M26/747351	undiff. Haupiri Group	marble	S_2, S_3				✓
RJ325	16145	M26/748351	undiff. Haupiri Group	phyllite sandy siltstone	S_2	004/29°E	✓	✓	
RJ326	16146	M26/748351	undiff. Haupiri Group	phyllitic siltstone/ sandstone	S_2, S_3	003/30°E	✓	✓	
RJ327	16147	M26/748351	undiff. Haupiri Group	phyllitic siltstone/ sandstone	S_2	360/30°E	✓	✓	
RJ328	16148	M26/749351	undiff. Haupiri Group	strained conglomerate	S_2	360/12°E	no thin-section		
RJ337	16149	M26/764326	undiff. Haupiri Group	strained conglomerate	S_1	002/66°E	no thin-section		
RJ338	16150	M26/765327	Devil River Volcanics Grp.	altered volcanic/ intrusive			unoriented thin-section		
RJ341	16151	M26/736323	undiff. Haupiri Group	crenulated slaty sandstone	S_2, S_3				✓
RJ342	16152	M26/737323	undiff. Haupiri Group	strained conglomerate	S_2	053/37°SE	no thin-section		
RJ355	16153	M26/767367	undiff. Haupiri Group	strained conglomerate	S_1	010/70°E	no thin-section		
RJ356	16154	M26/768365	undiff. Haupiri Group	strained conglomerate	S_1	360/00°	no thin-section		
RJ361	16155	M26/770351	undiff. Haupiri Group	strained conglomerate	S_1	341/84°W	no thin-section		
RJ362	16156	M26/770351	undiff. Haupiri Group	strained conglomerate	S_1	350/84°W	no thin-section		
RJ475	16157	M26/755348	Devil River Volcanics Grp.	metadolerite		unoriented	unoriented thin-section		
RJ477	16158	M26/753339	undiff. Haupiri Group	shale	S_1, S_3				✓
RJ483	16159	M26/752357	undiff. Haupiri Group	siltstone	S_1, S_3	011/52°E			✓
RJ487	16160	M26/745362	undiff. Haupiri Group	phyllite sandy siltstone	S_2, S_3		✓	✓	
RJ489	16161	M26/755346	undiff. Haupiri Group	siltstone	S_1, S_3				✓
RJ490	16162	M26/758348	undiff. Haupiri Group	shale/ sandstone	S_1, S_3(subtle)				✓ S_1
RJ491	16163	M26/752360	undiff. Haupiri Group	slaty shale	S_1, S_3				✓ S_1
RJ492	16164	M26/753360	undiff. Haupiri Group	slaty siltstone	S_1, S_3				✓
RJ493	16165	M26/755357	undiff. Haupiri Group	siltstone	S_1, S_3				✓

Adelaide Tarn and Lonely Lake domains: Buller terrane

Field no.	UC no.	Grid reference	Rock unit	Description	Main cleavage	handspecimen orientation	XZ section	YZ section	Section ⊥ to intersect lin
RJ42	16166	M26/717292	Douglas Formation	crenulated laminated slaty siltstone	S_1, S_3	066/57°SE			✓
RJ43A	16167	M26/710283	Douglas Formation	crenulated laminated slaty siltstone	S_1, S_3	unoriented			✓
RJ203	16168	M26/721292	Douglas Formation	crenulated laminated slaty siltstone	S_1, S_3	060/42°SE			✓
RJ208	16169	M26/724292	Douglas Formation	crenulated laminated slaty siltstone	S_1, S_3				✓
RJ211	16170	M26/709281	Douglas Formation	crenulated laminated slaty siltstone	S_1, S_3	093/71°S			✓
RJ212	16171	M26/710286	Douglas/Leslie Formation	crenulated laminated slaty siltstone	S_1, S_3				✓
RJ215	16172	M26/710291	Douglas Formation	crenulated laminated slaty siltstone	S_1, S_3				✓
RJ218	16173	M26/722302	Douglas Formation	crenulated laminated slaty siltstone	S_1, S_3				✓
RJ469	16174	M26/725259	Douglas Formation	crenulated laminated slaty siltstone	S_1, S_3	049/39°SE			✓
RJ472	16175	M26/721251	Douglas Formation	crenulated siltstone/ sandstone	S_1, S_3				✓
RJ473	16176	M26/727250	Douglas Formation	crenulated siltstone/ sandstone	S_1, S_3				✓
RJ474	16177	M26/722251	Douglas Formation	crenulated siltstone/ sandstone	S_1, S_3	335/40°NE			✓
RJ506	16178	M26/725307	Leslie Formation (?)	graphitic slaty siltstone	S_1, S_3				✓

Adelaide Tarn and Lonely Lake domains: Takaka terrane

Field no.	UC no.	Grid reference	Rock unit	Description	Main cleavage	handspecimen orientation	XZ section	YZ section	Section ⊥ to intersect lin
RJ204	16179	M26/727291	undiff. Haupiri Group	crenulated slaty siltstone	S_1, S_3	055/39°SE			✓
RJ205	16180	M26/726291	undiff. Haupiri Group	crenulated slaty pebbly siltstone	S_1, S_3	046/54°SE			✓
RJ221	16181	M26/724303	Devil River Volcanics Grp.	metadolerite	chloritic foliation	unoriented	✓(?)		
RJ449	16182	M26/729245	undiff. Haupiri Group	slaty sandstone/ siltstone	S_1, S_3				✓
RJ451	16183	M26/729246	undiff. Haupiri Group	slaty shale	S_1, S_3				✓
RJ454	16184	M26/729252	undiff. Haupiri Group	slaty sandstone/ shale	S_1	353/47°E	✓(?)		
RJ457	16185	M26/729253	undiff. Haupiri Group	slaty sandstone/ siltstone	S_1				✓
RJ460	16186	M26/728255	undiff. Haupiri Group	metasomatised shear zone rock	shear foliation, S_3		✓(?)		
RJ464	16187	M26/729253	Devil River Volcanics Grp.	metasomatised intrusive			unoriented thin-section		
RJ466	16188	M26/729255	undiff. Haupiri Group	slaty siltstone/ sandstone	S_1	336/70°NE	✓(?)		
RJ467	16189	M26/733256	undiff. Haupiri Group	slaty siltstone	S_1, S_3	309/39°NE			✓ S_1
RJ471	16190	M26/728257	undiff. Haupiri Group	slaty shale	S_1, S_3				✓✓
RJ495	16191	M26/729290	undiff. Haupiri Group	crenulated slaty shale	S_1, S_3	066/44°SE			✓✓
RJ499	16192	M26/726257	undiff. Haupiri Group	crenulated slaty sandstone	S_1, S_3				✓
RJ500	16193	M26/725256	undiff. Haupiri Group	slaty sandstone	S_1		✓		
RJ502	16194	M26/755261		metasomatised dolerite			unoriented thin-section		

Peak 1610 and Kakapo Peak domains: Buller terrane

Field no.	UC no.	Grid reference	Rock unit	Description	Main cleavage	handspecimen orientation	XZ section	YZ section	Section ⊥ to intersect lin
RJ184	16195	M26/721216	Douglas Formation	slaty laminated siltstone	S_1				✓ S_1
RJ186	16196	M26/723212	Leslie Formation (?)	dark grey slaty shale	S_1, S_{ii}				✓ S_{ii}
RJ426	16197	M26/723207	foliated fault breccia btw. Leslie Formation (?) and Douglas Formation				unoriented thin-section		
RJ427	16198	M26/725198	Leslie Formation (?)	slaty siltstone	S_1				✓✓ S_1
RJ433	16199	M26/724204	Leslie Formation (?)	dark grey slaty shale	S_1	335/71°E			✓ S_1

Peak 1610 and Kakapo Peak domains: Takaka terrane

Field no.	UC no.	Grid reference	Rock unit	Description	Main cleavage	handspecimen orientation	XZ section	YZ section	Section ⊥ to intersect lin
RJ146	16200	M26/722221	Summit Limestone	deformed limestone	S_1		unoriented thin-section		
RJ147	16201	M26/722221	Summit Limestone	metalimestone with chert	S_1		✓ (?)		
RJ148	16202	M26/722221	Buller terrane derived	foliated brittle shear zone rock		unoriented	no thin-section		
RJ149	16203	M26/722221	Summit Limestone	calc-mylonite	S_1	330/52°NE	✓		
RJ153	16204	M26/721226	undiff. Haupiri Group	slaty shale	S_1		✓		
RJ155	16205	M26/721226	undiff. Haupiri Group	slaty shale	S_1	346/62°E	✓		
RJ157	16206	M26/722224		altered dolerite			unoriented thin-section		
RJ159	16207	M26/722226	Devil River Volcanics Grp.	altered basic volcanic rock			unoriented thin-section		
RJ160	16208	M26/722226	undiff. Haupiri Group	metalimestone in volcanic horizon	S_1		✓		
RJ161	16209	M26/722226	Devil River Volcanics Grp.	altered basic volcanic rock	S_1	329/50°NE	unoriented thin-section		
RJ162	16210	M26/722226	Devil River Volcanics Grp.	tuff/ reworked tuff	S_1	324/62°NE	no thin-section		
RJ164	16211	M26/722226	undiff. Haupiri Group	metalimestone	S_1		✓		
RJ168	16212	M26/721228	undiff. Haupiri Group	slaty siltstone/ very fine sandstone	S_1	347/65°E	✓		✓ S_1
RJ169	16213	M26/721228	undiff. Haupiri Group	slaty shale	S_1	007/45°E	✓ (?)		
RJ171	16214	M26/724224	undiff. Haupiri Group	slaty shale	S_1	320/49°NE	✓	✓	
RJ174	16215	M26/722234	Devil River Volcanics Grp.	dolerite			unoriented thin-section		
RJ176	16216	M26/720230	undiff. Haupiri Group	slaty shale	S_1	322/57°NE	✓		✓ S_1
RJ177	16217	M26/721227	undiff. Haupiri Group	slaty shale	S_1	332/56°NE	✓		
RJ179	16218	M26/721227	undiff. Haupiri Group	deformed granule sandstone	S_1		✓		
RJ188	16219	M26/725221	Summit Limestone	deformed limestone	S_1	355/88°W	unoriented thin-section		
RJ191	16220	M26/725210	Summit Limestone	metalimestone	S_1	090/62°N	unoriented thin-section		
RJ194	16221	M26/724209	Summit Limestone	metalimestone	S_1		unoriented thin-section		
RJ198	16222	M26/725206	undiff. Haupiri Group	metasomatised tuff?	S_1		✓ (?)		
RJ200	16223	M26/725206	Summit Limestone	metalimestone	S_1		unoriented thin-section		
RJ408	16224	M26/725201	Summit Limestone	sandy metalimestone	S_1	359/74°E	✓	✓	
RJ409	16225	M26/725201	Summit Limestone	calc-mylonite	S_1		✓		
RJ410	16226	M26/725201	undiff. Haupiri Group	slaty sandy shale	S_1		✓		
RJ412	16227	M26/725201	undiff. Haupiri Group	limestone horizon rich in allochems	S_1		unoriented thin-section		
RJ413	16228	M26/725201	undiff. Haupiri Group	slaty shale	S_1	002/80°E	✓	✓	
RJ415a	16229	M26/726202	Devil River Volcanics Grp.	basalt with pyroxene phenocrysts			unoriented thin-section		

Peak 1610 and Kakapo Peak domains: Takaka terrane (continued)

Field no.	UC no.	Grid reference	Rock unit	Description	Main cleavage	handspecimen orientation	XZ section	YZ section	Section ⊥ to intersect lin
RJ417	16230	M26/726204	Devil River Volcanics Grp.	calcareous tuff/ reworked tuff	S_1		✓		
RJ418	16231	M26/726205	Devil River Volcanics Grp.	metasomatised intrusive/ volcanic			unoriented thin-section		
RJ420	16232	M26/726205	Devil River Volcanics Grp.	calcareous volcanic derived epiclastic	S_1		✓	✓	
RJ440	16233	M26/725201	undiff. Haupiri Group	slaty shale	S_1	355/70°E	✓	✓	
RJ442	16234	M26/727204	Devil River Volcanics Grp.	metasomatised intrusive/ volcanic			unoriented thin-section		
RJ443	16235	M26/728201	Devil River Volcanics Grp.	metasomatised intrusive/ volcanic			unoriented thin-section		

Mt Benson domain: Buller terranes

Field no.	UC no.	Grid reference	Rock unit	Description	Main cleavage	handspecimen orientation	XZ section	YZ section	Section ⊥ to intersect lin
RJ130	16236	M26/729156	Leslie Formation (?)	dark grey slaty shale	S_1	336/42°NE			✓ S_1
RJ131	16237	M26/729156	Leslie Formation (?)	dark grey slaty shale	S_1	337/48°NE			✓ S_1
RJ132	16238	M26/729156	Leslie Formation (?)	dark grey slaty shale	S_1				✓ S_1
RJ140	16239	M26/731157	Leslie Formation (?)	dark grey slaty shale	S_1				✓ S_1

Mt Benson domain: Takaka terrane

Field no.	UC no.	Grid reference	Rock unit	Description	Cleavage	handspecimen orientation	XZ section	YZ section	Section ⊥ to intersect lin
RJ57	16240	M26/732154	Summit Limestone	metalimestone	cleavage		✓		
RJ135	16241	M26/732154	adjacent to Summit L/S	calcareous slaty sandstone	cleavage		✓ (?)		
RJ136	16242	M26/732155	Summit Limestone	sandy metalimestone	cleavage		✓		
RJ137	16243	M26/732155	Summit Limestone	calc-mylonite	layering	360/73°E	✓		
RJ138	16244	M26/732157	adjacent to Summit L/S	slaty shale	slaty cleavage	346/85°E	unoriented thin-section		
RJ142	16245	M26/733154	adjacent to Summit L/S	metalimestone and slaty shale	cleavage	336/69°NE	✓		
RJ143	16246	M26/733154	adjacent to Summit L/S	metalimestone and slaty shale	cleavage	341/70°E	✓	✓	
RJ144	16247	M26/733154	adjacent to Summit L/S	metalimestone and slaty shale	cleavage		✓		

Crow River domain

Field no.	UC no.	Grid reference	Rock unit	Description	Cleavage	handspecimen orientation	XZ section	YZ section	Section ⊥ to intersect lin
RJ8G	16248	M27/704877	Crow Granite	Granite used for zircon dating		unoriented	no thin-section		
RJ220A	16249	M27/689887	Douglas Formation	slaty graphitic shale	S_1 (?)				✓ S_1 (?)
RJ222	16250	M27/695886	Douglas Formation	pelitic hornfels			unoriented thin-section		
RJ223	16251	M27/695886	Douglas Formation	semi-pelitic hornfels			unoriented thin-section		
RJ224	16252	M27/698872	Douglas Formation	semi-pelitic hornfels			unoriented thin-section		
RJ226	16253	M27/698872	Douglas Formation	pelitic hornfels			unoriented thin-section		
RJ228	16254	M27/712870	Summit Limestone	fine grained marble	layering		✓		
RJ229	16255	M27/711870	Summit Limestone	metalimestone	cleavage		unoriented thin-section		
RJ231	16256	M27/711870	Hornfelsed sediment	cemented fault breccia			unoriented thin-section		
RJ232	16257	M27/712876	Crow Granite	protocataclasite/ cataclasite			unoriented thin-section		
RJ234	16258	M27/714877	unknown	carbonate metasomatised acid volcanic			unoriented thin-section		
RJ235	16259	M27/714878	Hornfelsed sediment	very fine quartz sandstone			unoriented thin-section		
RJ237	16260	M27/713878	fault contact between Crow Granite and hornfelsed sediment			073/64°N	no thin-section		
RJ238	16261	M27/713878	Hornfelsed sediment	semi-pelitic hornfels		067/85°NW	unoriented thin-section		
RJ241	16262	M27/715881	Summit Limestone	fine grained marble	layering		✓ (?)		
RJ243	16263	M27/716883	Summit Limestone	metalimestone in brittle fault zone	cleavage		✓		
RJ247	16264	M27/705901	Crow Granite	protocataclasite/ cataclasite		010/83°W			
RJ248	16265	M27/ float	Crow Granite	protocataclasite					
RJ252	16266	M27/708904	Summit Limestone	fined grained marble	layering	095/63°N	✓	✓	
RJ253	16267	M27/708904	Summit Limestone	metalimestone	cleavage	331/48°NE	✓		
RJ254	16268	M27/708904	Summit Limestone	metalimestone	cleavage		✓		
RJ255	16269	M27/708905	Summit Limestone	fine grained marble	layering	310/54°NE	✓		
RJ257	16270	M27/708905	Summit Limestone	fine grained marble	layering	306/59°NE	✓	✓	
RJ258	16271	M27/708906	Summit Limestone	fine grained marble	layering	346/82°E	✓	✓	
RJ259	16272	M27/708906	Summit Limestone	fine grained marble	layering	325/58°NE	✓	✓	
RJ261	16273	M27/705911	Anatoki Formation	coarse sandstone	cleavage		unoriented thin-section		
RJ262	16274	M27/702909	Summit Limestone	fine grained marble	layering		✓		
RJ263	16275	M27/702908	Summit Limestone	sandy metalimestone	cleavage		✓		
RJ264	16276	M27/702908	Summit Limestone	sandy metalimestone	cleavage		✓		
RJ266	16277	M27/702909	Hornfelsed sediment	semi-pelitic hornfels			unoriented thin-section		

Balloon Mélange

Field no.	UC no.	Grid reference	Rock unit	Description	Cleavage	handspecimen orientation	XZ section	YZ section	XY section
RJ375	16278	M26/753201	Balloon Mélange	mélange	$S_{mél}$	002/72°E	✓		
RJ377	16279	M26/743200		dolerite			unoriented thin-section		
RJ381	16280	M26/733205		dolerite			unoriented thin-section		
RJ382	16281	M26/733205		carbonate metasomatised dolerite			unoriented thin-section		
RJ385	16282	M26/732205		carbonate metasomatised dolerite			unoriented thin-section		
RJ386	16283	M26/731206	Balloon Mélange	mélange	$S_{mél}$	025/60°SE	no thin-section		
RJ388	16284	M26/735205	Balloon Mélange	sandstone inclusion	$S_{mél}$	unoriented	unoriented thin-section		
RJ390	16285	M26/731206	Balloon Mélange	mélange	$S_{mél}$	332/68°E	✓	✓	✓
RJ391	16286	M26/731206	Balloon Mélange	mélange	$S_{mél}$		✓	✓	
RJ446	16287	M26/735249	Balloon Mélange	mélange	$S_{mél}$, S_3	359/38°E	✓	✓	
RJ447	16288	M26/733249	Balloon Mélange	mélange	$S_{mél}$		✓		
RJ452	16289	M26/730246	Balloon Mélange	mélange	$S_{mél}$		✓		
RJ508	16290	M26/750324	Balloon Mélange	mélange	$S_{mél}$, S_3		unoriented thin-section		

Reconnaissance fieldwork

Field no.	UC no.	Location	Grid reference	Rock unit	Description	Cleavage/ foliation	XZ section	Section ⊥ to intersect lin
RJ18	16291	Wangapeka Valley	M28/665709		Anatoki Fault shear zone rock		unoriented thin-section	
RJ511	16292	Knuckle Hill	M25/731608	Separation Point Suite	mylonitic granite	biotite foliation	✓	
RJ512	16293	Parapara Peak	M25/828402	Bay Schist	crenulated graphitic slate	slaty and crenulation cleavages		✓ cren
RJ513	16294	Parapara Peak	M25/824405	Flowers Formation	slaty sandstone/ siltstone	slaty cleavage	unoriented thin-section	
RJ515	16295	Parapara Peak	M25/824403	Flowers Formation (Parawhakaoho Slate)	graphitic sandy slate	slaty cleavage	unoriented thin-section	
RJ516	16296	Parapara Peak	M25/824403	Flowers Formation (Parawhakaoho Slate)	graphitic slate	slaty cleavage subtle crenulation cleavage		✓ cren.
RJ522	16297	Pakawau	M25/827667 (float)	Separation Point Suite	mylonitic granitoid	quartz foliation	✓	

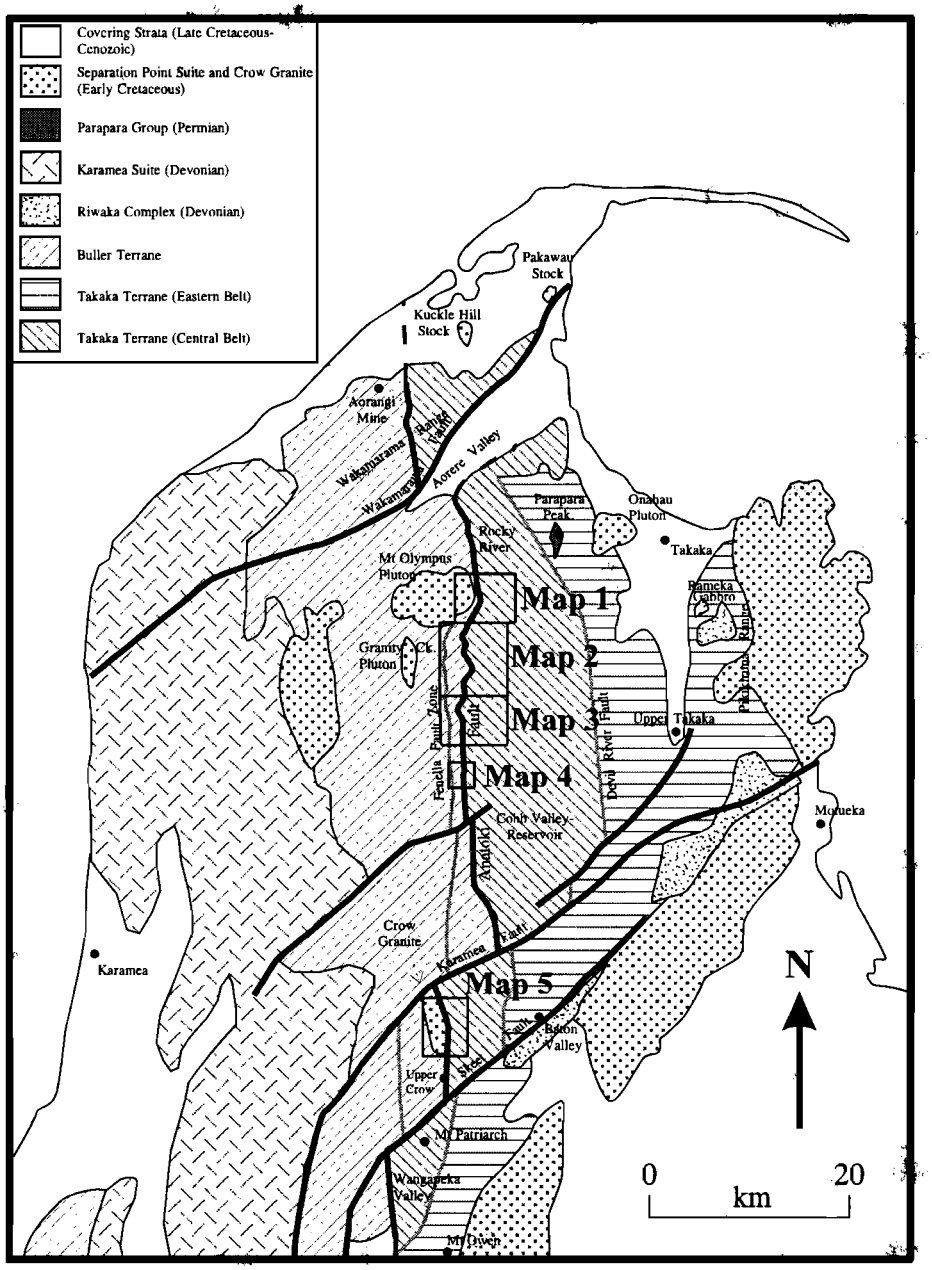

Location of Maps

Geological Legend for Maps 1 to 5

Rocks west of the Anatoki Fault

Early Cretaceous — Mt Olympus Granite

earliest Cretaceous — Crow Granite

Late Ordovician? — Hornfelsed sediment (Douglas Formation?)

Late Ordovician — Douglas Formation
sandy bedded Douglas Formation

Middle Ordovician? — Dark-grey to black shale/slate unit (Leslie Formation?)
thick quartzite bed

Middle Ordovician — Leslie Formation

Early Ordovician — Fenella Fault zone (Aorangi Mine Formation)
thick quartzite bed

Early Ordovician — Roaring Lion Formation

Rocks east of the Anatoki Fault

Age unknown — Doleitic dike

Early Ordovician — Summit Limestone

late Late Cambrian — Anatoki Formation

Late Cambrian — Balloon Mélange
Chert

Middle to early Late Cambrian — Undifferentiated Haupiri Group
coarse sandstone/grit dominated
marker horizon
conglomerate

Middle to early Late Cambrian — Devil River Volcanics Group
volcanics (lava pillow and flows, tuffs)
Volcanically derived epiclastics
(breccias, sandstones, siltstones)
Intrusives

early Middle Cambrian — Junction Formation

Planar structures

bedding (unknown facing)

upright bedding (face defined at outcrop)

overturned bedding (face defined at outcrop)

S_1
$S_{mél}$ in Balloon Mélange
S_{cren} in rocks west of the Anatoki Fault of Map 1.
Undesignated cleavage in Summit Limestone of Maps 3 and 4, and Douglas Formation of Map 5.

S_1 parallel to S_0
Undesignated cleavage parallel to S_0 in limestone sliver of Map 4.

S_2 (Map 1)
Calcite tectonite layering (Map 5)

S_2 parallel to S_0 (Map 1)

S_3 (Map 1 and 2)
S_{ii} (Map 3)

Locally developed cleavage which crenulates S_1 and/or S_2

Foliation in Mt Olympus Granite

Prominent joint set in Crow Granite

Outcrop

Contact located or located approximately

Contact inferred

Fault located or located approximately

Fault inferred

Brittle shear zone

Any symbol with "?" should be treated as speculative

Spot heights and contours are in metres
Contour interval is 100m

Lineations

L_0^1
L_2^{cren} in rocks west of the Anatoki Fault of Map 1

Mesoscale F_1

Mesoscale F_1 with vergence (this symbol shows anti-clockwise vergence when viewed down the fold axis)

L_0^3
L_2^3 in S_2 tectonites of Map 1

Mesoscale F_3 (Maps 1 and 2)
Mesoscale F_{ii} (Maps 3,4, and 5)

Mesoscale F_3 with vergence (this symbol shows anti-clockwise vergence when viewed down the fold axis)

Mesoscale fold associated with locally developed cleavage which crenulates S_1 and/or S_2

Stretching lineation

Axial plane traces

inferred — approximate

F_1 with or without plunge arrow

F_1 anticline (not overturned)

F_1 anticline (overturned)
F_i anticline (overturned) in Anatoki Fm of Map 5

F_1 syncline (not overturned)

F_1 syncline (overturned)
F_i syncline (overturned) in Anatoki Fm. of Map 5

F_1 anticline (open overturned)

F_1 syncline (open overturned)

F_3 antiform (overturned)

F_3 synform (overturned)

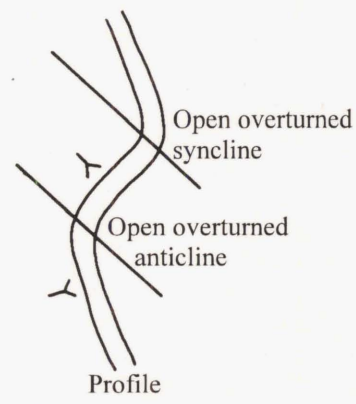

MAP 4: MT BENSON DOMAIN

1.2km

Waingaro Peak

1290

1390

1503

1672

Mt Be

0.2

N

Base map: NZMS260 Sheet M26

Scale 1:10 000

0 metres 1000

7

6

5

4

71

72

73